WL-TR-94-4094

# SDIO TRIBOMATERIALS / PRECISION GIMBAL DEMONSTRATION PROGRAM
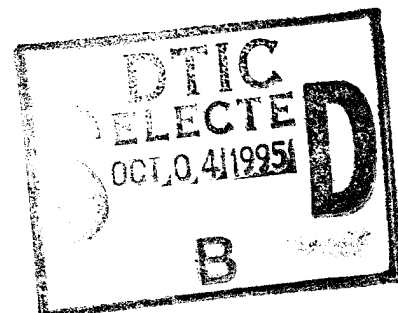
PHASE 2, FINAL REPORT

Stuart Loewenthal

Lockheed Missiles &Space Company
1111 Lockheed Way
Sunnyvale, Ca    94089

December 1993

Final Report For  02/28/93-09/30/93

Approved For Public Release;  Distribution Is Unlimited

MATERIALS DIRECTORATE
WRIGHT LABORATORY
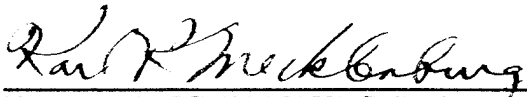AIR FORCE MATERIEL COMMAND
WRIGHT-PATTERSON AFB, OH 45343-7734

DTIC QUALITY INSPECTED 5

19951003 021

# NOTICE

When government drawings, specifications, or other data are used for any purpose other than in connection with a definitely related government procurement operation, the United States Government thereby incurs no responsibility nor any obligation whatsoever; and the fact that the government may have formulated, furnished, or in any way supplied the said drawings, specifications, or other data, is not to be regarded by implication or otherwise as in any manner licensing the holder or any other person or corporation, or conveying any rights or permission to manufacture, use, or sell any patented invention that may in any way be related thereto.
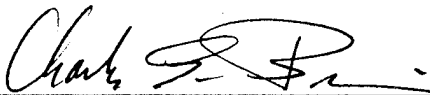
This technical report has been reviewed and is approved for publication.

KARL R. MECKLENBURG, Project Engineer
Nonstructural Materials Branch
Nonmetallic Materials Division

KENT J. EISENTRAUT, Chief
Nonstructural Materials Branch
Nonmetallic Materials Division

CHARLES E. BROWNING, Chief
Nonmetallic Materials Division
Materials Directorate

If your address has changed, if you wish to be removed from our mailing list, or if the addressee is no longer employed by your organization, please notify WL/MLBT, Bldg 654, 2941 P St, Ste 1, Wright-Patterson AFB OH 45433-7750 to help maintain a current mailing list.

Copies of this report should not be returned unless return is required by security considerations, contractual obligations, or notice on a specific document.

# REPORT DOCUMENTATION PAGE

Public reporting burden for this collection of information is estimated to average 1 hour per response, including the time for reviewing instructions, searching existing data sources, gathering and maintaining the data needed, and completing and reviewing the collection of information. Send comments regarding this burden estimate or any other aspect of this collection of information, including suggestions for reducing this burden, to Washington Headquarters Services, Directorate for Information Operations and Reports, 1215 Jefferson Davis Highway, Suite 1204, Arlington, VA 22202-4302, and to the Office of Management and Budget, Paperwork Reduction Project (0704-0188), Washington, DC 20503.

| 1. AGENCY USE ONLY (Leave blank) | 2. REPORT DATE | 3. REPORT TYPE AND DATES COVERED |
|---|---|---|
| | DEC 1993 | FINAL 02/28/93--09/30/93 |

**4. TITLE AND SUBTITLE**

SDIO TRIBOMATERIALS/PRECISION GIMBAL DEMONSTRATION PROGRAM PHASE 2, FINAL REPORT

**6. AUTHOR(S)**

STUART LOEWENTHAL

**5. FUNDING NUMBERS**

C SDIO84-89-C-0028
PE 63218
PR 1504
TA 00
WU 02

**7. PERFORMING ORGANIZATION NAME(S) AND ADDRESS(ES)**

LOCKHEED MISSILES & SPACE COMPANY
1111 LOCKHEED WAY
SUNNYVALE CA 94089

**8. PERFORMING ORGANIZATION REPORT NUMBER**

LMSC/F386643-33

**9. SPONSORING/MONITORING AGENCY NAME(S) AND ADDRESS(ES)**

MATERIALS DIRECTORATE
WRIGHT LABORATORY
AIR FORCE MATERIEL COMMAND
WRIGHT PATTERSON AFB OH 45433-7734

**10. SPONSORING/MONITORING AGENCY REPORT NUMBER**

WL-TR-94-4094

**11. SUPPLEMENTARY NOTES**

**12a. DISTRIBUTION/AVAILABILITY STATEMENT**

APPROVED FOR PUBLIC RELEASE; DISTRIBUTION UNLIMITED.

**12b. DISTRIBUTION CODE**

IS

**13. ABSTRACT (Maximum 200 words)**

The performance of high density, ion-sputtered molybdenum disulfide (MoS$_2$) films as long-life lubricants for precision gimbal bearing assemblies was demonstrated. These films show promise in terms of low friction, negligible outgassing, insensitivity to temperature, radiation resistance and absence of migration as associated with liquid space lubricants. Advances were sought to meet the stringent life, pointing and jitter requirements of SDIO gimbaled sensors, fine pointing antennas, CMG gimbals and other tribomechanisms.

A total of 270,000 life test hours were obtained in a vacuum on 55 pairs of precision angular contact ball bearings. Three sizes of bearings, lubricated with 33 different tribomaterial combinations (lubricant, bearing retainer material, ball material or coating) were tested. Benchmark life tests were conducted with liquid lubricants for space gimbals. Quality control issues with production MoS$_2$ films were identified.

Self-lubricating PTFE retainers were required for long life (> 40 million gimbal cycles). Bearings with polyimide retainers, silicon nitride ceramic balls or steel balls sputtered with MoS$_2$ film suffered early torque failure, irrespective of the type of race-sputtered MoS$_2$ film. Evidence of MoS$_2$ film fracture was found on most bearings from SEM examination. Six pairs of flight quality, 5 and 12 inch test bearings were life tested with a more fatigue resistant, high gold content, multilayer film. The torque performance associated with these larger gimbal bearings were more irregular than the 2 inch test bearings. Both the MoS$_2$ films and grease lubricated bearings produced long lives, although the torque with liquid lubricants was lower and less irregular. Gimbal pointing performance was directly related to bearing torque signature based on simulation.

**14. SUBJECT TERMS**

Bearings, Rolling Element, Gimbals, Lubrication, Life, Molydenum Disulfide, Spacecraft

**15. NUMBER OF PAGES**

260

**16. PRICE CODE**

| 17. SECURITY CLASSIFICATION OF REPORT | 18. SECURITY CLASSIFICATION OF THIS PAGE | 19. SECURITY CLASSIFICATION OF ABSTRACT | 20. LIMITATION OF ABSTRACT |
|---|---|---|---|
| UNCLASSIFIED | UNCLASSIFIED | UNCLASSIFIED | SAR |

NSN 7540-01-280-5500

# TABLE OF CONTENTS

## Section 1

# INTRODUCTION

This final report summarizes the work performed by Lockheed Missiles and Space Company, Inc. (LMSC), under SDIO Contract number SDIO84-89-C-0028, Tribomaterials/ Precision Gimbal Demonstration (T/PGD) program. The overall T/PGD goal is to demonstrate enhanced performance and life of Strategic Defense Initiative (SDI) vehicle systems via insertion of advanced tribomaterials into precision gimbal bearing assemblies. This is in recognition of the critical importance that bearings and lubricants have on the mission performance, reliability and survivability of SDI precision gimbals. In particular, tribomaterial advancements were needed to meet the stringent life and jitter requirements of SDIO gimbaled sensors, fine pointing antennas, CMG gimbals and other tribomechanisms.

LMSC T/PGD Program Plan is illustrated in Fig. 1-1. The program was structured into two phases plus an optional third phase. The 4-month Phase I conceptual design study was completed in October 1989. Current SDI tribomaterial limitations were identified, the performance of promising new solid and liquid lubricants were characterized, and their potential benefits to SDI gimbals were highlighted. This work was reported in the Phase I Final Report.

The Phase II effort covered the period of 28 February 1990 to 30 September 1993. The object of Phase II was to perform bearing component level validation tests in order to transition this technology into SDI spacecraft. At the beginning of the program these spacecraft were the Boost Surveillance and Tracking Satellite (BSTS) and Space Surveillance and Tracking Satellite (SSTS), both programs being resident at LMSC. Latter these programs were replaced by the Advanced Warning Satellite (AWS) and the Brilliant Eyes (BE) Satellite. However, at the time of this writing AWS has evolved into the Follow-on Early Warning System (FEWS) and SDIO has evolved into the Ballistic Missile Defense Organization (BMDO).

The work reported here covers the 3 year, Phase II component level demonstration effort. During this period 270,000 cumulative life test hours were obtained on 55 pairs of precision angular contact ball bearings lubricated with 33 different tribomaterial combinations (lubricant, bearing retainer material, ball material or coating). The main emphasis was on high density, ion-sputtered molybdenum disulfide ($MoS_2$) solid lubricant coatings which show promise in terms of low friction in a vacuum environment, negligible outgassing contamination, insensitivity to temperature, radiation resistance and absence of migration as associated with liquid space lubricants. Life tests were conducted in a vacuum over a simulated duty cycle for a space payload gimbal. Optimum retainer and ball material composition were investigated. Life tests were also conducted with comparable bearings lubricated with liquid space lubricants in order to directly compare the performance of the $MoS_2$ bearings with today's customary gimbal bearing lubricants. Such comparative benchmark tests were considered crucial in obtaining program acceptance for these advanced lubricants.

Screening tests were performed on smaller ($\approx$ 2-inch OD) high quality bearings in order to determine the best $MoS_2$ film - retainer & ball material combination for later testing in full scale, flight-quality gimbal bearings. These flight-like gimbal bearings were to two different sizes that enveloped those proposed for use in the Brilliant Eyes primary payload gimbals.

Scale-up performance and process quality control issues were to be addressed using these larger bearings ($\approx 5$ and 12 inch OD).

A goal of this work was to improve pointing performance of SDI gimbals through bearings which produced less drag disturbances. Gimbal pointing simulations performed in this investigation show that bearing torque ripple is a significant source of gimbal pointing jitter. The sensors aboard SDI spacecraft have stringent jitter requirements. An innovative LMSC bearing concept using a flexure showed that jitter levels could be reduced up by more than an order of magnitude under certain operating conditions.

A 2-year, Phase III gimbal system level demonstration was originally planned as an option to provide experimental "proof" of pointing performance improvements associated with advanced tribobearings. The validation testing was to be performed on large single and combined two axis gimbals, consistent with the large sensor gimbals aboard SDI satellites. However, the Phase III option was not exercised.

# TRIBOMATERIALS/PRECISION GIMBAL DEMONSTRATION (T/PGD)

**PROGRAM DESCRIPTION:**

BEARING / GIMBAL LEVEL DEMONSTRATION OF ADVANCED BEARING TRIBOMATERIALS TO MEET STRINGENT LIFE AND JITTER REQUIREMENTS OF MISSION CRITICAL SDI GIMBALLED SENSORS, FINE POINTING ANTENNAS, AND CMG GIMBALS



**APPLICATIONS**

- SENSORS AND SCAN MIRROR GIMBALS (BP, GSTS, BE)
- LASER X-LINK AND HIGH GAIN ANTENNA (ALL)
- CMG GIMBALS (BE, GSTS)     REACTION WHEELS (BP)
- OTHER TRIBO MECHANISMS (SOLAR ARRAY, DEPLOY)
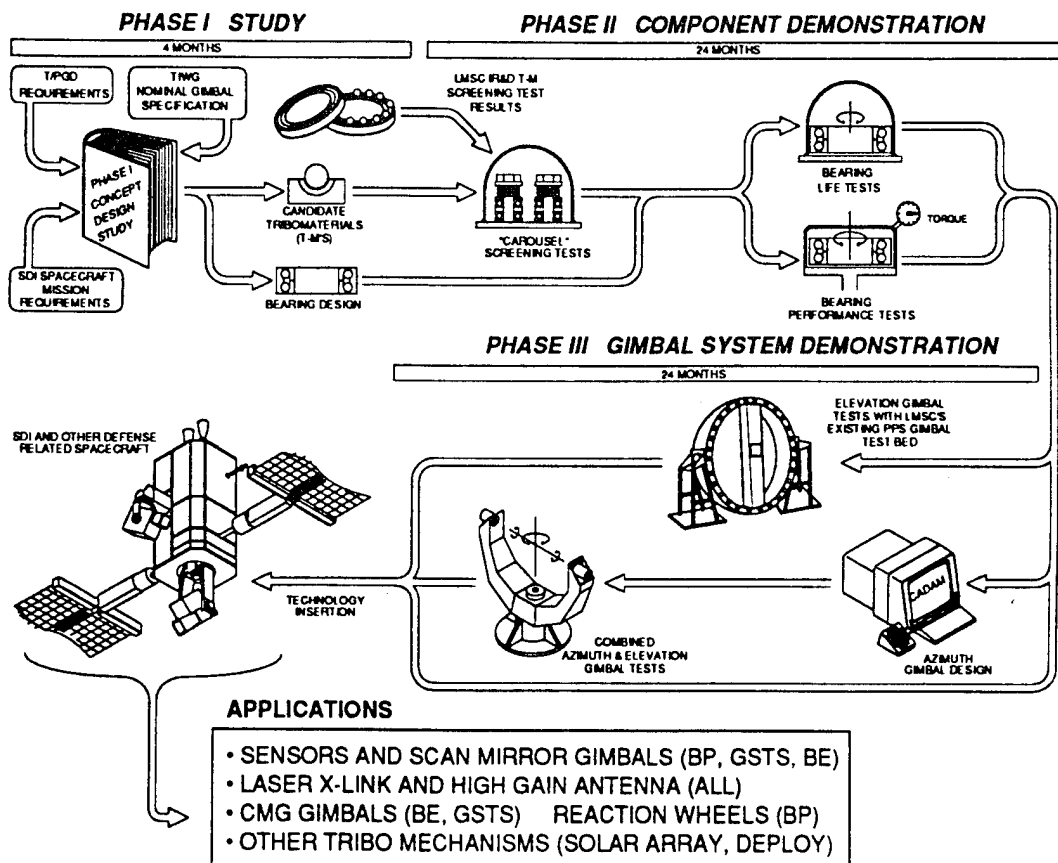
**PROBLEM STATEMENT**

- LOW TORQUE JITTER SIGNATURES CAN NOT BE GUARANTEED WITH TODAY'S TRIBOMATERIALS
- INSUFFICIENT TEST DATA BASE TO CONVINCE USERS OF FLIGHT WORTHINESS OF RECENT, ULTRA LOW FRICTION SOLID AND LIQUID LUBRICANTS
- GIMBAL BEARINGS ARE GENERALLY MISSION THREATENING SINGLE POINT FAILURE ELEMENTS

**APPROACH**

- IDENTIFY (PHASE I) AND SCREEN (PHASE II) CANDIDATE TRIBOMATERIALS
- COMPETIVELY LIFE AND PERFORMANCE TEST AGAINST TODAY'S FLIGHT LUBRICANTS
- VALIDATE PREDICTED GIMBAL POINTING IMPROVEMENTS WITH GIMBAL LEVEL PERFORMANCE TEST

**Fig. 1-1   LMSC's Tribomaterials/Precision Gimbal Demonstration Program**

# Section 2

# SUMMARY

The results of the T/PGD Phase II component demonstration are reported. The work covers test results from bearing lubricant screening life tests, producibility issues for advanced $MoS_2$ films, design and test of flight quality tribobearings, and the status of tribobearing technology transfer to SDI vehicles. Discussion is given of the results of a bearing disturbance gimbal simulation which shows improved pointing performance attendant with bearings having lower torque ripple. Also the gimbal jitter level reductions associated with the LMSC Passive Hybrid Flexure (PHF) bearing are quantified.

Early screening tests with thrust bearings indicated that high density, ion-sputtered $MoS_2$ films provided longer life in a vacuum than other solid film lubricants such as ion-plated lead or diamond-like carbon films. One hundred fifty thousand cumulated hours of test life were obtained on 27 pairs of high precision, 105 size angular contact ball bearings lubricated with sputtered $MoS_2$ and 14 pairs of liquid lubricated reference bearings. Self-lubricating PTFE retainers were required for long life (> 40 million gimbal cycles). Bearings with polyimide retainers, silicon nitride ceramic balls or steel balls sputtered with $MoS_2$ film suffered early torque failure, irrespective of the type of race-sputtered $MoS_2$ film. Failure generally resulted from excess film or retainer debris deposited in the ball track which tended to jam the bearing. Both grease lubricated and the better $MoS_2$ film lubricated bearings produced long lives, although the torque with liquid lubricants was lower and less irregular.

Evidence of film fracture and delamination was found from SEM examination of life tested bearings. A more fatigue resistant, multilayer film with a high gold content interlayer was cooperatively developed with the film producer. Six pairs of flight quality, 5- and 12-inch test bearings were life tested with this film.

The life and torque performance associated with these larger gimbal bearings were more irregular than the small test bearings. The high stiffness and larger diameter of these larger bearings is believed to increase their torque sensitivity to debris. Deposition of the multilayer film on large bearings required different fixturing which may have affected film quality. Torque performance with $MoS_2$ lubricated bearings were comparable to or better than similar bearings lubricated with synthetic greases at the start of life tests but quickly degraded with cycling. These synthetic greases, with the exception of the multiply-alkylated cyclopentane lubricant, gave long lives.

Pointing simulations with a high fidelity bearing disturbance model show that gimbal pointing performance is directly related to bearing performance. Bearing disturbance torques are a major, if not the largest, contributor to gimbal jitter and, subsequently, improved bearing tribomaterials could significantly improve the performance of a precision gimbal system. The bearing model used bearing characteristic test data generated at the beginning, middle and end of life testing.

A novel, low cost Hybrid Flexure Bearing developed by LMSC was analytically and experimentally evaluated for its jitter reduction potential. The passive HFB was found to reduce jitter by a factor of 3 to 10 for inertial pointing or staring applications while showing no improvement or even a performance penalty for sensor applications that image while scanning. An actively controlled version of the HFB provides one to two orders of magnitude jitter rejection under all gimbal modes at the expense of added complexity.

**Screening tests.** The test approach was to perform a large number of screening tests with small, relatively inexpensive, yet high quality bearings. This was to identify the best tribomaterial combinations for later test in the larger, more expensive flight-like gimbal bearings. Three computer controlled, vacuum bearing life testers were used. These rigs can concurrently test 36 pairs of 105-size ($\approx$ 2 inch OD) precision angular contact bearings over a composite gimbal scan duty cycle. Bearing torque and torque ripple were continuously monitored. The bearing's "hard" preload was measured and matched at the beginning of test and at the end of test to detect any loss due to wear. Each of the test bearings were thoroughly examined at the end of the test and their condition documented.

Earlier screening tests with more than 30 thrust ball bearings with $MoS_2$ films from 5 sources (some laser treated or with ceramic undercoats), ion-plated lead and diamond-like film lubricant coatings were conducted in Phase I and early Phase II. The $MoS_2$ films with PTFE composite retainers were clearly the best performers. However, the life potential of these films for bearings in spacecraft mechanisms could not be determined due to the poor quality of the thrust bearings. $MoS_2$ films produced from three different sources were selected for additional screening tests on more precise, angular contact ball bearings made for precision grinding spindle equipment. A wear model was proposed which related lubricant life to coating thickness, stress, and % slip.

Forty three pairs of 105-size precision angular contact bearings were tested over a composite gimbal duty cycle. Twenty seven of these test bearings were lubricated with advanced ion sputtered $MoS_2$ films from the 3 "commercial" sources: Ovonic Synthetic Materials (Ovonic), Hohman Plating (Hohman) and National Centre of Tribology (NCT). The remainder were lubricated with traditional and advanced liquid space lubricants for comparison purposes. Compared to earlier $MoS_2$ films, these new films are denser, more adherent and are very long lived. The bearings were equipped with 4 different ball retainer materials and some had solid ceramic ($Si_3N_4$) balls or those coated with $MoS_2$. Twelve pairs of the bearings with PTFE composite retainers, having $MoS_2$ films from each of the 3 sources, ran unfailed to test cutoff (35 to 48M cycles). On the other hand, only one of the 13 bearing pairs having either non-PTFE retainers, silicon nitride balls or balls coated with $MoS_2$ survived more than 2 million cycles.

From this it was concluded that bearing life is more strongly related to the retainer and ball material combination than to the actual producer of the film lubricant. The bearings having self-lubricating PTFE (Duroid™) or PTFE/bronze/$MoS_2$ composite (Salox™) do better than those having polyimide/$MoS_2$ (Vespel™) retainers. Special retainer material friction tests conducted at Battelle for Lockheed pointed out the significantly higher friction of dry retainers versus those that are grease lubricated and the need for PTFE-based ball retainers.

The formulated synthetic hydrocarbon and polyoester oil based greases having anti-wear additives performed very well showing little or no torque change over the test life of 35 to 40M cycles. These lubricants performed better than tradition perfluorinated space greases which showed torque increases at about the 30 million cycle point. Furthermore, the hydrocarbon and ester greases showed little deterioration at the end of life test, unlike the perfluorinated grease. A multiple-akylated cyclopentane grease formulated with a lead napthenate antiwear additive showed irregular torque performance. Replacing the steel balls with $Si_3N_4$ balls in perfluorinated grease lubricated bearings caused early torque failures. Also substituting ceramic sputtered coated (TiN) balls caused an early failure in one case and no change in performance on a second bearing sample. A single bearing pair lubricated with a perfluorinated oil containing a proprietary anti wear additive showed excellent performance until test suspension at 35 million cycle life.

Torque signature frequency analysis has proven to be a valuable diagnostic tool. Strong responses at the predicted ball defect frequencies were measured at start of the test for the bearings with $MoS_2$ coated balls that subsequently failed early. Similar traces obtained at failure showed significant inner race and outer race defects, consistent with large flakes of compacted $MoS_2$ debris found in the race track of the failed bearing. Pre and posttest bearing preload measurements on these bearings showed an increase in preload, consistent with the trapped debris found between the balls and race.

**$MoS_2$ producibility.** A goal of the LMSC T/PGD effort was to develop reliable commercial sources for advanced solid film lubricants. This requires that the lubricant film not only show consistently good bearing performance but, moreover, that the film deposition process from bearing to bearing meets traditional flight process control standards. In this regard, characterization of $MoS_2$ lubricant films deposited on witness plates that accompany the bearings during the sputter run has greatly contributed to our ability to identify uncontrolled variations. Film morphological structure, crystalline texture and composition have been evaluated on the films under study here. These "fingerprints" can assist in detecting process changes and potential causes for anomalous performance.

Bearing life appears to be strongly related to the thickness, adherence and fracture resistance of the films. Each of the film producers have significantly different processes to obtain "good" film properties. Each film has differing degrees of edge-plane versus basal-plane texture as determined from X-ray diffraction analysis. Some change in the X-ray spectra of the NCT film was also detected between early and later sputtered bearings, perhaps the result of improvements to their high-rate process. While each of the film producers were able to deposit films of relatively consistent thickness from run to run, only Ovonics was able to obtain the nominal requested race thickness of 1 micron.

The Hohman films containing antimony trioxide appeared harder than those from NCT from SEM analysis of a scribed mark across the film. However, both films sustained ball maximum contact stresses of 170,000 psi without detectable deformation. Considerable support was provided to Hohman in refining their $MoS_2+ Sb_2O_3$ film. The density and hardness of their films were found to be directly related to the sputtering current amplitude, while the high current films fractured more easily at the substrate interface. The optimum structure, density, ductility and rub block sliding life was obtained by alternating the sputtering current between medium low and medium high.

**Design / test of flight quality bearings** It is necessary to demonstrate that the advanced $MoS_2$ film lubricants can not only be consistently applied to flight-like bearings but also offer good torque and life performance while not sacrificing stiffness, runout accuracy or Dahl slope (torsional wind up). These last parameters are also important to gimbal performance.

The bearings to be tested were originally designed to the requirements of the Long Wave Infrared Sensor (LWIR) two axis gimbal on SVS. Spare bearings having the best advanced lubricant, upon successfully completion of qualification tests under the T/PGD program, were to be furnished to the SVS program for use on the SVS flight gimbals. The bearings were sized to be as small as possible yet able to meet launch loads and on-orbit stiffness requirements. Preload was selected as the best compromise between stiffness and torque. Bearings 12 inch outside diameter were selected for the azimuth axis and 7 inch OD for the elevation axis. (Later 5-inch OD bearings were substituted for the 7 inch OD inch bearings when the requirements for the smaller BE satellite came to light.) The 12-inch bearing

envelope is identical to currently produced LMSC flight gimbal bearings that have comparative life, torque, and Dahl friction test data.

Three carousel bearing life test fixtures, used for lubricant screening, were later modified to life test three pairs of medium (5-inch) and three pairs of large (12 inch) flight quality gimbal bearings. Two pairs of bearings of each size were lubricated with the best $MoS_2$ film/retainer/ball material combination. A pair of large and medium bearings were each lubricated with the best oil/grease to provide comparative bench mark data. All bearings at test start received an abbreviated torque, torque signature (Power Spectral Density or PSD) and preload functional test. The torque and torque signature were continually monitored throughout the life test and preload checked as necessary. The test bearings were gimbaled over a composite stop/start/dwell scan duty cycle in a $10^{-6}$ torr vacuum for up to 48 million cycles or failure.

A precision rate table supported on air bearings with integral brushless motor for low noise was used for torque ripple, angular runout and Dahl friction slope tests. The effects of rates of rotation, dwell, and bearing wear on torque, torque signature and preload was quantified. Comparisons were made with a passive Hybrid Flexure.

Additional beginning and end-of-life characterization tests include bearing angular runout and Dahl friction-displacement for the solid and liquid lubricated bearings. The bearing's minimum, maximum and non-repeatable angular runout was measured using the precision turntable with an autocolliminator/mirror system. Dahl friction measurements, which determine the torsional stiffness and breakaway torque of bearings with small dithering motion, was also measured. A proximity probe displacement measurement system and precise, smooth linear actuator generated the Dahl "hysteresis" loops.

The test data from both the screening and full scale life tests was used to validate proposed wear life models that can be used to optimize future gimbal bearing designs. This data in combination with parametric data was used to enhance the fidelity of a detailed disturbance model to better predict bearing effects on gimbal pointing performance.

**Tribobearing technology transfer**   Tribo technology transfer was accomplished by three mechanisms: (1) direct transfer into the SDIO programs at Lockheed, formerly SSTS and BSTS and later BE; (2) direct involvement of commercial tribomaterial/bearing vendors, such as Ovonics, Hohman, NCT and Industrial Tectonic Bearings; and (3) publication of the work in technical society journals, references [2-1] and [2-2].

A complete, fully integrated gimbal bearing design was completed for the LWIR sensor aboard SSTS validation satellite prior to its cancellation. The bearings, lubricated with an advanced $MoS_2$ film lubricant if warranted, were to be made available to the program for flight acceptance testing and flight demonstration. The same tribomaterial technology was also transferable to gimbals on other SDI programs, such as those listed in Table 2-1.

It was shown that improved tribomaterials were important to the development of gimbals for both SSTS and BSTS. These vehicles have large sensors that require quick accelerations, quick stopping and settling with minimum disturbances to the vehicle. Both satellites have jitter sensitive sensors. Similarly, gimbal generated disturbances are expected to be equally important to BE and BP size vehicles. The BP pan/tilt mirror gimbal is not only jitter sensitive but also sensitive to any contaminating outgassing products from the bearing lubricants. This scan mechanism performs a continuous step/stare surveillance scan with very short settling time; thus lubricant longevity and the elimination of stick slip bearing behavior becomes crucial.

**Table 2-1    SDI gimbal applications for Tribomaterial technology**

```
• SENSORS AND SCAN MIRROR GIMBALS (BP, GSTS, BE)

• X-LINK AND DOWN LINK ANTENNA (ALL)

• CMG GIMBALS (BE, GSTS)    REACTION WHEELS (BP)

• OTHER TRIBO MECHANISMS (SOLAR ARRAY, DEPLOY)
```

The BE satellite has cross/down link antennas and CMG gimbals which are essentially dormant over long periods of time or even years, except for periodic exercise. The BE system must become fully operational in a matter of seconds once notified that a target has been acquired. Thus, lubricant degradation during dwell periods is not tolerable.

To augment the application of improved tribobearings to a wide variety of gimbals, the test data base obtained under this contract, was incorporated into a gimbal/bearing disturbance simulation. The objective is to assess the potential pointing performance improvements attendant with "improved" tribobearings. The high fidelity bearing disturbance mode was augmented to include end-of-life bearing behavior. In addition, the disturbance model was incorporated into a Lockheed independently developed gimbal simulation which considers other gimbal disturbance sources such as motor cogging/ripple, power transfer device disturbance (e.g., cable wrap), guidance sensor errors as well as spacecraft born disturbances such as CMG vibration. The core bearing disturbance model includes torque, torque hash, Dahl friction, runout, structural stiffness, and damping.

Some of the important results from simulations indicated that bearing disturbance torque, compared with the other sources of disturbance, is a major contributor to gimbal jitter during constant velocity scans. The simulation also showed a precipitous increase in gimbal jitter as a bearing fails using actual torque failure data for one life test bearing. Additional results show that the LMSC Passive Hybrid Flexure (PHF) Bearing provides up to a 10 times reduction in gimbal jitter levels relative to a standard bearing for fine angle, inertial pointing. However, bearing start up torque transients render the PHF bearing ill suited for large angle scans.

# References For Section 2

[2-1]   Loewenthal, S.H., Chou, R.G., Hopple,G.B. and Wenger,W.L. "Evaluation of Ion-Sputtered Molybdenum Disulfide Bearings for Spacecraft Gimbals," STLE 93-TC-2D-1, Tribology Trans. 1994 (In press)

[2-2]   Hopple, G. B., Keem, J. E., and Loewenthal, S. H., "Development of Fracture Resistant, Multilayer Films for Precision Ball Bearings," Wear, Vol.162-164, 1993, pp. 919-924.

# Section 3

# T/PGD PROGRAM OVERVIEW

The next generation of SDI surveillance/interceptor spacecraft have critical sensor, antenna, CMG gimbals and other tribomechanisms containing single point failure bearings. In most cases, loss of these bearings is either mission threatening or at least mission limiting. Additional requirements, such as rapid resettling times, survivability in hostile environments, elimination of lubricant born optical contaminants and the need for low jitter producing bearings, raise specific tribomaterial concerns. Other space mechanism lubrication issues, such as ground testing and storage, also need to be addressed [3-1].

While recently developed ultra-low friction $MoS_2$ films have the potential of addressing many of these concerns, an insufficient test data base exists to establish their flight readiness or worthiness. Specifically, there is lack of a significant quantity of life and torque data on flight quality bearings of different configurations under simulated gimbal operation conditions. Furthermore, process controls that consistently produce high quality lubricant films on bearings of varying sizes have yet to be established. Finally, the ability to predict lubricant wear life or the effects of bearing disturbances on gimbal life and pointing performance are largely unavailable.

## 3.1 PROBLEM DESCRIPTION

The main thrust of the T/PGD effort was to demonstrate performance improvements associated with advanced solid film lubricants for precision gimbal bearings. Flight and test experience with traditional liquid and solid space lubricants uncovered certain performance limitations, as identified in Table 3-1. The stop/start (direction reversal) nature of oscillatory gimbals incurs boundary lubrication where significant asperity contact is encountered. The degree of torque signature degradation with traditional gimbal bearing lubricants, such as the perfluoroalkyl polyether (PFPE) oils, had not been established over a SDI mission life of 7+ years.

**Table 3-1  Tribomaterial performance limitations**

**LIQUID LUBRICANTS**
- MIGRATION, CREEP, DEPOLYERMERIZATION, DEBRIS FORMATION
- COLD TEMPERATURE PERFORMANCE
- OUTGASSING CONTAMINATION ON OPTICS
- POOR BOUNDARY FRICTION & FRICTION NOISE
- DIFFICULT TO ACCELERATE LIFE TESTING
- LOW TOLERANCE TO HAZARDOUS ENVIRONMENTS

**SOLID LUBRICANTS**
- SPOTTY WEAR LIFE TRACK PERFORMANCE
- NON GRACEFUL SUDDEN FAILURE MODE
- INCONSISTENCY OF PROCESS REPEATABILITY
- DEBRIS GENERATION
- FRICTIONAL EFFECTS OF DWELL AND STORAGE TIME
- HIGH SENSITIVITY TO AIR/HUMIDITY

Molybdenum disulfide's low friction in a vacuum environment, without the outgassing, migration and low temperature torque concerns of liquid lubricants, makes it a natural candidate for lubricating spacecraft mechanisms. Furthermore, its ability to lubricate at near zero rotational speeds, common to most space bearings, is a decided advantage since liquid lubricants form meager film thicknesses under such conditions. Despite such advantages, the use of $MoS_2$ has generally been restricted to low duty cycle applications, such as deployment pivot joints and lightly loaded bearings, where substantial torque margins exist [3-2].

### 3.1.1 Liquids
Liquid lubricants, primarily perfluoropolyalkylether (PFPE) greases have been the preferred lubricant for space applications due to their very low vapor pressure, wide temperature range, ease of application and considerable flight history. Their preference is also due to the past unavailability of reliable solid lubricant films. However, there are well recognized limitations with PFPE oils and greases, as well as other liquid lubricants. These include the tendency to migrate or creep out of the bearing contact zone and the concern that outgassed volatile components will contaminate cryogenically cooled, infrared sensors and thermal surfaces.

**Boundary Lubrication** Perhaps, the most serious concern is that PFPE oils have poor boundary lubrication performance since it has been difficult to introduce soluble antiwear additives. In addition, PFPE materials have been found to be chemically reactive (polymerize) in rubbing contact with ferrous and some nonferrous alloys (e.g., see Carre [3-3]. In low speed, oscillatory bearing applications, resulting wear debris can adversely affect torque and torque noise levels. The primary approach to combating PFPE's poor boundary performance has been to keep Hertzian stresses low. In some cases, nonreactive ceramic ball coatings such as CVD TiC have been used [3-4] , but mostly for small, high speed gyro bearings.*(Test bearings with ceramic $Si_3N_4$ balls and balls sputtered with TiN were evaluated with a PFPE grease.)* Contamination of the oil with a small amount of a synthetic hydrocarbon oil containing antiwear additives will also help for a time. The use of other types of antiwear additive containing synthetic oils, such as polyalphaolefins (PAO), have been also suggested for critical boundary lubricant applications [3-5]. *(Two pairs of test bearings are lubricated with a cabosil thickened PAO grease and two others with a neopentyl ester grease with excellent boundary performance).* However, acceptance of these somewhat higher vapor pressure materials will hinge on the required level of contamination control and the tolerance to higher pour point temperatures (higher cold temperature viscosity).

**Other factors** Other shortcomings of gimbal bearing liquid lubricants include the difficulty of performing greatly accelerated (speed) life tests. Too much of a test speed increase will shift the mode of lubrication from boundary to elastohydrodynamic (EHD) and thereby invalidate the results.

A final concern is tolerance to hazardous environments such as radiation, extreme temperatures, atomic oxygen etc., for SDI missions. Liquid lubricated bearings may require special shielding and thermal control considerations. Improving the performance of advanced tribomaterials for harsh space environments is the thrust of another SDIO L502 project. Understanding the long term effects of extreme environments on tribocomponent performance is critical for mission reliability.

### 3.1.2 Solid Lubricants
Solid lubricant films, ceramics, and ion beam surface modification techniques resolve many of these liquid lubricant problems but introduce some new ones as well. In oscillatory bearings (both dry and wet) the formation of debris at the ends of ball travel, particularly for motions of less than one ball spacing, has been shown to produce significant "torque bumps" [3-6]. This is a particular problem for bonded $MoS_2$ films which formed relatively thick

coatings that can shed large wear debris. In "hard" (i.e., non-spring) preloaded, thin section ball bearings, such as those used for large gimbals, debris buildup can produce a serious torque problem. The solid lubricant film must not only possess good adhesion to the surface but excellent cohesion (wear life) characteristics as well. This drives one into the direction of thinner films which generally produce lower friction at the expense of shorter wear life. Furthermore, thin films are needed to be compatible with the tight clearances in precision gimbal bearings. The most significant concern is limited endurance characteristics of the earlier sputtered $MoS_2$ films and their sudden "non-graceful" failure characteristics.

**Prior Studies** The inability of $MoS_2$ lubricant films to replenish themselves, unlike liquid lubricants, and questions of durability have impeded their application for long life and torque sensitive space applications. Attempts to use only PTFE composite ball retainers for transfer film lubrication of the ball and races produced excessive film buildup leading to high erratic bearing torque [3-7]. Matching retainer transfer rates to the wear rate of the film deposited on the bearing is critical to controlling the bearing's internal clearance, preload and torque [3-8]. For example, Christy and Barnett [3-6] report the use of PTFE composite retainers on scan mirror bearings for a meteorological satellite produced unacceptable torque bumps at the end of travel due to PTFE film over-transfer. A change to a non sacrificial retainer and very thin (700 Å), sputtered $MoS_2$ film reduced torque fluctuations but adversely affected life margins as the thin film wore through [3-9].

Similarly, very lightly loaded instrument bearings sputtered with $MoS_2$ exhibited high torque at the end of test when tested with non-replenishing, $MoS_2$ -sputtered phenolic and bronze retainers [3-10]. To extend life without PTFE retainers, Roberts [3-7] reported a four fold life increase by coating the balls as well as the races with $MoS_2$. However, this life improvement comes at the expense of more than double the torque. Adding PTFE retainers boosted bearing life by a factor of 20 and torque levels remained essentially unchanged [3-7]. Evidently, the PTFE transfer film worked synergistically with the $MoS_2$ coated balls and races. The average bearing torque was now reduced by 5 to 8 times compared with bearings using only PTFE retainers with no film coatings [3-7]. Clearly, a systems approach is required for achieving long life and minimum torque for solid film lubricated bearings.

**Flight Heritage** An excellent survey of the current status and future trends in European space tribology was prepared by Rowntree and Todd [3-11]. Solid lubricated bearings have been used in some European space positioning mechanisms, due to the extensive work performed at the European Space Tribology Laboratories in the early 1970's. However, their main application have been for non-critical pointing applications, unlike those of interest here. For example, Ref. [3-11] points out that more than 2 million accumulated flight hours have been logged on ion-plated lead, solar array drive bearings on several European spacecraft. Solid film lubricants are used far less frequently on U.S. spacecraft bearings and many of these have used bonded, rather than sputtered films [3-2]. The main spacecraft application of $MoS_2$ lubrication has been for release or deployment pivots, pins or springs where the shortcomings of bonded $MoS_2$ films are not critical.

**Advanced MoS2 films** Advances in deposition techniques (initially identified by Roberts [3-12] at the National Center of Tribology) lead to low friction ($\mu < 0.01$), high density, sputtered $MoS_2$ films which offered promise for long life in gimbal bearings. Based on thrust bearing screening tests on a whole host of solid lubricant films, our interest centered on Robert's film in addition to two others. Hohman Manufacturing & Plating Co. had a long commercial history of ion-sputtering $MoS_2$ on bearings. They developed co-sputtered metal/MoS2 films in the late 70's [3-13]. More recently, Ovonic Synthetic Materials Corp. developed a RF magnetron $MoS_2$ film that had been interlayered with gold or nickel. [3-14, 3-16]. In addition, Singer at NRL [3-15] developed ion beam assisted deposition techniques

for densifying $MoS_2$ films. However, the bulk of work on these new films has been conducted with simple sliding tribometers or spring-loaded, thrust bearing testers [3-16]. Reliable torque and life data for flight-quality, rolling element bearings were lacking. Insufficient data existed with regard to the best ball separator materials to use with these films and their effect on preload levels for bearings that can not use a spring loading system. Little was known about how these films effect the bearing torque signature as a function of cycle life or their failure mechanism. Furthermore, bearing data with stop/start oscillatory motion as generally required by pointing and scanning space systems were unavailable. Also, no comparative data for liquid lubricated bearings was available under identical conditions in order to judge relative performance. Resolution of these and other issues became the objective of the T/PGD investigation.

**Producibility** From a producibility standpoint, ease and consistency of application of dry lubricants are an important issue for user acceptability. Film performance is quite sensitive to the control of many sputtering parameters, such as sputtering power, argon levels, substrate temperature and specimen cleanliness. Sulphur content in films will affect their cohesive/adhesive character (e.g. see Roberts [3-7]). Strict control over processing is therefore required. Processing improvements and quality control issues associated with these films is discussed in Section 7. Hohman has made progress in improving their run-to-run consistency. The rub block[#] air and vacuum results of nearly 50 variable current depositions are shown in Fig. 3-2. Note that a few "poor" runs still occasionally occur, but there is still the option to strip the inferior coated parts and re-sputter. Ovonics films appear very uniform in thickness from batch to batch, but some variation in crystallinity was detected (see Section 7.3).

A special problem with $MoS_2$ film coated races and balls is the accurate setting of preload and contact angle on precision bearings by the bearing manufacturer. Setting preload generally requires adjustment grinding of the race face stickout which can't be done with $MoS_2$ films due to the need for grinding wheel fluid coolants. A cumbersome alternative is to manufacture multiple sets of balls in fine, say $10 \times 10^{-6}$ inch, diameter graduations about the nominal value for fine preload adjustment. In the case of large gimbal bearings like the 12 inch test unit, there are 104 balls per row or 208 balls total. Thus having 4 or 5 graduated sets of balls for each bearing becomes a fairly expensive proposition, particularly if they happened to be $MoS_2$ coated or even more expensive ceramic.

---

[#] *Note that the direct applicability of pure sliding rub block life data (adhesive wear) to the primary rolling/micro sliding contact of a ball against a race in a bearing (adhesive wear) still needs to be established.*
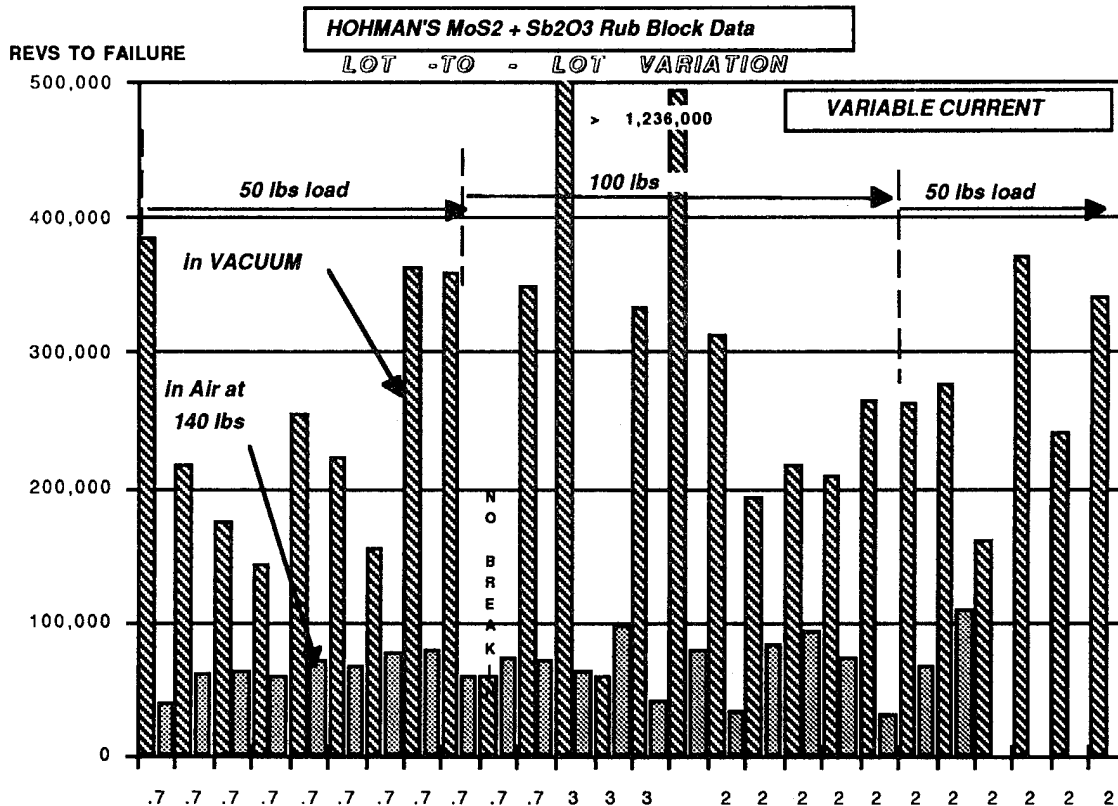
**Fig. 3-2** Variable current MoS$_2$ + Sb2O3 film consistency from Hohman rub block tests in air and vacuum

**Humidity** It is well known that the performance of MoS$_2$ films is adversely affected by the moisture in the air (e.g., see Roberts [3-7]). This is illustrated in Hohman's sliding tests shown in Fig. 3.2. Poor tribological performance in air limits ground testing of gimbals, although does not necessarily jeopardize on-orbit performance. The more moisture resistant MoS$_2$ films would also be more immune to increased friction upon start up after long periods of inactivity, due to the presence of small amounts of residual water vapor. Although not specifically tested, the more densified films and those interlayered would likely be much less sensitive to moisture than the older sputtered films.

**Retainer material** When solid lubricant films are thin ($\approx$ 1 $\mu$m or less), there is the question of wear-through. The need for a replenishment or transfer film mechanism, such as a PTFE composite sacrificial ball separator, becomes a consideration. Matching the retainer material transfer rate to the race film wear rate to maintain an equilibrium thickness is difficult. Too much transfer increases film thickness, bearing preload and thus torque. Too little transfer increases wear and wear debris, Grease thickener buildup in low oscillatory bearing contacts can also be a concern.

Furthermore, the friction of a non liquid lubricated ball against a dry retainer pocket will be significant. If the ball pocket friction is high, then bearing torque and torque ripple will also be high even if the ball race friction is low. For this reason, a special low speed, friction tests of potential bearing retainer materials were conducted at Battelle [3-17] under a subcontract from LMSC.

Toroids of polyimide+MoS$_2$ (Vespel), teflon (Duroid), bronze+teflon+MoS$_2$ composite (Salox) and steel sputtered with a MoS$_2$+ Sb$_2$O$_3$ film were tested either dry or lubricated with a PFPE grease (Bray 600). *(Toroids around every other ball have been successfully used as ball separators on several of LMSC's gimbal bearings).* Ball loads were varied from 50 to 200 gms at 15 rpm. The friction from the ball contact against the toroid's outside diameter versus contact with the inside diameter was separately measured. The results of these tests are summarized in Fig. 3-3. Measured friction levels with grease lubrication were significantly less than those that were dry, as expected. However, the self lubricating Salox material did achieve relatively low friction levels (μ <0.10) for some of the tests. Good friction performance was also achieved with the MoS$_2$ coated steel retainer, although coating wear through occurred in one test after only 8 minutes of running. Even with no wear through, the MoS$_2$ coated steel retainer showed a relatively large wear area, making it a risky choice for long life. The Vespel friction was comparable to Salox for the OD tests, but was significantly larger for the ID test. Contact load, over the range tested, seemed to have little effect on the friction coefficient.
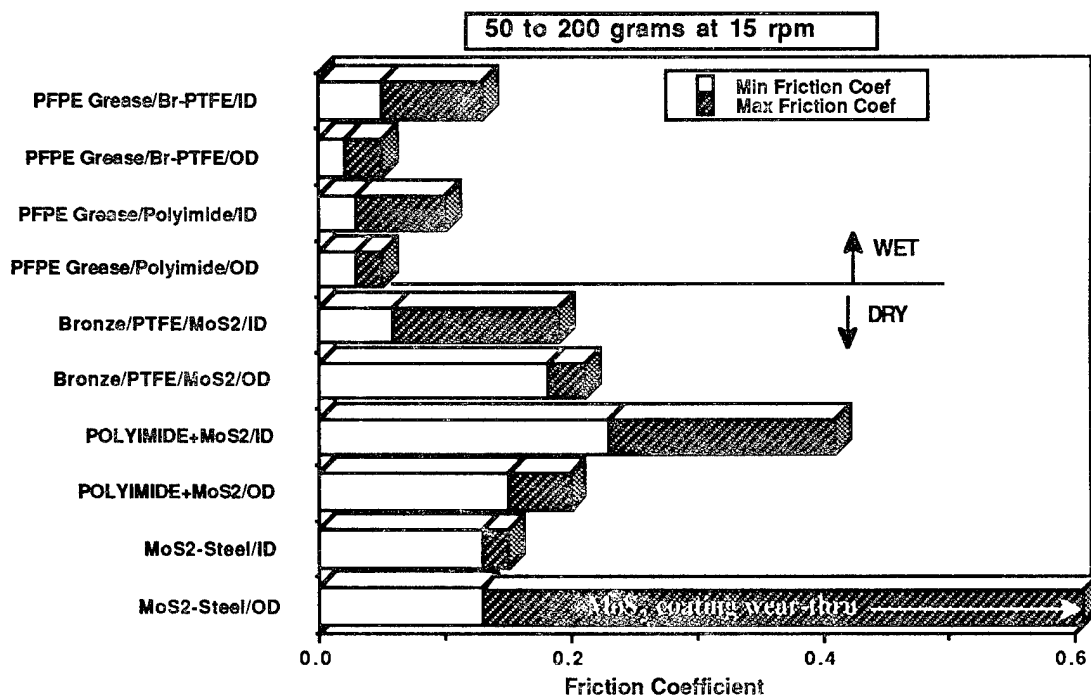


Fig. 3-3    Results from retainer material friction tests by Battelle

Based on the Battelle results and prior experience, the MoS$_2$ lubricated test bearings were evaluated with four retainer materials: Vespel, Salox, Duroid (a glass reinforced teflon material) and Vespel retainers sputtered with MoS$_2$ film (a less abrasive material than steel in the event of coating wear through).

## 3.2 BENEFITS WITH IMPROVED TRIBOCOMPONENTS

Benefits with improved lubricants and gimbal bearings will have significant impact on mission performance in a number of areas. Recognizing that SDI gimbals bearings are single point failure items, extending bearing cycle life through better tribomaterials will relax the need to limit payload operational cycles for a given mission life or the need for on-orbit replacement. Since many of the sensors on these vehicles have stringent jitter requirements, reduction of gimbal bearing torque disturbances through better tribo-components (lubricants/bearings) or advanced bearing concepts such as the LMSC Hybrid Flexure Bearing (see Section 8.4) will increase jitter margins and reduce the workload of fast steering mirrors. In the cases where jitter levels can be substantially reduced at the gimbal level, the reduction of the number of fast steering mirrors or their complete elimination is possible. This would have a significant payback in reduction of electronic complexity, cost, and reliability.

Extension of bearing lubricant temperature and radiation operational capabilities through the use of advanced $MoS_2$ film lubricants would have a direct payback in terms of reducing the need for shielding and active thermal control systems in order to meet survivability requirements from hostile attack. Potential degradation of optical sensor performance will benefit from a reduction of lubricant outgassing constituents, although these may be relatively small compared to other sources of contamination.

Enhancing the bearing lubricant's ability to resist torque degradation during long periods of inactivity, would be of large benefit for spacecraft like BE which must quickly spring into action after long periods of dormancy. Improvements for both $MoS_2$ film and liquid lubricants are sought in this area.

## 3.3 PROGRAM DESCRIPTION

In recognition of these factors, LMSC, under SDIO contract SDIO84-89-C-0028, formulated a three phase program described below.

| Description | | Period of Performance |
|---|---|---|
| Phase I | Component Design Study | 4 months |
| Phase II | Component Level Demonstration | 36 months |
| Phase III | (Option) Gimbal Level Demonstration | 24 months |

The major program objectives were to:

(1) Identify (Phase I) and screen (Phase II) the best tribomaterial candidates

(2) Demonstrate performance and life benefits in bearing component level (Phase II) then gimbal level (option, Phase III) hardware

(3) Evaluate the performance of LMSC's innovative Hybrid Flexure Bearing

(4) Insert enabling T/PGD technology into SDI spacecraft gimbals in time to impact designs

(5) Provide a mechanism to transfer this technology to U.S. commercial bearing and tribomaterial producers.

The two phase effort is illustrated pictorially in Fig. 3-4. In Phase I, candidate solid and liquid lubricants were evaluated in relation to SDI mission requirements. Bearing preliminary design specifications were prepared. A Phase II test plan was also prepared as well as a plan to insert this technology into SDI programs. In addition, Lockheed funded thrust bearing tests were conducted to provide early screening test data on candidate tribomaterials.

In the current Phase II, improved liquid and $MoS_2$ technology were competitively evaluated, first at the screening test level and later at the full scale bearing level (see Fig. 3-4). The main Phase II output is a substantial data base for precision, life-tested bearings having advanced tribomaterials. An additional product of this activity was the development of production methods for sputtering $MoS_2$ films on to flight bearings.
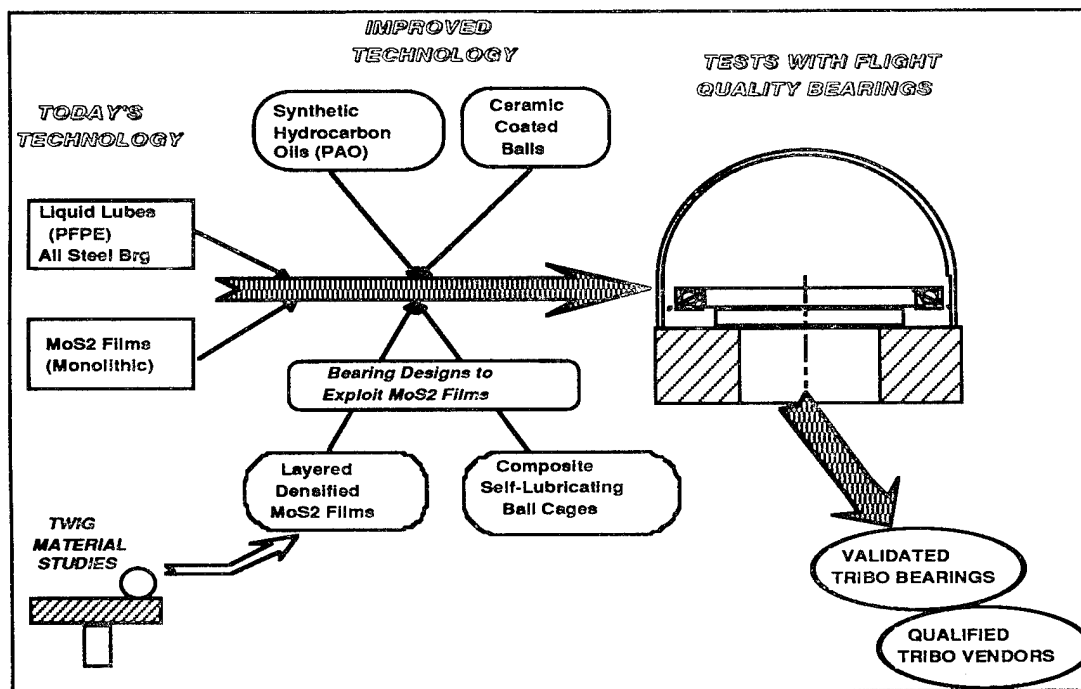


Fig. 3-4    Phase II : Tribo technology insertion into flight hardware

The Phase II tests consist of screening tests to determine the optimum lubricant/retainer/ball material combination. The best dry and liquid lubricants are to be applied to medium and large size flight quality bearings. Performance and life tests were then conducted to determine torque characteristics and life performance. The test data were also used to enhance the fidelity of detailed bearing disturbance simulation models (Fig. 3-5). Gimbal/bearing simulation studies with these bearing models were conducted to provide the potential user with expected gimbal performance benefits from the new technology.

The optional Phase III system tests are to incorporate bearings having advanced tribomaterials into full scale gimbals to provide confirmation of the expected benefits. In this regard, azimuth and elevation axis gimbals are to be designed and instrumented. A series of pointing, jitter and repeatability tests are to be performed. Bearing structural stiffness and gimbal modal frequencies are also to be determined. Comparisons with performance predictions from gimbal simulations are to be made.

| BEARING LIFE TESTS | | BEARING PRECISION TESTS | |
|---|---|---|---|

- LIFE DATA ON SMALL, MEDIUM, AND LARGE FLIGHT QUALITY GIMBAL BEARINGS

- TRACKING OF TORQUE, TORQUE RIPPLE, AND VIBRATION

- TORQUE SIGNATURES AS FUNCTION OF SPEED AND PRELOAD
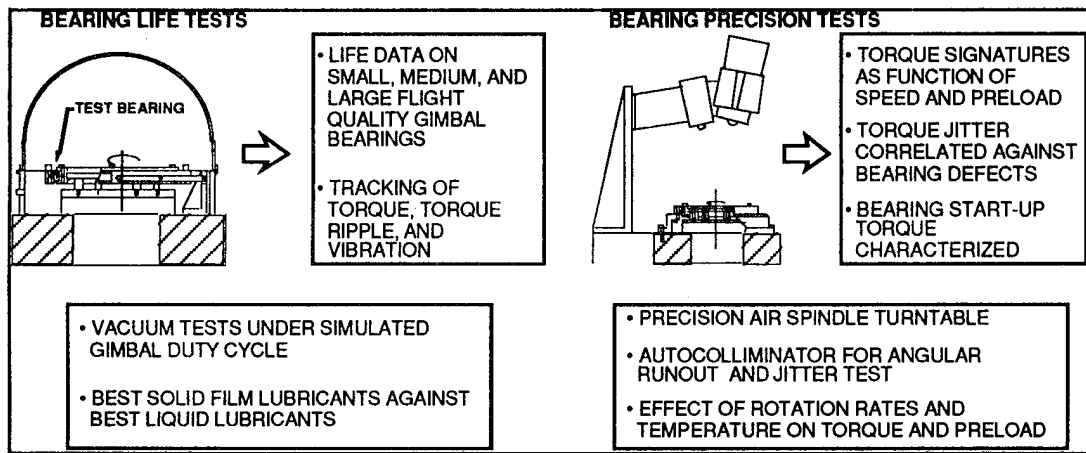
- TORQUE JITTER CORRELATED AGAINST BEARING DEFECTS

- BEARING START-UP TORQUE CHARACTERIZED

- VACUUM TESTS UNDER SIMULATED GIMBAL DUTY CYCLE

- BEST SOLID FILM LUBRICANTS AGAINST BEST LIQUID LUBRICANTS

- PRECISION AIR SPINDLE TURNTABLE

- AUTOCOLLIMINATOR FOR ANGULAR RUNOUT AND JITTER TEST

- EFFECT OF ROTATION RATES AND TEMPERATURE ON TORQUE AND PRELOAD

**Fig. 3-5    Bearing life and performance tests in Phase II**

## References for Section 3

[3-1]  Roberts, E. W., "Thin Solid Lubricants Films in Space," Tribology International, Vol. 23, No. 2, pp. 95-104, (1990).

[3-2]  Hilton, M. R., and Fleischauer, P.D., "Application of Solid Lubricant Films in Spacecraft," Surface Coatings Tech., Vol. 54-55, (1992) pp. 435-441.

[3-3]  Carre', David, "The Performance of Perfluoropolyalkylether Oils Under Boundary Lubrication," STLE Trans., Vol. 31, No. 4, 1987, pp. 437-441.

[3-4]  Boving, H., Hintermann, H.E., and Henni, W., "Ball Bearings with CVD-TiC Coated Components," Proc. of 3rd European Space Mechanisms & Tribology Symposium, Oct. 1987.

[3-5]  Fleischauer, Paul D., and Hilton, Michael R., "Assessment of the Tribological Requirements of Advanced Spacecraft Mechanisms," Proc. Mat. Res. Soc. Symp. Vol. 40, 1989.

[3-6]  Christy, R. I., and Barnett, G. C., "Sputtered $MoS_2$ Lubrication System for Spacecraft Gimbal Bearings," ASLE Lube Eng., Vol. 34, No. 8, pp. 437-443, (1978).

[3-7]  Roberts, E. W., "The Tribology of Sputtered Molybdenum Disulfide Films," Proc. Inst. of Mech. Eng., Tribology - Friction,Lubrication and Wear, Fifty Years On, Vol. I, (1987) pp. 503-510.

[3-8]  Meeks, C. R., "Theory and Practice of Self-Lubricated, Oscillatory Bearings for High Vacuum Applications - Part II," ASLE Lube Eng., Vol. 37 , 11,  pp. 657-667, (1980).

[3-9]  Bohner, J. J., and Conley, P. L., "On the Torque Behavior of Selected Thin Film $MoS_2$ Lubricated Gimbal Bearings," Proc. 22nd Aerospace Mechanisms Symp., NASA CP-2506, (1988) pp. 227-244.

[3-10] West, C. E., "Tests of a Sputtered MoS$_2$ Lubricant Film in Various Environments," ASLE 1976 Annual Meeting Preprint 76-AM-5C-4.

[3-11] Rowntree, R. A. and Todd, M. J., "A Review of European Trends in Space Tribology and its Application to Spacecraft Mechanism Design," Proc. Mat. Res. Soc. Symp. Vol. 140, 1989.

[3-12] Roberts, E. W., "Towards an Optimized Sputtered MoS$_2$ Lubricant Film," Proc. of 20th Aerospace Mechanisms Symposium, NASA CP-2423, May 1986.

[3-13] Stupp, B. C., "Synergistic Effects of Metals Co-Sputtered with MoS$_2$," Thin Solid Films, Vol. 84, (1981) pp. 257-256.

[3-14] Hopple, G. B., Keem, J. E., and Loewenthal, S. H., 1993, "Development of Fracture Resistant, Multilayer Films for Precision Ball Bearings," Wear, Vol. 162-164, pp. 919-924, (1993).

[3-15] Singer, I. L., "Solid Lubricating Films for Extreme Environments," New Materials Approaches to Tribology: Theory and Applications, Mat. Res. Soc. Proc., Vol. 140, (1989) pp. 215-226.

[3-16] Hilton, M. R., Bauer, R., Didziulis, S. V., Duggar, M. T., Keem, J. M. and Scholhamer, J., " Structural and Tribological Studies of MoS$_2$ Solid Lubricant Films Having Tailored Metal-Multilayer Nanostructure," Surface and Coatings Technology, Vol. 53, (1992) pp. 13-23.

[3-17] Gleeson, J.:, "Low Speed Tests of Gimbal Bearing Cage Materials," Battelle Final Report to Lockheed, Aug. 6, 1990.

## Section 4

## SDI GIMBAL APPLICATIONS

At the beginning of Phase II Lockheed had the prime responsibility for gimbal design and performance of four major SDI gimbals: BSTS, SSTS, Starlab and Ground Based Free Electron Laser. Of these, the flight gimbals in BSTS and SSTS, identified in Fig. 4-1, had the most demanding requirements.

The Long Wave Infrared (LWIR) sensor gimbal on SSTS and the visible/ultraviolet (V/UV) sensors on SSTS and BSTS Payload Two put great demands on the gimbal performance. *(Many similar demands are anticipated for the BE and BP spacecraft).* Servo-mechanism challenges include:

- high pointing accuracy and jitter stability
- large sensor payloads
- high servo bandwidths
- light, but stiff gimbal structures
- rapid retargeting
- quick resettling time
- need for ultra-low jitter disturbance feedback into sensor platforms
- constant surveillance for 7 years or more
- extended periods of standby, then rapid activation
- survivability in hostile environment

Exact values for most of these parameters are currently classified, but they are consistent with the very best gimbal technology that can now be provided.

Low torque and torque ripple under boundary lubrication, up to 15 million stop/start cycles for gimbal reversals, short resettling times, rapid retargeting scan rates after possible long periods of dormancy, and the use of cryogenic infrared optics severely hampers the use of today's space qualified liquid lubricants in certain SDI gimbal applications. When this is coupled with the awareness that the bearings represent a mission threatening, single point of failure, the need to investigate improved tribomaterials becomes even more apparent.

### 4.1 SVS GIMBAL

Early in Phase II, the flight program schedule of the SSTS Validation Satellite, SVS, was found to be very compatible with that of the T/PGD program. A coordinated program to transfer flight gimbal bearings with advanced tribomaterials for the SVS's Long Wave Infared Sensor (LWIR) was established. The plan was to competitively life/performance test, advanced ultra low friction $MoS_2$ film azimuth and elevation axis bearings against bearings lubricated with bench mark "standard" space greases and furnish flight bearings with the "winning" lubricant to the program in the May 1992 time frame.
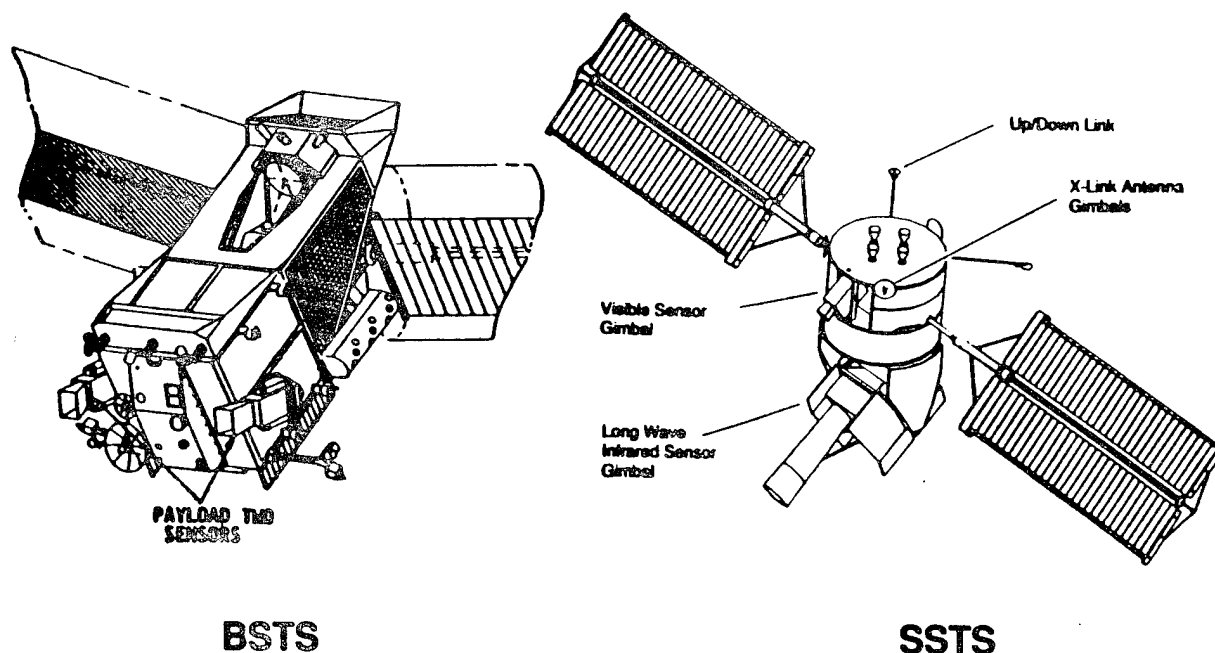
BSTS        SSTS

**Fig. 4-1 Critical BSTS & SSTS Gimbals**

### 4.1.1 Critical Gimbal Drivers

Major performance and reliability drivers for SVS gimbals appear in Fig. 4-2. These are also generally applicable to other spacecraft gimbals as well. Since constant surveillance over 7+ years was the primary mission of SVS and since many of the sensors were nearly in continuous use during most of the mission life, the life of the bearing assemblies becomes a prime concern. Sensor imaging and infrared targeting requirements demand low torque induced jitter imposed by bearings. This is especially important since sensors must operate at the same time while gimbaling. Some of the sensors are on active standby for long periods of time, requiring that lubricant performance not degrade during long periods of dormancy.

| SSTS MAJOR DRIVERS | | | | | | | |
|---|---|---|---|---|---|---|---|
| ITEM | LIFE | DORMANCY | TORQUE INDUCED JITTER | POINTING & TRACKING | CRITICAL GIMBAL RELIA. | POWER/ WEIGHT | CONTAM. FROM LUBRIC. |
| LONG WAVE INFRARED SENSOR | X | X | X | X | X | X | X |
| VISIBLE SENSOR | X | | X | X | X | X | X |
| X-LINK ANTENNA | X | | X | X | | X | X |
| CMGs | X | | X | | | X | |

**Fig. 4-2 SVS (SSTS) Gimbal Design Drivers**

Difficult pointing and tracking requirements encompass not only gimbal line of sight (LOS) errors but knowledge of the target position with reference to inertial space. Maximum allowable focal plane jitter levels are a direct function of pixel size and disturbance frequency, as shown in Fig. 4-3 for a typical sensor. Note that allowable jitter is much more restrictive at

the higher frequencies, beyond the frequency band width of the gimbal servo loop. Thus, even relatively low amplitude bearing disturbances may be objectionable if they occur in the mid to high range frequency region. The critical gimbal reliability column in Fig. 4-2 identifies those gimbals where bearings are single point failure items for which loss or serious degradation of mission performance is likely. In the case of antennas, Control Moment Gyros (CMG), redundant units allow failure of at least one single element without jeopardizing function. Power and weight improvements are also sought. Reduction in power consumption reduces demands on both solar arrays and battery storage and thus benefits both cost and weight. Finally optical surfaces, particularly those cryogenically cooled such as the LWIR sensor, require freedom from particulate and vapor contamination from not only lubricants but other surrounding spacecraft structural materials and propulsion devices.
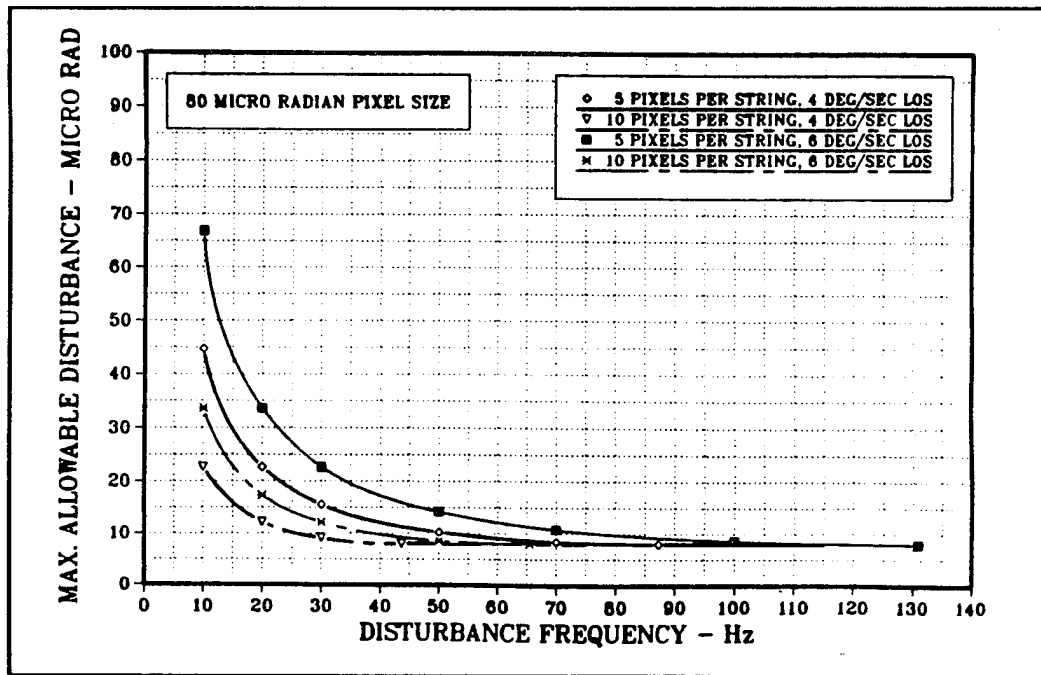


**Fig. 4-3  Typical allowable focal plane disturbance levels**

### 4.1.2 Gimbal Bearing Design Requirements
The original technology insertion objective was to provide flight quality bearings with advanced tribomaterials for the first SSTS flight vehicle. Test bearing design was therefore based on the SSTS gimbal concept shown in Fig. 4-4.

Derived bearing requirements are summarized in Fig. 4-5. The gimbal was supported by azimuth bearings that are mounted to a stationary shaft, end-mounted to the main spacecraft bus (stable section). Shaft bending stiffness of the bearing assembly became a key driver in meeting launch and on-orbit stiffness frequency minimums. The azimuth bearing size and preload were selected to meet both launch load and stiffness requirements. Fig. 4-6 shows the trade between acceptable stiffness and drag torque. The selected 11 x 12 " azimuth bearing pair had an axial stiffness of ≈ 0.8 million lb/in and a radial stiffness of ≈ 5 million lb/in at the nominal 200 lb preload. This bearing was the same size as a flight gimbal bearing from another Lockheed program, so that comparative life and performance test data were available. A finite element model of the SVS primary structure showed that the on-orbit modes of the selected azimuth bearing and shaft assembly met or exceeded the required 10 Hz frequencies, as illustrated in Fig. 4-7.
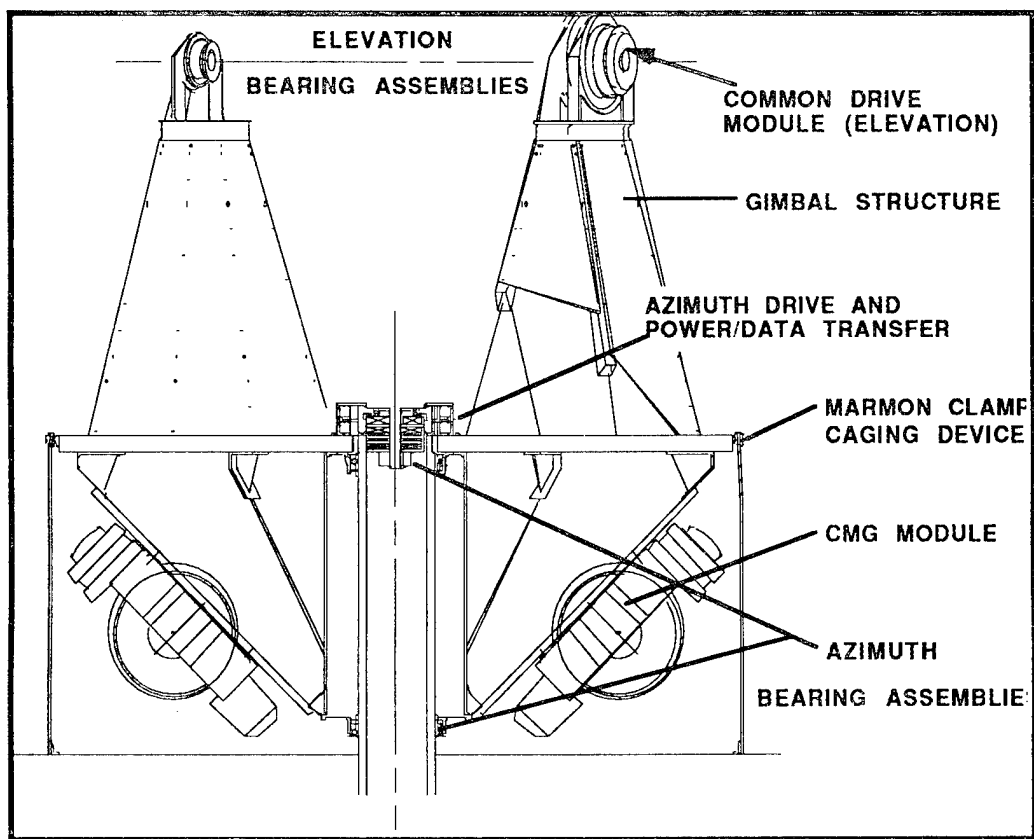
Fig. 4-4   SSTS Gimbal assembly showing azimuth & elevation bearings

**AZIMUTH AXIS**
- FIELD OF REGARD: ± 135 DEG
- SLEW RATE: 0.1 TO 6 DEG/SEC
- RATE JITTER: CLASSIFIED
- LIFE (7 YEARS) : 10 MILLION REVERSALS

**ELEVATION AXIS**
- FIELD OF REGARD: 0 TO 90 DEG
- SLEW RATE: 0.5 DEG/SEC
- RATE JITTER: CLASSIFIED

**TRIM CONTROL**
- ROLL CONTROL OF STABLE SPACECRAFT PLATFORM
- COMPENSATION FOR BEARING TORQUE & JITTER

**LWIR PAYLOAD**
- MASS:  971 KG
- INERTIA:  XX= 365 KG-M^2

**STIFFNESS REQUIREMENTS**
- LAUNCH LOADS: 15 g's AXIAL & LATERAL
- ON ORBIT FREQUENCIES: 10 HZ MIN
- STOWED FREQUENCIES: 15 HZ MIN AXIAL, 10 HZ MIN LATERAL

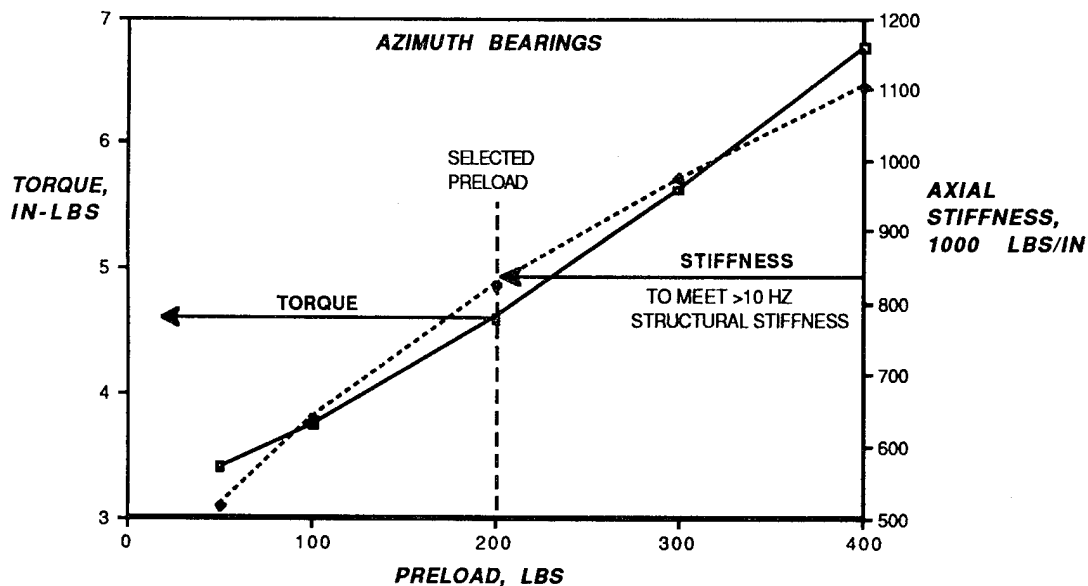Fig. 4-5   SVS LWIR gimbal requirements

**Fig. 4-6    Azimuth bearing preload trade**

The elevation axis bearing was sized in a similar fashion, viz. to meet load and stiffness requirements in the smallest package and provide the lowest torque. Bearings of 5.5 inch bore by 7 inch outside diameter were found to meet these objectives.
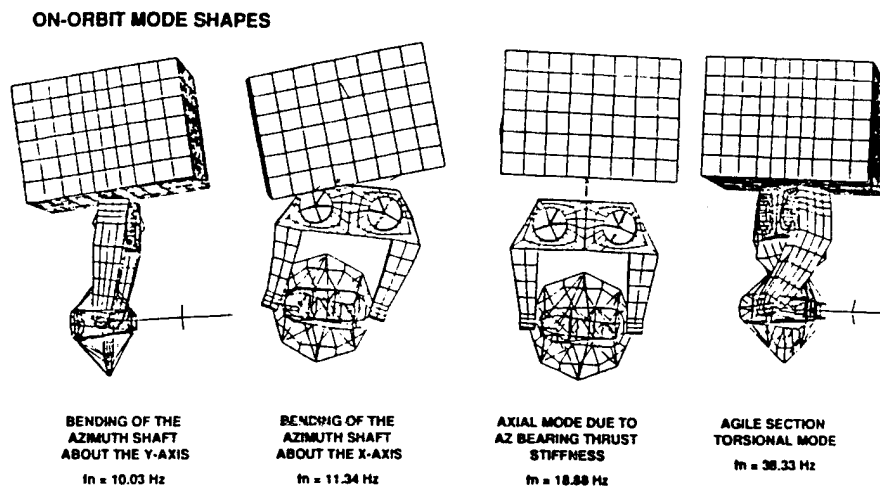


**Fig. 4-7    SVS On-orbit modes meet 10 Hz requirement**

## 4.2 BRILLIANT EYES

The Brilliant Eyes (BE) Satellite was added to the SDIO architecture in the fall of 1989. Its mission was one of mid-course booster detection and tracking, to complement the Brilliant Pebbles (BP) Satellite constellation. From a tribological point of view, the key concerns are similar to SVS in that low bearing jitter and good antenna pointing accuracy are important. However, BE's long periods of dormancy adds the burden that the various gimbal bearings must respond to rapid targeting demands after long periods of inactivity or very small motion. Also, the spin bearings in the 4 CMG units must be able to quickly ramp up in speed for battle maneuvers from their normal idle speed. The bearings in the CMG gimbals will also have to respond quickly after long periods of inactivity.

The antenna bearings (Fig. 4-8) associated with BE will be on the same size order as the 25 mm bore diameter screening bearings now on test. The switch from SSTS to BE came late in the procurement cycle for flight quality bearings. However, 7 pairs of a smaller, elevation axis bearing (3.3 x 5.1 inch) were procured to replace the 5.5 x 7 inch bearings, ear marked for the full scale life and functional tests. These replacement bearings have exceptional geometric accuracy and surface finish (better than AFBMA class 7 precision). Thus, with the current 11 x 12 inch bearing, the test data to be obtained in Phase II will be applicable to a wide range of SDI systems from a BE and BP class satellite up to a GSTS size vehicle.
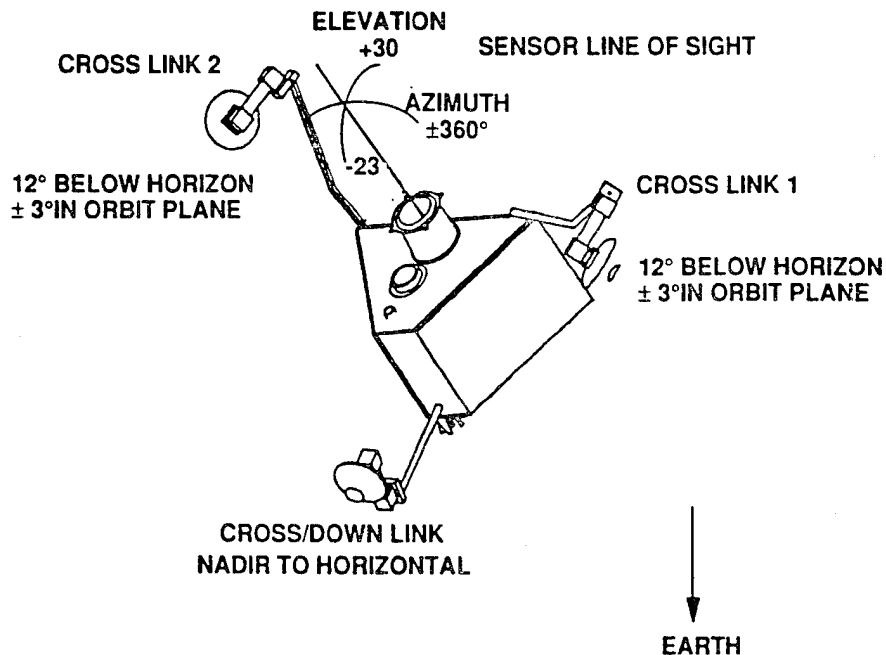
Fig. 4-8   Antenna gimbal angles for early monolith BE spacecraft

## 4.3 TEST PARAMETERS

### 4.3.1 Bearing Size

Three sizes of test bearings were selected to be able to quantify the effects of bearing size on both film performance and film quality control. Although limited test data had been obtained on these new high density films on small bearings, no test data were available on bearings of the size needed for the larger SDI payload gimbals. A comparison of the three sizes of test bearings with those proposed for the BE gimbals is shown in Fig. 4-9. The test bearings envelope the sizes anticipated for the BE gimbals, although the cross section of the middle size bearing is larger than that normally used for space gimbals. This was due to the non-availability of flight quality test bearings of this size needed to support the test schedule.



Fig. 4-9  Comparison of Test and Gimbal Bearing Sizes

## 4.3.2 Test Cycle

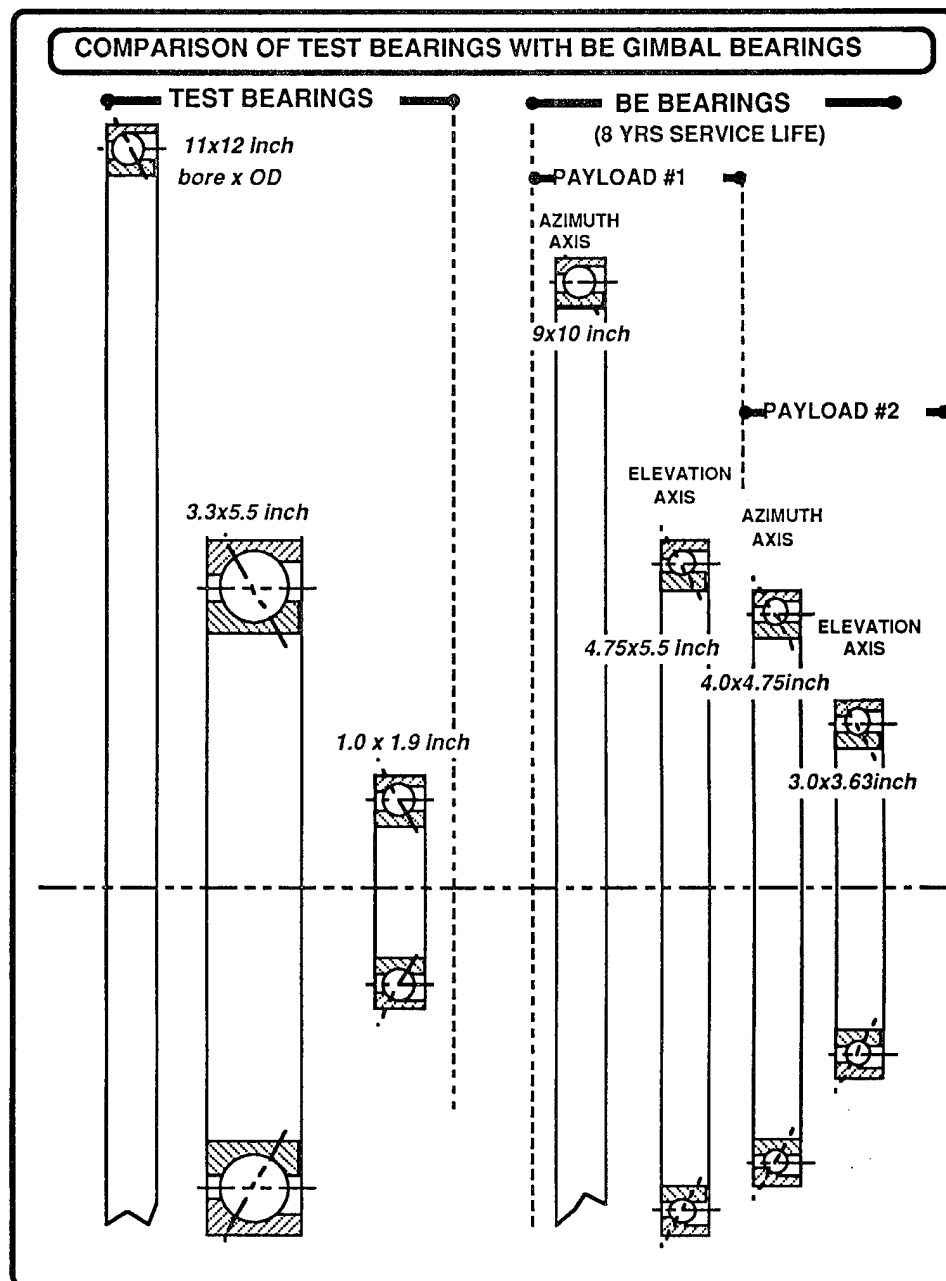A composite gimbal motion duty cycle was selected for the test in the interest of making the bearing life data as widely useful to as many gimbal applications as possible. For the 105-size ($\approx$ 2 inch OD) screening bearings, the test cycle consisted of a search mode of 50,000 continuous revolutions at 1 Hz (1 rev/sec), followed by 100,000 cycles of ± 80 degs of wide angle scan at 1 Hz and then 50,000 cycles of ± 10 degs of small angle pointing at 2 Hz.(see Fig. 4-10). This gimbal cycle repeated continuously through out the test. The 360 deg rotations are consistent with an acquisition sensor executing a 360 deg search pattern. The ± 80 degs of motion allowed for at least 2 ball overlap contacts in each direction (6 stress contacts per full cycle). It is consistent with an acquisition sensor gimbal doing a raster scan track. The ± 10 degs of motion permits no ball track overlap and thus represents a small angle dither type motion. Such motion is common for pan/tilt mirrors such as those on weather satellites. A concern for bearing motions that do not span at least one ball spacing is the occurrence of debris build up at end of travel. This can create "torque bumps" when the gimbal is commanded to point to a new sector as the bearing balls ride up over this debris. Thus the chosen test cycle is reflective of a wide variety of gimbal scan motions. Stop/start gimbal motion is particularly demanding for bearings since lubricant redistribution is generally nonuniform.

The gimbal angles for the grease-lubricated 105-size bearing was the same as that shown in Fig. 4-10, but the cycle rates were reduced (see Fig. 4-11) to keep the bearing lubrication condition primarily in the boundary regime. This is consistent with low speed gimbal operation, whereas higher tests speed would provide primarily elastohydrodynamic (EHD) lubrication which could artificially benefit bearing test life. The general rule of thumb is to keep the Lambda ratio (EHD minimum film thickness/RMS of surface composite roughness) well below one for boundary lubrication. As illustrated in Fig. 4-12, the stop-start nature of
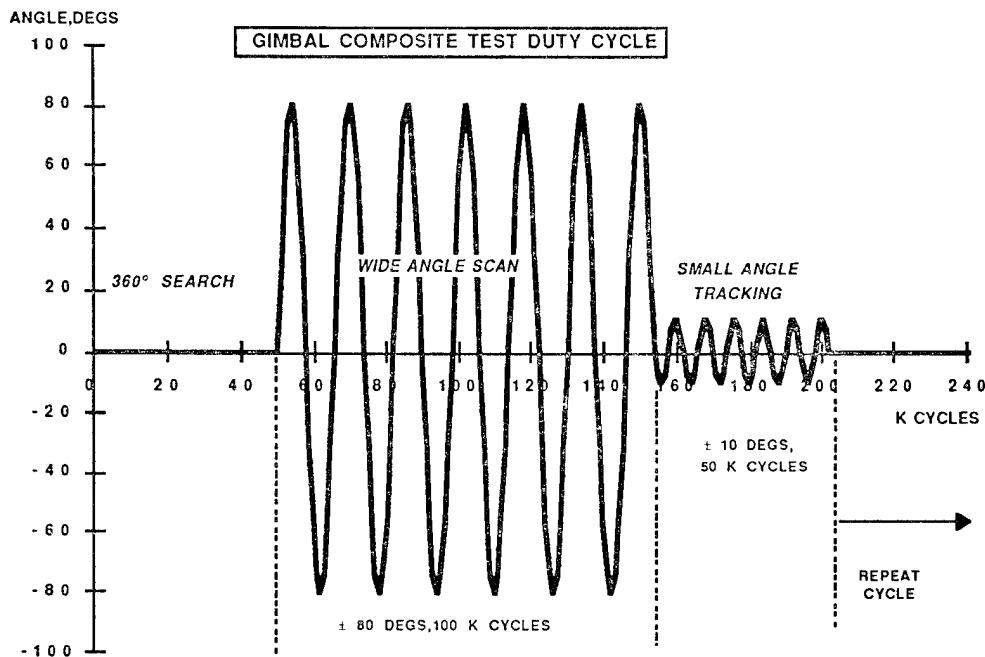


Fig. 4-10    Test duty cycle for 105-size MoS$_2$ test bearings

**105-Size BEARING LIFE TEST - MoS2 Lubricated**

| GIMBAL ANGLE, ±degs | CYCLES | *FREQ Hz | *Peak Ang Vel, deg/s |
|---|---|---|---|
| CONTINUOUS | 50,000 | 1 | 360 |
| 80 | 100,000 | 1 | 502 |
| 5 | 50,000 | 2 | 63 |

**105-Size BEARING LIFE TEST - Grease Lubricated**

| GIMBAL ANGLE, ±degs | CYCLES | *FREQ Hz | *Peak Ang Vel, deg/s | *Peak Lambda Ratio |
|---|---|---|---|---|
| CONTINUOUS | 50,000 | 0.6 | 216 | 0.90 |
| 80 | 100,000 | 0.5 | 251.3 | 1.00 |
| 5 | 50,000 | 2 | 62.8 | 0.36 |

*peak Ang Vel limited to 250°/sec for lambda <1.0*

**117-Size BEARING LIFE TEST - MoS2 Lubricated**

| GIMBAL ANGLE, ±degs | CYCLES | FREQ Hz | *Peak Ang Vel, deg/s |
|---|---|---|---|
| CONTINUOUS | | | |
| 60 | 100,000 | 0.5 | 188.5 |
| 5 | 400,000 | 2.5 | 78.5 |

**117-Size BEARING LIFE TEST - Grease Lubricated**

| GIMBAL ANGLE, ±degs | CYCLES | FREQ Hz | *Peak Ang Vel, deg/s | *Peak Lambda Ratio |
|---|---|---|---|---|
| CONTINUOUS | | | | |
| 60 | 100,000 | 0.28 | 105.6 | 0.86 |
| 5 | 400,000 | 2.5 | 78.5 | 0.69 |

*peak Ang Vel limited to 130°/sec for lambda <1.0*

**11X12 BEARING LIFE TEST- MoS2 Lubricated**

| GIMBAL ANGLE, ±degs | CYCLES | FREQ Hz | Peak Ang Vel, deg/s |
|---|---|---|---|
| CONTINUOUS | | | |
| 60 | 100,000 | 0.28 | 105.6 |
| 5 | 400,000 | 2 | 62.8 |

**11X12 BEARING LIFE TEST- Grease Lubricated**

| GIMBAL ANGLE, ±degs | CYCLES | FREQ Hz | *Peak Ang Vel, deg/s | *Peak Lambda Ratio |
|---|---|---|---|---|
| CONTINUOUS | | | | |
| 60 | 100,000 | 0.28 | 105.6 | 1.00 |
| 5 | 400,000 | 2.5 | 78.5 | 0.81 |

*peak Ang Vel limited to 105°/sec for lambda <1.0*

Fig. 4-11    Summary test duty cycle for all test bearings.

gimbaling assures boundary lubrication for a substantial period of test time. Cycles rates for all the liquid lubricated test bearings (see Fig. 4-11) were set so that Lambda ratios at even the peak velocities never exceed one. The test cycle for the larger 117-size ($\approx$ 5 inch OD) and 12 inch OD bearings were similar to that of the 105-size bearing, except that the continuous rotation segments were deleted. This is in recognition that the BE payload gimbals were primarily scanning and/or targeting rather than continuously rotating.
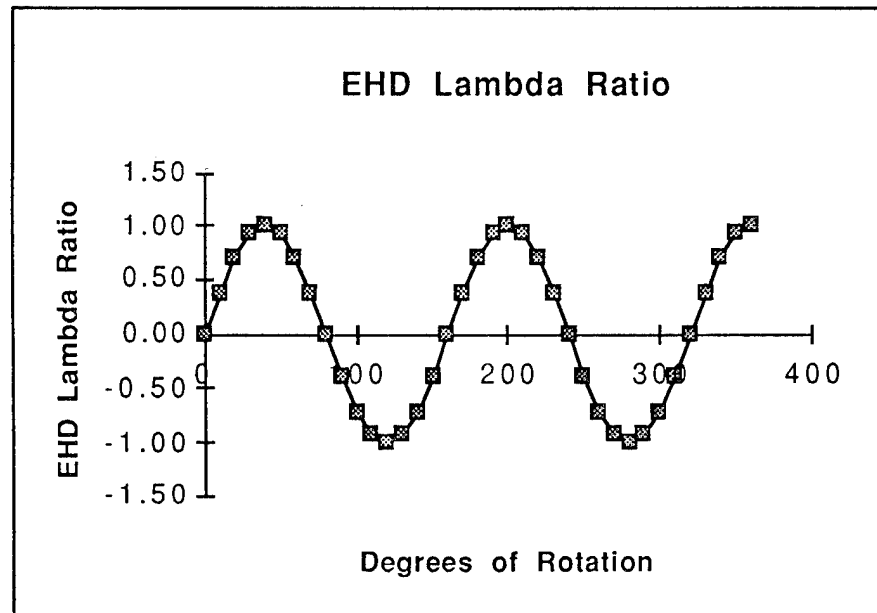


Fig. 4-12    105-size test bearings spend large percentage of time in boundary lubrication regime (low Lambda ratio)

### 4.3.3 Comparison with B.E. Duty Cycle

The B.E. gimbals were active between 15 and 25% of the time based on all orbits. When not in a surveillance or targeting mode, the remainder of the time was spent in a standby mode. The bearing cycle life for each payload gimbal was determined by integrating the total slew during active duty. The cycle life was converted to ball/race crossings or stress cycles to account for differences in the number of bearing balls and gimbal motions between the B.E. bearings and those used for the tests.

A comparison between required B.E. bearing life and those achieved during test can be found in Fig. 4-13. Comparing bearings of similar size, the test bearing lives generally exceeded those required except for the 4.75 inch OD, Payload 2 Azimuth bearing which had nearly 3 times the ball/race stress cycles of the other BE bearings. Only the 105-size ($\approx$ 2 inch OD) and 12-inch, grease lubricated test bearings had lives which were long enough.
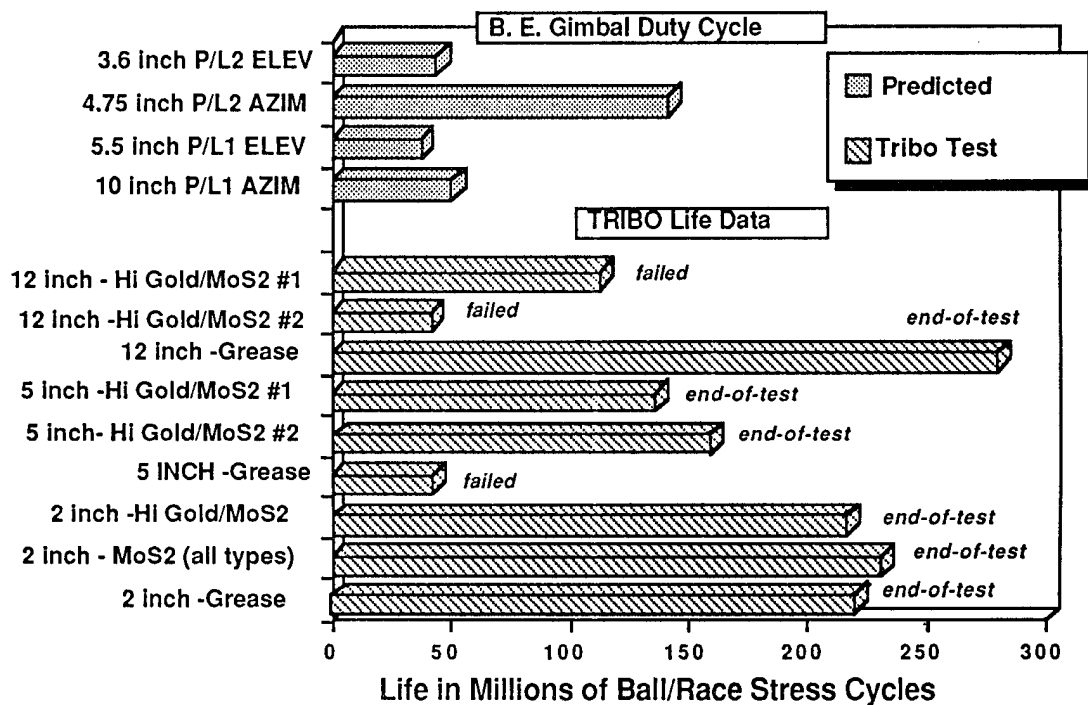


Fig. 4-13   Comparison of Test and Gimbal Bearing Application Lives

## 4.4 TEST BEARING MANUFACTURE

### 4.4.1 Accuracy

To achieve the high level gimbal performance sought under this program requires not only the best tribomaterials technology but the state-of-the art in bearing manufacturing technology as well. Careful attention to runout, surface waviness (lobing), preload control and internal geometry are mandatory. A case in point are the 5-inch OD bearings now on hand. A typical transverse cross race curvature profile and race deviation from true circularity (DFTC) plot appear in Figs. 4-14 and 4-15, respectively for one of the outer races. The peak to valley cross race curvature deviation is 26 $\mu$ in., transverse roughness 3 $\mu$ in. RMS and circumferential lobing (DFTC) is less than 19 $\mu$ in. In addition, the bearing bore and outside diameters of this bearing were grouped to within 50 $\mu$ inches from bearing to bearing. These numbers are extremely good for a bearing of this size. Complete acceptance data packages were obtained for all 5- and 12-inch test bearings.

| Mode | Traverse Length | Reference | Ignore |
|------|-----------------|-----------|--------|
| UNFILTERED | .83 in | CONCAVE | 0 % |
| 117848 D\R | NO 38 | | |
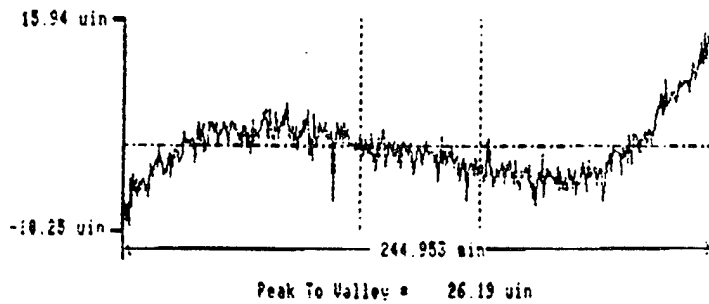
*Trans Roughness = 3.05 µm AA*

15.94 uin

-18.25 uin

244.953 uin

Peak To Valley = 26.19 uin

```
PFa    =    3.25 uin
PFq    =    4.95 uin
Pksk   =    1.8
PFku   =    4.7
PDelq  =     .49 Deg
PLarq  =    3.647 uin
PS     =    638.42 uin
PSa    =    3.591 uin
PRz    =    24.92 uin
```

Fig. 4-14 Typical cross race curvature data for the 5 inch test bearing

DFTC 19.3 µin

DFTC₅₀ 18.1 µin

$\text{Max}\dfrac{dR}{d\theta}$ 0.93 $\dfrac{\mu\text{in}}{\text{deg}}$

$\text{Av}\dfrac{dR}{d\theta}$ 0.30 $\dfrac{\mu\text{in}}{\text{deg}}$
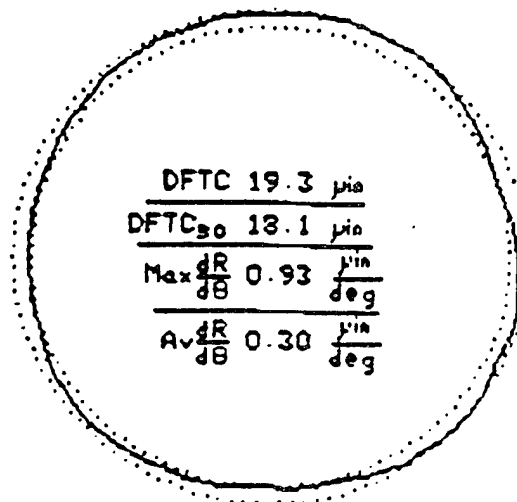
Fig. 4-15    Typical race circularity plot for 5 inch test bearing

## 4.4.2 Test Rings

Additional manufacturing considerations include accommodation of the solid lubricant coating thickness in terms of internal clearance control, preload (stickout), and contact angle. As an example, a nominal solid lubricant thickness of 1 μm or 0.000040 inch on the inner and outer races of the 12-inch OD bearing can increase normal preload by ≈ 70 lbs, more than 1/3 the initial preload. Special preload adjustments were used to ensure that the $MoS_2$ film lubricated and grease lubricated bearings have essentially equal preloads. These individual bearing adjustments are necessary to compensate not only for variation in ball-race track diameter but solid lubricant film thicknesses as well. First, the bearings were mounted in precision test rings that simulate the equivalent radial stiffness and expected fits of the shaft and housing of the chosen gimbal. This is necessary since the unmounted preload of a bearing as supplied by the bearing vendor will change when installed in the actual gimbal mounting structure. In the case of 12-inch bearings, precision test rings were manufactured and furnished to the bearing vendor to control the installed preload to spec. These precision gage rings were manufactured to diametral tolerance of less than 100 μ inch over a 11 or 12 inch diameter (see Table 4-16). The correctly preloaded bearing cartridges can then be conveniently mounted into the life and/or parametric bearing test fixtures. A similar approach was adopted with the 5-inch OD bearing, except the bearings were matched and mounted to test rings at Lockheed. In some cases it was necessary to replace the balls with incrementally larger or smaller balls to achieve uniformity of preload from bearing to bearing. A special bearing preload and stiffness fixture was built for this purpose.

**Table 4-16   Typical diametral tolerances of test rings at different clock positions in microinches**

| | | | | 11 X 12 | INNER TEST | RINGS | | |
|---|---|---|---|---|---|---|---|---|
| PART | DWG SIZE | TOL | position | axis 0° | axis 45° | axis 90° | axis 135° | |
| | | μ IN | | μ IN | μ IN | μ IN | μ IN | |
| IT-3 PAIR "E" | 10.9993 | ±0.0001 | left end | 50 | 60 | 70 | 30 | |
| ID | 9.40 | ±0.03 | middle | 120 | 130 | 150 | 130 | |
| width | 1.122 | | right end | 65 | 40 | 75 | 30 | AVERAGE |
| | | | AVG | 78 | 77 | 98 | 63 | 10.99938 |
| | | | | | | | | |
| IT-4 PAIR "F" | 10.9993 | ±0.0001 | left end | -25 | 10 | 20 | -25 | |
| ID | 9.40 | ±0.03 | middle | 40 | 55 | 55 | 50 | |
| width | 1.122 | | right end | 0 | -25 | -5 | 0 | AVERAGE |
| | | | AVG | 5 | 13 | 23 | 8 | 10.99931 |
| | | | | | | | | |
| IT-5 PAIR "G" | 10.9993 | ±0.0001 | left end | 15 | 15 | -30 | 0 | |
| ID | 9.40 | ±0.03 | middle | 50 | 65 | 55 | 65 | |
| width | 1.122 | | right end | -30 | 5 | 60 | 0 | AVERAGE |
| | | | AVG | 12 | 28 | 28 | 22 | 10.99932 |
| | | | | | | | | |
| IT-6 PAIR "H" | 10.9993 | ±0.0001 | left end | -40 | 0 | -40 | -30 | |
| ID | 9.40 | ±0.03 | middle | 50 | 60 | 50 | 50 | |
| width | 1.122 | | right end | -20 | 0 | -30 | -30 | AVERAGE |
| | | | AVG | -3 | 20 | -7 | -3 | 10.99930 |

## 4.4.3 Bearing Specification

Detail bearing specifications were prepared for both 5-inch and 12-inch O.D. test bearings. The 12-inch bearing document contain detailed manufacturing specifications, bearing dimensions and quality assurance provisions (acceptance criteria and verification matrix) consistent with flight bearings, as required for space flight applications. Required measured bearing parameters for acceptance included: bearing preload, contact angle, breakaway/ running torque, axial stiffness, angular runout, surface finish, transverse curvatures, and actual critical dimensions. The 5-inch bearing specification was to set to match that of a commercial precision class 7-9 bearing, having a separable inner race. Seven duplex pairs of this bearing were available with relatively short lead times. The bearing came with complete

dimensional certifications including preload, deviation from true circularity, surface finish, transverse curvatures, and actual critical dimensions. All test bearings were again functionally tested at LMSC to determine torque signatures, preload, axial stiffness and angular runout prior to life testing. This was done to confirm installed performance of the bearings when mounted in rig hardware and to establish a beginning-of-life basis for post-life comparisons.

## 4.5 WEAR LIFE MODEL

In the interest of applying life test data for a bearing of one size, load, and motion to another bearing for a different application, it is desirable to develop a model which relates the fundamental film and bearing parameters to life. Also modeling the effect of contact stress on life was needed to account for the unavoidable variations in preload, hence contact stress, of test bearings having $MoS_2$ films of differing thicknesses and those with $MoS_2$ films on the balls.

The starting point is the well known Archard wear life equation for adhesive wear given in Fig. 4-17. These equations relate material hardness, load and the material wear coefficient to wear rate for a sliding *continuous contact*, such as a pin on a disk.
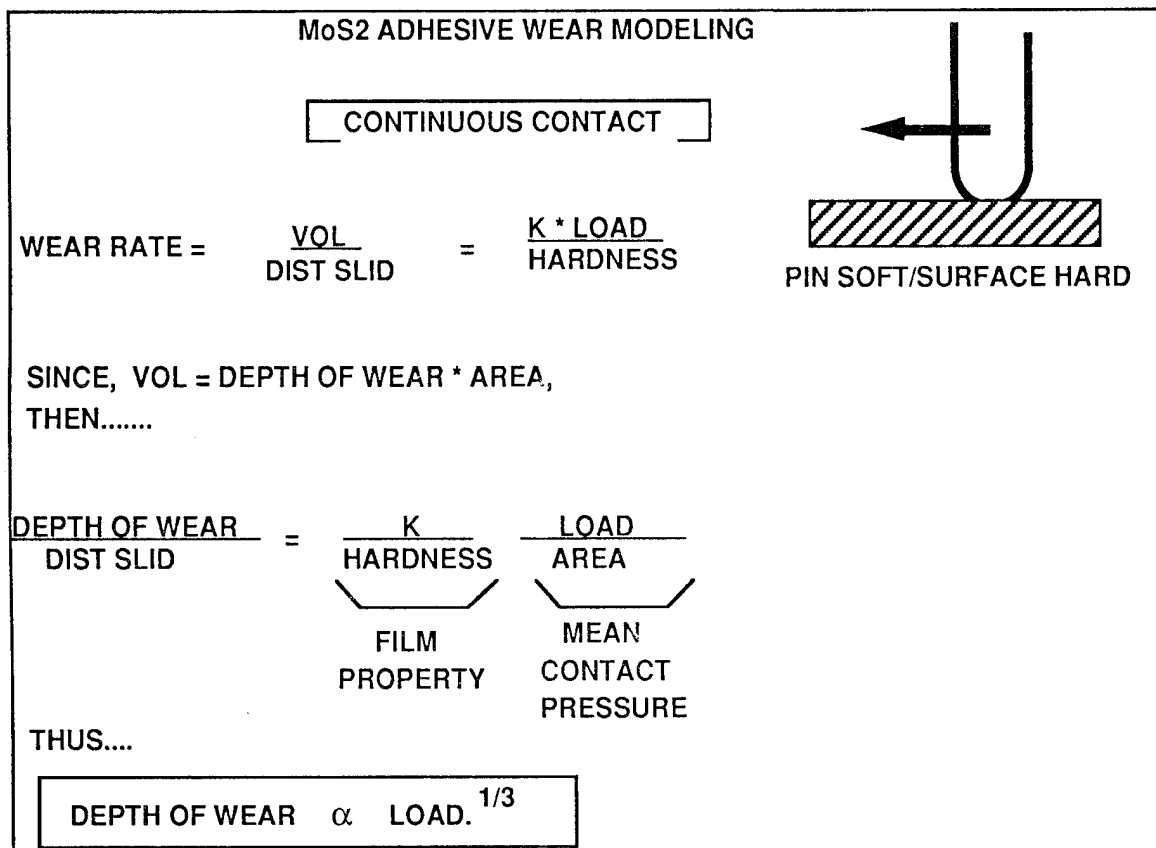


Fig. 4-17   Continuous contact wear model

However, a bearing ball rolling over a race coated with an MoS$_2$ film is an example of a non-continuous contact problem. This is equivalent to a hard pin sliding over a soft surface as illustrated in Fig. 4-18. The wearing surface is now sensitive to the number of the times the hard pin slides over the same spot. The wear rate and subsequently number of cycles to failure can be related to coating thickness, hardness, load, % slip and number of passes or contacts per cycle as shown. Note that theoretically life is inversely related to load to the 2/3 power. However, pin-on-disk test data from Roberts [4-1] (see Fig. 4-19) as well as Hohman rub block data (see Fig. 4-20) show that MoS$_2$ film life is more strongly effected by load, approximately to the 1.4 power.

Therefore adjusting the load-life exponent based on experimental data, we get the following MoS$_2$ film life model as shown in Fig. 4-21. Note that a reverse scanning life knock down factor Ø has been included to account for the expected damaging effect of reverse shear stress during gimbaling. The life model is based on MoS$_2$ sliding wear life alone and does not consider the effects of a replenishing transfer film from the ball retainer.
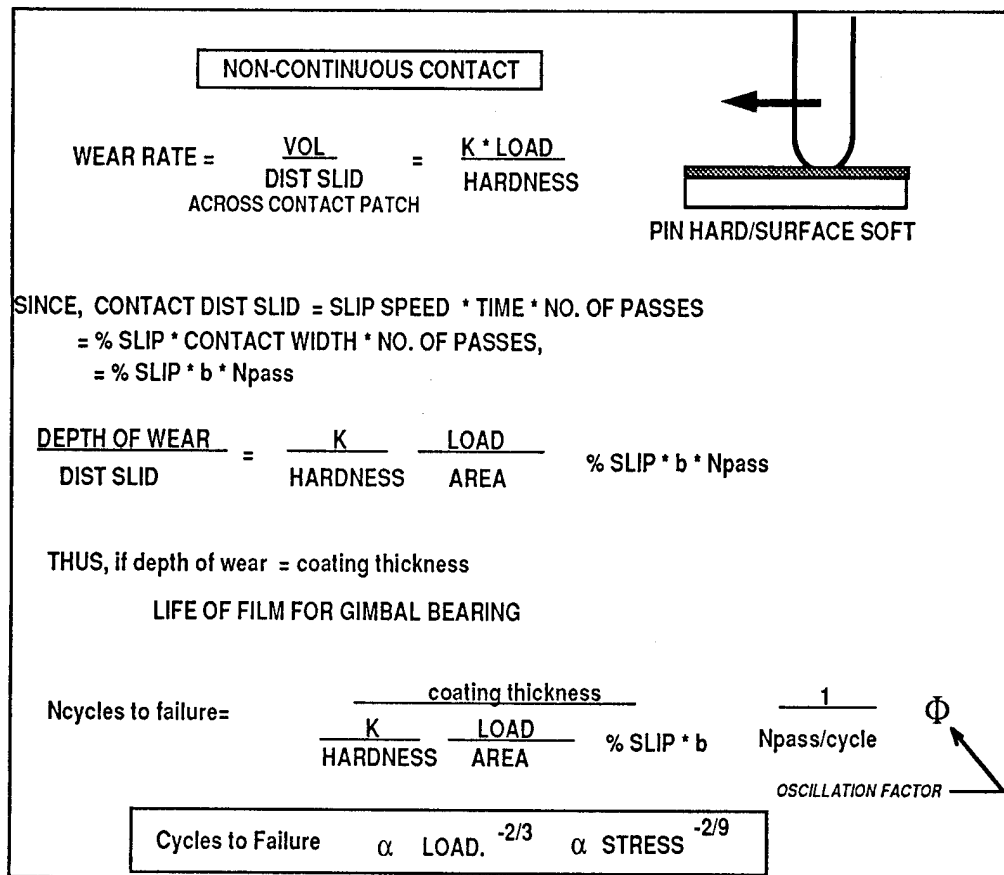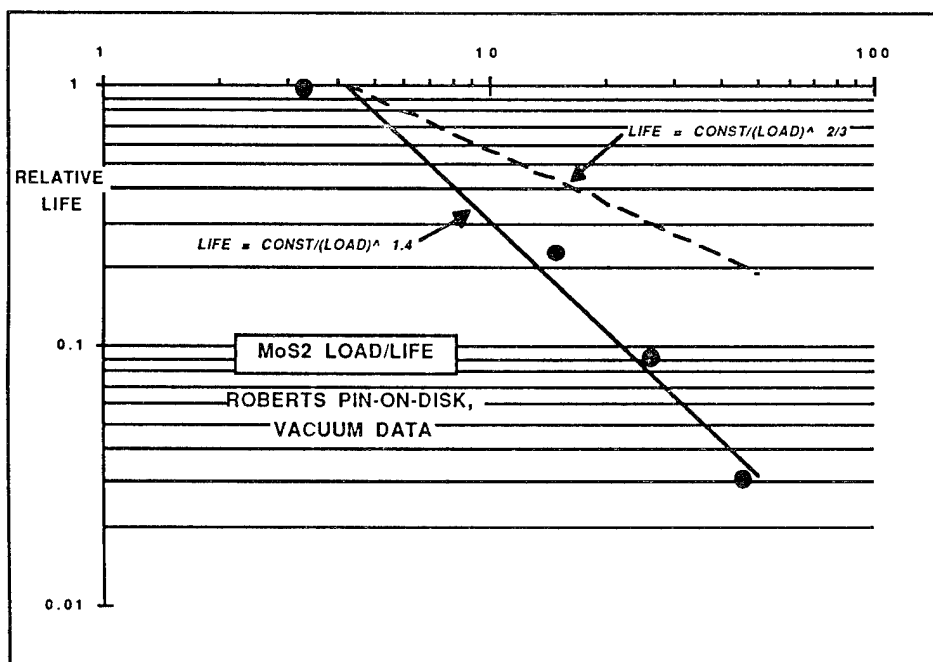


Fig. 4-18 Bearing MoS$_2$ film wear model

- 33 -

**Fig. 4-19 Roberts MoS₂ film load-life Data [4-1]**

Figure content:
- Axis: RELATIVE LIFE (1, 0.1, 0.01)
- Top axis: 1, 10, 100
- LIFE = CONST/(LOAD)^ 2/3
- LIFE = CONST/(LOAD)^ 1.4
- MoS2 LOAD/LIFE
- ROBERTS PIN-ON-DISK, VACUUM DATA
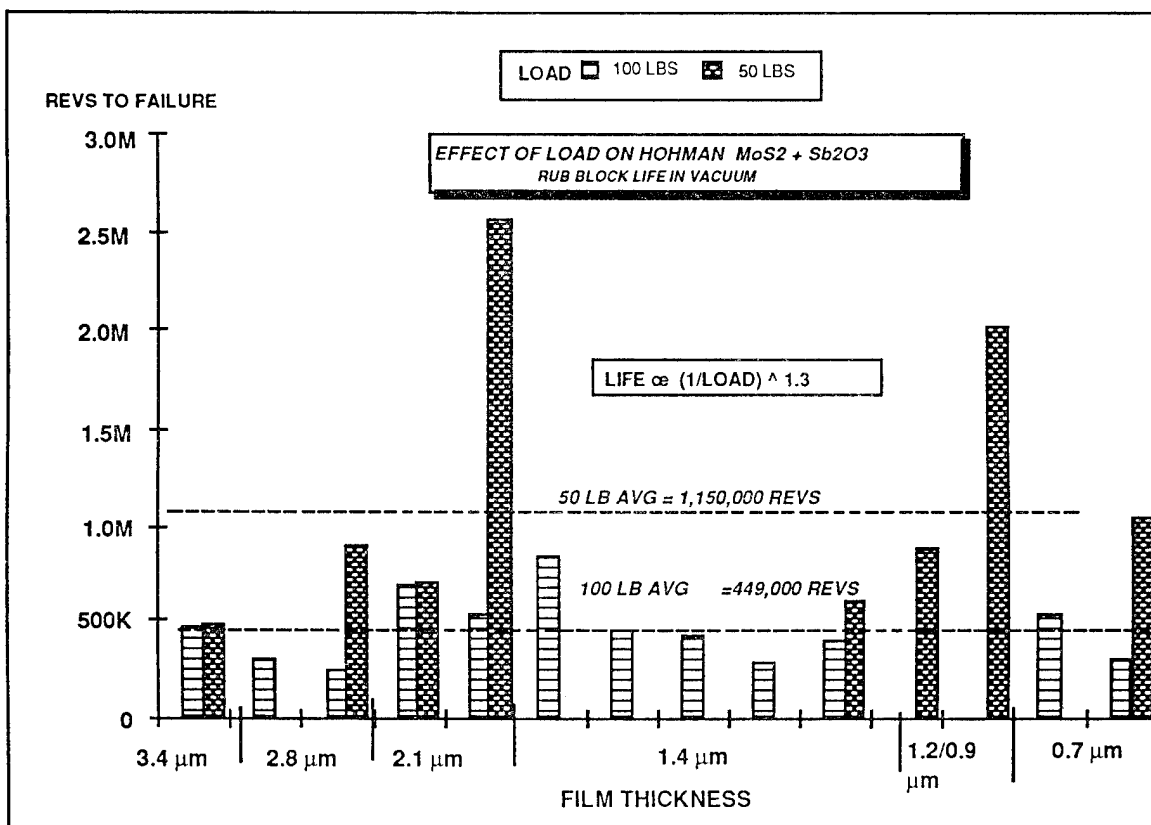


**Fig. 4-20 Hohman MoS₂ film load-life data**

Figure content:
- LOAD □ 100 LBS ▨ 50 LBS
- REVS TO FAILURE (3.0M, 2.5M, 2.0M, 1.5M, 1.0M, 500K, 0)
- EFFECT OF LOAD ON HOHMAN MoS2 + Sb2O3 RUB BLOCK LIFE IN VACUUM
- LIFE œ (1/LOAD) ^ 1.3
- 50 LB AVG = 1,150,000 REVS
- 100 LB AVG = 449,000 REVS
- FILM THICKNESS: 3.4 μm, 2.8 μm, 2.1 μm, 1.4 μm, 1.2/0.9 μm, 0.7 μm

```
From Test Data

Cycles to Failure    α Load $^{-1.4}$    α Stress $^{-4.2}$


Therefore


Cycles to Failure  α  $\dfrac{\text{Coating Thickness}}{(\text{Stress }^{4.2})\,(\%\text{ Slip})\,(\text{Npass/Cycle})}$  Φ


Where


        Φ =   Life Knock Down Factor for Reverse
                   Stress during Scanning
```

Fig. 4-21     Hohman MoS$_2$ film load-life data

Fig. 4-22 illustrates the effect of axial load and ball number on theoretical life for the 105 size test bearings at ± 45 deg stroke. Note that bearing preload will have a noticeable effect on life.  It is instructive that cutting the number of bearing balls in half from 12 to 6 significantly increases contact stress but has a more modest effect on life.  This is because reducing the number of balls also reduces the number of stress cycles each spot on the inner and outer race thereby partially offsetting the increased stress effect on life.

| | | 105 ANG CONTACT BEARINGS | | |
|---|---|---|---|---|
| LOAD,LBS | NUMBER BALLS | MEAN HERTZ STRESS,KSI | #CONTACTS PER CYCLE | RELATIVE WEAR LIFE |
| 20 | 12 | 93 | 4 | 1.78 |
| 20 | 9 | 103 | 4 | 1.19 |
| 20 | 6 | 118 | 2 | 1.35 |
| 30 | 12 | 107 | 4 | 1.00 |
| 30 | 9 | 118 | 4 | 0.67 |
| 30 | 6 | 135 | 2 | 0.76 |
| 40 | 12 | 118 | 4 | 0.67 |
| 40 | 9 | 129 | 4 | 0.45 |
| 40 | 6 | 148 | 2 | 0.51 |

Fig. 4-22     Hohman MoS$_2$ film load-life data


# References For Section 4

[4-1]   Roberts, E. W., "The Tribology of Sputtered Molybdenum Disulfide Films," Proc. Inst. of Mech. Eng., Tribology - Friction,Lubrication and Wear, Fifty Years On, Vol. I, (1987) pp. 503-510.

## Section 5

# PHASE II BEARING TESTS

The work to be performed under the T/PGD program is to provide a test data base to establish that tribomaterial technology : (a) provides significant performance/life advantages over today's materials and (b) is sufficiently mature to warrant use in critical space flight gimbals.

These objectives are satisfied by :

(1)  Running a statistically significant number of advanced vs. conventional lubricant, precision bearing screening tests under simulated space gimbal conditions.

(2)  Developing bearing life and performance models for user assessment that have been validated with *hard* test data.

(3)  Proving, through test, that advanced tribo film producers can *consistently* coat flight quality bearings of various sizes.

(4)  Establishing the expected gimbal performance payoffs with better tribo bearings for the user's specific application from an experimentally validated gimbal/bearing simulation.

This section described the results of tests to meet the first three of the objectives above. Section 8 addresses the question of potential gimbal performance payoffs for the user of tribo technology.

## 5.1  THRUST BEARING

As reported in LMSC Phase I Final Report [5-1], 1" bore diameter by 2" OD thrust bearings were used to provide early screening data on the advanced $MoS_2$ films and liquid lubricants. These tests were generally conducted at a ball/race maximum contact stress of 161 ksi, an oscillatory stroke of $\pm 45°$, in a $10^{-6}$ torr vacuum. The thrust bearing geometry allowed easy disassembly for sputtering and analysis. Preloading through a coil spring was also easily accomplished. However, commercial thrust test bearings, normally used for automotive applications, were geometrically crude compared to aerospace bearings. Furthermore, their $90°$ contact angle geometry generated a large amount of spin microslip which accelerated the wear process and aggravated turn-around torque signature. Figs. 5-1 & 5-2 show typical results from the thrust bearing tests with Ovonic Synthetic Material Inc (Ovonic), The Aerospace Corp., and National Center of Tribology (NCT) as well as those from Hohman Plating & Manufacturing (Hohman).
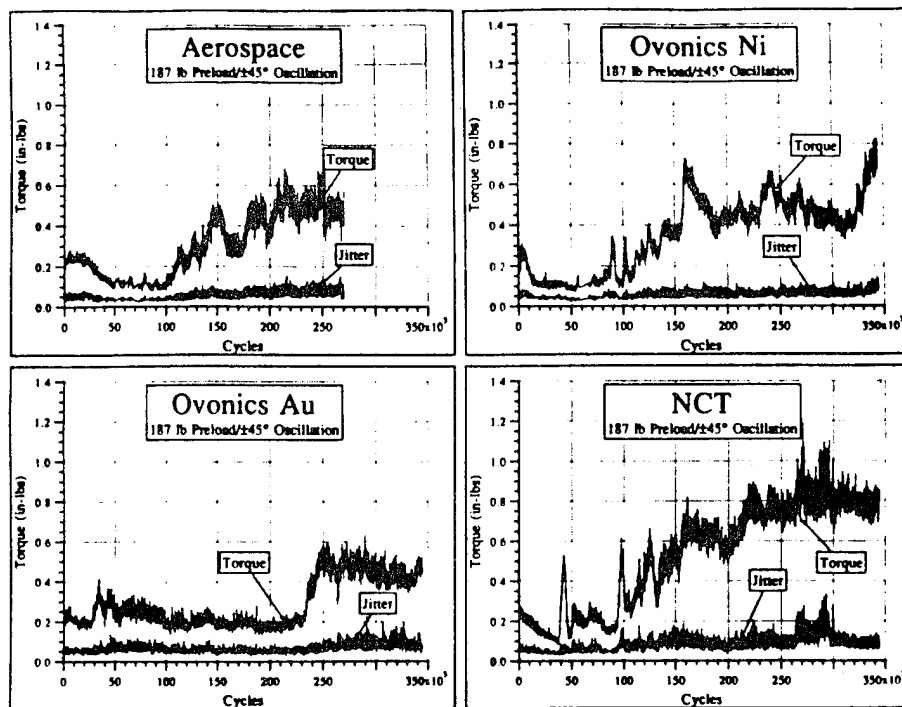
**Fig. 5-1  Thrust bearing results with Aerospace, Ovonics & NCT films**

The torque signatures in Fig. 5-1[#] , appear to show some sort of break-in improvement up to about 100,000 cycles, then start to fail. The only exception being the Ovonics film multilayered with gold, which lasted about 230,000 cycles before failing.

Two sets of bearings (4 singles) were sputtered coated with $MoS_2$+ $Sb_2O_3$ film in two separate deposition runs, A & B.  The performance of these films were remarkably similar, as shown in Fig. 5-2. This lent some credence to Hoh'man's ability to produce consistent films from batch to batch. However, the rub block tests that accompanied these runs indicated that film B would be vastly superior to film A. It would appear from the bearing results that there was a problem with this particular rub block test.

---

[#] In Fig. 5-1 and most subsequent plots, both the steady or average value of torque is plotted together with the RMS value of the fluctuating component of torque(width of torque hash band) which is referred to as "ripple".  The bearing torque ripple is very important to the quality of sensor imaging since jitter can degrade performance, as will be discussed later.
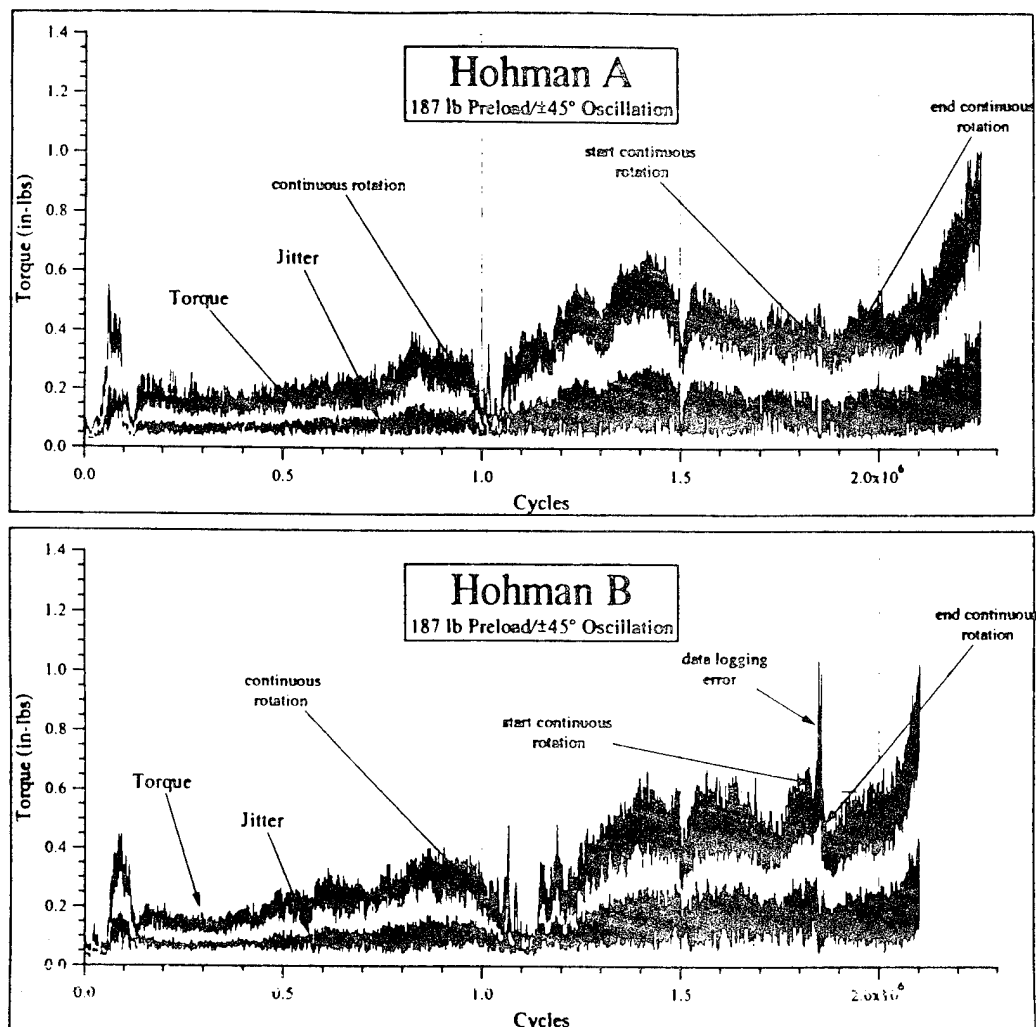
**Fig. 5-2 Thrust bearing results with Hohman films**

### 5.2.1 Blocking

One can clearly notice a drop in torque at about 1 million cycles in Fig. 5-2. This corresponds to a point where continuous rotation was substituted for the normal ±45° gimbaling during the test. This is believed due to a phenomena referred to as "blocking" in Ref.[5-2]. Blocking is build up of torque when the bearing reverses direction due to some of the balls pinching the ball separator. The thrust bearing's spin producing geometry and its relative tight raceway cross curvatures (standard conformity = 52%) clearly aggravates this effect. The benefits of continuous rotation which "resets' the blocking torque is clearly evident in Fig. 5-3 for the test thrust bearing lubricated with a polyalphaoelifin oil (PAO).
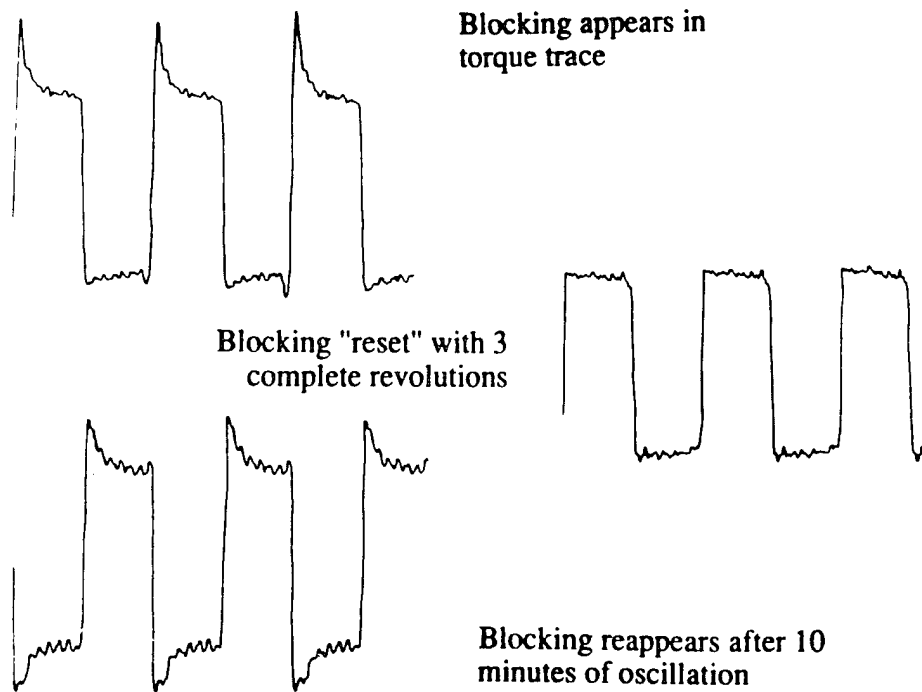
- 38 -

Blocking appears in
torque trace

Blocking "reset" with 3
complete revolutions

Blocking reappears after 10
minutes of oscillation

**Fig. 5-3   Thrust bearing Blocking reset with continuous rotation**

### 5.1.2 Liquids versus MoS2 films

The potential of low torque with bearings lubricated with $MoS_2$ films is apparent from Fig. 5-4 which shows the Ovonics multilayer film versus a PAO oil and neopentyl ester grease. In the case of the PAO oil, the $MoS_2$ film shows about a 3 to 1 lower torque advantage up to 100,000 cycles before starting to fail. There was less of an advantage in terms of torque ripple (Fig. 5-5), probably because of the thrust bearings relatively coarse surface finish (16 $\mu$ inch AA). Although both of the liquid lubricants are very long lived, $MoS_2$ films can show adequate life in bearings of better quality than the relatively crude thrust bearings. In fact, as will be discussed in the next section, 105 size, precision angular contact ball bearings coated with these films have maintained very low torque signatures for more than many million gimbal cycles.

### 5.1.3 Load Effects

An important concern is the effect of preload, hence contact stress on bearings lubricated with $MoS_2$ films. Bearing preloads for gimbals need to be sufficiently large so that the bearing stiffness does not compromise the margin between structural frequency modes and the operating frequencies of the gimbal (bandwidth). As discussed in Section 4.5, sliding test data with the $MoS_2$ films suggest that life $\approx$ (load) $^{-1.4}$ However, this data was for pure sliding and may not strictly hold for bearings that are primarily in rolling (adhesive wear).
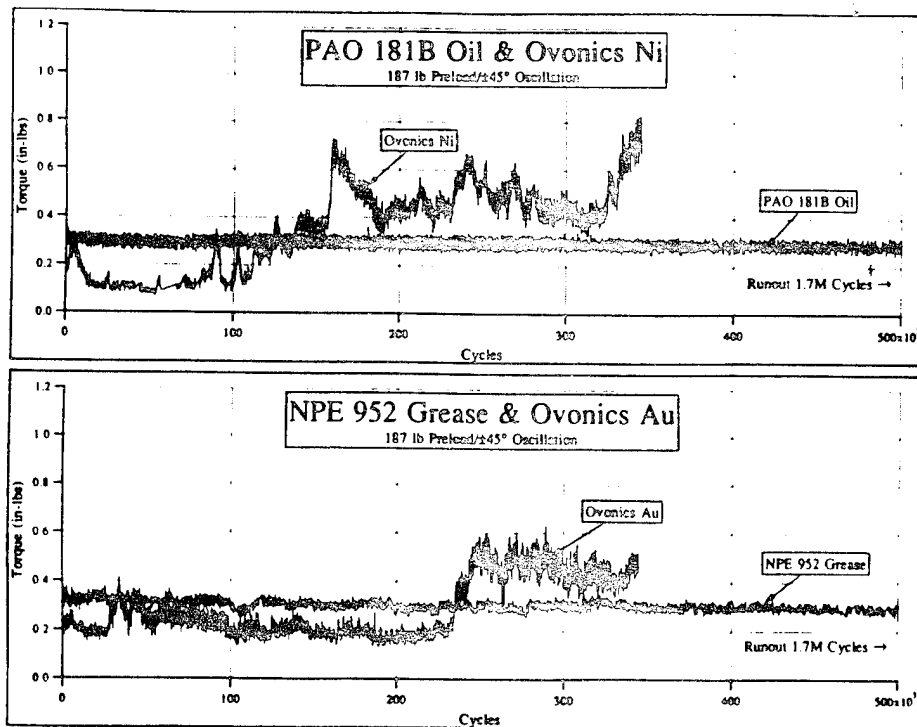
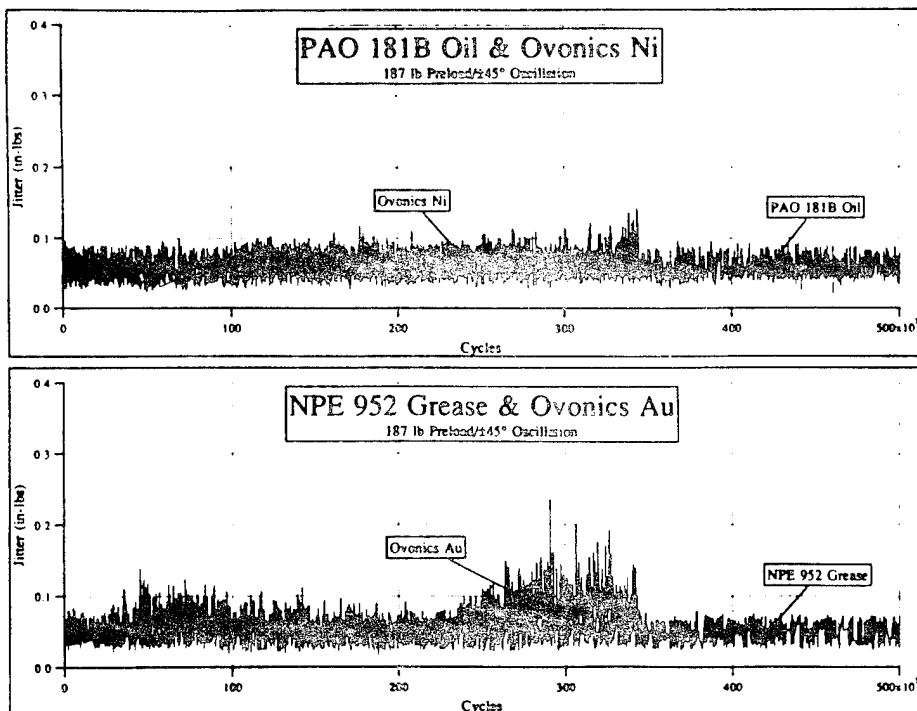**Fig. 5-4 Thrust bearing torque: Liquids vs. MoS₂ films**



**Fig. 5-5 Thrust bearing torque ripple: Liquids vs. MoS₂**

Load-life thrust bearing tests were conducted with Aerospace (Fig. 5-6) and Hohman films (Fig. 5-7) at preloads of 187 and 112 lbs (mean Hertz stresses of 107 and 91 ksi, respectively). Note that the X-axis scales are very different. Although the tests at 112 lbs preload were not run to failure, the life of the Aerospace film has improved by a factor of 5 at test cutoff.
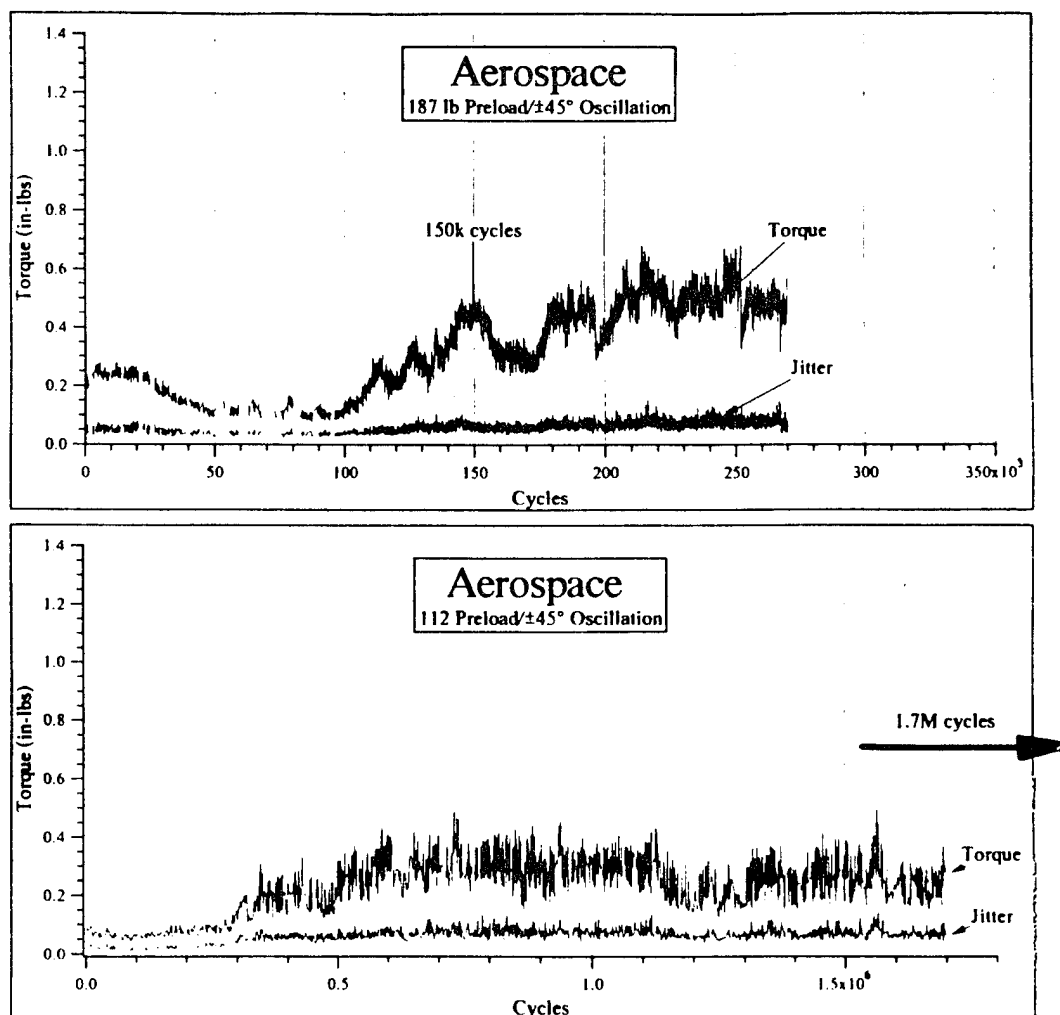


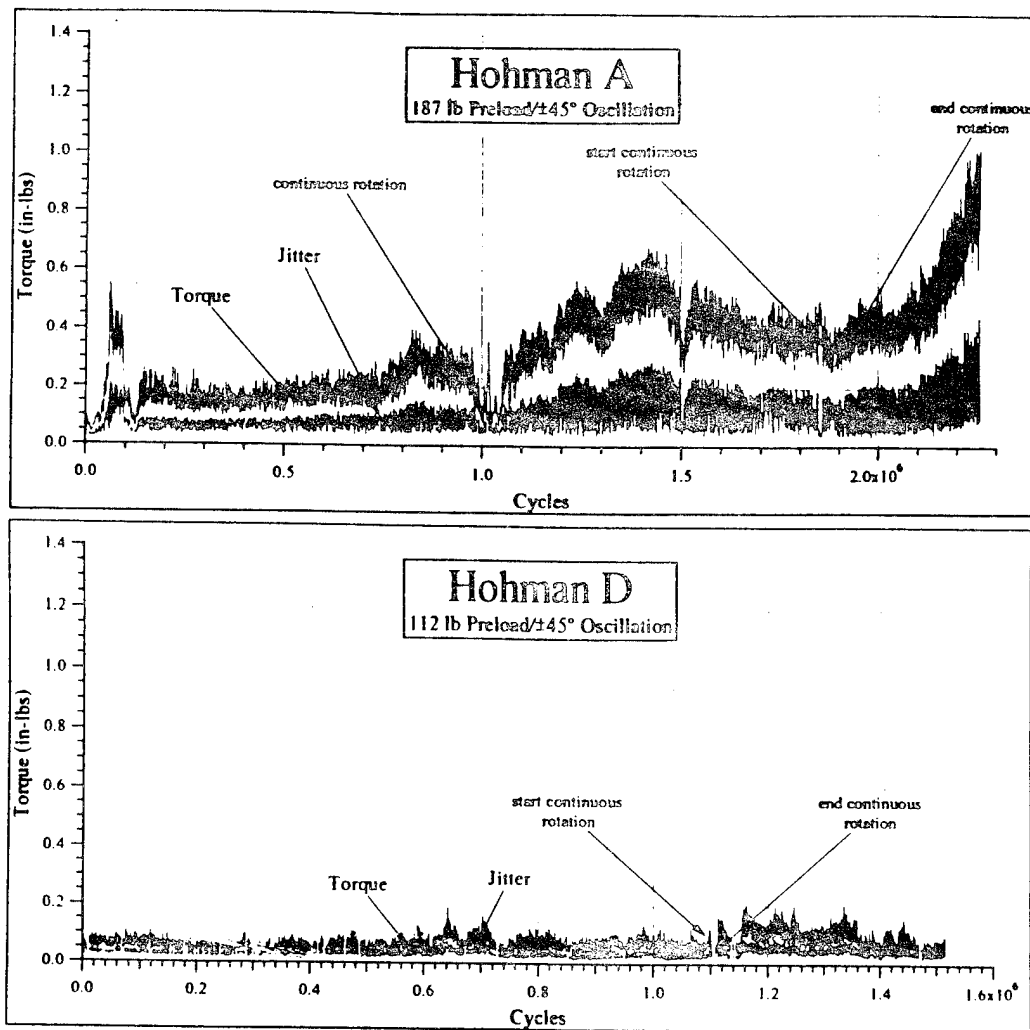**Fig. 5-6 Thrust bearing load results with Aerospace films**

**Fig. 5-7 Thrust bearing load results with Hohman films**

### 5.1.4 Thrust Bearing Results

Thrust bearing tests conducted early in Phase II set the basis for selecting ion-sputtered $MoS_2$ film lubrication over ion-platted lead or diamond-like film lubrication. Fig. 5-8 summarizes the results for fourteen different solid film lubricants. These included Hohman $MoS_2$ films cosputtered with metal (3 & 7% Au, 3&9% Ni) and with 35% $Sb_2O_3$, those from NCT (RF Magnetron) and those from Aerospace (RF AT). Also ion-plated Pb and diamond-like carbon films were tested, as were $MoS_2$ films coated over sputtered ceramic underlayers of either $TiB_2$ or TiC. Some representative "good and bad" torque signature traces are shown in the attached Fig. 5-9. The NCT magnetron film and Hohman $Sb_2O_3$ film and +7% Au films gave consistently low torque for many stop/start cycles. Some of the thin films such as the "diamond-like" coating and those that were post laser treated showed torque deterioration almost immediately. The TiC and $TiB_2$ sputtered under-coated races with $MoS_2$+3% Au also started to fail almost immediately. Perhaps these ceramic coatings were too thin to support the load.

The 7% Au film had surprisingly long relative life, but it was significantly thicker (2.1 μm) than all of the other films. In general, life was found to increase with the thicker films. The Hohman $Sb_2O_3$ film was the third longest lived film but it's measured thickness was only 0.6 μm compared with the NCT film of 1.7 μm. Normalizing these films on the basis of thickness, the $Sb_2O_3$ film provided the most life (see Fig. 5-10).
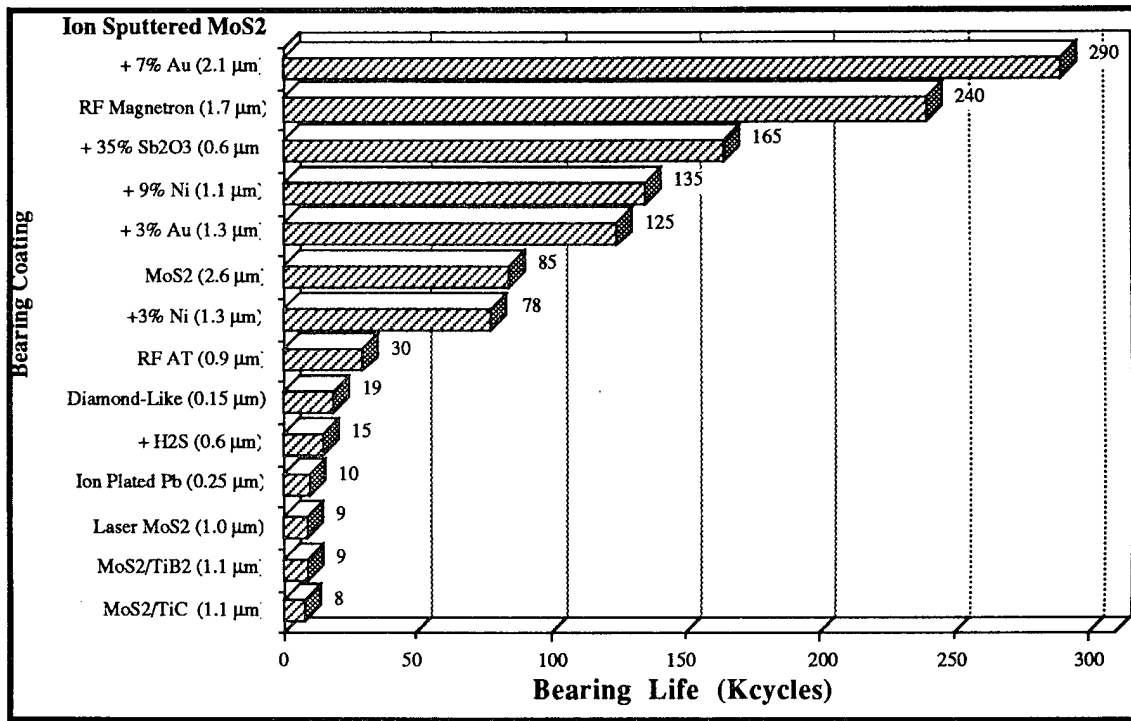
- 42 -

**Fig. 5-8** Thrust bearing life summary from early tests. Failure criteria was 0.3 in-lbs of torque.
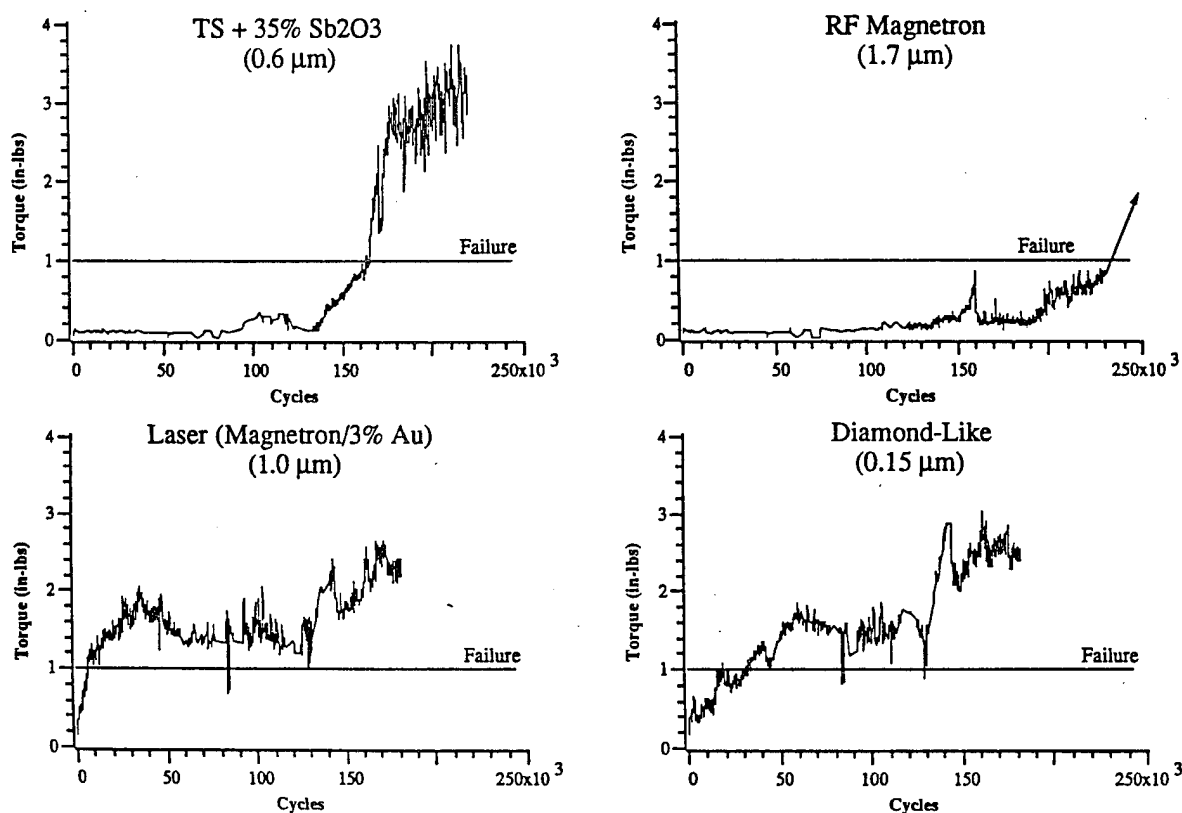


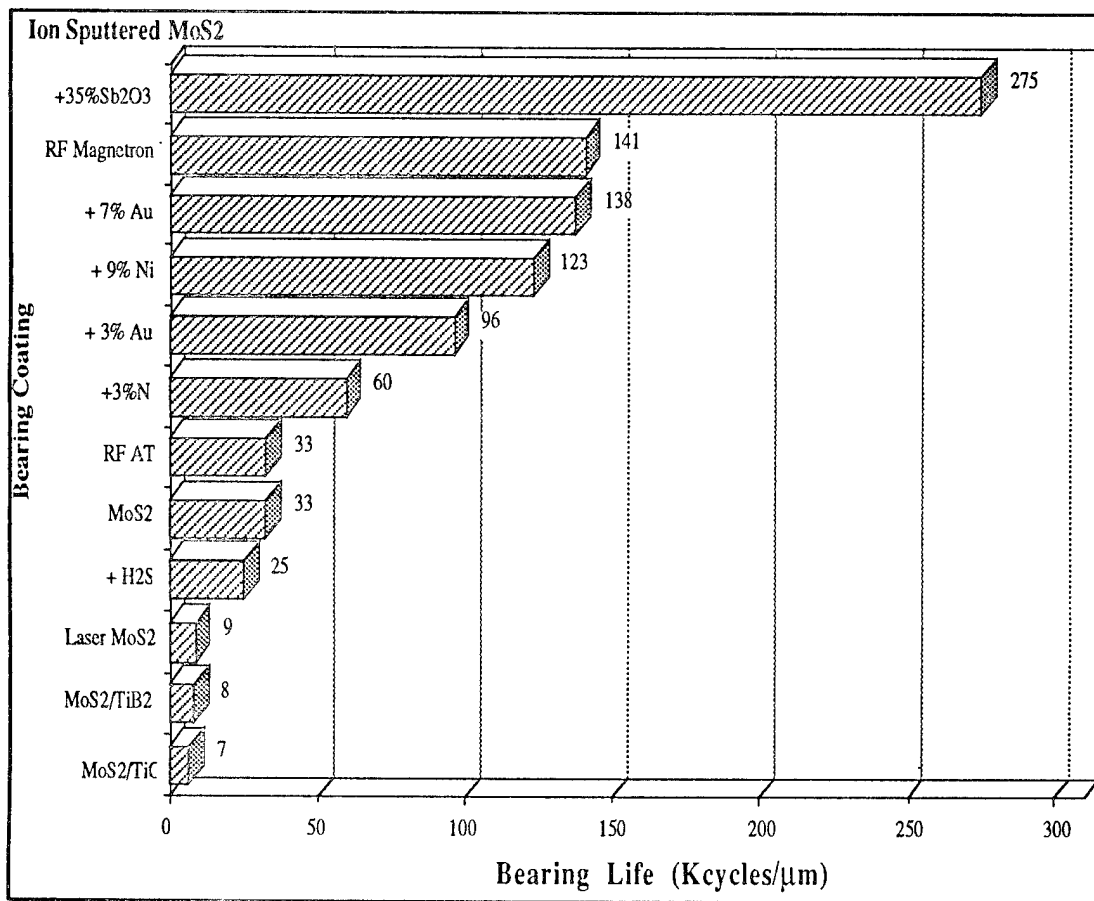**Fig. 5-9** Examples of good and bad thrust bearing torque histories.

Fig. 5-10   Normalized thrust bearing life

## 5.2 105-SIZE BEARING TESTS

Screening tests were performed on 105-size ($\approx$ 2 inch OD) precision bearings in order to determine the best $MoS_2$ film - retainer & ball material combination for later testing in more-expensive, flight-like gimbal bearings. Precision 105-size, angular contact ball bearings were selected for the screening test bearing for several reasons. The thrust bearings tested in Phase I were convenient and easy to inspect, but had poor surface finish, geometrical inaccuracies and a 90 degree contact angle which produced excessive spin microslip. These factors lead to short film lives and high ball separator wear.  The 105-size bearings, were geometrically accurate (ABEC class 7) and had an excellent surface finish (honed). Their internal geometry, relative size and quality were consistent with bearings that could be used on a small space gimbal, such as  an antenna or a scanner. In addition, the selected bearings had separable inner races for ease of disassembly. Also the bearings were mass produced in large quantities for commercial grinding spindles, making them both affordable and available.

The 105-size bearing torque/life screening tests were planned to satisfy the following objectives:

(1)  High fidelity evaluation of the optimum film, retainer material and ball combination for $MoS_2$ film coating the flight-quality gimbal bearings to be parametrically and life tested later in Phase II.

- 44 -

(2) Assessment of film producer's ability to consistently coat small, bearing races and balls, as well as our ability to non-destructively identify good sputtering batches from bad ones.

(3) Head-to-head comparison of the best $MoS_2$ film lubricated bearings against those lubricated with conventional and advanced oils and greases.

(4) Characterization of bearing performance (torque signature, PSD's and preload) degradation with time, particularly beginning of life versus end-of-life behavior.

(5) Generation of test data to validate the bearing wear model and provide data for the gimbal/bearing disturbance simulation model.

### 5.2.1 Bearing Test Rigs

Four computer controlled, bell jar, bearing test rigs were used for the life tests (Fig. 5-11). Turbo-molecular pumps provide clean vacuum levels from $10^{-6}$ to $10^{-7}$ Torr. (see Section 5.4 for Residual Gas Analysis of pumping system). Bearing torque and torque ripple were continuously monitored. A computer was used to drive the test stand motors over a simulated composite gimbal scan cycle and to record torque signature data on disk for later analysis. Three of these bell jar testers were first used to test the 105-size bearings and then later reconfigured to test the larger, gimbal bearings.
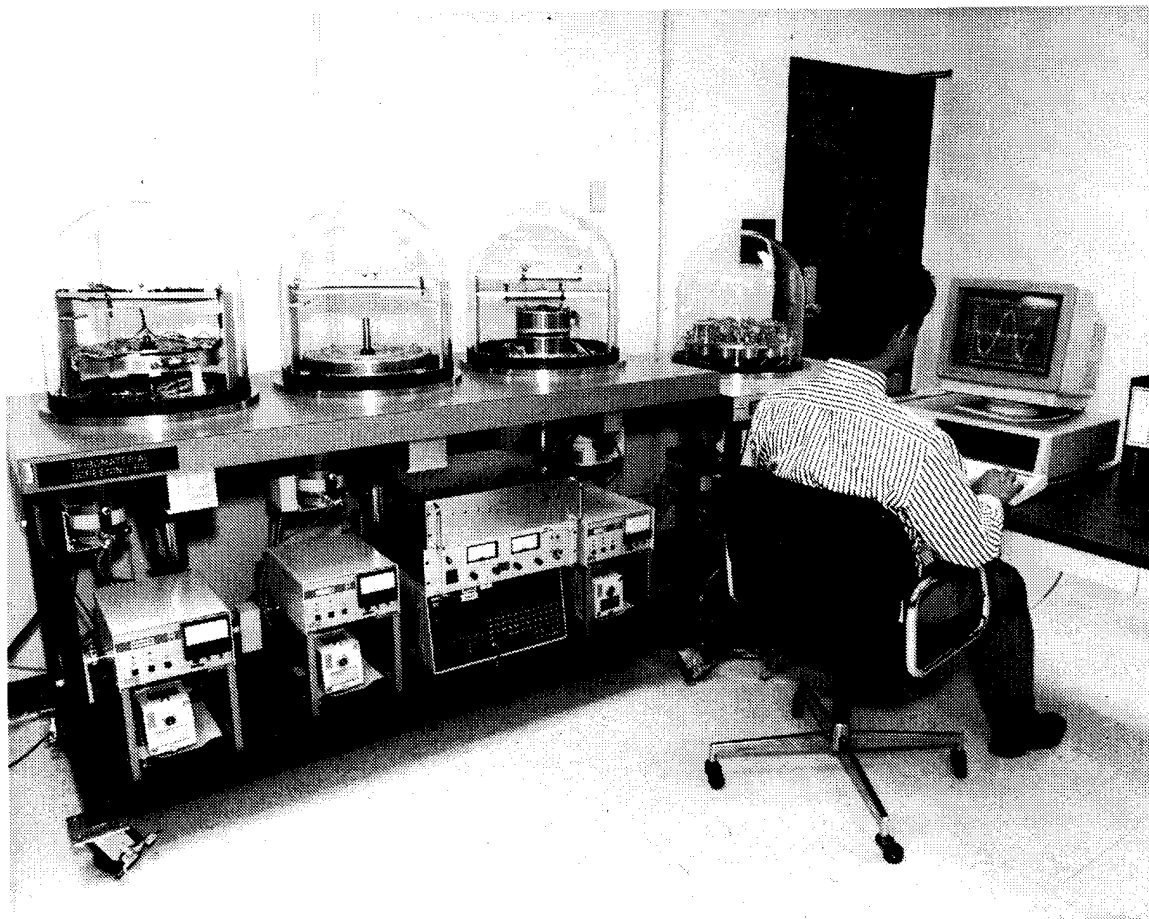


**Fig. 5-11   Overall view of bearing life test rigs showing turbo-pumps and computer controller.**

Twelve pairs of hard-preloaded (rigidly clamped), 105-size ball bearings are circumferentially spaced inside each vacuum bell jar tester (Fig. 5-12). The bearings are fitted into individual bearing cartridges. Each cartridge is grounded to the base plate through a strain gage flexure system which measures the reaction torque acting on the bearing pair. A central drive motor system drives a large collector gear through a rotary, ferrofluidic vacuum feedthrough. The collector gear meshes with gear pinions fixed to the bearing cartridge spindle and thus provide inner race rotation (Fig. 5- 13).

## 5.2.2 105-Size Test Bearings

Sixty, hard-preloaded, duplex pairs of 105 size (25 mm x 47 mm), AFBMA class 7 ball bearings were procured for the screening tests. The bearings contained 12 balls, 0.25 inch in diameter, grade 5 quality. Raceway transverse curvatures are nominally 54%. The bearing races were manufactured from CVM AISI 52100 bearing steel, hardness > 60 Rc, and were honed to a maximum transverse surface roughness of 2 $\mu$ in AA. Ball roughness was 0.6 $\mu$ in AA or better. Ceramic (silicon nitride) grade 5 balls were substituted for the steel ones in two of the bearing pairs. Ball roughness was 0.2 $\mu$ in AA or better.

The standard phenolic retainers of the 105 bearings were replaced with either Vespel™ (polyimide + 15% $MoS_2$), Duroid™ (60% PTFE / 40% chopped fiber glass with $MoS_2$ filler), and Salox™ (60% PTFE / 40% bronze composite). In one case, the Vespel retainer was sputter-coated with an approximate 1 $\mu$m thick, multi-layered $MoS_2$ film. The number of balls was reduced from 13 to 12 to improve retainer web strength and the retainer pocket and land clearances were enlarged to reduce the potential for a "blocking" type of torque anomaly. The photograph in Fig. 5-14 shows the separable inner race of the 105 test bearing and custom designed ball retainer.
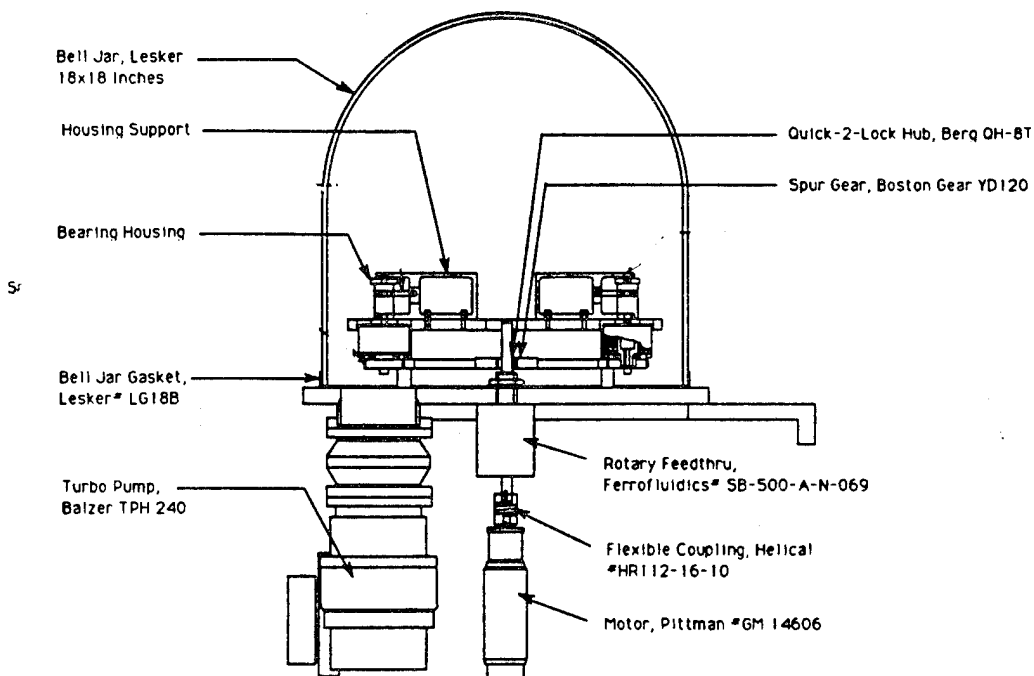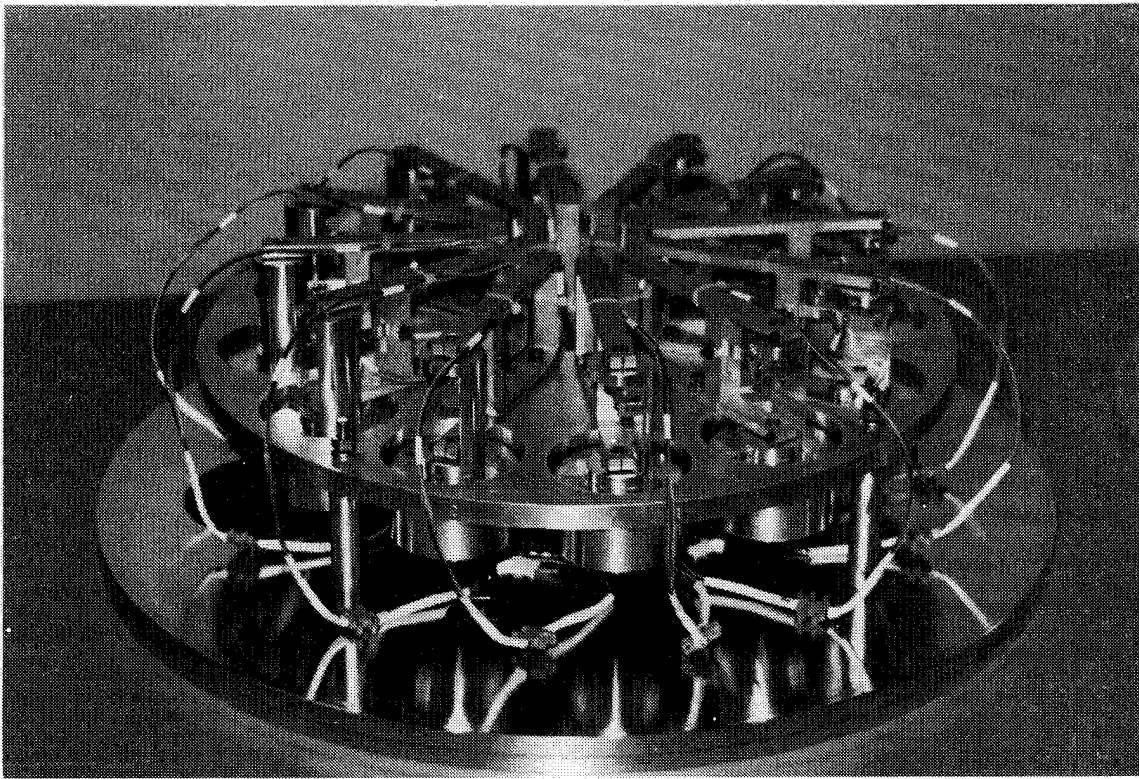


**Fig. 5-12 Carousel bearing tester schematic**

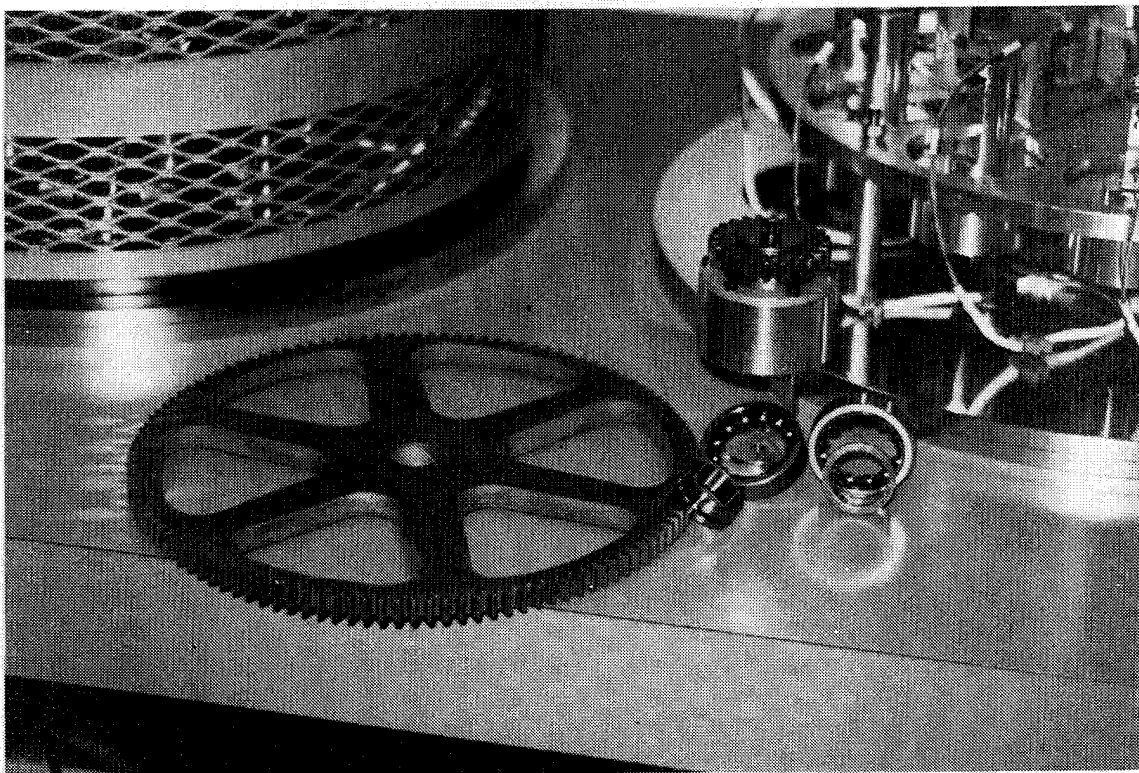(a) Bearing test spindles with strain gage torque arms
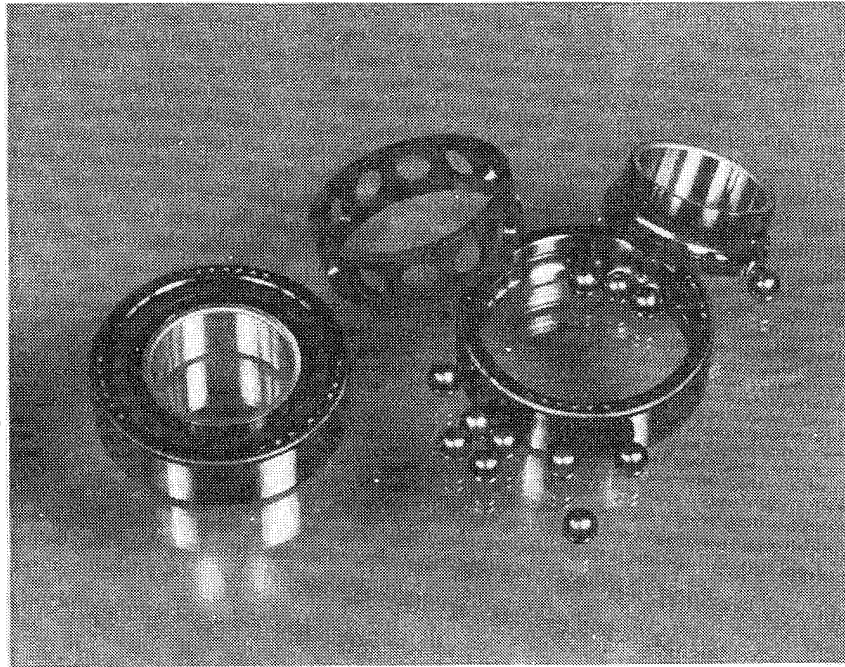


Fig. 5-13 Close up view of Carousel tester

**Fig. 5-14   Photo of 105 test bearing with custom retainer.**

### 5.2.3 Solid Lubricant Films.

Based on the results of thrust bearing screening tests (see Section 5.1.4), the three best $MoS_2$ films were ion-sputtered on the test bearing components by the three different vendors. Each used a different ion deposition process. These included Hohman's DC triode, NCT's radio frequency magnetron and Ovonic's multi-layer radio frequency magnetron sputtered MoS2 films. Hohman's DC triode sputtering (DCS) process used a 65% $MoS_2$ - 35% $Sb_2O_3$ target material combined with a oscillating deposition current to produce dense films. The NCT radio frequency magnetron sputtering (RFMS) process enabled high rate and density deposition with a pure $MoS_2$ target. The multi-layer sputtering (MLS) process by Ovonics incorporated two radio frequency magnetron targets which alternately deposited 10 nm layers of $MoS_2$ followed by 1 nm layers of nickel to produce dense films for 10% Ni films or 4.5 nm layers of gold-paladium for 45% Au-Pd films. Section 7.0 presents a more complete description of the films and their characteristics.

Actual film thickness was measured on the inner and outer race shoulders by indenting the film and viewing the fractured film in a SEM at a high angle. Although a nominal film thickness of 1 μm was requested, the Hohman films measured 1.8 μm in thickness on the inner race, while ranging from 0.9 to 0.2 μm in thickness on the outer race. The NCT film was 0.4 μm thick on all parts. Only the Ovonic film was consistently 1 μm thick, as requested.

Witness plates that accompanied bearing components during film deposition were characterized by x-ray diffraction (XRD), x-ray photoelectron spectroscopy (XPS) and

- 48 -

microhardness. XRD analysis indicated all of the films had either no observable texture or weak basal plane film orientations. Elemental compositions of the films (as determined by XPS) indicated that all three films had sulfur to molybdenum atom ratios that were much less than two. Moreover, the three films contained substantial amounts of carbon and oxygen, up to 20% in some cases. An ultra-microhardness test of the films using a 250 mg indention load indicated a 150 Vickers hardness number for both the DCS and RFMS films. The MLS films were substantially harder at 570 Vickers hardness number.

### 5.2.4 Test Bearing Summary

Table 5-15 summarizes the 29 pairs (20 different combinations) of $MoS_2$ films, retainer and ball materials tested, together with preload and maximum Hertz stress. All but one of the bearings had $MoS_2$ sputtered races. Six of the bearing pairs had both balls and races coated. In general, each of the retainer/ball combinations were tested once with each of the three different film types. However, the Ovonic's MLS film with Br-PTFE (Salox) retainers and steel balls was tested on three bearings. Also, duplicate tests were conducted with PTFE (Duroid) retainers with all three film types and the Ovonics high gold film was also tested twice. One comparative test was conducted with bearings having uncoated races with Br-PTFE retainers. Also the MLS film was tested at high preload (52 lbs).

### 5.2.5 Preload

As explained in section 4.1.2, bearings were originally sized to provide adequate bending stiffness and launch load capability for the SVS satellite sensor gimbals. A trade was made between bearing size, preload, stiffness and torque. Similar analysis was performed when the SVS gimbals were superseded by those for Brilliant Eyes. In both cases, necessary preloads resulted in on-orbit contact stress levels on the order of 160 to 180 ksi maximum Hertz stress (equivalent to 107 to 123 ksi mean Hertz stress) with due consideration of operating temperatures and temperature gradients. These stress levels were also consistent with previous LMSC flight gimbal bearings. In keeping with the philosophy that the advanced tribomaterials should be tested at stress levels consistent with prior practice, preloads for the Phase II test bearings were selected to provide equivalent contact stress levels. Secondly, the SVS, and later, B.E. gimbal design required high structural frequencies which necessitate the use of hard-preloaded ( i.e., clamped without springs) bearings. This design approach was also adopted in the Phase II tests.

In theory, coating a 1 μm $MoS_2$ film* on the inner and outer races of the 105-size bearings having a manufactured preload of 17 lb would produce an inner race mean Hertz stress of 108 ksi (Fig. 5-16) However, it was necessary to measure actual bearing preload because of the variability of $MoS_2$ film thicknesses, ball and race treatments. This was also useful to determine the drop in preload due to $MoS_2$ film wear at end of life. Maintenance of preload is important to ensure that bearing stiffness, hence critical structural frequencies are not significantly degraded. A preload fixture was used to determine the "knee" in the bearing load/deflection curve (Fig. 5-17). In principle, the knee of the curve corresponds to the preload at the point where the factory ground-in race gap bottoms out. Shims provide some limited adjustment in preload for differences in $MoS_2$ film coating thicknesses. Some

---

* This effectively increased the internal preload to ≈ 30 lbs. The 1 μm film thickness was selected because it was the nominal thickness used for the TWIG pin-on-disk tests. For the same reason, it also was used for the LMSC thrust bearing tests. However, later in the test program, the 1 μm film was believed too thick for precision ball bearings, being more susceptible to fracture and delamination. Stress levels of the liquid lubricated bearings, which used a stock 30 lb preload were comparable to the dry film bearings.

**Table 5.15  Summary of 105-size MoS$_2$ test bearing combinations**

| Post | †Film | Cage | Ball | Preload Start lbs | Initial Mean Hertz Strs KSI | | |
|------|-------|------|------|------|------|------|------|
| **Ovonics + 10% Ni Films** | | | | | | preload | stress |
| 4.6 | MLS | BrPTFE | Bare | 31 | 109 | Average | |
| 4.11 | MLS | BrPTFE | Bare | 40 | 119 | 34 | 113 |
| 4.9 | MLS | BrPTFE | Bare | 32 | 111 | one-sigma | |
| 4.2 | MLS | PTFE | Bare | 41 | 120 | 4.1 | 4 |
| 2.2 | MLS | PTFE | Bare | 31 | 110 | | |
| 2.6 | MLS | PTFE | MoS | 31 | 109 | | |
| 2.4 | MLS | PTFE | SiN | 32 | 127 | | |
| 2.8 | MLS | PI | Bare | 38 | 117 | | |
| 2.12 | MLS | PI | MoS | 30 | 108 | | |
| 3.11 | MLS | PI+MoS | Bare | 34 | 113 | | |
| **52 lb Preload** | | | | | | | |
| 4.1 | MLS | BrPTFE | Bare | 52 | 130 | | |
| **Ovonics + 45% Au-Pd Films** | | | | | | preload | stress |
| 4.3a | MLS+Au | BrPTFE | Bare | 33 | 112 | Average | |
| 4.12 | MLS+Au | BrPTFE | Bare | 29 | 107 | 26 | 104 |
| **NCT Films** | | | | | | preload | stress |
| 4.8 | RFMS | BrPTFE | Bare | 25 | 102 | Average | |
| 4.1 | RFMS | PTFE | Bare | 27 | 105 | 29 | 107 |
| 2.1 | RFMS | PTFE | Bare | 19 | 93 | one-sigma | |
| 2.5 | RFMS | PTFE | MoS | 26 | 103 | 3.3 | 4 |
| 2.3 | RFMS | PTFE | SiN | 28 | 122 | | |
| 2.7 | RFMS | PI | Bare | 22 | 98 | | |
| 2.11 | RFMS | PI | MoS | 28 | 106 | | |
| **Hohman + 35% Sb2O3 Films** | | | | | | preload | stress |
| 4.5 | DCS | BrPTFE | Bare | 37 | 116 | Average | |
| 4.4 | DCS | PTFE | Bare | 37 | 116 | 36 | 115 |
| 4.3 | DCS | PTFE | Bare | 34 | 113 | one-sigma | |
| 3.5 | DCS | PTFE | MoS | 36 | 115 | 3.8 | 4 |
| 3.4 | DCS | PTFE | SiN | 29 | 123 | | |
| 3.6 | DCS | PI | Bare | 39 | 118 | | |
| 3.9 | DCS | PI | MoS | 41 | 120 | **All Combinations** | |
| **No MoS2 Film** | | | | | | preload | stress |
| 4.7 | none | BrPTFE | Bare | 32 | 111 | Average | |
| †Film: MLS=Multi-layer, RFMS= RF magnetron, DCS=Direct Current | | | | | | 31 | 110 |

rounding of the "knee" was observed for MoS$_2$ film coated bearings due to coating compliance and the balls being seated in a staggered fashion rather than all at once. This required that the preload be interpreted from initial and final slope intersections.

As shown in Table 5.15, preload was reasonably uniform ($\approx$10% one-sigma) from group to group although the bearings with the thinner NCT films, averaging 0.3 $\mu$m in thickness, were about 20% lower in preload. Despite some possible interpretation inaccuracies, preload could be set within a range of 31 lb $\pm$5 lb (one-sigma) for the 27 pairs of solid-lubricated bearings and 30 lb $\pm$4.3 lb (one-sigma) for the 14 pairs of liquid-lubricated bearings (Table 5.48).

```
                        PROG   *****BEARING*****
        CALC BRG LOADS;STIFFNESS;DEFLECT & TORQUE FOR ANG CONTACT BALL BEARINGS
            MOUNTED IN HOLLOW FLEXIBLE STRUCTURE WITH THERMAL GRADIENTS
                  $$$$ VERSION 31 JAN 1989  BY STU LOEWENTHAL $$$$$$

 TRIBO 105 Bearing + 1 um Coating on I/R & O/R              [    OUTPUT    ]

                                         ##########DATA FOR MANUFACTURED FITS AT ROOM TEMP ##########

 BETA0=FREE MANUF CONT ANG 15.2             ITER= 20              79.7                    66.9
 BETA1=LOADED CONT ANG 0
THRUST=APPLIED THRUST OR PRELOAD  17       >>>>>>>>>>>>>>>>>>>>> CONTACT ANGLES,DEGREES<<<<<<<<<<<<<<<<<<<<
 TBULK=O/R TEMP 70                          FREE= 15.2           15.200        LOADED= 16.171
 DELT=TEMP I/R -TEMP O/R 0                  PRELOAD= 17.0        0.00035       DIA CLEAR= 1.40E-03
 TAMB=AMBIENT TEMP AT MANUFAC 70                        INNER RACE     OUTER RACE
 MU=BALL CONT SLIDING FRIC COEF 0.22                    ........       ........
 GDRAG=GREASE DRAG PER ROW 0
 SPEED= 'SPEED IN DEGS/SEC 0.5              TEMP;°F= 70           70
 VISC='KINEM VISC cS @ OPER TEMP 0          MANUF INTERF;IN= 0.00000   0.00000
         ************BRG  GEOM***********   DIAM DEFLECT;IN= 0.00000   0.00000
 NROW=NO. OF BRG ROWS 2                     Mean HERTZ STRESS;KSI= 89.5    76.7
 NBALL=NO OF BALLS/ROW 12                   SEMI MAJ ELLIPSE;IN= 0.01035  0.00999
 D= BALL DIA 0.25                           ELLIPSE RATIO;IN= 5.93        4.72
 DB= BORE DIA 0.9843                       ***AXIAL STIFF(BRG PAIR);LBS/IN= 161,548
 DOD= BRG OD 1.8504                        +++ BRG TORQ @ SLIDING FRIC COEF= 0.22   0.00      PER ROW
 L= BRG ROW WIDTH 0.4724                   $$ BRG PAIR TORQ ;IN-LBS (OZ-IN)= 0.04  (    0.63
 S=AX STRADDLE BETW BALL ROWS 0.47         $$ BRG PAIR TORQ ;IN-LBS (OZ-IN)= 0.01  (    0.15
 CONFIG=FACE TO FACE,BACK TO BACK B        VISCOUS(SPEED) TORQ COMP;IN-LBS= 0.00   (    0.00   )
 FI= I/R CONFORMITY 0.54
 FO= O/R CONFORMITY 0.54
 SHIR%=%;(I/R SHOULDER HT/D) 20
 SHOR%=%;(O/R SHOULDER HT/D) 20
 DS= SHAFT BORE DIA 0.1                    **********OUTPUT FOR THERMAL CASE WITH RINGS CLAMPED**********
 DH= HOUSING OD 2.5
         ************FITS***************    ITER= 19              79.7                    66.9
 I/R & O/R CLAMPING FORCE;LBS 500    500
 IIR=MANUF SHAFT TO I/R PRESS FIT 0        >>>>>>>>>>>>>>>>>>>>> CONTACT ANGLES,DEGREES<<<<<<<<<<<<<<<<<<<<
 IOR=MANUF O/R TO HOUSING PRESS FIT 0       FREE= 15.2           14.678        LOADED= 16.136
 IIRINST=INSTALLED SHAFT TO I/R FIT 0.00016 PRELOAD= 30.1       5.28E-04      DIA CLEAR= 1.31E-03
 IORINST=INSTALLED O/R TO HSG FIT -0.00005              INNER RACE     OUTER RACE
         **********MAT'L PROPERTIES;***********          ........       ........
 NUS=POISSON'S RATIO SHAFT 0.29             TEMP;°F= 70           70
 NUB= POISSON'S RATIO BEARING 0.25          MANUF INTERF;IN= 0         0
 NUH=POISSON'S RATIO HOUSING 0.29           OPERAT INTERF@R.T.;IN= 0.00016   -0.00005
 ES=MODULUS SHAFT 2.80E+07                  OPERT INTERF@TEMP;IN= 0.00016    -0.00005
 EB=MODULUS BEARING 2.90E+07                DIAM DEFLECT;IN= 0.00000   0.00001
 EH=MODULUS HOUSING 2.80E+07                Mean HERTZ STRESS;KSI= 108.4     92.9
 CTES=CTE SHAFT 6.00E-06                    SEMI MAJ ELLIPSE;IN= 1.25E-02    1.21E-02
 CTEB=CTE BEARING 5.70E-06                  ELLIPSE RATIO;IN= 5.93        4.72
 CTEH=CTE HOUSING 6.00E-06                 ***AXIAL STIFF(BRG PAIR);LBS/IN= 192,943
                                           +++ BRG TORQ @ SLIDING FRIC COEF= 0.22   0        PER ROW
 SDI=I/R SHOULDER DIA) 1.26735             $$ BRG PAIR TORQ ;IN-LBS (OZ-IN)= 0.09  (    1.41   ) O/R CONTROL
 SDO=O/R SHOULDER DIA) 1.56735             $$ BRG PAIR TORQ ;IN-LBS (OZ-IN)= 0.02  (    0.36
                                           VISCOUS(SPEED) TORQ COMP;IN-LBS= 0.00   (    0.00   )

                                           MAX SHOULD ANGL;DEG= 51.0      51.0
                                           CONT EDGE ANGL;DEG= 21.5       21.3
```
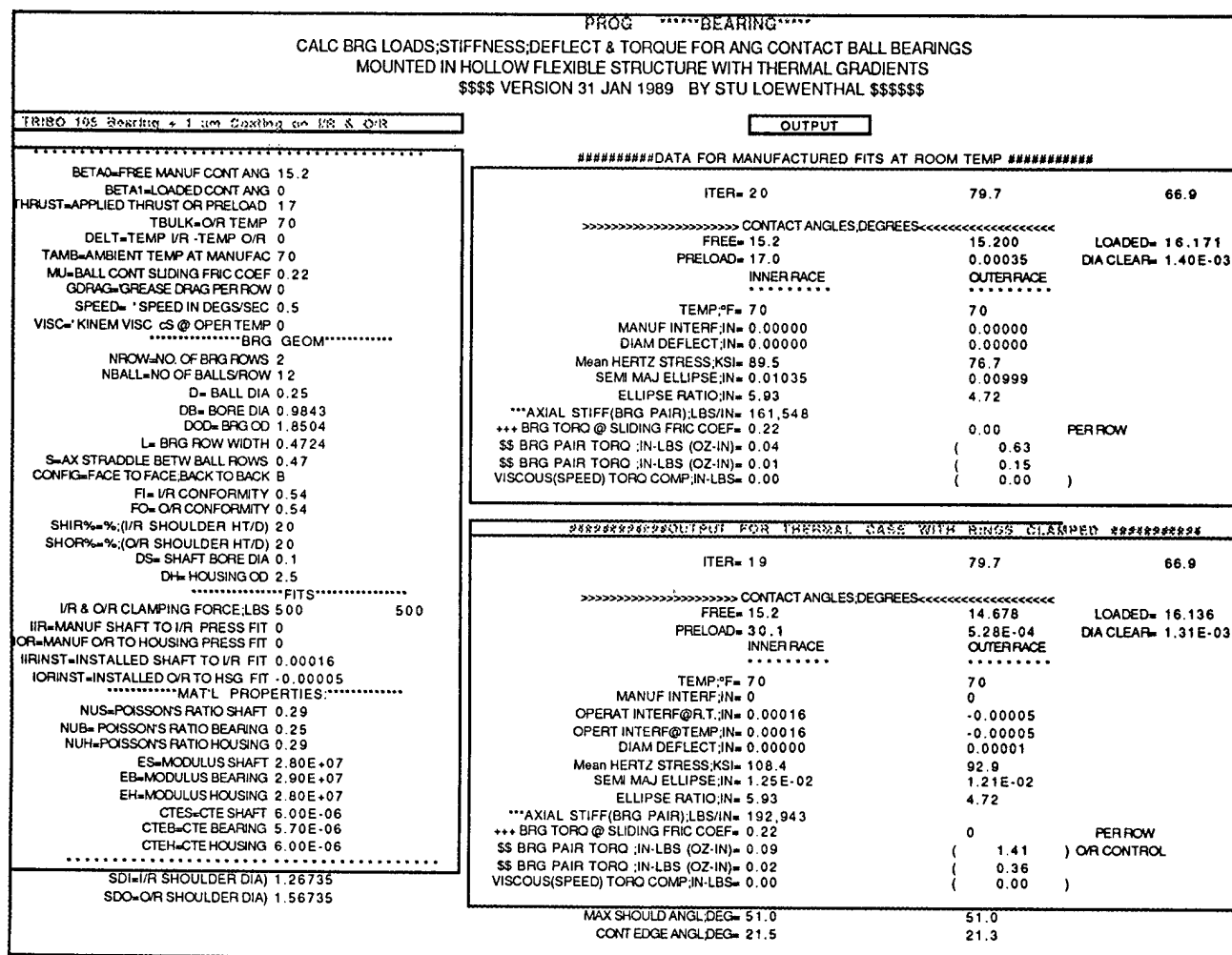
Fig. 5-16    Predicted 108 KSI inner race mean Hertz stress for 105-size test bearing sputtered with 1 $\mu$m film on inner and outer races
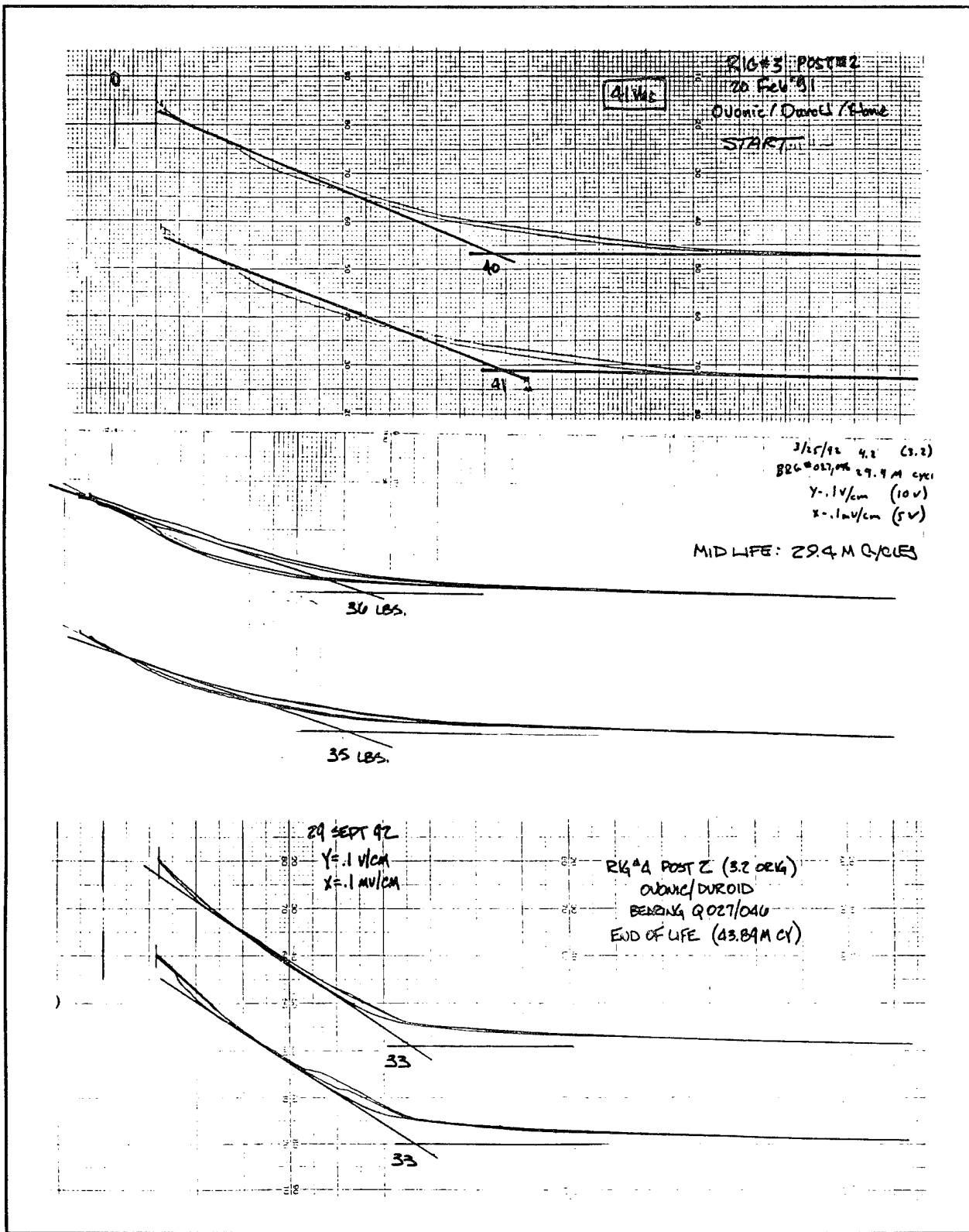
**Fig. 5-17** Examples of start, mid life (29M cycles) and end of life (44M cycles) preload traces for MoS2 film bearing ( #4.2, Ovonic Duroid)

## 5.2.6 Bearing Preparation.

The 105 test bearings with $MoS_2$ film coated races were assembled with their appropriate retainer and balls (bare, $MoS_2$ film coated or uncoated $Si_3N_4$) in a clean room (better than class 10,000). Shims were used to set preload as closely as possible to nominal levels. The liquid lubricated bearings were assembled in the same fashion, except that the bearing races were grease plated in a freon bath with the test lubricant (approximately 15% by weight) and then vacuum dried in an oven for several hours to evaporate any remaining freon. Before and after lubricant weights were recorded.

## 5.3 105-SIZE BEARING TEST RESULTS

### 5.3.1 Torque Histories.

The rms value of peak torque and torque ripple (hash band) of each test bearing was digitally recorded approximately every 2 minutes while the bearings continuously cycled through the prescribed test cycle. Examples of the torque histories for the three types of $MoS_2$ films with Br-PTFE or PTFE retainers and uncoated steel balls appears in Figs. 5-18 and 5-19[#]. These bearings generally exhibited very long lives, no matter which type of film was used. A bearing was considered failed when its peak torque reached a level of 50 N-mm (0.44 in-lb). This arbitrary level, set for comparison purposes, was roughly 3 to 4 times normal peak operating torque levels.

PTFE containing retainers can replenish lost $MoS_2$ film via the ball film transfer mechanism. Occasional, large torque excursions were observed.[##] One bearing pair (post # 4.11), however, showed three momentary torque excursions to about 0.5 in-lb around 1.8 million cycles, before returning to normal levels for the remainder of the test. Long life was also achieved with the single test bearing pair lubricated by only Br-PTFE retainers (no race film) but its torque was higher and more erratic than those used with $MoS_2$ film coated races, Fig. 5-18(d). Furthermore, its loss in preload was the highest ($\approx$ 40%) of all the bearings tested, except one.

---

[#] These torque histories compress a very large number of data points over a span of 30 to 40 million cycles, giving a jagged appearance to the test data. Expanding the data over a shorter interval (see Fig. 5-20), shows that peak torque levels generally fluctuated over time with changes in gimbaling mode. In Fig. 5-20, the bearing torque is lower during the wide ($\pm 80°$) and narrow ($\pm10°$) cycling than during the 360 degree rotations. This is attributed to the build-up of debris at the end of stroke which is rolled-over during continuous rotation. End-of-stroke debris bumps is a problem previously identified with $MoS_2$-lubricated bearings that gimbal [5-3]. Elevated torques generally persisted through the entire 50,000 revolutions before resetting to lower values during the next gimbal cycle.

[##] These variations are likely the result of excess film/cage wear debris trapped between the ball and race. Switching modes of operation from short stroke (no ball track overlap) to large stroke or continuous rotation often increased torque temporarily until any end-of-stroke debris was redistributed. Much less cycle-to-cycle variation would be expected if the bearing operated exclusively in either continuous rotation or over a short stroke, rather than periodically cycling between such modes. The introduction of spring rather than hard preload would also be of benefit.

In contrast to PTFE-containing retainers, the bearings tested with polyimide retainers exhibited relatively short lives (1.6, 4.5 and 1 million cycles), irrespective of film type (Fig. 5-21 a,c,e). This supports the need for a replenishment PTFE transfer film from the retainer for long life [5-4]. Subsequent examination of the bearings with Vespel retainers showed considerable debris (Section 7.4) which evidently contributed to increased preload and torque. Coating the PI retainer with $MoS_2$ film offered no real life improvement (Fig. 5-21g) nor did $MoS_2$ film coating the balls.

Short lives (< 1.2 million cycles) were consistently obtained with balls that were either $MoS_2$ film coated or uncoated balls made from silicon nitride ($Si_3N_4$). This was true for bearings with either Br-PTFE or PTFE ball retainers, no matter which type of $MoS_2$ film (Fig. 5-22 ). *(Note that the torque scale has been increased in Figs 5-21 & -22 because of the higher torque levels)*. Shedding of the poorly adherent $MoS_2$ film on the balls was believed responsible for debris jamming and subsequent torque increase. Indeed, scanning electron microscope (SEM) inspection of untested balls from all three film sources showed clear defects in the films (see Section 7.4.1). The reason for the poor performance of the silicon nitride balls is less clear. The very short lives do not seem completely explainable on the basis of higher contact stress from the ceramic's high modulus. The mean Hertz stresses of some of the long-lived bearings (e.g., posts 4.2, 4.11 and 4.5) were nearly as high as those short-lived bearings having silicon nitride balls (see Table 5.15). Subsequent visual inspection of these bearings showed considerable wear debris which contributes to erratic torque behavior. Perhaps the very smooth surface finish (<0.2 $\mu$ in AA) of the silicon nitride balls inhibited the PTFE transfer process which normal occurs through asperities rubbing off the PTFE retainer.
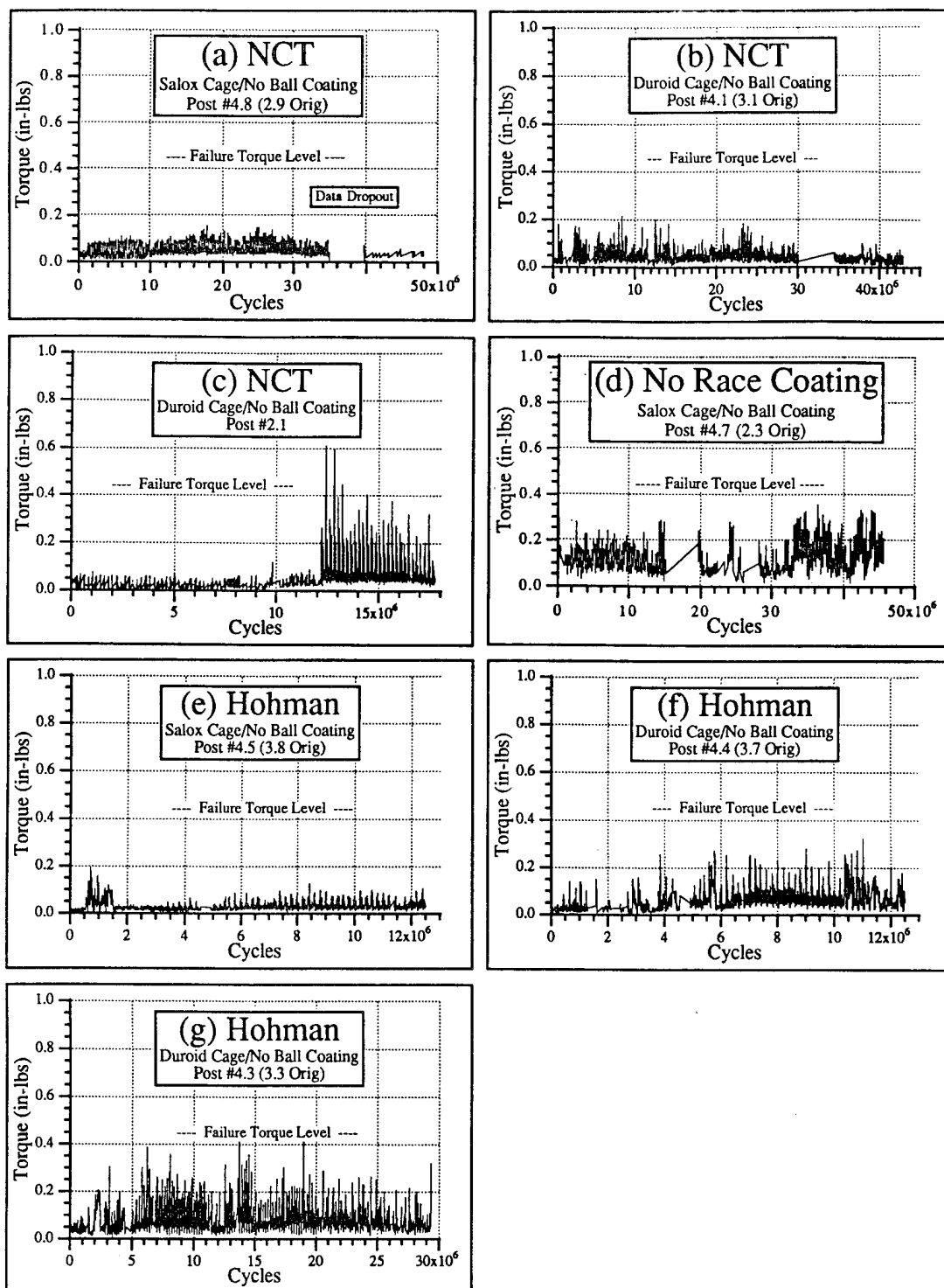
**Fig. 5-18** **Long-lived 105-size bearings with NCT and Hohman films having Br-PTFE and PTFE retainers**
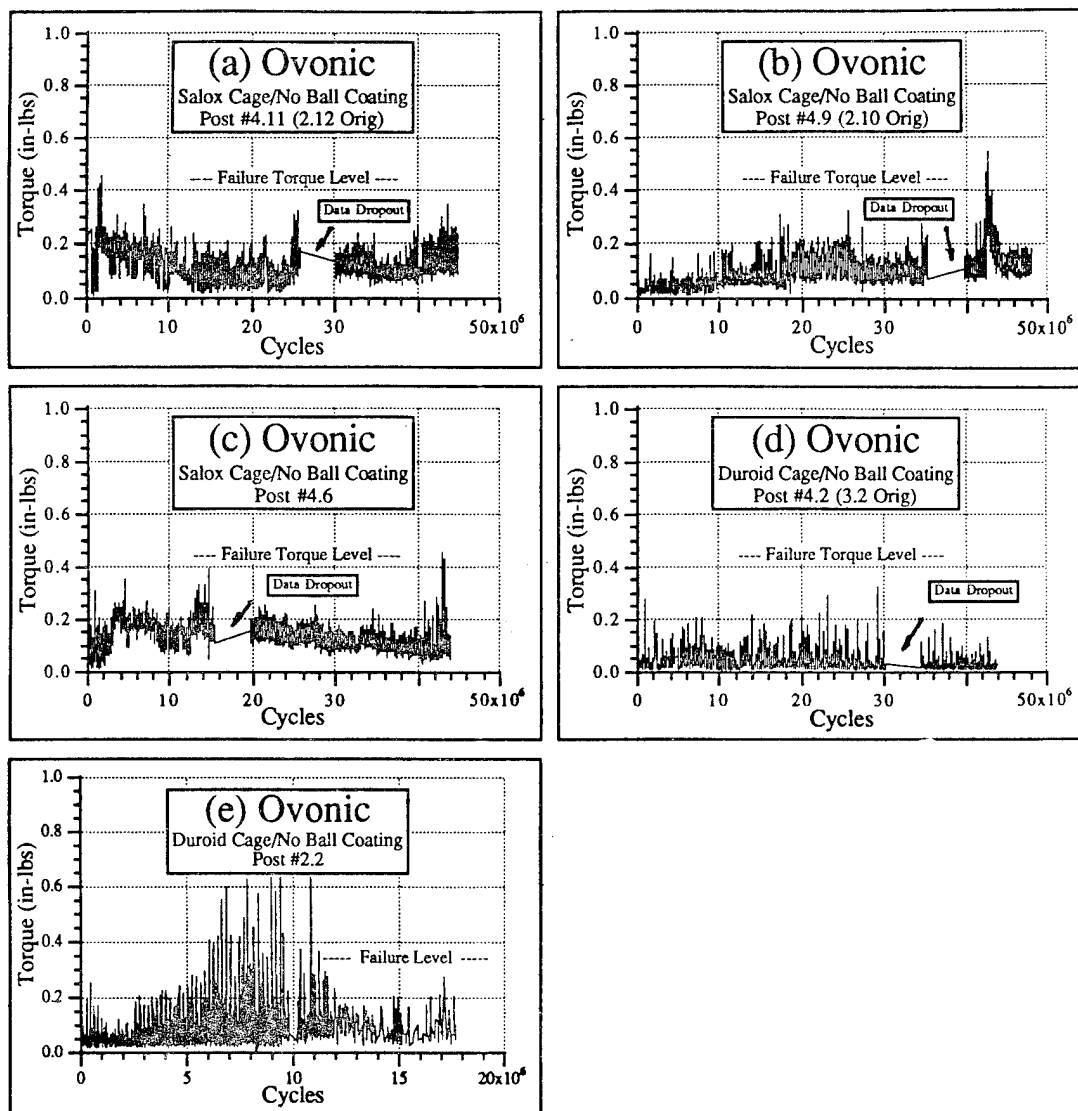
**Fig. 5-19    Long-lived 105-size bearings with Ovonics films having Br-PTFE and PTFE retainers**
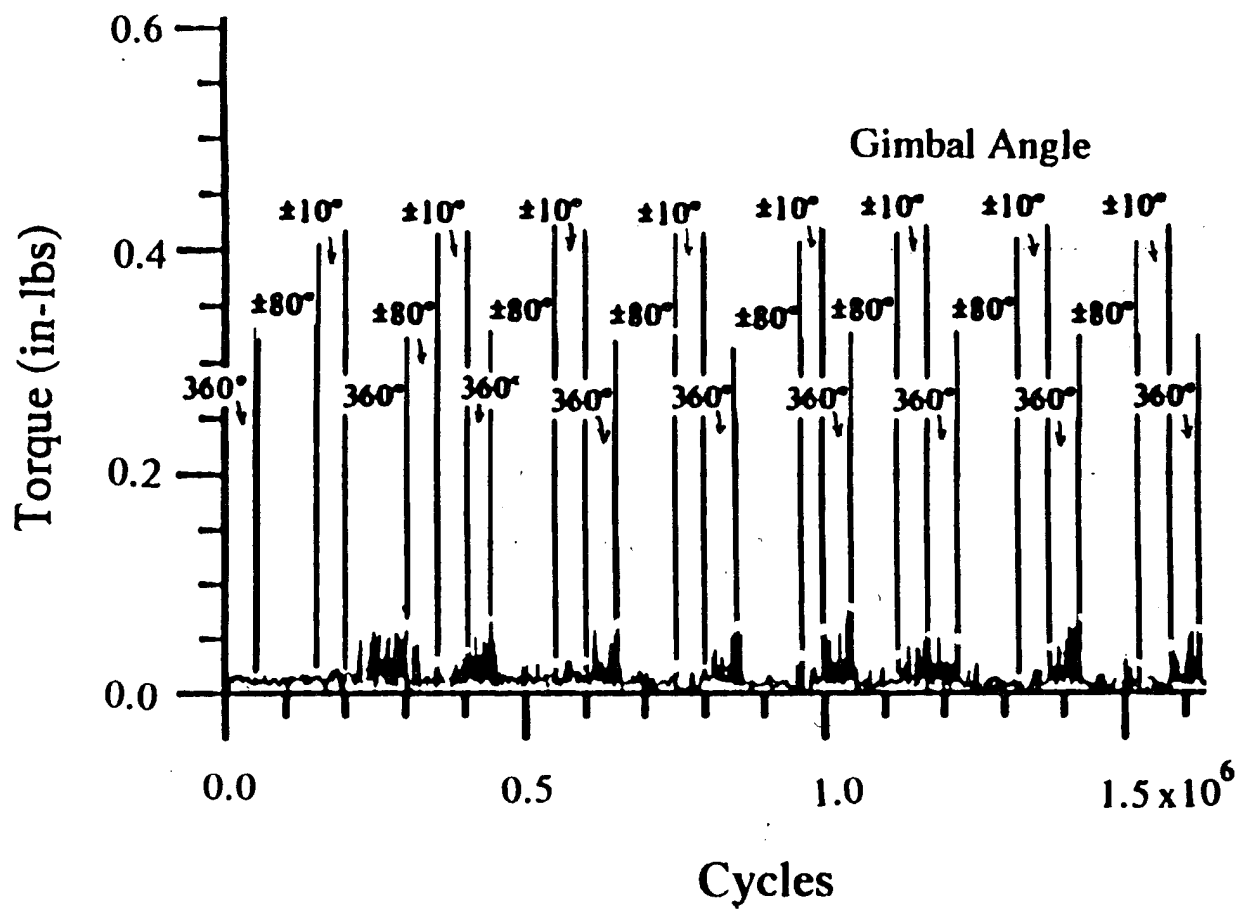
Fig. 5-20   Torque variation with gimbaling mode showing elevated torque
during 360 rotations from end-of-gimbal-stroke debris
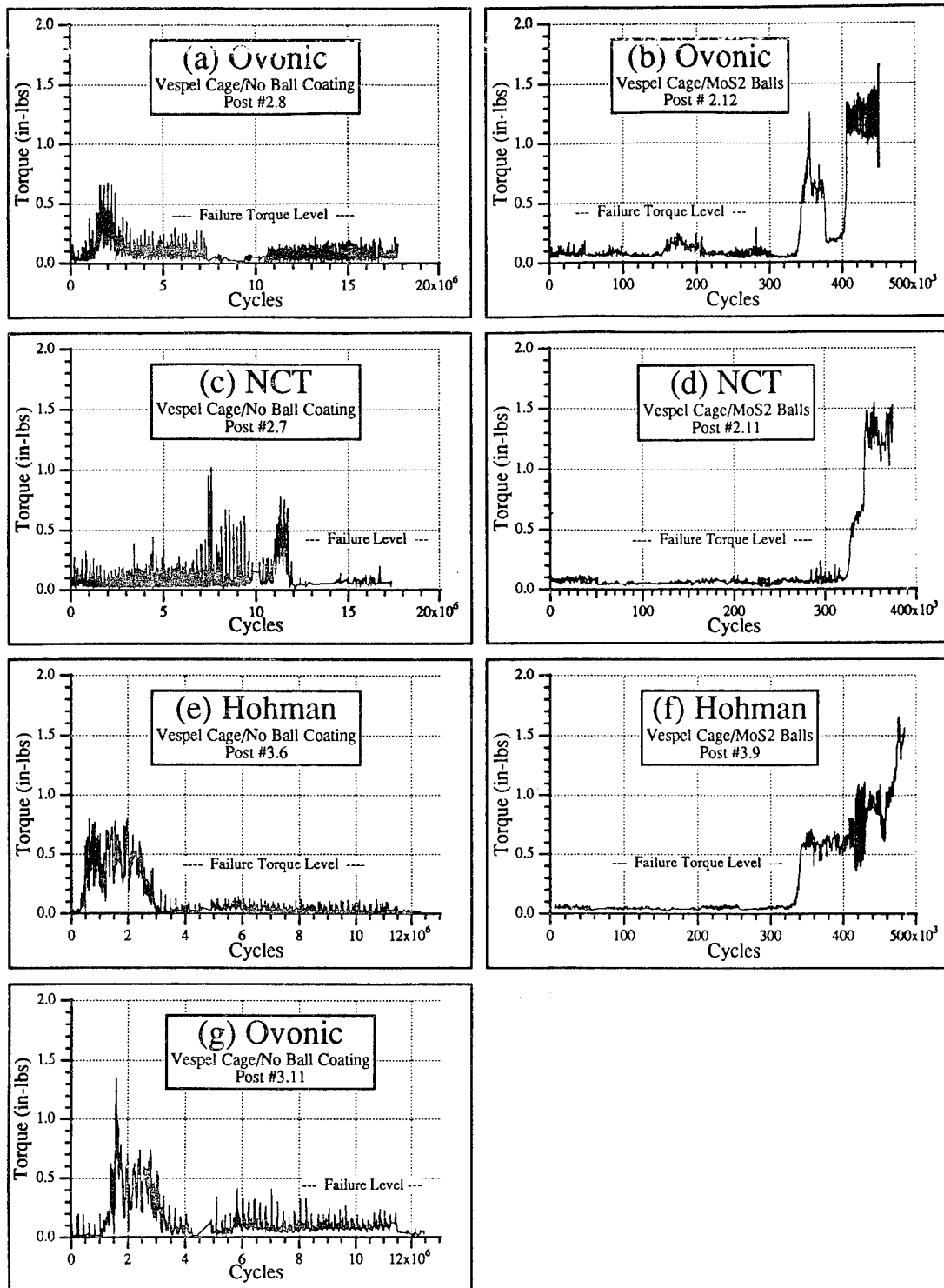
**Fig. 5-21** Short-lived 105-size bearings with polyimide retainers and plain or MoS$_2$ coated balls
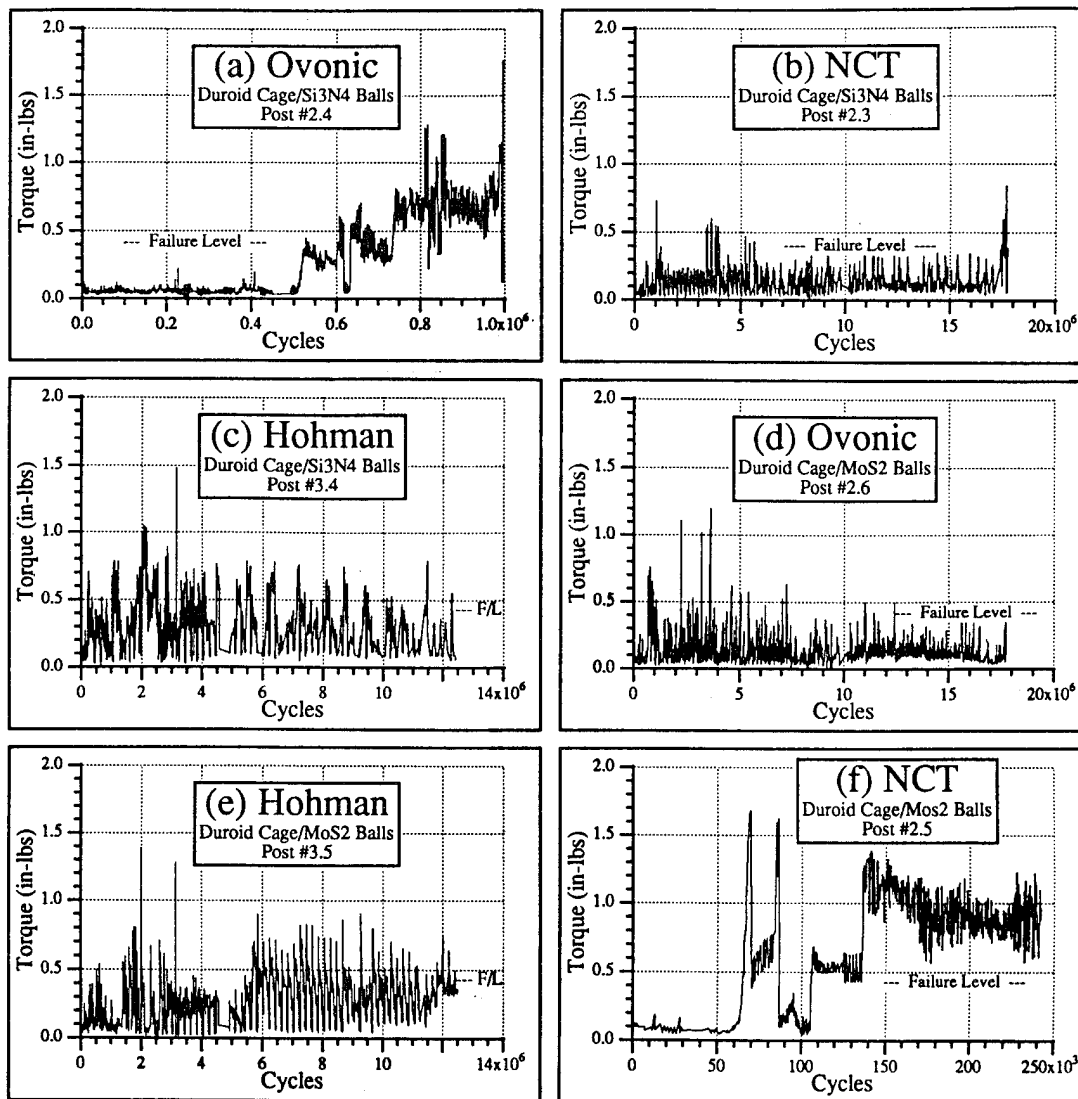
**Fig. 5-22** **Short-lived 105-size bearings with PTFE retainers and MoS2 coated or Si3N4 balls**

Fig. 5-23 presents a summary of bearing test lives. It is apparent that bearings with PTFE impregnated retainers and bare steel balls produced the longest lives, no matter which film type. Ceramic coated or monolithic balls and/or Vespel retainers produced the shortest lives, no matter which film type.

Cycle life to 0.44 in-lb in addition to detailed preload, wear and torque data is summarized in Table 5-24. Typical bearing running torques are listed which reflect the normal expected torque range while gimbaling. Peak excursion values are generally torque levels at failure or relatively short duration torque blips that were observed during the course of life. These excursions, often occurring between gimbal modes due to roll-over of end-of-stroke debris, can be seen on some of the torque histories appearing in Figs. 5-18 to 5-22. End of test torque reflect either failure torque or torque when the bearing was taken off of test. In some cases the torque at end of test was relatively low because of wear and subsequent reduction in preload.

In general, the lower running torques were associated with the smaller oscillating motions ($\pm$ 10°) where debris could be deposited between the ball paths and retainer material transfer to the ball/race contact was minimal. Higher torques (2 to 3X) were experienced during wide angle gimbaling and continuous rotation where debris entrapment could occur. Compared to these factors, initial preload appeared to have less effect on life. Both long and short lived bearing groups had about the same statistical distribution of high and low preload.



†Film: MLS=Multi-layer (Ovonic), RFMS= RF magnetron (NCT), DCS=Direct Current (Hohman)
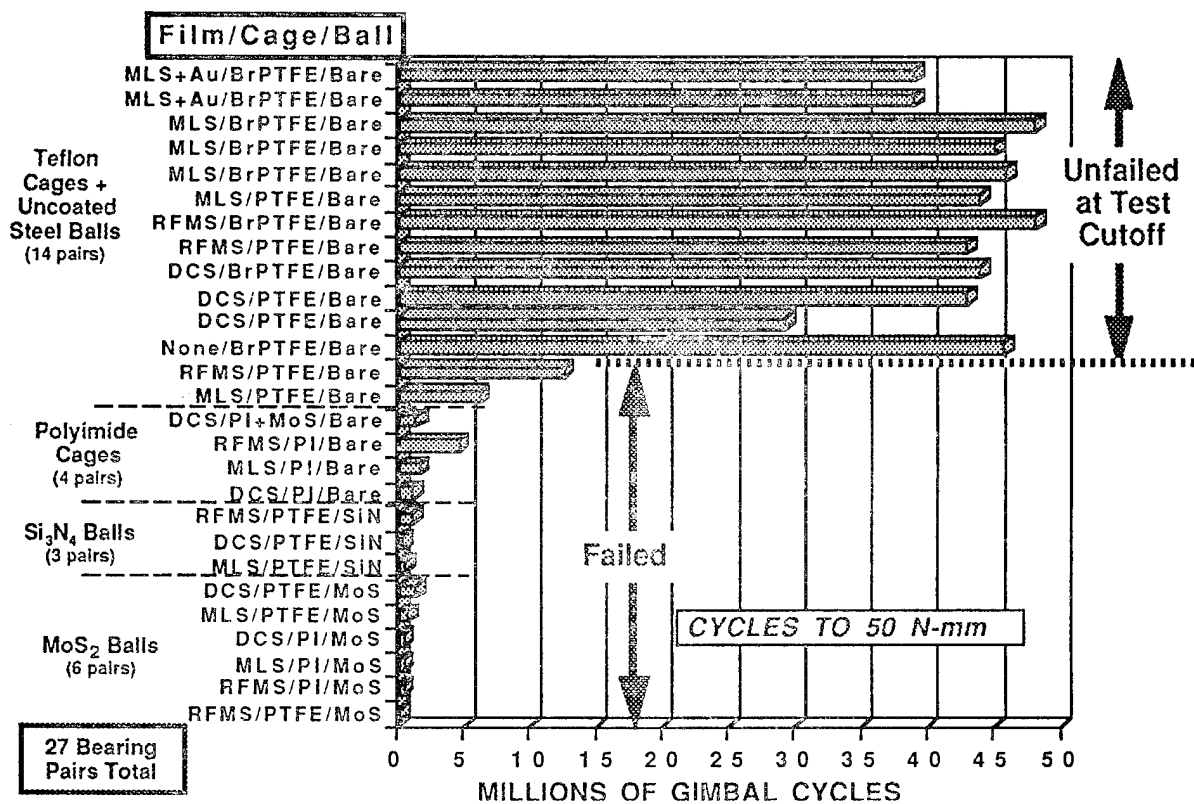
Fig. 5-23    Summary of MoS₂ coated, 105-size bearing lives to peak torque of 50 N-mm (0.44 in-lb)

## Table 5-24  Summary of 105 size bearing performance with MoS2 films

| Post | †Film | Cage | Ball | *Status | Life in Mcycles to 0.44 in-lbs | at Test Cutoff | Typ. Running low | high | Peak Excurs | End of test | Preload Start | End | Change | #Ball/Inner Race Track Width at end of test | Hertzian calculated | Increase | Δ Track Width mils/M cyc | Initial Max Hertz Strs KSI |
|---|---|---|---|---|---|---|---|---|---|---|---|---|---|---|---|---|---|---|
| *Ovonics + 10% Ni Films* | | | | | | | | | | | | | | | | | | |
| 4.6 | MLS | BrPTFE | Bare | F | 42.5 | 45.7 | 0.07 | 0.18 | 0.45 | 0.2 | 31 | 26 | -5 | 0.0475 | 0.026 | 0.022 | 0.5 | 164 |
| 4.11 | MLS | BrPTFE | Bare | TC | 1.8†† | 45.1 | 0.06 | 0.20 | 0.5 | 0.26 | 40 | 34 | -6 | 0.051 | 0.028 | 0.023 | 0.5 | 179 |
| 4.9 | MLS | BrPTFE | Bare | F | 43 | 48.2 | 0.03 | 0.14 | 0.3 | 0.54 | 32 | 23 | -9 | 0.047 | 0.026 | 0.021 | 0.4 | 166 |
| 4.2 | MLS | PTFE | Bare | TC | | 43.9 | 0.02 | 0.10 | 0.34 | 0.05 | 41 | 33 | -8 | 0.051 | 0.028 | 0.023 | 0.5 | 180 |
| 2.2 | MLS | PTFE | Bare | F | 6.1 | 17.7 | 0.04 | 0.12 | 0.6 | 0.2 | 31 | 31 | 0 | 0.049 | 0.026 | 0.023 | 1.3 | 164 |
| 2.6 | MLS | PTFE | MoS | F | 0.7 | 17.7 | 0.06 | 0.26 | 0.8 | 0.38 | 31 | 29 | -2 | 0.047 | 0.026 | 0.021 | 1.2 | 164 |
| 2.4 | MLS | PTFE | SiN | F | 0.6 | 1 | 0.07 | 0.30 | 1.7 | 1.7 | 32 | 40 | 8 | 0.048 | 0.026 | 0.022 | 21.8 | 191 |
| 2.8 | MLS | PI | Bare | F | 1.6 | 17.7 | 0.07 | 0.24 | 0.7 | 0.4 | 38 | 28 | -10 | 0.07 | 0.028 | 0.042 | 2.4 | 176 |
| 2.12 | MLS | PI | MoS | F | 0.3 | 0.5 | 0.08 | 0.40 | 1.7 | 1.7 | 30 | 36 | 6 | 0.052 | 0.027 | 0.025 | 49.5 | 162 |
| 3.11 | MLS | PI+MoS | Bare | F | 1.4 | 12.5 | 0.04 | 0.30 | 0.8 | 0.15 | 34 | 27 | -7 | 0.066 | 0.027 | 0.039 | 3.1 | 169 |
| *52 lb Preload* | | | | | | | | | | | | | | | | | | |
| 4.1 | MLS | BrPTFE | Bare | TC | Hi Preload | 45.8 | 0.2 | 0.60 | 0.8 | 0.2 | 52 | 26 | -26 | 0.065 | 0.031 | 0.034 | 0.7 | 195 |
| *Ovonics + 45% Au-Pd Films* | | | | | | | | | | | | | | | | | | |
| 4.3a | MLS+Au | BrPTFE | Bare | F | 5.2 | 38.9 | 0.03 | 0.10 | 0.47 | 0.07 | 33 | 20 | -13 | 0.052 | 0.026 | 0.026 | 0.7 | 168 |
| 4.12 | MLS+Au | BrPTFE | Bare | TC | | 38.9 | 0.04 | 0.13 | 0.32 | 0.05 | 29 | 23 | -6 | 0.047 | 0.025 | 0.022 | 0.6 | 161 |
| *NCT Films* | | | | | | | | | | | | | | | | | | |
| 4.8 | RFMS | BrPTFE | Bare | TC | | 48.1 | 0.03 | 0.10 | 0.2 | 0.05 | 25 | 35 | 10 | 0.033 | 0.027 | 0.006 | 0.1 | 153 |
| 4.1 | RFMS | PTFE | Bare | TC | | 42.9 | 0.03 | 0.10 | 0.35 | 0.07 | 27 | 27 | 0 | 0.039 | 0.025 | 0.014 | 0.3 | 157 |
| 2.1 | RFMS | PTFE | Bare | F | 12.5 | 42.9 | 0.03 | 0.06 | 0.6 | 0.35 | 19 | 22 | 3 | 0.028 | 0.023 | 0.005 | 0.1 | 140 |
| 2.5 | RFMS | PTFE | MoS | F | 0.07 | 0.24 | 0.10 | 0.20 | 1.3 | 1.2 | 26 | 40 | 14 | 0.052 | 0.028 | 0.024 | 99.0 | 155 |
| 2.3 | RFMS | PTFE | SiN | F | 1 | 17.7 | 0.07 | 0.24 | 0.7 | 0.4 | 28 | 41 | 13 | 0.0645 | 0.028 | 0.036 | 2.0 | 183 |
| 2.7 | RFMS | PI | Bare | F | 4.5 | 17.7 | 0.06 | 0.20 | 0.25 | 0.7 | 22 | 26 | 4 | 0.063 | 0.023 | 0.040 | 2.3 | 147 |
| 2.11 | RFMS | PI | MoS | F | 0.3 | 0.38 | 0.05 | 0.20 | 1.7 | 1.7 | 28 | 40 | 12 | 0.051 | 0.028 | 0.023 | 59.9 | 159 |
| *Hohman + 35% Sb2O3 Films* | | | | | | | | | | | | | | | | | | |
| 4.5 | DCS | BrPTFE | Bare | TC | | 43.3 | 0.03 | 0.10 | 0.3 | 0.18 | 37 | 29 | -8 | 0.048 | 0.028 | 0.020 | 0.5 | 174 |
| 4.4 | DCS | PTFE | Bare | TC | | 42.9 | 0.04 | 0.17 | 0.42 | 0.14 | 37 | 33 | -4 | 0.051 | 0.028 | 0.023 | 0.5 | 174 |
| 4.3 | DCS | PTFE | Bare | TC | | 29.3 | 0.04 | 0.16 | 0.43 | 0.16 | 34 | 36 | 2 | 0.047 | 0.027 | 0.020 | 0.7 | 169 |
| 3.5 | DCS | PTFE | MoS | F | 1.2 | 12.5 | 0.08 | 0.38 | 1 | 0.45 | 36 | 60 | 24 | 0.05 | 0.032 | 0.018 | 1.4 | 173 |
| 3.4 | DCS | PTFE | SiN | F | 0.2 | 12.5 | 0.12 | 0.40 | 1.2 | 0.6 | 29 | 52 | 23 | 0.056 | 0.029 | 0.027 | 2.2 | 185 |
| 3.6 | DCS | PI | Bare | F | 1 | 12.5 | 0.03 | 0.50 | 1 | 0.06 | 39 | 21 | -18 | 0.069 | 0.028 | 0.041 | 3.3 | 177 |
| 3.9 | DCS | PI | MoS | F | 0.3 | 0.5 | 0.05 | 0.06 | 1.7 | 1.7 | 41 | 47 | 6 | 0.046 | 0.030 | 0.016 | 32.4 | 180 |
| *No MoS2 Film* | | | | | | | | | | | | | | | | | | |
| 4.7 | none | BrPTFE | Bare | TC | 44.13 | | 0.10 | 0.22 | 0.39 | 0.35 | 32 | 20 | -12 | 0.046 | 0.026 | 0.020 | 0.5 | 166 |

†Film:  MLS=Multi-layer (Ovonic), RFMS= RF magnetron (NCT), DCS=Direct Current (Hohman)

*Status:  F=failed at 0.44 in-lb, TC= test cutoff, R= still running on test.

**Max Torque:  Typ. Running= Typical bearing torque range from low to high, Peak Excursion = highest torque recorded during run, End of Test = torque at test cutoff or failure.

- 61 -

## 5.3.2 Torque Signatures

Torque/time signatures of the test bearings were periodically recorded throughout life to characterize performance. A gimbal angle of ± 45° at a sinusoidal slew rate of 0.25 Hz (1 cycle / 4 seconds) was used.

**Short-Lived Bearings** Typical torque signatures for bearings having silicon nitride balls and those with balls coated with $MoS_2$ appear in Figs. 5-25 to 5-29. Large increases in torque were observed early in life due to debris jamming. Bearings with uncoated (bare) steel balls having polyimide retainers (Vespel™) also showing significant torque increases due to debris (Figs. 5-30 and 5-31). These bearings were found to be heavily worn from the abrasive Vespel debris (see Section 7.4). Occasionally the torque signature improved with additional running from the loss in preload produced by wear (see Fig. 5-30, for example).
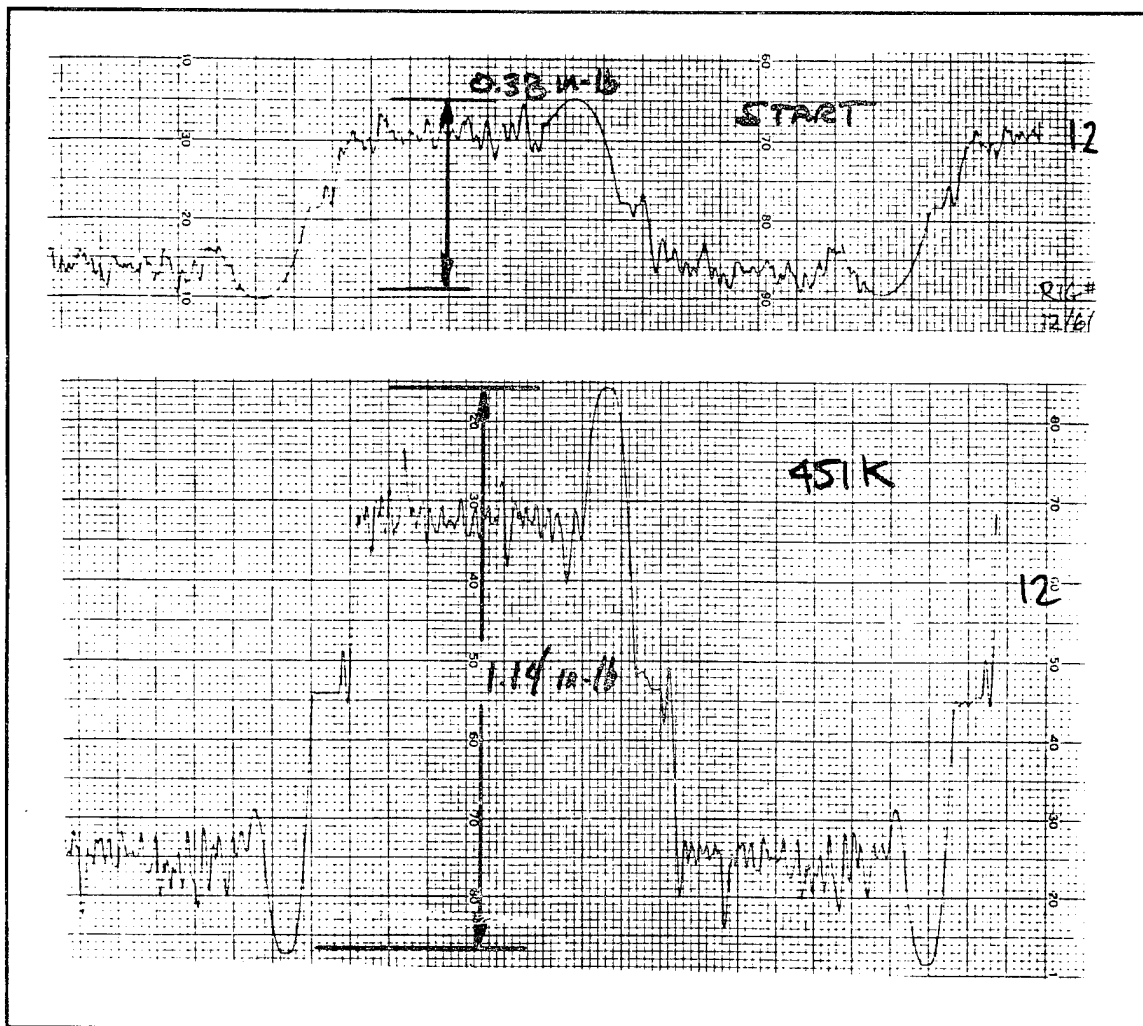


Fig. 5-25   Large torque increase with $MoS_2$ coated balls.
*(Note pronounced debris torque bump at end of stroke)*
(Post 2.12 Ovonics/Vespel/$MoS_2$ balls)
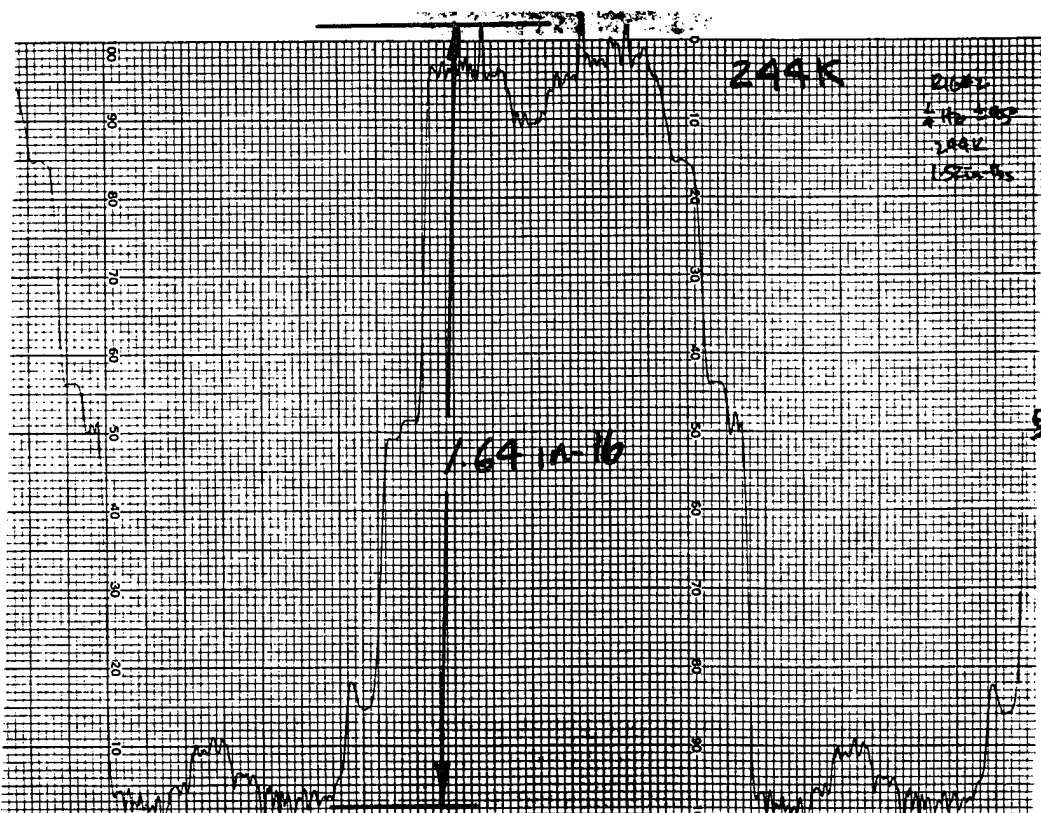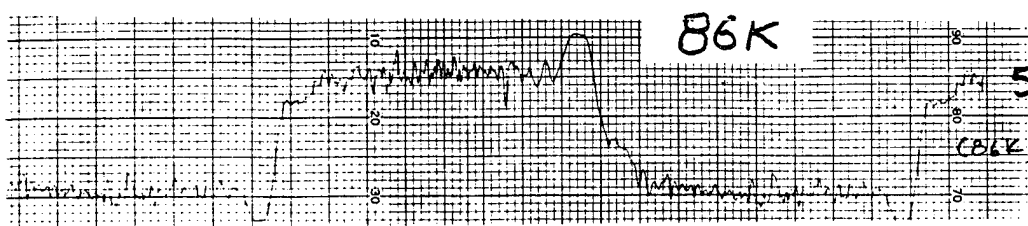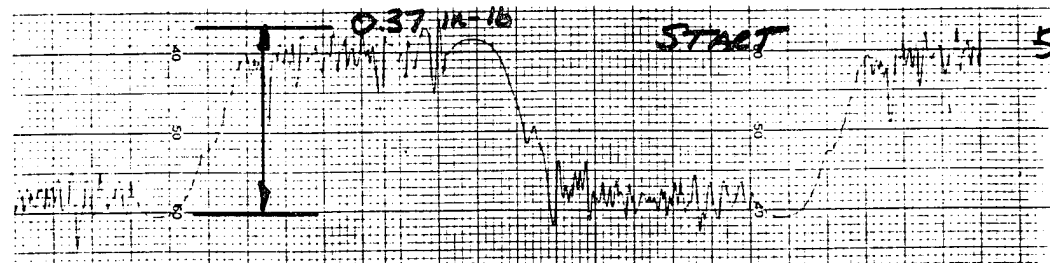
**Fig. 5-26** **Large torque increase with MoS₂ coated balls.**
(Post 2.5 NCT/Duroid/MoS2 balls)
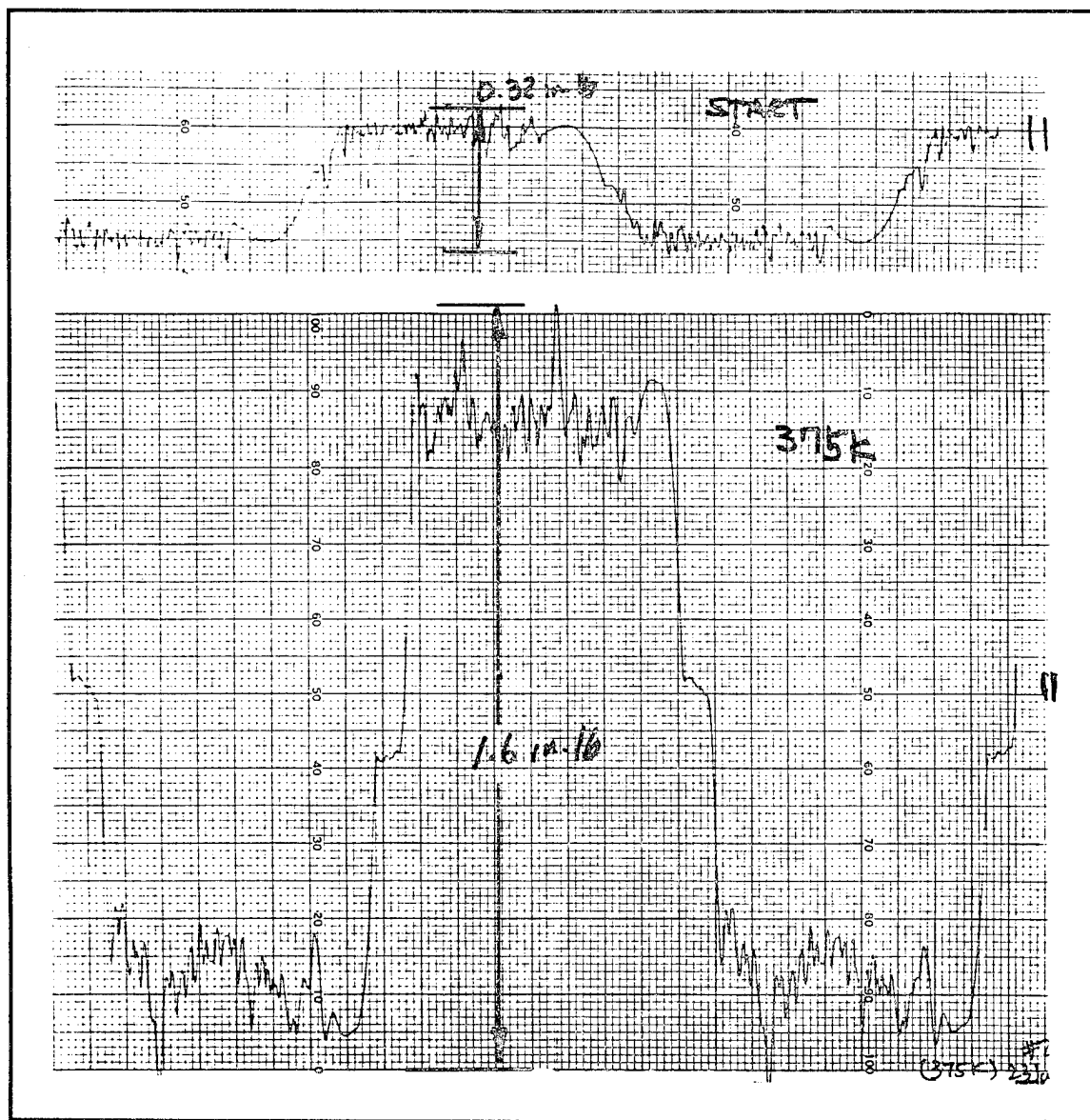
**Fig. 5-27** Large torque increase with MoS2 coated balls.
(Post 2.11 NCT/Vespel/MoS2 balls)
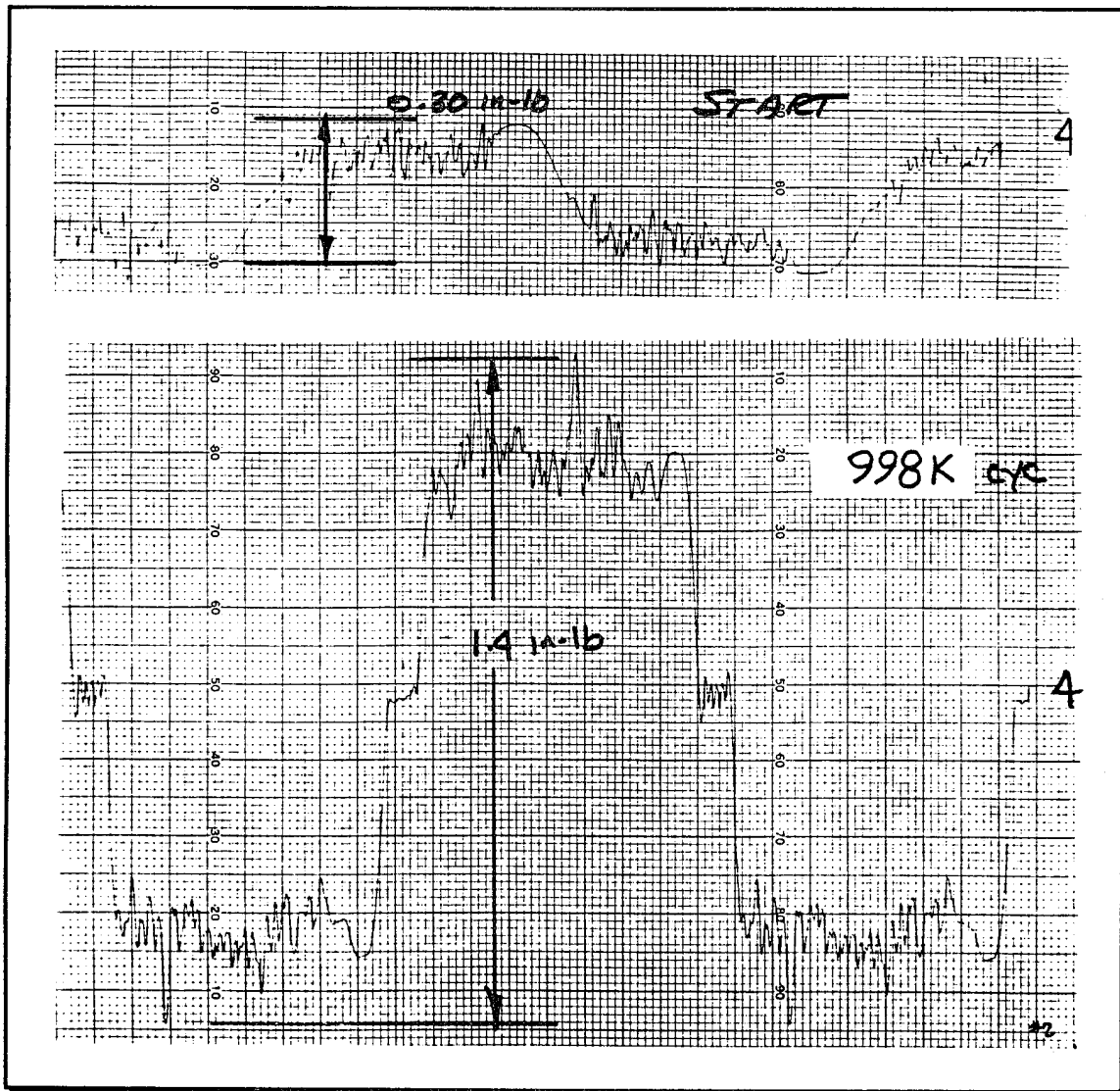
**Fig. 5-28    Large torque increase with Si3N4 balls.**
(Post 2.4  Ovonic/Vespel/Si3N4 balls)
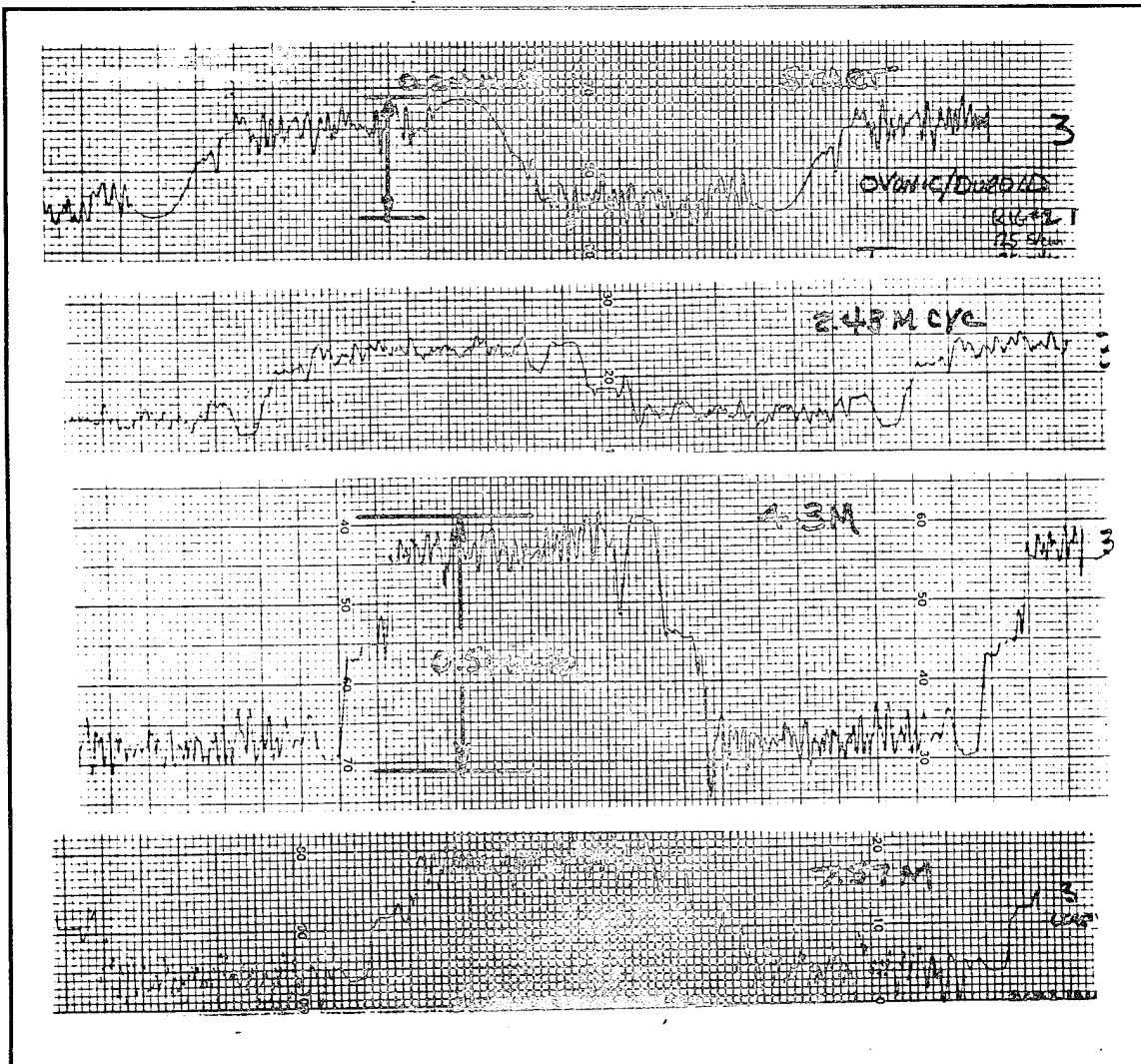
**Fig. 5-29** Torque increase with $Si_3N_4$ balls.
(Post 2.3 NCT/Duroid/$Si_3N_4$ balls)
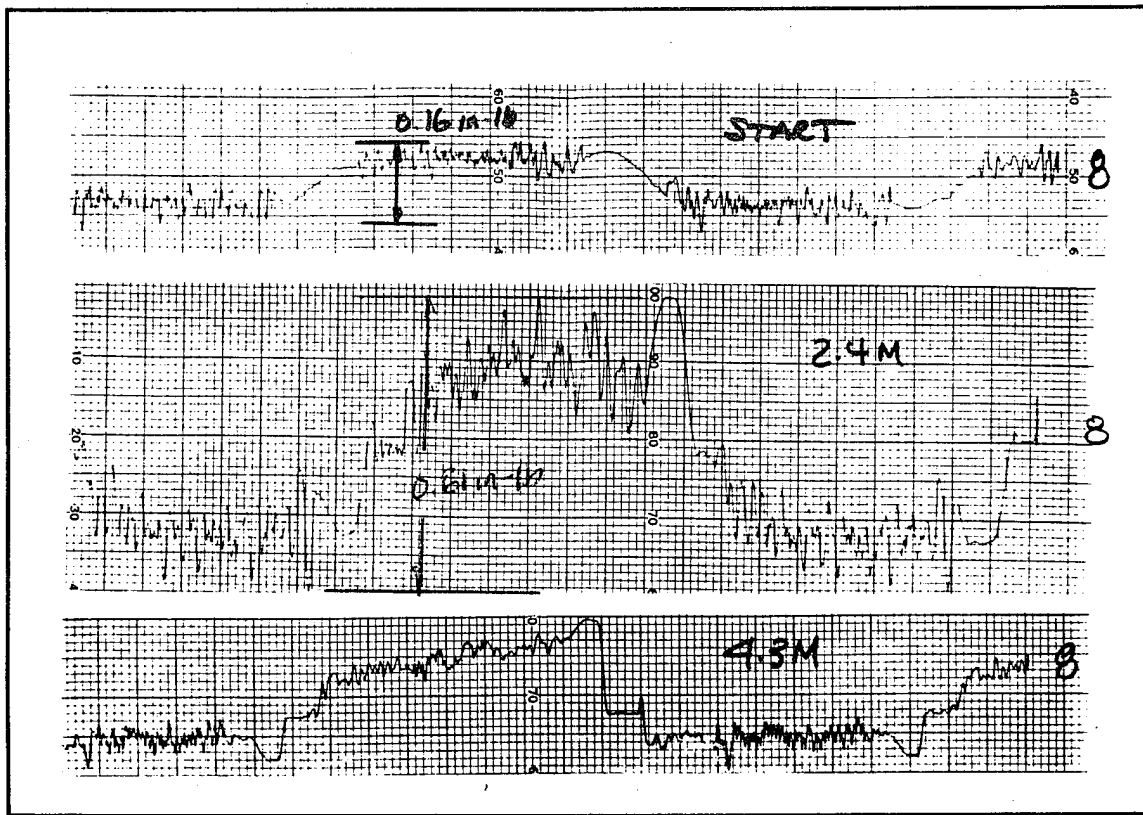
**Fig. 5-30** **Torque increase with Vespel retainer.** *(Note torque improvement at 4.3 M cycles due to wear and reduced preload)*
(Post 2.4 Ovonic/Vespel/bare balls)
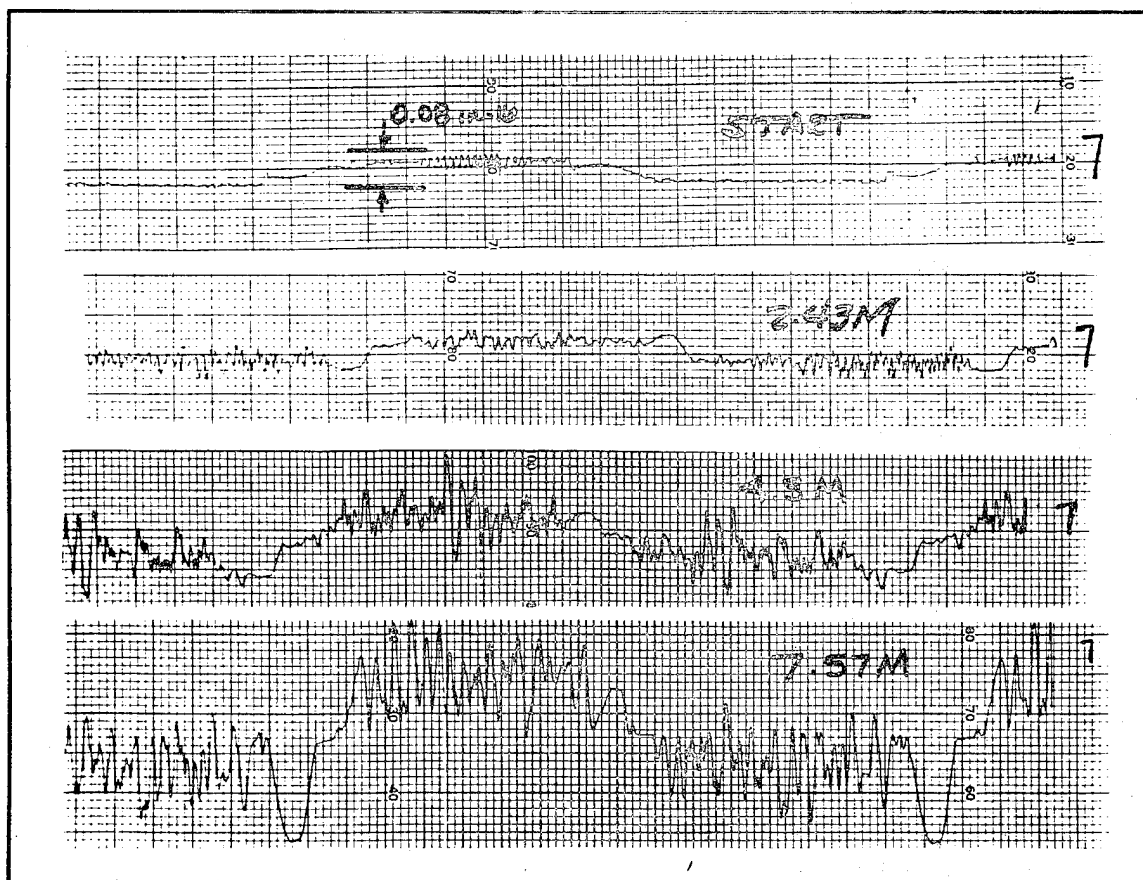
**Fig. 5-31  Torque increase with Vespel retainer.**
(Post 2.7 NCT/Vespel/bare balls)

**Long-Lived Bearings** Torque signature traces for the long-lived (48 million cycles) bearings having PTFE containing retainers (Salox™ or Duroid™) and bare steel balls appear in Figs. 5-32 to 5-37. Variation in torque appears relatively small during life from these traces. However, torque excursions can be significantly larger during gimbaling from occasional excess debris build-up as shown in the torque history plots appearing in Figs. 5-18 and 5-19. Some of the traces (Figs 5-34 and 5-35) also show the ripple component of bearing torque taken over 3 revolutions at 0.25 Hz or 1 rev/ seconds.
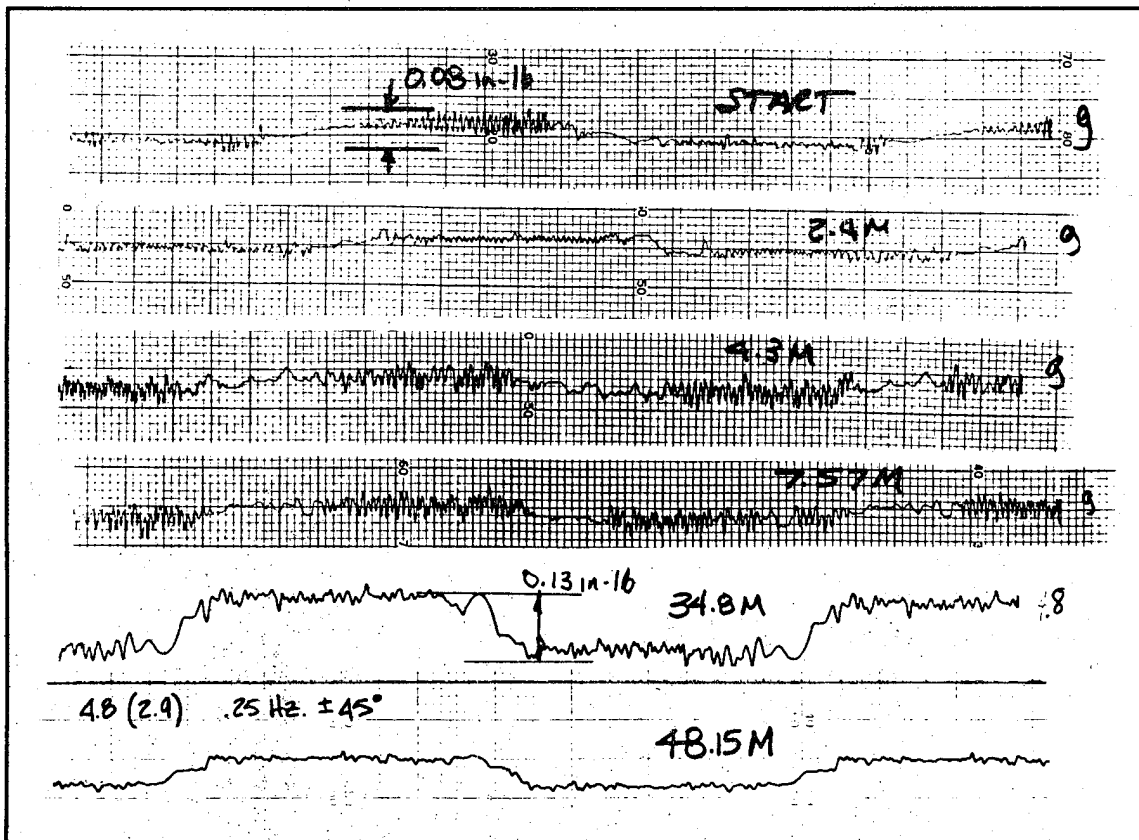


**Fig. 5-32 Torque traces with Salox retainers to 48 million cycles.**
(Post 4.8 NCT/Salox/bare balls)
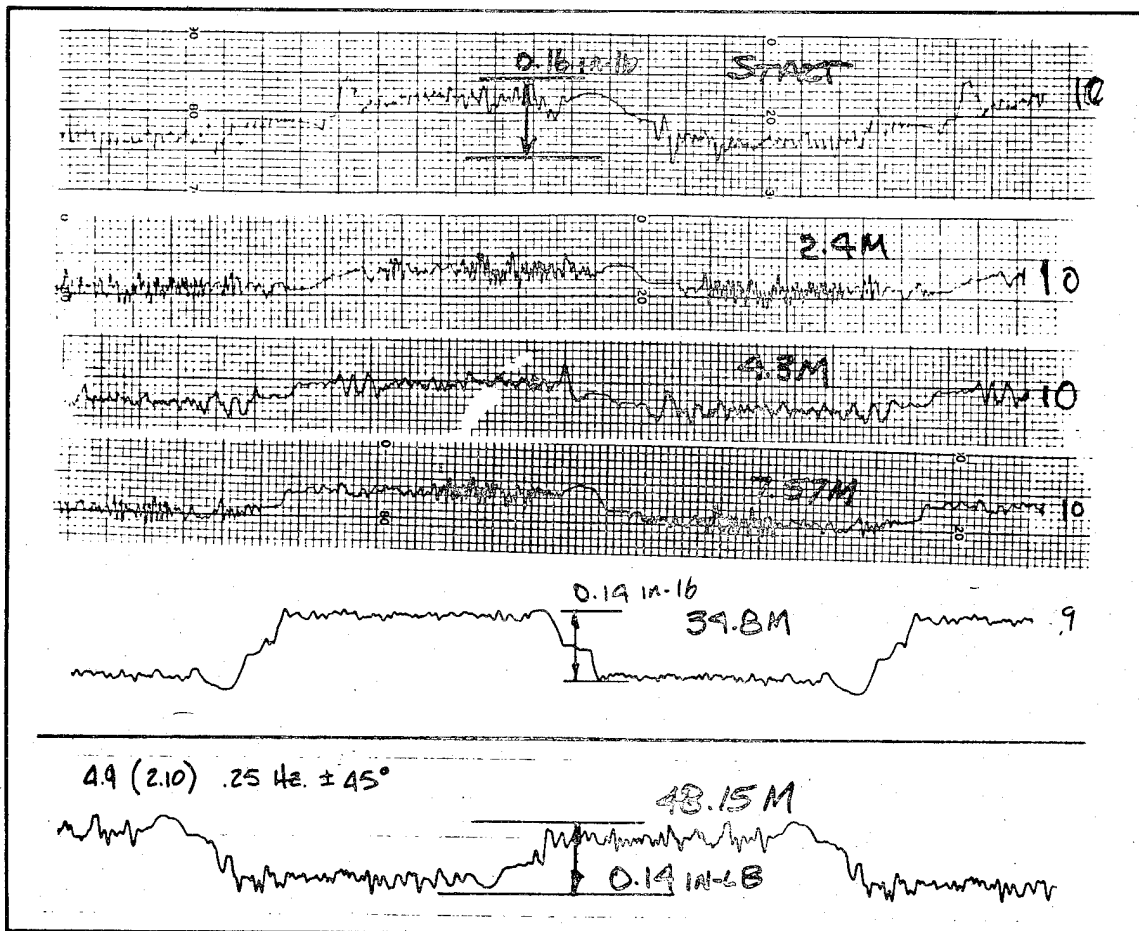
**Fig. 5-33** Torque traces with Salox retainers to 48 million cycles.
(Post 4.9 Ovonics/Salox/bare balls)
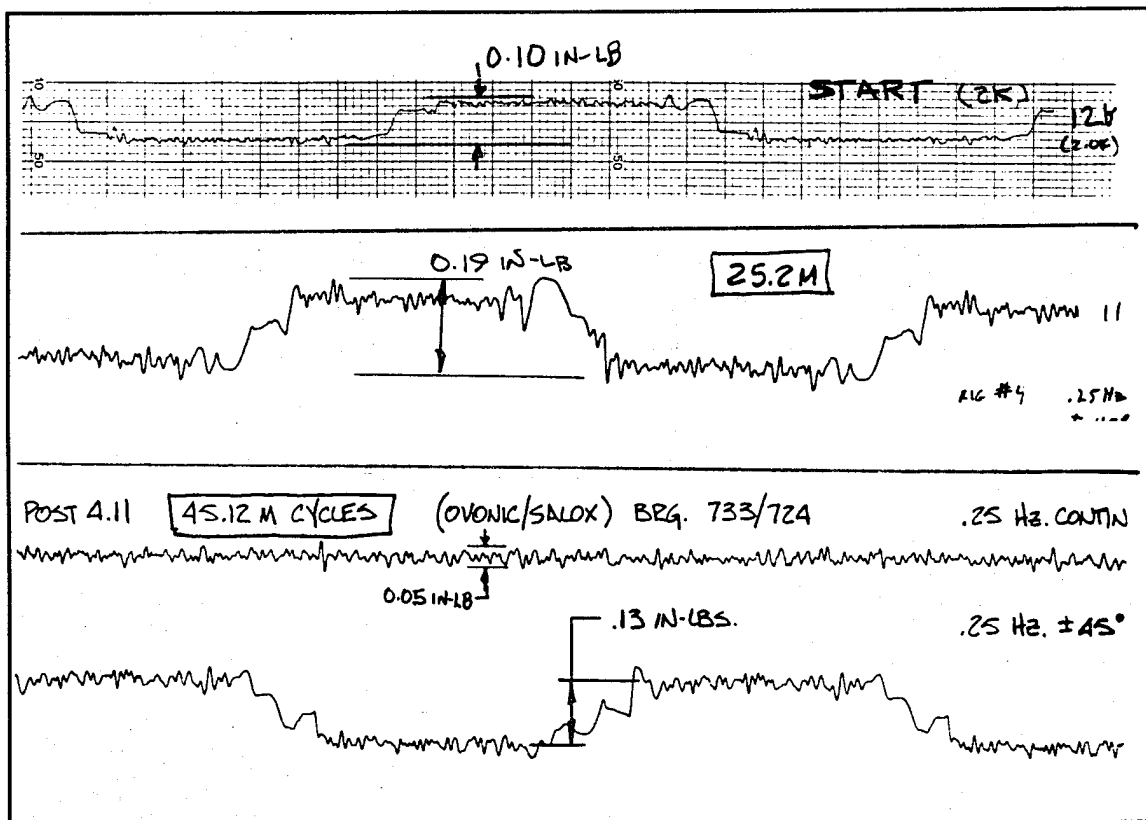
**Fig. 5-34  Torque traces with Salox retainers to 48 million cycles.**
(Post 4.11  Ovonics/Salox/bare balls)
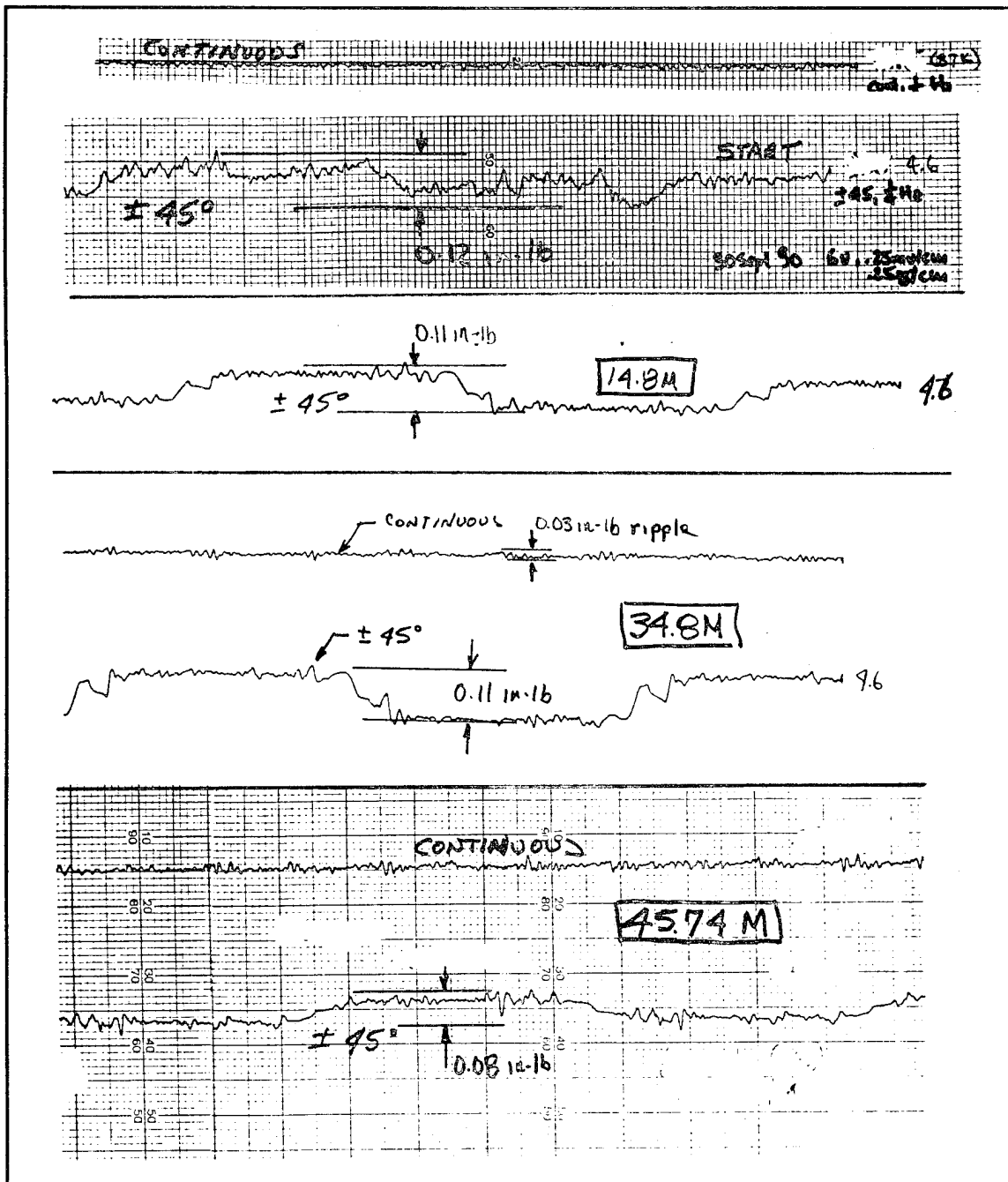
**Fig. 5-35  Torque traces with Salox retainers to 48 million cycles showing starting and ending torque ripple.**
(Post 4.6 Ovonics/Salox/bare balls)
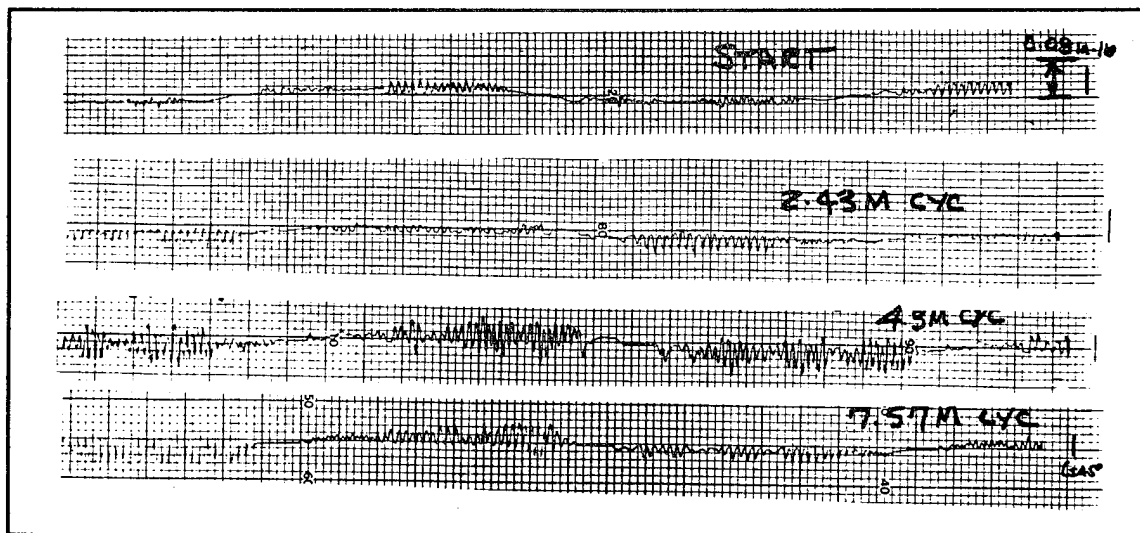
(a) Post 2.1 NCT/Duroid/bare balls)
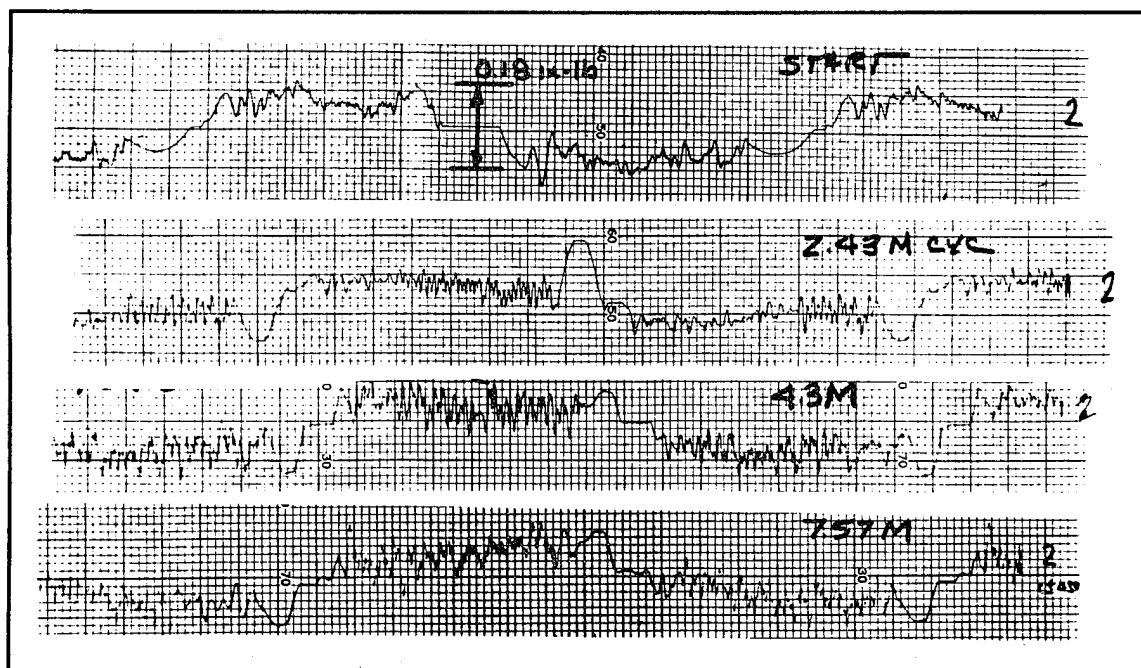


(b) Post 2.2 Ovonic/Duroid/bare balls)

Fig. 5-36 Torque traces with Duroid retainers.
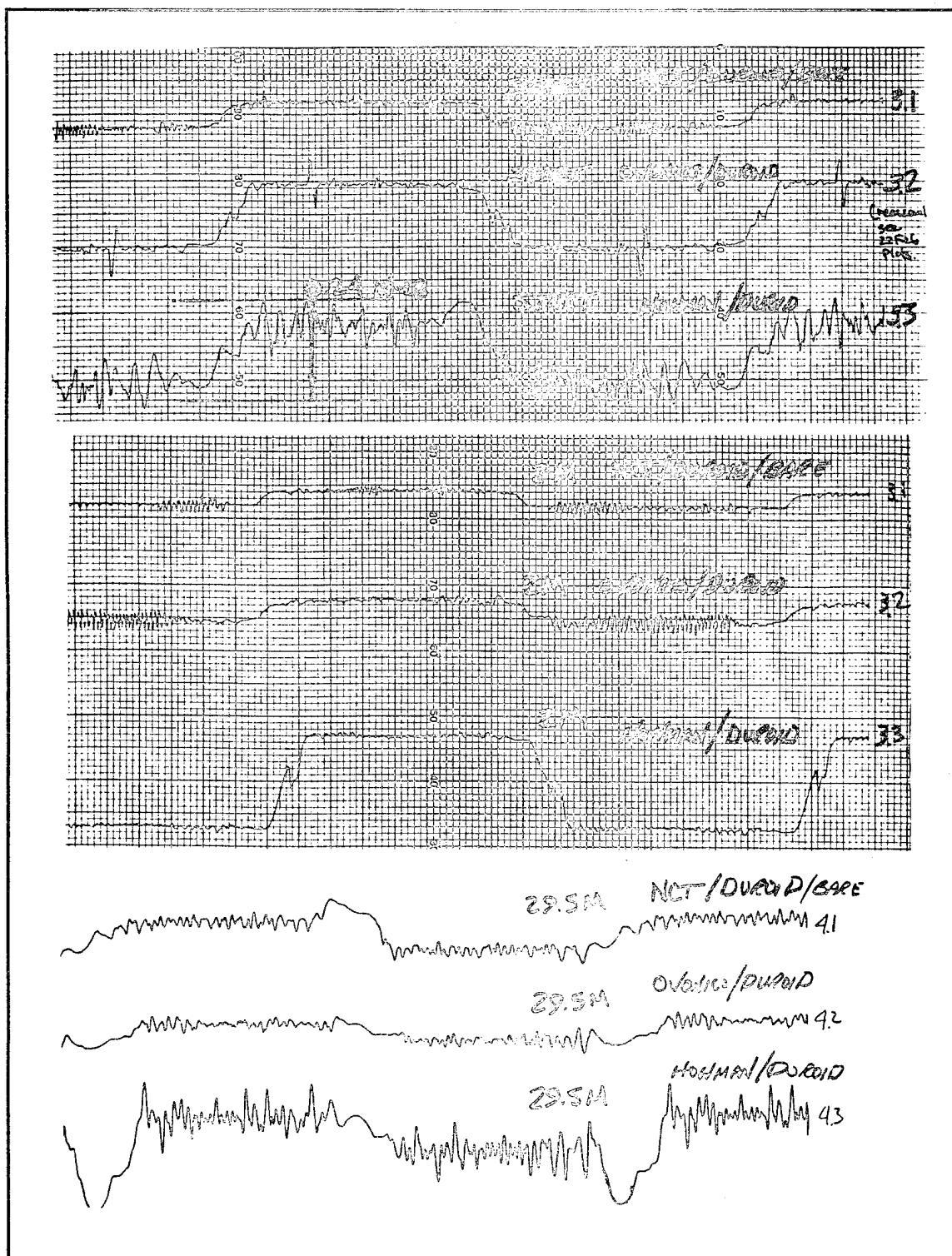
**Fig. 5-37** Torque traces with Duroid retainers and 3 different MoS2 films

(Posts #3.1 NCT / #3.2 Ovonics / #3.3 Hohman)

**Effect of PTFE Retainer Material** It is clear that the self-lubricating PTFE-containing bearing retainers provided much more life than the non-active lubricating polyimide retainer. A special test was performed to determine if the $MoS_2$ film sputtered on the races was important to performance or whether the self-lubricating retainers by themselves were sufficient. Fig. 5-38 shows a direct torque signature comparison between a bearing pair without $MoS_2$ film ( Fig. 5-38a) and one with (Fig. 5-38b). Note that both bearings have Salox retainers and have initial bearing preloads of 32 and 31 lbs for the bare and $MoS_2$ coated bearings, respectively. While both bearings start off with about the same torque, the bare bearing has nearly 3x the torque of the coated bearing after 14 million cycles. The same is true at 35 million cycles with the bare bearing showing significantly higher torque ripple compared with the $MoS_2$ bearing. The presence of $MoS_2$ film appears to have a synergistic effect on film transfer rate moderating the build up of material and, in turn, moderating torque irregularities.

**Effect of High Preload** A special test on one bearing pair was conducted at high preload. Bearing life exceeded 40 million cycles although torque performance for the bearing with 52 lbs preload (Fig. 5-39) is more than 3x higher than the 31 lb preloaded bearing (Fig. 5-36) with the same Ovonics film and Salox retainer . Also note that there is a substantial drop in torque between 40.8 million and 45.8 million cycles (see Fig. 5-39), suggesting wear out and loss in preload. It is important to recognize that despite this wear, no hard jam failure was produced unlike bearings with either $MoS_2$ coated or $Si_3N_4$ balls.
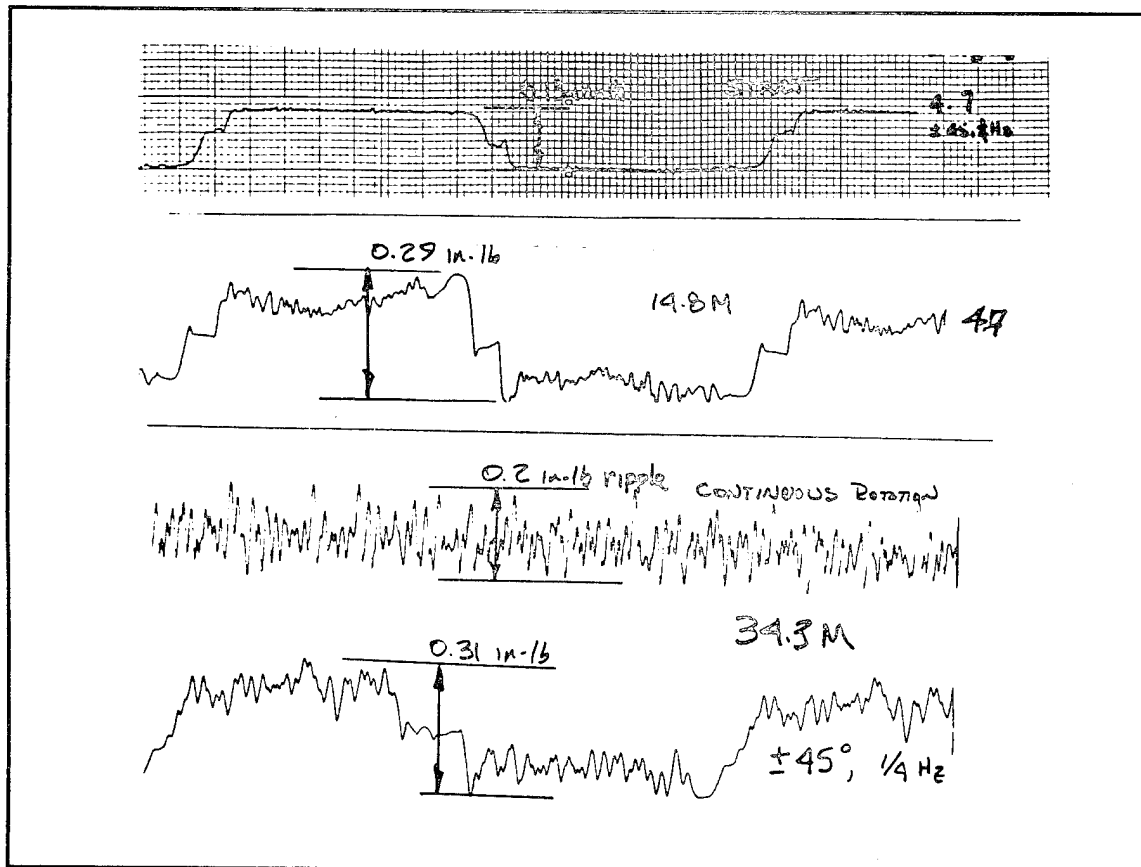
(a) No MoS2 film with Salox retainers (32 lbs initial preload)
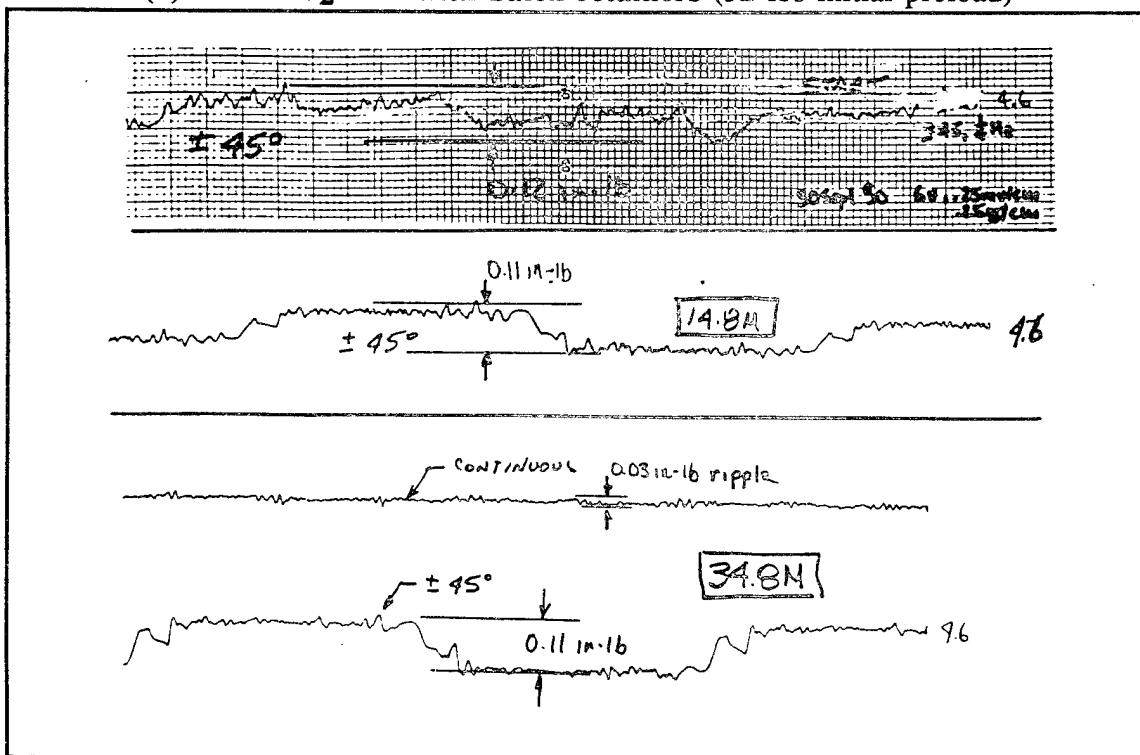


(b) Ovonics film with Salox retainer (31 lbs initial preload)

Fig. 5-38 PTFE cage torque performance degrades without MoS2 film on races.
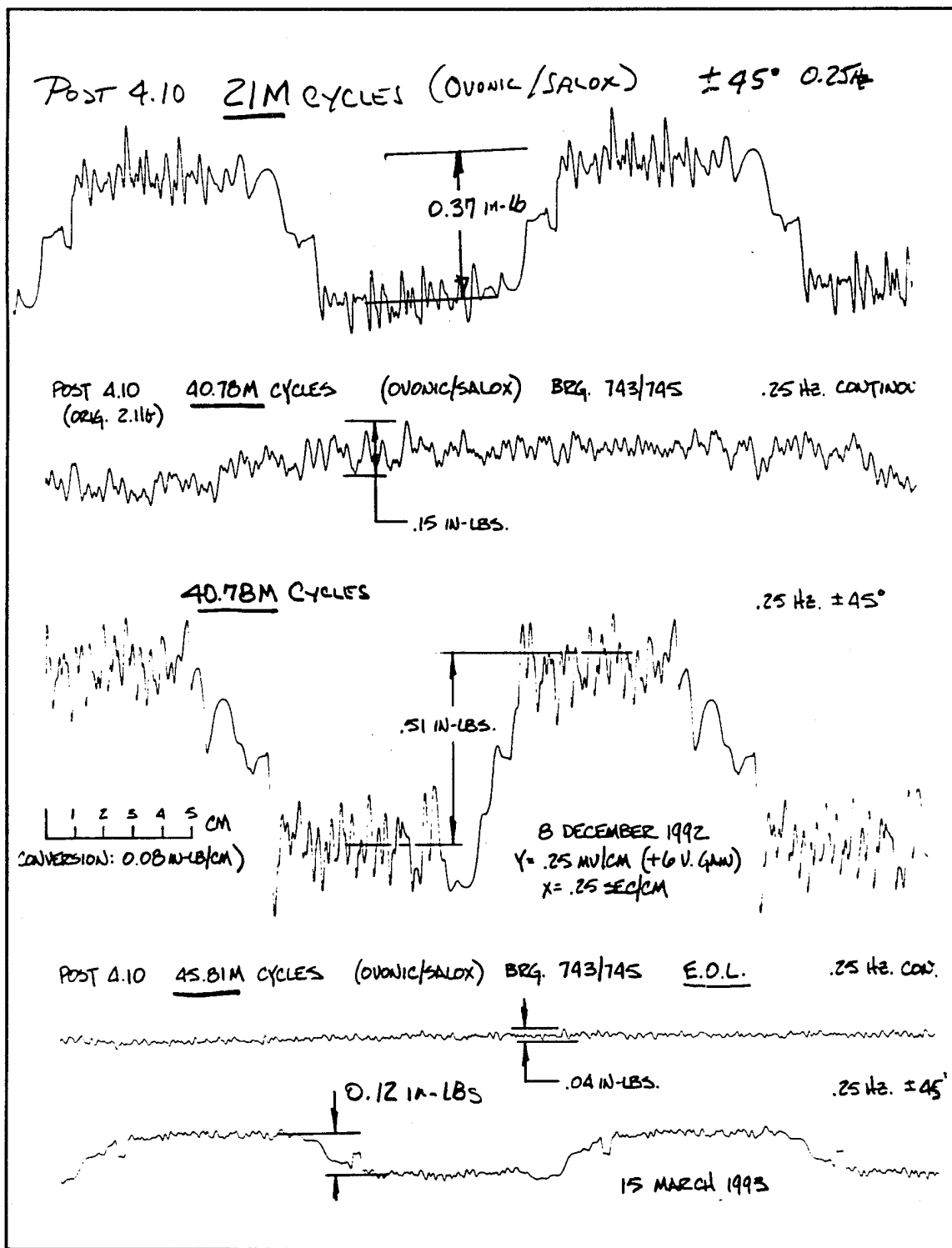
**Fig. 5-39 Torque signature of high preload (52 lbs initial) bearing showing suspected loss in preload between 41 and 46 million cycles**
(Post 4.10 Ovonic / Salox / bare balls)

### 5.3.3 Torque Ripple

The torque magnitude and, specifically, torque ripple of the support bearings generally affect the performance of precision pointing servo-mechanisms. Frequencies associated with bearing torque disturbances, often multiples of the ball pass frequencies, can exceed the bandwidth limits of the servo-controller. It is usually easier to compensate for slow changing bearing torque levels (DC or average component) than fluctuating disturbances (ripple).

In the case of many optical and infared sensors, special fast steering mirrors, supported on flexures, are used for "dejittering" high frequency vibratory disturbances. Groups of mirrors and attendant controls, as many as 7, are occasionally needed to satisfy packaging and pointing requirements. Reduction of all sources of vibration, mostly from rotating and gimbaling mechanisms containing bearings (gimbals, CMG's, solar array drives, etc.), will lessen the burden, hence complexity and cost of the electro-optic compensation system. Thus, the torque ripple character of bearings lubricated with advanced tribomaterials and the manner which it changes with time is an important evaluation factor.

Figs. 5-40 and 5-41 show the early progress of the torque ripple component of 12 NCT and Ovonic $MoS_2$ film coated bearings at start (7k cycles), 3M and 4.3M cycles. The data were taken with the bearings rotating in one direction at a rate of 1/4 Hz or 90°/sec. Note from Fig. 5-40 that the ripple of some films (posts #3,8 &10) has improved, some have degraded (posts #1,6 & 7) or failed (posts #4,5,11&12) and the others are pretty much the same (posts #2 & 9). Between 3M and 4.3M cycles (see Fig. 5-41), all of the films, except post #6, are about the same. In general, the quietest bearings were those with PTFE composite retainers and plain steel balls. Bearings with $MoS_2$ coated balls were among the noisiest, presumably due to debris shedding and unevenness in coating thickness.

1. NCT+Duroid +No Ball Coating
2. Ovonic+Duroid +No Ball Coating
3. NCT+Duroid +Si3N4 Balls
4. Ovonic+Duroid +Si3N4 Balls
5. NCT Duroid +MoS2 Balls
6. Ovonic+Duroid +MoS2 Balls
7. NCT+Vespel +No Ball Coating
8. Ovonic+Vespel +No Ball Coating
9. NCT+Salox +No Ball Coating
10. Ovonic+Salox +No Ball Coating
11. NCT+Vespel +MoS2 Balls
12. Ovonic+Vespel +MoS2 Balls
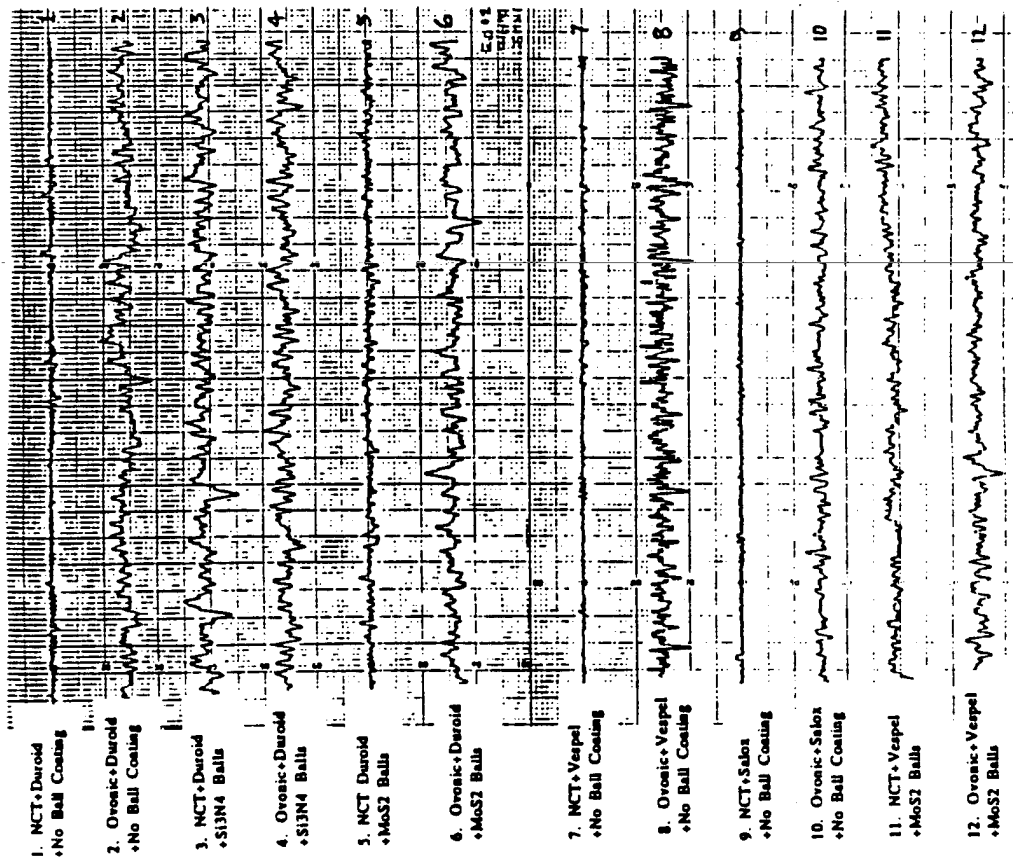
1/4 Hz Continuous, 7k cycles
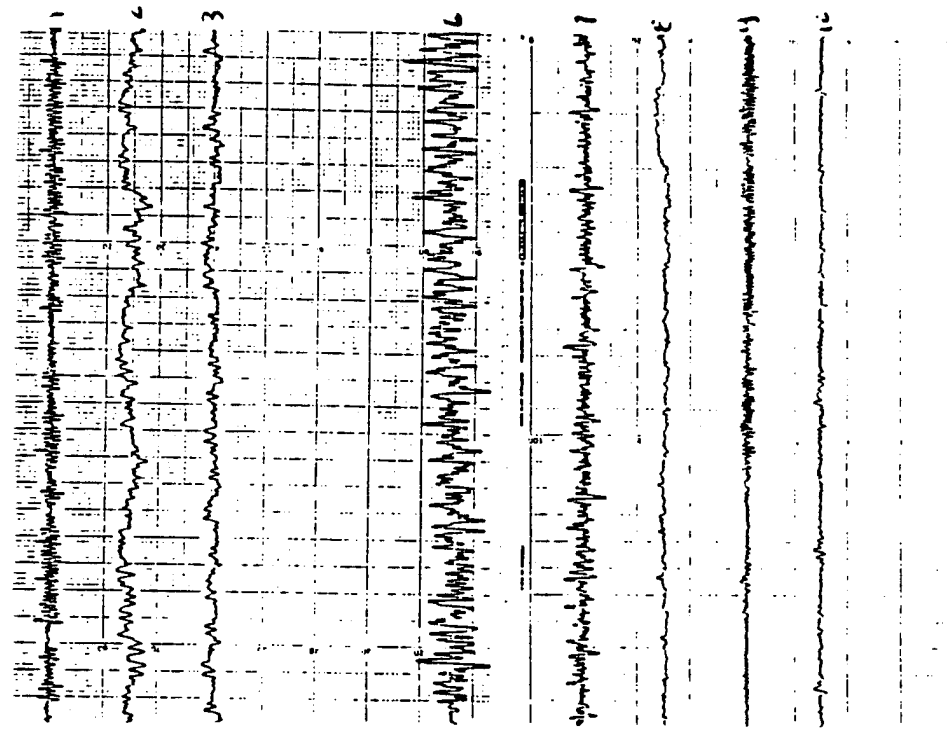
1/4 Hz Continuous, 3M cycles

Fig. 5-40 Torque Signatures of NCT & Ovonics MoS2 films

- 79 -

1. NCT+Duroid
+No Ball Coating

2. Ovonic+Duroid
+No Ball Coating

3. NCT+Duroid
+Si3N4 Balls

6. Ovonic+Duroid
+MoS2 Balls

7. NCT+Vespel
+No Ball Coating

8. Ovonic+Vespel
+No Ball Coating

9. NCT+Salox
+No Ball Coating

10. Ovonic+Salox
+No Ball Coating

1/4 Hz Continuous, 4.3M cycles

1/4 Hz Continuous, 2.9M cycles
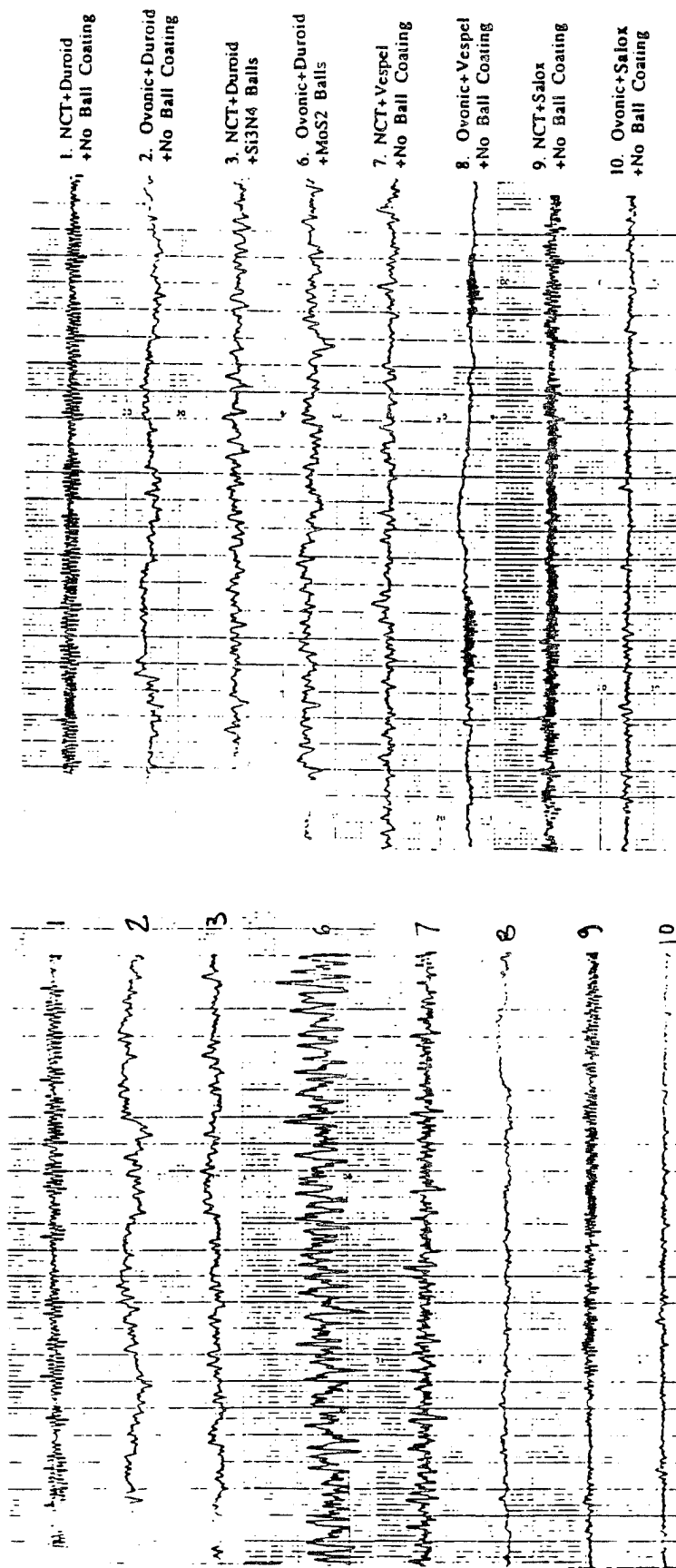
Fig. 5-41    Torque   Signatures   of   NCT   &   Ovonics   MoS2   films

### 5.3.4 Preload

Preload was measured for bearings at both the start and end of test (see examples, Figs 5-42 and 5-43). Compared to the choice of retainer material and ball treatment, initial preload had less of an effect on life. Preload levels and variations were comparable for the groups of long and short lived bearings (see Table 5-15).

Preload levels increased for all but one of the bearings incorporating either $Si_3N_4$ balls or steel balls coated with $MoS_2$ at the time of failure. This coupled with the observation of copious amounts of $MoS_2$ dust in these bearings indicated that debris jamming contributed to torque failure. On the other hand, two of the three bearings containing retainers lost preload. These bearings contained significant amounts of polyimide wear particles (Section 7.4.1) which evidently contributed to $MoS_2$ film and race wear, resulting in a loss of preload.

With one exception, long-lived bearings (> 40 million cycles) having PTFE or Br-PTFE type retainers with plain balls experienced some preload reduction or remained essentially unchanged (Fig. 5-44). Posttest inspection showed that the $MoS_2$ film was found removed from the races in certain spots and replaced with bronze and/or PTFE deposits from the retainer. This double transfer mechanism is well known. A loss in bearing preload would suggest that insufficient retainer transfer film occurred to offset wear of $MoS_2$ film, race and balls.

It was often difficult to decide when to terminate the long-lived bearing tests since no "hard" failures were encountered. Consequently, some of the bearings may have been tested too long resulting in additional wear and preload loss. Despite this, preload losses of less than 20% were measured in several cases on bearings with more than 40 million gimbal test cycles. Because of the hard preload nature of these tests, a 20% loss in preload represents a modest 6% reduction in stiffness since stiffness is proportional to the cube root of preload.
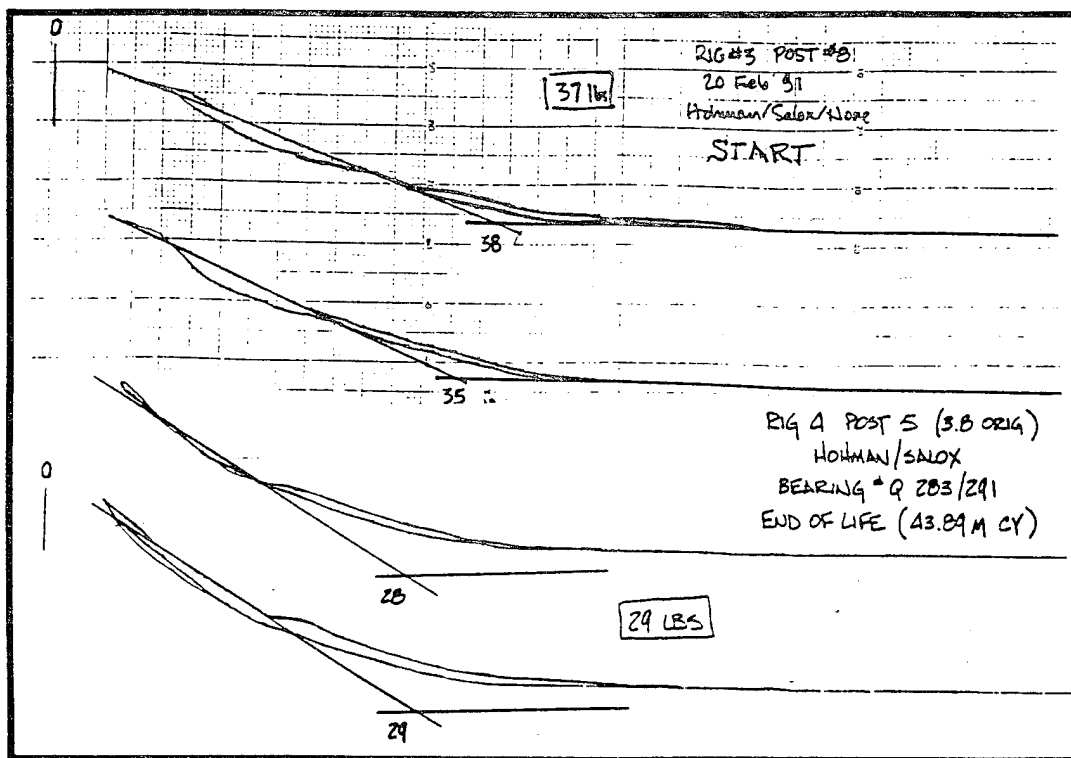
(a) Hohman Film/Salox Retainer (43.84M cycles)
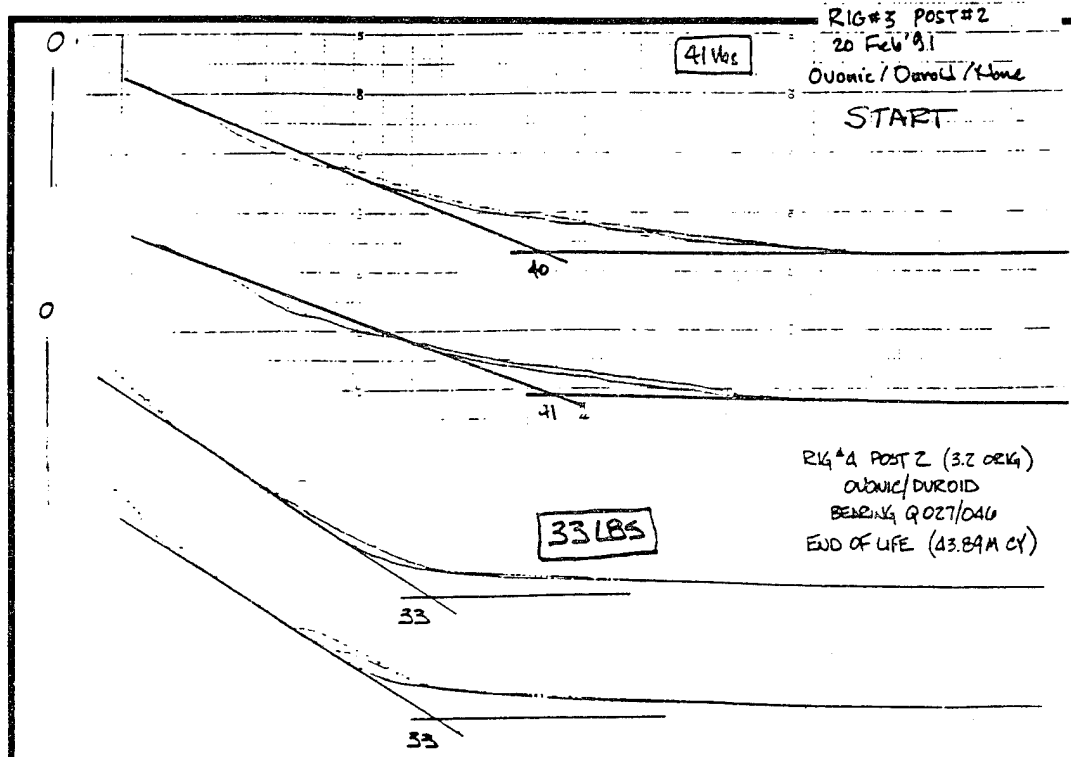


(b) Ovonic Film/Duroid Retainer (43.84M cycles)

Fig. 5-42 Typical start and end preload traces for Hohman & Ovonic MoS2 lubricated 105 size bearings .
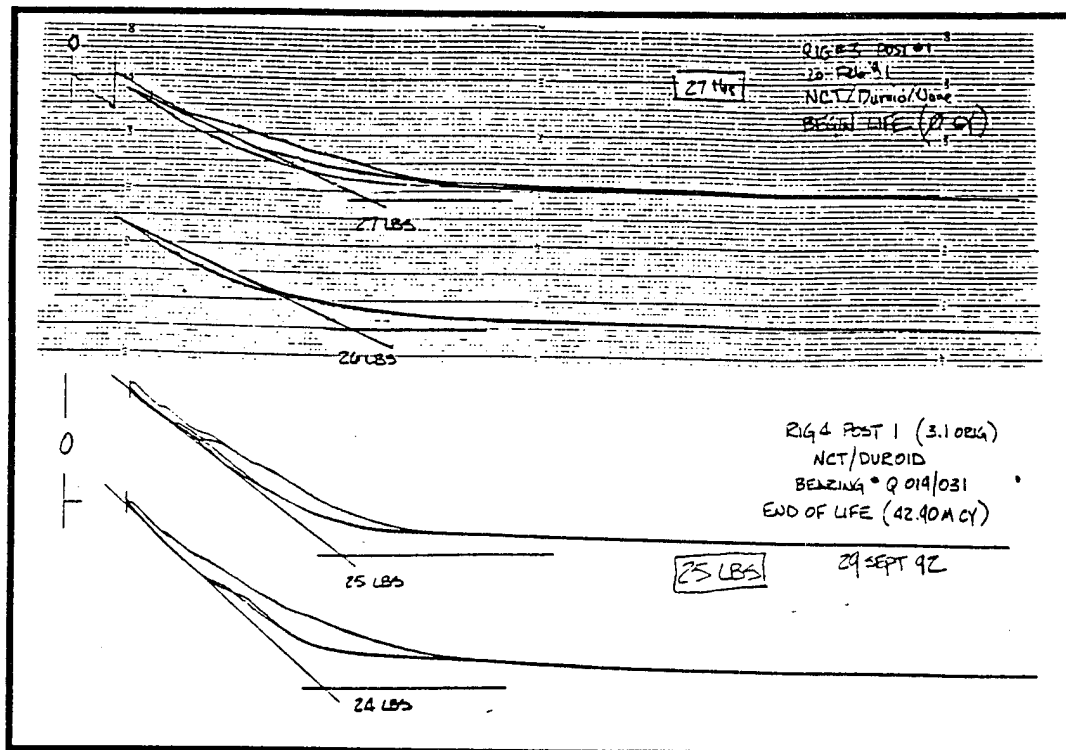
(a) NCT Film/Duroid Retainer (42.9M cycles)
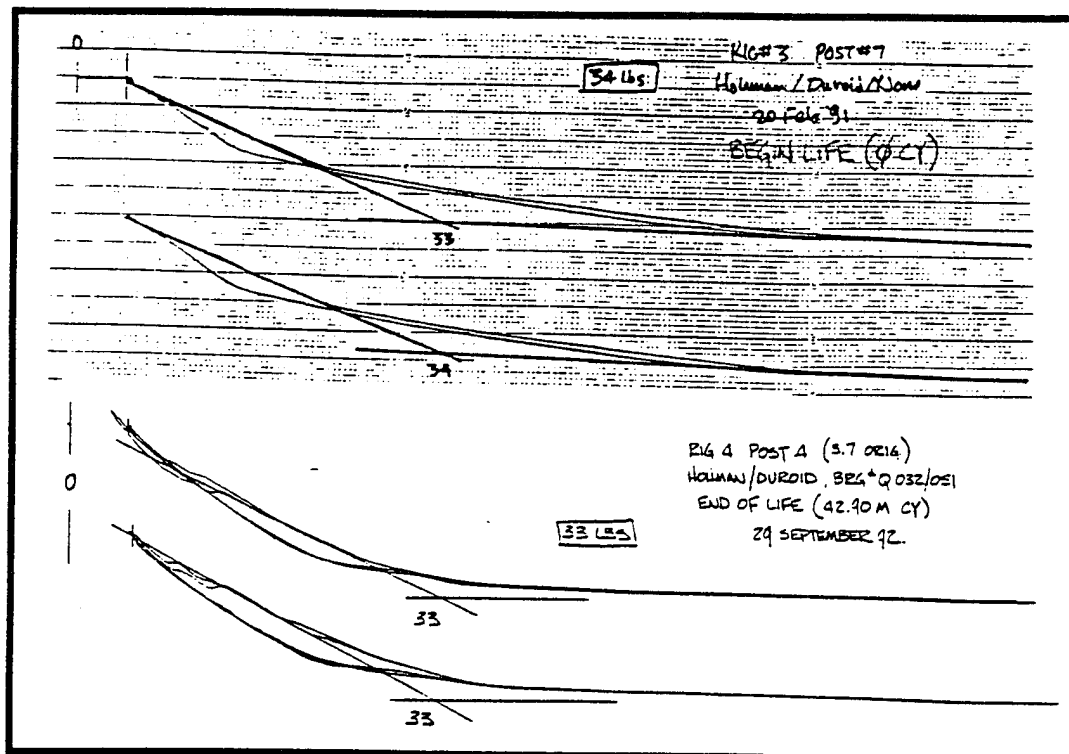


(b) Hohman Film/Duroid Retainer (42.9M cycles)

Fig. 5-43  Typical start and end preload traces for NCT & Hohman MoS$_2$
lubricated 105 size bearings.
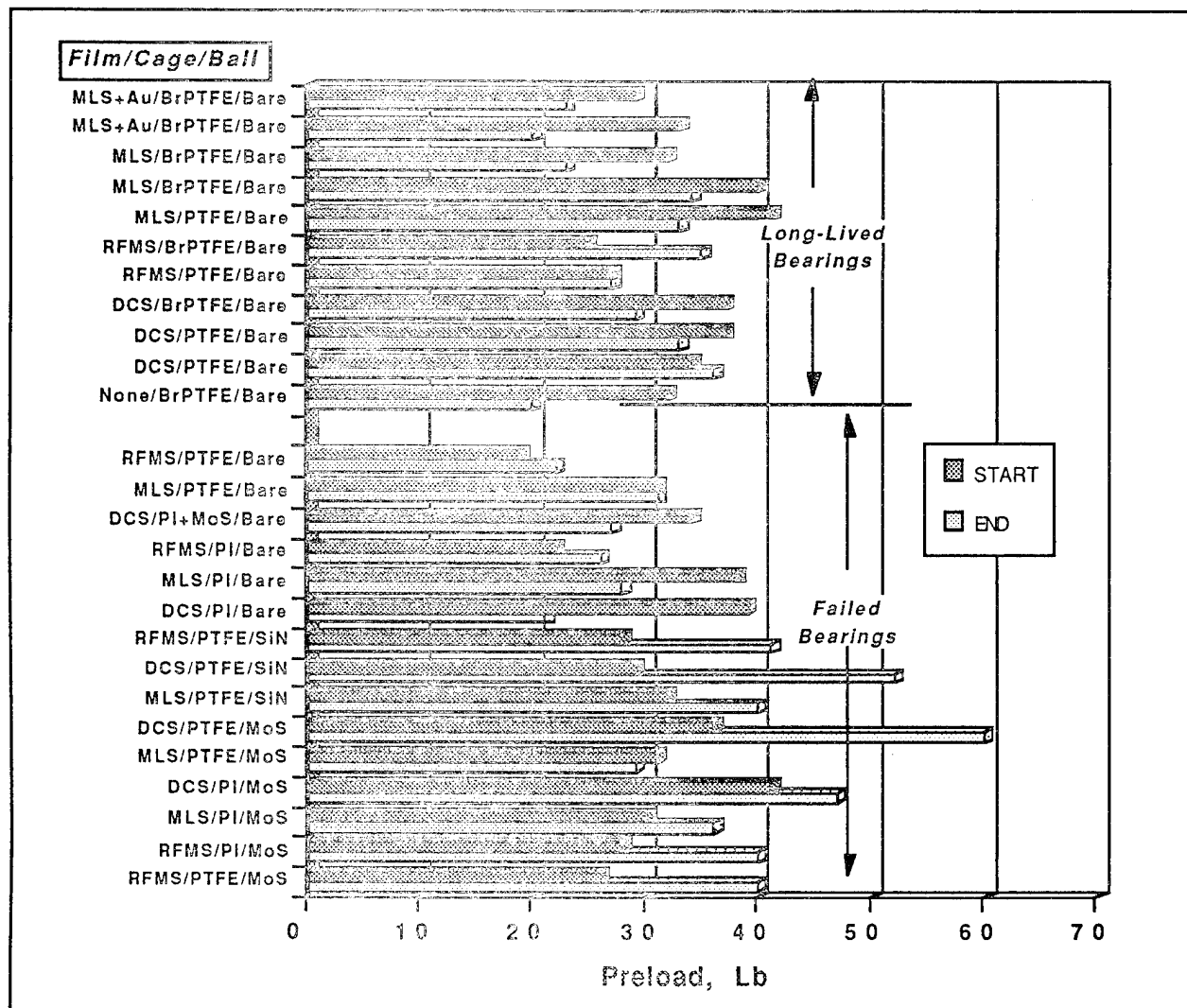
Fig. 5-44  Summary of bearing preload changes over life.

## 5.3.5 Track Widths

The tested bearings were disassembled and the components examined visually and/or by scanning electron microscopy, as described in detail in Section 7.4. Backscattered electron imaging combined with X-ray elemental microanalysis revealed compositional variations in the ball tracks on the races. The track width, a relative indication of film loss and race wear, was clearly defined. The increase in track width of the examined test bearings was a reasonable indicator of film loss (delamination/wear) and race wear. The increase in track width was determined by subtracting the theoretical Hertzian contact width at the inner race under the initial preload from the measured track width at the time of examination (see Table 5-24). Fig. 5-45 shows that self-lubricating retainers provided the lowest wear rates based on the increase in track width per million gimbal cycles. Bearings having $MoS_2$ film coated balls suffered the highest wear rates due to considerable debris generation and their relatively short lives.

The increase in track width of long lived bearings show a reasonable correlation with initial preload and changes in preload. The trends shown in Fig. 5-46 indicate that the increase in bearing track width is proportional to preload, as might be expected from the classical wear equations. Furthermore, bearings tested with Salox retainers exhibited less inner race wear

Film/Cage/Ball

MLS/BrPTFE/Bare
MLS/BrPTFE/Bare
MLS/BrPTFE/Bare
RFMS/BrPTFE/Bare
DCS/BrPTFE/Bare
None/BrPTFE/Bare
MLS/PTFE/Bare
RFMS/PTFE/Bare
RFMS/PTFE/Bare
DCS/PTFE/Bare
MLS/PTFE/Bare
MLS/PI/Bare
RFMS/PI/Bare
DCS/PI/Bare
MLS/PI+MoS/Bare
RFMS/PTFE/SiN
DCS/PTFE/SiN
MLS/PTFE/SiN
DCS/PTFE/MoS
MLS/PTFE/MoS
RFMS/PTFE/MoS
DCS/PI/MoS
MLS/PI/MoS
RFMS/PI/MoS

BrPTFE & PTFE retainers + plain balls

Polyimide retainers

Silicon Nitride balls

MoS2 coated balls

0.0 0.1 0.2 0.3 0.4 0.5 0.6 0.7 0.8 0.9 1.0

Δ track width/million cycles, mm/1E6 cycles

Fig. 5-45 Increase of ball/inner race track width per million test cycles.

than those tested with Duroid retainers when coated with the same $MoS_2$ film (Fig. 5-46). The abrasive nature of the chopped, glass fiber reinforcement used in the Duroid retainers may of contributed to wear. In contrast, the Salox retainer material, which contains only bronze in addition to the PTFE, is not as likely to abrade the metal surfaces.

The loss in preload generally correlates with the increase in track width (see Fig. 5-47). This is a consequence of the internal clearance change of the hard (built-in) preloaded test bearings and its affect on contact angle variation. Apparently, the retainer film transfer rate was insufficient to offset the race film loss and any metal wear. An imbalance in this process could account for occasional periods of torque increase observed during life where the retainer temporarily over-transfers a thicker deposits and torque decrease when the transfer film does not keep up with film loss.

Internal preload of the hard preloaded, test bearing is quite sensitive to losses in race coating thickness. For example, a loss of 50% of a nominal 1 μm thick film on both races reduces preload by approximately 9 lb based on preload measurements. Thinner films would thus be preferred from this point of view. The remaining thickness of $MoS_2$ plus retainer transfer film left on post-test examined bearings generally agrees with the observed loss in preload.
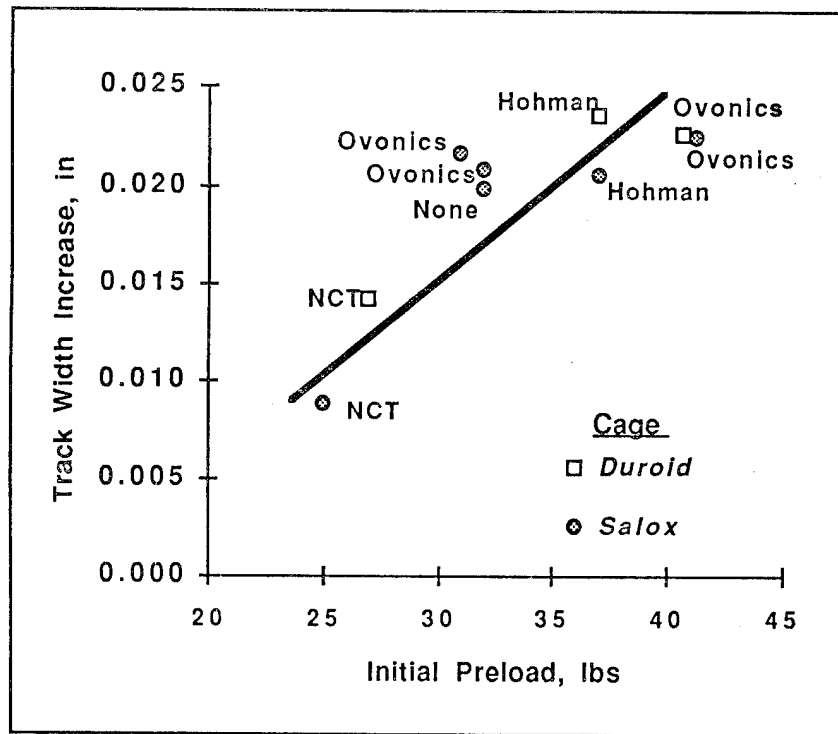
Fig. 5-46  Correlation of track width increase with initial preload for long-lived bearings. Note that wear is proportional to initial preload
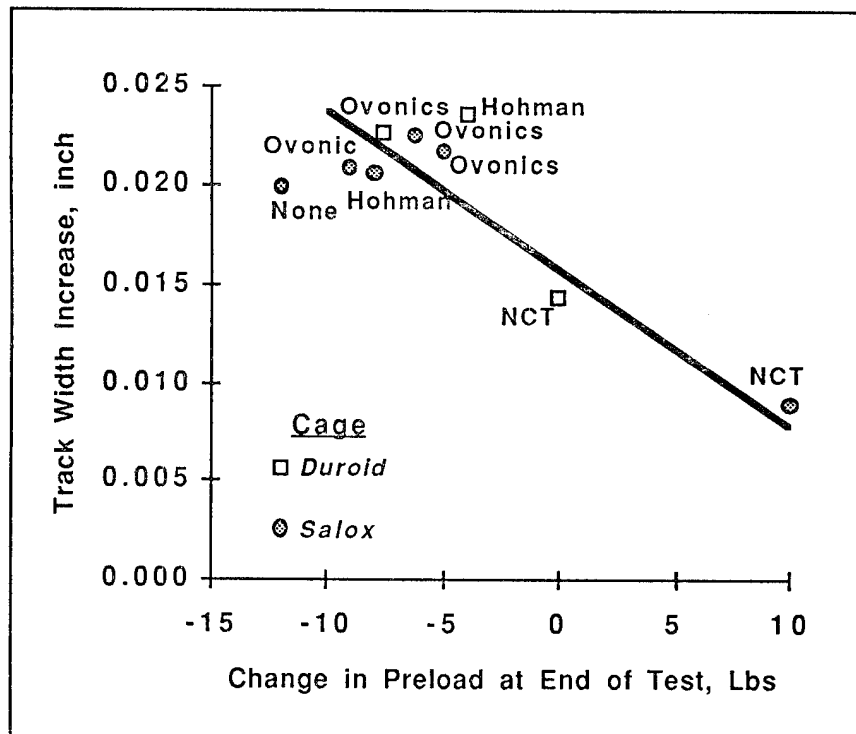


Fig. 5-47  Correlation of track width increase with preload change for long-lived bearings

From an application standpoint, the torque and preload performance of MoS$_2$ lubricated bearings would benefit from spring rather than hard preload. Spring-preloading would reduce debris-related torque excursions and mitigate preload variations. However, spring loading is not always compatible with stiffness driven applications, such as rapid scanning space gimbals, where high structural natural frequencies are generally desired.

### 5.3.6 Comparison with Liquid Lubricants

Comparative life tests were conducted with 105 size bearings lubricated with traditional space gimbal bearing greases and those being considered for near future applications. These tests were to serve as a "benchmark" to judge the relative performance of the MoS$_2$ film bearings. Four synthetic, vacuum stable lubricants were tested with either plain steel balls, those ion-sputtered with titanium nitride (TiN) or with solid Si$_3$N$_4$ balls (Table 5-48). The test greases consisted of a 148 cS at 40°C perfluoro polyalkylether oil in a PTFE thickener (PFPE grease or Bray 600™), a 60 cS neopentyl ester oil in lithium sterate thickener +1% TCP (NPE grease or Rheolube 952™), a 56 cS polyalphaolefin oil (181B™) in a cabosil thickener +1% TCP (PAO grease) and a 110 cS multiply-alkylated cyclopentane (MAC or Pennzane 2000™) oil in a sodium octadecyl terephthalanate thickener (Rheolube 2000™) with 3.5% lead naphthanate (PbNp) for antiwear. All bearings were tested with polyimide ball retainers (Vespel™).

**Table 5-48  Summary of comparative 105-size liquid lubricated test bearing combinations**

| Post | †Lube | ††Ball | #Race | Preload Start lbs | Initial Mean Hertz Strs KSI | | |
|---|---|---|---|---|---|---|---|
| | *Bray 600 Grease (PTFE thickener)* | | | | | preload | stress |
| 4.1a | PFPE | Bare | Bare | 26 | 103 | Average | |
| 4.6a | PFPE | Bare | Bare | 25 | 102 | 31 | 109 |
| 1.12 | PFPE | Bare | TCP | 25 | 102 | one-sigma | |
| 1.6 | PFPE | SiN | Bare | 34 | 130 | 4.9 | 6 |
| 1.5 | PFPE | SiN | Bare | 35 | 131 | | |
| 1.3 | PFPE | TiN | Bare | 35 | 114 | | |
| 4.2b | PFPE | TiN | Bare | 34 | 113 | | |
| | *Bray 815Z Oil + antiwear additive* | | | | | | |
| 4.4a | PFPE | Bare | Bare | 27 | 105 | | |
| | *PAO Grease (181B oil + Cabosil thickener)* | | | | | | |
| 4.11b | PAO | Bare | Bare | 25 | | | |
| 4.9a | PAO | Bare | Bare | 29 | 107 | | |
| | *Rheolube 952 Grease (UC9 oil + lithium thickener)* | | | | | | |
| 4.7a | NPE | Bare | Bare | 28 | 106 | | |
| 4.8a | NPE | Bare | Bare | 25 | 102 | | |
| | *Rheolube 2000 Grease (Pennzane + Na thickener)* | | | | | | |
| 4.5a | MAC | Bare | Bare | 32 | 111 | | |
| 4.2a | MAC | Bare | Bare | 35 | 114 | preload | stress |
| †Lube: *PFPE=Perfluoropolyalkyl ether, PAO=* | | | | | | Average | |
| *Polyalphaoelifin, NPE= Neopentyl ether,* | | | | | | 30 | 108 |
| *MAC=Multiple alkylated cyclopentane* | | | | | | one-sigma | |
| ††Ball: | | | | | | 4.3 | 5 |

titanium nitride coating, SiN=Monolithic silicon nitride

#Race: *Bare= Untreated 52100 steel, TCP=Tricrysl phosphate treatment*

- 87 -

PFPE greases have considerable space flight heritage due to their very low vapor pressure and low pour point. They are considered the traditional standard for the industry. Polyether and polyalphaolefin lubricants have also been used in space but not as extensively as the PFPE lubricants. The MAC lubricant is relatively new with no current flight data but has received some limited ground testing. The MAC lubricant is considered as a potential replacement to the PFPE oils because of its ability to accept antiwear additives and its very low outgassing capabilities. Its cold temperature performance while on a par with the other synthetic oils is not as good as with the PFPE fluids. This lubricant was introduced relatively late in the test program at about the same time it was started on test in the 5-inch OD test bearing.

**Test Conditions** The liquid lubricated bearings were assembled in the same fashion as those for the $MoS_2$ tests, except that the bearing races were grease plated in a freon bath with the test lubricant (approximately 15% by weight) and then vacuum dried. Bearing preloads were comparable to those used in the $MoS_2$ tests (see Table 5-48). Mean Hertzian stress levels averaged 110 ksi and 108 ksi for the dry and wet 105-size test bearings, respectively.

The test cycle was the same as before except that the test speed was reduced by about 50% to ensure that the bearings operated primarily in the boundary lubrication regime (see Section 4.3.2 Test Cycle). The stop/start, oscillatory nature during gimbaling provided substantial periods where the elastohydrodynamic film thickness was much smaller than the composite surface roughness or lambda ratio. Lambda ratio ranged from zero at end of stroke to a peak of 1.1, 0.4 and 0.4 at mid stroke for the PFPE, NPE and PAO greases, respectively.

All four greases were life tested with plain steel balls while just the PFPE grease was also tested with ceramic and ceramic coated balls (see Table 5-48). Each combination was tested twice for a total of 10 bearing tests. A PFPE oil (Bray 815Z) with a special antiwear additive was also tested.

**Test Results** All of the greased lubricated bearing pairs with plain balls showed steady low torque for the first 30 million test cycles (see Fig. 5-49). The only exception is the two bearings lubricated with the MAC grease, Fig. 5-49(g)-(h). While the influence of gimbal cycle mode is apparent for all grease lubricated bearings, it is however very strong for the MAC bearings. The high, intermittent bearing torque in MAC lubricated bearings appeared to be associated with deposits of wear products, degraded lubricant, lubricant thickener and/or antiwear additive in the ball track. They generally occur during the 360° rotation of the duty cycle. On the other hand, the NPE and PAO grease bearings showed low, steady torque performance to beyond 35 million cycles, Fig. 5-49(c)-(e). The PFPE grease started to show signs of degradation at ≈ 20 million cycles and hard failure at about 30 million cycles, Fig. 5-49(a).

In contrast, both PFPE lubricated bearing pairs with silicon nitride balls showed erratic torque, Fig. 5-50(c)-(d), as did one of the two pairs of TiN coated balls, Fig. 5-50(a). Post test inspection showed that the sputtered TiN ball coating had failed in one of the bearings. The other bearing, Fig. 5-50(b), showed no such problem. Quality control for ceramic coated balls is quite demanding since a defect on any one ball in the ball set can lead to gross failure and non-destructive inspection is not currently possible.
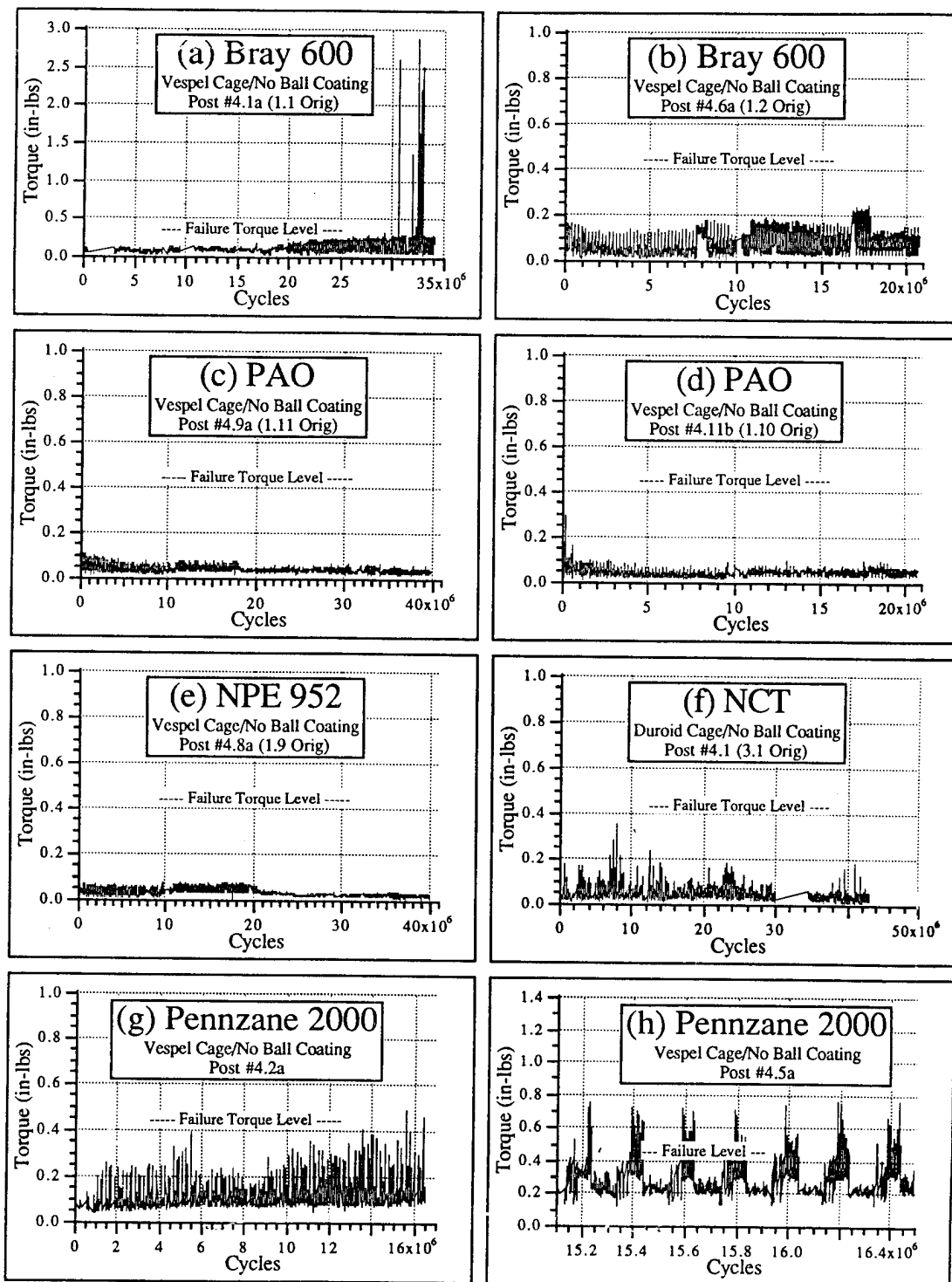
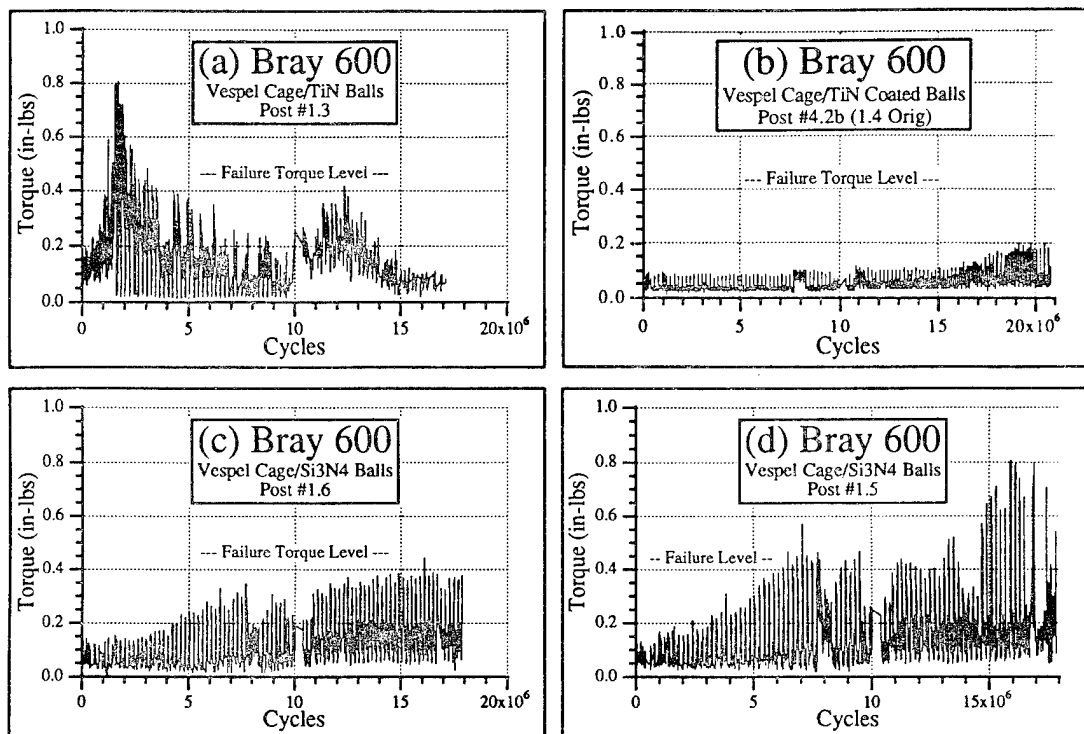**Fig. 5-49  Torque histories of grease lubricated 105 size bearings having plain balls.**

**Fig. 5-50** **Torque histories of grease lubricated 105 size bearings having ceramic balls showing reduced lives**

**Torque Signatures** Representative torque signatures for the greased 105 size bearings appear in Figs. 5-51 to 5-55. The NPE and PAO lubricated bearings show little change in torque signature over life. The PFPE greased bearing torque signature is clearly degraded at 34.09 million cycles but unchanged at 17.9 million (Fig. 5-53). In contrast, the PFPE greased bearings with TiN coated or silicon nitride balls showed inferior torque signatures (Fig. 5-54). Degradation in torque performance is also evident with the MAC greased bearings (Fig. 5-55).

**Comparison with MoS2 Film Bearings** Cycle life to 0.44 in-lb in addition to detailed preload, wear and torque data is summarized in Table 5-56 for the liquid lubricated bearings. Preload changes and wear track width increases are relatively small for the non-failed bearings compared with those lubricated with $MoS_2$ film (Table 5-24).

Torque signatures associated with the liquid lubricated bearings were generally superior to those solid film lubricated. Fig. 5-57 shows a direct torque history comparison between $MoS_2$ and grease lubricated bearings. Fig. 5-58 shows a representative middle of life (13 to 20 M cycles) torque signature comparison. Some of this torque smoothness advantage is due to less debris and lower retainer friction associated with the wet bearings.
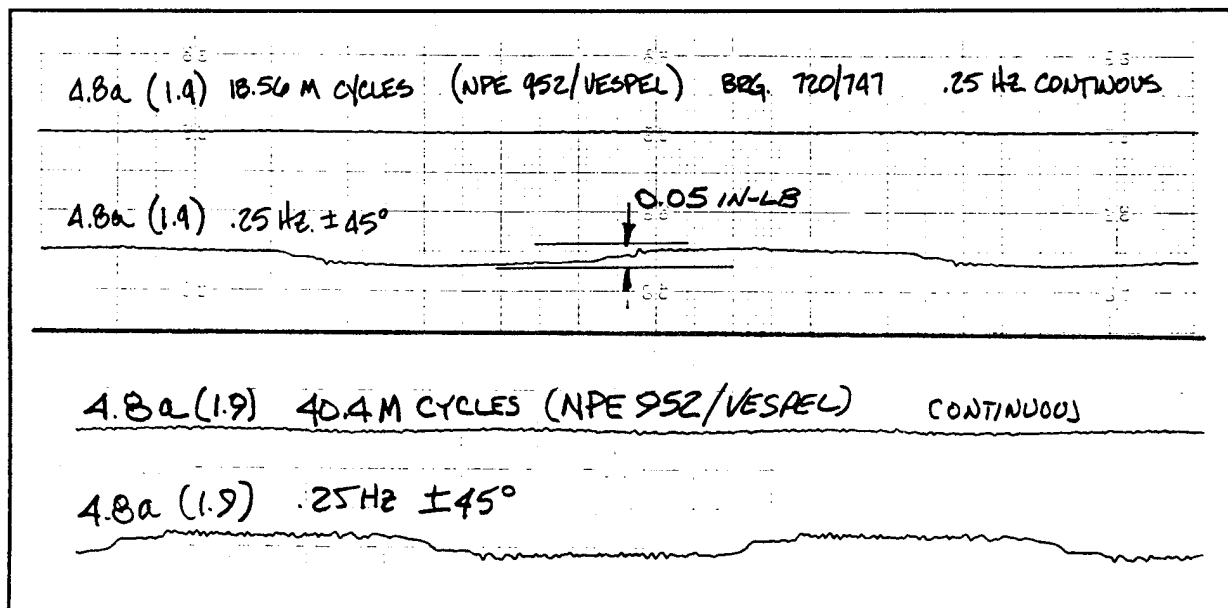
Fig. 5-51   Torque signatures for NPE greased bearing at 18.6M & 40.4M cycles
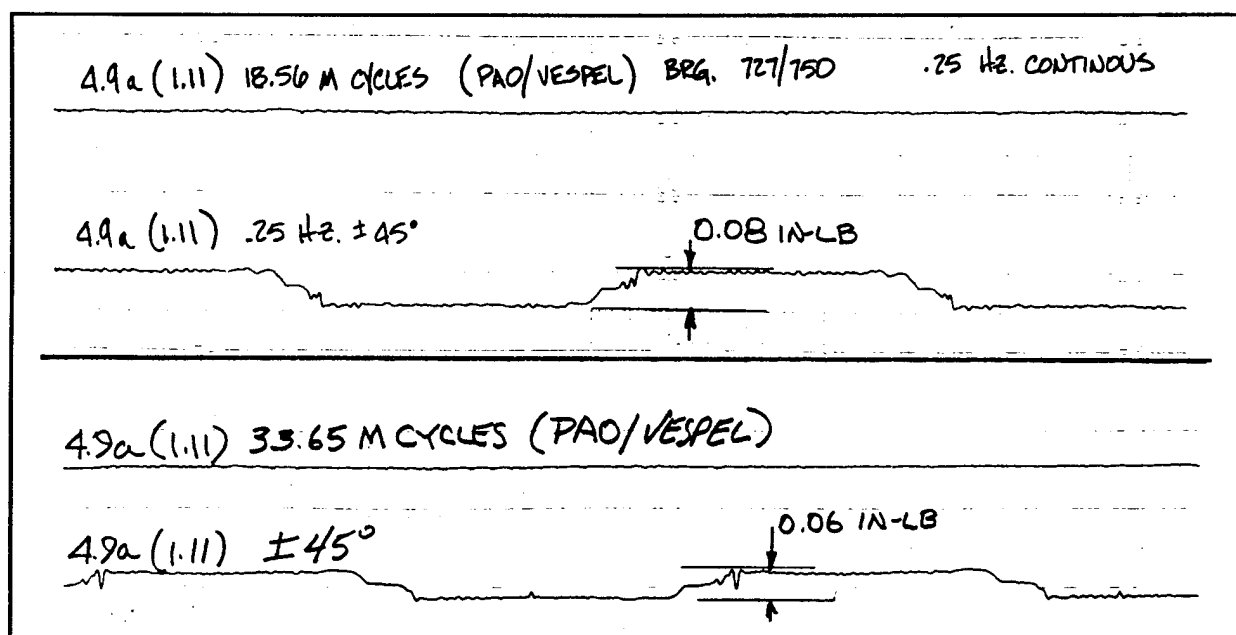


Fig. 5-52   Torque signatures for NPE greased bearing at 18.6M & 33.7M cycles
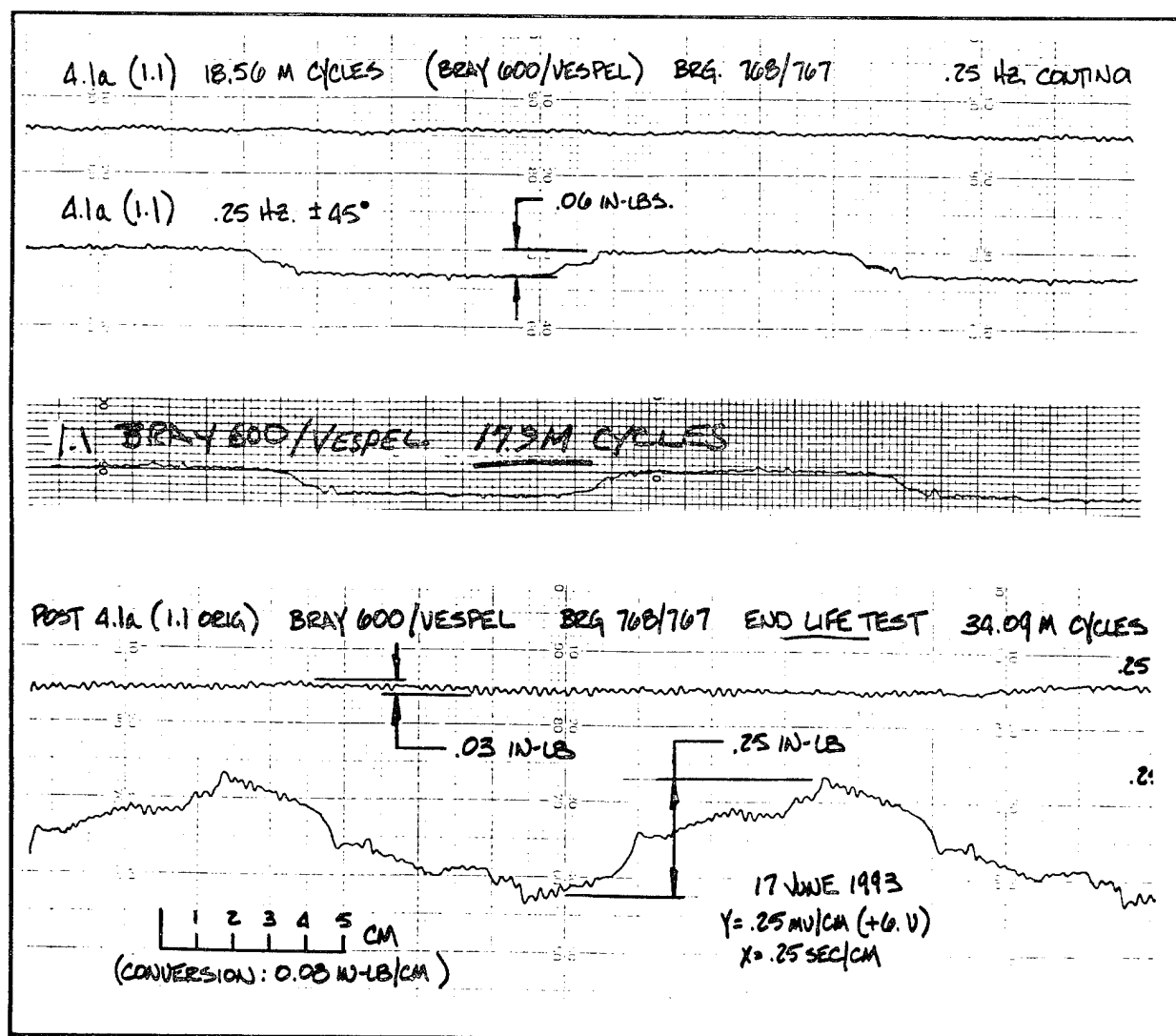
Fig. 5-53 Torque signatures for PFPE greased bearing at 0, 18M and 34 M cycles
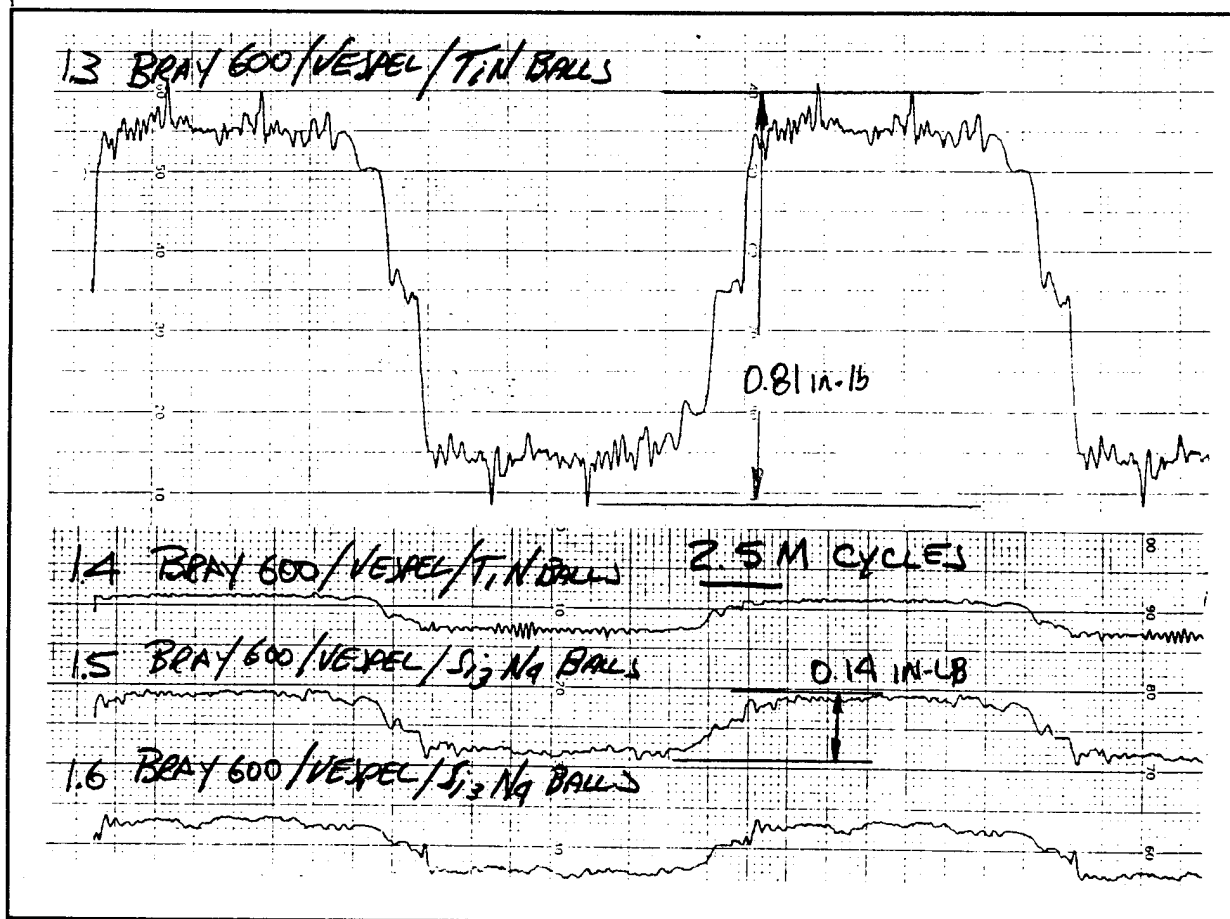
(a)  2.5 Million test cycles
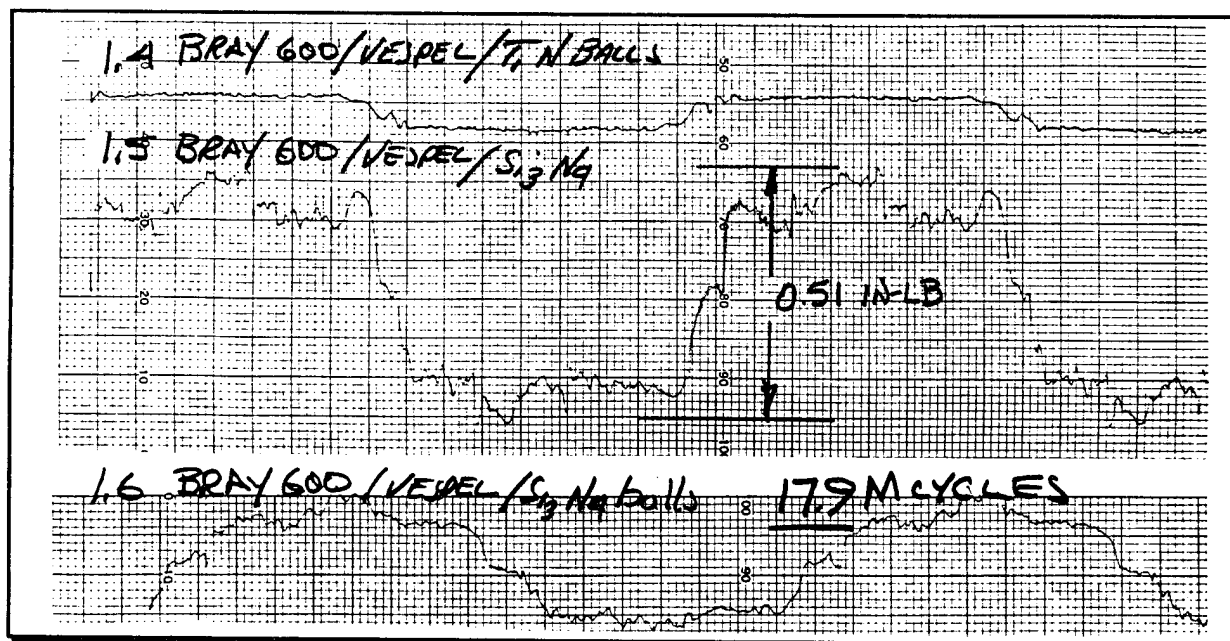


(b)  17.9 Million test cycles

**Fig. 5-54  Torque signatures for ceramic treated balls in PFPE greased bearings**

- 93 -
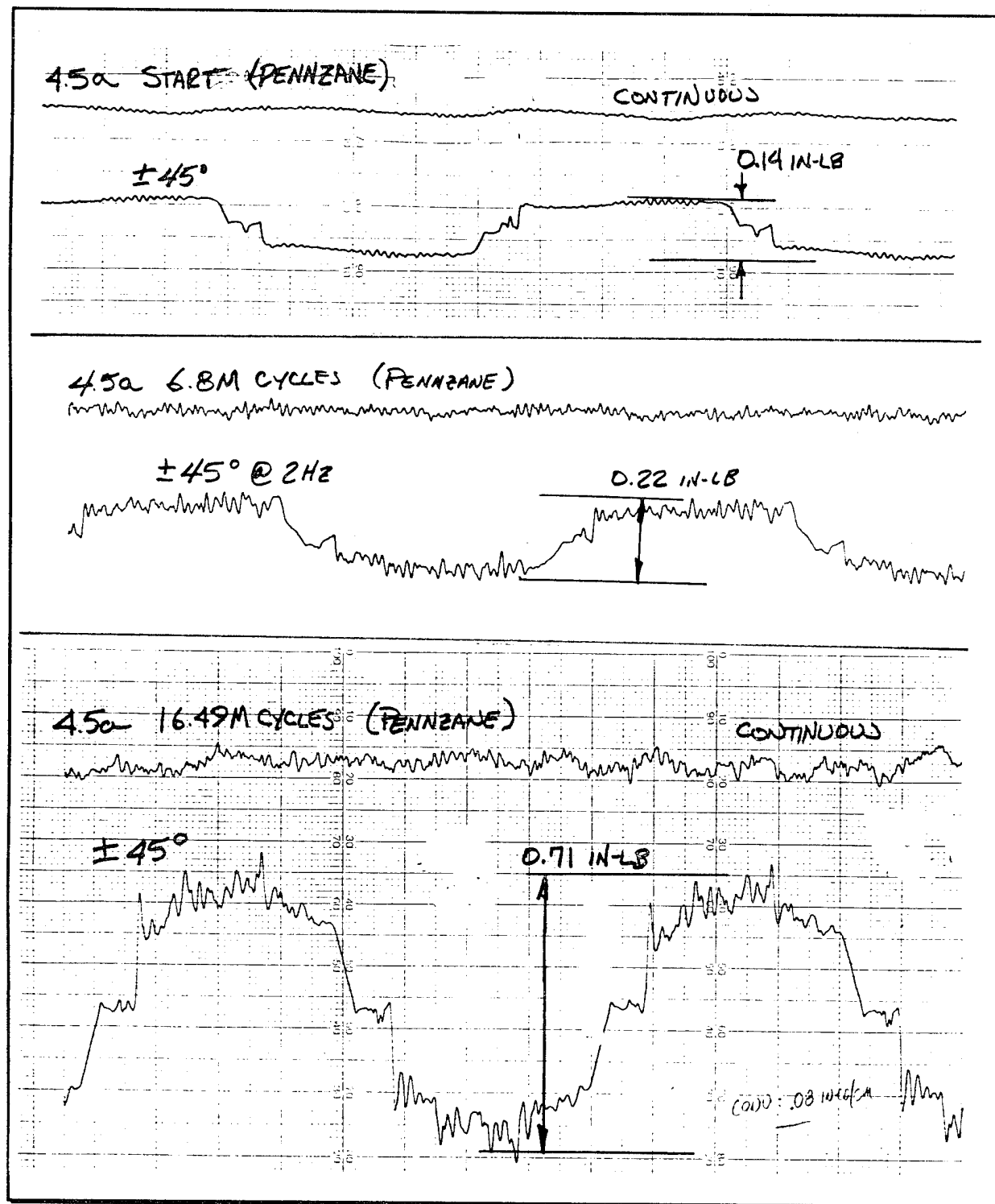
**Fig. 5-55   Torque signatures for MAC greased bearing at 0, 6.8M and 16.5 M cycles**

## Table 5-56 Summary of 105-size bearing performance with liquid lubricants

| Post | †Lube | ††Ball | #Race | *Status | Life in Mcycles to 0.44 in-lbs Cutoff | Life in Mcycles to at Test Cutoff | **Max Torque, in-lbs Typ. Running low | high | Peak Excurs | End of test | Preload, lbs Start | End | Change | #Ball/Inner Race Track Width, in at end of test | Hertzian calculated | Increase | Initial Mean Hertz Strs KSI |
|---|---|---|---|---|---|---|---|---|---|---|---|---|---|---|---|---|---|
| *Bray 600 Grease (PTFE thickener)* | | | | | | | | | | | | | | | | | |
| 4.1a | PFPE | Bare | Bare | F | 30.6 | 34.1 | 0.05 | 0.12 | 2.6 | 0.3 | 26 | 22 | | 0.03 | 0.024 | 0.006 | 103 |
| 4.6a | PFPE | Bare | Bare | R | | 24.5 | 0.03 | 0.16 | 0.23 | 0.18 | 25 | | | N/A | 0.024 | | 102 |
| 4.2b | PFPE | Bare | TiN | R | | 17.8 | 0.05 | 0.09 | 0.2 | | 34 | | | 0.031 | 0.025 | 0.006 | 113 |
| 1.12 | PFPE | Bare | TCP | F | 8 | | 0.05 | 0.30 | 1.2 | 1 | 25 | | | 0.039 | 0.024 | 0.015 | 102 |
| 1.5 | PFPE | SiN | Bare | F | 6.2 | | 0.07 | 0.20 | 0.6 | 1 | 35 | | | N/A | 0.027 | | 131 |
| 1.6 | PFPE | SiN | Bare | F | 3.7 | | 0.07 | 0.15 | 0.42 | 0.38 | 34 | | | 0.038 | 0.027 | 0.011 | 130 |
| 1.3 | PFPE | Bare | TiN | F | 1 | | 0.16 | 0.30 | 0.90 | 0.1 | 35 | | | 0.067 | 0.027 | 0.040 | 114 |
| *Bray 815Z Oil + Antiwear additive* | | | | | | | | | | | | | | | | | |
| 4.4a | PFPE | Bare | Bare | TC | | 37.3 | 0.05 | 0.09 | 0.15 | 0.22 | 27 | 22 | -5 | 0.029 | 0.025 | 0.004 | 105 |
| *PAO Grease (181B oil + Cabosil SiO2 Thickener)* | | | | | | | | | | | | | | | | | |
| 4.9a | PAO | Bare | Bare | TC | | 40.4 | 0.02 | 0.05 | ††0.11 | 0.05 | 29 | | | 0.029 | 0.025 | 0.004 | 107 |
| 4.11b | PAO | Bare | Bare | R | | 24.5 | 0.03 | 0.08 | †0.16 | 0.06 | 25 | | | N/A | 0.024 | | 102 |
| *Rheolube 952 Grease (UC9 oil + lithium thickener)* | | | | | | | | | | | | | | | | | |
| 4.8a | NPE | Bare | Bare | TC | | 40.4 | 0.03 | 0.07 | 0.08 | 0.03 | 25 | | | 0.028 | 0.024 | 0.004 | 102 |
| 4.7a | NPE | Bare | Bare | R | | 24.5 | 0.03 | 0.07 | 0.11 | 0.04 | 28 | | | N/A | | | 106 |
| *Rheolube 2000 Grease (Pennzane + Na thickener)* | | | | | | | | | | | | | | | | | |
| 4.5a | MAC | Bare | Bare | F | 16.5 | 16.5 | 0.2 | 0.50 | 0.7 | 0.8 | 32 | 36 | 4 | 0.046 | 0.027 | 0.019 | 111 |
| 4.2a | MAC | Bare | Bare | F | 1.1 | 16.5 | 0.08 | 0.28 | 0.4 | | 35 | 30 | -5 | 0.032 | 0.027 | 0.005 | 114 |

†0.16:   Two startup torque excursions of .8 and .42 in-lb observed at 100K and 600K, respectively for PAO

††0.11:   Two startup torque excursions of .44 and .16in-lb observed at 100K and 600K, respectively for PAO

†Lube:   PFPE=Perfluoropolyalkyl ether, PAO= Polyalphaolefin, NPE= Neopentyl ether, MAC=Multible Alkylated Cyclopentane

††Ball:   Bare= Untreated 52100 steel, TiN=Ion-sputtered titanium nitride coating, SiN=Monolithic silicon nitride

#Race:   Bare= Untreated 52100 steel, TCP=Tricrysl phosphate treatment

*Status:   F=failed at 0.44 in-lb, TC= test cutoff, R= still running on test.

**Max Torque:   Typ. Running= Typical bearing torque range from low to high, Peak Excursion = highest torque recorded during run, End of Test = torque at test cutoff or failure.

#Ball/Inner Race Track Width:   Averaged upper and lower bearing track width
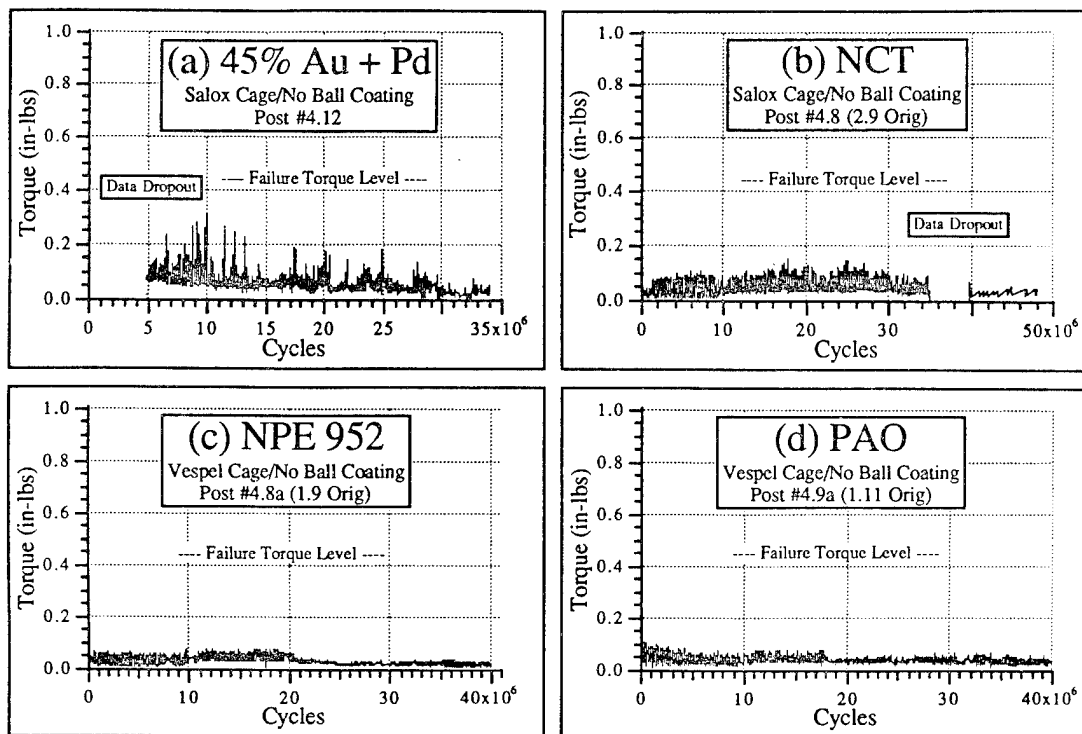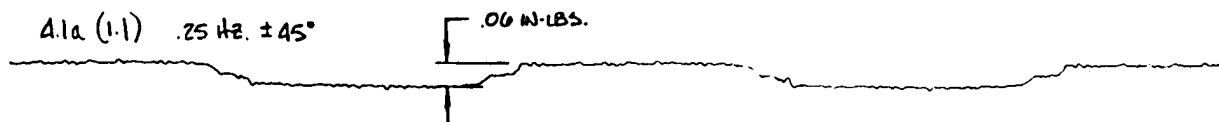
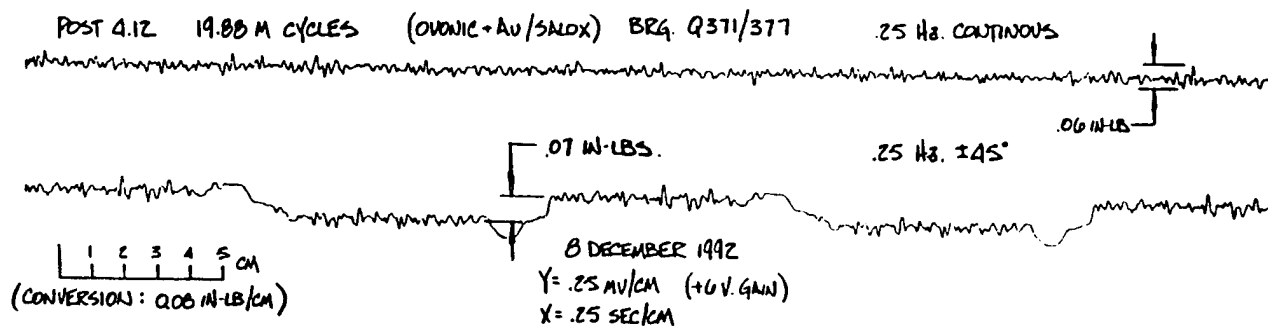**Fig. 5-57  Torque history comparison of MoS2 and Grease Lubricated 105 bearings**

At approximately 12 million cycles, the torque and torque ripple of the best MoS2 coated bearings from each of the three sources is quite competitive with the Bray 600 grease as shown in Fig. 5-59. These signatures, taken at about 12 million cycles for 3 of the lubricants, show ± 45 ° gimbaling torque together with torque under continuous CW and CCW rotation at 1 Hz (90 °/s).

The effect of slew rate on bearing torque was investigated. Fig. 5-60(a) shows that peak to peak torque of MoS2 coated bearings (Ovonics #2.10) are relatively insensitive to gimbal rate unlike the grease lubricated bearings (Bray 600 #1.1) are quite sensitive, Fig. 5-60(b). Rate increases from 0.1 Hz (± 8 deg/sec) to 1 Hz (± 80 deg/sec) can triple drive torque, due to viscous grease effects, according to the data in Fig. 5-61. Thus, the torque levels with MoS2 bearings become more attractive than grease lubricated bearings for applications with high scan rates and/or cold temperature operation.

- 96 -

4.1a (1.1) 13.56 M CYCLES (BRAY 600/VESPEL) BRG. 768/767     .25 Hz. CONTINOUS

4.1a (1.1)   .25 Hz. ±45°         .06 IN·LBS.

**Torque Signature (Peak & Ripple) of Bray 600
105-Size Bearing at 13.56M Cycles**

POST 4.12   19.88 M CYCLES   (OVONIC+AU/SALOX) BRG. Q371/377     .25 Hz. CONTINOUS

.06 IN·LB

.07 IN·LBS.                    .25 Hz. ±45°

1 2 3 4 5 CM
(CONVERSION: 0.08 IN·LB/CM)

8 DECEMBER 1992
Y= .25 MV/CM  (+6 V. GAIN)
X= .25 SEC/CM

**Torque Signature (Peak & Ripple) of Ovonics + Au
105-Size Bearing at 19.88M Cycles**

**Fig. 5-58   Comparison of Grease and MoS2 lubricated 105 size bearing
torque signature at mid-life**
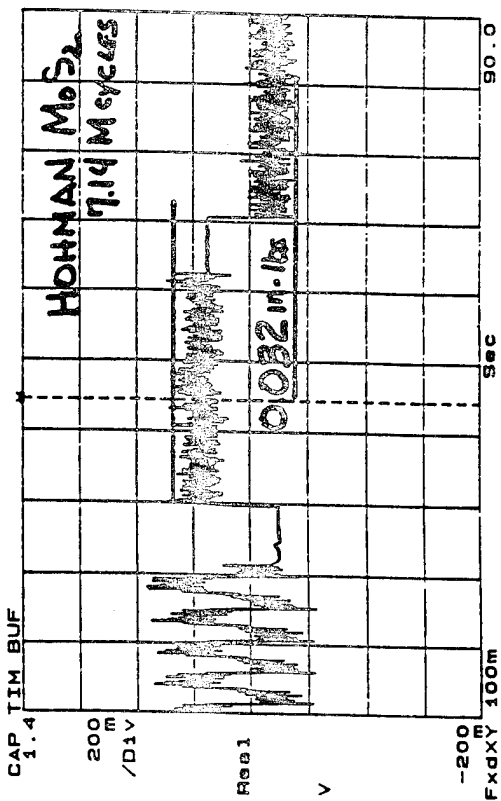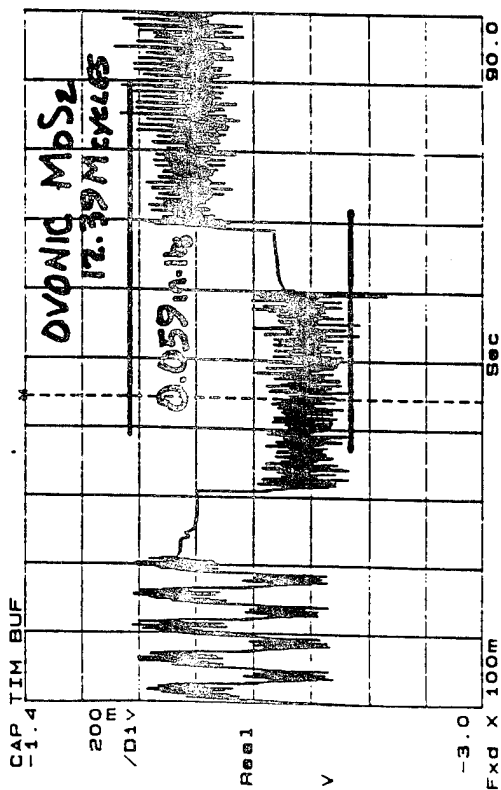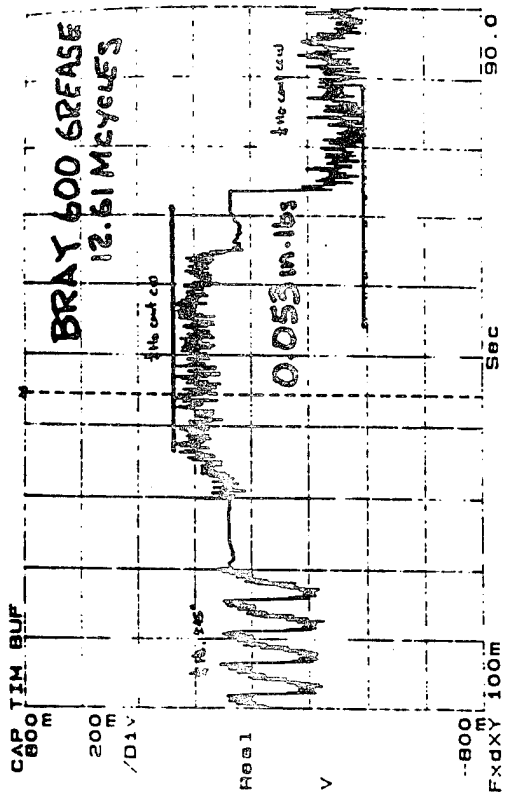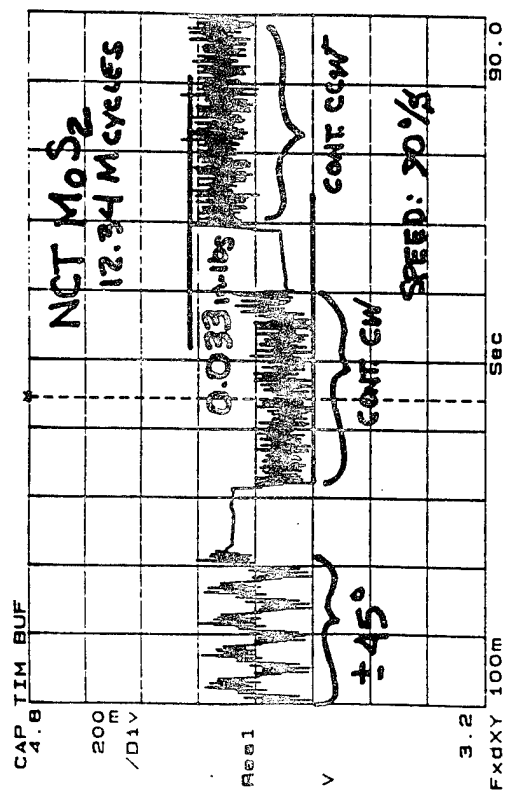
Fig. 5-59 Torque signature comparison of MoS2 & greased bearings at 12 million cycles

CAP TIM BUF
-1.4

200 m /Div

0.1Hz, ±80°       0.25Hz, ±80°       1Hz, ±80°

Real

V

0.108 in-lb pk-pk       0.105 in-lb pk-pk       0.081 in-lb pk-pk

-3.0

FxdXY 100m       Sec       90.0
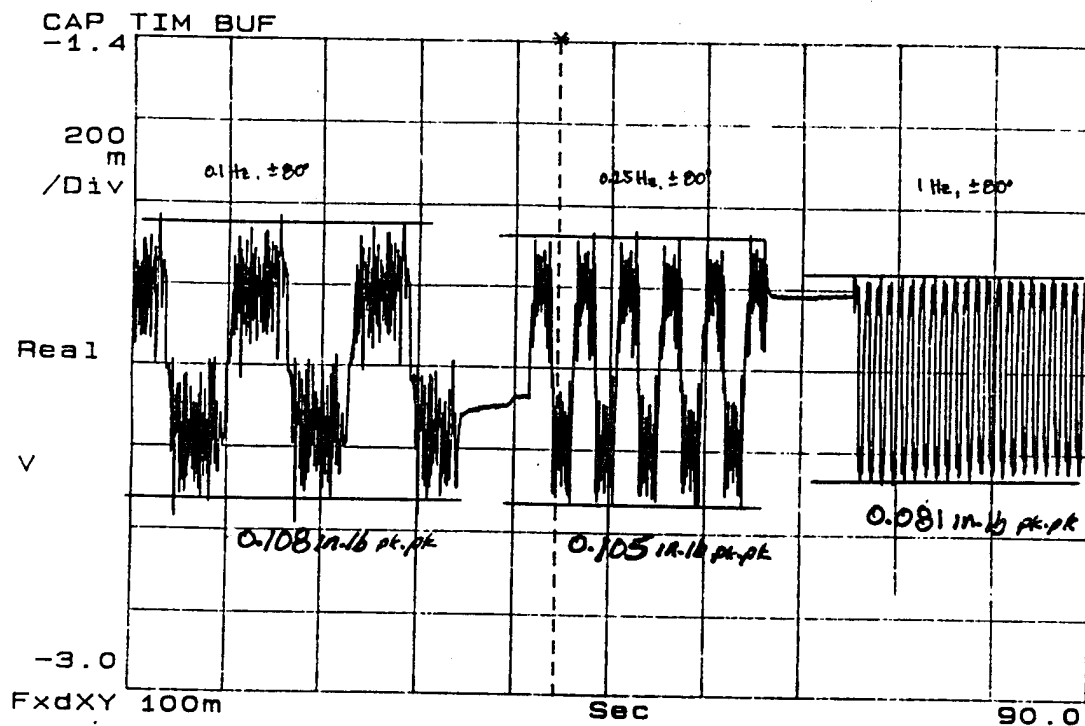
**(a) Ovonics MoS$_2$ film bearing, post #2.10   @12.34 M cycles**

CAP TIM BUF
800 m

200 m /Div

0.1Hz, ±80       0.25Hz, ±80°       1Hz, ±80°

Real

/

0.060 in-lb pk-pk       0.093 in-lb       0.183 in-lb pk-pk

-800 m

FxdXY 100m       Sec       90.0
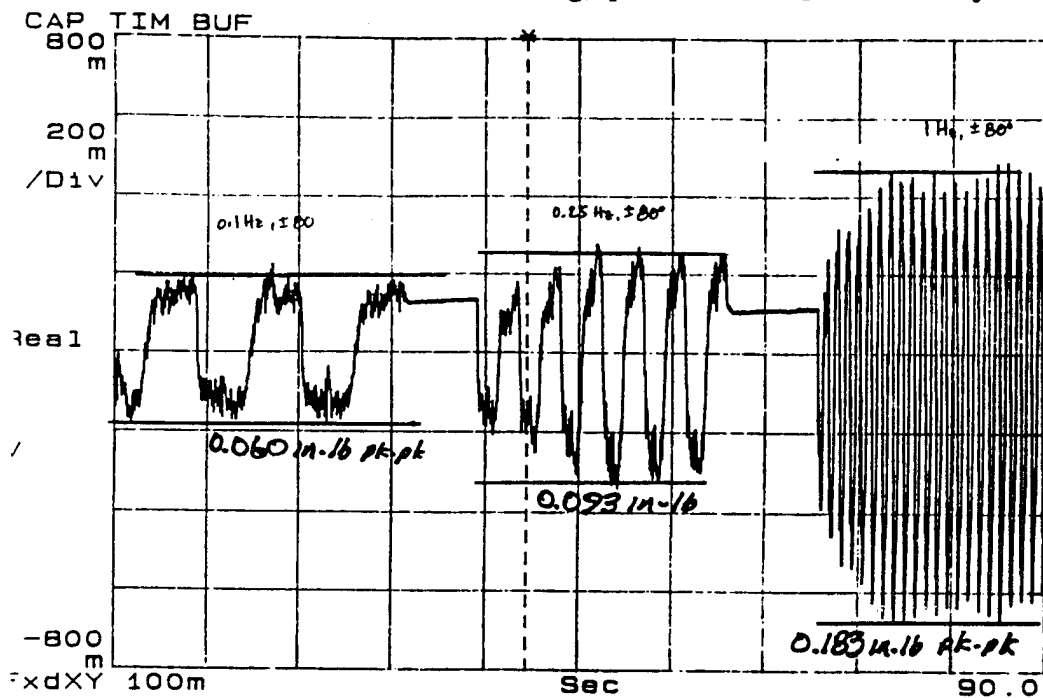
**(b) Bray 600 grease bearing, post #1.1   @12.61 M cycles**

**Fig. 5-60 Torque sensitivity to gimbal rate at ± 80 deg gimbal angle**
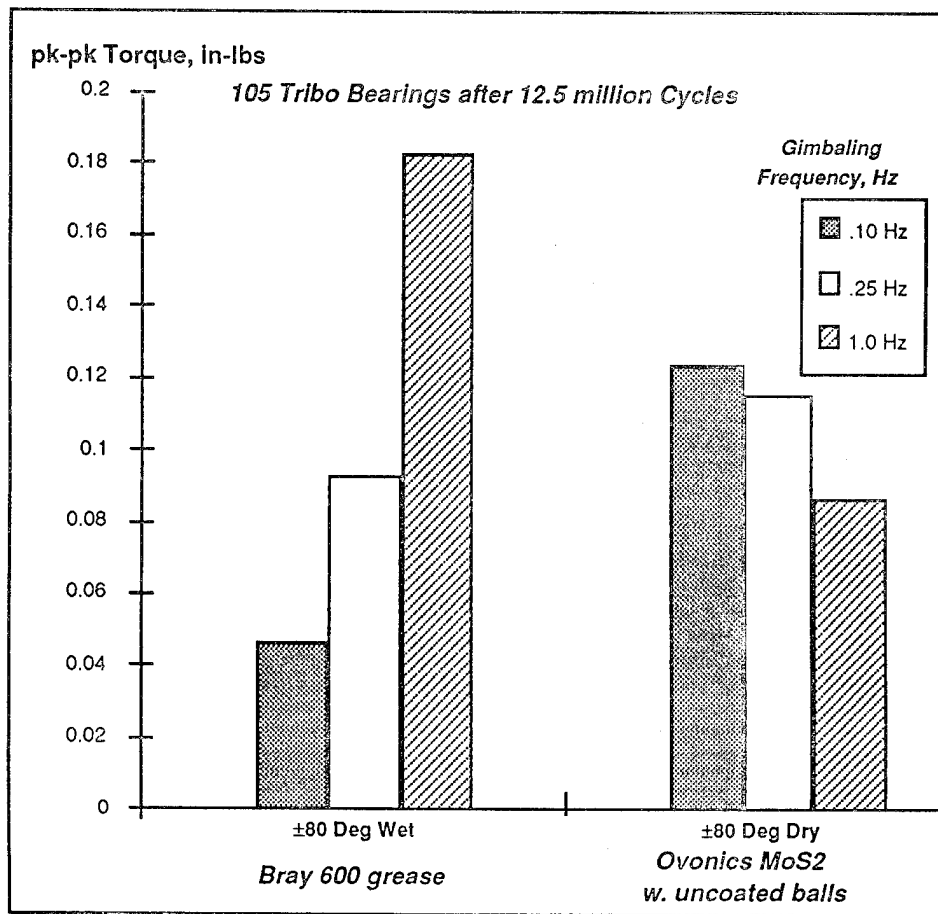
**Fig. 5-61 Gimbal rate has significant effect on grease lubricated bearing torque**

## 5.4 RESIDUAL GAS ANALYSIS (RGA) OF TEST CHAMBERS

In the course of the bearing life tests, the atmosphere of two test chambers was analyzed by mass spectroscopy (residual gas analysis). This was to assure that there was no significant presence of any high molecular weight species, such as oils, to contaminate the $MoS_2$ film test bearings. A portable quadrapole sensor head replaced the cold cathode vacuum gage (the RGA has vacuum measuring capability). The RGA mass range of 300 atomic mass units (AMU) was sufficiently high to capture high molecular weight species such as Freon.

The system was also attached to the test chamber with the liquid lubricated 105-sized bearings. Eight hours after venting and pump down, the vacuum level was in the $10^{-7}$ torr range. This vacuum level is consistent with expected gimbal usage. While initial spectra (obtained within an hour of pump down) contained some components from gasket, finger oils and cleaning solvents, these high molecular weight components were practically eliminated after the first day. Water vapor was by far the largest component in the atmosphere with smaller amounts of hydrogen and nitrogen also present (Fig. 5-62). The peak heights in the spectra provide a rough indication of quantities of residual gas present. High molecular weight species (> 40 amu) appear to be very small. This indicates the outgassing from gaskets, wire insulation, and lubricants are small and/or efficiently eliminated by the turbomolecular pump. Note that efficiency of turbomolecular pumps increase with gas molecular weight; the heavier the molecular weight of the residual gas the more efficiently it is pumped away by the turbopump. This vacuum environment is typical of

a clean, un-baked turbomolecular pumped system. After a few days at vacuum, only water vapor, hydrogen, and nitrogen were detected (Fig. 5-63). The RGA was also attached to the test chamber containing two 117-sized (5 inch OD) bearings with the Ovonics multilayer, fracture resistant films. As expected, the results were essentially the same.
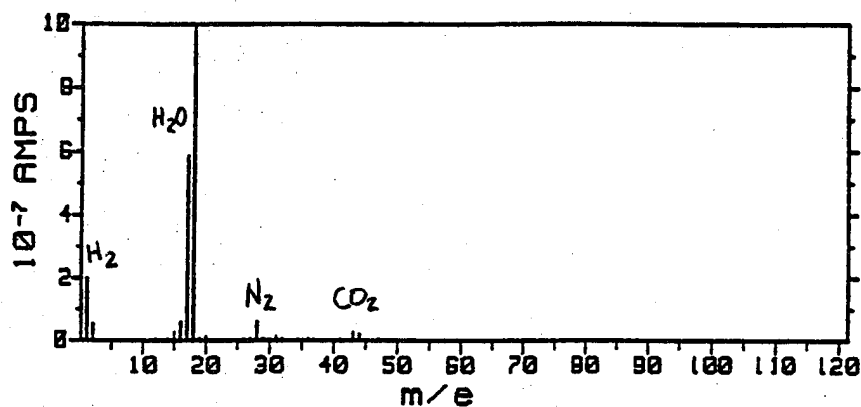


Fig. 5-62    Residual gas analysis of vacuum chamber containing 105-sized thin film bearings after initial pump down. Spectral peaks associated with hydrogen ($H_2$) , water vapor ($H_2O$),nitrogen ($N_2$) and carbon dioxide ($CO_2$) are denoted.
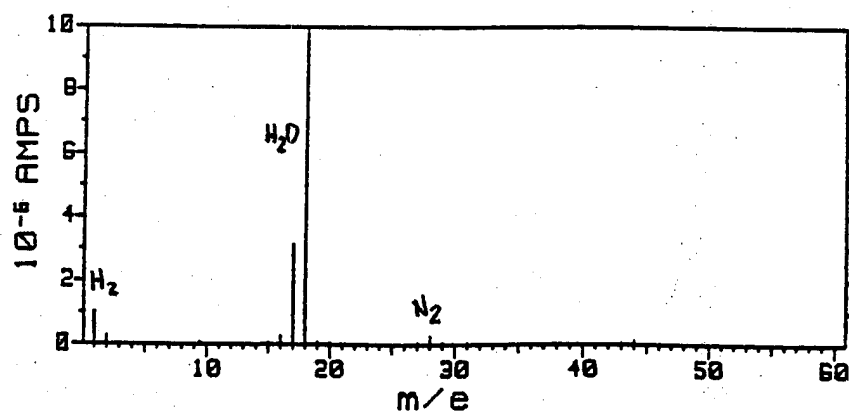


Fig. 5-63    Residual gas analysis of vacuum chamber containing 105-sized thin film bearings after a few days of operation. Spectral peaks associated with hydrogen ($H_2$) , water vapor ($H_2O$), and nitrogen ($N_2$) dominate

- 101 -

## 5.5 KEY FINDINGS

**Thrust Bearings (5.1)** Thrust bearings provided an early, quick, inexpensive test specimen to evaluate different tribomaterials. However, their poor quality accelerated the wear process and resulted in early failures. Of the 14 different solid film lubricants, the NCT and Hohman $MoS_2$ films were the best performers and selected for subsequent tests. Diamond-like carbon films and ion-plated lead bearings gave poor performance.

**Life (5.3)** PTFE and/or PTFE-bronze composite retainers were required for long life (>40 million cycles) no matter which $MoS_2$ film deposition process was used. On the other hand, polyimide retainers, ceramic balls or those coated with $MoS_2$ had short lives, irrespective of the deposition process.

**Failure Mechanism (5.3)** Elevated torque were attributed to excess debris from film delamination and retainer transfer film material. Occasionally large torque excursions occurred between short stroke and long stroke modes due to rolled-over end of stroke debris and perhaps over-transfer of retainer transfer material. The match between retainer transfer rate and rate of film loss is critical for long life with reasonably constant torque.

**Torque Excursions (5.3.2)** Although torque excursions of 3 or 4X were occasionally encountered during test, the internally-generated high preload apparently accelerated film wear providing some self-limiting effect on torque. None of the long lived bearings, that is those with PTFE based retainers and uncoated steel balls, produced a hard jam torque failure (>10X torque), unlike bearings with $MoS_2$ coated balls or those with $Si_3N_4$. Torque levels on some bearings improved with test cycles as the bearing film wore and the internal preload was relaxed. For example, the 52 lb high preload bearing had a high torque up until 41 million cycles and then dropped substantially from wear out. The bearing never jammed.

**Torque Signatures (5.3.2)** In general, lower gimbaling torques were associated with the smaller gimbaling motions ($\pm 10°$) where debris could be deposited between the ball paths and retainer material transfer to the ball/race contact was minimal. Large torque bumps from end-of-stroke debris was observed with large debris producing combinations, such as $MoS_2$ coated balls or polyimide retainers. The better long-lived $MoS_2$ bearings produced reasonably constant ( $\Delta < 25\%$) torque signatures through out life. However, the torque signature test taken at very long intervals rarely captured the transient torque excursion observed occasionally during the gimbaling life test. Thus real time torque monitoring during life testing is considered a must.

**Preload (5.3.4)** Compared to the choice of retainers and ball treatments, initial preload appeared to have less effect on life. Both long and short lived bearing groups had about the same statistical distribution of high and low preload values.

Preload levels increased for all but one of the bearings incorporating either $Si_3N_4$ balls or steel balls coated with $MoS_2$ at the time of failure. This coupled with the observation of copious amounts of $MoS_2$ dust in these bearings indicates that debris jamming contributed to torque failure. With one exception, long-lived bearings (> 40 million cycles) having PTFE or Br-PTFE type retainers with plain balls experienced some preload reduction or remained essentially unchanged. Preload losses of less than 20% were measured on some bearings with more than 40 million gimbal test cycles or about a 6% loss in stiffness.

From an application standpoint, the torque and preload performance of $MoS_2$ lubricated bearings would benefit from spring rather than hard preload. Spring-preloading would reduce debris-related torque excursions and mitigate preload variations. However, spring loading is not always compatible with stiffness driven applications, such as rapid scanning space gimbals, where high structural natural frequencies are generally desired.

**Track Widths (5.3.5)** Post test measured bearing track width was proportionately larger for bearings with higher initial preload, as might be expected from the classical wear equations. The loss in preload generally correlates with the increase in track width. This is a consequence of the internal clearance change of the hard (built-in) preloaded test bearings and its affect on contact angle variation.

**Comparison with Liquid Lubricants (5.3.6)** Torque signatures associated with the liquid lubricated bearings were generally superior to those solid film lubricated. However, the torque levels of the liquid lubricants were clearly speed sensitive where those $MoS_2$ lubricated were not. Combinations of cold temperature and high slew rates favor $MoS_2$ lubrication. The NPE and PAO lubricated bearings show little change in torque signature over life as did the PFPE greased bearing up until about 34 million cycles when torque degradation was observed. In contrast, the PFPE greased bearings with TiN coated or silicon nitride balls showed inferior torque signatures, and degradation in torque performance was also evident with the MAC greased bearings.

# References For Section 5

[5-1] Lockheed Missile and Space Co., "SDIO Tribomaterials/Precision Gimbal Demonstration Program Phase I Final Report," LMSC F279291, under SDIO Contract SDIO84-89-C-0028, 16 October 1989.

[5-2] Loewenthal, S.H.,"Two Gimbal Bearing Case Studies: Some Lessons Learned," NASA CP-2506, May 1988.

[5-3] Bauer, R., and Fleischauer, P.D.,"Torque Characteristics of Solid Lubricated Precision Bearings During Oscillatory Motion," Trib Trans. #93-002(in press) 1993.

[5-4] Roberts, E. W., "The Tribology of Sputtered Molybdenum Disulfide Films," Proc. Inst. of Mech. Eng., Tribology - Friction,Lubrication and Wear, Fifty Years On, Vol. I, (1987) pp. 503-510.

# Section 6  PRECISION GIMBAL BEARING TESTS

The 105-size bearing tests were used to identify the most promising $MoS_2$ film to be carried forward for full-scale, gimbal bearing tests. As discussed in Section 4.3, bearing sizes were picked to envelope those proposed for the Brilliant Eyes payload gimbals. The intent was to quantify the effects of bearing size on both film performance and film quality control, since no test data were available on bearings of the size needed for the larger SDI payload gimbals.

Life tests with torque monitored were conducted on seven pairs of 117-size (5 inch OD) bearings and four pairs of 12 inch OD size bearings. The test matrix and summary of performance appears in Table 6-1. The multilayer Ovonics $MoS_2$ film with Salox retainers was selected for full scale evaluation based on its long term performance and consistency of the deposition process as described in Section 7.3. The two alternate films, Hohman and NCT, also showed long lives with poly-tetrafluoroethylene (PTFE) based retainers and were close second choices. The neopentyl ester based grease was selected as the benchmark liquid lubricant for the 12-inch bearing tests based on its exceptionally low torque throughout life. Its performance was closely paralleled by the polyalphaolefin grease. The MAC grease was selected for the 5-inch OD (117-size) bearings relatively late in the test program based on reports of good performance from outside sources, although no 105-size bearing test data were yet available.

**Table 6-1  Summary of precision gimbal bearing performance with MoS2 and grease lubrication.**

**117-Size and 12 inch Ovonics MoS2 Lubricated Bearings**

| S/N | Post | †Film | Status | Life at Test Cutoff Mcycles | ** Max Gimb Torq, in-lbs Typical low | Typical high | Peak Excurs | End of test | ††Torq@1°/s, 3 revs, in-lbs Start Avg. | Start #hash | End or Failure Avg. | End or Failure hash | Preload, lbs Start | End | Change | Initial Mean Hertz Strs KSI | Axial Stiffness 10^3 lbs/in start | end |
|---|---|---|---|---|---|---|---|---|---|---|---|---|---|---|---|---|---|---|
| | | | **12 inch Bearing** | | | | | | | | | | | | | | | |
| #5a | 1.2a | MLS+Au | suspended 3/93 | 12.72 | 3.0 | 5.0 | 27.0 | 7.0 | 1.2 | 1.7 | 2.3 | 4.1 | 222 | 188 | -34 | 99 | 1,010 | 890 |
| #3 | 1.1a | MLS+Au | failed/10/92 (re-cleaned) | 4.5 | 3.0 | 5.0 | 13.0 | | 1.3 | 2.5 | 6.4 | 3.1 | 241 | 293 | 52 | 102 | - | 992 |
| #4 | 1.1 | MLS+Au | fail excess speed/2/3/92 | 2.11 | 5.0 | 12.0 | 15.0 | 35.0 | 1.0 | 1.0 | - | - | 225 | 329 | 104 | 100 | 1,100 | - |
| #5 | 1.2 | MLS+Au | fail excess speed/1/16/92 | 1.39 | | | | | 1.2 | 1.7 | 2.8 | 1.6 | 212 | 303 | 91 | 98 | - | - |
| #6 | | MLS+Ni | delaminated functional 11/91 | | | | | | 0.6 | 0.9 | 1.0 | 2.3 | 225 | - | - | 100 | 960 | - |
| | | | **117-Size Bearing** | | | | | | | | | | | | | | | |
| 60/61 | 3.1b | MLS+Au | end of test 6/93 | 47.87 | 1.6 | 2.0 | 8.5 | 2.0 | 0.8 | 0.16 | 1.3 | 1.3 | 215 | 152 | -63 | 108 | 343 | *397 |
| 64/65 | 3.2a | MLS+Au | end of test 6/93 | 41.76 | 2.0 | 6.5 | 12.5 | 3.5 | 1.0 | 0.14 | 0.9 | 1.2 | 195 | 175 | -20 | 104 | 394 | 368 |
| 18/57 | 3.1a | MLS+Ni | failed 1/92 | 2.44 | 2.0 | 4.8 | 8.2 | 4.0 | - | - | - | - | 195 | 286 | 91 | 104 | *262 | 347 |
| 66/67 | 3.2 | MLS+Au | failed 2/92 (oversize ball) | 0.04 | 1.2 | 3.2 | 2.6 | | 1.0 | 0.14 | - | - | 218 | 286 | - | 108 | 394 | 368 |

* suspect value

†Film:  MLS+AU=Multi-layer (Ovonic) with 45% Au-Pd, MLS+Ni=Multi-layer with 10% Ni

†† Torq= Running torque from strip chart at 1 deg/sec

#hash = pk-pk

**117-Size and 12 inch Grease Lubricated Bearings**

| S/N | Post | †Lube | Status | Life at Test Cutoff Mcycles | ** Max Gimb Torq, in-lbs Typical low | Typical high | Peak Excurs | End of test | ††Torq@1°/s, 3 revs, in-lbs Start Avg. | Start #hash | End or Failure Avg. | End or Failure hash | Preload, lbs Start | End | Change | Initial Mean Hertz Strs KSI | Axial Stiffness 10^3 lbs/in start | end |
|---|---|---|---|---|---|---|---|---|---|---|---|---|---|---|---|---|---|---|
| | | | **12 inch Bearing** | | | | | | | | | | | | | | | |
| #2 | 2.1 | NPE | end of test 9/93 | 38.9 | 7.0 | 12.0 | 17.0 | 14.0 | 1.8 | 0.9 | 1.4 | 0.9 | 199 | 193 | -6 | 96 | 1,200 | 920 |
| | | | **117-Size Bearing** | | | | | | | | | | | | | | | |
| 32/49 | 2.2 | MAC | test stop 6/92, Hi Torq | 8.1 | 1.0 | 8.5 | 8.2 | 5.6 | 1.00 | 0.14 | - | - | 247 | - | - | 113 | - | - |
| 11/41 | 2.2a | NPE | test stop 10/92, Hi Torq | 4.2 | 2.0 | 3.0 | 6.0 | 4.5 | 0.65 | 0.10 | 0.5 | 0.2 | 247 | - | - | 113 | 420 | - |
| 41/58 | 2.2b | MAC | xtra grease, test end 6/93 | 12.8 | 1.2 | 3.4 | 3.4 | 11.5 | 0.50 | 0.12 | 1.1 | 0.5 | 260 | 260 | 0 | 115 | 302 | - |

†Lube:  NPE= Neopentyl ether, MAC=Multible Alkylated Cyclopentane (Pennzane)

†† Torq= Running torque from strip chart at 1 deg/sec

#hash = pk-pk

## 6.1 LIFE TEST SETUP

### 6.1.1 Test Rig
The full scale bearing life tests were conducted on the same fixtures used to perform the special screening tests. Each fixture was modified to accommodate two full scale elevation size or azimuth size duplex bearing (Fig. 6-2). The bearings were mounted and clamped in precision inner and outer test rings which simulated expected rotor and housing stiffness and fits. The test rings were manufactured to diametral tolerance of less than 100 $\mu$ inch (see Table 4-16). After bearing pre-life functional tests, the bearing cartridges were mounted on to drive spindles in the vacuum bell jars. The bearing cartridges extra weight was off-loaded by suspension cables. Precision load cells restrained the bearing outer race/housing providing direct torque readings.
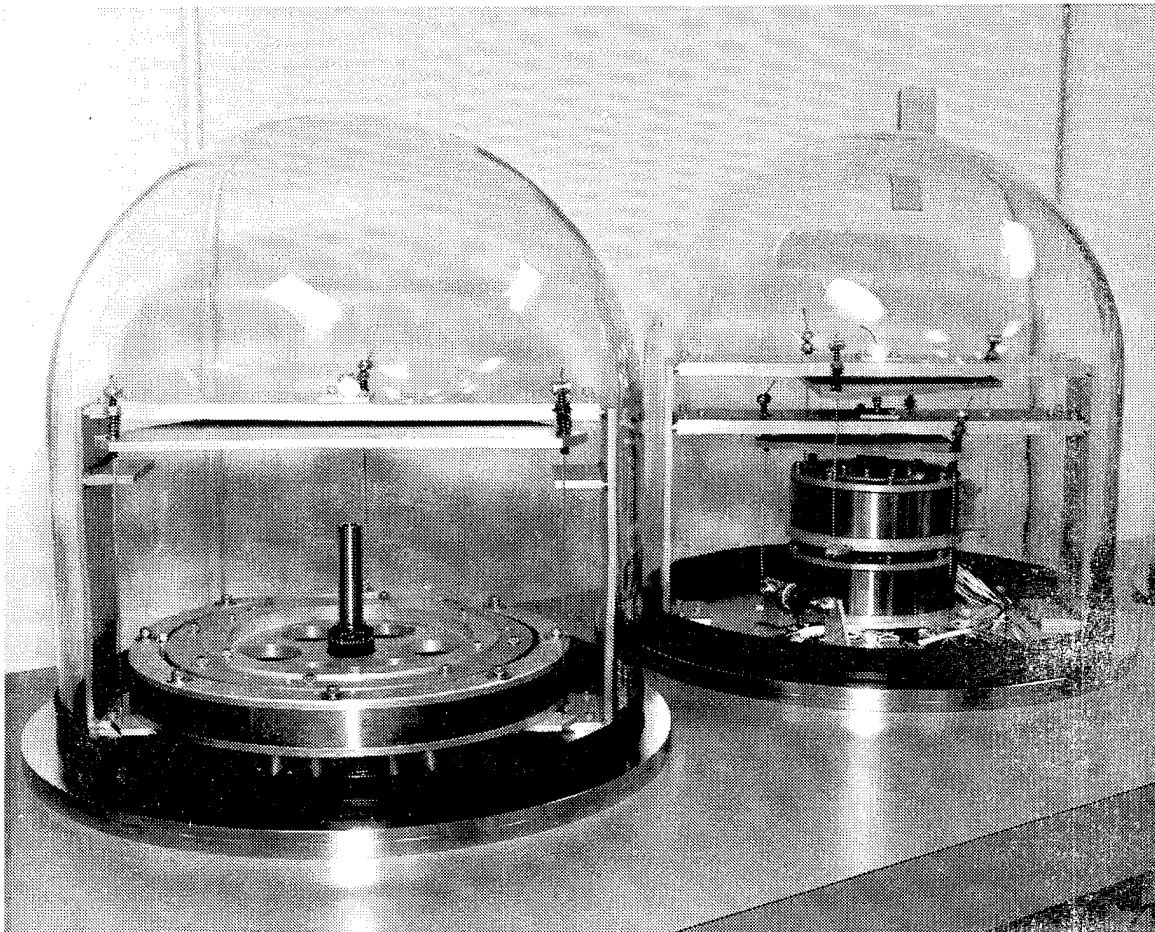


Fig. 6-2   Gimbal bearing life test rigs

### 6.1.2 Test Cycle
The test cycle was similar to that used for the 105 size bearing tests, except the gimbal angles were reduced to ± 60 degrees and ± 5 degrees. The larger angle provided 34 and 8 ball/inner race stress cycles for the 12 and 5 inch bearings, respectively. The ± 5 degree stroke was less than one ball path over lap for either bearing. The cycling rate was reduced according to bearing size and type of lubrication (see Fig. 4-11). The grease lubricated bearing rates were

lowered to keep peak EHD lambda ratios less than one. The stop-start nature of gimbaling assures boundary lubrication for a substantial period of the test time.

### 6.1.3 Test Bearings

As described in Section 4.4.1, test bearing geometry and surface finish were made to flight quality. Each bearing was delivered with dimensional and performance acceptance test data. A comparison of bearing sizes, geometry and typical acceptance test data can be found in Fig. 6.3.

| | | |
|---|---|---|
| **• Angular Contact, Duplex Ball Bearings**<br>**• Class 7 Precision / Grade 5 balls**<br>**• Built-in Hard Preload**<br>**• Honed Races (roughness < 2 $\mu$ in rms)** | | |
| **105 Size** | **117 Size** | **12 inch** |
| • 25 X 47 mm | • 85 X 130mm | • 280 x 305 mm |
| • 15 ° Contact Angle | • 15 ° Contact Angle | • 15 ° Contact Angle |
| • 12 balls (0.25 in) | • 20 balls (0.56 in) | • 104 balls (0.25 in) |
| • 30 lbs Nom Preload | • 210 lbs Nom Preload | • 225 lbs Nom Preload |
| • 108 Ksi (Mean Hertz) | • 105 Ksi (Mean Hertz) | • 100 Ksi (Mean Hertz) |
| • AISI 52100 | • AISI 52100 | • AISI 440-C |
| **Bearing Acceptance Tests Parameters** | | |
| • Preload | • Axial Stiffness | • Starting Torque |
| • Contact Angle | • Angular Runout | • Running Torque |
| • Surface Roughness | • Deviat from True Circle | • Transverse Curvature |

Fig. 6-3    Gimbal bearing comparison and acceptance parameters

### 6.2 PARAMETRIC TESTS

Parametric functional tests were performed on the full-scale gimbal bearings prior to life test. This provided a start of life reference to compare end-of-life performance to as well as provide a check on bearing quality, specifically running torque, angular runout, mounted preload and axial stiffness. In addition, these functional tests provided critical bearing data for predicting gimbal performance at not only beginning of life but, more importantly, end-of-life as well. Key bearing characterization data is illustrated in Fig. 6-4. Details of the test setup can be found in Section 8.2.

## 6.2.1 Torque Signature

The torque and torque ripple measurements are performed on a precision rate table, supported on air bearings. (Fig. 6-5). The rate table, having less than 25 μ inch radial runout, is driven by a brushless DC motor/encoder servo with < 1 arc second resolution. The motion of the table is completely flexible, being controlled by a PC. Bearing torque is directly measured using a reaction load cell mount to the outer test ring.



**Precision Bearing Testers**

Angular Runout Test    Torque Ripple Test    Dahl Friction Slope Test

**Bearing Torque Disturbance Mode**

| Dahl Friction | Torque Hash | Runout |
|---|---|---|
| • velocity reversal errors | • high frequency scanning errors | • repeatable and nonrepeatable LOS pointng errors |
| • hybrid flexure damping | | |

Turnaround Torque

Torque Bump    Torque Blocking

• high stiffness and impulse type disturbance errors

**Fig. 6-4    Precision Bearing Torque Ripple Test**

Fig. 6-5    Torque signature measurement on precision rate table

### 6.2.2 Angular Runout

Bearing angular runouts use an X-Y autocollimator with a rotating alignment mirror as shown in Fig. 6-6. The bearing inner race is driven by the rate table through a soft drive coupling. The system is calibrated via an optical wedge, which determined bearing precision. Minimum, maximum repeatable and non-repeatable angular runout down to 0.25 arc second can be determined.

A typical angular runout plot for the 5-inch bearing showing 1.2 arc sec repeatable runout and 0.8 arc sec non-repeatable runout appears in Fig. 6-7. The repeatable runout is attributed to race grinding inaccuracies. It is the maximum minus the minimum deviation from true circularity of the angular runout plot. The non-repeatable runout is due to mismatches in ball diameters. It is the maximum thickness of the trace at one location after several turns due to nonuniform ball tumbling. Repeatable and non-repeatable runouts were typically less than 1.5 and 1 arc sec for the 5-inch bearings and 4.5 and 1.5 arc second for the 12-inch bearings.
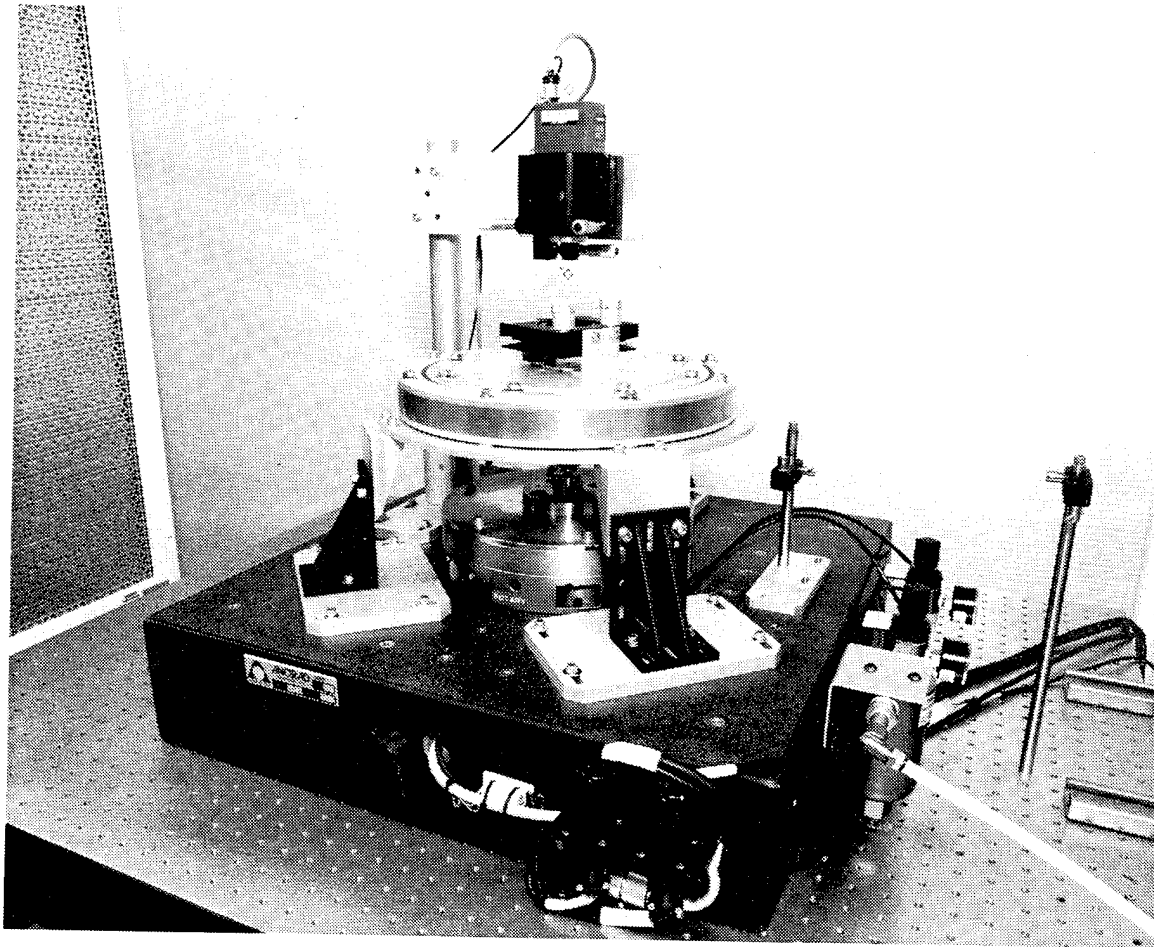


**Fig. 6-6    Angular runout setup**
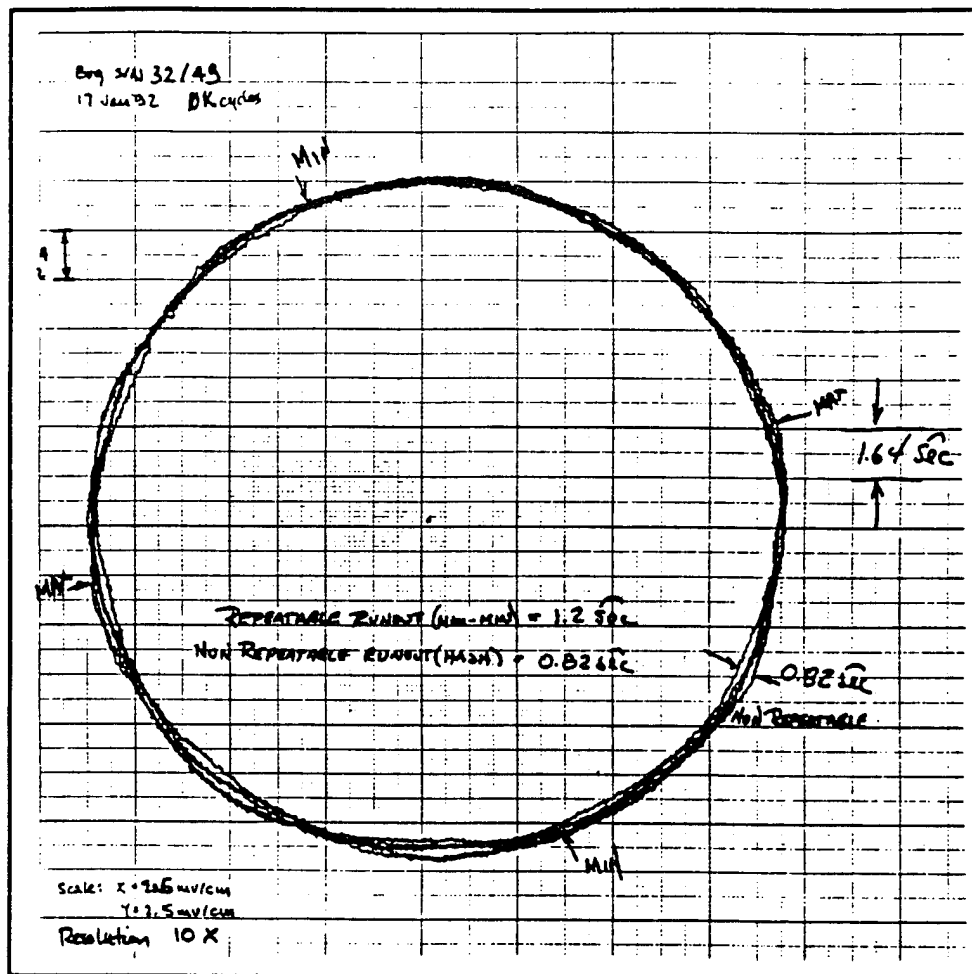
**Fig. 6-7** Typical Angular Runout Data for 5 inch bearing showing 1.2 and 0.8 arc sec repeatable and non-repeatable angular runouts

### 6.2.3 Preload and Stiffness

The preload of both 5 inch and 12 inch bearings were specified to the bearing vendor. The bearing vendor measured and controlled the preload of the 12 inch bearing as mounted in the precision test rings which formed the bearing cartridge. Adjustments were made for the thickness of the $MoS_2$ film for the solid lubricated bearings. The starting preloads of the as delivered 12 inch bearings were remeasured at LMSC. Preload averaged 225 lb ± 10 lb one sigma at an average mean Hertz stress level of 100 KSI (see Table 6-1). A typical preload plot appears in Fig. 6-8.

The preload of the as delivered 117 size or 5 inch bearing was nominally 75 lbs in the unmounted condition without any $MoS_2$ film coating. This preload when fitted into the test rings with $MoS_2$ typically exceeded 200 lbs. It was necessary to order several sets of replacement balls graduated 20, 50 and 100 microinches, some over sized and some under sized, to adjust preload. In this way, starting preload averaged 206 lb ± 12 lb one sigma (106 KSI) for the $MoS_2$ bearings and 251 lb ± 8 lb one sigma (114 KSI) for those grease lubricated (see Table 6-1).

As mentioned in Section 4.1.2, bearing on-orbit and launch stiffness are typically design drivers. The 12 inch bearing's acceptance data package typically included axial stiffness for the hard preloaded, bearing cartridge. These stiffness numbers were reconfirmed at LMSC to provide a reference to compare with end of life stiffness. The axial stiffness of the 12 inch bearings typically ranged from 1 to 1.2 million lb/inch (see Fig. 6-9). Similarly, the stiffness of the 117-size bearings were found to range between 300K to 400K lb/in (see Table 6-1).



+17 LB. FIXTURE WGT.

7 July 92  BRG +Sa (∮ cycles)
X:(LC) .25 mv/cm
Y:(LVDT) .01 v/cm

(w/IT-4 inner test ring)

222 LBS.          RETURN

221 LBS.
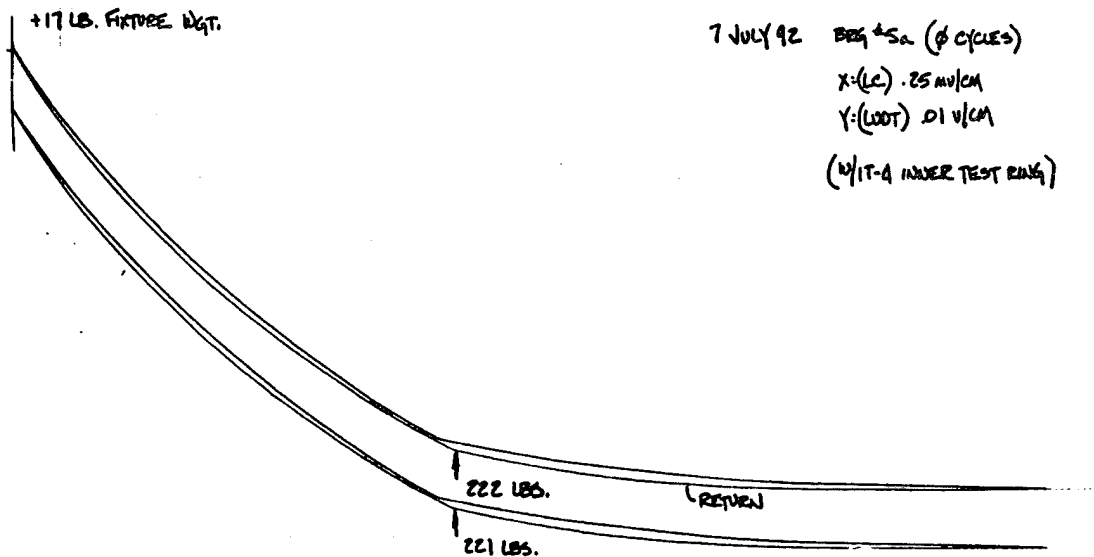
**Fig. 6-8     Typical preload trace for a 12 inch test bearing (222 lbs).**



STIFFNESS = 1.066 x10⁶ LB/N.
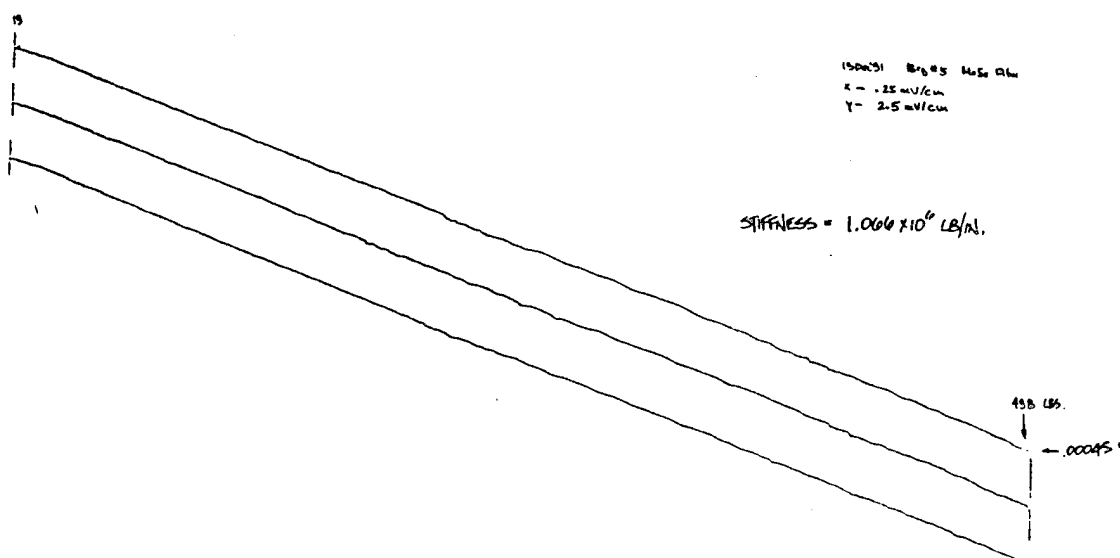
**Fig. 6-9     Typical axial stiffness trace for a 12 inch test bearing. (1.1 million lb/in).**

- 112 -

### 6.2.4 Dahl Friction

For pointing type gimbals, the small angle torque displacement characteristics of a bearing, particularly its torsional stiffness, are important from a servo-control stand point (see Section 8.1.1). In this region, referred to as Dahl friction after Phil Dahl who was the first to attempt to model it [6-1], the traction in the ball/race contact has yet to reach its limiting value before gross slip. Thus the ball is in a "windup" mode before it actually starts to roll. The tangential elastic compliance of the contact governs the bearing "windup" stiffness [6-2]. Since the shear modulus of the $MoS_2$ films is much lower than the steel bearing race substrate, the application of $MoS_2$ film lubricants to bearings was expected to lower the Dahl friction slope.

The bearing rate table setup shown in Fig. 6-6 was modified with a high precision linear actuator to generate "hysteresis loops." A proximity probe displacement system was installed to get angular resolution down to the arc second level.

As expected, the $MoS_2$ bearings were more torsionally compliant than those grease lubricated. Fig. 6-10 shows representative small angle hysteresis loops for the 117-size (5-inch) bearings with both wet and dry lubricants. The windup angle before breakaway is significantly larger for the $MoS_2$ bearing, while the initial slope is lower.

Grease Lubricated
117 Size Bearing

Ion-Sputtered MoS2
117 Size Bearing
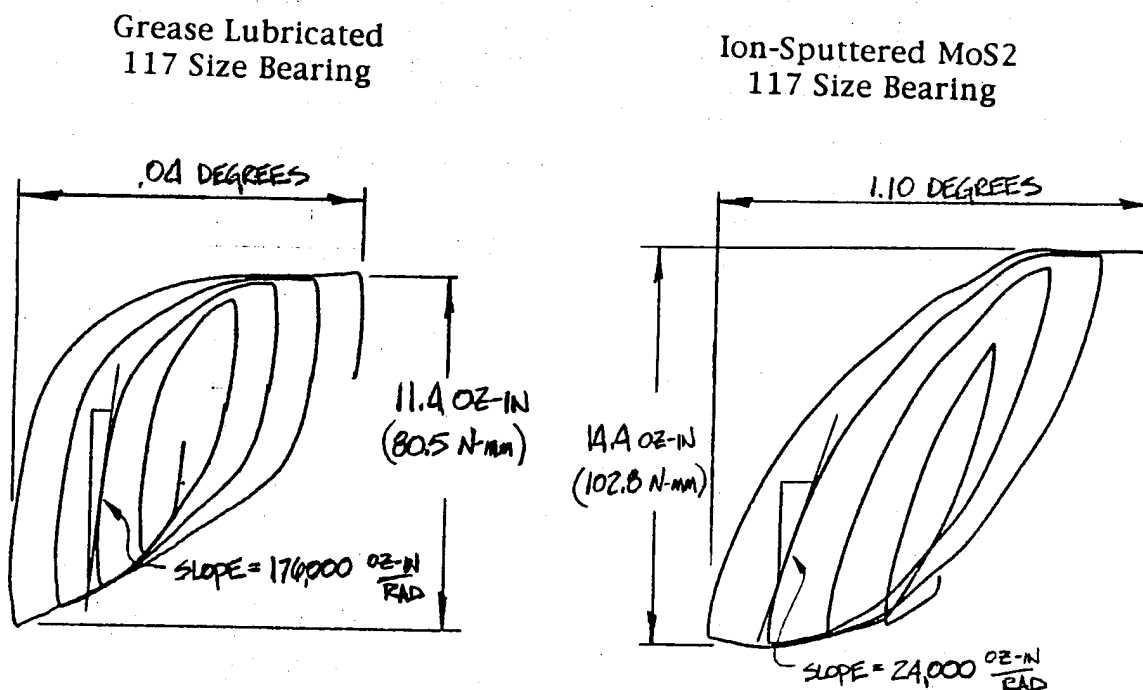


**Fig. 6-10    Dahl Torque Trace for Flight Bearing**

## 6.3 TWELVE INCH BEARINGS WITH NICKEL/MULTILAYER FILMS

A problem with $MoS_2$ film delamination was encountered with the 12-inch bearings during prelife functional tests. Initially, the torque performance of the $MoS_2$ film lubricated 12-inch bearings was exceptional good in comparison with the 12-inch grease lubricated bearing based on the bearing vendor's acceptance torque traces. (see Fig. 6-11). However, after a small amount of additional testing both torque and torque ripple essentially doubled in value

as shown in Fig. 6-12. Visual inspection of the bearing races showed that the film had delaminated. (see Section 7.5) In addition, one of the 5-inch (117-sized) bearings deposited with multilayer Ni/MoS$_2$ films also exhibited failure during prefuntional testing. Disassembly and examination of this bearing revealed MoS$_2$ debris in the retainer ball pocket (Fig. 7-26) that had spalled from the races.

### 6.3.1 Fracture Resistant Films

As described in Section 7.5.1, a joint effort was undertaken with Ovonics Synthetic Materials to develop an MoS$_2$ film with more fracture resistance than the 10% nickel multilayer films used in the 105- bearing tests. A simple, ball-on-plate tester was developed to evaluate the film's resistance to cracking. Gold-Paladium, replaced nickel as the interlayer and the thickness of the interlayer and total film was varied. Specimens with different roughness levels were also evaluated. Surface roughness was found to play a surprisingly large role in film delamination. Films with 10% Au-Pd interlayer thicknesses quickly developed incipient cracks along the grinding mark ridges of the test plate with ground surface finish at maximum contact stress levels of 236 ksi. These cracks quickly led to large scale film delamination. Surface roughness effects were not previously appreciated by prior experimenters with these films who generally used polished, pin-on-disk test specimens in their work. Furthermore, rolling contact film delamination was much different from the wear through failure modes associated with pure sliding pin-on-disk testers. The net result was that optimum film composition and thickness found from lightly load, pure sliding tribometers were much less than optimum for ball bearing applications. Recommended films based on sliding tribometer data are very dense, hard and relatively thick to extend wear life. On the other hand, films for rolling contact bearings should be less brittle and thinner to reduce the tendency to spall.

The work at Ovonics indicated that a multilayer film with about 45% Au-Pd and a thickness of approximately 0.3 μm would have considerably more fracture toughness in a bearing contact. (see Section 7.5.1). As a result, the film was changed to this "high" gold film for the 5- and 12-inch life test bearings and the nominal film thickness was reduced from 1 μm to 0.3 μm. In addition, two pairs of 105-size test bearings were also coated with the thinner, Ovonics "high" gold films to get comparative data against the other MoS$_2$ films.

### 6.3.2 105 Size Bearing Tests with Fracture Resistant Films

The 105-size bearings having the new MoS$_2$ gold film were tested in parallel with the 5 and 12-inch bearings. Thus 105-bearing life test results with the new films were not available prior to beginning the large gimbal bearing tests. Fig. 6-13 shows a torque history comparison between the low nickel and high gold films. Although, improvements in torque are noted in the mid to end-of-test region, torque excursions were still observed early in the life test[†]. On the other hand, torque signatures were quite good at various points through life (see traces at start, 20M and 35M cycles in Figs. 6-14 and 6-15). Such results were observed with other screening test bearings, suggesting that transient debris buildup was still the likely root cause of the torque excursions. As discussed in Section 7.6.1, although evidence of fracture fracture was not found during posttest SEM examination, the ball track on the inner race was well defined by the edges of the film where the film had been worn off (Fig. 7-37b).

---

[†] Unfortunately, a glitch in the data recording equipment caused a data drop out for the first 5 million cycles.
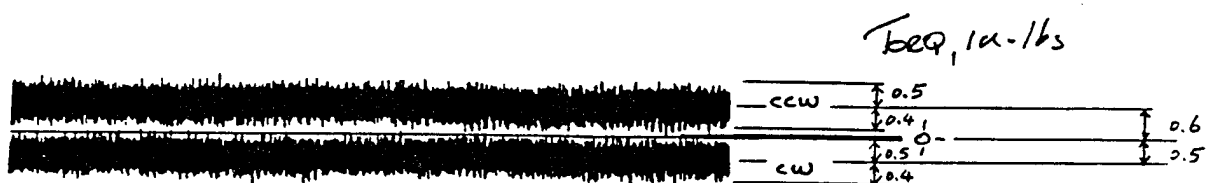
(a) Torque signature of MoS$_2$ film lubricated, 12 inch bearing
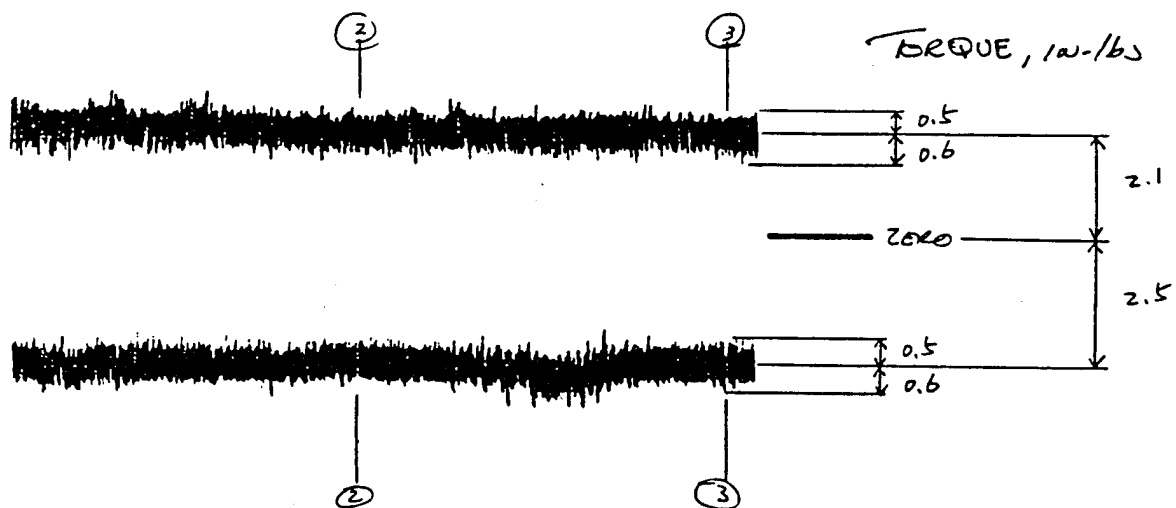


(b) Torque signature of grease lubricated, 12 inch bearing

Fig. 6-11   MoS$_2$/Ni film had excellent torque signature performance on as delivered test bearings before film delamination.
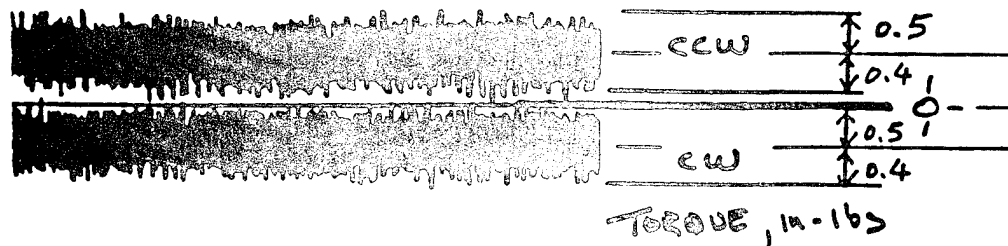
**(a) Torque signature of 12 inch bearing (s/n 06) before film delamination**
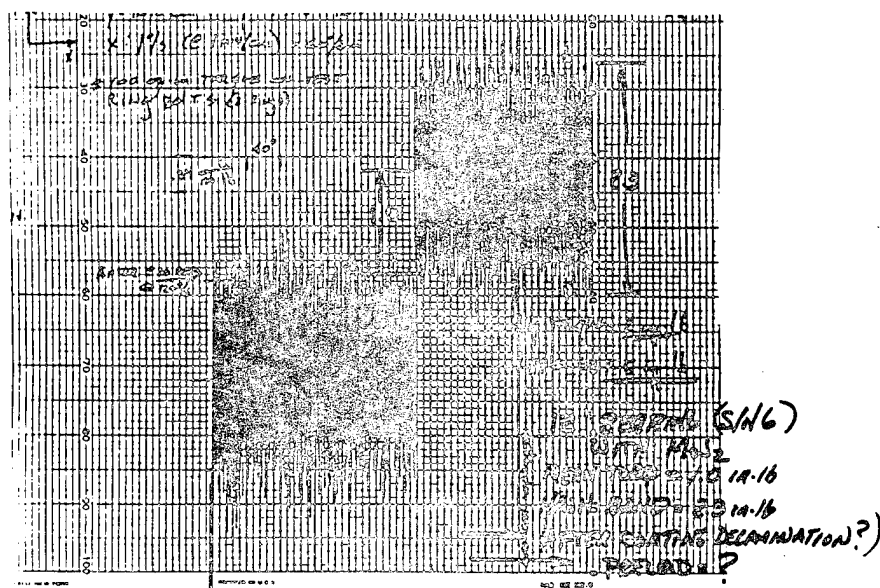


**(b) Torque signature of 12 inch bearing (s/n 06) after film delamination**

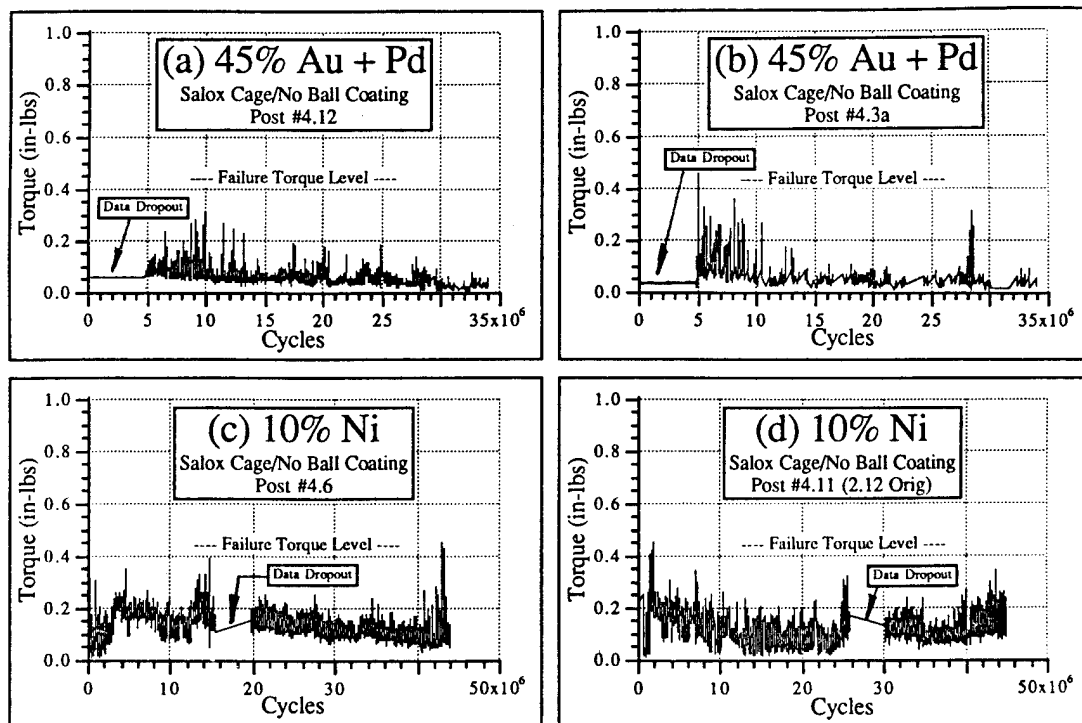**Fig. 6-12    Effect of MoS$_2$ film delamination on torque signature**

**Fig. 6-13 Comparison of torque histories of high gold and low nickel multi-layer film 105-size test bearings.** *(Note data drop out due to equipment problem)*
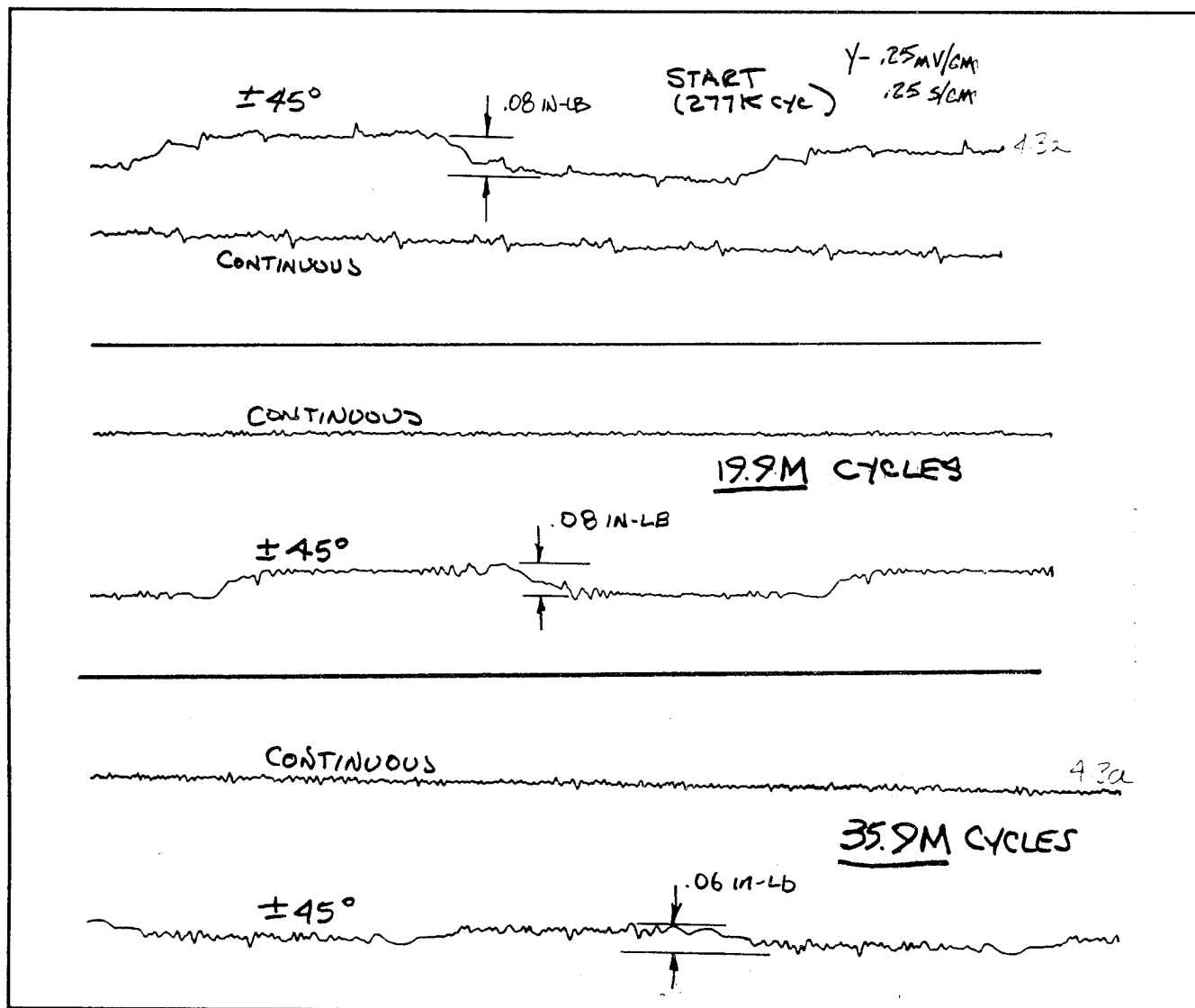
**Fig. 6-14** 105-Size bearing torque traces at start, middle (19.9M) and end-of-test (35.4M)with high gold Ovonics film (post 4.3a)
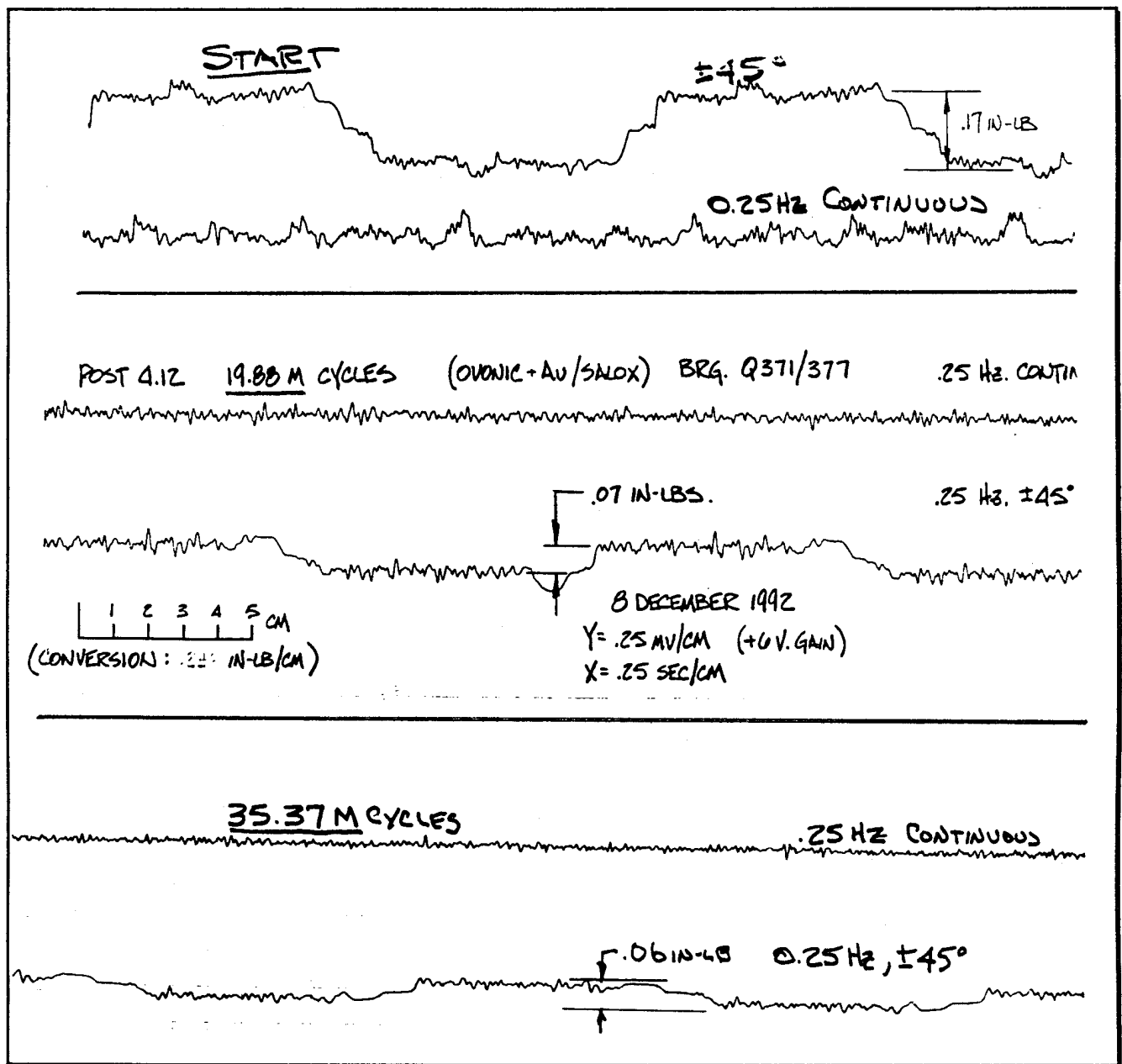
Fig. 6-15  105-Size bearing torque traces at start, middle (19.9M) and end-of-test (35.4M)with high gold Ovonics film (post 4.12)

## 6.4  TORQUE CHARACTERIZATION OF 12 INCH BEARINGS

Twelve inch test bearings were prepared with the gold Ovonics films and pre-life functionally tested.  These functional tests include characterization of the beginning-of-life torque signatures on the precision rate table. These signatures were obtained by rotating the bearing 3 revolutions in each direction at a rate of 1 deg/sec.  To provide a standard starting condition, the bearing was preconditioned by rotating 3 revolutions in the reverse direction at 5 deg/sec. Rotating the bearing through several revolutions tended to redistribute debris, lessening the jamming effect that was occasionally observed during the gimbaling tests.

### 6.4.1 Torque Signature Comparison

Fig. 6-16 shows that the average torque levels of the bearings with the new $MoS_2$ film were quite low compared to the as-delivered bearings. A direct comparison with the new NPE greased bearing appears in Fig. 6-17. Note that although the $MoS_2$ bearing has somewhat higher torque ripple, it shows virtually no torque/speed sensitivity, unlike the grease lubricated bearing.

A torque signature power spectral density (PSD) plot shows that the $MoS_2$ bearing has a higher harmonic component than the greased bearing. (Fig. 6-18). Its disturbances occur at the ball / outer race defect frequency, suggesting nonuniformity of the film coating on the outer race.

ITB BEARING #3 BASELINE

PRECONDITIONED:
720° CCW @ 5°/sec

```
|   1   2   3   4  5cm
|___|___|___|___|___|
```
(CONVERSION: 2.18 IN·LB/CM)

(CW ROTATION)                1.9 IN·LBS.                    2.83 IN·LBS

(CCW ROTATION)
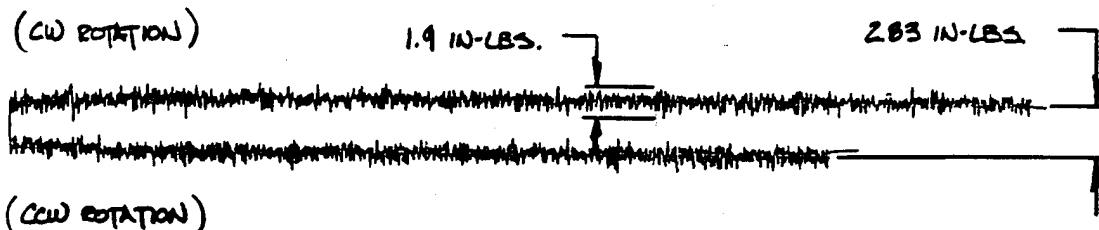
INNER TEST RING : IT-5
OUTER TEST RING: OT-4

27 JULY 1992
Y = .25 MU/CM
X = 50 SEC/CM
VEL. = .07°/SEC, ±60°
(±.1666 REV)

PRECONDITIONED:
720° CCW @ 5°/sec

BEARING S/N : BRG #5
(P/N: F381091)

```
|   1   2   3   4  5CM
|___|___|___|___|___|
```
(CONVERSION: 2.18 IN·LB/CM)

(CW ROTATION)                          1.3 IN·LBS.

(CCW ROTATION)

INNER TEST RING # IT-6
OUTER TEST RING # OT-5

21 JULY 1992                    3.4 IN·LBS.
Y = .25 MU/CM
X = 50 SEC/CM
VEL. = .07°/SEC, ±60°
(±.1666 REV)

Fig. 6-16  Starting torque traces for the two MoS$_2$ lubricated 12 inch
bearings at very low speeds (0.07 deg/sec)

Brg #4, MoS2+Salox Retainer+No Ball Coating, 1°/s

$MoS_2$ film at 1 deg/sec

Brg #4, MoS2+Salox Retainer+No Ball Coating, 5°/s

$MoS_2$ film at 5 deg/sec

Brg #2, NPE 952+Vespel Retainer+No Ball Coating, 1°/s

NPE grease at 1 deg/sec

Brg #2, NPE 952+Vespel Retainer+No Ball Coating, 5°/s
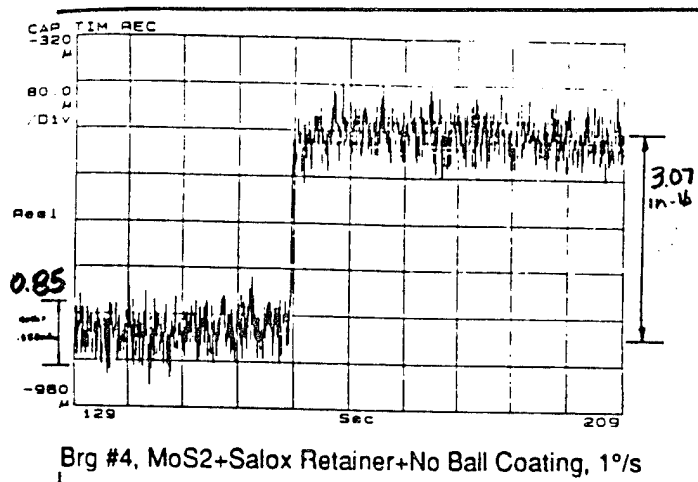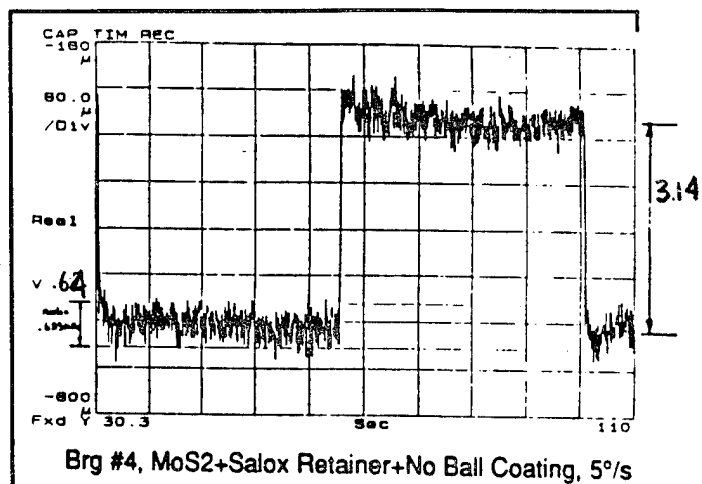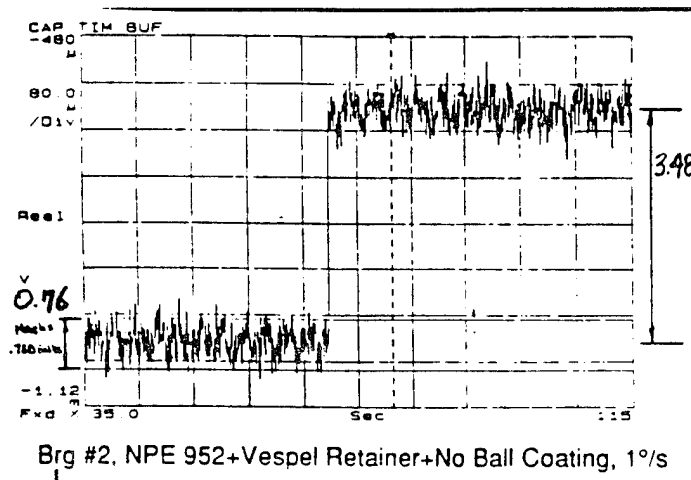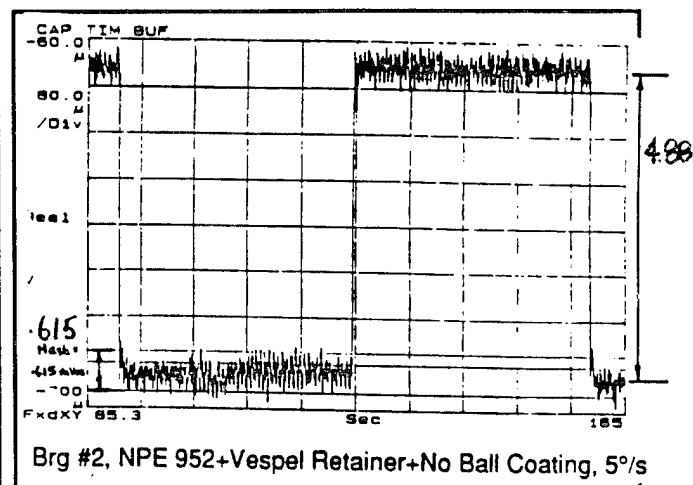
NPE grease at 5 deg/sec

Fig. 6-17   Dry and wet lubricated 12 inch bearing torque are comparable at start of life test. Greased bearing torque is slightly quieter but more speed sensitive
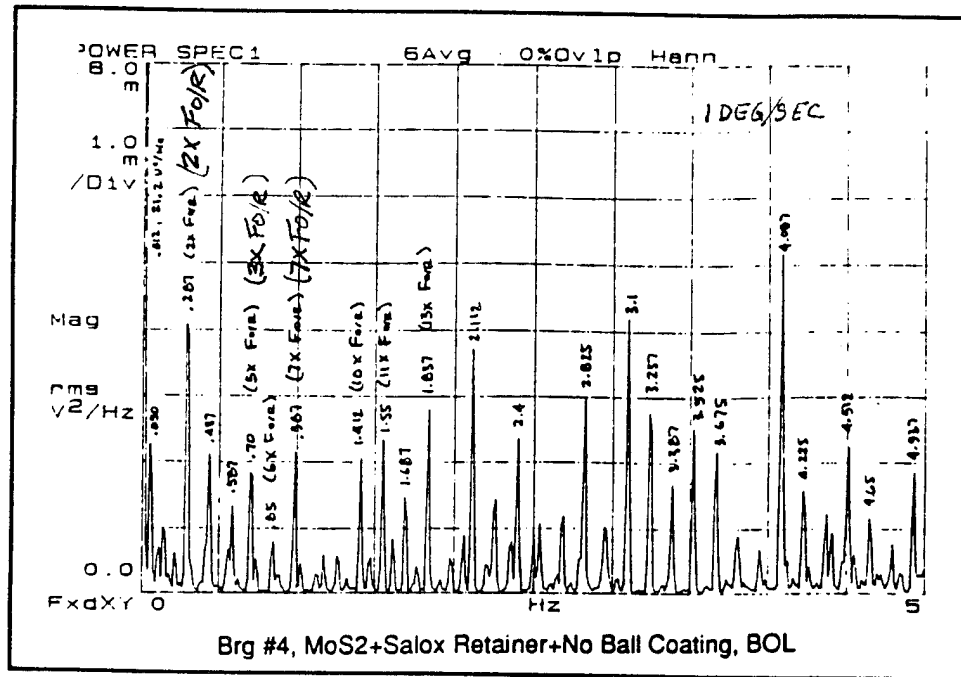
**MoS₂ film 12 inch bearing**
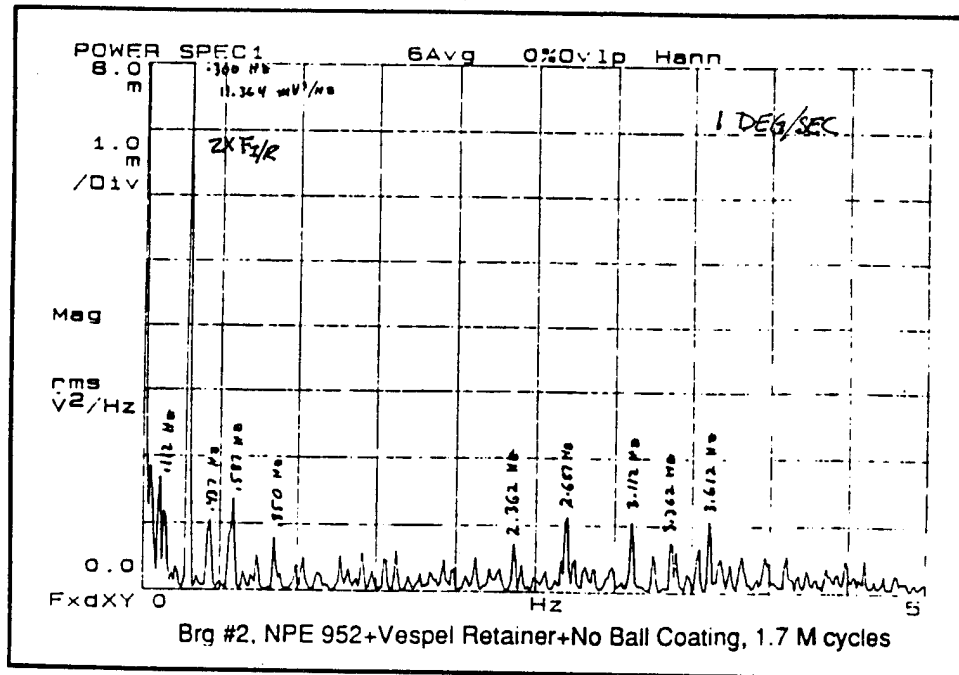


**NPE Grease 12 inch bearing**

Fig. 6-18  Power spectral density plots show less torque ripple with the greased 12 inch bearing.  Harmonics of ball/outer race defect frequency are dominant for the MoS₂ bearing

## 6.4.2 Speed Effect

The first two pairs of 12-inch bearings with multilayer/gold films *(posts #1.1 and #1.2 )* experienced high torque levels (> 30 in-lbs) after 2.1 and 1.4 million (see Fig. 6-19) test gimbal cycles, respectively. It was suspected that a buildup in torque occurred due to an over-transfer of Teflon film from the Teflon/bronze composite retainer. This buildup in film thickness caused an increase in preload with a corresponding increase in bearing drag torque. Measured torques were noticeably higher during continuous rotation and ± 60 deg gimbaling where retainer rubbing speeds were high (9 to 11 inch/sec) compared with ± 5 deg operation where sliding speeds were low (3 in/sec peak) as shown in Fig. 6-19. A noticeable torque buildup with time was observed at constant slew rates above 120 deg/sec with the 12-inch bearing (Fig. 6-20). Bearing torque more than doubled from its 4.4 in-lb starting level after approximately 2 minutes or 44 revolutions.

Retainer film over-transfer was confirmed when post-test preload measurements indicated that preload increased from 225 to 329 lbs and excessive retainer wear on the OD of the toroid ball separators was found during a tear down visual inspection. Because of these results, the continuous rotation mode was removed from the test cycle and the ± 60° gimbaling rate was reduced from 0.6 Hz to 0.28 Hz so that peak speeds were less than 120 deg/sec as shown in the duty cycle table appearing in Fig. 4-11. At the same time, the gimbaling rate for the 5-inch bearing was also reduced from 0.8 to 0.5 Hz.
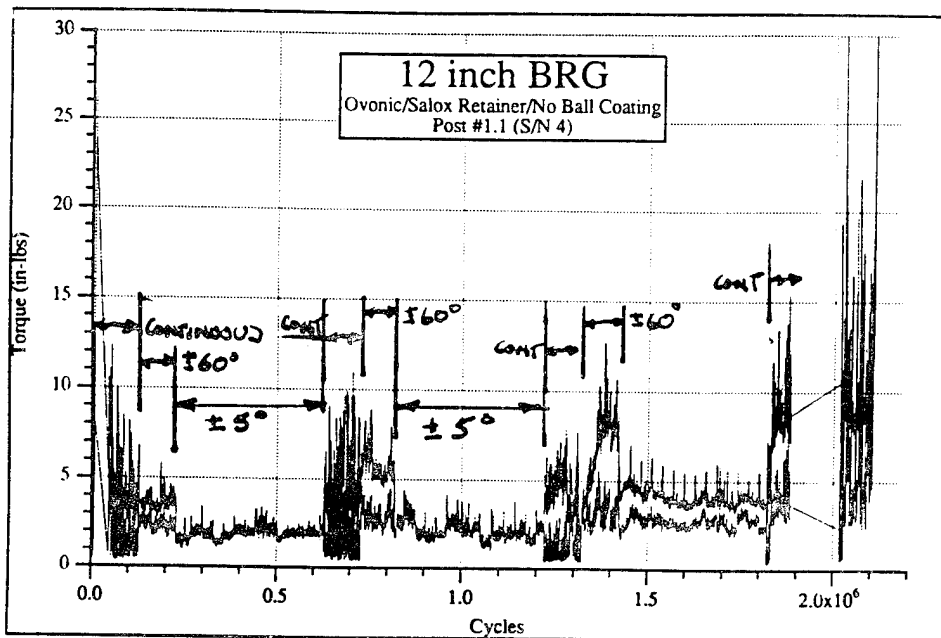


Fig. 6-19    Torque buildup from believed Teflon film over-transfer from higher cage speeds during large angle gimbaling and continuous rotation. (12-inch bearing #4 post 1.1)

- 124 -
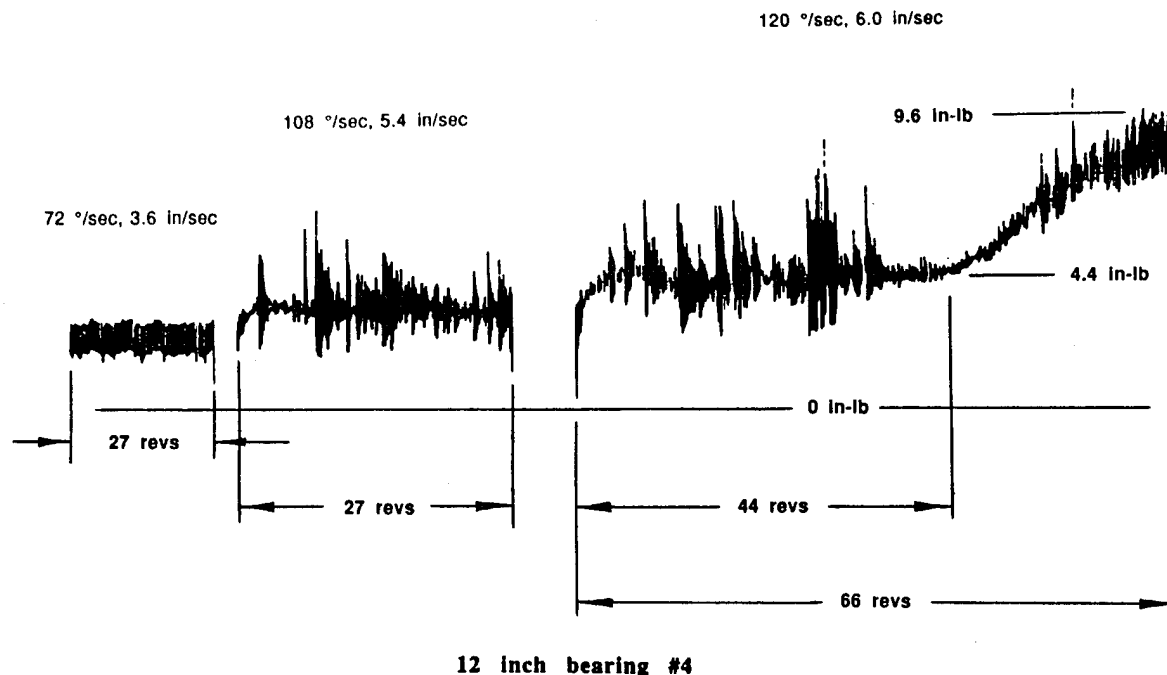
**Fig. 6-20** Spin test at constant 120 deg/sec shows torque buildup from Teflon film over-transfer after 44 revolutions (12-inch bearing #4 post 1.1)

## 6.5 TWELVE INCH BEARING LIFE TEST RESULTS

Two pairs of 12-inch bearings with the new high gold Ovonics films were put on life test at the reduced cycle rate. Erratic torque behavior was observed within the first million test cycles.(Fig. 6-21). The tests were continued to determine whether the torque irregularities would diminish with time. However, both bearings continued to show large torque excursions with bearing S/N #3 (post 1.1a) suspended from test at 4.5 million cycles for very large torque (> 30 in-lbs). Fig. 6-22 shows the torque history for the other bearing (S/N 5a). While low torque levels were present during small angle ±5° dither of less than one ball track overlap (see Fig. 6-22b), large angle slews of ± 60°, involving overlap of many balls (17 balls), produced high torque excursions. This is again believed to be due to rolled over $MoS_2$/retainer debris that accumulated at the end-of-stroke during periods of small angle dither. The effect of debris on torque is amplified for a large, thin torque tube type of bearing since they are very stiff and have many small balls with relatively small Hertzian deformations.

Posttest examination of the failed bearing (see Section 7.6.1), showed a considerable amount of retainer debris present on the balls, races, and retainers. The visual appearance of the ball track was similar to that of the 5- and 105-size bearings, where the $MoS_2$ film was lost at the edge of the track and had combined with a relatively thick deposit of retainer transfer film in the center of the track.
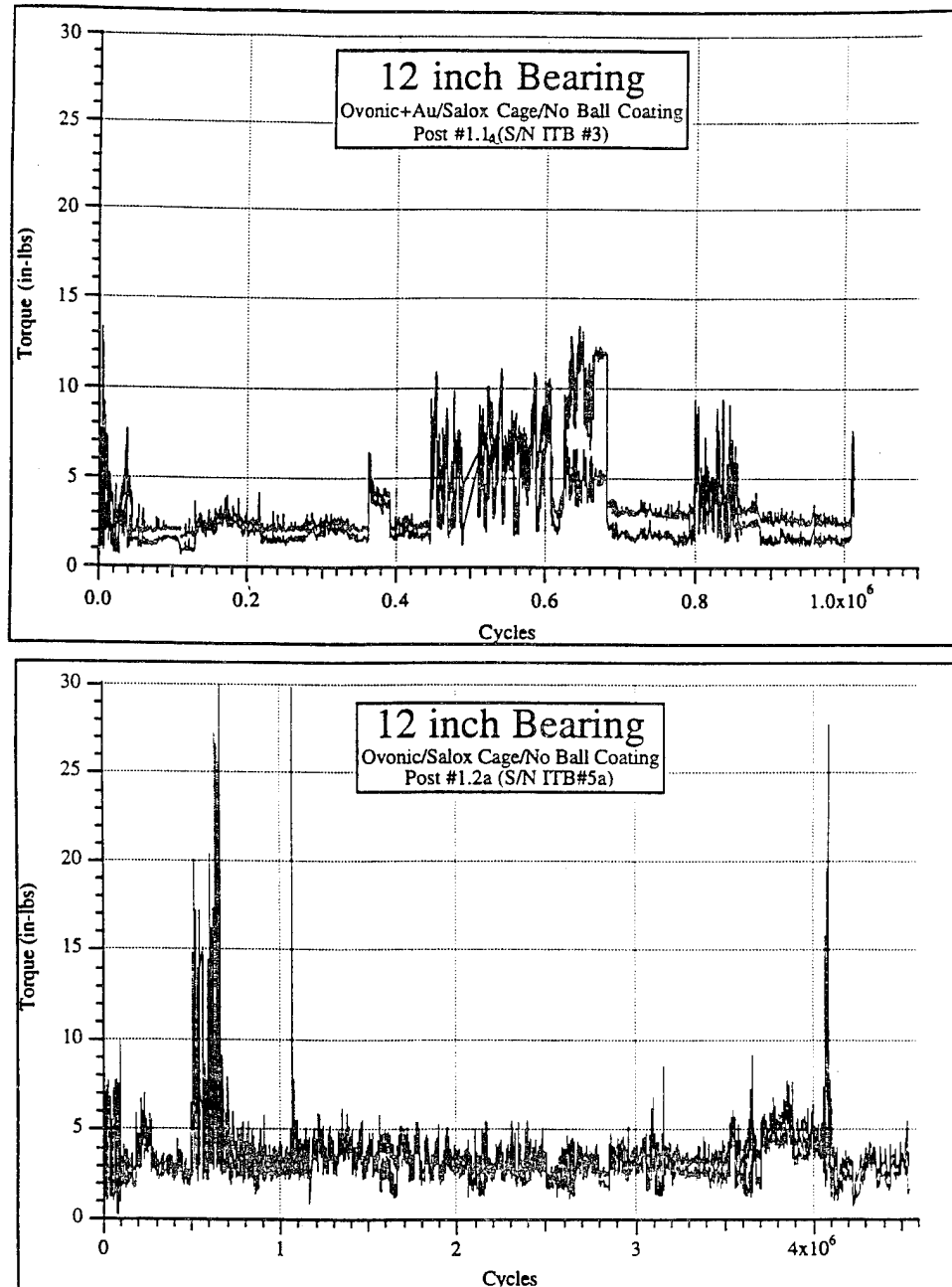
**Fig. 6-21** Early torque histories of high gold MoS₂ 12 inch bearing showing erratic torque behavior.
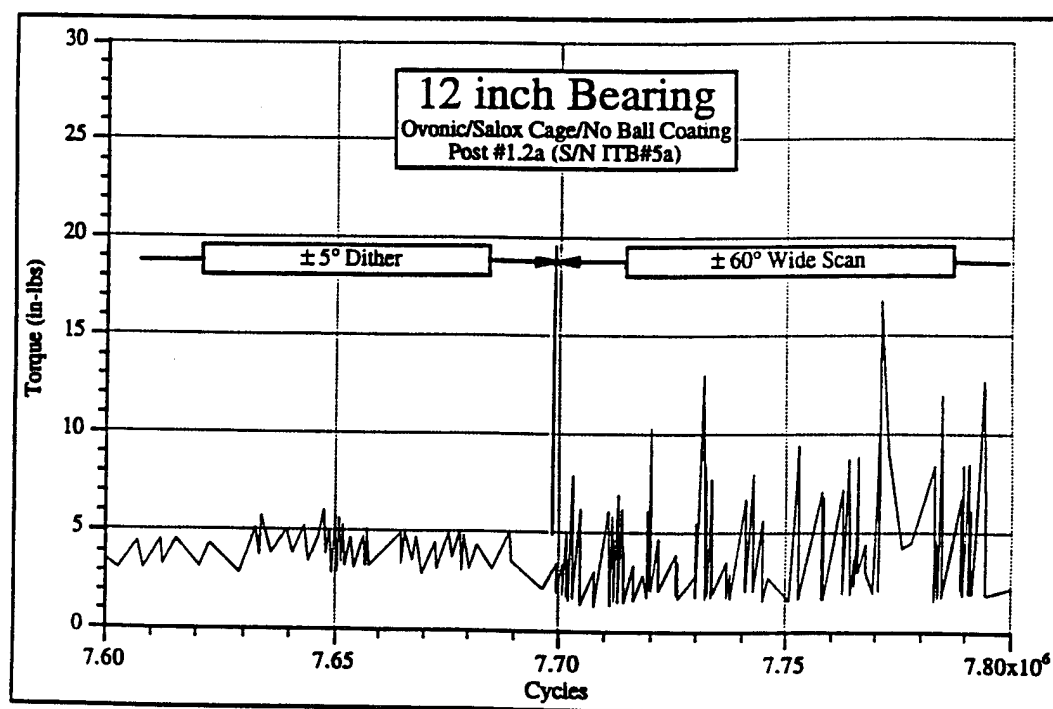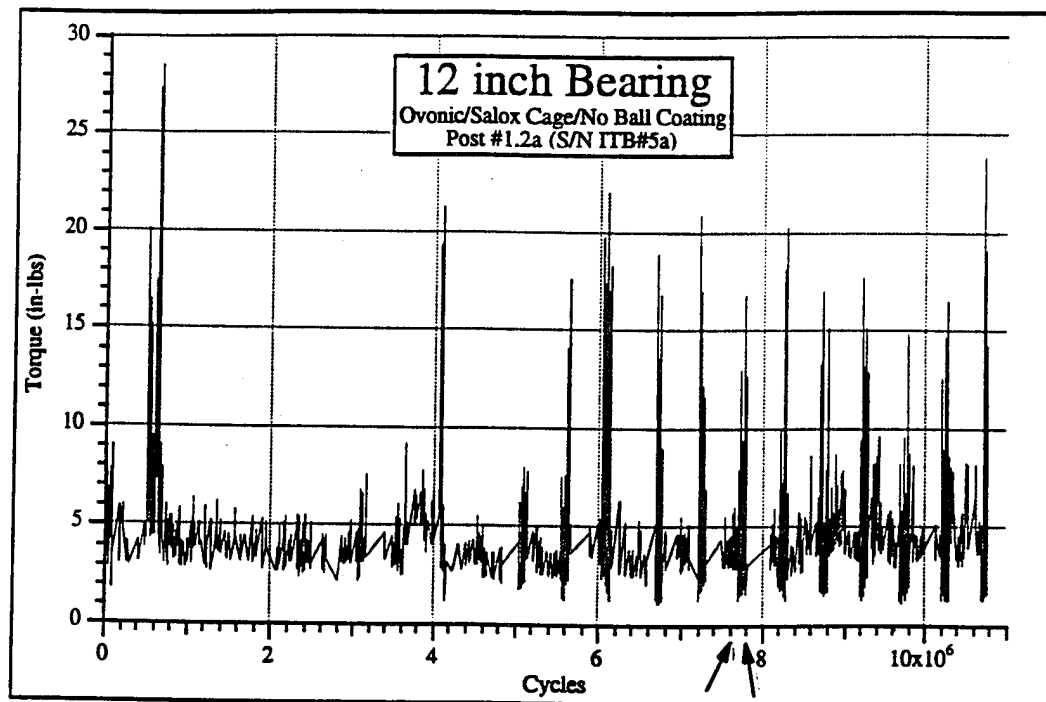
**Fig. 6-22** Debris-related torque excursion observed during ±60 degree slew as shown in expanded lower view

### 6.5.1 Soft Preload

The torque excursions exhibited by the 12 inch bearing (ITB #5a) from debris was believed to be accentuated by the high stiffness of the "hard" clamped preload arrangement. A stiffly-loaded bearing can not easily accommodate displacements due to rolled-over debris. Preload and torque increases are the result. A spring clamping or "soft" preload screening test was initiated to investigate its potential torque mitigating effects on the 12 inch (ITB #5a) bearing. It is recognized that the "soft" mount maybe unacceptable for certain gimbal applications where stiffness is a factor.

Functional Tests- Before life testing, the soft preload bearing received the standard end-of-life functional tests. Bearing mean torque measured ±2.25 in-lbs and torque ripple measured 4.1 in-lbs (Fig. 6-23) after 12.7M test cycles. This is approximately twice the mean torque level at start of test and approximately 2.5 times the starting torque ripple. Although the mean torque levels are not particularly high relative to the end-of-test, grease lubricated 12 inch bearing , the torque ripple component is more than 3 times greater ( 4.1 in-lb vs. 1.2 in-lb) (see Fig. 6-24 and note change in Y-scale).

Modest changes in measured preload and stiffness were also noted for this 12 inch bearing at 12.7M cycles. Bearing preload dropped about 10% from 215 lbs at the start to 189 lbs (Fig. 6-25). The axial stiffness also decreased slightly from 1.06 x10$^6$ lb/in at test start to 0.89 x10$^6$ lb/in at 12.7M cycles (Fig. 6-26).

Life Tests- Torque shows a significant reduction at the start of soft preload life test as shown in Fig. 6-27(a). However, the reduced torque only lasted another 1 million cycles or so before the high torque returned during the ± 60 ° gimbaling, Fig. 6-27(b). It is likely that the introduction of soft preload was implemented too late in life to be of much benefit for a bearing that had already failed from excess debris. Soft preload remains a promising approach to help extend the life of large MoS$_2$ sputtered gimbal bearings.
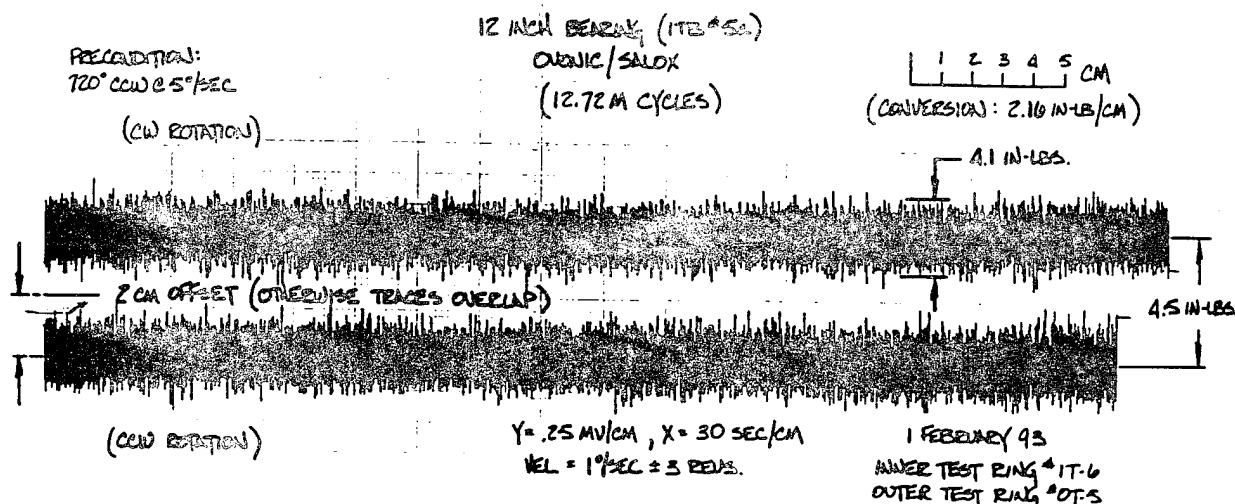


**Fig. 6-23  Torque Signature of 12 inch Bearing with Ovonics Film at 12.7M cycles.**

PRECONDITION:
720° CCW @ 5°/sec

(CW ROTATION)

12 INCH BEARING (ITB 2)
NPE GREASE
(38.93M CYCLES)

1.2 IN-LB

3.0
.IN-LB

1.2 IN-LB

(CCW ROTATION)

Y=.05 MV/CM
X= 30 CM/SEC
VEL= 1%/SEC ± 3 REVS
CONV = 0.4/35 IN-LB/CM

1 OCT 93
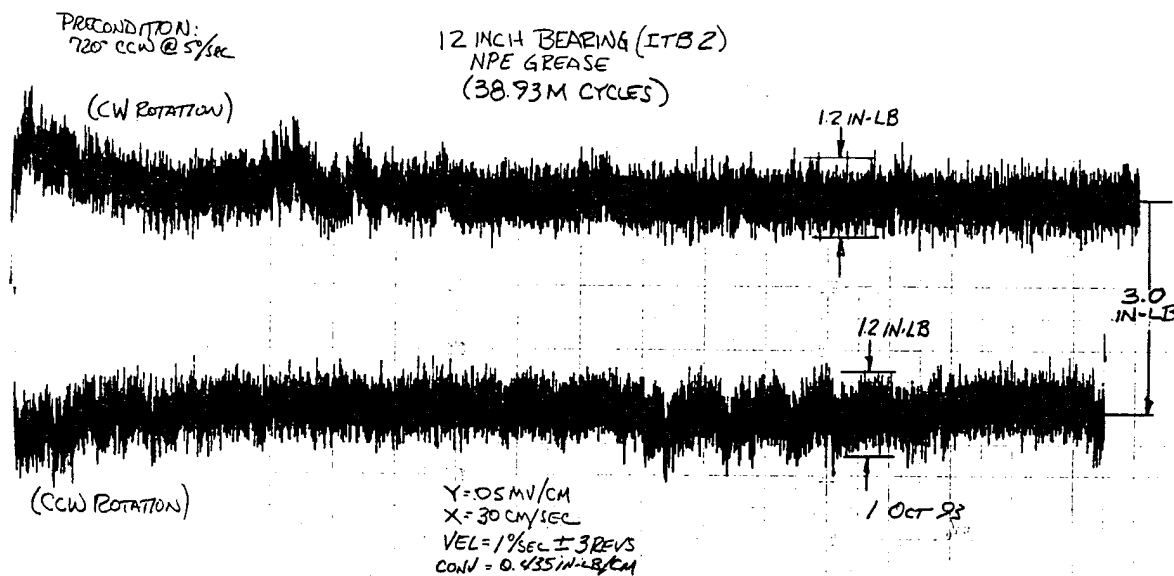
**Fig. 6-24** **Comparative torque signature of grease lubricated 12 inch Bearing at end-of-test (38.9M cycles).** *(Note change in Y-scale)*

+17 LB
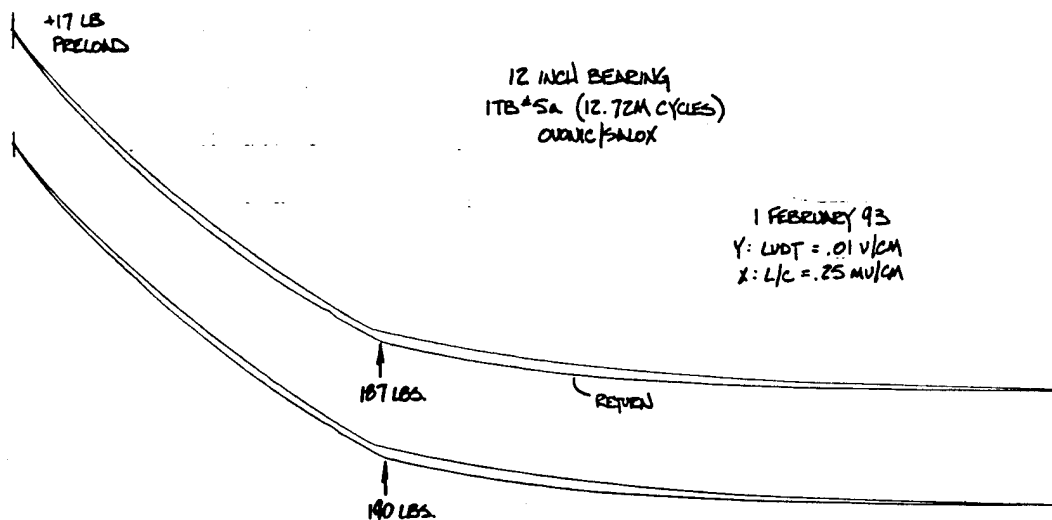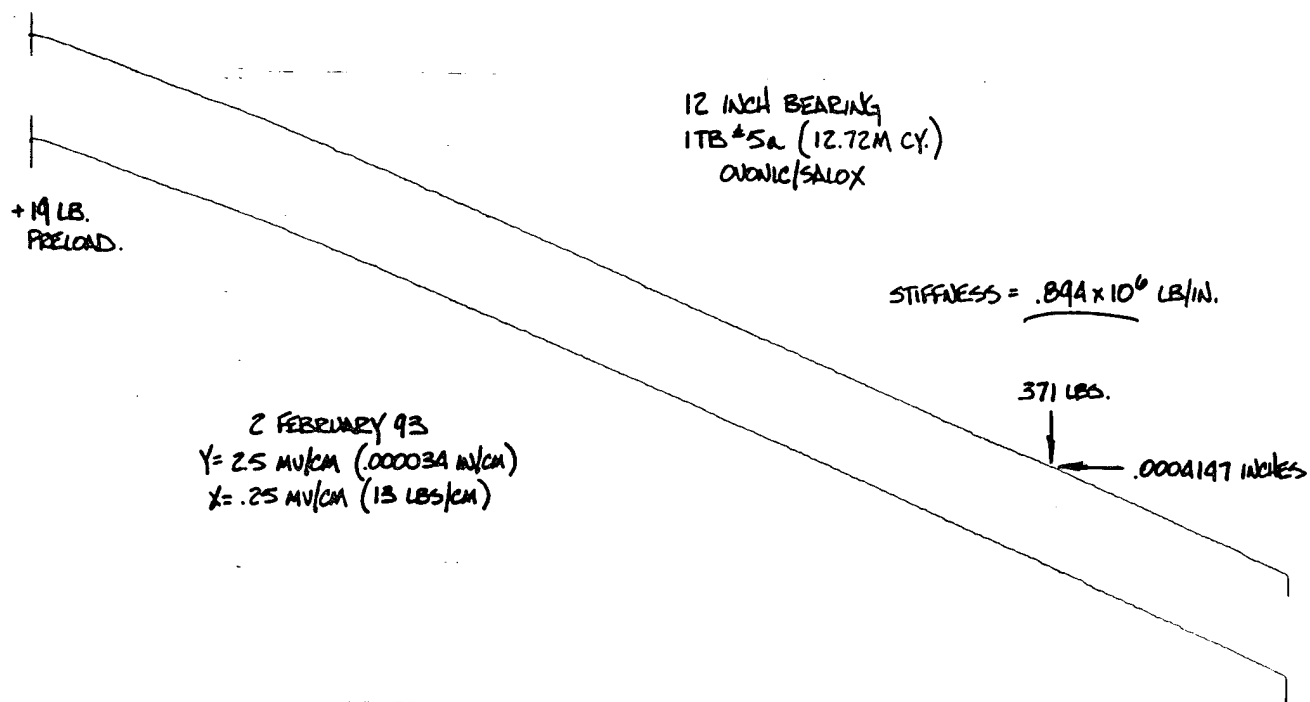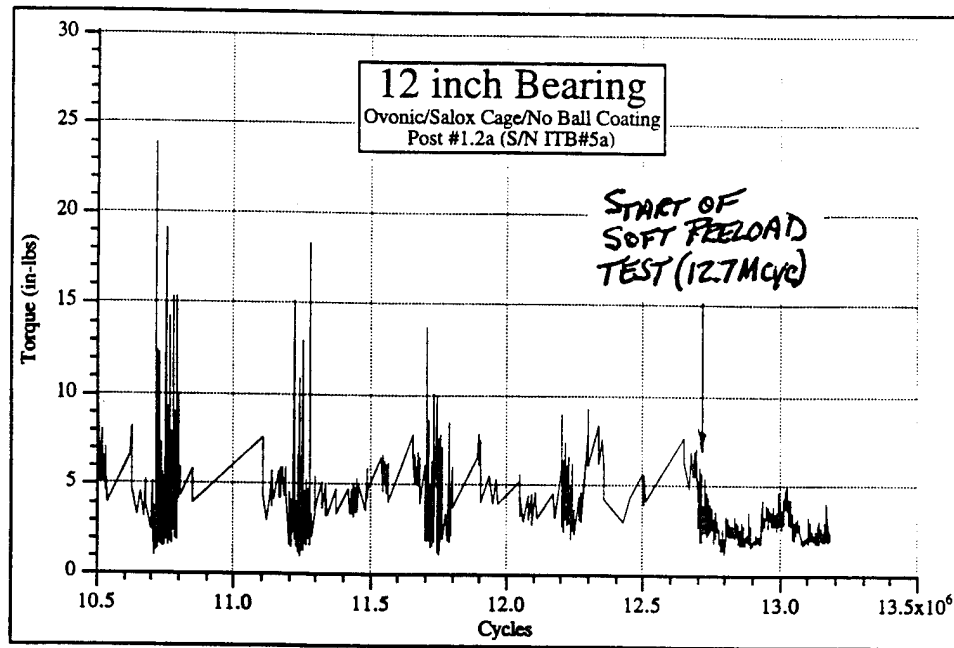PRELOAD

12 INCH BEARING
ITB #5a (12.72M CYCLES)
OVONIC/SNLOX

1 FEBRUARY 93
Y: LVDT = .01 V/CM
X: L/C = .25 MV/CM

187 LBS.

RETURN

140 LBS.

**Fig. 6-25  Preload of 12 inch Bearing with Ovonics Film at 12.7M cycles.**

**Fig. 6-26    Axial Stiffness of 12 inch Bearing with Ovonics Film at 12.7M cycles.**

**(a)** Soft preload test started at 12.7M cycles.
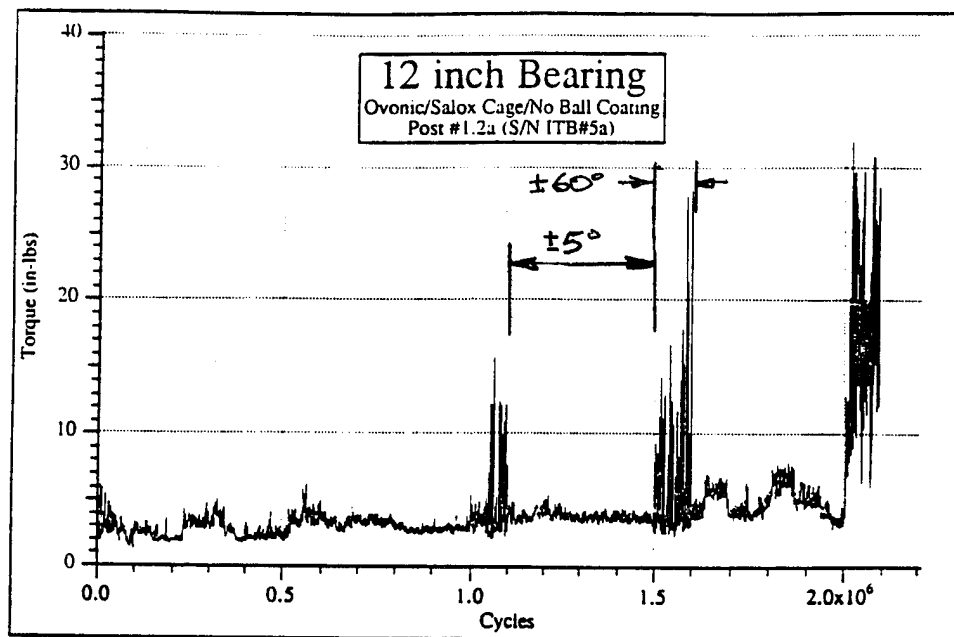


**(b)** Additional cycle life after 12.7M cycles

**Fig. 6-27** Soft preload extended life about one million cycles on Ovonics film bearing that previously failed at 12.7M cycles.

- 131 -

## 6.5.2 Comparison with NPE Greased Bearing

The 12-inch bearing (ITB #2) lubricated with the neopentylester grease was tested to nearly 39 million cycles. Gimbaling torques typically ranged from 5 to 12 in-lb, although excursions to 16 in-lbs occurred in mid-life. (see Fig. 6-28). These excursions were small compared with the $MoS_2$ bearings.

The posttest visuals showed the NPE 12-inch bearing to be in very good condition, little wear was found on either the balls or races, and the retainer ball pockets showed little or no damage. Copious amounts of free oil was still available on the bearing races. This is consistent with virtually no change in preload over life (201 lbs at test start and 193 lbs at test end) and little change in torque signature (see Fig. 6-24).
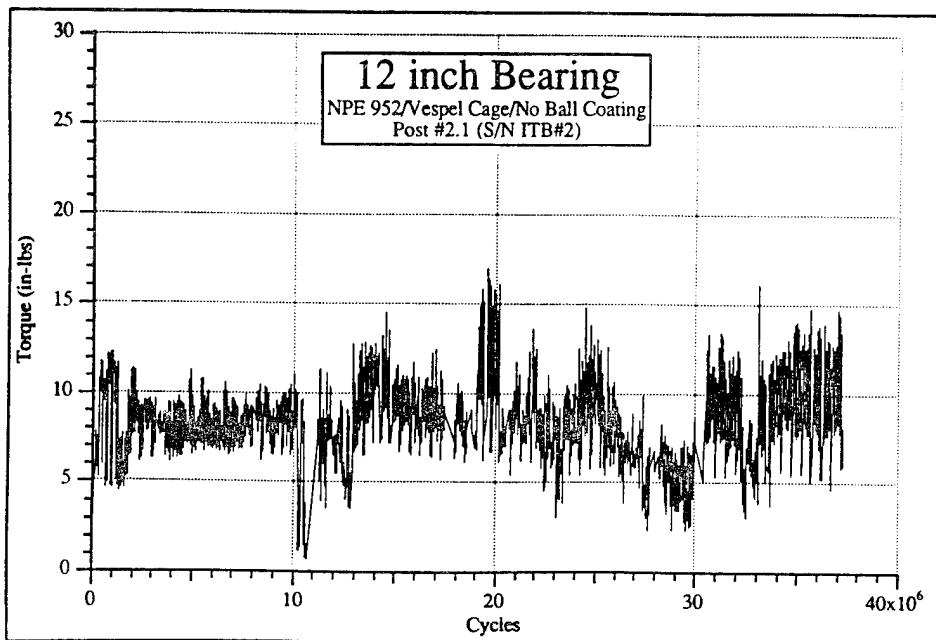


**Fig. 6-28    NPE-greased lubricated 12-inch bearing showed good torque performance throughout life. Test suspended at 39M cycles.**

## 6.6   FIVE INCH BEARING LIFE TEST RESULTS

### 6.6.1 $MoS_2$ Sputtered Bearings

Like the 12-inch bearing, the first pair of 5-inch or 117-size bearings with the nickel/Ovonics film showed high torque early in life. This bearing (post #3.1a) was suspended from test at 2.44 million cycles ( Table 6-1).

All subsequent bearings were then coated with the Ovonic high gold films. A second early failure (bearing on post #3.2) occurred at 40,000 cycles due to an oversized bearing ball that was 300 $\mu$ inch larger in diameter than the rest of the ball set. This put undue contact stress on the film which appear to have spalled off the race.

- 132 -

## 6.6.2 Life Tests

Torque histories for the high gold MoS$_2$, 5 inch bearings appears in Fig. 6-29. The bearing on post #3.1b showed relatively steady torque early in life, but experienced high torque excursions at 16 and 24 million cycles, Fig. 6-29(a). The post #3.2a bearing showed unusually high torque early in life that diminished with time, Fig. 6-29(b).
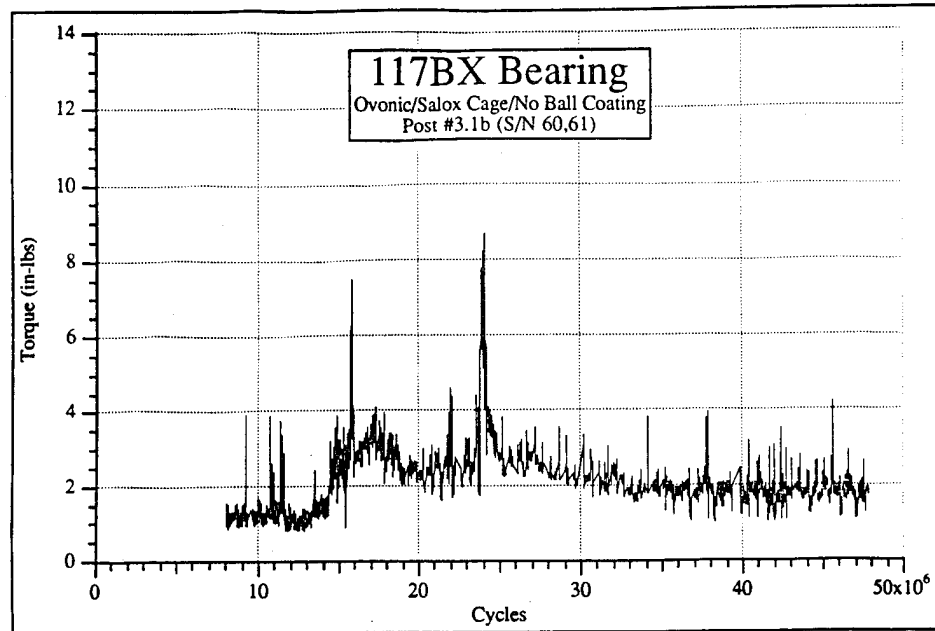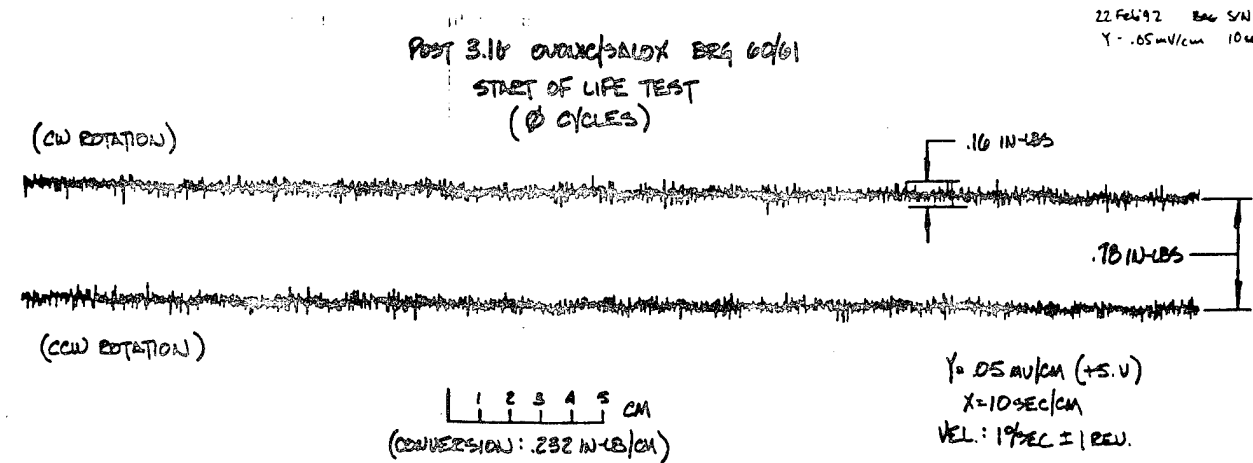


**(a)** Post #3.1b at 47.9M cycles
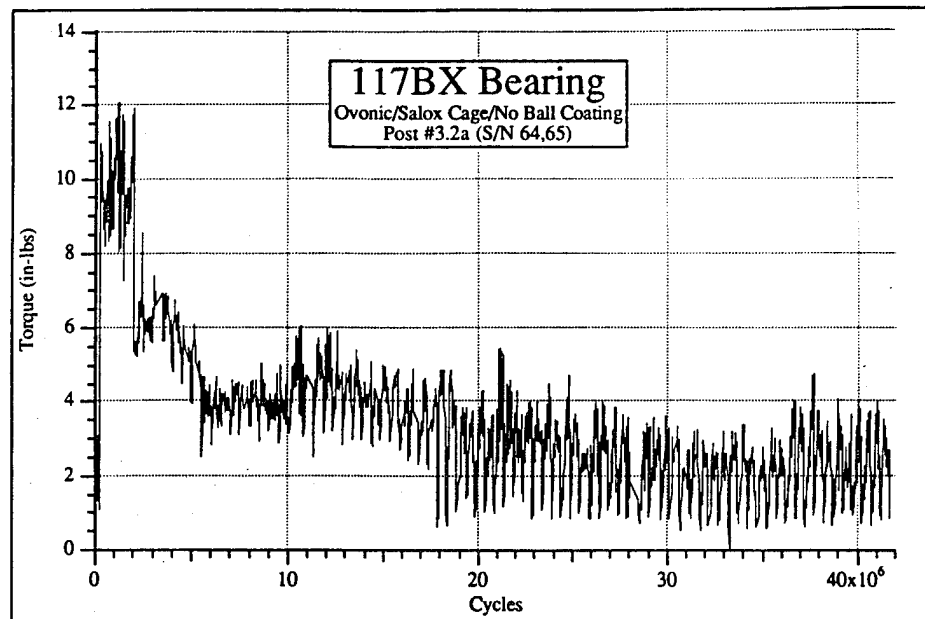


**(b)** Post #3.2a at 41.8M cycles

**Fig. 6-29 Torque history of high gold-MoS$_2$ lubricated, 117 size bearings**

- 133 -

Both bearings were found to have wear patterns similar to those on the 105-size bearings. The MoS2 film was clearly fractured or worn off at the edges of the ball track with some residual film, together with bands of retainer transfer film in the center region of the track (See 7.6).

Similar to the 12-inch bearings, a noticeable increase in torque and torque ripple was measured from the posttest torque signatures (Fig. 6-30). The torque ripple component is very large compared with starting trace values. The preload of #3.1b showed a substantial drop from 215 lbs at the start of testing to ≈ 150 lbs at end of life. The second 5-inch bearing showed a more modest loss in preload from 195 lbs to 175 lbs at test end. Preload changes are a net difference between film loss through wear and film replenishment from the transfer of film from the retainer.



(a) Beginning of Life
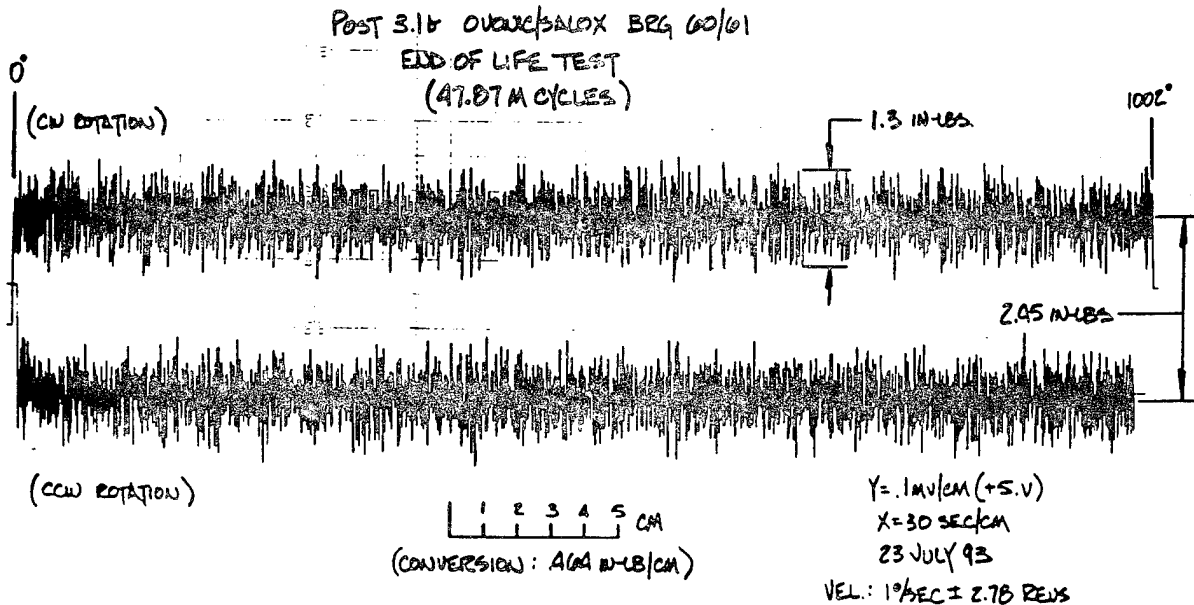


(b) End of Life (47.9M cycles)

Fig. 6-30    Comparison of Start and End of Life Test Torque Signatures of High Gold MoS2 Lubricated 117 Size Bearing (post #3.1b), Removed from Test Unfailed After 47.9M Cycles

- 134 -

POST 3.1b OVONIC/SALOX BRG 60/61 END LIFE TEST (47.87 M CYLES.)

Y=25mv/cm (+su.)
X=.25mv/cm
27 JULY 93

152 LBS.

147 LBS.
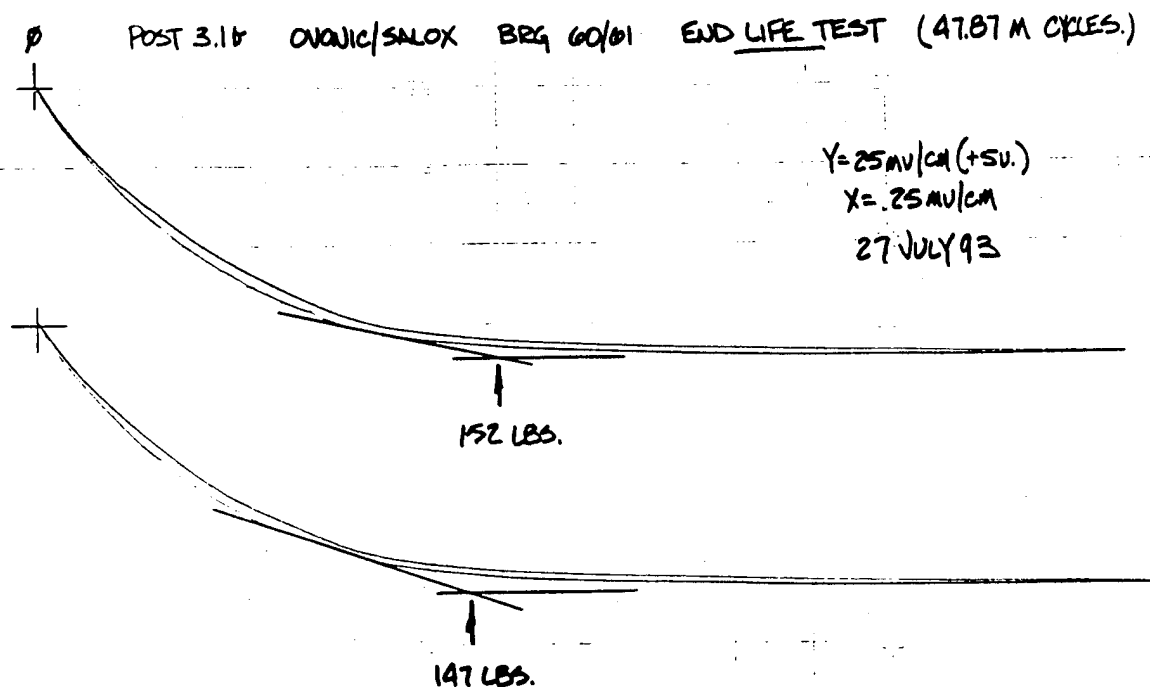
**Fig. 6-31** The post #3.1b, MoS$_2$ Lubricated 117 Size Bearing showed a significant drop ($\approx$ 25%) in preload at test end (47.9M cycles)

### 6.6.3 Comparison with Grease Lubrication

The multiple-alkylated cyclopentane (MAC) grease used in these tests contained Pennzane 2000™ oil in a sodium based thickener incorporating 3.5% lead naphthanate for antiwear protection. The first test bearing (post #2.2) showed erratic torque behavior, first only during the ± 5 deg cycle. As the life test progressed, erratic torque occurred for both small and wide angle slews (Fig. 6-32). It was first theorized that there was a problem with this particular grease so it was decided to rerun the test with the NPE grease, a known good performer.

When the test was rerun with NPE grease, a similar torque pattern resulted (Fig. 6-33). Again escalated torque was first observed for the ± 5° dither cycle only and later for both small and wide angles. Since both the MAC and NPE bearings looked dry during posttest examination, it was hypothesized that there may not have been enough grease in the bearing at start of test. Up until this point all 105-size, 5- and 12-inch bearings had received the standard grease plate procedure where bearing races and balls were submerged in a freon/grease bath comprised of approximately 15% by weight of the test lubricant. It was thought that the high torque encountered during ± 5 degree gimbaling was likely the result of the ball/race contact drying out, since a ± 5 degree angle is too small to replenish the contact with fresh grease that had been squeezed out.

To test this hypothesis, a third pair of 5-inch bearings was prepared with 2.5 gms of additional grease per bearing ( 5 gms per pair) injected by a syringe. This was in addition to the 0.4 gms of grease that is normally supplied by the grease plating process. This represents a grease fill of about 15%; considered an ample supply of grease to rule out grease starvation as the problem. Furthermore, more grease would cause a bearing drag torque problem (Fig.

6-34). The extra grease did help, but the same torque problem reappeared after about 8 million cycles (Fig. 6-35).

The posttest torque signature of this bearing showed considerably more bearing torque noise compared with the starting torque trace in Fig. 6-36. However, this running torque trace does not happen to catch the bearing producing the abnormally high peak torque as observed in Fig. 6-36. This suggests that the source of high torque may be debris which can be occasionally trapped between the balls and race.

Post-life test visual examination indicated that the bearings were relatively wet with lubricant. Darkened grease of a gelatinous consistency was found in the ball pockets and along the ball track on the inner race. The retainer ball pockets were not worn. The carbonaceous lead deposits found in the inner race ball tracks appear to be sufficiently thick (at least a micrometer) to increase bearing torque. Other investigators [6-3] have reported that the lead naphthanate antiwear additive will form thick deposits in the ball wear track under high stress and elevated temperature conditions. The deposit no doubt forms from reduction/ decomposition of the lead naphthanate antiwear additive. Although this reduction/ decomposition of the lead naphthanate is the reason for its addition (which minimizes bearing wear), a high rate of reduction/decomposition will cause deposit build-up, increased preload and hence an increase an bearing torque.
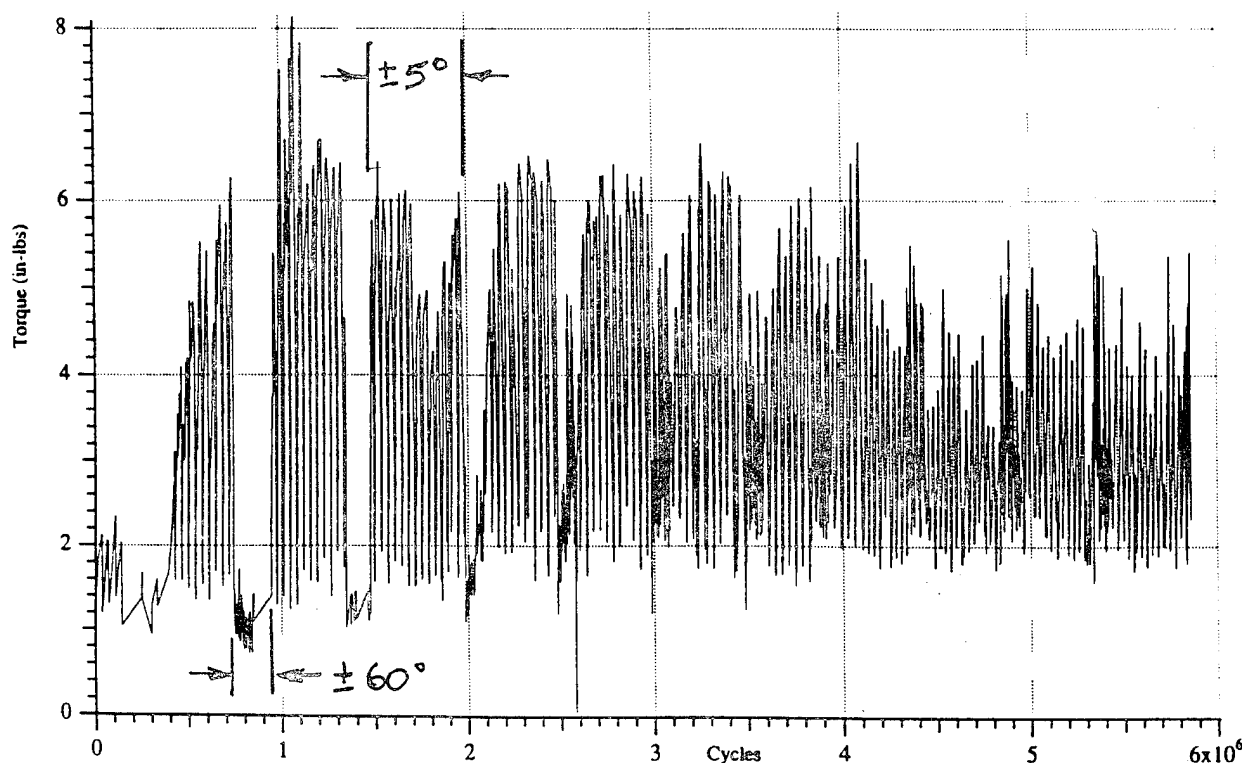


Fig. 6-32 Torque profile for the MAC greased, 5-inch bearings showing erratic torque behavior for small angle slews and later for both large and small angle slews
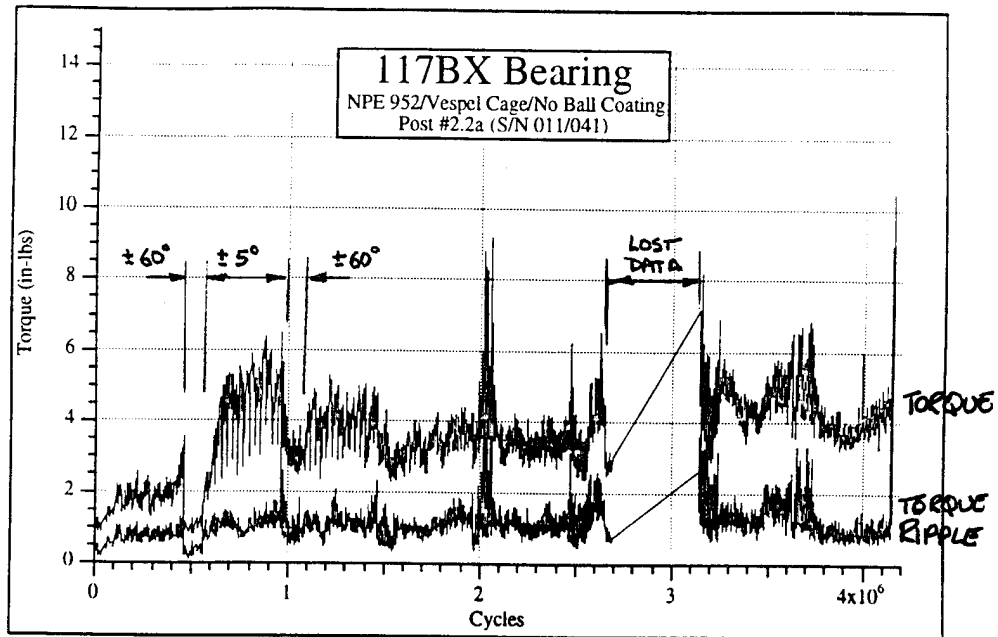
- 136 -

**Fig. 6-33** NPE greased, 5 inch bearing showed similar erratic torque profile to the MAC greased bearing suggesting insufficient grease amount.
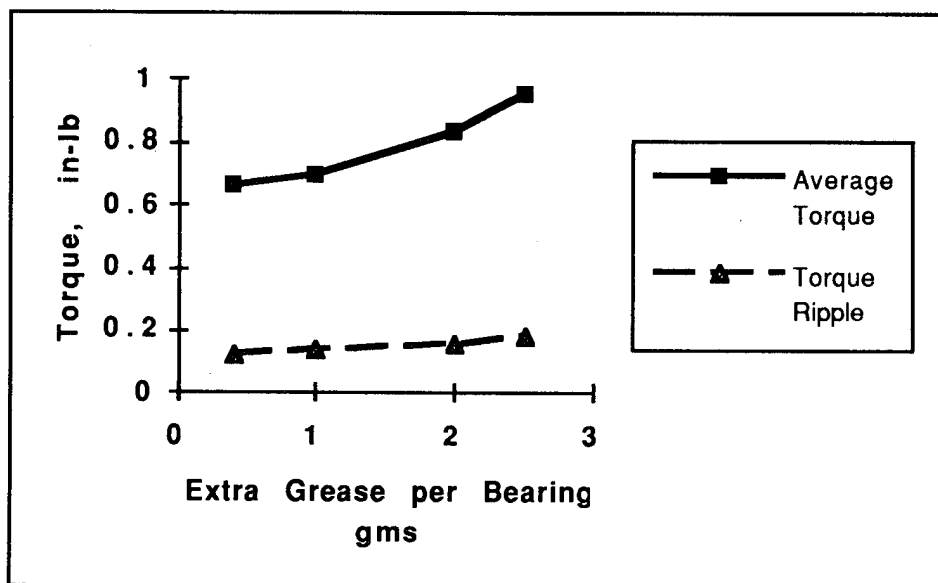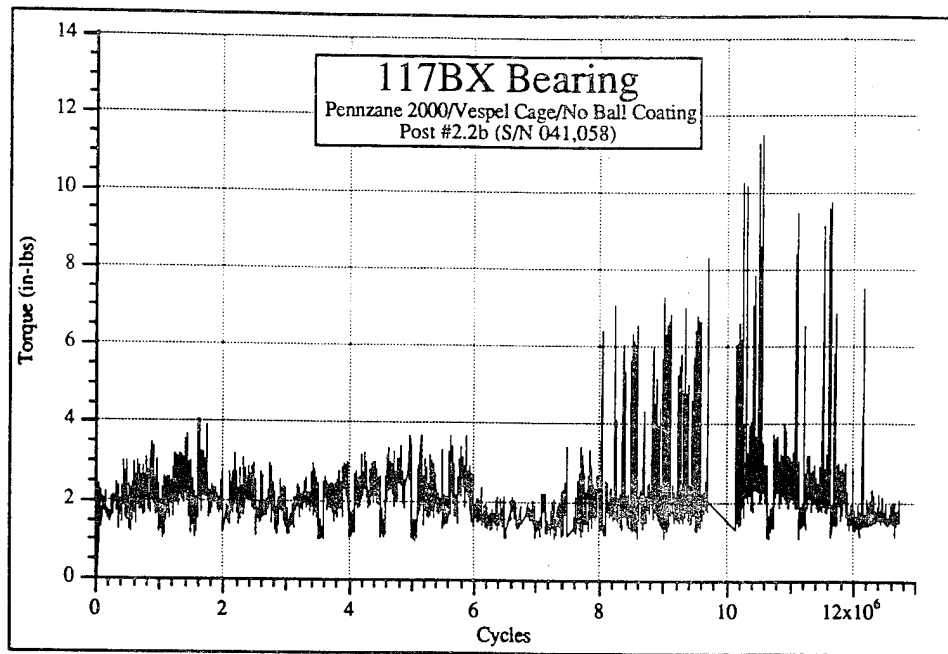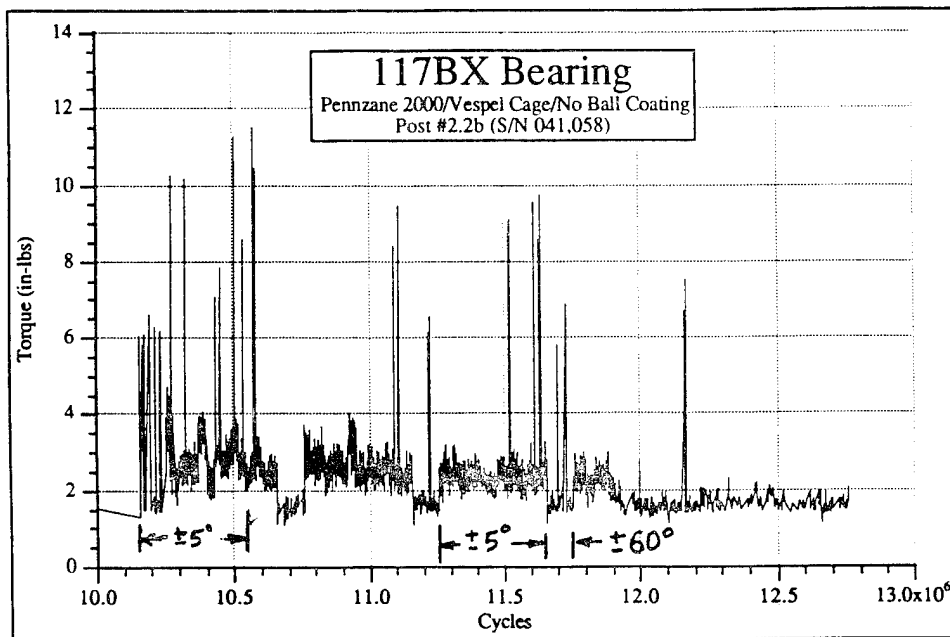


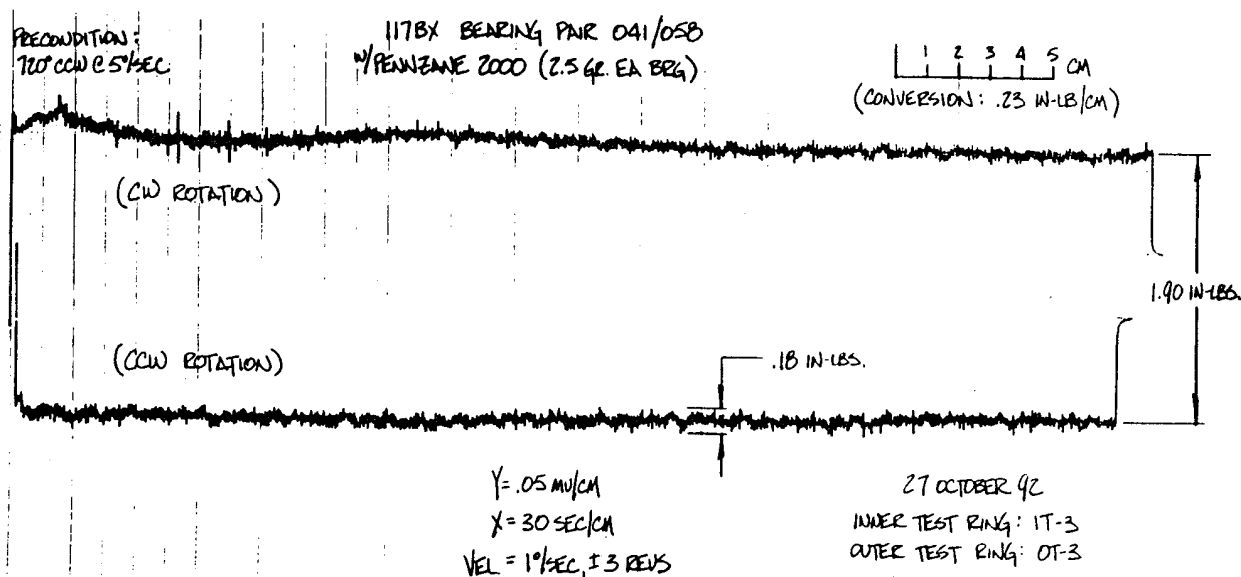**Fig. 6-34** Effect of grease amount on torque for MAC lubricated, 5 inch bearing at 1 deg/sec.
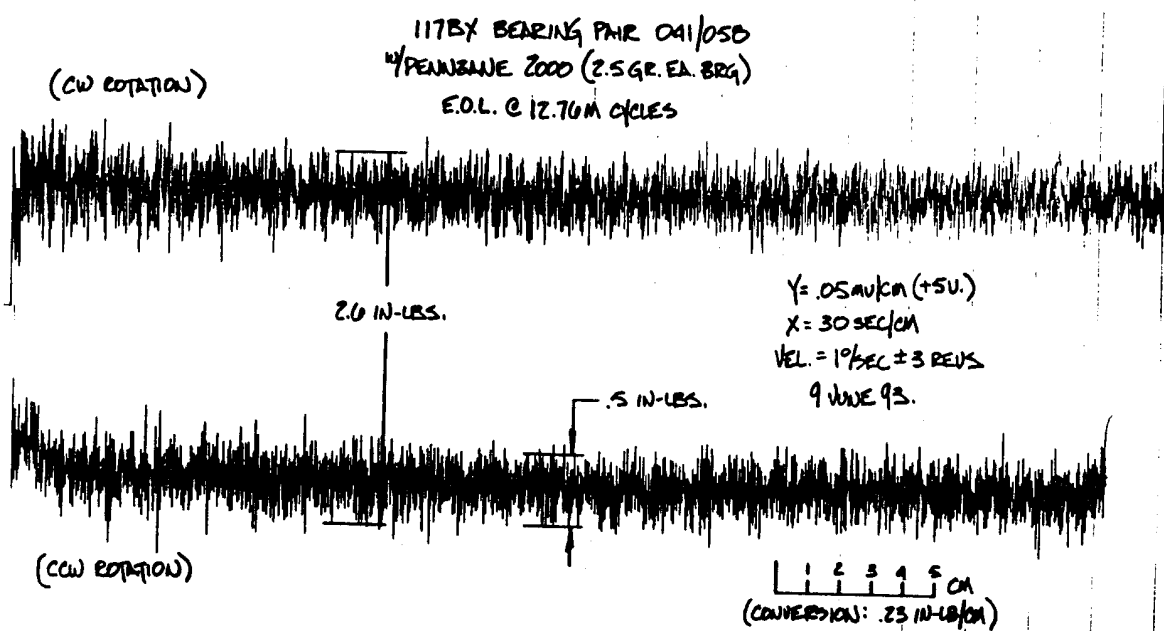
(a) Torque peaks start at ≈ 8M cycles



(b) Expanded scale showing torque peaks during
both short and wide gimbal strokes

Fig. 6-35    Repeat test with MAC greased, 5 inch bearing pair with 10
grams of extra grease, showing delay of torque spikes to 8
million cycles.

- 138 -

117BX BEARING PAIR 041/058
W/PENNZANE 2000 (2.5 GR. EA BRG)

| 1 | 2 | 3 | 4 | 5 | CM |

(CONVERSION: .23 IN-LB/CM)

(CW ROTATION)

1.90 IN-LBS.

(CCW ROTATION)

.18 IN-LBS.

Y = .05 MV/CM
X = 30 SEC/CM
VEL = 1°/SEC, ± 3 REVS

27 OCTOBER 92
INNER TEST RING: IT-3
OUTER TEST RING: OT-3

**(a)** Starting torque signature

(CW ROTATION)

117BX BEARING PAIR 041/058
W/PENNZANE 2000 (2.5 GR. EA. BRG)
E.O.L. @ 12.76M CYCLES

2.6 IN-LBS.

.5 IN-LBS.

Y = .05 MV/CM (+5V.)
X = 30 SEC/CM
VEL. = 1°/SEC ± 3 REVS
9 JUNE 93.

(CCW ROTATION)

| 1 | 2 | 3 | 4 | 5 | CM |

(CONVERSION: .23 IN-LB/CM)

**(b)** Post test torque trace

**Fig. 6-36  Running torque trace comparison with damaged MAC - greased bearings. Note considerable degradation of torque smoothness.**

## 6.7 SCALE UP

The bearing lives with the larger bearings having the high gold Ovonic films were much shorter than those obtained with the 105-size screening bearings (Fig. 6-37). Furthermore, torque excursions were more severe. Scale up of the deposition process for larger bearings and the design of fixturing required several iterations (Section 7.6.1). Higher quality films are more achievable in the smaller bearings.

The larger diameter, thin section gimbal bearing geometry is inherently more debris sensitive, hence a poorer candidate for solid lubricant films. This is due to their very stiff construction and the relatively small Hertzian deflection associated with a large number of small balls. Also, the large pitch diameter amplifies frictional forces in terms of torque irregularities.

Relative increases in torque between small and large bearings are also shown in Fig. 6-37. Torque increases of 10 to 20 times were measured between the two bearing sizes when lubricated with either MoS2 film or grease.
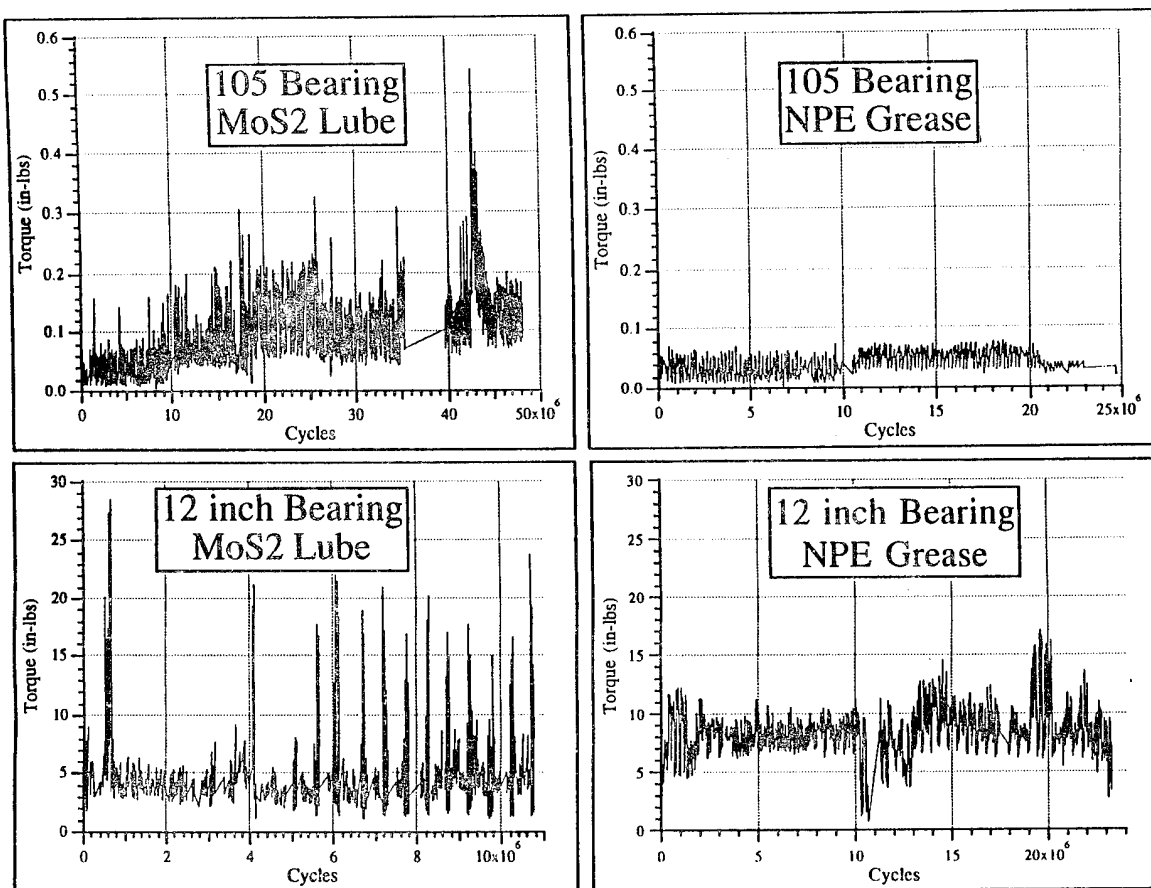


Fig. 6-37  Effects of bearing size on torque and life of Ovonics/Au MoS2 and NPE grease lubricated bearings

## 6.8 KEY FINDINGS

**Film Delamination (6.3)** A problem with $MoS_2$ film delamination was encountered with both the 12- and 5-inch bearings deposited with multilayer $Ni/MoS_2$ films. Thinner films with 45% Au-Pd interlayers were found to be more fracture resistant based on a ball/plate tester. However, these films did not totally eliminate film delamination in either the large or the small bearings.

**Speed Effect (6.4)** A torque build up with rotational speed was observed with the 12-inch bearings. This was attributed to an over-transfer of PTFE film from the PTFE/bronze composite retainer, causing a buildup in film thickness, hence preload. A large preload increase at the end of test and excessive wear of the Br-PTFE toroidal ball separators helped confirm this observation. It was necessary to reduce the test cycling rate in order to inhibit retainer material over transfer. The balance between race film wear and replenishment by the retainer's transfer film is critical.

**Debris Sensitivity (6.5 & 6.6)** Large periodic torque excursions were recorded for both 5- and 12-inch $MoS_2$ bearings. The 12-inch bearings exhibited the highest torque excursions during the transition from $\pm 5$ deg cycling (< one ball track spacing) to $\pm 60$ deg (many ball track overlaps). These excursions were attributed to rolled over $MoS_2$/retainer debris which caused large increases in preload. A spring or "soft" preload test was devised to desensitize the relationship between preload and debris. An immediate torque reduction for the next million cycles resulted, indicating that spring preload would be preferred for bearings using $MoS_2$ film lubrication. However, such an approach would likely be restricted to nonstiffness driven gimbal applications.

**Torque Performance (6.4.1)** The torque performance of new $MoS_2$ bearings is comparable to or better than those grease lubricated at low speeds (Fig. 6-37). At higher speeds and presumably colder temperatures the $MoS_2$ coated bearing has an advantage due to its low torque/speed sensitivity. On the other hand, the torque signature of the $MoS_2$ lubricated bearings degraded more quickly with time than those grease lubricated. This is likely a result of unevenness of the film coating/retainer transfer deposits in combination with higher retainer friction. The large torque excursions observed during the gimbal life test did not always occur during a multi-rev torque signature test. Rotating the bearing through several revolutions in each direction tended to redistribute debris and smooth out the torque. Such a technique might prove to be a reasonable on-orbit maintenance procedure for improving dry film bearing torque performance.

**Life (6.5, 6.6 and 6.7)** The life of 12-inch bearings with $MoS_2$ lubrication was relatively short compared with the comparable grease lubricated bearings and the smaller $MoS_2$ test bearings. The two pair of $MoS_2$ coated 5-inch bearings, although having some major torque excursions, were still tested to more than 40 million test cycles. The bearings experienced some wear and loss in preload The 12-inch bearing was judged particularly sensitive to $MoS_2$/retainer debris because of its high stiffness, large torque arm and small ball Hertzian deflections.
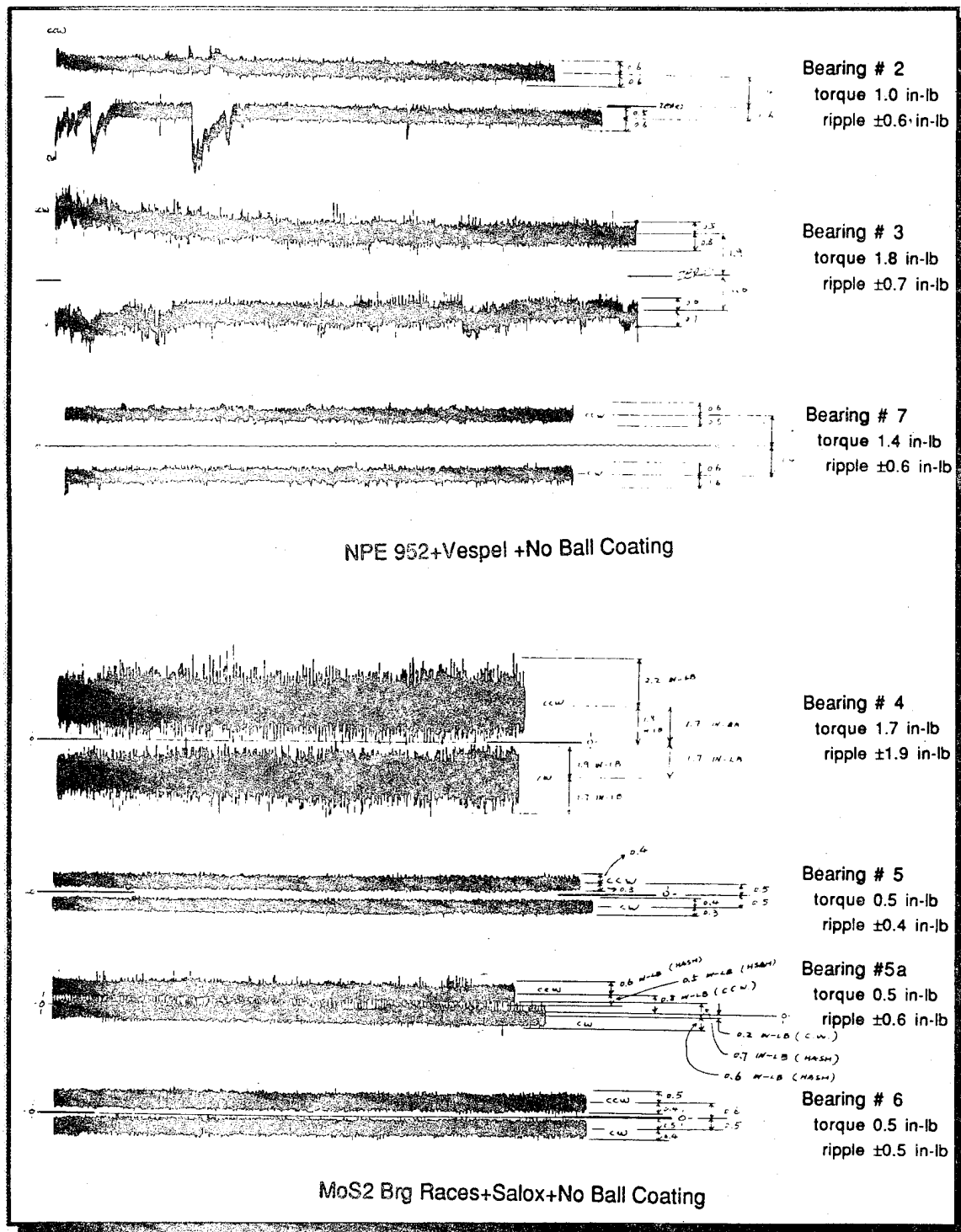
Bearing # 2
torque 1.0 in-lb
ripple ±0.6 in-lb

Bearing # 3
torque 1.8 in-lb
ripple ±0.7 in-lb

Bearing # 7
torque 1.4 in-lb
ripple ±0.6 in-lb

NPE 952+Vespel +No Ball Coating

Bearing # 4
torque 1.7 in-lb
ripple ±1.9 in-lb

Bearing # 5
torque 0.5 in-lb
ripple ±0.4 in-lb

Bearing #5a
torque 0.5 in-lb
ripple ±0.6 in-lb

Bearing # 6
torque 0.5 in-lb
ripple ±0.5 in-lb

MoS2 Brg Races+Salox+No Ball Coating

Fig. 6-38  Comparison of torque signatures of new 12 inch bearings lubricated with NPE grease (top) and Ovonics/Au MoS$_2$ (bottom)

# References For Section 6

[6-1]   Dahl, P.R., "A Solid Friction Model," AFO 4695-67-C-D158, Aerospace Corp.,
        May 1968.

[6-2]   Rohn, D. A. and Loewenthal, S. H.,  "An Analysis of Traction Drive Torsional
        Stiffness, " Trans. of ASME, Journal of Mechanisms, Transmissions, and
        Automation in  Design, Vol. 107, No. 4, Dec 1985, pp. 573-581.

[6-3]   Hilton, M.R., Kalogeras, C.G., and Didziulis, S. V., "Investigation of Multiply
        Alkylated Cylopentane Synthetic Oil and Lead Naphthenate Additive Under Boundary
        Contact Interactions," Aerospace Report No. ATR-93(8361)-1, (1993).

# Section 7

# CHARACTERIZATION OF THIN FILMS AND TESTED BEARING COMPONENTS

This section presents the results of detailed examination of the tested bearing components. In addition, thin films deposited on specialized test samples and witness plates were characterized in order to optimize the deposition process and improve thin film properties. Films tested on small thrust bearings were deposited by Aerospace Corporation, Hohman Plating & Mfg., National Center of Tribology (NCT), Naval Research Laboratories (NRL) and Ovonics Synthetic Materials Co. Hohman, NCT, and Ovonics were chosen to deposit films on the 105-size angular contact bearings for the comprehensive screening tests. Ovonics was selected to deposit films on the 5- and 12-inch bearings. Perfluoroalkyl polyether, synthetic hydrocarbon and ester greases that were tested in angular contact bearings were also examined for comparison.

## 7.1 THRUST BEARINGS

The thrust bearings were disassembled after testing and examined visually with a light microscope and in a SEM. All of the worn films appeared similar with two exceptions:

1. One of the bearing sets coated by Naval Research Laboratories (NRL) using the ion beam assisted deposition (IBAD) process still had shiny balls after testing, thus indicating transfer of the film from race to balls had not occurred. Examination of the races revealed a polymer deposit in the ball path (Fig. 7-1a). Infrared analysis of the deposit indicated it was poly-tetrafluoroethylene which matched an analysis of the Salox-M retainer. Examination of the retainers did not reveal any pieces missing; however flakes of materials were found suggesting abrasion was occurring somewhere on the retainer.

2. One set of the Hohman C thrust bearings (Hohman C) performed poorly during tribo-testing. Examination of the bearings showed at least three balls in each set of twelve were shiny thus indicating film transfer had not occurred. Moreover, one of the shiny balls could be moved by merely tilting the bearing shaft assembly. This movement is clear evidence of zero preload on those balls. Disassembly of the bearings revealed ball wear paths that were not concentric with the race ball path (Fig. 7-1b). These eccentric wear paths are typically caused by misaligned parts or unspecified dimensional changes.

The races of the remaining thrust bearings generally had an even distribution of debris around the circumference of the ball track (Fig. 7-2a). The ball paths were typically well delineated by the absence of grinding scratches which get worn off or ironed over by ball travel (Fig. 7-2a). This ball track can easily be seen in backscattered electron micrographs in which image contrast is more sensitive to atomic number than topography (Fig. 7-2b). In this case the $MoS_2$ film is much lighter in contrast than the underlying steel. The heaviest wear occurred in the center third of the ball track, where exposed iron carbides could be observed (Fig. 7-3). Heavy wear in the center of the ball track suggests an adhesive wear (rather than abrasive) mechanism, considering stress is highest in the center of the ball track.

Salox-M retainers exhibited much less wear than the retainers made from Vespel. The Vespel retainers typically had deep pockets ground into the retainer faces as a result of ball contact. This high degree of wear was not observed on the Salox-M retainers. However, debris

This high degree of wear was not observed on the Salox-M retainers. However, debris analysis indicated some abrasion of the Salox-M retainers had occurred. Elemental analysis of the debris from the thrust bearings using Salox-M ball separators revealed copper, tin and fluorine present. These elements are the retainer composite: bronze (copper-tin) particles in a polytetrafluoroethylene (Teflon) matrix.

The thicknesses of the films on the thrust bearings were determined by indenting the film (Rockwell C) on a flat adjacent to the ball-path groove. This indentation fractures the film adjacent to the indent. The thickness of film can then be directly measured by examination of the film cross-section at high tilt (Table 7-1)

## Table 7-1

| Film | Film Thickness (µm) |
|---|---|
| Aerospace | 0.8 |
| Hohman | 2.1 |
| National Center for Tribology | 0.6 |
| Naval Research Laboratories | 0.7 |
| Ovonics - Nickel | 1.1 |
| Ovonics - Gold | 0.9 |
| Requested | 1.0 |

These film thicknesses were consistent for each of the film manufacturers. That is, the film thickness variation for an individual manufacturer or process was typically within 0.1 micrometers. However, only Ovonics exhibited high accuracy considering a one micro-meter film was requested from all of the film producers.
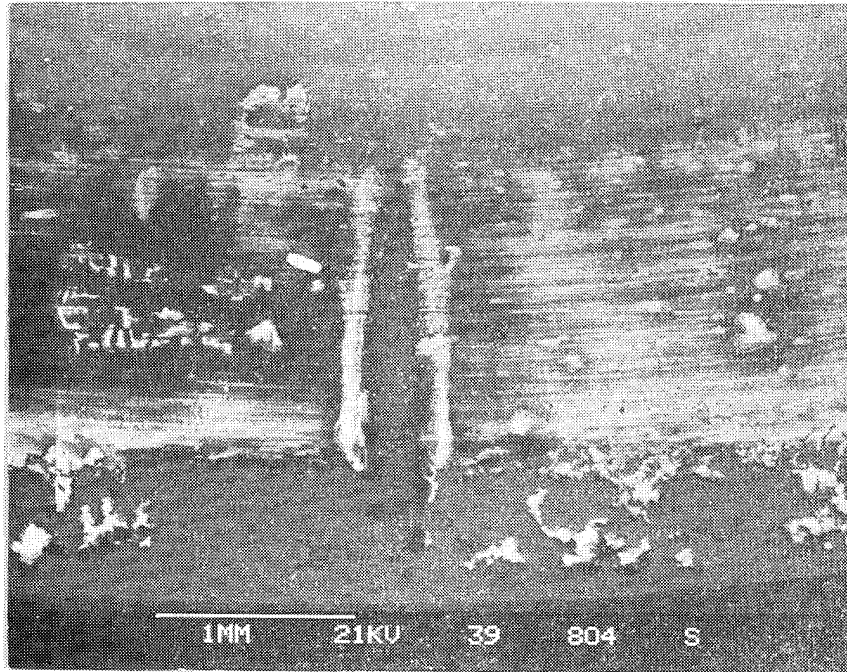
(a)            15X
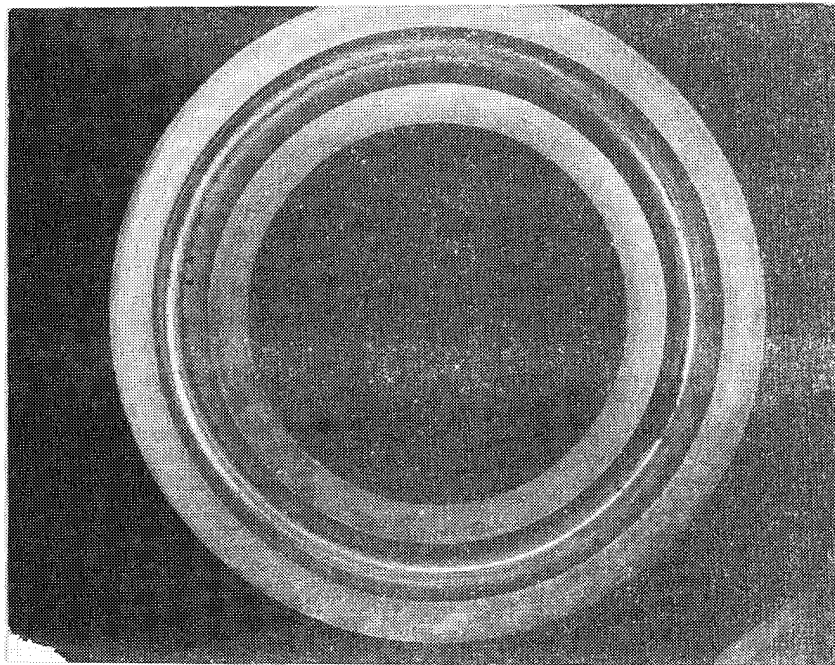


(b)            2X

Fig. 7-1 Deposit in the ball track of the NRL bearing was retainer material (a). Eccentric ball tracks on the Hohman C races suggests misalignment (b).
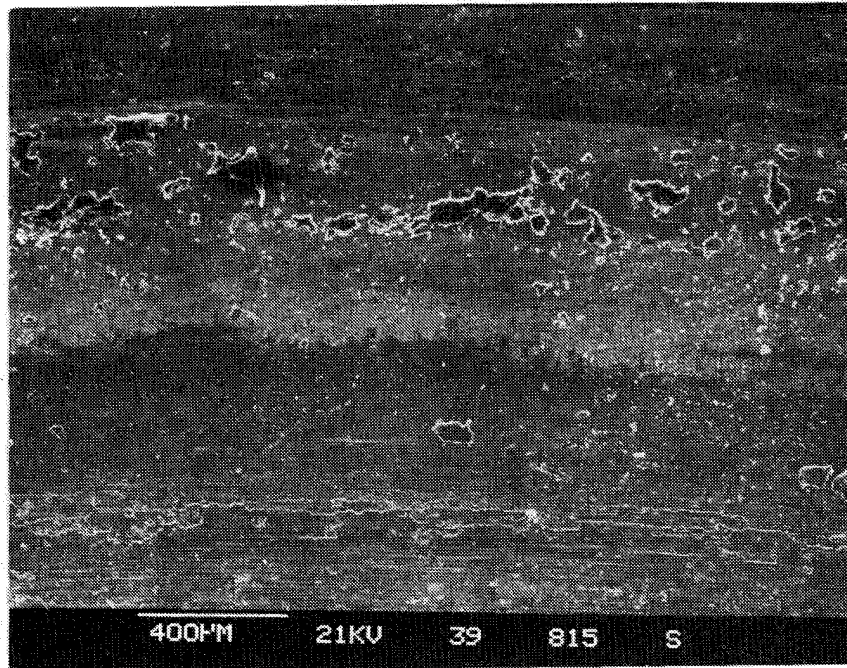
(a)             50X
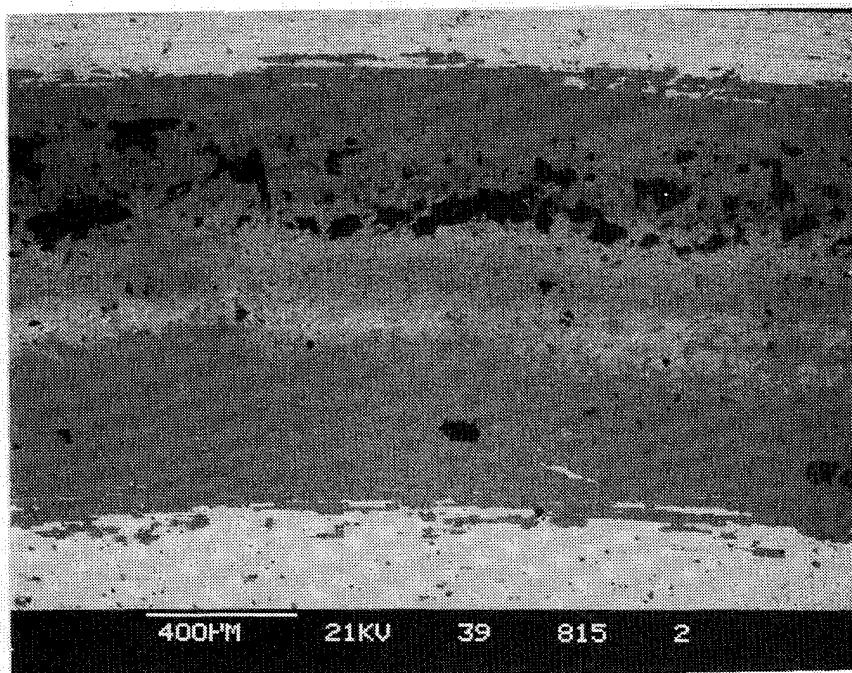


(b)             50X

**Fig. 7-2**   **Debris was evenly distributed along ball track circumference (a). Ball track was well delineated in the backscattered electron image (b).**
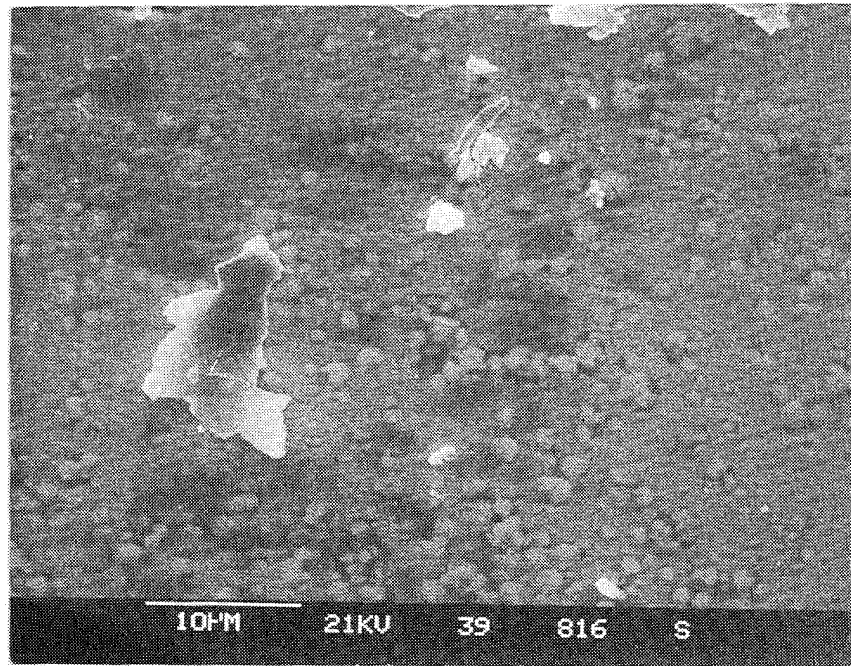
**Fig. 7-3    Extreme wear in the ball track center exposes carbides from the steel alloy races**

## 7.2 HOHMAN MoS$_2$/Sb$_2$O$_3$ DEPOSITION PROCESS SUPPORT

Lockheed's Materials & Process Laboratory supported the refinement of Hohman's MoS$_2$/Sb$_2$O$_3$ deposition process. Hohman reported that the current setting on the plasma power supply was the process variable that affected the endurance of the films the most. Films produced with lower currents tended to exhibit greater endurance on the Hohman A-6 tester. To understand the effect of these current settings on the film structure, witness plates were exposed to depositions at three different current settings and then analyzed. The films were scribed and indented, then examined in a scanning electron microscope (SEM) to characterize the morphology. Crystallinity was determined by X-ray diffraction.

The morphology of the films changed significantly with current levels. The film produced with a low current had a columnar-plate morphology (Fig. 7-4), whereas the higher current films had more of a "mounded" morphology (Fig. 7-5 and 7-6). Using the structure-zone models, the low current films had a zone 2 morphology whereas the higher current films had a zone 1 morphology.

An interesting feature of the low current film morphology is that the columnar plates appear to be grouped or organized into colonies about 0.2 μm in diameter. Note this size range is similar to the size of the mounds in the higher current films (Figs. 7-5 and 7-6). Moreover, the mounds in film 2 appear to be made up of smaller (0.05 μm) particles. This consistency in macro-morphology with changes in micro-morphology suggests the diameter of the mounds may be a function of the film nucleation and final thickness rather than the plasma process.
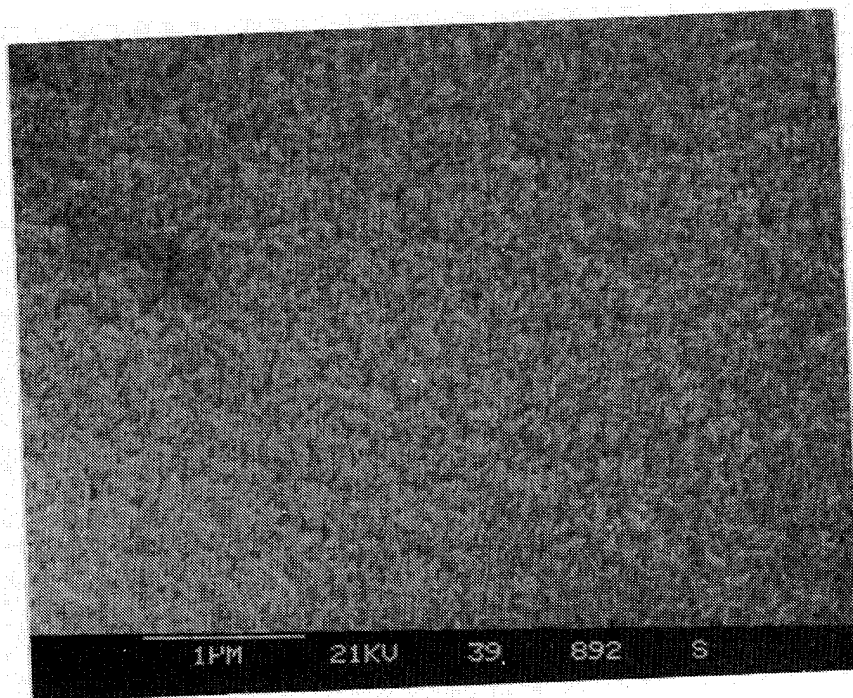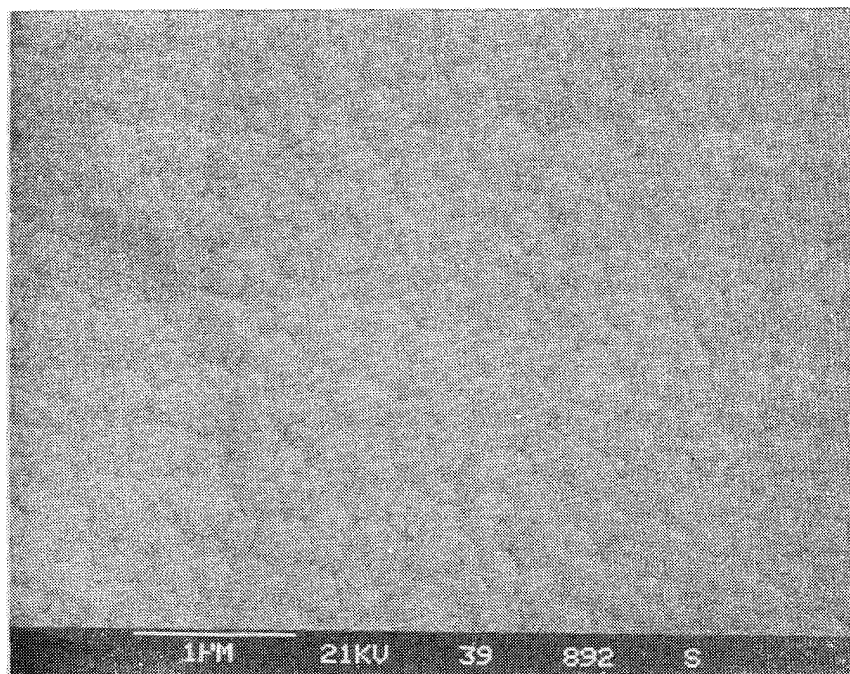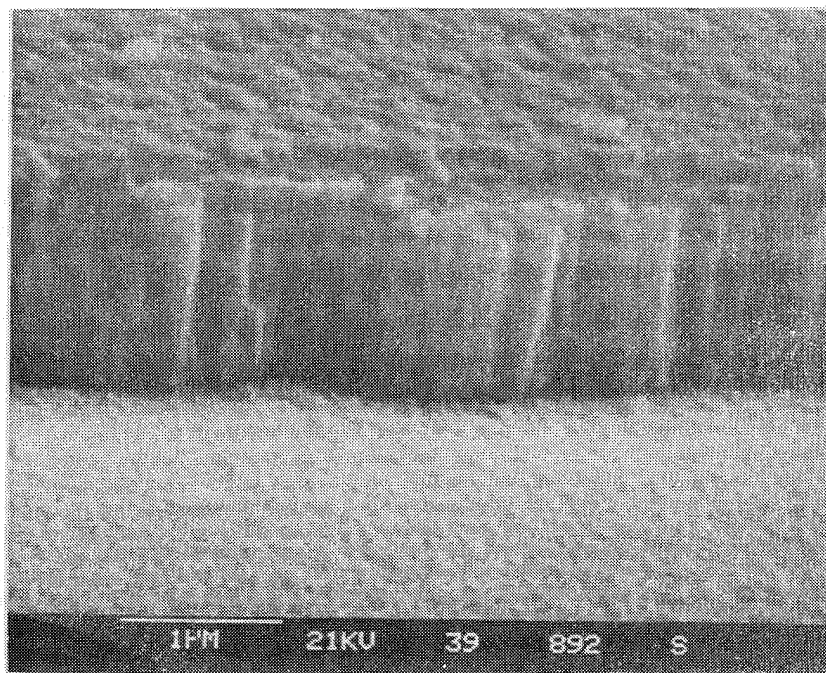
(a)            No Tilt



(b)            High Tilt

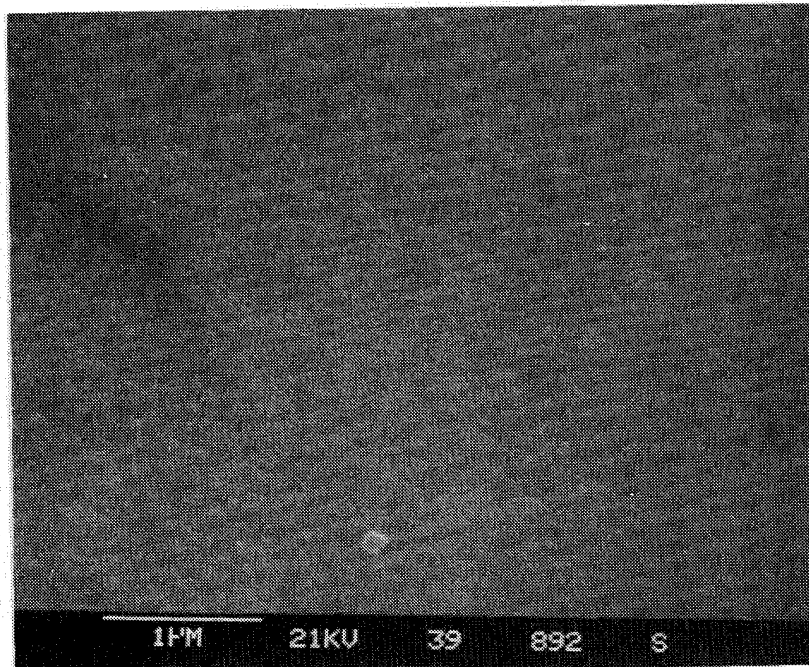**Fig. 7-4**     **Film deposited at low current had a columnar-plate morphology. 20,000X.**

(a)                No Tilt

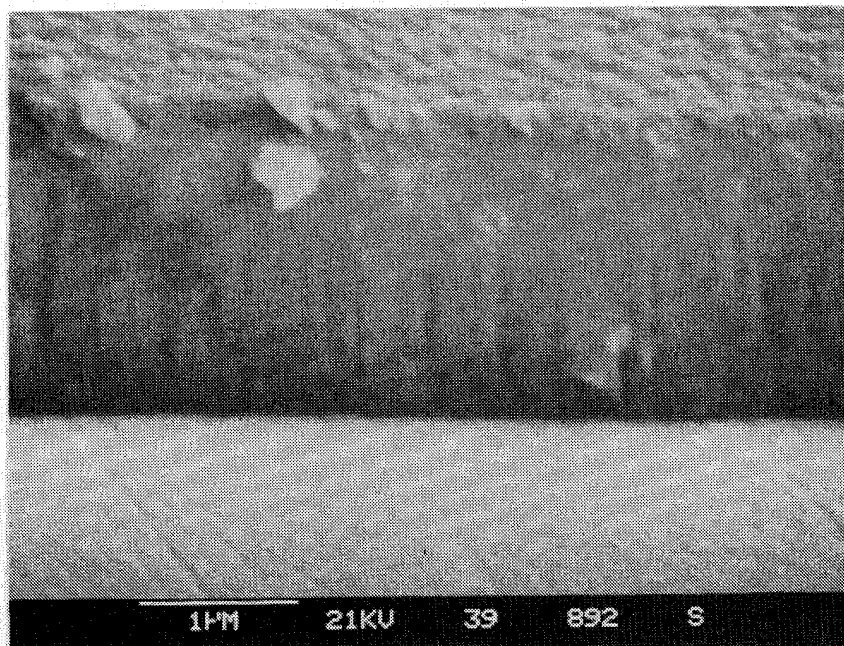

(b)                High Tilt

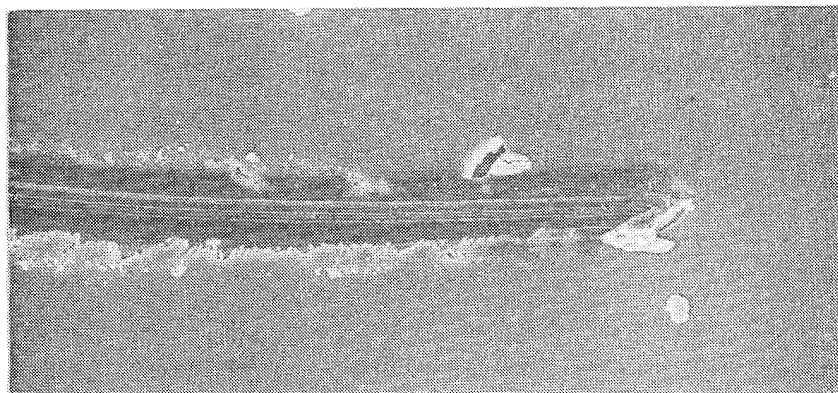**Fig. 7-5**    **Film deposited at medium current had a mounded morphology.   20,000X.**
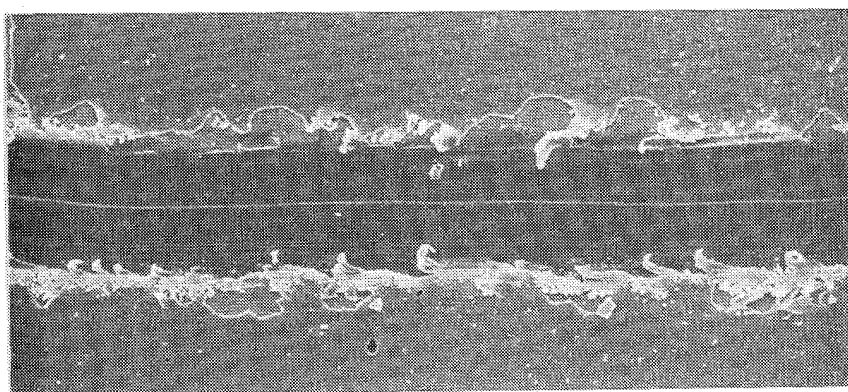
(a)    No Tilt



(b)    High Tilt

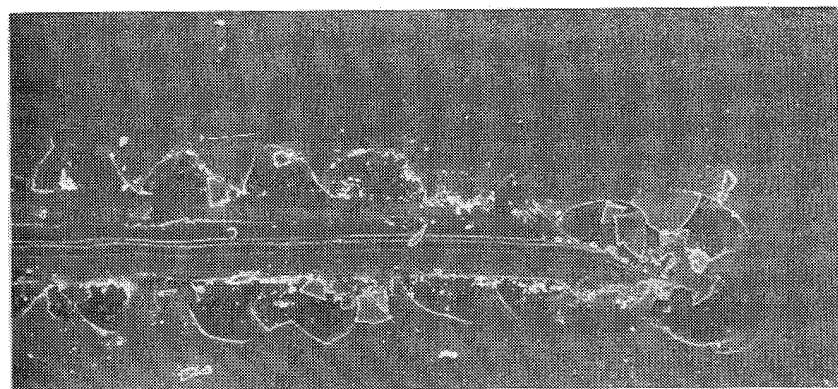**Fig. 7-6** **Film deposited at high current had a less distinct mounded morphology.   20,000X.**
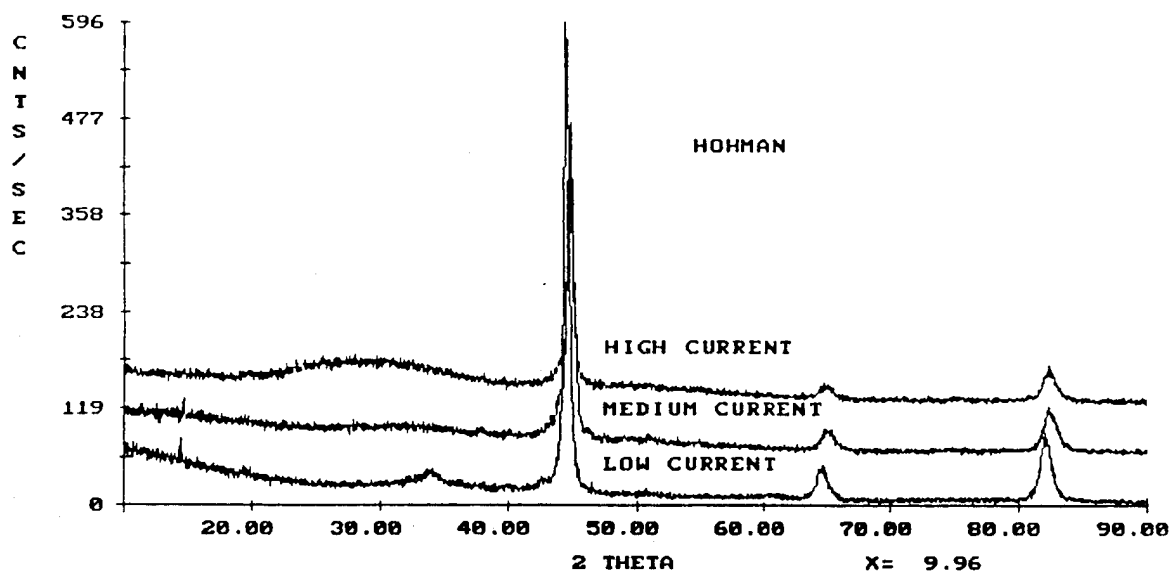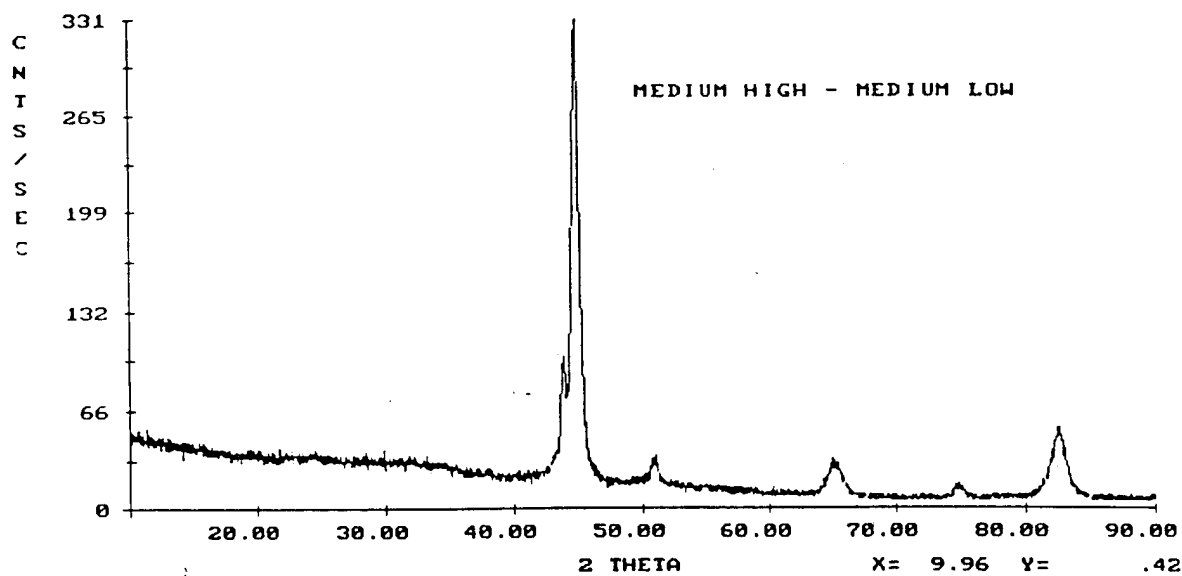
Low Current



Medium Current



High Current

**Fig. 7-7    Fractures generated by scribing the film indicated lower
deposition current produced better adhesion.   250X**

(a)



(b)

**Fig. 7-8**     X-ray diffraction results show changes in crystalline structure with deposition current (a). Film produced by alternating current did not exhibit crystallinity (b).

The fracture and delamination of the films adjacent scribe marks indicates film adhesion also varied with current levels (Fig. 7-7). More brittle film fracture and delamination occurred with higher current. This may be a result of film thickness and/or density. This variation in adhesion also can be observed in the high tilt views of the films. The high current films tend to fracture more often at the film to substrate interface rather than leaving a small amount of residual material on the substrate (Figs. 7-4 to 7-6).

X-ray diffraction supported the structural analysis gained from the SEM examination. Only the film produced at low current exhibited significant crystallinity - a small (100) peak was detected (Fig. 7-8a). This result is consistent with the existence of a zone 2 columnar plate film morphology. Note the film produced at a high current exhibited a broad peak or "hump" between 25 and 35 degrees ($2\theta$ scale). The hump is actually a broad peak that is typical of a non crystalline material or amorphous. Note also this humped region is flat in the lower current films. The physical explanation for broad peaks in non crystalline materials is that a range of atom interatomic distances exists, similar to glass.

The optimum structure for this film may be between amorphous or non crystalline and the textured (show diffraction peaks) perhaps micro- or nano- crystalline would be a good term. Amorphous $MoS_2$ films are reportedly poor lubricants [7-1]. Also, a high degree of texture and associated porosity due to columnar-plate growth is generally not favorable [7-2]. Maybe this nanocrystalline region between the two extremes is best. IBAD films reportedly had 10 to 20 nanometer (nanometer = 10 angstroms) sized "crystallites" [7-3]. Structure this fine is probably not detectable by X-ray diffraction which requires about 100 atomic layers ( ~ 100 nm sized crystallites).

The relative density of the films increased linearly with increasing deposition current. However, the film thickness reached a minima at medium density. Note these results were all with identical deposition times:

## Table II

| ID | Thickness (µm) | Density |
|---|---|---|
| Low | 2.2 | 1 |
| Medium low | 1.5 | 1.9 |
| Medium | 1.6 | 2.5 |
| Medium high | 1.4 | 3.2 |
| High | 2.1 | 3.6 |
| Alternating | 0.8 | 3.6 |

The morphology of the films produced at medium low current appears to be more fibrous than the film produced at medium high current. Moreover, the film produced at the medium low current seems to be less brittle when examining fractures upon scribing. The film densities produced at these current levels are as expected in the rankings shown in Table II.
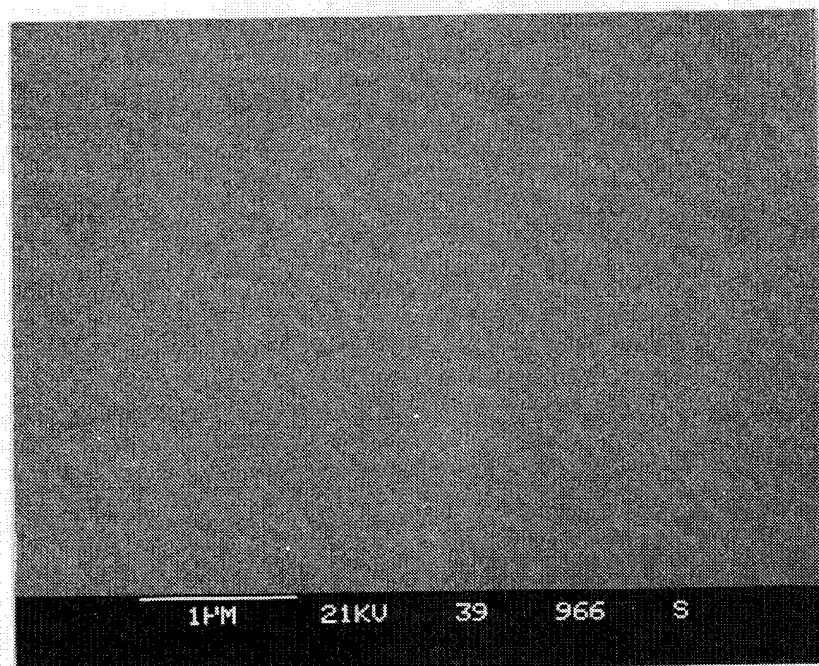
(a)     No Tilt



(b)  High Tilt

**Fig. 7-9    Film produced by alternating the deposition current had a refined structure.   20,000X.**

- 155 -

By changing or alternating the plasma current power level between medium high and medium low current for 10 minutes, a very dense structure was produced. This thin film not only has the density of last year's successful films (within error), but also the morphological refinement. The zone 1 "mounded" structure was extremely fine, on the order of 0.05 μm (Fig. 7-9a). This refined structure is evident in the cross-section. The fracture of this film is also similarly produced upon scribing and is similar to the film produced last year (Fig. 7-9b).

In addition, the X-ray spectra of the alternating current film also looks like the film produced last year (Fig. 7-8b). Neither the (110) "texture" peak or the "amorphous" hump are evident. Perhaps this is a more "nanocrystalline" film as compared to films produced at a single current. Unfortunately, the existence of this fine structure is difficult to prove.

Additional analyses indicate current levels also affects the composition of the films. The film compositions were determined by removing and weighing films deposited on glass slides. Chemical analysis involved peroxide fusion followed by inductively coupled plasma (ICP) analysis. The results in weight percent are as follows:

Table 7-3

| Current Level | Mo | S | Sb | Rem. |
|---|---|---|---|---|
| Med Low | 36.6 | 23.3 | 15.6 | 24.5 |
| Med High | 26.6 | 18.1 | 33.8 | 21.9 |
| Alternating | 26.7 | 17.8 | 24.3 | 31.2 |

Although these results should be double checked (accuracy reportedly is better than a percent), the composition clearly changes with current levels. This result is somewhat surprising considering the composition of the film should be similar to the target (by most theoretical accounts). Perhaps a higher deposition current is more likely to "bury" the antimony. Note the sulfur to molybdenum ratio stays the same for the medium high and medium low current levels. The remaining or balance of the film is oxygen and probably carbon.

These favorable results suggest the films might be improved even more by optimizing the period or dwell and/or the amplitude of the current oscillation. If morphological refinement is the most important film characteristic governing endurance, reducing the period of oscillation may provide a even more refined structure. However, reducing the period too much may make the structure too amorphous with concomitant poor endurance. On the other hand, if composition is more of a factor, amplitude changes may have an effect.

In addition to developing the alternating current deposition process, Hohman also "mapped" film thickness locations in the chamber as a function of part composition and configuration. The film thickness of different components all given the same deposition time is presented in Table 7-4.

Table 7-4

| Component | Thickness, μm |
|---|---|
| Glass Slide Witness Plate | 1.2 |
| Steel Witness Plate  -Flat | 2.5 |
| Perpendicular | 2.0 |
| Thrust Bearing | 1.5 |
| A-6 Test Ring | 1.0 |

The same (planetary) fixture was used for deposition on the witness plates and thrust bearing. The A-6 test ring was on a rotating spindle. Variation in the thermal conductivity of the components appears to be the most likely reasons for the differences in thicknesses considering that the location of the parts on the fixture was similar. Although electrical conductivity was originally thought to be the cause of the widely different results between glass and steel witness plates, metallizing the glass before deposition of the film did not change the thickness. These results were used to determine deposition times for the angular contact bearings.

## 7.3 THIN FILM CHARACTERIZATION

### 7.3.1 Witness Plates

One inch diameter plates made of 440C steel polished plates were placed in the chamber along with bearing components in order to witness the deposition of the films with the small angular contact bearings. The films were then characterized by x-ray diffraction (XRD), X-ray photoelectron spectroscopy (XPS), and microhardness.

### X-Ray Diffraction

X ray diffraction (XRD) scans of an uncoated 440C witness plate provided substrate background peaks (metal and carbides) for comparison with the coated plates (Fig. 7-10a). The X- ray spectra of the film produced by the National Center for Tribology (NCT) revealed only a small (002) peak which is indicative of a weak basal-plane film orientation (Fig 7-10b). This rather broad, low-angle peak is more obvious when the substrate spectra is subtracted from the film on substrate spectra. Note this film texture is much different than the films produced by NCT in the past. The film produced by NCT used on the thrust bearings had an edge-plane texture.

Films produced by Ovonics were also characterized by XRD. Both edge-plane and basal-plane orientations were detected (Fig. 7-11a). However, no multifilm peaks that are typical of a layered synthetic microstructure were detected. Moreover, the film textures appeared to change with the separate deposition runs as evidenced by the variation in peak heights. The variation in the basal-plane or (002) peak was especially obvious. This change in texture probably results from the variation of the witness plate location and exposure to the atom flux in the deposition chamber. Ovonics reported that the witness plates were not fixtured for the multilayer films as were the bearings; witness plates were placed in convenient locations.

Hohman films deposited on the 440C substrates exhibited extremely weak and variable edge-plane and even weaker basal-plane texture (Fig. 7-11b). For one deposition run, the edge-plane peak (100) was not even detectable. Due to the broadness of the basal-plane peak, possible variations in the size were difficult to observe.

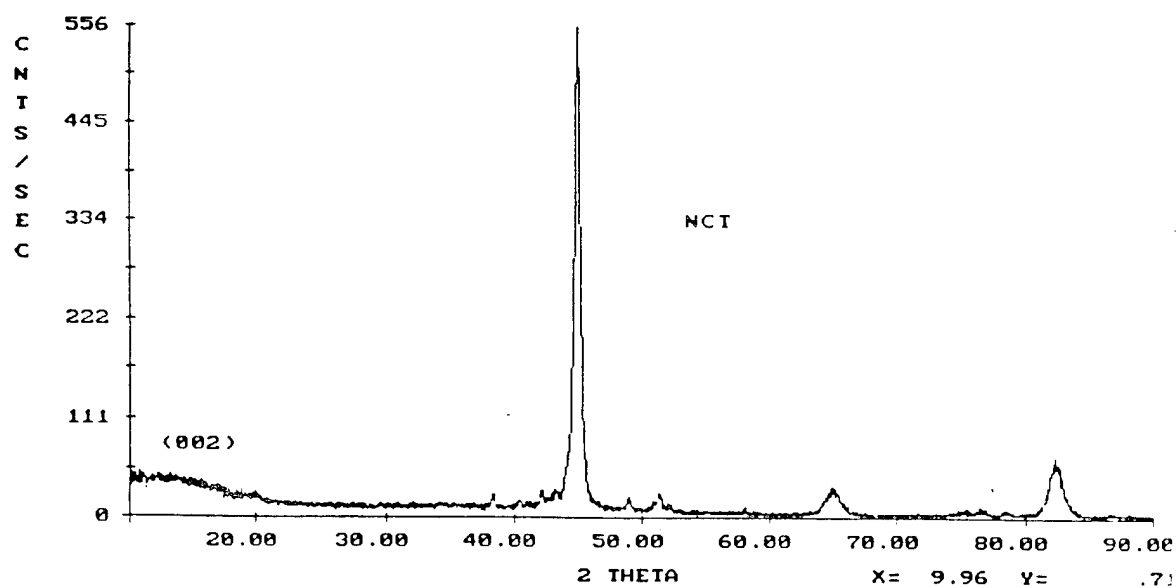### X-Ray Photoelectron Spectroscopy (XPS)

Elemental compositions of the films determined by XPS after a 2 minute ion etch are as follows (compositions in atom %) :

**TABLE 7-5**

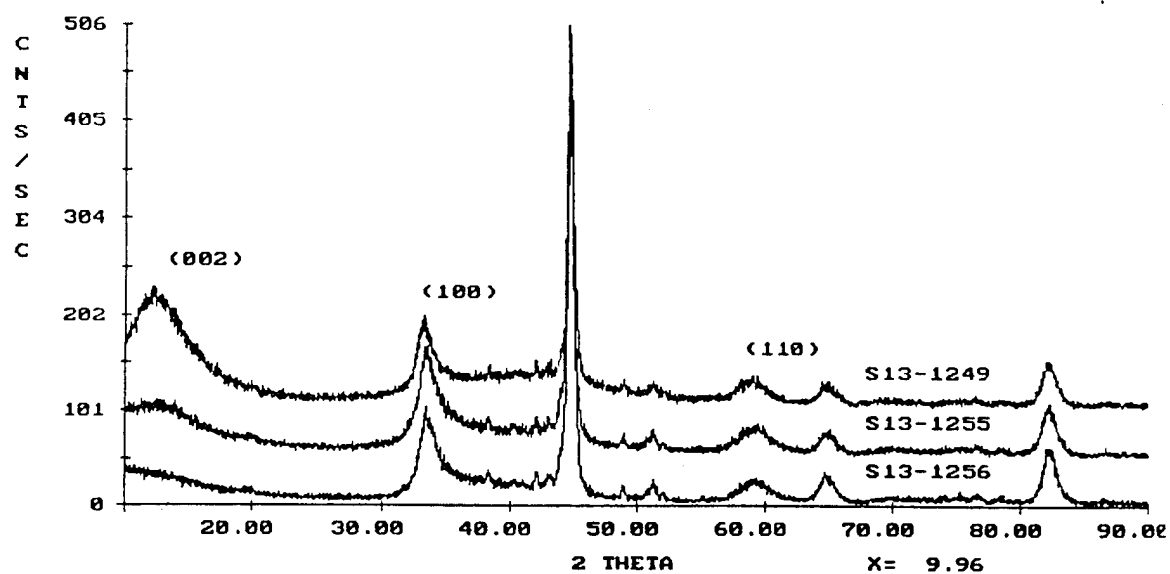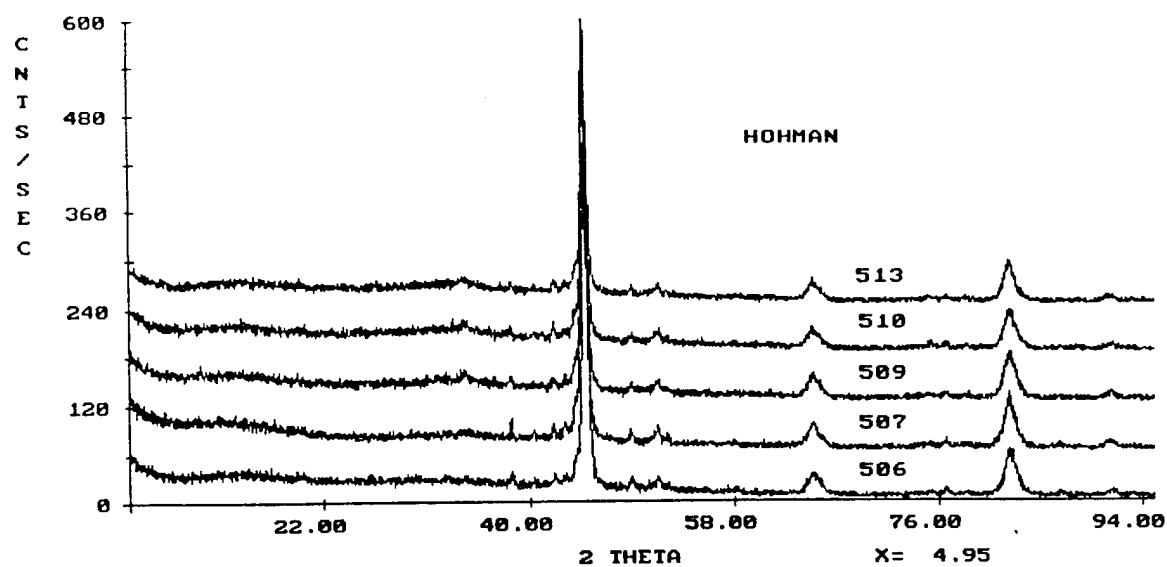| Film | Sulfur | Molybdenum | Carbon | Oxygen | Antimony |
|------|--------|------------|--------|--------|----------|
| Hohman | 27 | 25 | 26 | 13 | 10 |
| NCT | 33 | 38 | 8 | 21 | - |
| Ovonics | 40 | 45 | 12 | 4 | - |
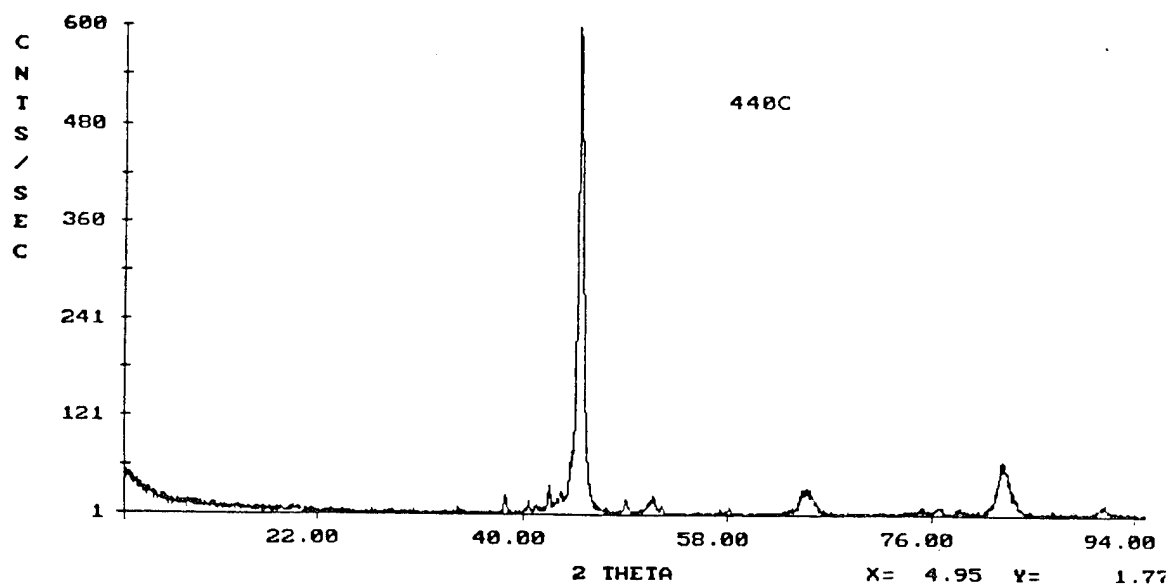
(a)



(b)

**Fig. 7-10** Comparison of the X-ray diffraction spectra of the bare 440C
substrate (a) with the NCT film (b) reveals a weak (002)
basal film texture.

Fig. 7-11   X-ray diffraction of films deposited by Ovonics revealed
variable and non oriented crystallographic textures (a).
Hohman films had weak basal plane   texture (b).

Elemental compositions of the films indicated that all three films had sulfur to molybdenum atom ratios that were much less than two, which is typical of sputtered $MoS_2$ films. Moreover, the three films contained substantial amounts of carbon and oxygen, up to 20% in some cases. Relatively high amounts of carbon and oxygen contaminants are also typically found in sputtered $MoS_2$ films.

The type of vacuum systems used to pump-down the deposition chamber affects the carbon and oxygen present. Ovonics uses a cyropump which pumps water vapor efficiently and the resulting films have relatively low oxygen contents. The low carbon content in the NCT films is due to turbomolecular pumped vacuum system which has a high rate of hydrocarbon removal, but poor water vapor pumping capability. Finally, Hohman uses a diffusion vacuum pumped system which is well known for introducing high hydrocarbon contamination.

## Morphology/Hardness

Microhardness measurements were taken on the witness samples with an Anton Paar ultramicrohardness tester model MHT-4 mounted on a SEM stage [7-4]. Vickers diamond indenter (136° pyramid with a 0.3 mm radius tip) impressions were made using loads 0.25 grams force (250 x $10^{-5}$ N). Thicknesses of the films were obtained by indenting or scribing the films and examining the edge at high tilt. The thickness of the films on the witness plates was not representative of the film thickness on the actual bearings (discussed in next section). Considering intact film could be found on the bearing race shoulders, film thickness and morphology were assessed on the bearing components. Hardness results along with film thickness and indenter penetration depths are as follows:

### Table 7-6

| Film | Vickers Hardness | Thickness (μm) | Penetration (%) |
|------|------------------|----------------|-----------------|
| Hohman | 160 | 1.1 | 33 |
| NCT | 143 | 0.8 | 43 |
| Ovonics | 570 | 2.2 | 8 |

Ideally, the penetration of the indenter into the film should be less than 10%. Considering the substrate has a Vickers hardness of about 700 VHN, penetrations greater than 10% may produce hardness numbers greater than the actual film hardness. Therefore, the Hohman and NCT film hardnesses may be even less than the low values reported in Table 7-6. The hardness in these films probably reflect low density.

## 7.3.2 Mechanical Tests of Thin Films on Races

Considering that a large portion of the film deposited on actual bearings does not interact with the rolling elements and does contribute to bearing lubrication, destructive tests of this unused film provides a method of film quality assessment. The most useful location of intact film is on the inner and outer race shoulders. If the indentation diameters are relatively small (as with Rockwell hardness indentations), the bearing curvature in these regions has little effect on the fracture properties. In other words, these shoulder regions are relatively flat. In addition to fracture properties, tilting the part to high tilts provides an accurate way to measure the thickness of the coating.

### Film Thickness

The film thickness was measured on angular contact bearings by indenting the film with a Rockwell C hardness tester and examining the film edge in a scanning electron microscope (Figs 7-12). Measurements were taken on the inner race shoulder adjacent the ball track and of both outer race shoulders. Results (in micrometers) are as follows:

**Table 7-7**

| Film | Inner Race | Outer Race Film Thickness, $\mu$m Side 1 | Side 2 | Witness Plate |
|------|-----------|-------------|--------|---------------|
| Hohman | 1.8 | 0.9 | 0.2 | 1.1 |
| NCT | 0.4 | 0.3 | 0.4 | 0.8 |
| Ovonics | 0.9 | 0.9 | 1.0 | 2.2 |

These thickness measurements were very consistent for each of the film types for a number of bearings. The accuracy of the measurements was about 0.1 $\mu$m. Comparison of these thicknesses on the bearing races is quite different than thicknesses on the witness plates (reported earlier and added to the above table). This result is consistent with the results reported in section 7.2 on optimizing the Hohman deposition process. Clearly, for all deposition processes, the witness plate does not provide an accurate thickness measurement of the coating on the actual bearing parts.

Hohman Film
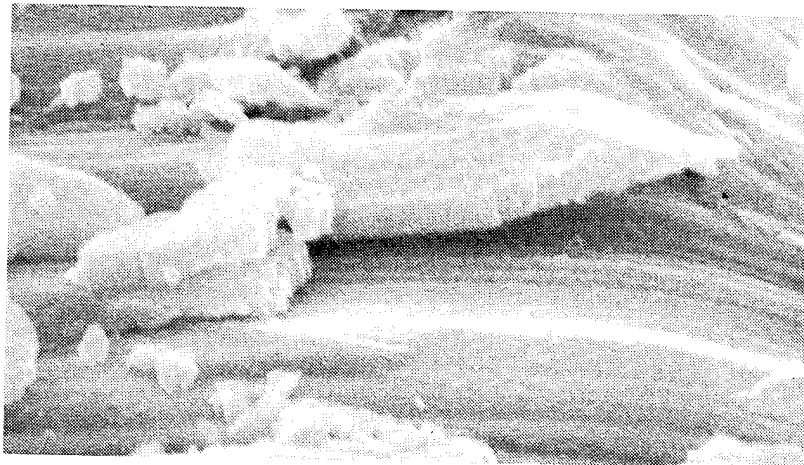

NCT Film
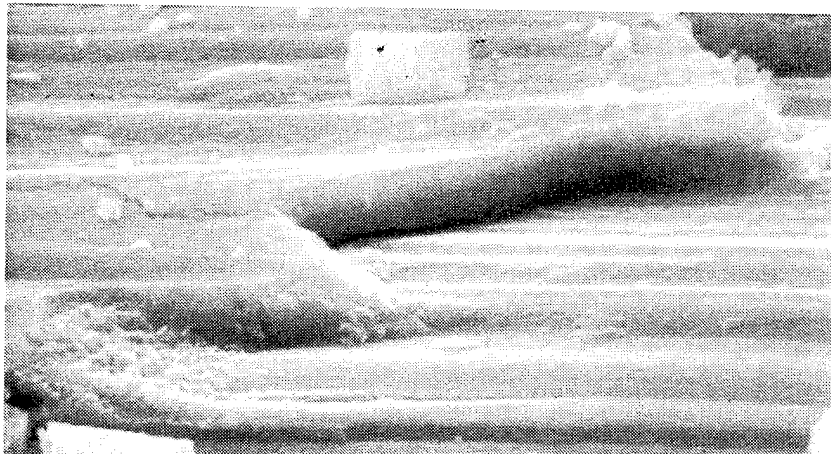

Ovonics Film

Fig. 7-12    Film edges exposed by indenting the inner races shoulder and examining the edge at high tile in the SEM.   10,000X magnification.

## Indentation Tests

In order to predict the performance of a film in a precision bearing, indentation testing was performed on the recently tested bearings. The extent of lateral film cracking at the periphery of an indent reportedly can provide an indication of film adhesion or interface fracture toughness [7-5].

Three indents were made on the inner race shoulders using a Rockwell "C" indenter at 60, 100 and 160 kilogram loads. The extent of film fracture associated with the indents was determined by examining the indent in a scanning electron microscope in the backscattered electron (compositional) imaging mode. Regions of film delamination were easily delineated in the Ovonics (Fig. 7-13) and Hohman (Fig. 7-14) films. The NCT film, however, did not show delamination (Fig. 7-15). The lack of continuous cracking in the NCT film is likely to be associated with the thickness. Very thin $MoS_2$ films of less than 0.5 micrometers thick reportedly exhibit multiple buckling rather than the continuous radial cracking. The buckling is difficult to discern in the compositional image mode.
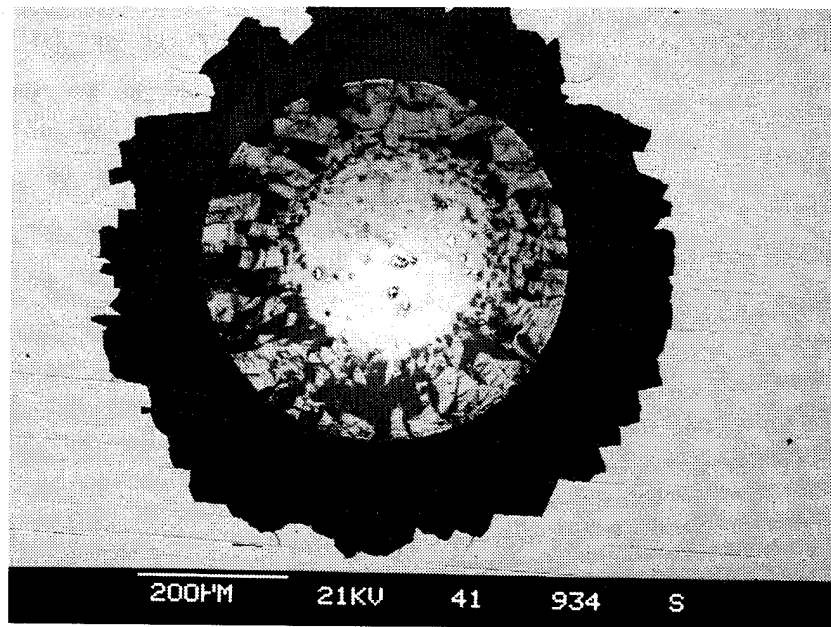


**Fig. 7-13 Compositional image of the film delamination associated with Rockwell "C" indent in the Ovonics coating.**
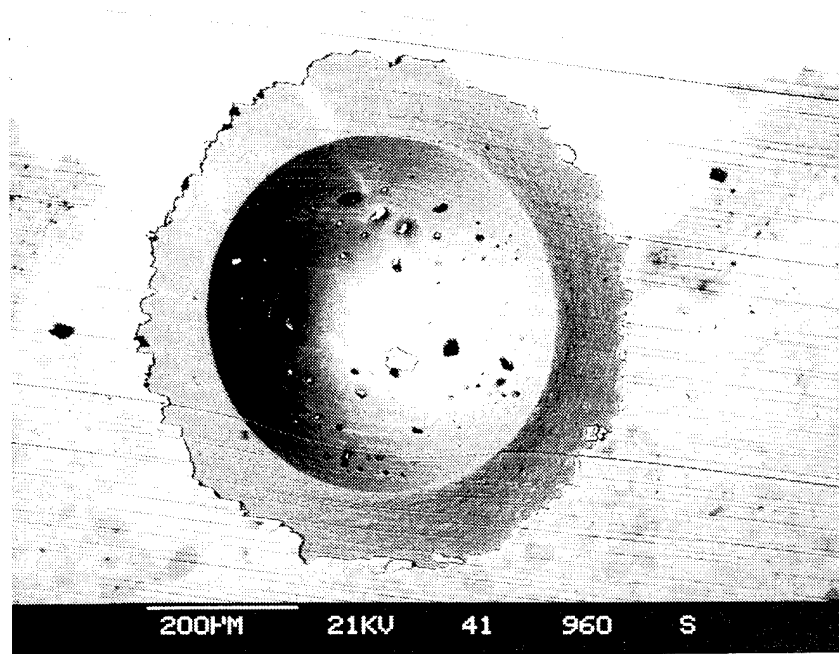
**Fig. 7-14** Compositional image of the film delamination associated with an Rockwell "C" indent in the Hohman coating.
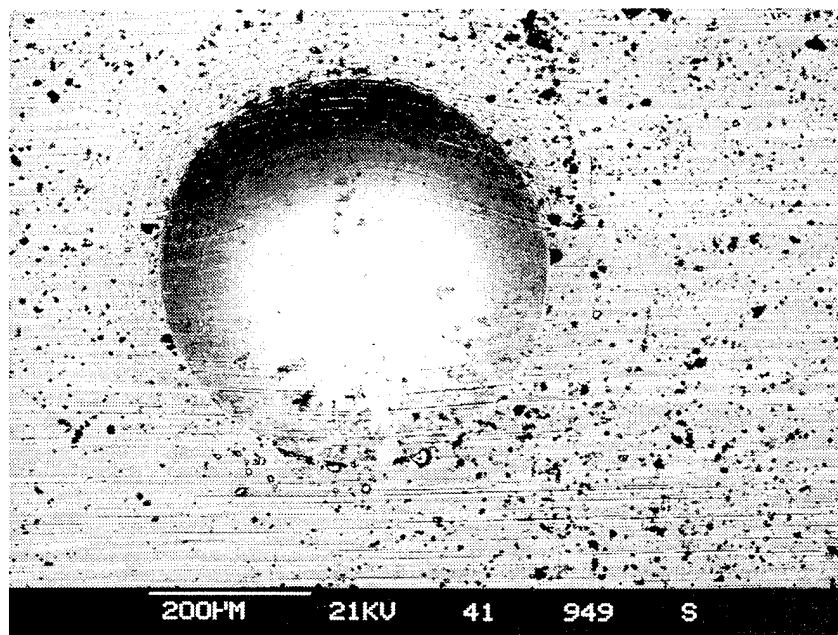


**Fig. 7-15** Compositional image of an indent in the NCT coating did not show film delamination although microbuckling is evident.

The amount of radial cracking associated with the indents in the Hohman and Ovonics films was quantified by measuring the radial crack length at six positions around each indent. These results were averaged for each load and inner race, then plotted (Figs. 7-16 and 7-17). The type of retainer and inner race ball track widths are also shown for a given inner race on the graphs along with the corresponding film interface fracture toughness (described in next section). Note that the two retainers, either Salox or Duroid, were from the same bearing post. On the average, the Hohman films exhibited greater interfacial toughness than the Ovonics films even though they were much thicker: Hohman films were 1.8 μm thick, whereas the Ovonics films were 1.0 μm thick.

While the film fracture toughness exhibited by the Ovonics films were reasonably consistent, the film on one of the Hohman-coated inner races exhibited much poorer film toughness than the other three. The ball track width of this bearing (0.051 in.- after testing) was also much wider than the track width on the mating bearing (0.045 in.) on the test post. In this case, the results of the film fracture toughness test correlates well with track width, and hence, appears to be a relative predictor of film loss. Note that the ball track widths would be expected to be similar for given retainers if the films were identical in quality.

These film fracture toughness results suggests the Hohman deposition process exhibited variability in the films and the indentation test could be implemented in film quality control. Considering the indentation is performed on the race shoulder and does not affect the bearing, it is nondestructive and could be performed on precision flight bearings.
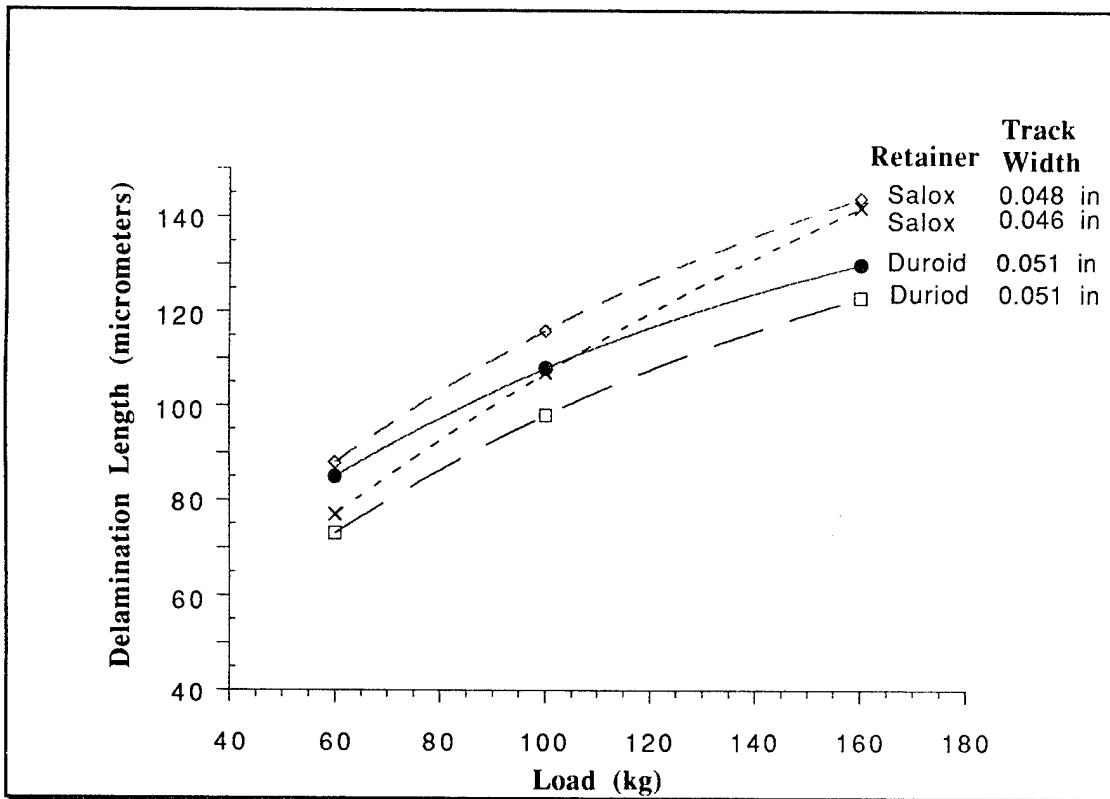
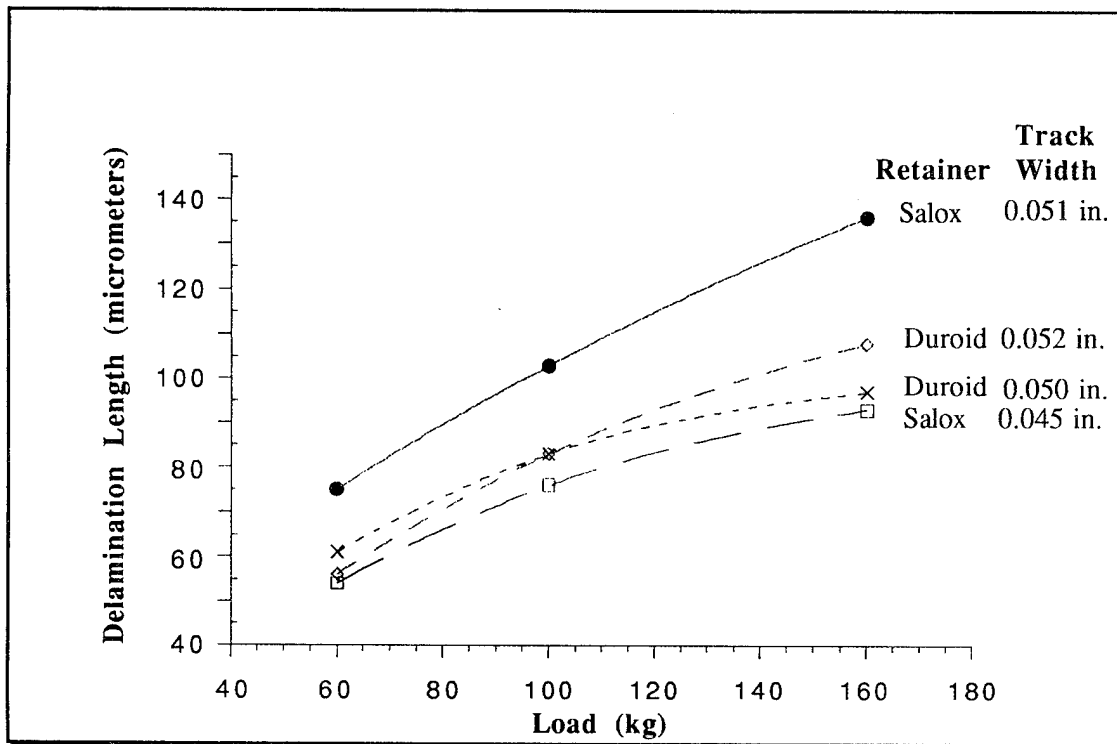**Fig. 7-16  Interface fracture toughness of Ovonics film on inner races.**



**Fig. 7-17  Interface fracture toughness of Hohman film on inner races.**

## 7.4 EXAMINATION OF TESTED ANGULAR CONTACT BEARINGS

The tested small angular contact bearings were disassembled and the components examined visually and by scanning electron microscopy. Backscattered electron imaging combined with x-ray elemental microanalysis revealed compositional variations in the ball tracks on the races which were defined by the width of the ball track on the races. The inner race ball track width and bearing identification and test results are reported in Table 7-8.

### Table 7-8

| Test Post | Thin Film | Retainer Material | Ball Material | Preload (lbs) | Cycles (millions) | Ball Track Width (in) |
|---|---|---|---|---|---|---|
| *Short Lived Bearings* | | | | | | |
| 2.4 | Ovonics | Duroid | $Si_3N_4$ | 32 | 1.0* | 0.048 / 0.048 |
| 2.3 | NCT | Duroid | $Si_3N_4$ | 28 | 17.7 | 0.072 / 0.057 |
| 3.4 | Hohman | Duroid | $Si_3N_4$ | 29 | 12.5 | 0.051 / 0.061 |
| 2.6 | Ovonics | Duroid | $MoS_2$ | 31 | 17.7 | 0.047 / 0.048 |
| 2.5 | NCT | Duroid | $MoS_2$ | 26 | 0.1* | 0.051 / 0.052 |
| 3.5 | Hohman | Duroid | $MoS_2$ | 36 | 12.5 | 0.049 / 0.050 |
| 2.12 | Ovonics | Vespel | $MoS_2$ | 30 | 0.5* | 0.054 / 0.049 |
| 2.11 | NCT | Vespel | $MoS_2$ | 28 | 0.4* | 0.052 / 0.050 |
| 3.9 | Hohman | Vespel | $MoS_2$ | 41 | 0.5* | 0.043 / 0.048 |
| 2.8 | Ovonics | Vespel | 52100 | 38 | 17.7 | 0.067 / 0.073 |
| 2.7 | NCT | Vespel | 52100 | 22 | 17.7 | 0.064 / 0.062 |
| 3.6 | Hohman | Vespel | 52100 | 39 | 12.5 | 0.076 / 0.061 |
| 3.11 | Ovonics | $MoS_2$ on Vespel | 52100 | 34 | 12.5 | 0.073 / 0.059 |
| *Long Lived Bearings* | | | | | | |
| 2.2 | Ovonics | Duroid | 52100 | 31 | 18 | 0.049 / 0.048 |
| 4.2 | Ovonics | Duroid | 52100 | 41 | 44 | 0.051 / 0.051 |
| 2.1 | NCT | Duroid | 52100 | 19 | 18 | 0.022 / 0.033 |
| 4.1 | NCT | Duroid | 52100 | 27 | 43 | 0.036 / 0.043 |
| 3.3 | Hohman | Duroid | 52100 | 34 | 29 | 0.043 / 0.051 |
| 4.4 | Hohman | Duroid | 52100 | 41 | 43 | 0.050 / 0.052 |
| 4.9 | Ovonics | Salox | 52100 | 32 | 48 | 0.046 / 0.048 |
| 4.6 | Ovonics | Salox | 52100 | 31 | 46 | 0.046 / 0.049 |
| 4.11 | Ovonics | Salox | 52100 | 41 | 45 | 0.049 / 0.052 |
| 4.10 | Ovonics | Salox | 52100 | 52 | 46 | 0.058 / 0.071 |
| 4.8 | NCT | Salox | 52100 | 25 | 48 | 0.033 / 0.033 |
| 4.5 | Hohman | Salox | 52100 | 37 | 44 | 0.045 / 0.051 |
| 4.7 | No Film | Salox | 52100 | 32 | 46 | 0.053 / 0.064 |
| *Fracture Resistant Film Bearings* | | | | | | |
| 4.3a | Ovonics | Salox | 52100 | 33 | 40 | 0.047 / 0.057 |
| 4.12 | Ovonics | Salox | 52100 | 33 | 40 | 0.045 / 0.048 |

\* Indicates hard failure (bearings jammed drive motor)

The identification of the bearing test post, and explanation of total test cycles and initial bearing preload can be found in section 5. The balls were either as-received with the bearings (52100), $Si_3N_4$ or 52100 with a $MoS_2$ thin film. The short and long lived bearing test results are discussed in the following subsections. The description and results of the fracture resistant films are discussed in Section 7.7.

### 7.4.1 Short-Lived Bearings

Bearings that incorporated either $MoS_2$-coated or $Si_3N_4$ balls and/or polyimide retainers typically resulted in early high torque failure.

### MoS₂ Coated Balls

Examination of failed bearings that had $MoS_2$-coated balls typically had a thick, compacted debris in the track of both the inner and outer races (Fig. 7-18). The coating appears to have come off the balls early in the test. The added material in the ball track increased the race deposit thickness which in turn increased the bearing preload and resulting torques. An inspection of the unused, as-coated balls by the three different manufacturers showed spalling, bare regions and infused particles (of spalled film) on the balls
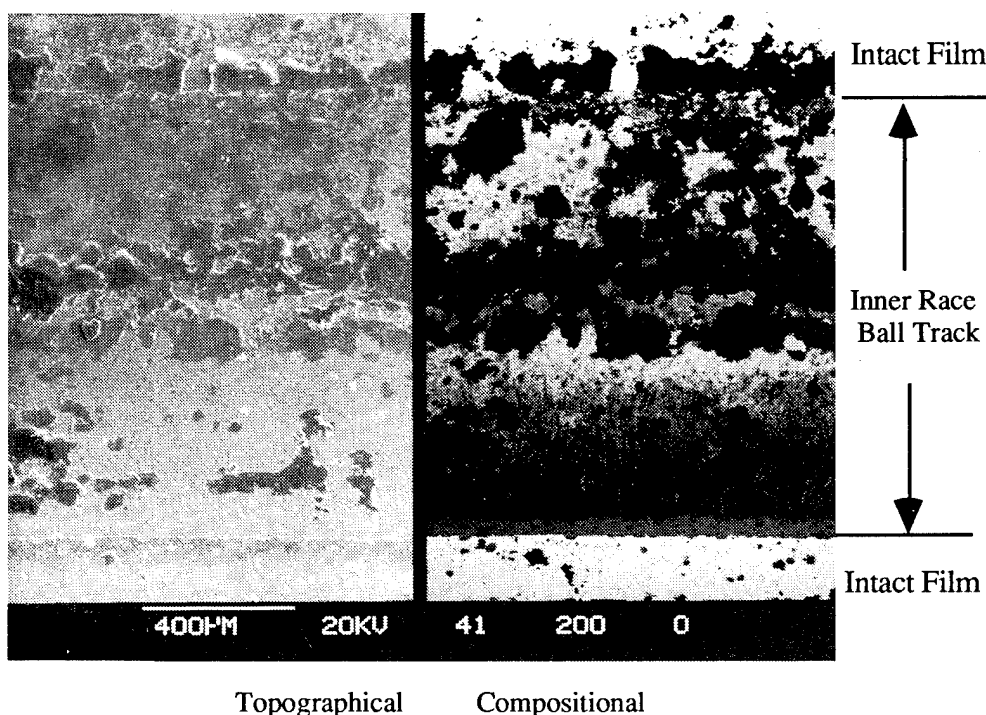


Topographical          Compositional

Fig. 7-18    Thick, compacted debris was found on the inner race ball
track of bearings with $MoS_2$ coated balls.

- 168 -

The film deposited by Ovonics had regions on the ball where 100 micrometer diameter portions of the coating had flaked off (Fig. 7-19). On one of the balls, these regions of spalling appeared to encompass half the ball surface area. Microanalysis indicated no molybdenum or sulfur present in the dark regions in the backscattered (compositional) electron image.

The coating on the balls deposited by Hohman had incorporated macroparticles of $MoS_2$ film in addition to flaked areas. Both macroparticles and spalled regions were typically on the order of ten micrometers in size (Fig. 7-20a). The mottled appearance of the film in the backscattered electron image indicated the coating varied considerably in thickness. In addition to the dark contrasting areas which revealed a spalled coating, the very light areas suggests a much thicker coating. When this film was viewed at high angle, flattened particles of coating (macroparticles) could be found (Fig. 7-20b).

The film deposited by NCT also contained macroparticles and spalled areas. As with the Hohman film, the macroparticles on the NCT film were best observed at a high tilt angle (Fig. 7-21b). The backscattered electron image showed regions typically 5 μm in diameter that were spalled (Fig. 7-21a).
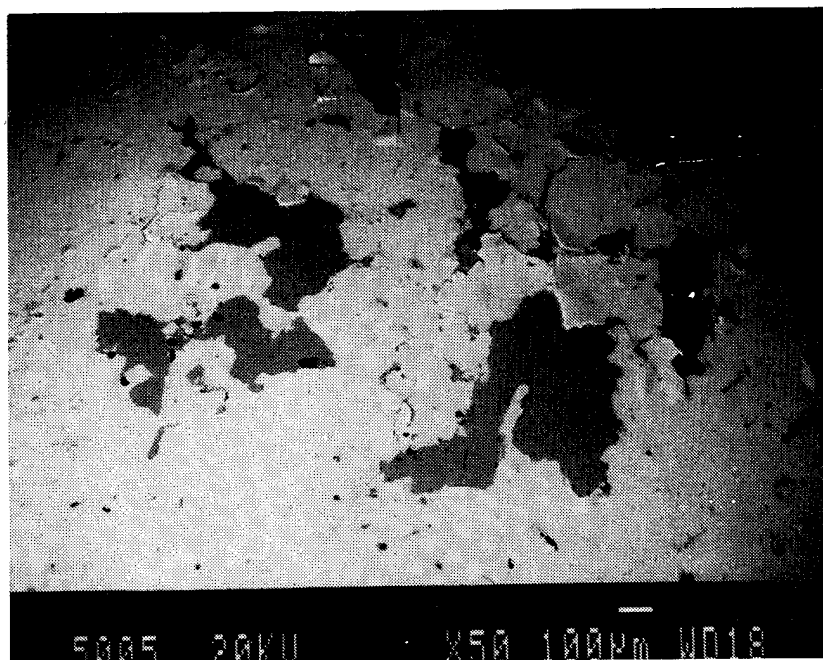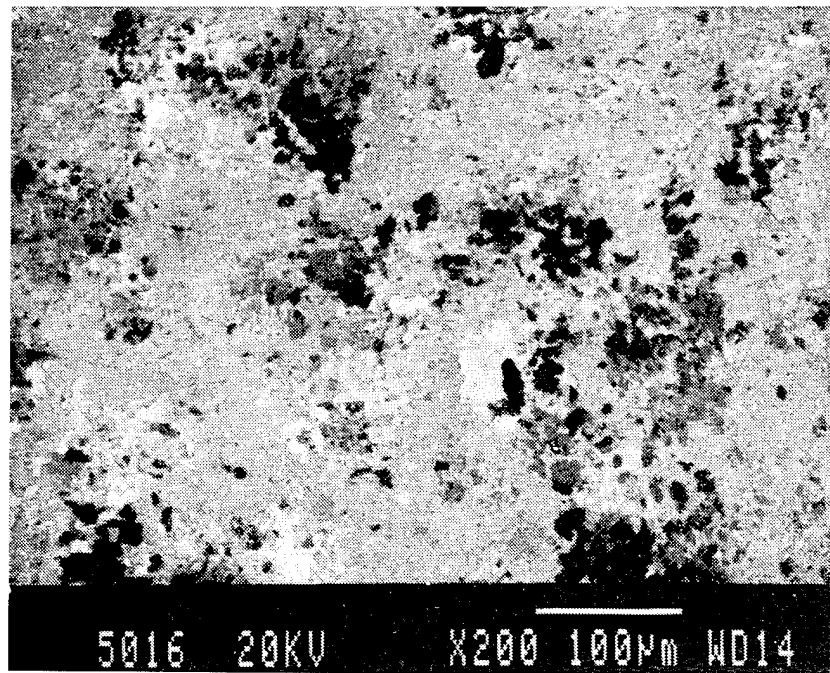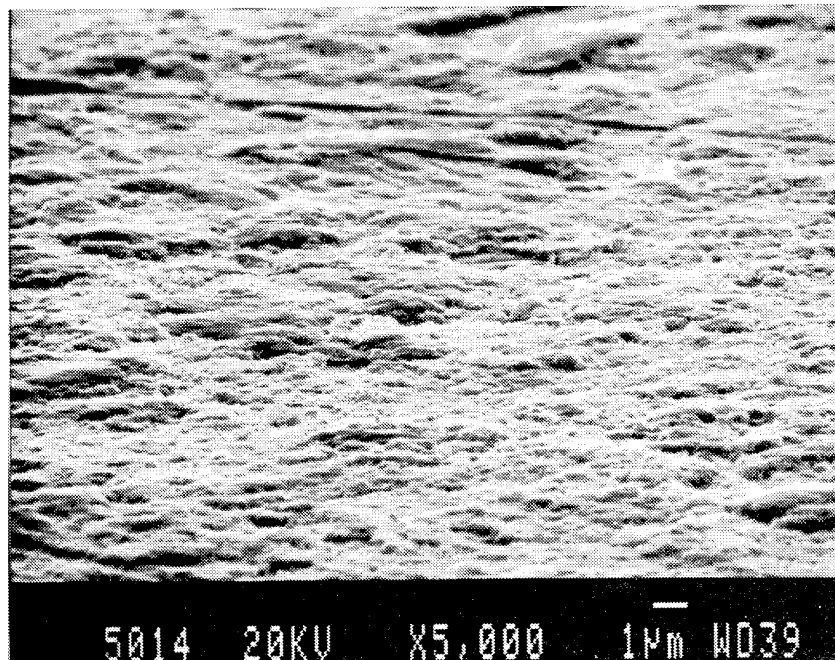


**Fig. 7-19 Backscattered (compositional) image of as-coated Ovonics ball shows spalling.**
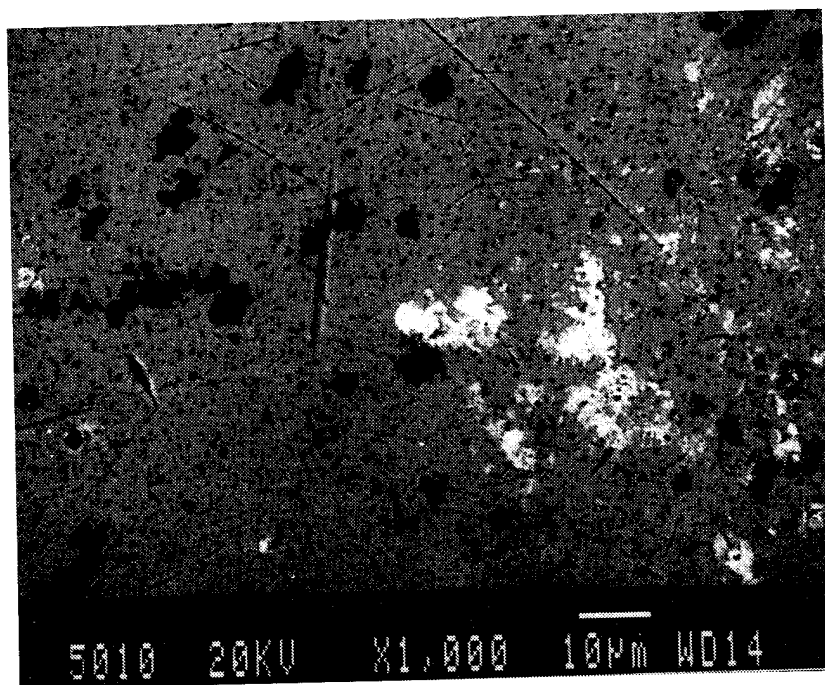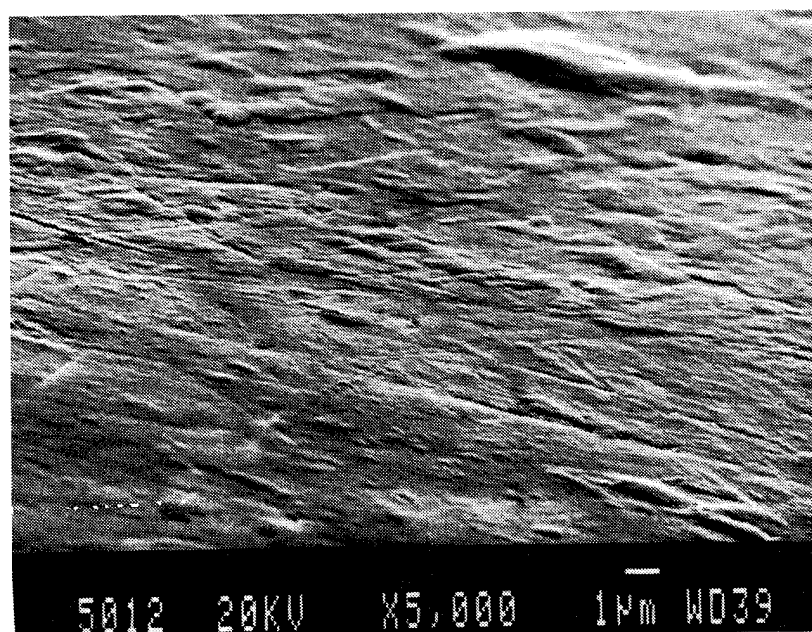
(a)



(b)

Fig. 7-20   Backscattered (a) and high tilt images of as-coated Hohman ball shows macroparticles.

(a)



(b)

**Fig. 7-21   Backscattered (a) and high tilt images of as-coated NCT ball shows macroparticles.**

Depositing a uniform $MoS_2$ film on a ball is apparently much more difficult than on the races. Balls have to be rotated in some manner to ensure the sphere surface is exposed to the deposition target (to some degree). During this rotation, contact with a fixture or other balls dislodges film particles off both the balls and the fixtures. On the ball, this region becomes a spall. The particles generated can also become incorporated in the coating. Since film on the races is not physically in contact with any fixture, spalling and macroparticle incorporation is much less likely to occur. Compared to races, coating balls is an inherently dirty process.

The film deposition method employed to coat the ball surface influenced the type of film produced (and defects). The three film producers each used a different process to coat the balls.

Ovonics coated the balls while rotating them between thrust washers. The large areas of spalling suggest adhesion was poor, perhaps the result of contamination from the fixture. However, note the film was buckling prior to spalling. This film deformation suggests sliding stresses from thrust race contact overcame the interface shear strength.

Hohman stirred the balls in a dish with a paddle during deposition. The balls contacted each other and the container constantly, thus generating particles from spalls that become part of the film.

Although NCT suspended the balls over the target on a coarse net screen (thereby minimizing macroparticle incorporation into the film), screen contact apparently removed small flakes of the film. Macroparticle incorporation into the film also occurred, albeit to a lessor degree than the Hohman film.
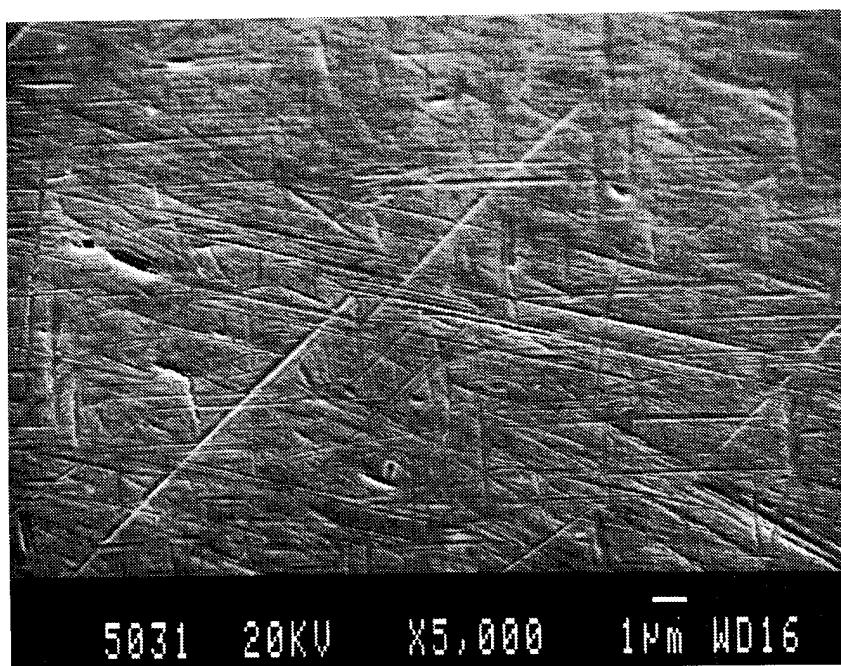
## Si3N4 Balls

Although the reason why bearings with $Si_3N_4$ balls exhibited high torque is not entirely clear, subsequent examination of the inner races showed that ball tracks were up to 20% wider than bearings with steel balls. This extreme wear by $Si_3N_4$ balls suggests a combination of high stress (due to the higher modulus than steel), higher hardness (the tested balls did not show wear when examined by SEM ), and lack of adequate transfer of retainer material to the balls (poor adhesion) accounted for the poor performance.

Silicon nitride bearing balls appear to have a much higher quality surface finish as compared to the original 52100 steel balls (Fig. 7-22). The polishing scratches are much less pronounced in the silicon nitride balls, although small, micrometer sized pits are common.
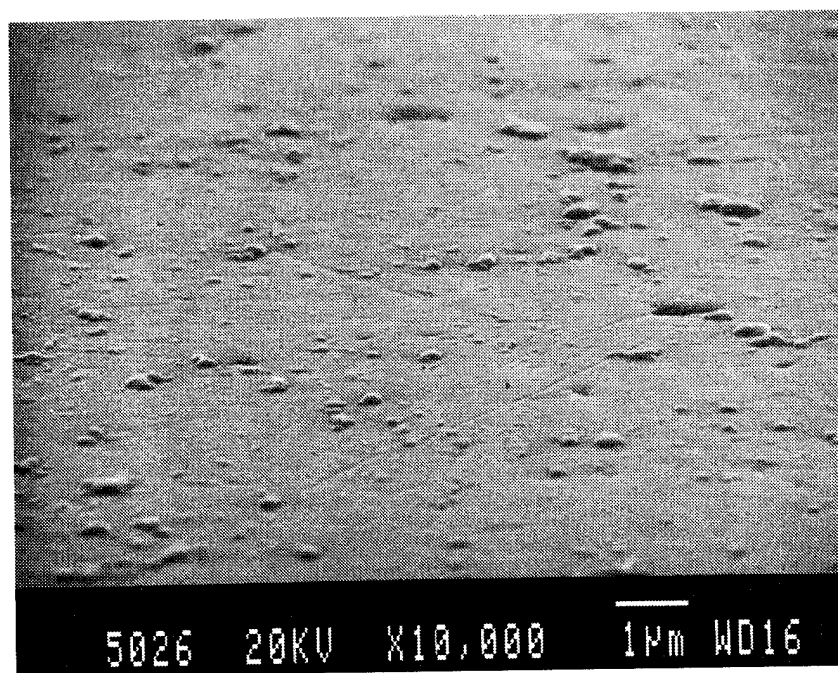
(a)



(b)

**Fig. 7-22** Highly tilted SEM image shows the surface finish of a new Si3N4 ball (a) was much better than the finish of the average 52100 steel ball (b).

Examination of the worn $Si_3N_4$ balls and the debris generated in the bearing indicate that the races and the retainer are exhibiting most of the wear. Polishing scratches could still be found on the worn silicon nitride balls, along with small amounts of debris.

Excessive debris generated by use of $Si_3N_4$ bearing balls appears to be the associated with the failure of the bearings. The debris is a mixture of the $MoS_2$ coating, steel races and retainer material. As detailed previously, this debris deposited in the race ball track results in increased preload and high torque.

Higher bearing stress that results from use of silicon nitride balls may have contributed to the poor bearing performance exhibited by these hybrid bearings. The higher elastic modulus of $Si_3N_4$ (46 Msi as opposed to steel, 28 Msi) increases the contact stress between the silicon ball and steel race by about 18 percent. However, steel balls tested at stress levels greater than this 18 percent did not exhibit the wide wear tracks (as had the $Si_3N_4$ bearings).

Wear between the balls and retainer contributes to the debris and this wear process could also be excessive. Although the loads between the retainer and ball are much less than the ball and race, abrasive wear of the retainer may be more a function of hardness. The hardness of silicon nitride ($R_c$ 80) is much higher than steel ($R_c$ 60) and this higher hardness may cause greater abrasion of the retainer, especially if little $MoS_2$ transfer film is adhering to the ball for lubrication. Note excessive wear was observed in the ball pockets of Duroid retainers when used with $Si_3N_4$ balls.

## Polyimide Retainers
Retainer and race wear was excessive with a polyimide (Vespel) retainer. The balls ground a large wear scar into the retainer generating considerable abrasive debris (Fig. 7-23a and 7-23b). All of the bearings that used Vespel retainers generated copious amounts of debris as a result of abrasion of the retainer. This debris not only coated the inner race shoulder, but also deposited a pile in a ring geometry below the bearing test post. This debris was marginally lubricating, and created a thick compacted deposit in the ball track that caused debris preload failure. Moreover, ball tracks were approximately 40% wider than bearings with Salox retainers. A bearing incorporating a polyimide retainer sputtered with an $MoS_2$ film was tested in an attempt to minimize the excessive retainer wear. Although initial bearing torques were very low, a dramatic rise in bearing torque signaled retainer film failure. Subsequent examination of the bearing revealed excessive wear of both the retainer and races. .
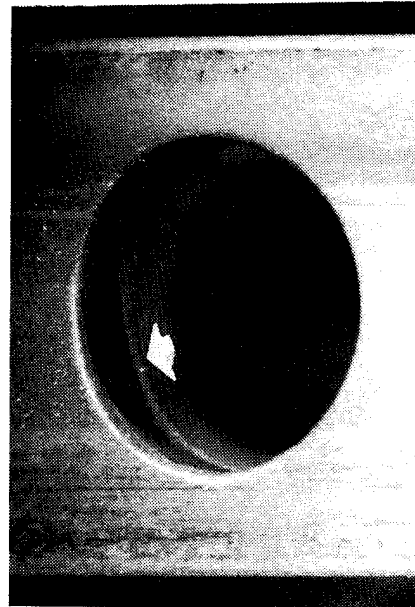
Vespel Retainer                    Salox Retainer

**Fig. 7-23(a)   Ball pocket wear (arrows) of the Vespel retainer was much greater than the Salox retainer ball pocket.**
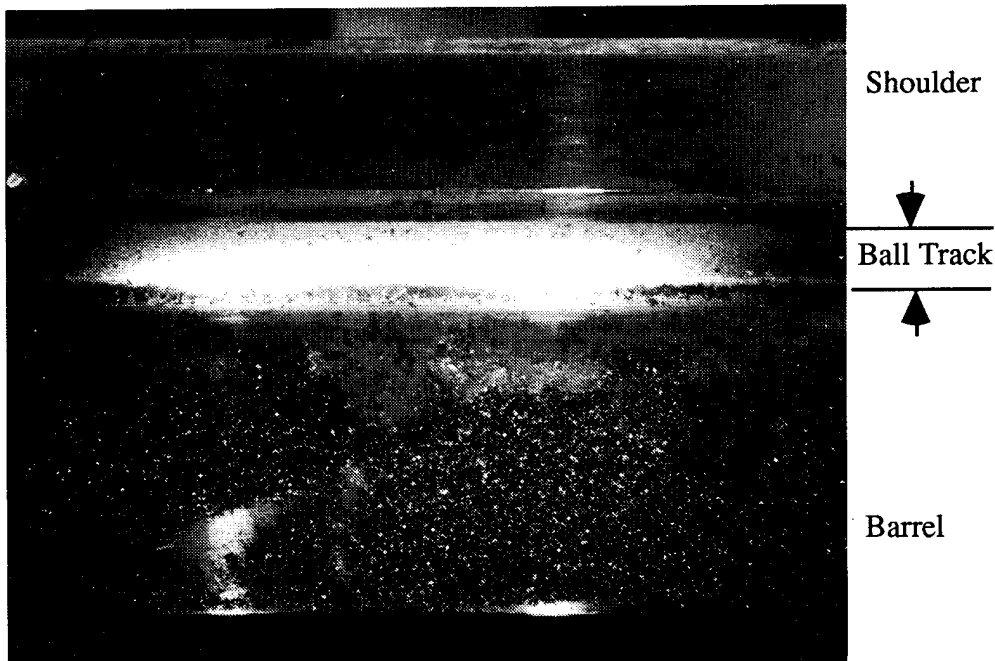


Shoulder

Ball Track

Barrel

**Fig. 7-23(b) Inner race from bearing with Vespel retainer had large amounts of retainer debris on the barrel.**
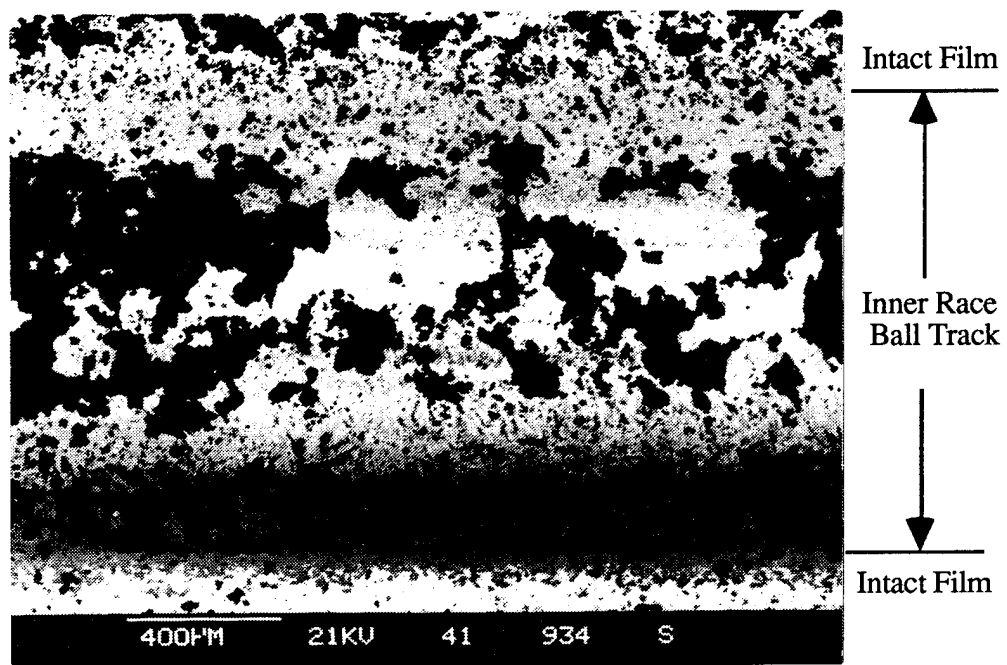
### 7.4.2 Long-lived Bearings

Bearings that contained either Duroid or Salox retainers and uncoated balls exhibited only limited wear of retainers and races, irrespective of the film type. The inner race ball tracks typically had a residual film of $MoS_2$ that formed a band in the track center (Fig. 7-24). Retainer transfer film was also found in the ball track but was much more discontinuous. The thickness of this transfer film was variable, but typically ranged up to 1 μm thick. The edges of the ball track were well defined by the absences of $MoS_2$ film. The film appeared distinctly fractured at this boundary. Lack of film fracture resistance contributes to film delamination which was observed along the outboard edges of the track. Similar film loss results were reported by Hilton et al. [7-6].

The tracks widths of the long-lived bearings as corrected by Hertzian stress on the inner race show reasonable correlation with initial preload and changes in preload (Fig. 7-25). Although preload loss is typically thought to be a direct indication of wear of $MoS_2$ film, a number of other factors affect this relationship. Theoretically, a preload loss on the order of 12 lbs would be expected if a nominal 1 μm film on inner and outer races were worn through without any wear of the metal races themselves. The fact that the preload loss was less than 12 lbs is indicative of transfer film and debris buildup from the ball retainers which is consistent with the observed deposits.

Examination of the long-lived bearings clearly indicates that a transfer film of predominately Duroid (along with bronze in the case of Salox) is depositing on the balls and races while some metal wear is occurring. It is not clear whether this occurs intermittently or simultaneously. The imbalance in this process could account for occasional periods of torque increase observed during life where the retainer temporarily over-transfers a thicker deposit which subsequently worn down due to the attendant increase in preload.
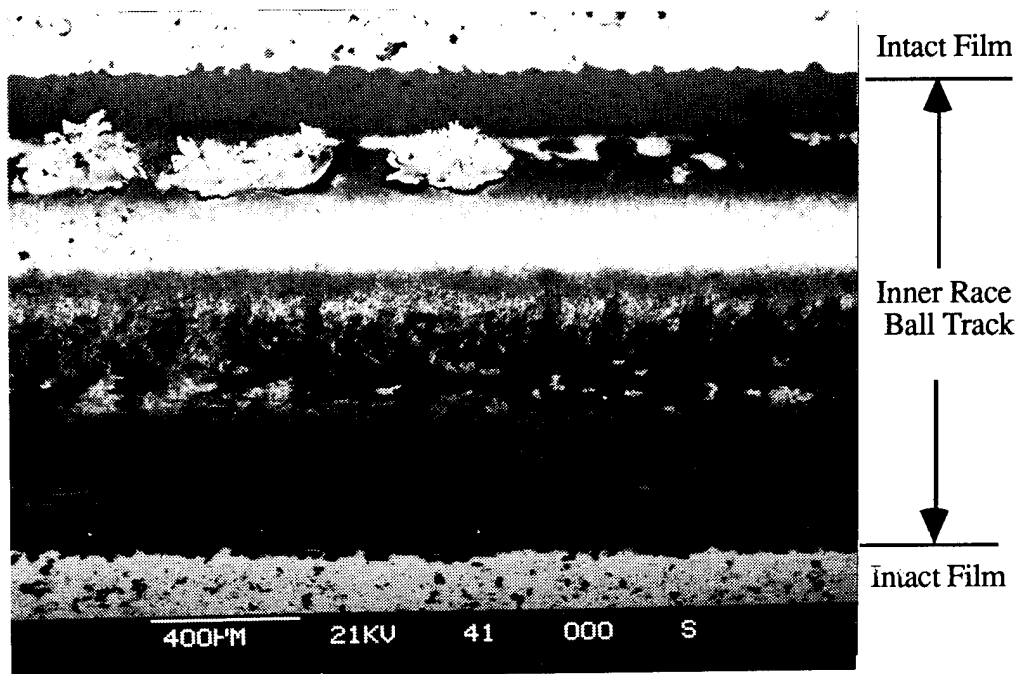
**Fig. 7-24** Backscattered (compositional) electron image of the inner race ball track of long-lived bearings with Ovonics (a) and Hohman (b) films. Light region in track center is residual MoS2 film in track center. Dark patches are retainer transfer film. 50X Magnification.

- 177 -
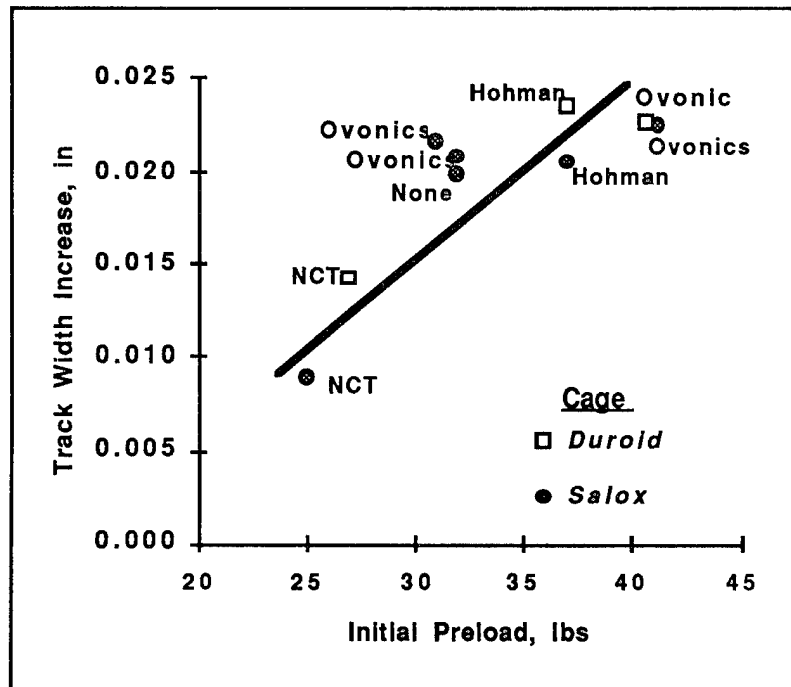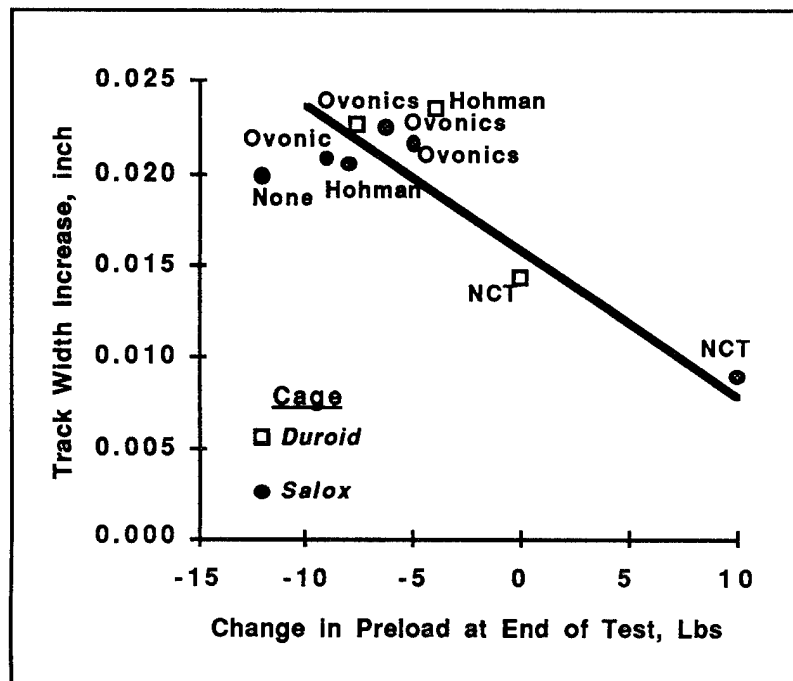
Fig. 7-25 Correlation of changes in inner race track widths of the long-lived bearings to initial preload (a) and changes in preload over bearing life (b)

## 7.5 OVONICS PROCESS SUPPORT

### Fracture of Ni/MoS2 Multilayer Film Deposited on Large Bearings

Multilayer Ni/MoS2 films that provided long lives on the 105-sized screening bearings fractured during prefunctional testing of the large bearings. When fitting the 12-inch bearings with different sized ball sets in the process of adjusting the bearing preload, debris was found in the bearing. The debris was identified as MoS2. Moreover, torque plots before and after debris was noticed showed a definite increase in torque and torque ripple (Section 6.5).

One of the 5-inch (117-sized) bearings deposited with multilayer Ni/MoS2 film also exhibited failure during prefuntional testing. Disassembly and examination of this bearing revealed debris consisting of rather large (millimeter-sized) pieces of film in the retainer ball pocket (Fig. 7-26). This debris was identified as MoS2 by EDS.

One 117 bearing set did, however, acquire about 2 million cycles prior to failure. Examination of the inner race by scanning electron microscopy revealed a wear morphology similar to that found in the smaller 105-size bearings. The wear track was well defined by backscattered electron (compositional) imaging (Fig. 7-27a). The edge of the intact film clearly delineates the edge of the wear track (Fig. 7-27b). Microanalysis showed little evidence of the MoS2 film components in this region adjacent the intact film. The amount of intact film generally increased towards the center of the wear track. A circumferential deposit that was centered in the track contained detectable amount of copper and fluorine. This result suggests the source of the deposit is primarily the retainer which is a mixture of PTFE and bronze. The center deposit appeared to vary in thickness, judging from the contrast variation (translucent appearance) in the compositional images. The thickness of the center deposit was estimated by examining peeled or partially delaminated pieces of the deposit at high sample tilt (along the edge of the inner race - Fig. 7.28). The maximum thickness of the deposit appeared to be about 3 $\mu$m.
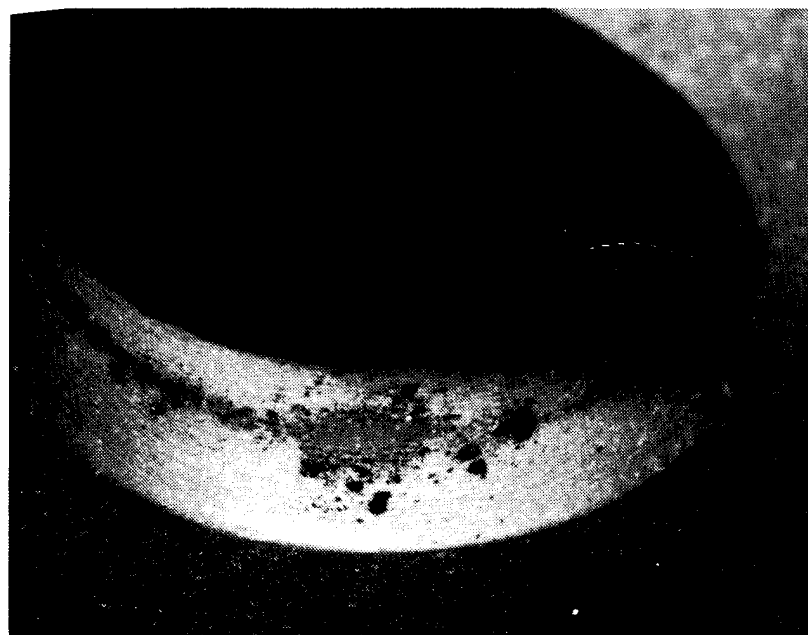


**Fig. 7-26**  **Thin film debris in the retainer ball pocket of the Ni/MoS2 multilayer film bearing indicated film failed during prefunctional testing.**

Intact Film

Inner Race
Ball Track

Intact Film

1MM    21KV    41    565    0

Topography    (a)    Composition    25X



Intact Film

Inner Race
Ball Track
Edge

100PM    20KV    01    507    0
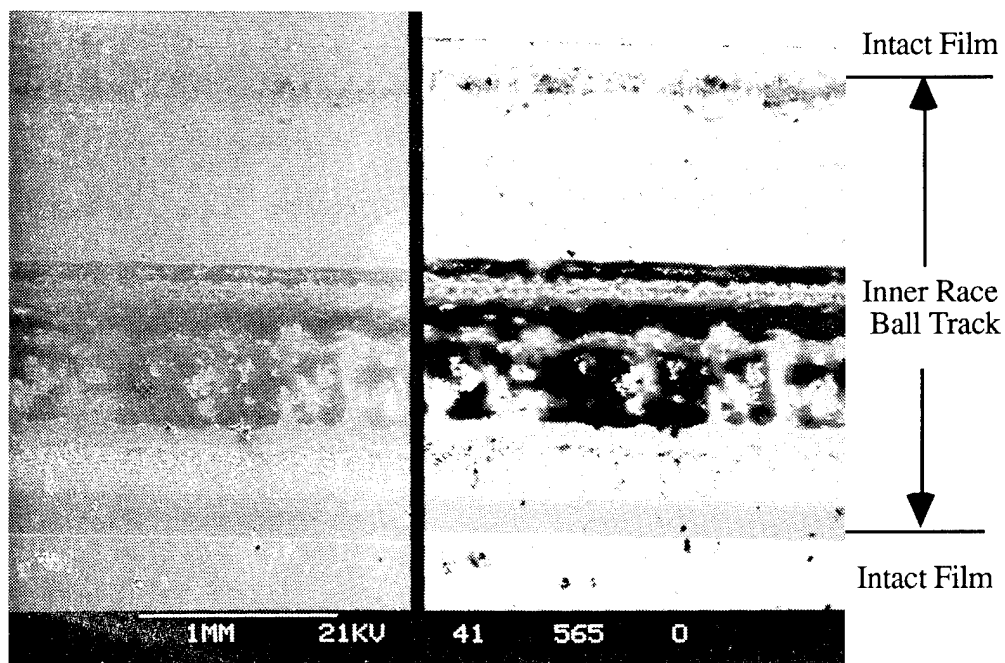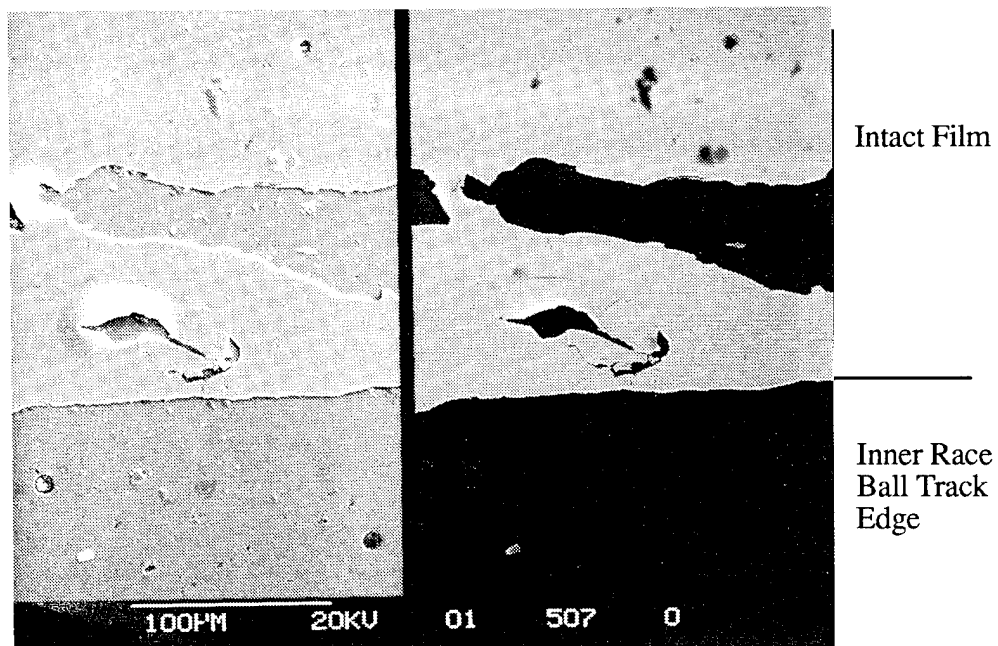
Topography    (b)    Composition    250X

Fig. 7-27    Ball track on 117-sized bearing inner race (a). Dark band in ball
track center is a retainer transfer film. Loss of Ni/MoS$_2$
multilayer film at upper track edge is clearly illustrated (b).

- 180 -
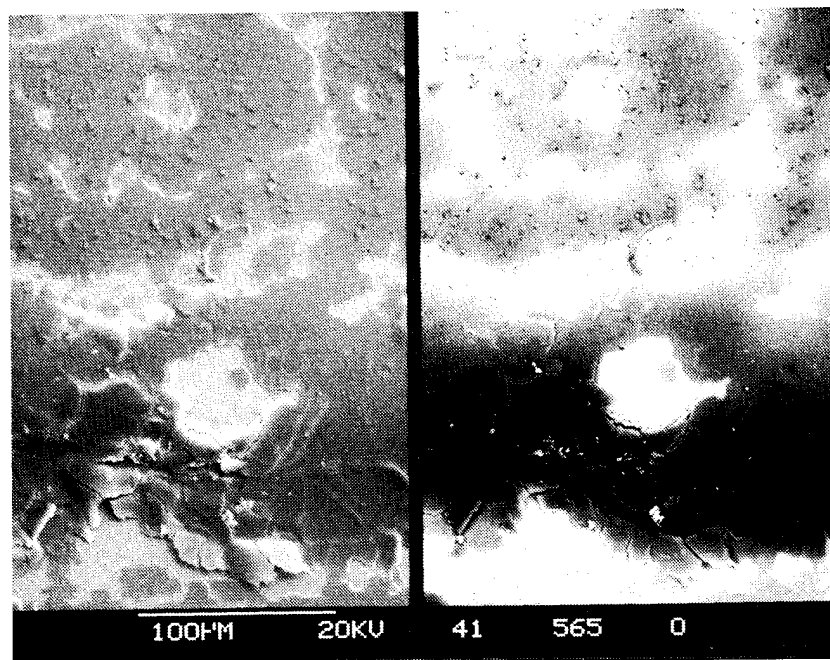
(a)       250X
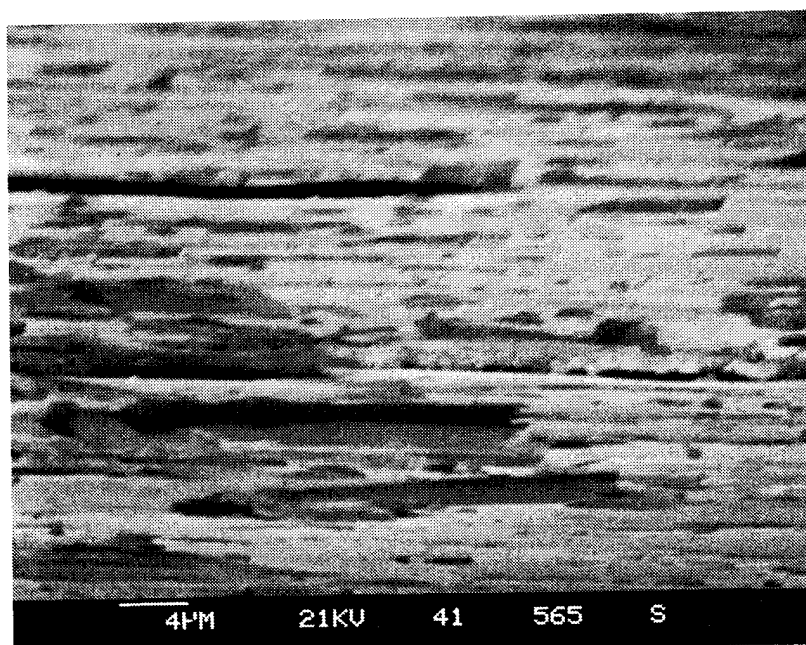


(b)       2,500X

Fig. 7-28. Close-up of the retainer transfer film in ball track center (a - see Fig. 7.27a). High angle view of edge indicates film was a few μm thick (b).

## Duplicate Film Fracture: 105-sized Bearing Short Test

In order to determine if Ni/MoS$_2$ multilayer film fracture was occurring on the smaller bearings, 105-sized bearings with less than 90,000 cycles were disassembled and examined. The film had delaminated at the ball track edges a similar to the that observed on the large bearings (Fig. 7-29). Moreover, flakes of the film were found in the ball pockets of the bearing retainers as was observed on the 117-sized bearings.



Topography          (b)          Composition          25X

Intact Film

Inner Race
Ball Track

Intact Film

Topography          (b)          Composition          250X

Intact Film

Inner Race
Ball Track
Edge
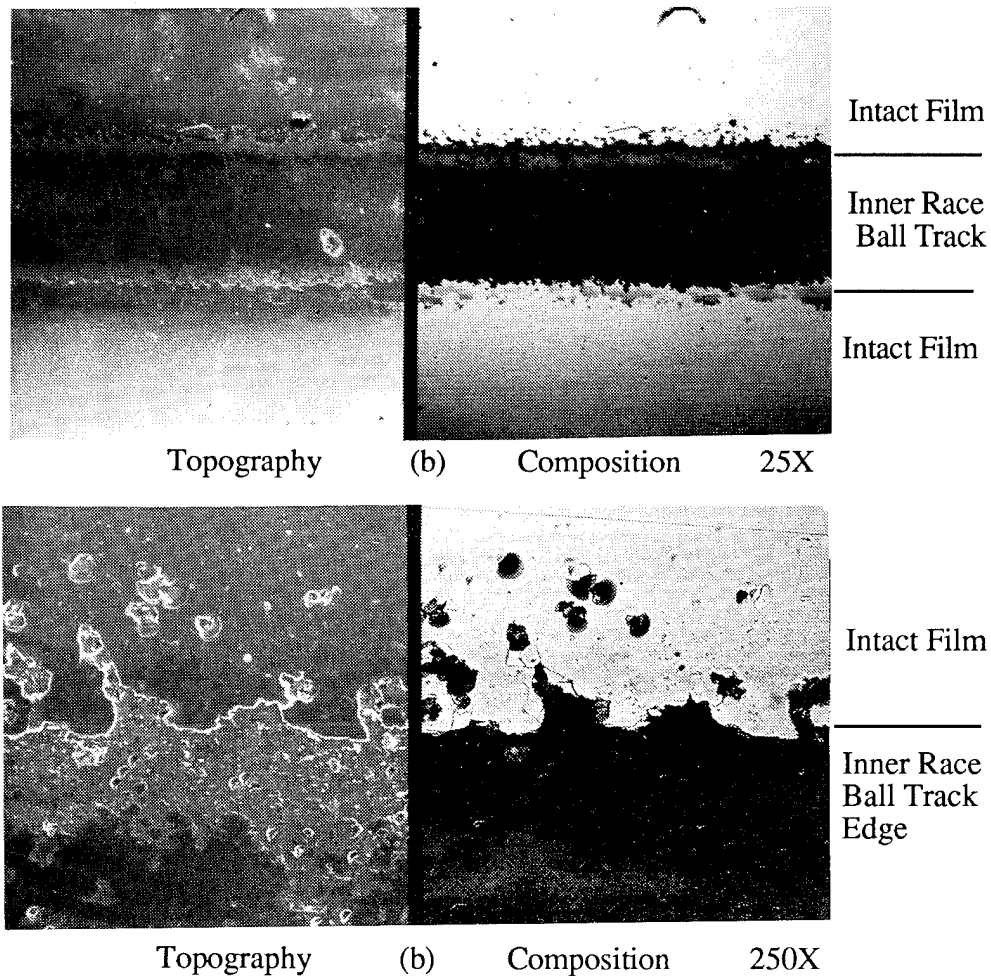
Fig. 7-29    Well-delineated ball track on the inner race of a Ni/MoS$_2$ multilayer thin film bearing (a) reveals film was lost. Fractured upper edge of track is shown in (b).

Although a portion of the MoS$_2$ film appears to have delaminated from the bearing race ball track, bearing failure (as measured by torque level or ripple) was not evident, although the smaller bearings may not be as sensitive to this film loss as the larger bearings. Lubrication occurs from the resulting residual (burnished) MoS$_2$ film. In addition, the retainer contributes to bearing lubrication due to a double transfer process from the retainer to ball, then ball to race as was observed in the other bearings with Salox retainers.

## 7.5.1 Development of Fracture Resistant Multilayer Film

As a result of the observation that the nickel multilayer films had fractured early in the bearing life, a combined effort with Ovonics Synthetic Materials was undertaken to develop a more fracture resistant film. Gold-Paladium, instead of nickel, was used as the interlayer, and the thickness of the interlayer was increased. In addition, the thickness of the entire film was decreased. The effect of these changes was assessed by a rolling contact test devised to directly test the capability of the film to resist fracture.

The thin films were deposited on 440C substrates that were finished by three different methods: grinding, lapping, and polishing. The ground surface had a 4.6 microinch ($\mu$in) rms finish, 28 $\mu$in peak to peak - similar to the finish on a high quality bearing race. The lapped surfaces had 2.0 $\mu$in rms finish, 4 $\mu$in peak to peak, comparable to special bearings finished by honing. The polished surface was obtained using standard metallographic techniques.

The films were prepared by radio frequency magnetron sputtering from individual targets onto substrates attached to a rotating carousel. The substrates were periodically rotated in front of one target or another. The thickness of the Au-Pd interlayers and $MoS_2$ layers was controlled by deposition rate, carousel bias, and carousel rotation rate. The entire film thickness was defined by the total number of carousel revolutions.

Three different thicknesses of the Au-Pd interlayers were deposited on the substrates while the $MoS_2$ layers were held constant at 10 nanometers (nm). The three Au-Pd interlayer thicknesses were 1.5, 3.0, and 4.5 nm thick. The thicknesses of the films deposited on the lapped and ground surfaces were 0.1, 0.3, and 1.0 $\mu$m. The polished substrates received a 1.0 $\mu$m thick film for microhardness testing and X-ray diffraction.

## Film Characterization

Extensive microstructural characterization of $MoS_2$/Au-Pd multilayer films similar to those developed here has been reported previously [7-7]. Considering the films in this study vary only in the interlayer metal thickness, detailed characterization was deemed unnecessary. However, X-ray diffraction was undertaken to verify multilayer spacing and texture. Actual multilayer spacings were slightly different than the theoretical attempts. Although the Au-Pd interlayers were accurate, the $MoS_2$ layers were slightly thicker (11 nm instead of 10 nm). Compositions were approximated by analyzing the pattern of intensity levels of the higher order reflections from the multilayer structure [7-8]. Results showed a weak (002) basal plane crystallographic texture as was reported previously for these multilayer films.

The relative hardnesses of films were measured using an Anton Paar ultramicrohardness tester model MHT-4, mounted on a SEM stage. Vickers diamond indenter (136° pyramid with a 0.3 mm radius tip) impressions were made using loads ranging from 0.25 to 2 milligrams force (250 to 2000 x $10^{-5}$ N). The thicknesses of the films prepared for hardness testing were typically greater than those for rolling contact testing in order to improve accuracy of the hardness measurement. In addition, a polished substrate improves the accuracy of the hardness measurement because the impressions are more square on a polished surface than on a rough, ground surface. Generally, the penetration of the indenter into the film ideally should be less than 10% [7-6]. Indenter penetration depth can be readily calculated from the geometry of the indenter. The 0.3 $\mu$m films used for most of the rolling contact tests would have required loads less than 0.1 milligrams to minimize substrate effects.
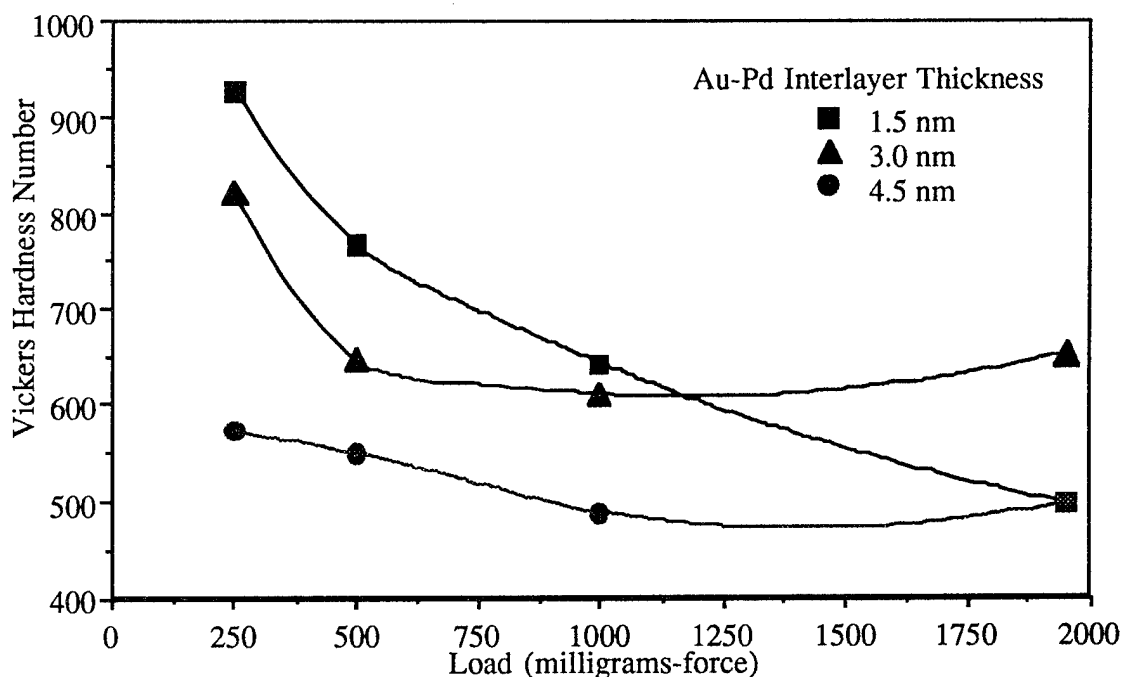
**Fig. 7-30    Results of Ultramicrohardness tests indicated thicker Au-Pd interlayers reduced hardness.**

Results indicate the greater amount of Au-Pd incorporated in the film (the thicker the inter-layer) the softer the film (Fig. 7-30). The increase in hardness at very low loads has been observed by others and is generally attributed to the finite shape of the indenter [7-7]. In addi-tion, the difficulty in imaging the impressions at the low load (100 milligrams) makes the accuracy questionable. The gradual rise in hardness at the higher loads is probably due to the hard substrate considering the substrate hardness was over 900 VHN. The 1.5 nm film appears to have been thicker than expected considering the drop-off in hardness at the higher loads.

## Indentation Tests

Indentation testing was performed on the films that were deposited by Ovonics during the development of the fracture resistant films. This type of thin film mechanical test may predict the performance of a film in a precision bearing. The extent of lateral film cracking at the periphery of an indent reportedly can provide an indication of film adhesion or interface fracture toughness.

Indents were made on 1.0 μm thick films that had been deposited on polished witness plate using a Rockwell "C" indenter. The extent of film fracture associated with the indents was determined by examining the indent in a scanning electron microscope in the backscattered electron (compositional) imaging mode. The area of fracture associated with the indents was similar for the 1.5 nm and 4.5 nm interlayer films (Fig. 7-31).
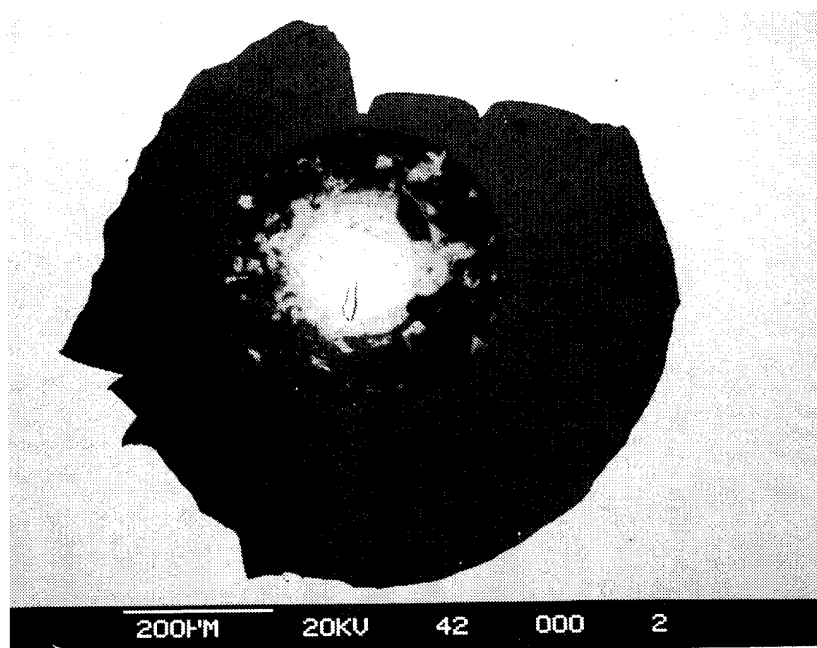
(a)
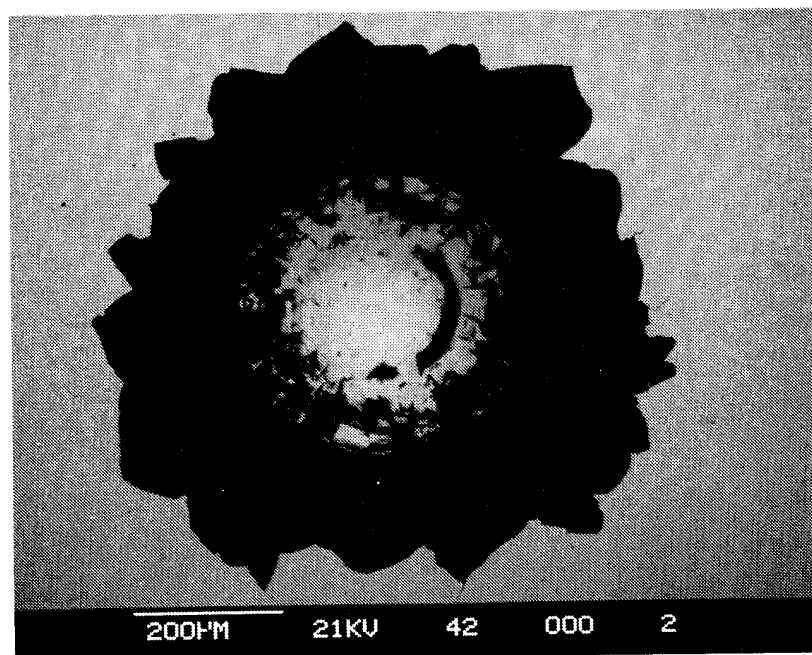


(b)

Fig. 7-31    Compositional electron images of film fractures associated with
Rockwell "C" indent in 1.0 μm thick 1.5 nm (a) and 4.5 nm (b)
interlayer thick   films on polished substrates.   100X magnification

- 185 -
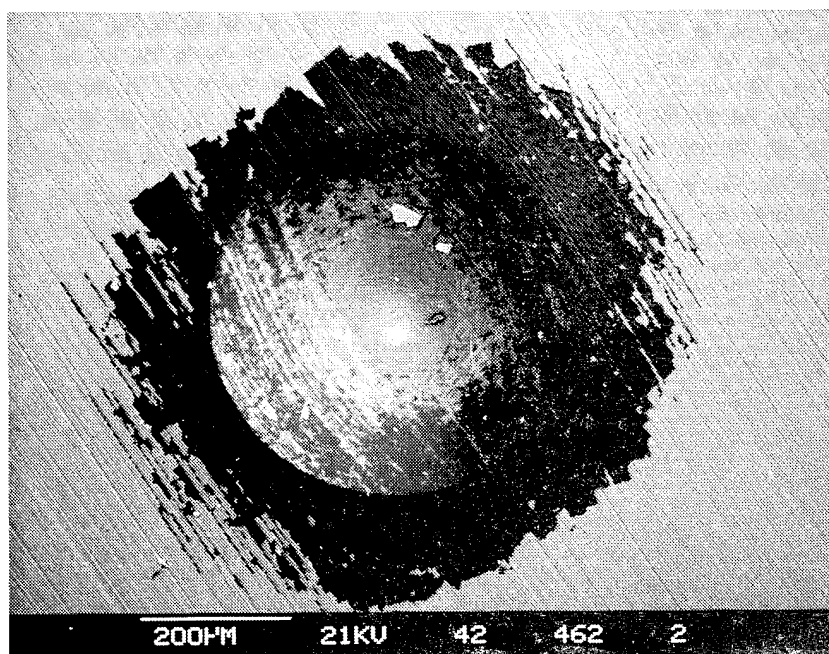
(a)
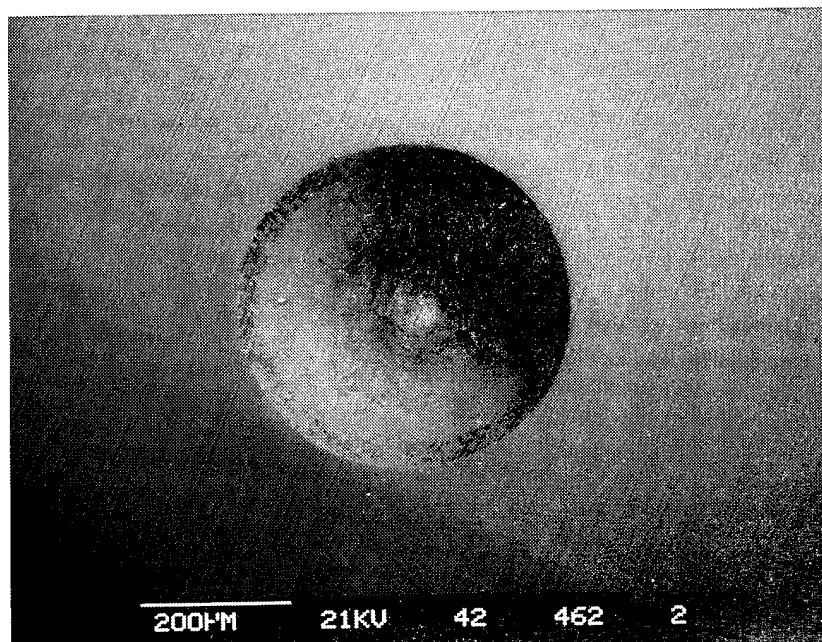


(b)

**Fig. 7-32** Compositional electron images of film fractures associated with Rockwell "C" indent in 0.3 μm thick 1.5 nm (a) and 4.5 nm (b) interlayer thick films on ground substrates. 100X magnification

The fracture associated with indents of 0.3 μm thick films that were deposited on ground and lapped 440C substrates revealed dramatic differences between the 1.5 nm and 4.5 nm Au-Pd films (Fig. 7.32). No evidence of lateral cracking was detected on either of the 4.5 nm Au-Pd films deposited on the ground substrates (Fig. 7-32). However, both of the 1.5 nm Au-Pd films on ground substrate exhibited extensive cracking. Films on lapped substrates showed similar results. The only difference was that cracking on the film deposited on the lapped substrate was discontinuous whereas the cracking on the ground surface was continuous.

## Rolling Contact Test

Rolling contact tests were initiated in order to investigate the effect of film variables on the delamination of the film. Three 0.25 inch diameter, hardened AISI 52100 (Rc 60) steel bearing balls were oscillated or dithered about 10 degrees in rotation between two discs, one of which was coated (Fig. 7-33). After about 100 dithers at 8 lbs/ball normal load (285 ksi maximum Hertz stress), the plates were examined.



24 lb Load

10 Degree Rotation
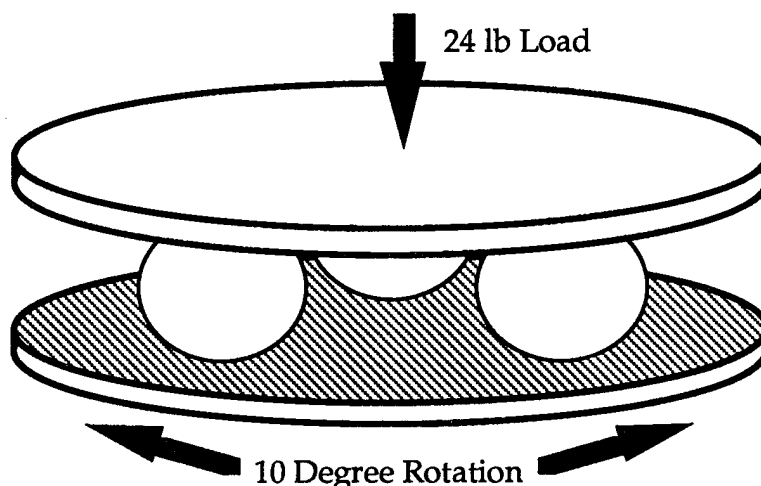
**Fig. 7-33    Rolling Contact Test Configuration**

Results indicated that many of the films deposited on ground surfaces typically failed by cracking and delamination; whereas films on lapped surfaces did not crack or delaminate under any conditions. More importantly, film cracking and delamination that occurred on the ground surface was suppressed when the Au-Pd interlayer was increased to 4.5 nm (Table 7-9).

**Table 7-9**

| Film Thickness | Au-Pd Interlayer thickness (nm) | | |
|---|---|---|---|
| | **1.5** | **3.0** | **4.5** |
| 0.1 μm | Cracking | Not tested | Fine Cracking |
| 0.3 μm | Cracking* | Not tested | No Cracking* |
| 1.0 μm | Not Tested | Some Cracking | Not Tested |

Although the film thickness effects were not fully investigated, these initial results suggest that 0.3 μm thick films with a thick Au-Pd interlayer were optimum in forestalling fracture on a ground surface.

## 7.5.2 Film Fracture Characterization

The 0.3 μm films that were deposited on the ground surfaces and then tested as described above were examined by scanning electron microscopy (SEM) in order to investigate the nature of the film failures. Backscattered electron (compositional) imaging revealed the delaminated regions on the test disc with the 1.5 nm Au-Pd interlayer film (Fig 7-34a). The delaminated or flaked regions were clearly associated with the ridges of the grinding grooves as evidenced by the linear delamination configuration. A higher magnification view of the edges of these flaked regions indicates the fractures were rather brittle with little evidence of plastic deformation (Fig. 7-34b). Within the flaked regions, a residual amount of film could still be detected (as evidenced by the light contrasting material visible on the substrate surface - Fig. 7-34b). This result was confirmed by elemental microanalysis.

Incipient film delamination could be observed in the 1.5 nm Au-Pd interlayer film by tilting the disc to a high angle (Fig. 7-35). A gap that develops between the film and substrate after repeated asperity deformations (rolling the ball over the film) suggests the steel substrate was exhibiting greater plastic deformation than the $MoS_2$ film. Subsequent film fracture appears to be associated with this difference in material response. The fracture appeared to initiate along the edge or sidewall of the grinding groove.

The 4.5 nm Au-Pd interlayer film content did not exhibit any delamination or cracking upon rolling contact testing. Defects that occurred where the ball tracked appeared to have resulted from particles embedded in the film (Fig. 7-36a) or organic contamination (black spots in the backscattered electron image). The particulate contamination probably occurred as a result of the dirty test environment. Higher magnification views of the "rolled over" film suggests increased ductility as a result of thicker Au-Pd interlayers. This increased ductility is apparent in a high tilt, high magnification view of a rolled over region (Fig. 7-36b).

## Assessment

The rolling contact coating tests indicate the ground surfaces (typical of bearings) are more susceptible to delamination-type fracture than the lapped surfaces. High surface roughness places severe mechanical demands on the film. As a ball at bearing loads rolls over a ground surface, high points associated with the grinding grooves (asperities) plastically deform. If the film does not plastically deform in a similar manner, fracture inevitably results. This lack of film deformation is evident in the high tilt view of the fractured low Au-Pd content film (Fig. 7-35). On lapped surfaces, the bearing loads are more evenly distributed due to the low asperity heights. Thus, film stresses are reduced. Only limited plastic deformation apparently occurs on a lapped surface when rolled over by a ball.

The suppression of this delamination fracture by use of the thick Au-Pd interlayers film is clear evidence of improved fracture toughness. Hilton [7-9] reports that the fracture toughness of multilayer films improves with increasing metal content. Using the brale indentation method of measuring fracture toughness, it was shown that decreasing the $MoS_2$ layer spacing between nickel interlayers and increasing metal content resulted in less film delamination. Although not reported, films with thin $MoS_2$ layers (resulting in high Au-Pd content) were also tested by the brale indentation method. Those films exhibited little delamination during indentation.
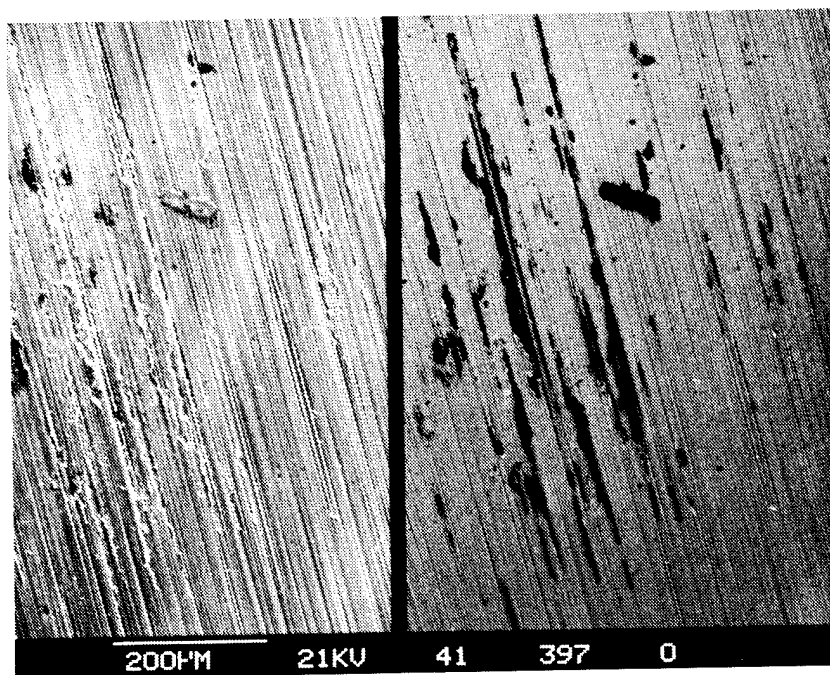
Topography   (a)   Composition         100X
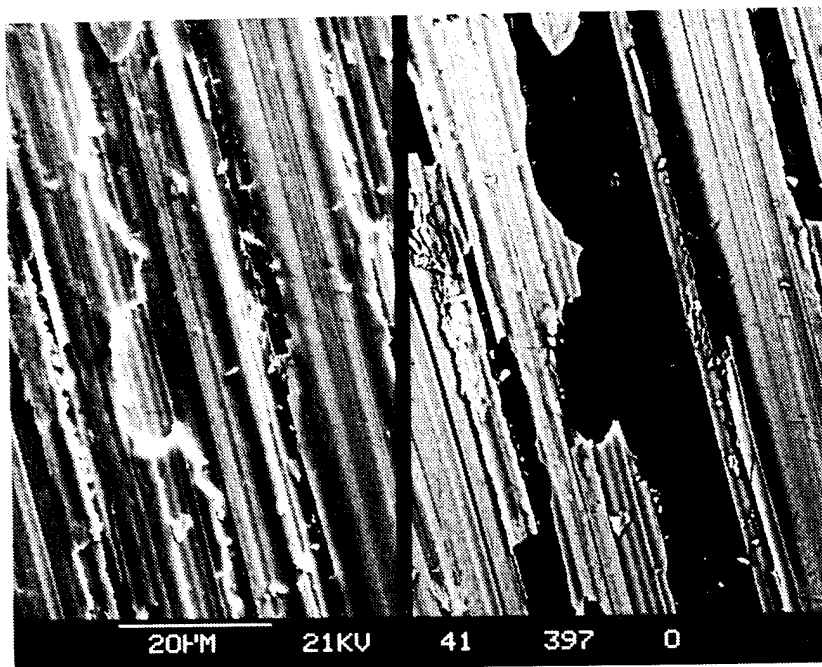
Topography   (b)      Composition      1000X

Fig. 7-34   Backscattered (compositional) image clearly shows the (dark
            contrasting) delaminated regions in the 1.5 nm Au-Pd
            interlayer film (a).   These delaminated regions were
            associated with the grinding grooves (b).
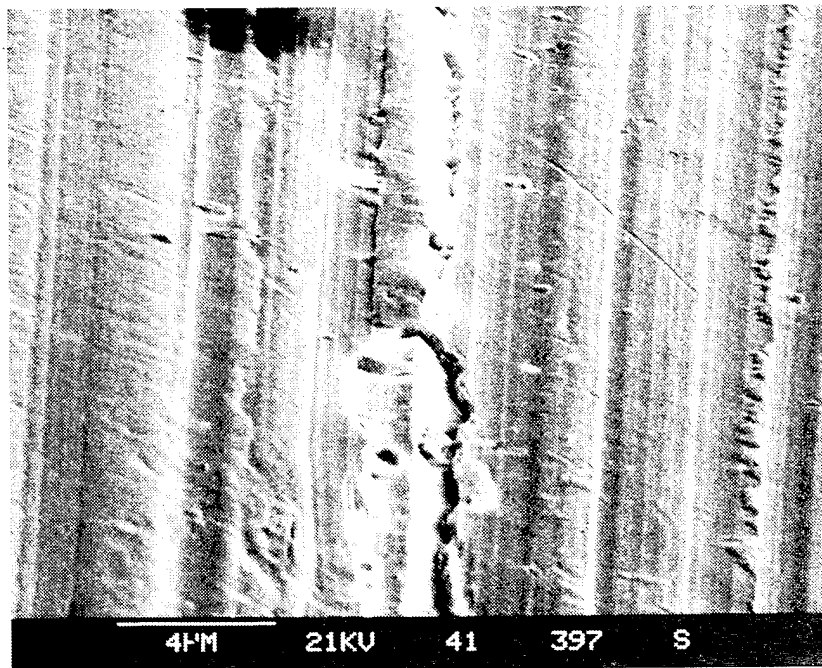
(a)                         5,000X



(b)                         20,000X

**Fig. 7-35   At high tilt, incipient film delamination was observed in the
1.5 nm Au-Pd interlayer film (a).   The gap under the
deformed region suggests a large difference in material
response between film and substrate (b).**
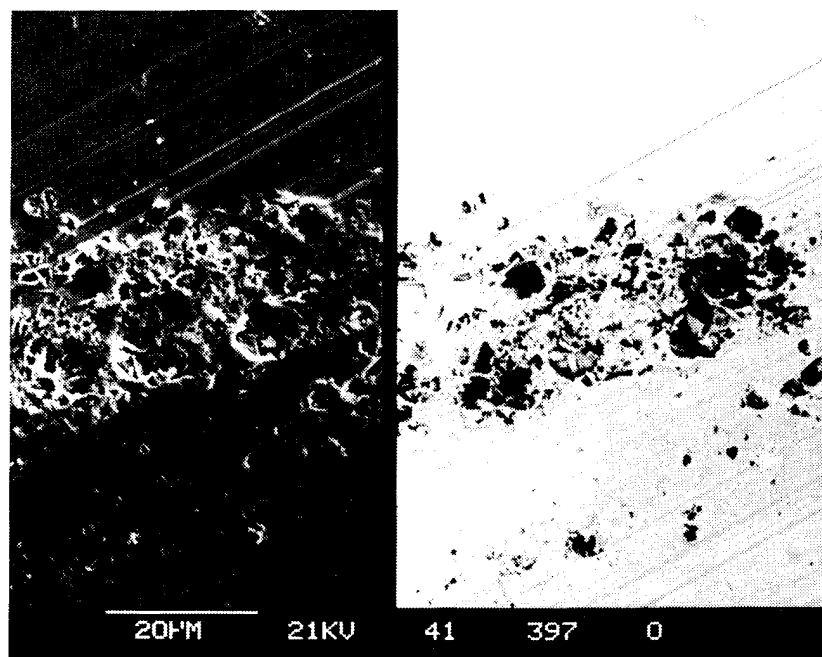
Topography    (a)    Composition    1000X
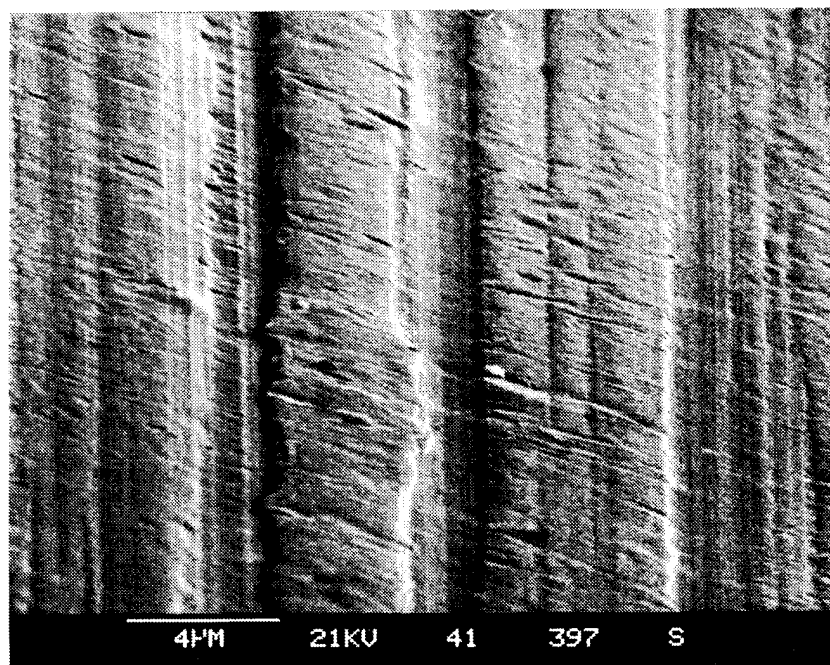


(b)                    5000X

Fig. 7-36  The only damage found on the 4.5 nm Au-Pd interlayer  film test
area   appeared to result from particles (contamination) indenting
the film (a).  A high tilt, high magnification view of the film
shows considerable deformation occurred at grinding ridge(b).

The observed improvement in fracture toughness of thick Au-Pd interlayer films may be a consequence of an energy absorption mechanism such as crack blunting. Cracks still probably initiate along the asperity sidewalls; however, they may be blunted by the thick Au-Pd interlayer. The Au-Pd interlayer, having isotropic properties, has the same deformation response regardless of orientation (i.e., sidewall or top of asperity). Incorporating soft, ductile and isotropic interlayers between lamina is a well known method of improving fracture toughness of fiber reinforced composites typically at the expense of strength [7-10].

The suppression of delamination may also be due in part to the lower yield stress and higher ductility exhibited by the thick interlayer film. Ultramicrohardness measurements indicate the thicker Au-Pd interlayer films are indeed softer. Considering hardness is directly related to yield stress [7-11], the thicker Au-Pd interlayer films are no doubt yielding at a lower stress. As occurs in most metallic materials, ductility is inversely proportional to strength.

The high Au-Pd content of the thick metal interlayer film may increase friction of the film, although composition of the interlayer apparently controls the friction. Hilton [7-7] reports that high gold contents in IBAD $MoS_2$ films exhibited lower friction and performed far better in endurance than the high nickel (sputtered) counterpart when tested in a thrust washer configuration. However, these results were not as good as pure $MoS_2$ or low (0.1 nm) metal interlayers (gold and nickel). Although the high gold films were not tested in a rolling element bearing configuration, these results suggests that there would be only a minor penalty in friction.

## 7.6 EXAMINATION OF BEARINGS INCORPORATING THE FRACTURE RESISTANT FILM

### 7.6.1 Scale-up of Deposition System for Large Bearings

Significant modification of the Ovonics deposition chamber was required to deposit multilayers on the large 5- and 12-inch bearings as compared to the smaller, 105-sized bearings. Scale-up of the deposition system for inner races was much simpler than for the outer races. The inner races are rotated in front of large (4 x 5 in.) magnetron sputtering targets and are periodically moved in front of one target or the other to obtain the appropriate layer thickness. Deposition on larger inner races entailed building a larger chamber and fixturing to accommodate the size of the inner race.

Depositing multilayer films on the large outer races required a significant change in the deposition system. The smaller 105-sized outer races could be coated by rotating the race in front of the large targets. The "throwing power" of the RF magnetron targets was sufficient to deposit on the inside diameter surface of the outer races which was only about two inches from the target (diameter of the outer race is about 1.5 inches). This fixturing set-up could not be used on the 5 or 12-inch bearings because the inner diameter surface was too far from the targets for efficient deposition. The 12-inch outer races were more easily accommodated by placing both Au-Pd and $MoS_2$ magnetron targets back to back inside the races and switching on when needed. Unfortunately, the 5-inch outer race required developing 1 inch targets because existing 2 inch targets were to large too fit inside the outer race ring. This development effort resulted in a significant delay in the program. Moreover, the effect of this change in deposition targets and geometry on film properties was unknown.

### Large Bearing Witness of Deposition Process: Problems

Control of the process through analysis of deposition witness plates was extremely limited on the larger bearings. For the 105-sized bearings, the quality of the thin films was monitored using witness plates that were placed on the fixture that held the bearing components. These fixtures were relatively close to the sputter targets. While this process control system was not useful in assessing the film thickness on the actual bearing components (described in section 7.4), other material properties such as composition, texture and hardness could be assessed.

Unfortunately the witness plates could not accompany the larger races in the deposition chamber. Fixturing of the bearing components did not allow room for the witness samples, especially during deposition on the outer races. The fixtures were not close to the targets. An attempt was made to attach witness plates on the edge of the races, however, these plates were only on the edge of the ion flux path. The resulting films were very thin. In order to deposit a film on a witness plate that is identical in ion flux to the film on the inner or outer race, additional, dedicated fixtures would have to been developed and separate deposition runs undertaken. The expense of a dedicated deposition run precluded this fixture development. Moreover, the witness plate would not "witness" the actual deposition. A satisfactory solution to this lack of process control was not determined. For actual flight application, expense of separate witness fixturing would probably be required in order to verify film properties.

The fracture resistant film developed in cooperation with Ovonics was applied to three sizes of bearings. The 0.3 μm thick Au-Pd/$MoS_2$ multilayer (4.5 nm Au-Pd interlayers) film was applied to inner and outer races and Salox retainers were used. After life testing, these bearings were disassembled and the films characterized.

## Examination of 2-inch, 105-Sized Bearings

The small bearings with the fracture resistant, multilayer film were similar in appearance to the small screening bearings that had Salox retainers previously reported (section 7.5). The retainer ball pockets revealed small wear scars with wear debris on the edges of the scar. The balls and ball tracks on the races were copper colored, indicating transfer of the bronze in the retainer to these components. Debris generated mostly from the contact between the ball and retainer covered the components.

SEM examination of the inner races showed a wear appearance similar to other screening bearings. The ball track was well-defined by the edges of the film (Fig. 7-37a). Although evidence of fracture was not found, the film was clearly worn from the ball track edge (Fig. 7-37b). Circumferential bands of retainer transfer film was evident and a highly tilted view of these transferred films reveals a thickness that averaged about 0.5 $\mu$m (Fig 7.38). The ball track widths of the four inner races, (0.047, 0.057, 0.048 and 0.045 inch) were comparable to other bearings with polytetrafluoroethylene retainers (section 7.5).
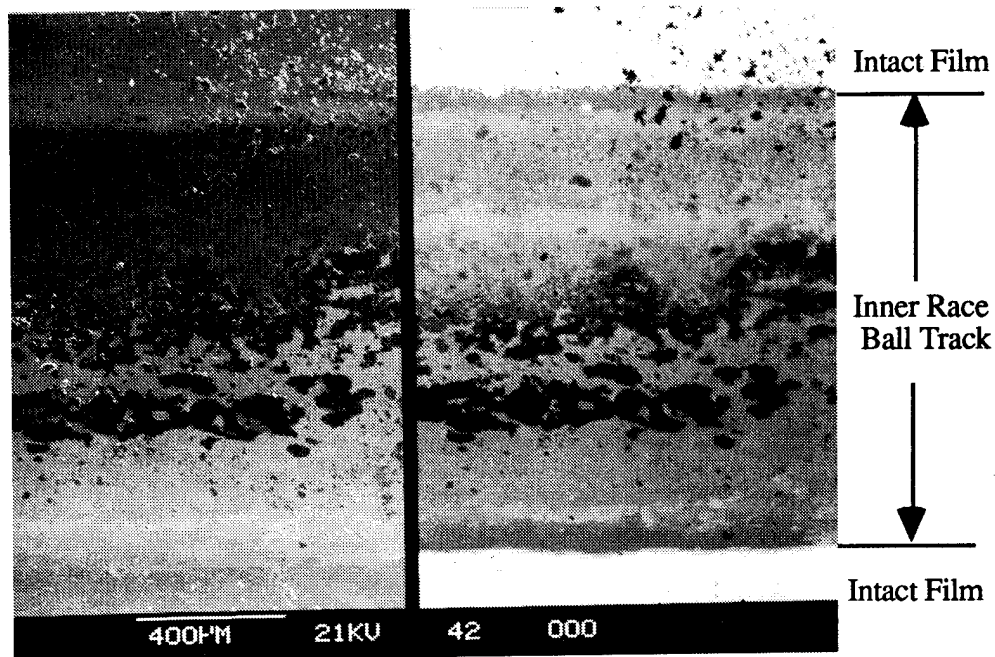
## Examination of 5-inch (117-sized) bearings

Examination of the two sets of 5-inch bearings incorporating the 0.3 $\mu$m, multilayer fracture resistant coating revealed a wear appearance similar to the smaller, 105-size bearings. Moreover, little difference between the individual bearings was observed. The retainer ball pockets revealed small wear scars with wear debris on the edges of the scar. This wear debris was also collected along the outside diameter of the retainer that contacted the outer race land. The inner and outer races and balls were copper-colored, indicating a transfer of the bronze in the Salox material to these components.

SEM examination of the inner races showed a wear appearance similar to previously examined parts. The ball track was well-defined by the edges of the film (Fig. 7-39a). Although MoS$_2$ can be detected in the track, the film was clearly worn-off or fractured at the edge (Fig. 7-39b). Circumferential bands of retainer transfer film were evident and a highly tilted view of these transferred films reveals a thickness of about 3 $\mu$m (Fig. 7-40).

## Examination of the 12-inch Bearing with Fracture Resistant Film

The 12-inch bearings incorporating the fracture resistant films and Salox retainers were disassembled and examined in order to determine the source of the intermittent high torque. The periodic increases in bearing torque exhibited by these bearings are suspected to result from a high transfer rate of retainer material to the ball race interface (Fig. 6-21).

As observed on the smaller bearings, considerable amount of retainer debris was evident on the balls, races, and retainers. All of the balls (in both the top and bottom rows) were copper colored which indicated the bronze component of the retainer material transferred to balls. The bronze had also transferred to the races as evidenced by the copper color of the ball track. The loose debris could easily be wiped-off with a Q-tip swab. However, the bronze was quite adherent and could not be removed. Close inspection of a cleaned region of the ball track did not reveal a fractured edge of the film along the ball track that had been observed in the past (Fig. 7-41). Although these large bearings were too large to fit into the SEM chamber for evaluation of the film, visual appearance was similar to the five and 105-size bearings. The ball track was probably very similar to the smaller bearings; loss of film at the edges combined with a relatively thick deposit of transfer film.

Intact Film

Inner Race
Ball Track

Intact Film

400I'M   21KV   42   000

Topography   (a)   Composition   50X



Inner Race
Ball Track
Edge

Intact Film

100I'M   21KV   42   000
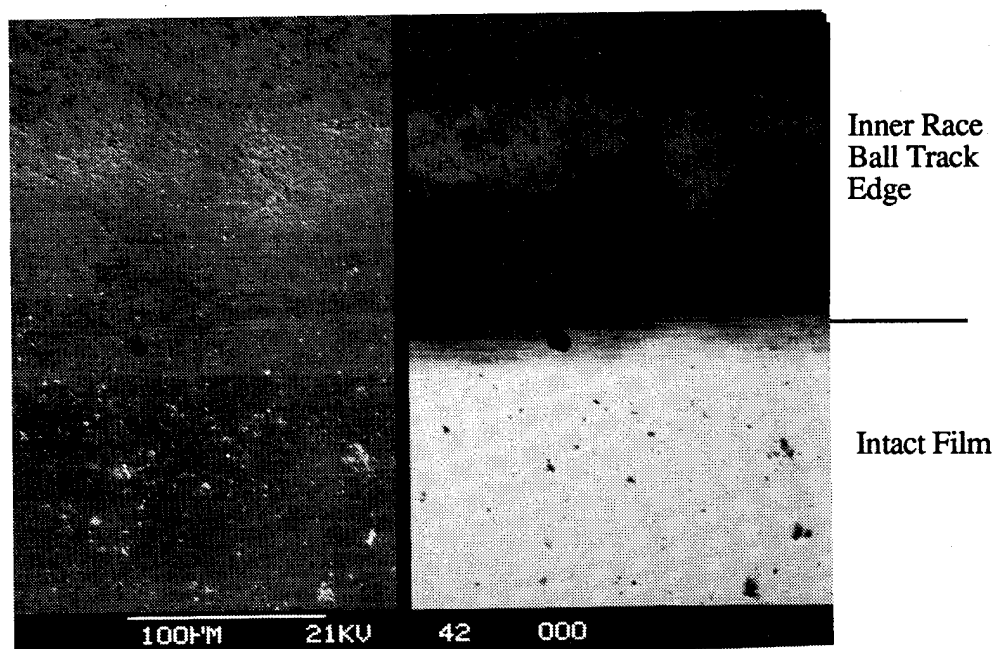
Topography   (b)   Composition   250X

Fig. 7-37   Ball track on 105-sized bearing inner race (a). Dark band in
ball track center is a  retainer transfer film.  Loss of
multilayer film  at lower track edge is shown (b).
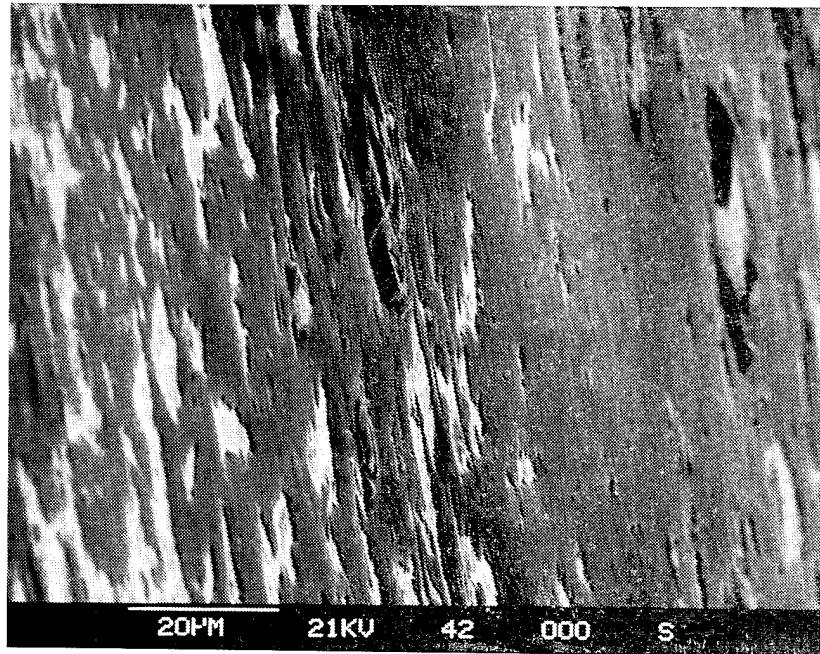
(a)                1000X
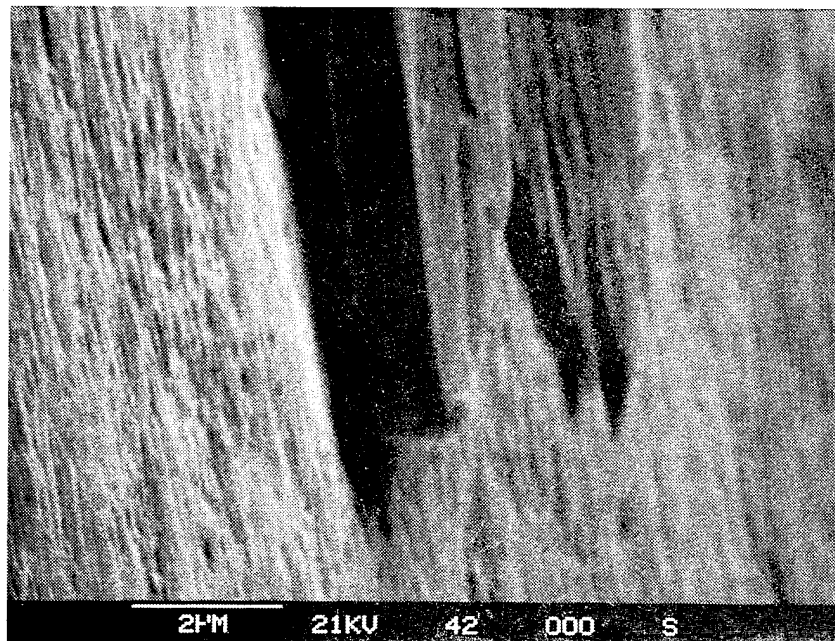


(b)                10,000X

Fig. 7-38    Highly tilted image of the retainer transfer film in ball track
center (a - see Fig. 7-37a).  High angle view of transfer film
edge indicates film was about a micrometer thick (b).
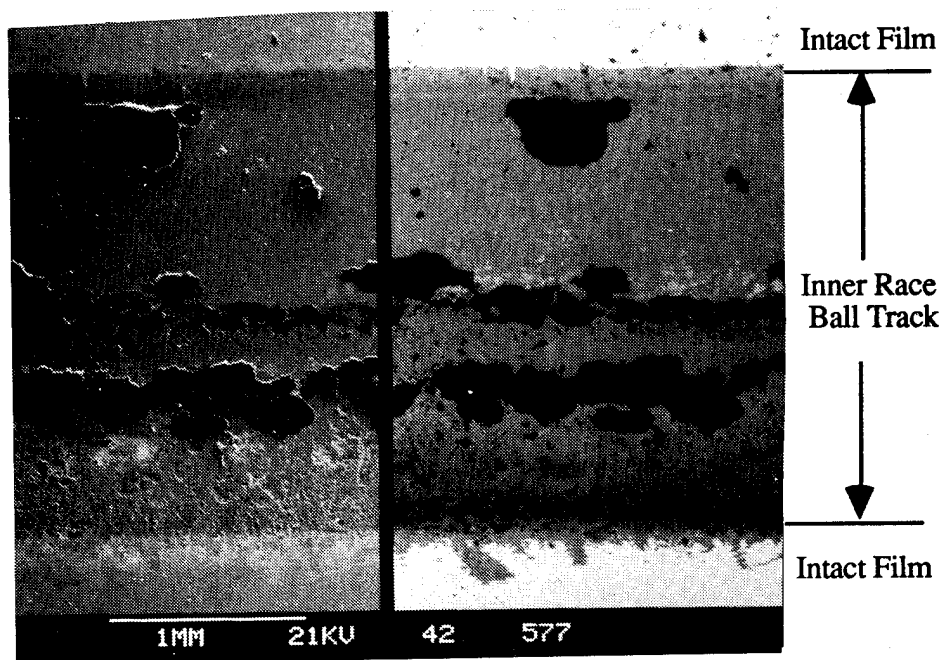
Topography     (a)     Composition     25X
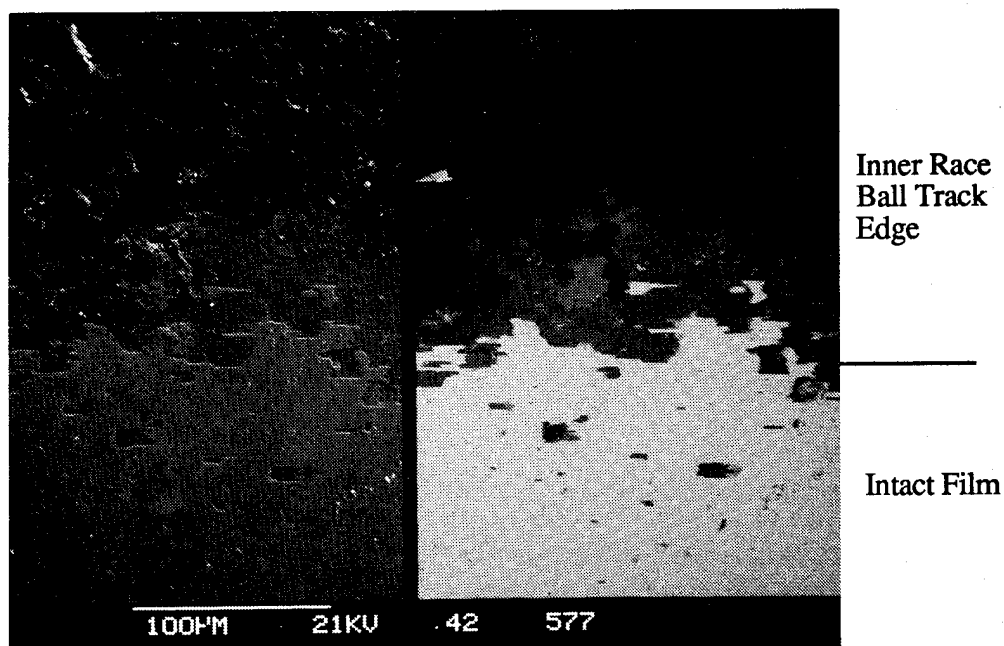


Topography     (b)     Composition     250X

Fig. 7-39 Ball track on 117-sized bearing inner race (a). Dark band in ball track center is a retainer transfer film. Loss of multilayer film at lower track edge is shown (b).

- 197 -
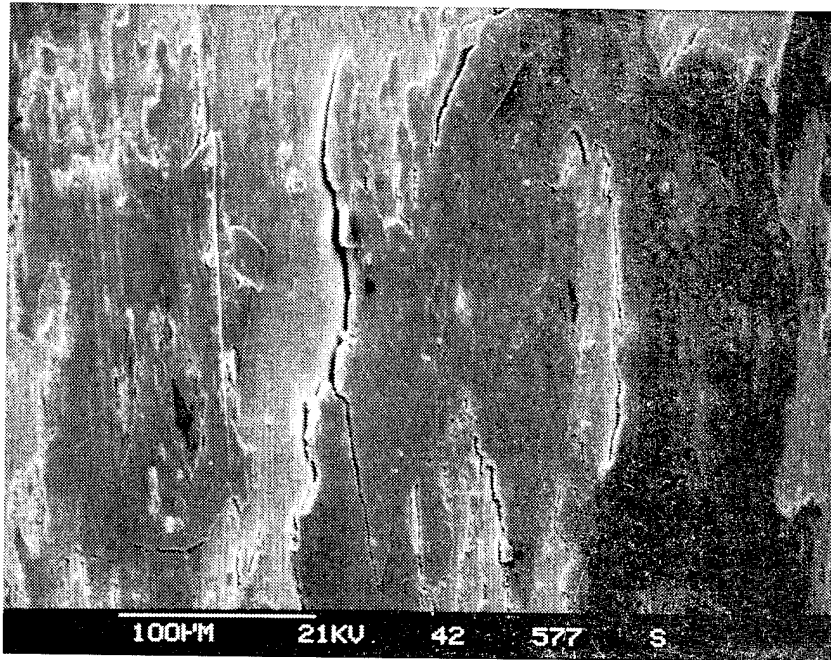
(a)                              250X
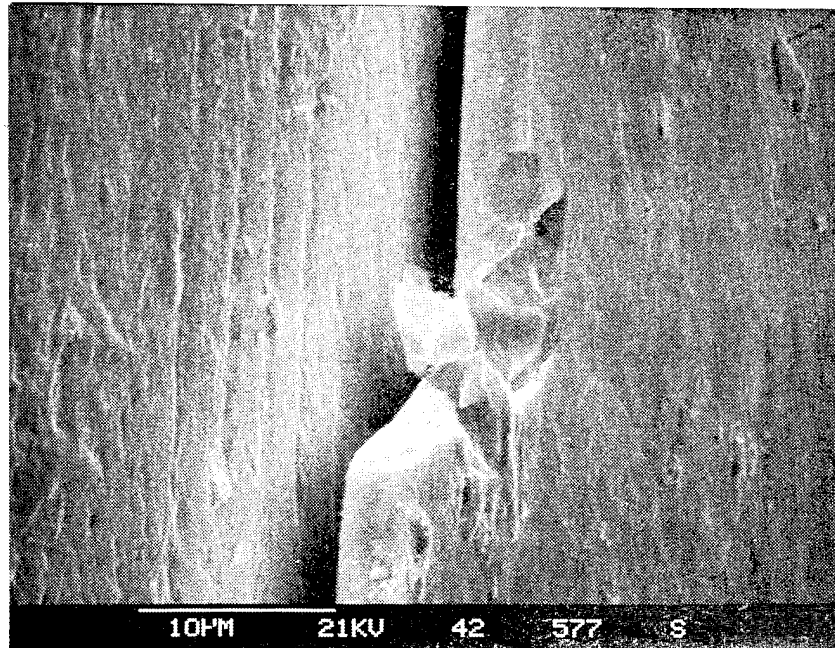


(b)                              2.500X

**Fig. 7-40**   **Highly tilted image of the retainer transfer film in ball track center (a - see Fig. 7-39a). High angle view of transfer film edge indicates film was about a 3 μm thick (b).**
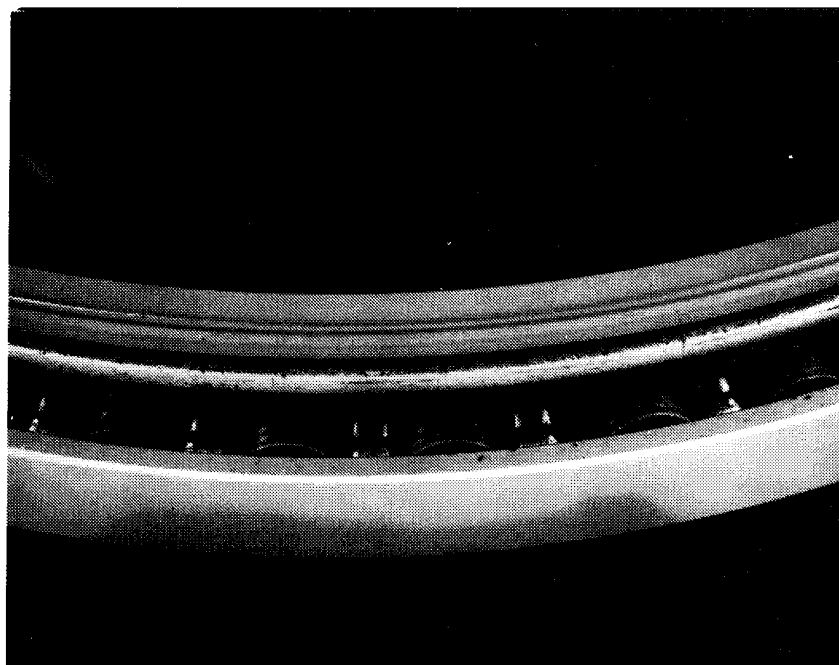
(a)            1 X
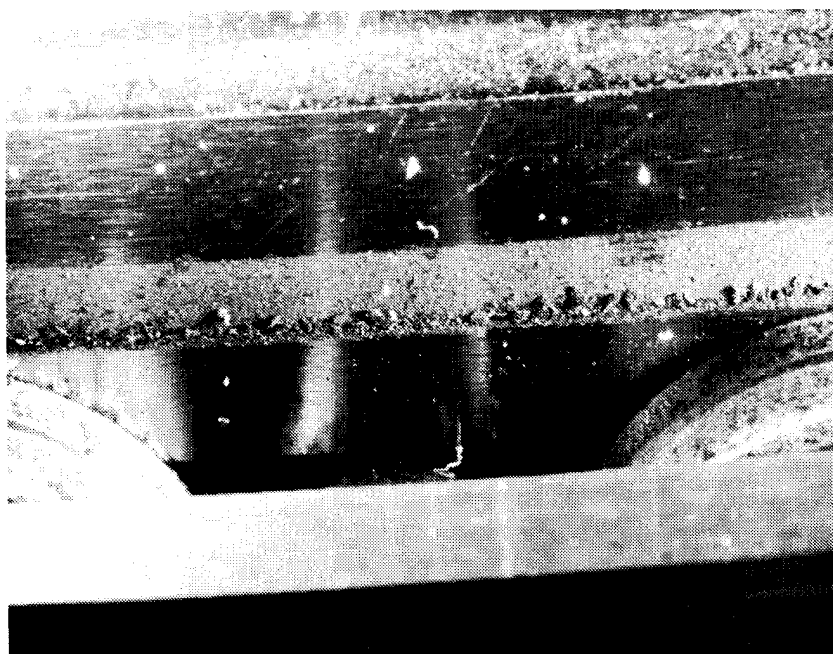


(b)            8 X

Fig. 7-41    Twelve inch duplex bearing with top row of balls removed shows bottom row of balls and retainer toroids (a). Considerable retainer debris was evident along inner race shoulder (b).

### 7.6.2 Assessment:   Fracture Resistant Thin Films

The significant portion of the $MoS_2$ thin film on the bearing is lost or, more accurately, converted to a burnished film during the early stages of the bearing life. Although high gold film on the bearings improved ductility and fracture resistance as a result of thick Au-Pd interlayers, these improvements may have only forestalled eventual film loss and relatively little of the film remained in the ball wear tracks when examined at the end of life. The mechanics associated with this loss of film are not clear although fatigue and associated fracture of the film still appears to be dominant mechanism for film loss.

Eventually, bearing lubrication is primarily due to (double) transfer of retainer material (retainer to ball, then ball to race), rather than the burnished thin film. Unfortunately, this transfer process is not particularly stable and appears to cause occasional high torques (spikes). Excessive debris generation from retainer wear appears to be the primary source of the intermittent high torques, although thin film and metal wear particulate also contribute to torque spikes. For reasons not quite clearly understood, overtransfer of the retainer will occur sometimes and the increase in preload associated with the overtransfer will increase the bearing torque. Perhaps the gradual loss of the thin film increases bearing friction, which increases the transfer rate. Conversely, the retainer material may transfer at too great a rate, which consequently increases the film loss rate. In any event, the copper color of the balls and race tracks, organic deposits in the ball track, and wear of the ball pockets is the clear evidence of transfer film in all of the bearings.

## 7.7 PRODUCIBILITY OF THIN FILMS:   PROCESS REQUIREMENTS FOR THIN-FILM BEARINGS

### Film Thickness

Obtaining an accurate film thickness appears to be probably the most important process requirement for these precision bearings. A consequence of the film conversion is a loss of preload and concomitant loss of bearing stiffness. Although the retainer transfer film deposits help to offset the film loss, the transfer film thickness appears to be uneven and unstable. The amount of stiffness loss that is acceptable determines the maximum allowable thickness of film on the bearing. The thinner film is acceptable in view of the observation that the retainer provides a considerable amount of lubrication.

Experience gained during the analysis of the tested bearings and Hohman process optimization suggest that obtaining the required thickness of coating is difficult for most of the different types of thin films examined in the thrust bearing screening tests. As can be seen in Table 7-1, the thicknesses of the various films on the thrust bearings varied between 60% to 200% of the nominal. This variability in thickness also occurred in films deposited on angular contact bearings by NCT and Hohman.

Only Ovonics has consistently deposited films on bearing races with very accurate film thickness. Perhaps this accuracy is inherent in the multilayer approach to film deposition or due to their considerable experience in coating components used in X-ray diffraction. In any event, additional bearing components from all sources remain to be examined to confirm these observations.

Film thickness accuracy was typically poor for film suppliers other than Ovonics. Most film producers apparently predict film thicknesses based upon witness plates rather than from practice runs on actual components which are more accurate. The reason for this poor accuracy becomes apparent by examining the results of the film thickness "mapping" in the Hohman deposition chamber (Table 7-4). Film thickness varies not only with component

orientation, but also size and composition of the substrate. Even after this mapping, the thicknesses of Hohman films on the races were off by up to 100%.

Despite these inaccuracies in absolute film thickness accuracy, the repeatability was high, indicating that deposition runs for each film producer were reproducible. No doubt accurate film thickness could be obtained for all films if repeat calibration runs on actual bearing components were run. This extra step, no doubt, adds considerably to the cost of deposition. However, at this level of process development, component witness plates are a necessity,although future experience may prove otherwise.

## Mechanical Tests: Indentation, Hardness

Tests that provide an indication of film mechanical properties could be correlated with film life, considering film fracture and conversion to a burnished film is associated with bearing life. Extent of film fracture that results during a Rockwell indentation was clearly related to resistance of the film in the rolling contact test. Large differences observed in indentation film fracture between the thin and thick Au-Pd interlayer films were also observed in the rolling contact tests. Considering that both the rolling contact and the indentation tests appear to reveal similar fracture toughness "properties" of a thin film, the simpler, indentation method may be a preferable test for developing more fracture resistant films.

The indentation test could be implemented in film quality control. The test could be performed on the race shoulder and not affect bearing operation; and, therefore, be done on precision flight bearings to ensure quality. However, imaging the indent on a flight bearing may be the difficult. Although nondestructive, electron microscopes generally have chamber size limitations which would limit the size of the bearing that could be placed in the chamber to about 6 inches in diameter. Perhaps some other optical microscopic method could be utilized to image the film fracture.

Thin, ductile films however, do not necessary provide useful fracture data. Neither the thick 4.5 nm Au-Pd interlayer films at 0.3 $\mu$m nor the 0.3 $\mu$m NCT films on the screening bearings showed any detectable radial fracture. If thin, ductile films are used in bearings, subtle differences in the fracture resistance of these films may not detectable in the indentation test.

Film hardness (determined by ultramicrohardness testing) may also provide an indication of the film life. Hardness was inversely correlated with extent of film fracture in the rolling contact test: the softer the film, the greater the fracture resistance. If soft, ductile films are required for long film life, hardness tests appear to be useful in film characterization. Unfortunately, ultramicrohardness testing requires specialized witness plates and adequate film thickness.

## Film Chemistry, Texture, Morphology

The effect of specific film characteristics, such as crystalline texture and composition on the friction and endurance of rolling element bearings, remains to be established. These film characteristics may have little effect on film properties in a rolling element environment. Never-the-less, characterization of the films to confirm run-to-run deposition consistency should be undertaken until these characteristics are conclusively shown to be nonessential (especially at this stage in process development).

X-ray diffraction has clearly revealed changes in the film texture  as a result of intentional process changes. Deposition current levels can be determined by texture (albeit subtle) in the Hohman films. A texture change in the apparently optimized NCT film was observed in the diffraction spectra, although this may have little effect on film endurance.

- 201 -

Morphological characterization of the film by SEM also reveals process changes. This was clearly evident in both the Hohman and NCT films. However, this morphology characterization can be performed on the witness plates that accompany the bearing components, at the same time thickness is measured.

The utility of compositional analysis appears to be less important than texture or morphology. However, gross changes in composition are likely to alter film behavior. Composition can also be determined by X-ray photoelectron spectroscopy (XPS) on witness plates. Note that other analyses could also be subsequently performed on accompanying witness plates, if the film quality were suspect as a result of subsequent anomalous bearing behavior.

## Accelerated Film Life Testing: A-6 & Rolling Contact

Accelerated testing of thin films in a simple wear tester provides both a method of quickly testing new thin films in development and subsequent quality control of film lots. However, sliding wear testers such as the well know pin-on-disc test clearly do not simulate the rolling element environment. Development of improved testers, such as the described rolling contact tester, that quickly assess how well a thin film will perform in an angular contact bearing are needed to improve the existing films and provide adequate quality control.

Hohman used an A-6 tester configured as a rub block with a thin film loaded against a rotating cylinder to assess films. The test rig was instrumented to detect film failure by a sudden increase torque. While this test method provided an assessment of film endurance typically in less than a day, the film was tested only in pure sliding. Considering the thin films in angular contact bearings failed from fracture associated with cyclic loading in rolling contact, sliding endurance of a film may not be relevant. Moreover, a hard film that is optimized for sliding may perform poorly in a rolling application that requires high toughness.

The rolling element tester collectively developed by Ovonics and LMSC provided rolling element motion to assess films (see section 7.6). While this test method more accurately simulated an angular contact bearing environment (compared to the A-6 or a pin on disc tester), film failure was determined by a somewhat subjective means. After 100 dithers, the degree of wear was assessed by visual and/or SEM examination of the test coupon. This test method duplicated the fracture observed on angular contact bearings. The technique could be improved in order to determine endurance in more ductile (fracture resistant) films. Instrumenting the test to detect a torque increase from film loss would be one method to improve the test.

## Improving the Thin Film Bearings (Summary)

Results to date show considerable progress towards developing flight bearings that exhibit a predictably long endurance and low friction; however, a number of design issues remain to be resolved. Although producing an accurate film thickness was resolved, the relationship between thickness and life still appears to be a function of the film fracture toughness. Conversion of the intact film to a burnished film controls the useful life of the film. Transfer films from the retainer that also provide bearing lubrication obscure this transition of the intact film to a burnished film. Interval testing (examination of the wear tracks at intervals during the life test) could be one method of determining the wear mechanism.

Polytetrafluoroethylene-based retainers appear to be required for long bearing life. After some unknown interval, the thin films on the bearings are converted to a burnished film, and additional lubricant is supplied by the PTFE retainers. However, improved fracture

resistance of thin films could delay or minimize the amount of retainer film transferred to the race. Angular contact screening bearings that had only the Salox retainers (no MoS$_2$ thin film) did not exhibit substantially worse torque than the bearings incorporating thin films and Salox retainers. The thin films may have been primarily responsible for the initial low torque, but after about 10 million cycles, little difference between the bearings with or without thin films was observed, although greater track wear was observed.

Considering that retainer transfer films both provide lubrication extending thin film bearing life, and at the same time, cause an occasional high torque from debris build-up, research into improving retainer materials may be worthwhile. A retainer material that provides a consistent amount of transfer film under various bearing speeds, loads, cycle rates, temperature, etc. may be more beneficial than a thin film that doesn't fracture.

## 7.8 CHARACTERIZATION OF LIQUID LUBRICANTS

A important component of the tribomaterials development program is testing and characterization of lubricant greases. Considering that liquid lubricants are presently used in precision gimbal bearings, they offer a necessary standard to which the dry films should be compared (especially under similar test conditions).

A major weakness of liquid lubricants for space applications is volatility or outgassing properties. Loss of the bearing lubricant in the vacuum (space) environment is detrimental not only because in time there may be insufficient lubricant quantity to provide low friction, but also the volatile components may contaminate other critical spacecraft components such as optics. Bearing sealing techniques, lubricant quantity, instrument wavelength sensitivity, and line-of-sight location are factors that determine if outgassing is a problem. Outgassing tests were performed on three greases that are presently under test in large precision bearings:

1. Nye Rheolube 952 is a neopentylester (NPE) oil with a lithium stearate thickener. Additives also in this grease are tricresylphosphate (TCP) for antiwear and dibutylated hydroxy toluene (BHT[2]) as an antioxidant. This grease provided the lowest consistent torque of all the liquid lubricants tested in the 105-sized bearing tester.

2. Nye Rheolube 2000 is a multiply-alkylated cyclopentane (MAC) oil with a sodium octadecyl terephthalanate thickener. Lead naphthanate (PbNp) in a 3.5% concentration is added for antiwear. Two antioxidants: thiodiethylene bis 3,5 di-tertiary butyl -4- hydroxy hydrocinnamate and dioctyldiphenylamine, are also in the grease formulation.

3. Braycote 600 is a perfluoropolyalkylether (PFPE) oil with a polytetrafluoroethylene (PTFE) thickener. This synthetic grease is the most widely used lubricant in flight bearings at LMSC. However, Braycote 600 has some limitations such as a lack of solubility for commonly used antiwear or antioxidant additives. Moreover, under some conditions, the lubricant reportedly will polymerize under extreme pressure.

### Outgassing Tests
The outgassing properties of the three greases were determined using an effusion cell combined with four quartz crystal microbalances (QCM). A 2-gram grease sample in a 25°C (temperature controlled) effusion cell is placed in a high vacuum (1 x 10$^{-9}$ torr) chamber. The outgassing flux is monitored by the four QCM's held at 85°K, 160°K, 220°K, and 298°K. The low temperature QCM (at 85°K) determines the outgassing rate and total mass loss

(TML). The other three QCM's determine volatile condensable material (VCM). In addition, the test chamber is equipped with a mass spectrometer in order to identify chemical species in the volatile component of the grease. Note that this test method is in the process of becoming an ASTM standard (ASTM E21.05).

The Rheolube 952 had an order of magnitude higher outgassing rate than the Rheolube 2000 which in turn was an order of magnitude higher than the Braycote 600 (Fig. 7-42). The high initial mass loss of the greases in the first 2 hours of the test is probably due in part to moisture absorbed form the atmosphere. After this initial loss, the outgassing rate decreased linearly for the remaining 46 hours of the test.
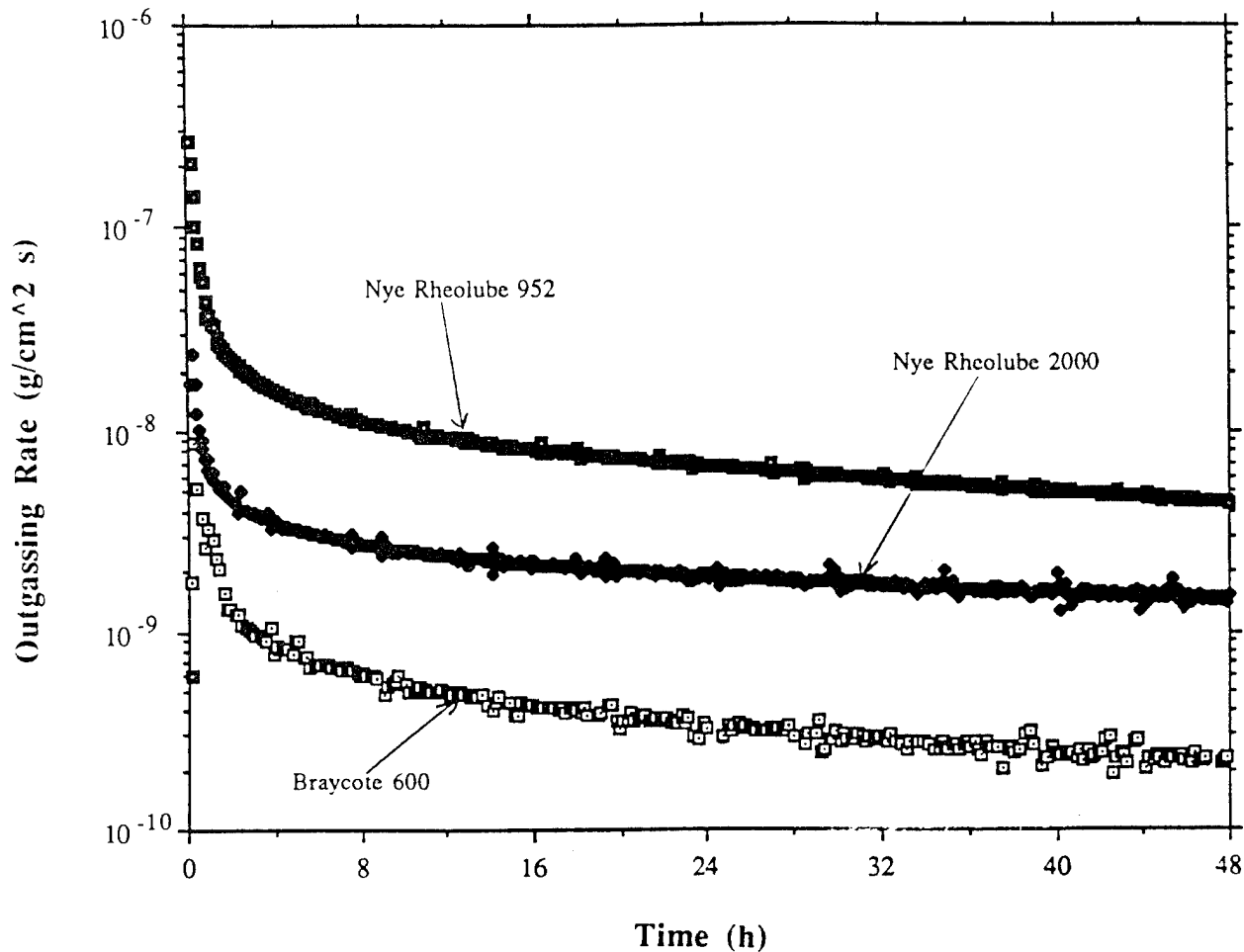


**Fig. 7-42      Outgassing rate of greases at 25°C and 1 x 10$^{-9}$ torr.**

This loss rate can be integrated over the initial 24 hour test time to provide the % TML. The same integration was undertaken with the other three QCM's to provide the % VCM. These results are presented in Table 7-10.

**Table 7-10**

|                  | Rheolube 952 | Rheolube 2000 | Braycote 600 |
|------------------|-------------|---------------|--------------|
| TML (%)          | 0.46        | 0.124         | 0.0123       |
| VCM (%) @ 160°K  | 0.36        | 0.104         | 0.007        |
| VCM (%) @ 220°K  | 0.0015      | 0.044         | 0.0014       |
| VCM (%) @ 298°K  | 0.0003      | 0.0003        | 0.0003       |

These values are relatively low when compared to the ASTM-E595 requirements of TML ≤1.0% and VCM @ 298°K ≤0.1%. However, the ASTM requires the tested material to be held at 125°C for 24 hours. These measurements were obtained at 25°C, which is a more realistic operational temperature for a precision gimbal bearing. The 0.0003 % VCM rate in the 298°K row is the lower limit of detection of the QCM.

Identification of condensed material on the QCM was partially successful for the volatile compounds from the Rheolube 952. However, less information was obtained from the other two greases. This result was mostly due to the greater amount of collected material available for analysis on the Rheolube 952 QCM.

When the 85°K QCM that collected Rheolube 952 volatiles was reheated, butylated hydroxy toluene, dimethyl phenol isomers, and o-cresol were detected. The butylated hydroxy toluene and o-cresol are from the antioxidant (BHT[2]) and antiwear (TCP) additives. The source of the dimethyl phenol isomers is unknown, although it may be a byproduct of grease manufacture.

Reheating the QCM containing the Rheolube 2000 volatiles released a continuum of chemical species which made individual identification of the species difficult. However, aliphatic hydrocarbons and aliphatic amines were detected. Both the aliphatic hydrocarbons and the aliphatic amines are probably contaminants in the grease thickener.

The Braycote 600 QCM released mostly aliphatic hydrocarbon and fluorocarbon when reheated. Again, these species were detected against a background of unidentifiable chemical species. The aliphatic hydrocarbon is an oil contaminant; the fluorocarbon is no doubt a byproduct of the fluorocarbon oil manufacturing process.

## Outgassing Requirements of a Bearing Grease

These outgassing results suggest that the lubricant additives are responsible for the poorer performances of the Rheolube greases in comparison to the Bray 600 lubricant (which contains no additives).

The volatiles of the base oils in these synthetic greases are sufficiently low so that there is little concern that insufficient oil will remain for lubrication for the life of the bearing. However, loss of some additives, such as TCP and BHT[2], may result in the significantly reduced lubrication properties. Loss of the antiwear additive TCP may be especially detrimental in high load, slow speed bearing operation such as a gimbal. Under these bearing conditions, TCP is known to reduce wear.

The loss of the TCP and BHT[2] additives has been observed in other lubricants. For example, when a poly-α-olefin oil containing a few percent of these additives was exposed to a mild vacuum of 10 millitorr at 200 °F for 100 hours, less than 10% of these original additives remained. Clearly, these additives only provide bearing protection under ambient

(nonvacuum) conditions. Much of the testing of the bearing mechanism is done in air so that these additives would provide protection during the early phase of bearing life.

The lead naphthanate antiwear additive in the Rheolube 2000 appears to offer a significant improvement to the TCP due to its low volatility. Note that this additive was not detected in the outgassed products from the Rheolube 2000 grease. Considering vapor pressure is typically a function of molecular weight, the vapor pressure of lead naphthanate is likely to be extremely low due to the presence of the lead in the molecular composition. In any event, addition wear testing is required to determine if the antiwear properties are equal to TCP.

The order of magnitude higher outgassing rate of the Rheolube 2000 in comparison to the Bray 600 appears to be due to the amine antioxidant additive. The phenolic-base antioxidant may also have contributed but was lost in the background spectra. The cyclic synthetic hydrocarbon oil in the Rheolube 2000 (Pennzane SHF 2000) reportedly has a vapor pressure equal to or better than the perfluorinated polyether base oil in the Bray 600. However, no additives were in the tested oil. Higher molecular weight (low vapor pressure) antioxidants are clearly needed to improve the outgassing properties of this synthetic hydrocarbon grease.

The grease manufacturing process can also introduce hydrocarbon contaminates that increase the outgassing rate of these greases. Both the Rheolube 2000 and the Bray 600 had some of these contaminates present. To remove these, some type of vacuum stripping procedure is probably required (similar to this outgassing test) in order to ensure the grease has low volatility.

## Infrared Characterization of Liquid Lubricants

Contamination of optical devices is generally considered one of the more serious drawbacks in the use of liquid lubricated gimbal bearings. In order to determine the extent of this potential contamination, lubricant outgassing rates and infrared absorption spectra were measured on the three lubricants presently being tested in precision bearings. Determining the quantity of volatile contaminants that may deposit on an optical device is only a part of the contamination assessment. In addition, the absorbance of the infared spectral bands (of the optical devices) by this contamination is also required.

The spectral bands (wavelength in micrometers ($\mu$m)) corresponding to infrared detection elements are listed Table 7-11 although the boundaries are more or less established by convention. Generally, a separate detector is required for each spectral region.

**Table 7-11**

| | |
|---|---|
| Short Wave Infrared (SWIR) | 2 - 3 $\mu$m |
| Medium Wave Infrared (MWIR) | 3 - 5 $\mu$m |
| Long Wave Infrared (LWIR) | 5 - 20 $\mu$m |
| Very Long Wave Infared (VLWIR) | > 20 $\mu$m |

## Infared Absorbance

The infrared absorbance of the greases was determined by irradiating a small quantity of the grease on a KBr pellet with infrared light. A Fourier transform of the transmitted light was then plotted in the 2.5 to 15.55 micrometer ($\mu$m) range. Considering only the liquid component of the grease was likely to volatilize and contaminate optics, an attempt was made to separate the oil from the thickener component. Results were only partially successful, although careful interpretation of the spectra shows which bands are associated with the specific component.

1. Nye Rheolube 952 is a neopentylester oil with a lithium stearate thickener. Examination of the IR spectra of the grease, oil and thickener components indicates the oil is likely to absorb mostly in the LWIR, especially sharp at the 5.9 μm band (Fig. 7-43). The oil component also had a number of less intense spectral peaks, from 6.8 to about 10 μm, also in the LWIR region. While some of these other absorption peaks may be a portion of the thickener component not completely removed during centrifuging, most of this absorption is probably associated with the complex (poly)ester structure.

2. Nye Rheolube 2000 is a multiply-alkylated cyclopentane (MAC) oil with a sodium octadecyl terephthalanate thickener. The oil component of this grease had an intense absorption in the 3.4 to 3.5 μm range (Fig. 7-44). This region is sharp and on the edge of the MWIR region. As occurred with the 952 grease, not all of the thickener was separated from the oil component thus probably accounting for most of the peaks in the LWIR region, although these peaks may be part of the oil spectrum.

3. Braycote 600 is a perfluoropolyalkylether (PFPE) oil with a polytetrafluoroethylene (PTFE) thickener. The oil component of this grease was available for testing. (This lubricant is probably the most widely used at LMSC). A rather intense, wide band is evident in the LWIR region (Fig. 7-45).
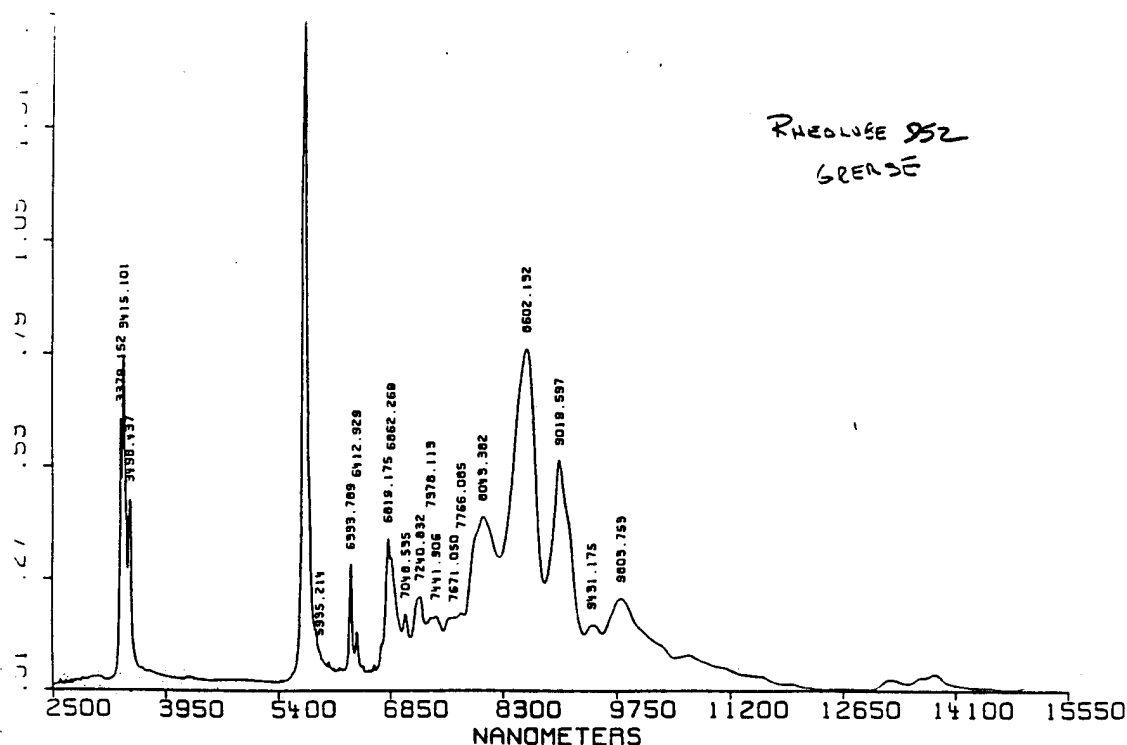


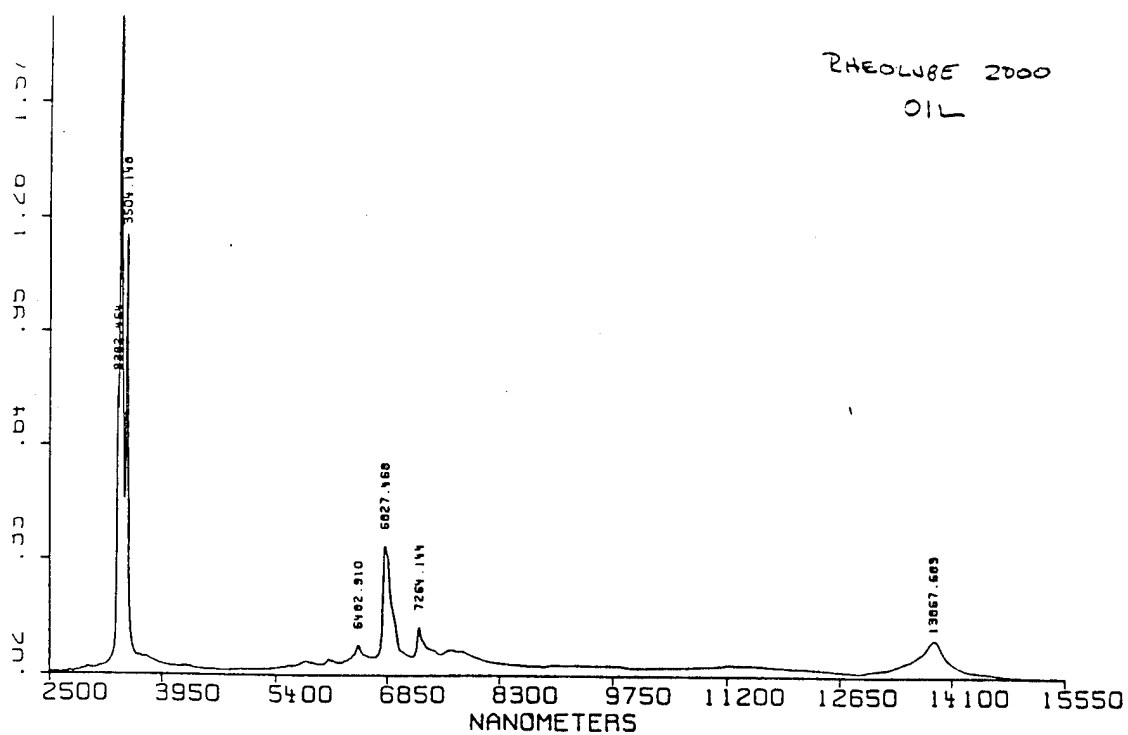Fig. 7-43   Oil component of the Rheolube 952 Grease   (1000 nm = 1 μm)

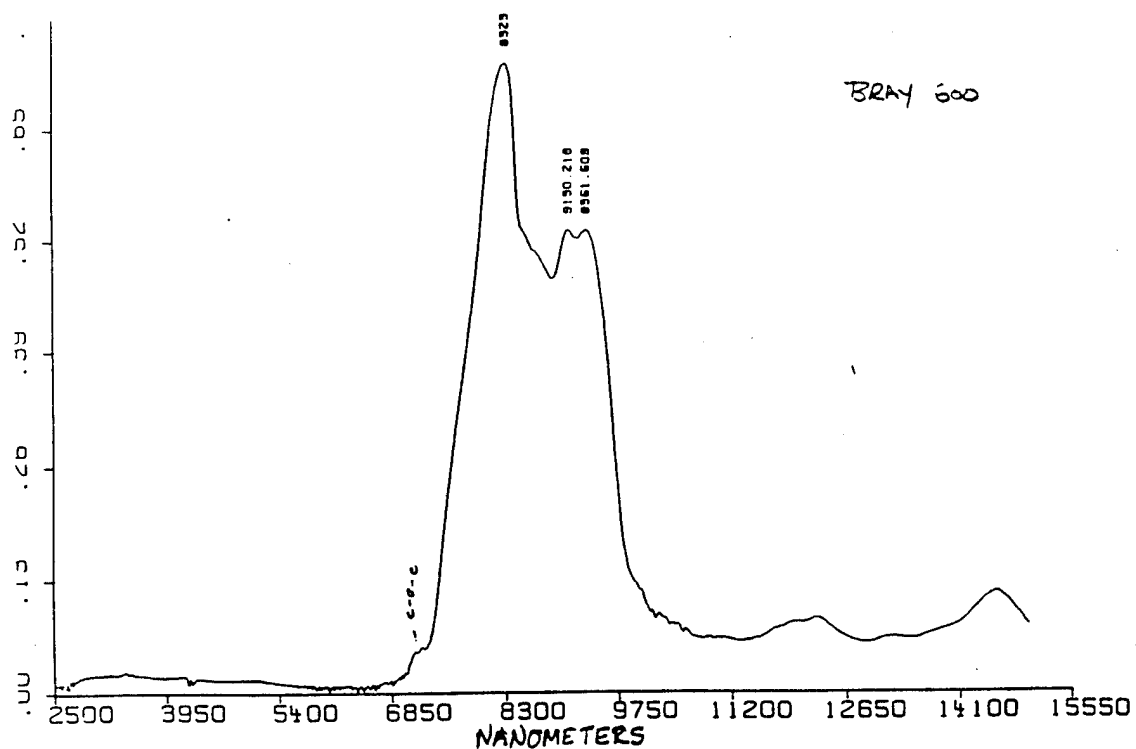**Fig. 7-44  Oil component of the Rheolube 2000 Grease   (1000 nm = 1 μm)**



**Fig. 7-45  Oil component of Braycote Grease, Bray 815Z   (1000 nm = 1 μm).**

Although the IR absorption data generated in this experiment are useful as an initial assessment of the contamination potential of the various greases, more accurate and realistic information could be gained by a more elaborate test. For example, testing just the oil component of the grease may eliminate the thickener interference. However, unreacted thickener components may also be volatile and contaminate optical devices. Perhaps the best method of determining the contaminating potential of the greases would be to collect the volatilized portion of the grease for analysis. This could be done by exposing a witness plate designed specifically for IR analysis (such as a KBr pellet) to the vapor species generated during an outgassing test (such as with the quartz crystal microbalance).

## Contamination Potential

The potential contamination of an optical device by a synthetic grease is probably more a function of bearing location relative to the optical device than the volatility or composition of the grease. Only when the detector is in the direct path of the bearing is significant contamination likely. While this configuration does occur when bearings are used within the optical detection device such as a scanning mirror, precision bearings that gimbal the optics package are obviously on the outside of the package (such as the present application of this program, Brilliant Eyes) present only a small contamination potential. Moreover, bearing cartridges incorporating (labyrinth) seals reduce contamination potential. Typically, volatilized grease components would have to be reflected twice from the space atmosphere to be directed towards the optical device. Some estimates of this reflected material are less than 0.05% of the volatilized component. In any event, to assess the contamination potential, the location of the bearings relative to the detectors has to be determined for the specific application.

Once the geometry is defined, the actual outgassing atom flux and composition from a specific grease can be converted into probable thickness on a detector and IR absorption of that deposit. Both thickness and wavelength absorption affect attenuation of the incident light and, hence, efficiency of the detector. Moreover, the range of radiation that is detected is variable depending on the purpose of the detector. These sort of considerations are best examined by trade-off. For example, when choosing a lubricant for use near a LWIR detector, Rheolube 2000 may be less risk than Braycote 600 even though Braycote 600 has an order of magnitude lower outgassing rate than Rheolube 2000. A small quantity (thickness) of Braycote 600 would attenuate more incident light than a thick coating of the Rheolube 2000 as a result of absorption. On the other hand, Braycote 600 is extremely clean up to $\approx$ 8 $\mu$m, making it quite suitable for SWIR and MWIR sensors.

IR detector ranges also effect the potential of grease volatiles attenuating incident light. Moreover, narrow spectral peaks may be more of an advantage than broad spectral absorption peaks. For example, even though the Rheolube 2000 strongly absorbs IR radiation at 3.4 $\mu$m wavelength (within the MWIR detection range), a specific MWIR detector may only detect radiation in the 4 to 5 $\mu$m range and therefore be unaffected by contamination. This rather intense, narrow absorption of the Rheolube 2000 synthetic hydrocarbon oil is due to the simplicity of the molecular structure; only the hydrocarbon "stretch" is evident. As long as an optical detector is not in this range, this would be an ideal lubricant (from a contamination point-of-view). The broader ranges exhibited by the Braycote 600 and the Rheolube 952 are due to the more complex molecular structure and may be more likely to overlap a detector range.

The volatiles from all three greases absorb radiation at various spectral wavelengths in the Infrared spectrum and optical devices detect in all four of the infared spectral ranges. Once the specific optical detectors are chosen and detection ranges established, contamination potential can be assessed.

## 7.9 EXAMINATION OF ANGULAR CONTACT BEARINGS

The procedures used in the disassembly and analysis of grease lubricated bearings is somewhat different than used for the thin film lubricants. The bearings were visually examined to assess the degree of wetness of the residual lubricant, color, etc. Generally, the blackened grease would accumulate in the retainer ball pockets and along the ball track edges. A sample of the blackened grease was removed from each of the bearings and analyzed by X-ray microanalysis. The balls from the bearings were washed with solvent to remove the grease/debris which was subsequently removed from the solution by filtering through a 0.5 μm silver filter. Both the filtered material and the resulting solution were retained for further analysis if necessary.

The inner races were soaked in solvent for a few minutes for a number of cycles and dried. This procedure was undertaken to remove the oil component of the lubricant with minimal disruption of the deposits that may be adhering to the inner race track. The inner races were then examined in a scanning electron microscope. On both inner races, the ball track was well delineated by grease thickener deposits on either side of the track. These thickener deposits form as the balls roll along the track and thickener is pushed out of the contact zone.

The inner races were then ultrasonically cleaned in solvent and examined a second time in the SEM to assess the degree of wear. The width of the wear track was delineated by location where the grinding or machining scratches ended. These ball track widths for top and bottom bearings are summarized in Table 7-12.

### Table 7-12

| Post | Lubricant | Balls | Cycles (millions) | Lubricant Condition | Ball Track Width (in) |
|------|-----------|-------|-------------------|---------------------|----------------------|
| 4.1a | PFPE | Uncoated | 34 | tar | 0.030 / 0.031 |
| 4.4a | PFPE+AW | Uncoated | 37 | tar | 0.029 / 0.029 |
| 4.2b | PFPE | TiN coated | 18 | tar | 0.029 / 0.033 |
| 1.3 | PFPE | TiN coated | 1* | dry | 0.066 / 0.068 |
| 1.6 | PFPE | Si3N4 | 4* | dry tar | 0.038 / 0.037 |
| 1.12 | Clean+PFPE | Uncoated | 8* | dry tar | 0.039 / 0.040 |
| 4.2a | MAC | Uncoated | 17* | gel | 0.032 / 0.031 |
| 4.5a | MAC | Uncoated | 17* | gel | 0.050 / 0.042 |
| 4.9a | PAO | Uncoated | 40 | gel | 0.029 / 0.028 |
| 4.8a | NPE | Uncoated | 40 | gel | 0.028 / 0.028 |

\* indicates test discontinued due to high torque failure

| |
|---|
| PFPE: perfluoropolyalkylether (Castrol Braycote 600) |
| PFPE+AW: experimental antiwear additive added to perfluoropolyalkylether |
| Clean+PFPE: races extensively cleaned prior to lubrication (see text) |
| MAC: multiply-alkylated cyclopentane (Nye Rheolube 2000) |
| PAO: poly-alpha-olefin (Nye 181B + Cab-o-sil thickener) |
| NPE: neopentyl ester (Nye 952) |

The width of the ball track provides a quantitative assessment of wear, similar to the wear assessment of the thin film bearings described in Section 7.4. Excessive track wear (> 0.31 inch width) was exhibited by PFPE lubricated bearings with Si3N4 balls and one of bearings with TiN-coated balls as well as a PFPE bearing that was extensively cleaned. The lubricant

was dry in these bearings. One of the MAC-lubricated bearings also had significantly wider wear tracks as well. The remaining (nonfailed) bearings had similar, small ball track widths. Preload tolerances and ball width measurement accuracy probably accounts for errors up to $\pm$ 0.002 inches. Even though the lubricant in the nonfailed PFPE lubricated bearings was tar-like, the amount of track wear was not significantly different than the NPE or PAO lubricated bearings. Note that some of the bearings were tested for a low number of cycles but did not fail from high torque. These bearings were not tested as long because only a limited number of test posts were available and higher priority was given to the thin film bearings.

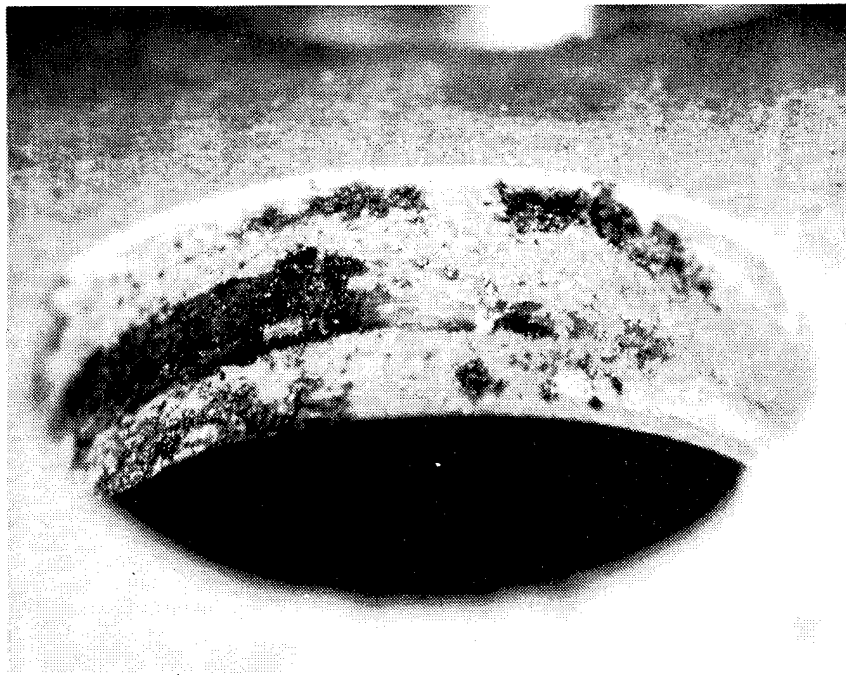## Long lived Braycote 600 Lubricated Bearings

Braycote 600-lubricated bearings with uncoated balls or antiwear (AW) additive in the lubricant had long lives and appeared similar when disassembled. One of the bearings with TiN-coating was also similar in appearance to the bearings with uncoated balls but was not tested as long.

Visual examination of the PFPE-lubricated bearings generally indicated they were only slightly wet with lubricant. The balls were typically gray as opposed to shiny when new. Blackened grease with a tar-like consistency was detected in the retainer ball pockets and along the race ball tracks of both bearings (Fig. 7-46a). The retainer ball pockets did not exhibit appreciable wear. Tar-like grease particles were found on practically all of the bearing inner race (Fig. 7-46b). Elemental analysis of this blackened grease indicated mostly fluorine present with lessor amounts of iron, oxygen, and carbon also found. White, unused grease could be occasionally found in the ball pockets and on the barrel of the inner race. This white grease appeared somewhat dry, perhaps depleted in the oil phase.

After the light rinse with Freon solvent, the inner races frequently had blocky, thin film deposits in the center of the ball track (Fig. 7-47a). When examined at higher magnification, the deposits appeared to be a "broken-up" thin film (Fig. 7-47b). Compositional analysis of the deposits indicated considerable fluorine present, suggesting they were the thickener component of the grease. The film deposits appeared to be less than a micrometer thick when examined at high tilt.

After ultrasonic cleaning in Freon, subsequent SEM examination revealed lightly discolored regions adjacent the ball track (Fig. 7-48a). While grinding scratches are visible through these lightly discolored regions adjacent the ball track, the discolored regions about 0.5 mm beyond the ball track edge concealed scratches. At high tilt, these discolored regions appear to be a well adhered deposit (Fig. 7-48b). Only iron and oxygen were detected in this region. (Note in x-ray microanalysis high levels of iron obscures small of amounts of fluorine that may be present.)

Analysis of the inner races by X-ray Photoelectron Spectroscopy indicated substantial quantities ($\sim$35%) of fluorine present in and adjacent to the wear track. While only about 15% of the fluorine was initially found to be ionically bonded (the remaining proportion of the fluorine was covalently bonded), argon etching to remove residual fluorocarbon lubricant on the surface shifted the ratio of ionic to covalently bonded fluorine from about 1/6 to 5/1. The greatest amount of ionic fluorine was found in the wear track (about 20%). A lessor amount was found adjacent the track (11%), and only a few (3) percent was in the corrosion free regions on the inner race barrel. In addition to the fluorine, carbon, oxygen, iron and chromium were detected all these areas. A high resolution scan of the iron peak indicated iron oxide, hydroxides, and $FeF_2$ may be present, however; no evidence of $FeF_3$ was detected.

(a)            15X
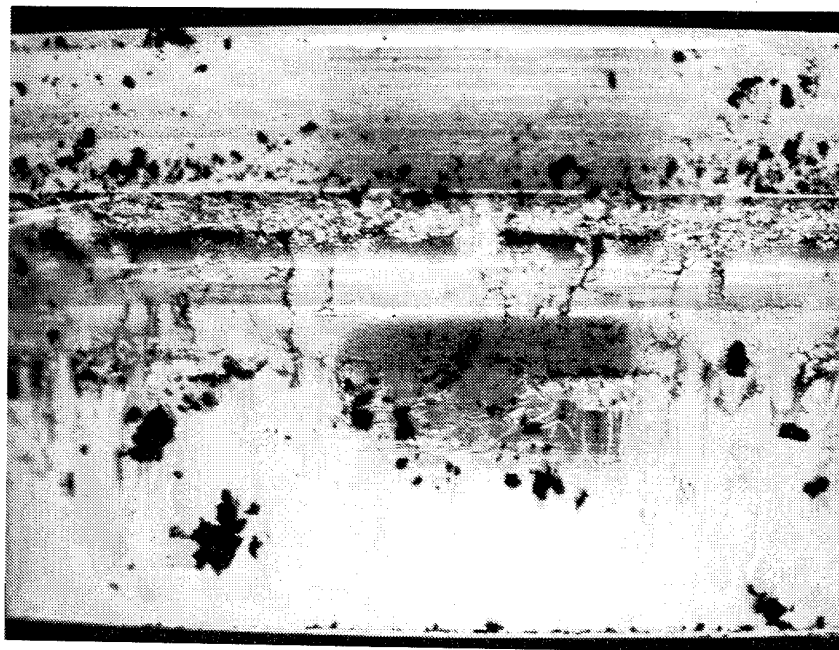


(b)            6X

**Fig. 7-46**     **Blackened, tar-like lubricant deposits were found in the retainer ball pocket (a) and on the inner race barrel of the Braycote 600 lubricated bearings after 34M gimbal cycles.**

Inner Race
Ball Track
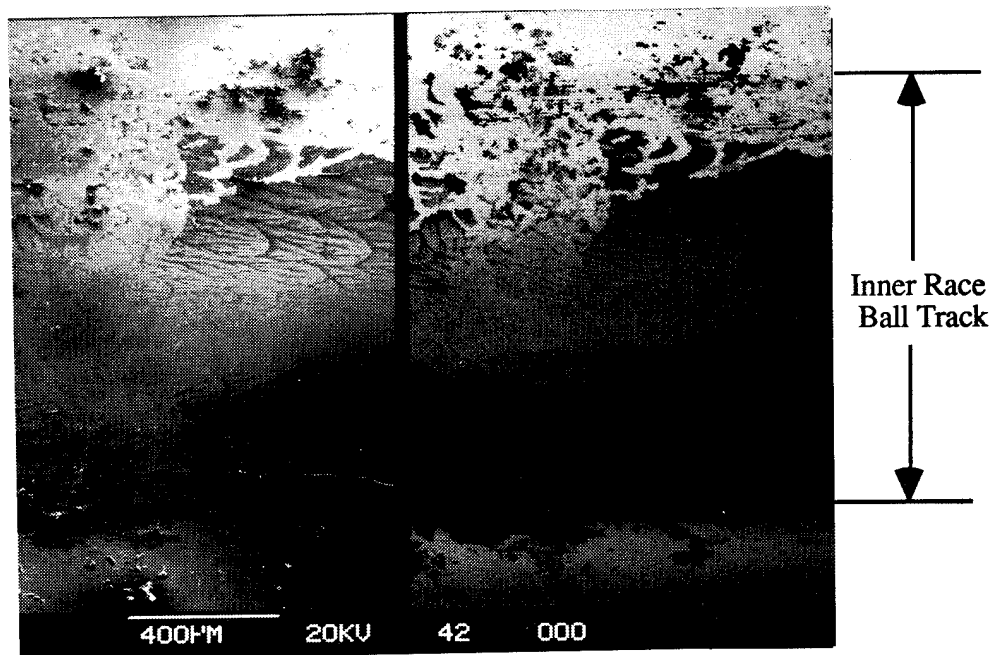
Topography　　(a)　　Composition　　50X
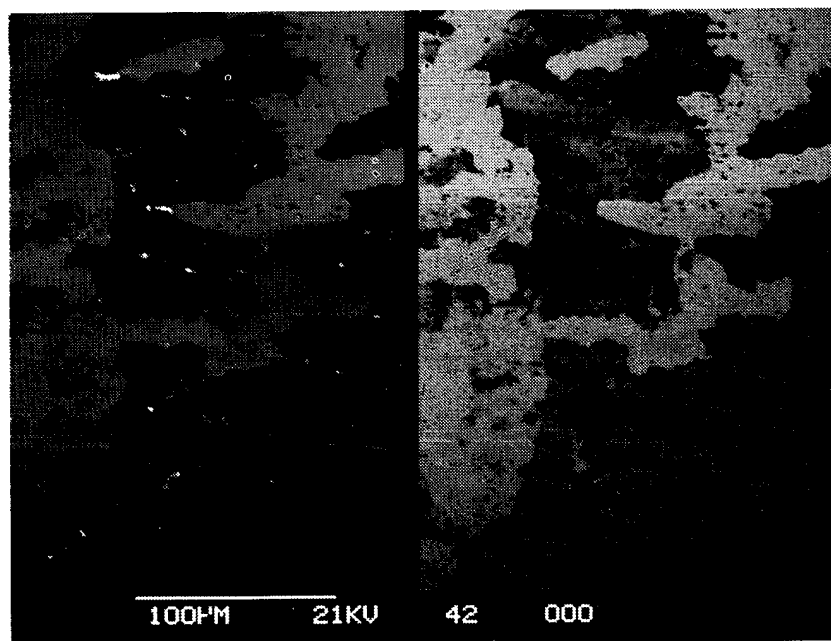


Topography　　(b)　　Composition　　250X

Fig.　7-47　Braycote 600 lubricated bearings had thin films of primarily
Teflon thickener in the ball track (a).　Close-up shows
blocky appearance of the films (b).

Scattered Corrosion Deposits

Heavy Corrosion Deposits

Inner Race Ball Track

1MM    21KV    42    554    S

(a)                          20X



10HM    21KV    42    554    S
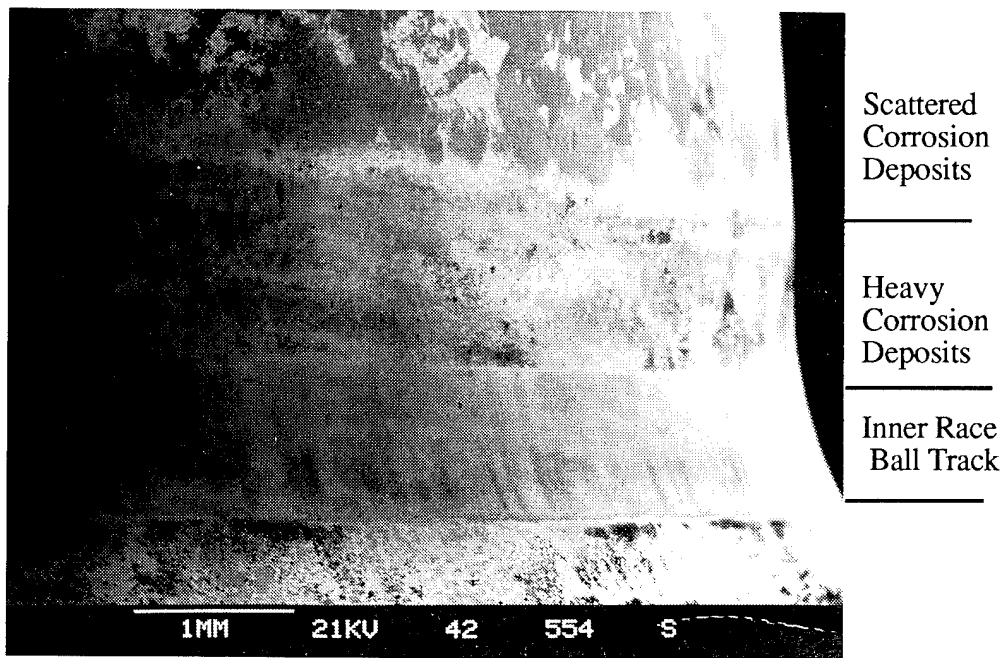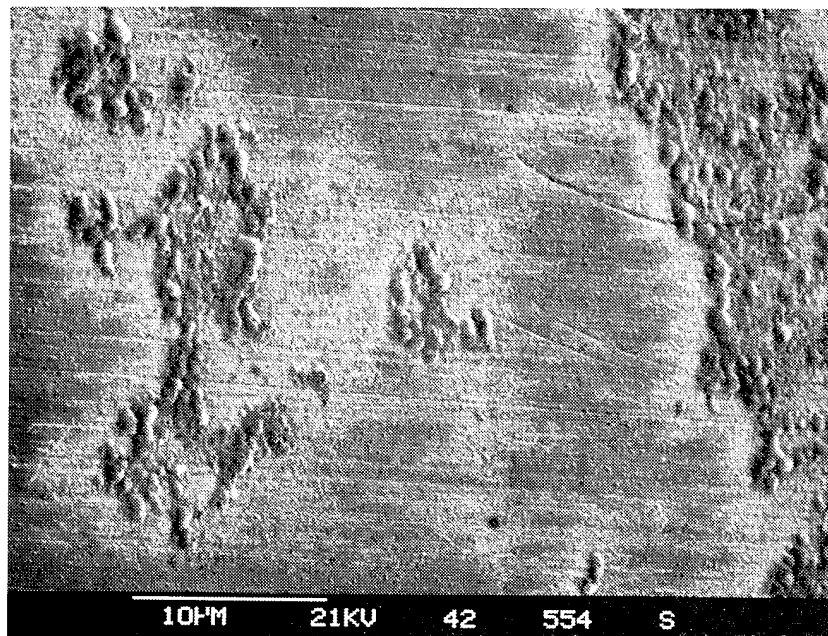
(b)                          2,500X

Fig. 7-48    Corrosion products were located along the edges of the inner
race ball track in Braycote 600 lubricated bearings (a).
Close-up shows corrosion morphology   (b).

## Short Lived Bearings: TiN-coated balls

Two sets of bearings had 0.5 µm TiN sputter-coated balls with Braycote 600 grease. One set failed relatively soon after testing was initiated, the other set performed similar to or better than bearings with Braycote grease and uncoated balls.

The failed bearings were dry. Dry black powder covered the bearing components. The retainer ball pockets were heavily worn (Fig. 7-49). None of the other grease-lubricated bearings exhibited this high level of wear. No white, unused grease was detected. Elemental analysis of the powder revealed mostly iron, carbon, oxygen and small quantities of titanium. Additional x-ray analysis indicated the source of the molybdenum and/or sulfur is the Vespel retainer.

Examination of the balls revealed a rough surface morphology and a mottled compositional image. The light contrasting regions in the compositional image were devoid of titanium which indicates the original 0.5 mm coating "wore off." Intact titanium was detected in the dark contrasting regions. Iron, chromium, and molybdenum/sulfur were also detected in both light and dark contrasting areas. The high chromium content indicated the balls were made from 440C steel.

The loss of the thin film on the balls is associated with the high torque exhibited by the bearings incorporating the TiN coatings. The TiN then functions as a grinding media which ground a wide wear track on the race and heavily abraded the retainer ball pockets. The lubricant became loaded with a large quantity of iron and retainer debris as evidenced by the high iron and organic composition.
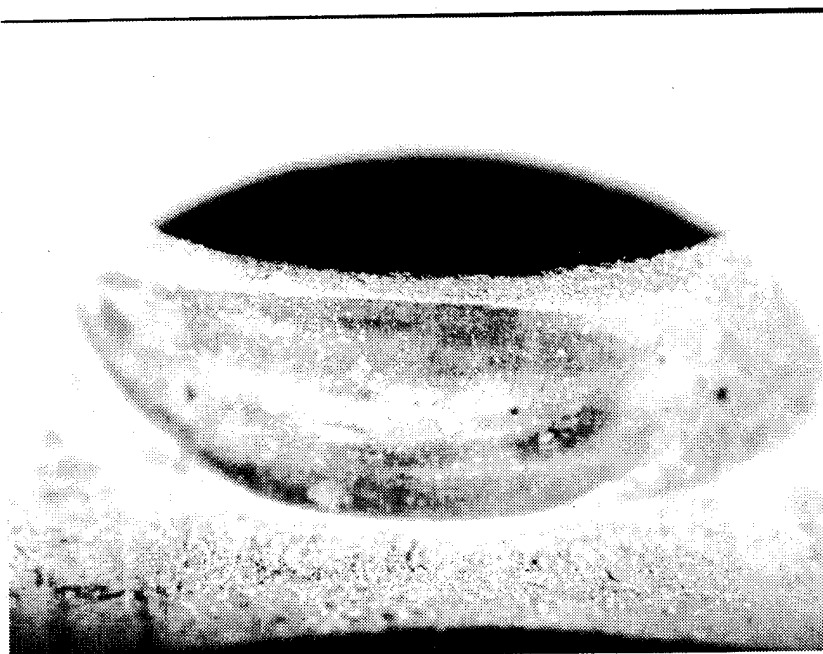


Fig. 7-49 One of the bearings with TiN coated balls and Braycote 600 lubrication exhibited heavy wear of the retainer pocket.

## Short Lived Bearings:  Si3N4 balls

Cause of the high torque in the bearings with the substituted Si3N4 balls is not entirely clear. The blackened grease in the ball pockets of the retainers from bearings with Si3N4 balls was dryer than the long lived bearings with steel balls.  The bearings had evidence of more extensive corrosion along the ball track than was observed on Braycote 600-lubricated bearings with steel balls, but no evidence of "thin film" debris deposits in the ball track as observed in the other Braycote 600 lubricated bearings.  The amount of ionic fluorine present in the ball track was also about the same for the Si3N4 bearings as steel ball bearings.

The high stresses that are generated in bearings with Si3N4 balls (modulus effects) may simply have consumed the oil in the grease a higher rate.  The gradual increase in torque this bearing exhibited over time is consistent with a gradual consumption of lubricant.  Friction (hence, torque) increases may simply be a reflection of the lubricant loss.  Note the amount of wear exhibited by the bearing pair was large considering the ball tracks were initially narrower than steel balls (modulus effect).

## Short lived Bearings:  Extensive Cleaning (TCP)

One bearing set was subject to cleaning and tricresyl phosphate (TCP) treatment using procedures developed by Charles Stark Draper Laboratory (GA-300 and GA-564).  The rather elaborate cleaning procedure involved ultrasonic cleaning the bearing in successive solutions of toluene, trifluorotrichloroethane, methanol and acetone-methanol mixtures with intermediate vacuum drying steps.  The bearings were then soaked in TCP at 225 $^\circ$F for 14 days; however, subsequent analysis of the bearing surfaces (after testing) did not indicate phosphorous present.  A review of the procedure indicates the oven used in the soaking was probably not set at the proper temperature.

The high torque and corrosion exhibited by the bearings examined in this report do not appear to be associated with TCP.  The lack of TCP on even the unworn regions of the inner race clearly indicates the TCP pretreatment of these bearings was unsuccessful.  One of the bearings had rather thick, discontinuous deposits in the ball track combined with detectable wear of the retainer pocket (Fig 7-50).  This suggests the lubricant was consumed at an excessive rate and eventually, the retainer was transferred to the ball track.  Indeed, XPS analysis of the discontinuous track deposits revealed nitrogen from the polyimide retainer material.  As observed in the dry film bearings with polyimide (Vespel) retainers , high torque and track wear were associated with these retainers.

X-ray diffraction indicated FeF3 was present in the tar-like lubricant.  Blackened grease from the retainer pockets was collected and analyzed by X-ray diffraction. Spectra from this bearing grease was compared to new, unused grease. While the diffraction peaks were barely above background, the grease deposit indicated a cubic form of FeF3 was present in some of the bearing greases (Fig. 7-51).

The high torque and corrosion exhibited by the bearing that did not have TCP properly applied is probably due to the extensive cleaning this bearing received.  Ordinarily, bearings to be lubricated with Bray grease are ultrasonically cleaned in Freon TF, then grease-plated with a Freon-Bray mixture and dried.  Perhaps the additional cleaning steps with toluene, methanol, and acetone removed a protective contaminant.  Contamination of PFPE oils with only a few per cent of formulated hydrocarbon lubricant is thought to increase bearing life [7-12].  Generation of the Lewis acid, FeF3, was thought to contribute to the breakdown of the PFPE lubricants: the detection of FeF3 adds credence to this degradation mechanism.
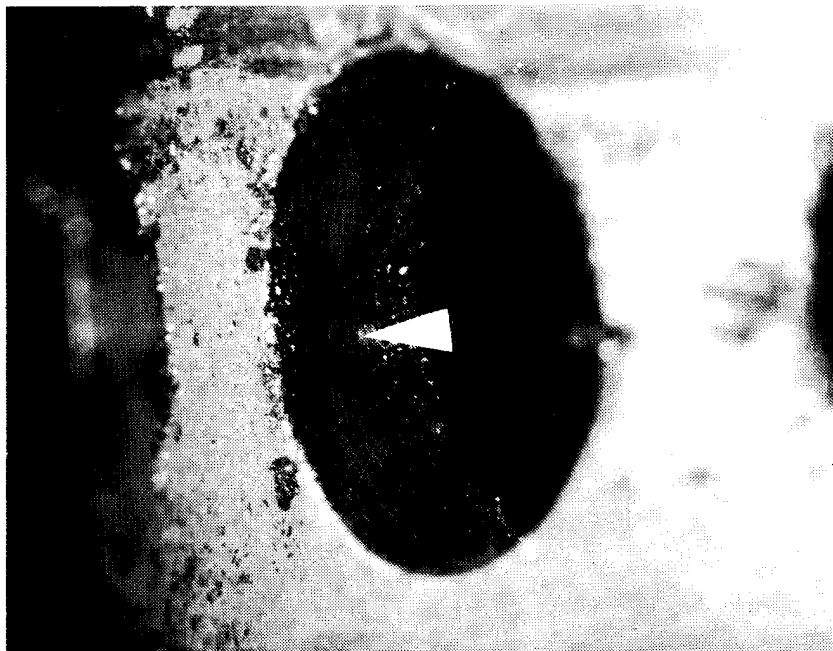
(a)            10X
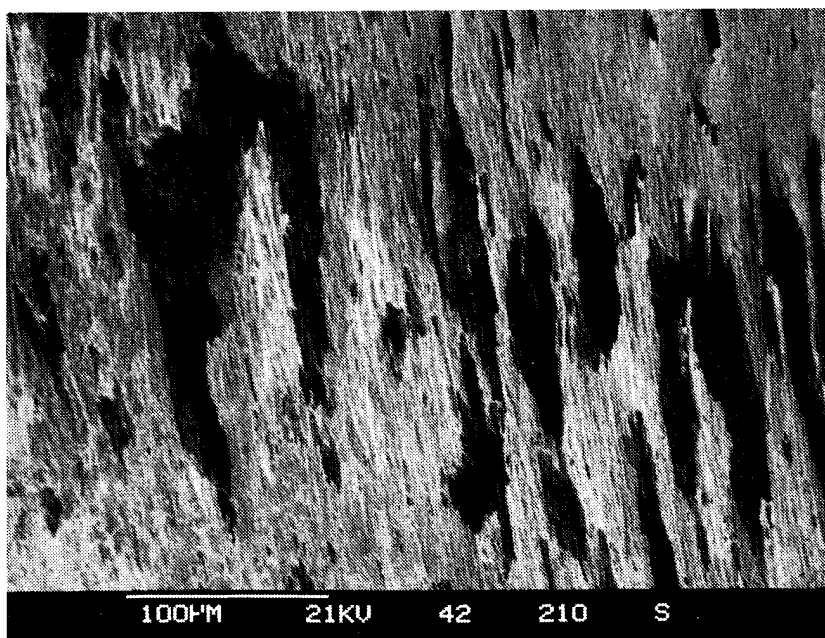


(b)            250X

Fig. 7-50   Wear of the ball pocket (arrow, a) caused high torque in the extensively cleaned, Braycote 600 lubricated bearing by depositing polyimide debris on the inner race ball track (b).

**Fig. 7-51** When compared with unused grease (a) the three additional peaks in the X-ray diffraction spectra of the grease from the Braycote 600 lubricated bearings indicated FeF$_3$ was present.

## Short Lived Rheolube 2000 Lubricated Bearings

Visual examination indicated the bearings were relatively wet with lubricant. Darkened grease of a gelatinous consistency was found in the ball pockets and along the ball track on the inner race (Fig. 7-52). The retainer ball pockets were not worn. White, unused grease was frequently detected on the inner race barrel and 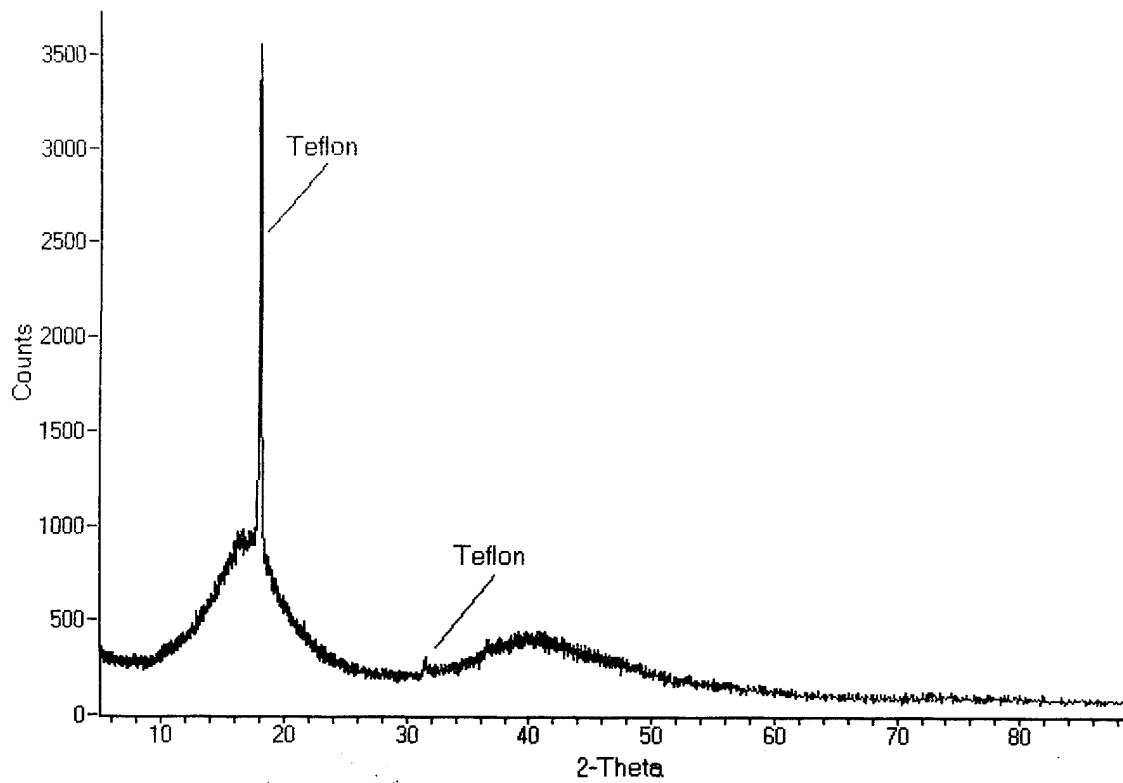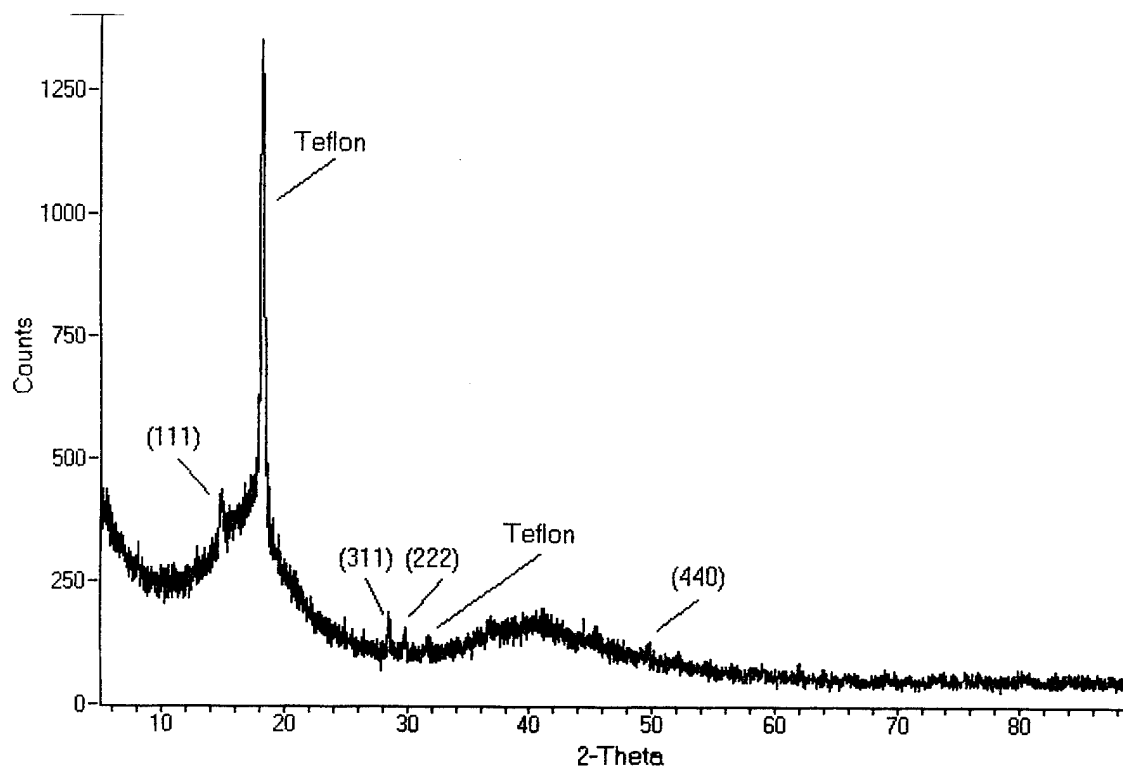in the ball pockets. Elemental analysis of the darkened grease revealed mostly carbon with small quantities of iron, sodium, oxygen and lead. Note sodium and lead are grease constituents, while iron debris is generated as a result of (adhesive) wear.

As with the Braycote-lubricated bearings, the bearings were soaked in hexane to remove the oil component of the lubricant with minimal disruption of the deposits adhering to the inner race track. The inner races were then examined in the SEM. A dark band delineated the ball track on the inner race in the backscattered electron (compositional) image (Fig. 7-53a). While residual grease thickener on the races typically had a thin, web-like appearance which results from a receding solvent meniscus, some blocky thickener particles were also observed on both races. At high tilt, the track deposit appears to be rather thick and somewhat lumpy in texture (Fig. 7-53b).

XPS analysis of the deposit in the track showed a few percent of lead present combined with large amounts of oxygen and iron. High resolution scans of the lead revealed it was in oxide rather than metallic form. An etch profile of the ball track indicates the carbonaceous lead layer is about 5 nm thick. This is in contrast to the SEM images of the deposit which suggests the deposit is over at least 100 nm thick. Perhaps a surface analysis with high spatial resolution, such as Auger electron spectroscopy, would reveal a distribution of the lead in the ball track.

Examination of the 117-sized bearings showed similar results to the smaller 105-sized bearings; lead deposits were located the ball tracks.

## Long-lived Synthetic Lubricants: NPE and PAO

Bearings with NPE and PAO greases were very wet with lubricant and the balls were still shiny as if new. Some blackened, gelatinous lubricant was detected in the ball pockets (Fig. 7-54a). The inner races were covered with white gelatinous grease (Fig. 7-54b). SEM examination of the inner races showed extremely thin surface deposits. As observed in Table 7-12, bearings with these synthetic lubricants had the narrowest ball wear tracks suggesting little wear.
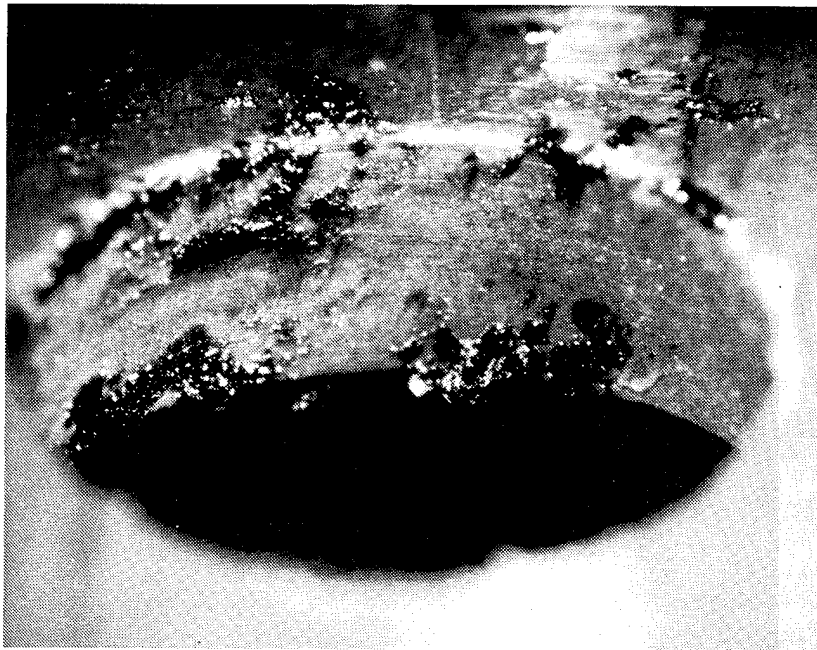
(a)                         15X
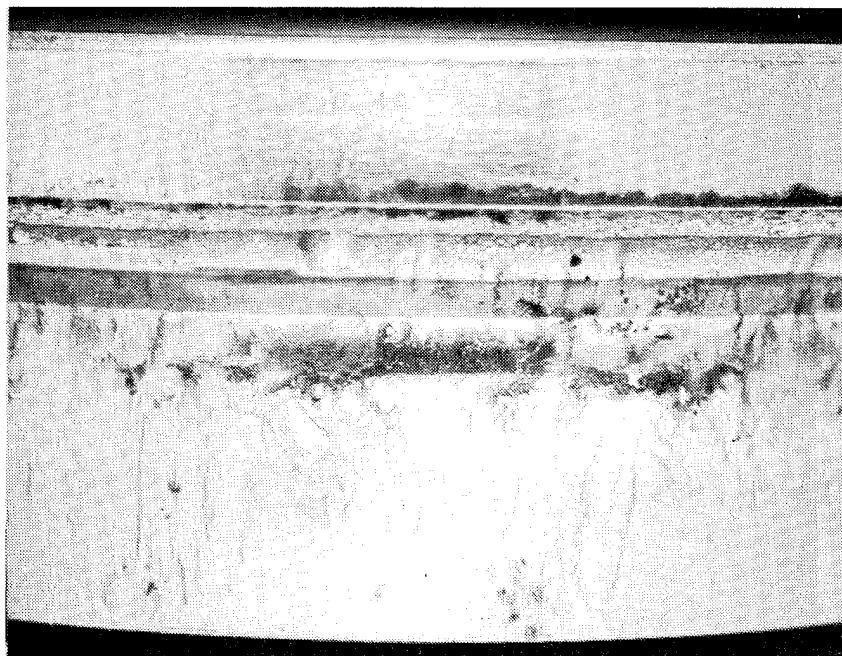


Shoulder

Ball Track

Barrel

(b)                         6X

Fig. 7-52    Blackened, gelatinous lubricant deposits were found in the
retainer ball pocket (a), however, the  inner race barrel of the
Rheolube 2000 lubricated bearings was relatively clean (b).
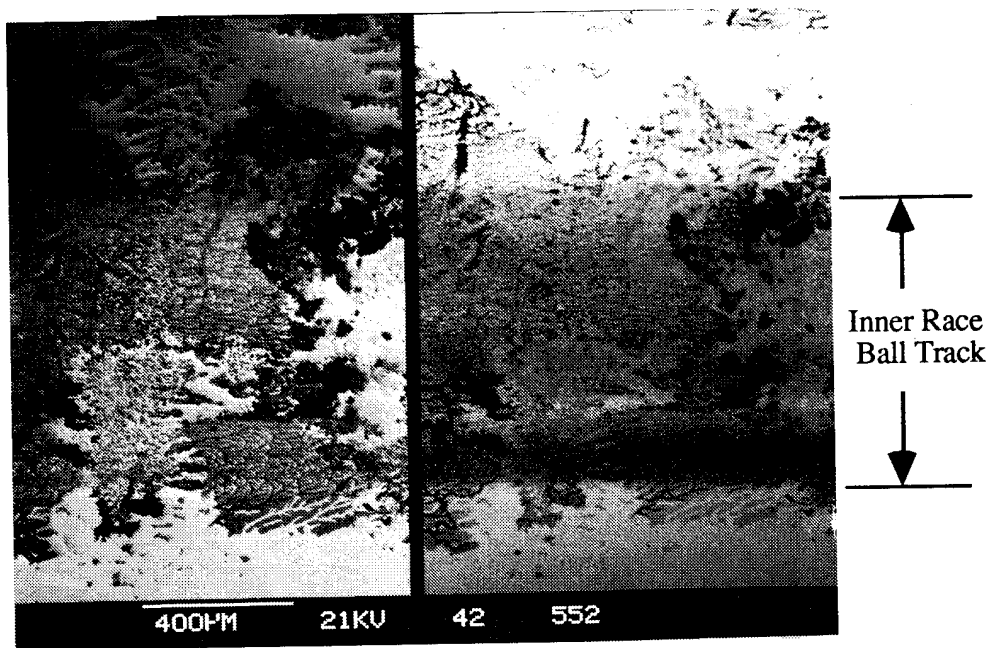
Topography    (a)    Composition    50X
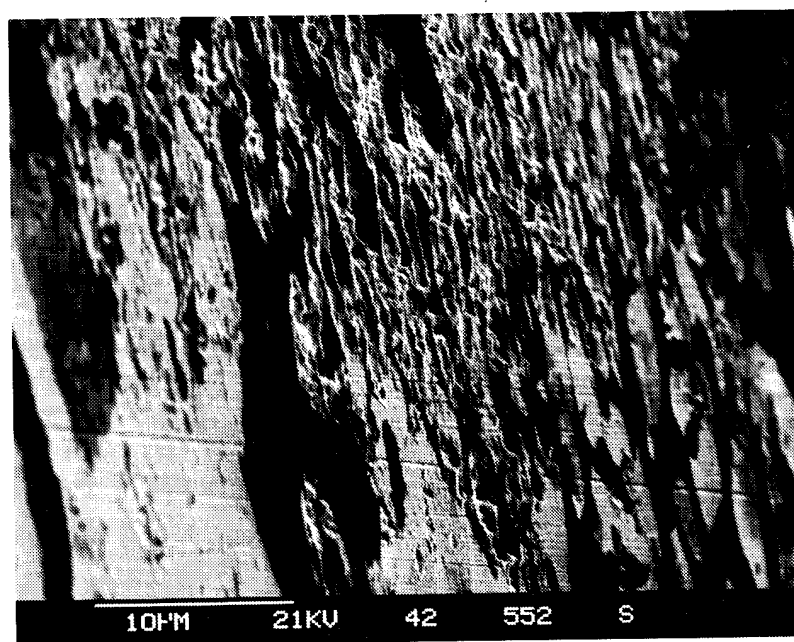


(b)        2,500X

Fig. 7-53 Ball track on the inner race of the Rheolube 2000 lubricated bearing had dark deposit in the compositional image (a). High tilt view shows deposit at the ball track edge (b).
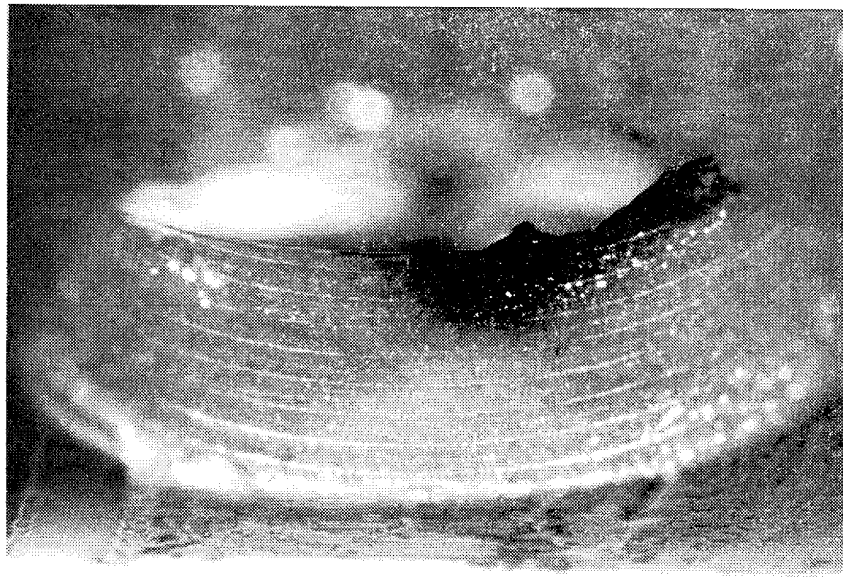
(a)                    10X
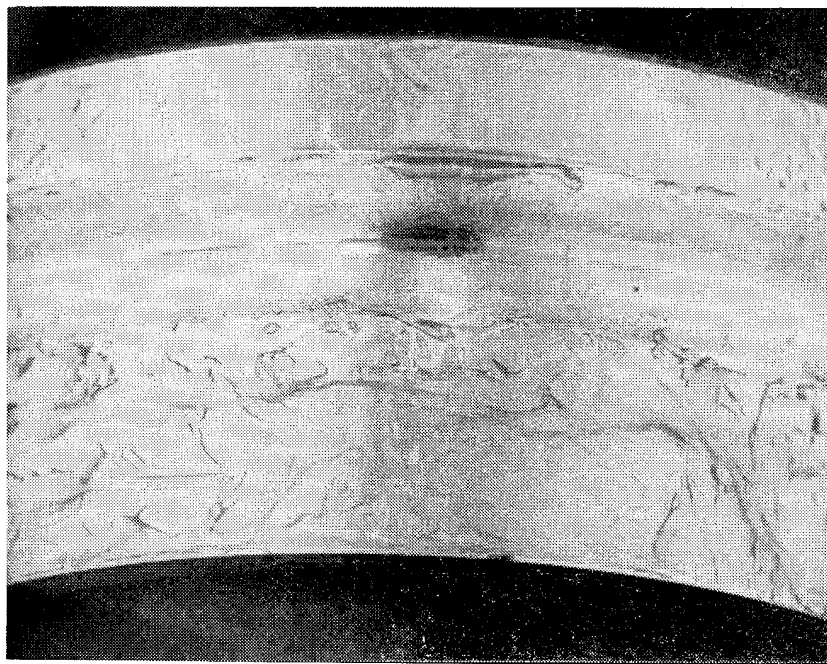


(b)                        6X

**Fig. 7-54** Retainer ball pocket from the neopentyl ester bearing had
only a small amount of blackened, gelatinous lubricant (a).
Inner races were wet with lubricant (b)

## Effects of Ionic Fluorine:  Corrosion

All of the 105-size Braycote 600 lubricated bearings exhibited some corrosion products in and along the ball tracks. The location and composition of the deposits on the inner race ball track, according to ball spacing intervals, suggest it resulted from corrosion that occurred during interuption of testing or after the life testing was completed but before the bearings were examined. Perpendicular "strips" without corrosive deposits were noticed at locations where the balls covered the inner race when the bearing test was stopped. The AISI 52100 steel used in these bearings are notoriously susceptible to corrision. The large amounts of ionic fluorine detected by XPS clearly contributed to this corrosion. However, for this corrosion process to sustain, the presence of moisture is required from laboratory air and thus inhibited by the vacuum provided during the test.

Because of this corrosion, the life of the PFPE bearings (post #4,1a) was adversely affected by a 26 month pause in testing when the bearings were stored due to test rig unavailability. As shown in Fig. 5-49a, the torque of these bearings began to increase immediately after being put back on test at 20 million cycles. Despite being stored with desiccant, corrosion apparently took place causing additional lubricant deterioration. Therefore, caution should be exercised when storing Braycote 600 lubricated flight bearings that have received extensive ground testing in a laboratory environment prior to flight.

## Effects of Ionic Fluorine:  Lubricant Breakdown

Research on performance of PFPE lubricants has shown that the Lewis acid, $FeF_3$, can be generated as a result of tribological breakdown of the lubricant [7-13]. This compound has been identified in the blackened grease of some of the PFPE-lubricated bearings by X-ray diffraction. Ionic fluorine generated by tribological severing of the fluorine atom from PFPE molecule would be expected to combine with the metallic iron generated from wear (in the absence of oxygen or moisture).

However, except for a few instances, the Braycote lubricated bearings generally exhibited long life. Some protection results from the "partial" cleaning of the metal surfaces before lubrication; Freon apparently does not affect surface preservatives such as esters, phosphates, etc. in the oil applied to the bearing for shipping. This hypothesis was indirectly supported by the fact that bearings well cleaned in preparation for TCP application exhibited poor torque performance.

The rates of lubricant degradation and generation of ionic fluorine probably affect bearing life. Recent literature suggests that the reaction rate of $FeF_3$ with the PFPE lubricants may be relatively slow and require a tribocatalytic (rubbing) effect for the reaction to occur at all [7-14]. This result may explain why the higher stresses associated with $Si_3N_4$ bearings may have resulted in a faster lubricant breakdown. Low stresses associated with metal balls may have generated less $FeF_3$ and thus, a very low rate of lubricant degradation. Consequently, the bearings with original metal balls provided low torque for over 35 million cycles.

## Ball Track Deposits:  Mechanism of High, Intermittent  Bearing Torque

The blocky, thin film of grease thickener on the ball tracks of even the long lived Braycote-lubricated bearings may be the source of the torque increase observed in those bearings. Teflon thickener films formed in bearings that were tested at very slow speeds have been shown to increase bearing torque in excess of three times the running torque. The thickener films observed in the 105-sized bearings may be similarly responsible for the intermittent torque increases even at relatively high bearing speeds. Loss and consumption of the oil in the grease will decrease the oil to thickener ratio and may make the grease more susceptible to film formation. Bearings with the thin films were observed to be only slightly wet with oil.

- 223 -

Moreover, incorporation of iron wear products in the grease will also cause thickening to an even greater extent. This thickening, in turn, is likely to increase the film formation susceptibility.

Deposits in the ball track are also the likely reason for the high running torque of the MAC-lubricated bearings. The carbonaceous lead deposits in the inner race ball tracks appear to be sufficiently thick (at least a micrometer) to increase bearing torque. Other investigators [7-15] have reported that the lead naphthanate antiwear additive will form thick deposits in the ball wear track under high stress and elevated temperature conditions. The deposit no doubt forms from the reduction/decomposition of the lead naphthanate antiwear additive. Although this reduction/ decomposition of the lead naphthanate is the reason for its addition (which minimizes bearing wear), a high rate of reduction/decomposition will cause deposit build-up and increase bearing torque. Deposits in the ball track will increase the bearing torque by effectively increasing bearing preloads. Loss, consumption and thickening of the grease may also contribute to the thickness of the deposit in the ball track.

Another source of intermittent high torque in MAC lubricated bearings may be due to an agglomeration of the grease thickener. Blocky structures observed on inner race ball tracks may be agglomerated thickener. These structures could in turn become caught in the ball track and increase bearing torque. It is not clear how the blocky structures would form although the excess aliphatic amine (dimethyl phthalamate) in the grease (detected during outgassing tests) may play a catalytic role. Note that the sodium octadecylterephthalanate is a rather uncommon grease thickener in the aerospace industry and there is little experience with failure mechanisms involving this grease thickener.

## Bearing Torque

Increases in torque during the life of a grease lubricated bearing appears to have two primary causes: 1) material debris in the ball/track interface and 2) friction at the ball /retainer and ball/race interface(s). The material debris is generally an agglomerated mixture of wear products from the races, balls and retainer, and lubricant sources such as thickeners, additives, and deteriorated lubricant. Corrosion products can also contribute. This material debris physically increases the distance between ball and race, and perhaps increases rolling resistance as well, both of which in turn increases the preload and concomitant torque. The torque effects of this debris would also account for the spikes in torque sometimes observed in the bearings during cycling.

Friction in the sliding regions in the ball/race contact zone and between the retainer and balls also contributes to the torque. The torque from this "sliding" friction can not be entirely separated from the material debris, although it probably can be estimated on a completely dry bearing. High torque in the bearing with $Si_3N_4$ balls seems to have been the result of this sliding friction because it appeared dry.

## 7.10 KEY FINDINGS:

**Thrust Bearings (7.1)** The ball wear tracks on all bearing races exhibited similar wear patterns with the greatest wear in the track center. Salox™ retainer wear was much less than Vespel™ wear. Deposited film thicknesses on the races varied between 60 to 200 % of requested. Wear patterns and ball movement indicate misalignment of the bearings can occur. Poor surface finish and bearing geometry resulted in short lives of the thrust bearing thin films.

**Hohman Deposition Process Support (7.2)** Varying the deposition current changed the density, texture, morphology and composition of the thin film. Alternating current was identified as providing optimal films. Correlation between part composition, configuration and location in the deposition chamber and resulting film thickness were demonstrated.

**Thin Film Characterization (7.3)** Witness plates that accompanied the small angular contact bearings were characterized by X-ray diffraction, X-ray photoelectron spectroscopy, and morphology. The thickness and fracture toughness of the thin film was evaluated on the bearing race shoulders.

**Examination of the Screening Angular Contact Bearings (7.4)** Reasons why bearings exhibited short life with $MoS_2$-coated or $Si_3N_4$ balls, or polyimide (Vespel™) retainers were identified. The poor quality of thin films deposited on balls caused excessive debris and increased bearing preload. Inadequate transfer of retainer film to $Si_3N_4$ balls combined with high hardness and stress resulted in high race wear. Bearings with polyimide retainers generated excessive debris which caused high wear.

All bearings with polytetrafluoroethylene-based (Salox and Duroid) retainers had long lives irrespective of type of thin films. Approximately 1.0 micrometer thick, discontinuous retainer transfer films found in the ball tracks appeared to be the primary bearing lubrication. Although residual $MoS_2$ was found in the ball track center, virtually no film was found at the ball track edges.

**Ovonics Process Support: Fracture Resistant Film Development (7.5)**
The recognition of the film fracture and conversion to a burnished film early in the bearing life initiated development of a more fracture resistant film. Increasing the gold interlayer thickness in the multilayer film was shown to decrease the hardness and increase the toughness as measured by indentation testing and also by a unique rolling contact tester.

**Deposition and Testing of the Fracture Resistant Film (7.6)** Depositing the fracture resistant, multilayer film on large bearings required different fixturing than was used for the small bearings. The effect of the fixturing and deposition targets may result in different film properties. Lack of witness plate capability is also a concern.

Large diameter bearings with the fracture resistant film show similar wear morphology to the small angular contact bearings used in the screening tests. Film loss at the ball track edges was consistently observed. Toward the end of bearing life, retainer transfer films appear to be the primary lubricant.

**Process Requirements for Thin Film Bearings (7.7)**
Because the potential loss of the film and resulting stiffness loss, thin films less than 0.5 μm thick are preferred. While the multilayer films developed by Ovonics have accurate thicknesses, more detailed characterization of other film deposition systems would have to be established for film thickness control.

Considering that film fracture is the primary bearing failure mechanism, tests that measure mechanical properties such as fracture toughness, hardness, and rolling contact resistance appear to be more important in process control than chemistry, texture or morphology.

## Characterization of Liquid Lubricants (7.8)
The outgasing rates and infrared signatures of perfluoropolyalkylether (PFPE), multiply-alkylated cyclopentane (MAC) and neopentyl ester (NPE) lubricants were determined.

## Examination of Liquid Lubricated Bearings (7.9)
The PFPE grease lubricated bearings exhibited long life but had blackened tar-like lubricant in the ball pockets and corrosion of bearing steel from ionic fluorine. The corrosion probably occurred after the bearing test when moisture was absorbed from the ambient air. Despite the darkening and thickening of the grease, the wear track width and torque performance of the PFPE-lubricated bearings was comparable to the long-lived, neopentylester (NPE) and polyalphaolefin (PAO) lubricated bearings. PFPE lubricated TiN-coated balls had short lives when the coating failed. PFPE lubricated bearings with $Si_3N_4$ balls generally performed poorly from excessive lubricant degradation. Extensive cleaning of the bearings prior to application of the lubricant is suspected to increase lubricant degradation rate.

High, intermittent bearing torque in MAC lubricated bearings appeared to be associated with deposits of wear products, degraded lubricant, lubricant thickener and/or antiwear additive in the ball track. Darkened grease of a gelatinous consistency was found in the ball pockets and along the ball track.

Bearings with NPE and PAO greases were very wet with lubricant and the balls were still shiny as if new. The lubricant was gelatinous in appearance and the metal parts exhibited little evidence of wear.

# References

[7-1]   T. Spalvins, "Structure of Sputtered Molybdenum Disulfide Films at Various Substrate Temperatures," ASLE Trans., 17,1 (1973).

[7-2]   P. D. Fleischauer, "Effect of Crystallite Orientation on the Environmental Stability and Lubrication Properties of Sputtered $MoS_2$ Films," ASLE Trans., 27, 1, 82 (1983)

[7-3]   Bolster, R. N., Singer, I. L., Wegand, J. C., Fayeulle, S., and Gossett, C.R., "Preparation by Ion-Beam-Assisted Deposition, Analysis, and Tribological Behavior of $MoS_2$ Films," Surf. and Coat. Technol., 46 (1991) 207-216.

[7-4]   Bangert, H., Cai, X., Wagendristel, A., and Kaminitachek, A., "Low Load Vickers Hardness Measurements of Nonconducting Materials in a Scanning Electron Microscope," Scanning Electron Microscopy, 1,1 (1987).

[7-5]   Hilton, M. R., and Fleischauer, P. D., "On The Use Of A Brale Indenter To Evaluate The Cross-Sectional Morphology Of Sputter-Deposited $MoS_2$ Solid Lubricant Films," Thin Solid Films, 172, (1989), L81.

[7-6]   Hilton, M. R., Bauer, R., Didziulis, S. V., "Deformation and Wear of Sputtered $MoS_2$ on Curved Surfaces", presented at the International Conference on Metallurgical Thin Films ICMCTF-92, April 7-10, 1992, San Diego, CA.

[7-7]   Hilton, M. R., Bauer, R., Didziulis, S. V., Dugger, M. T., Keem, J. M. and Scholhamer, J., "Structural and Tribological Studies of $MoS_2$ Solid Lubricant Films having Tailored Metal-Multilayer Nanostructure," Surface and Coatings Technology, 53, (1992) 13-23.

[7-8]   Henke, B. L., et. al., Atomic Data and Nuclear Data Tables, 27, 10, (1982).

[7-9]   Hilton, M. R., Bauer, R., and Fleischauer, P.D. "Tribological Performance of Sputter-Deposited $MoS_2$ Solid Lubricant Films During Sliding Wear and Indentation Contact ," Thin Solid Films, 188, (1990)

[7-10]  Mai, Y.W., and Castino, F., Materials Sci. 12, (1977), 43.

[7-11]  Hill, R., *The Mathematical Theory of Plasticity*, Clarendon, London, 1950.

[7-12]  Stevens, K.T. "Some Observations on the Performance of Fomblin Z25 Oil and Braycote 3L-38RP Grease in Ball Bearings and Gear Boxes," Proceedings of the 1st European Symposium on Space Mechanisms and Tribology, ESA SP-196, (1983)

[7-13]  Carre, D. J., "The Performance of Perfluoropolyalkylether Oils under Boundary Lubrication Conditions," Tribology Transactions, vol. 31, 4, (1987) 437-441.

[7-14]  Herrera-Fierro, P. C., Jones, W. R., and Pepper, S. V., "Interfacial Chemistry of a Perfluoropolyether Lubricant Studied by XPS and TDS," NASA Technical Memorandum 105840 (1992).

[7-15]  Hilton, M.R., Kalogeras, C.G., and Didziulis, S. V., "Investigation of Multiply Alkylated Cylopentane Synthetic Oil and Lead Naphthenate Additive Under Boundary Contact Interactions," Aerospace Report No. ATR-93(8361)-1, (1993).

# GIMBAL/BEARING SIMULATION STUDY

Advanced bearing tribomaterials may improve bearing life and/or decrease bearing torque but if they don't also improve gimbal pointing performance their implementation in precision spacecraft gimbal systems may not be worthwhile. At the beginning of the T/PGD program, the only way to evaluate the benefit of improved tribomaterials for gimbal performance was through expensive system level tests. The bearing test data generated during this investigation when coupled to LMSC in-house gimbal simulation provides a method of quantifying the benefits of improved bearing tribomaterials.

The LMSC gimbal simulation can model unrestricted large gimbal motions that occur during gimbal slew maneuvers, as well as very small micro-positioning gimbal motions that occur during gimbal inertial pointing. It includes the coupled two axis gimbal dynamics, sensor payload and actuator models, and spacecraft disturbance sources that occur in both the small and large angle regions. The detailed bearing sub-model includes large angle effects such as torque ripple and runout as well as small angle effects such as the Dahl friction slope. As a result, the gimbal/bearing simulation can be used to investigate the effects of improved bearing tribomaterials over the entire spectrum of gimbal operating conditions.

The following sections detail the T/PGD simulation work, including the development of the bearing disturbance model, the development of the gimbal system simulation, the investigation of the effects of bearing torque on gimbal performance, and a discussion of LMSC Hybrid Flexure Bearing. In addition, the validation of the gimbal/bearing simulation through the incorporation of bearing and gimbal test data is discussed.

<u>Overview</u> Figure 8-1 presents an overview of the LMSC gimbal simulation and its key elements and products. These key elements consist of: 1) gimbal design, specifically the dimensions, mass properties; 2) control system block diagram showing position command generator; 3) motor and payload dynamics; 4) the gimbal flexible body modes; 5) the bearing disturbance model; and 6) the spacecraft disturbance torques (not shown in diagram). Also shown in Fig. 8-1 are typical gimbal torque and jitter predictions.

Early in design, reasonable jitter predictions are possible with rigid body modes utilizing the bearing disturbance torque model. This assumes that the flexible body structural modes are well separated from the control system bandwidth. However, introducing the gimbal flexible modes are important since they can be excited by the bearing disturbance torque. Ordinarily, gimbal pointing performance is simulated with beginning-of-life bearing data since end-of-life data is unavailable. The characterization of bearing torque performance as various points through life, as obtained in this investigation, affords a special opportunity to illustrate how the sensor performance is linked to bearing life.
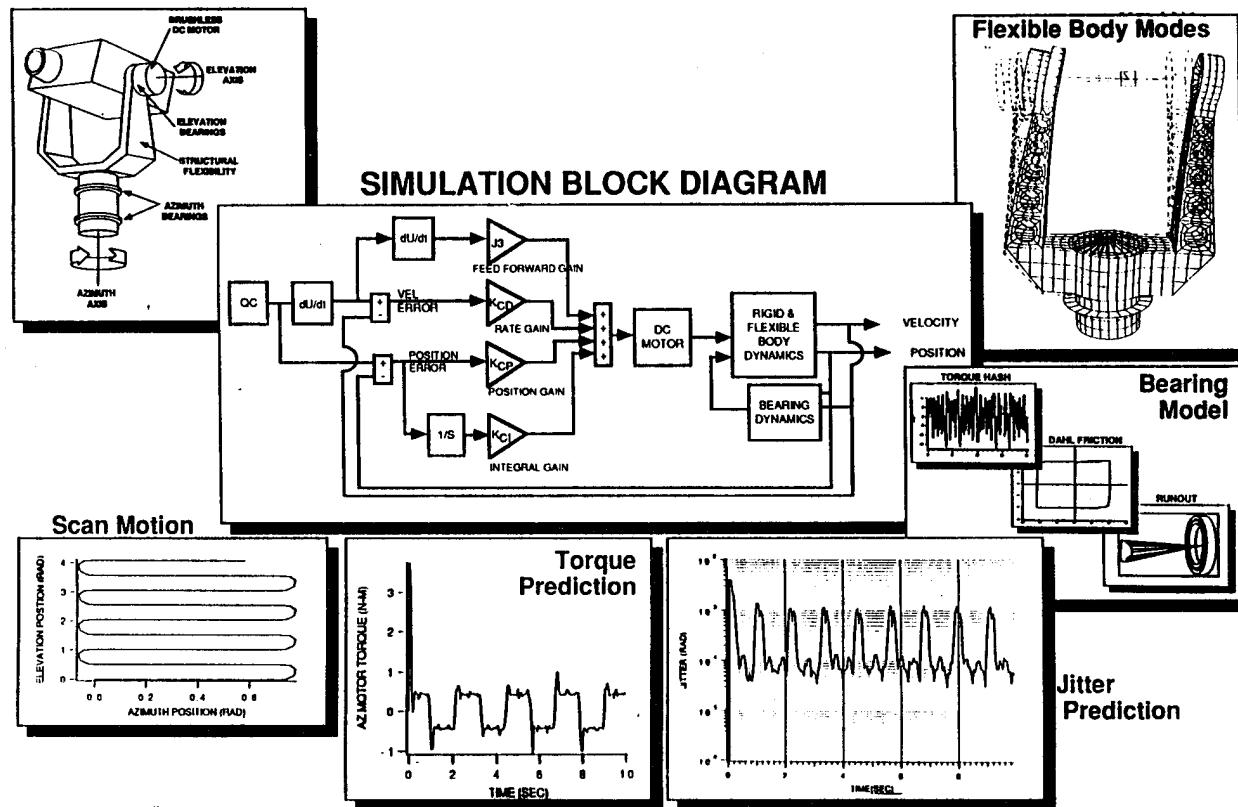
**SIMULATION BLOCK DIAGRAM**

**Flexible Body Modes**

**Scan Motion**

**Torque Prediction**

**Bearing Model**

**Jitter Prediction**

**Fig. 8-1   Gimbal Simulation Components and Products**

Products of the simulation consist of: 1) Optical jitter; 2) actuator torque levels; 3) actuator power levels (not show in the diagram).   While we tend to focus a lot of our attention on the optical jitter prediction, other useful information is available through the simulation.  The torque, power, and velocity predictions are used to select or verify the selection of the actuators and sensors.

## 8.1 BEARING DISTURBANCE MODELING

The bearing disturbance model is made up of a number of sub-models which simulate specific bearing torque disturbance phenomena.  These sub-models have been grouped into three categories: the primary bearing model, the secondary bearing model, and the end-of-life bearing model (see Fig. 8-2).  The primary bearing model contains the sub-models for Dahl friction, torque hash or ripple, bearing runout, and viscous friction.  The secondary bearing model contains the sub-models for the bearing structural stiffness and damping and the cable wrap wind-up torque.  The primary and secondary bearing models represent the core elements of the bearing model and are used to model the behavior of flight quality bearings. The end-of-life bearing model contains the sub-models for torque blocking, torque bump, and reversal torque phenomenon.  The end-of-life model represents the additional torque anomalies that may occur as a bearing approaches end-of-life conditions.

### 8.1.1 Primary Bearing Model
**Dahl Friction**  The torque profile of a bearing rotating at a constant velocity can be described by the sum of a DC torque that opposes the bearing rotation and torque hash that models the variations in torque as the bearing rotates.  However, the torque slope for a

bearing starting from rest in a step-stare gimbal or during a velocity reversal for a scanning gimbal is very large. These large torque slopes have a significant impact on the ability of the control system to accurately point and move the gimbal. Adequately modeling the transition in bearing torque that takes place during bearing "wind-up" or during a velocity reversal is crucial in assessing the impact of bearing performance on gimbal performance.
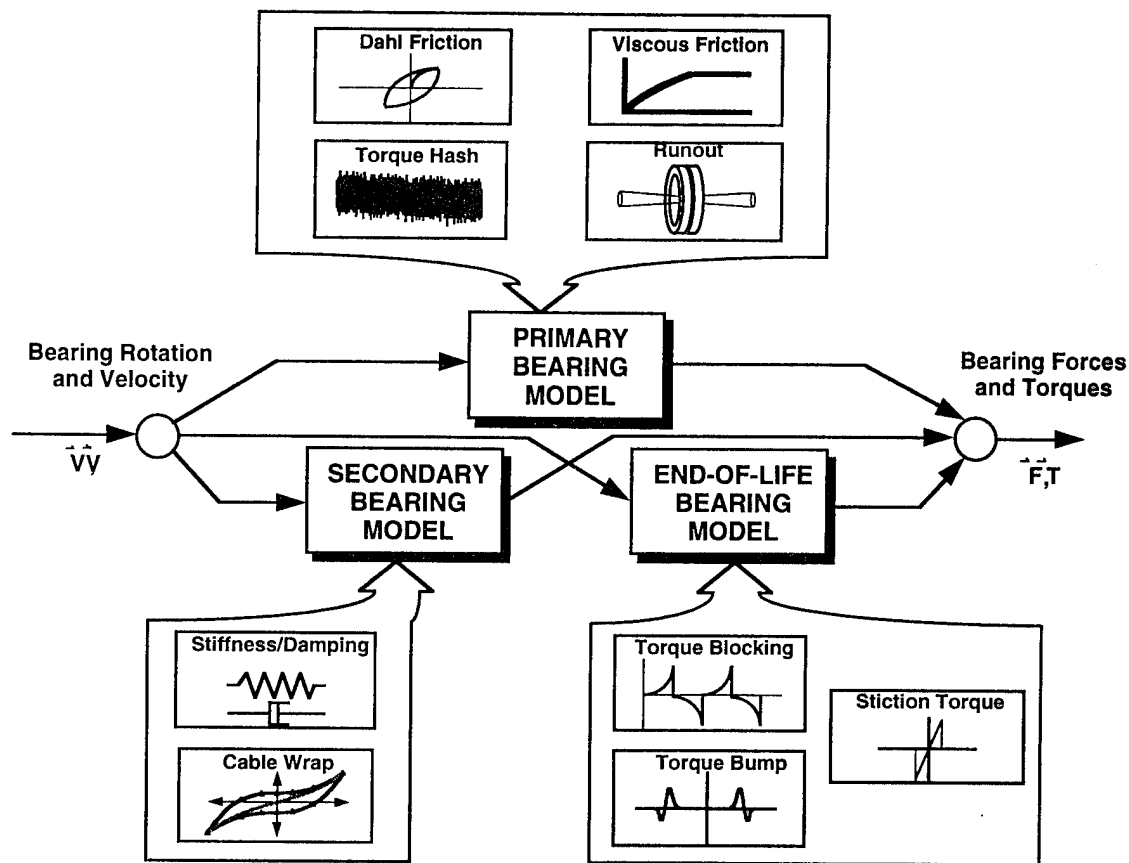


**Fig. 8-2    Bearing Disturbance Simulation**

As a bearing begins to rotate, the frictional torque grows from zero to some steady state value within a small but finite rotation. Upon reversal of rotation, a similar transient behavior is observed. If the bearing undergoes oscillatory motion, the torque-rotation relation displays hysteretic looping where the area between loading and unloading curves is equal to the energy lost in one cycle. Through experimental evidence, Dahl [8-1] proposed a mathematical expression to describe the torque change during a velocity reversal. Further experimental and theoretical work has led to the idea that the frictional torque-rotation relation can be defined with two parameters: the slope or gradient of the torque-rotation curve when the direction of rotation is reversed and the steady-state torque value that is asymptotically approached as the bearing rotation becomes large [8-2]. From experimental data it has been shown that the initial and reversal torque gradients are constant and are determined, for the most part, by the torsional elasticity of the bearing materials [8-2, 8-3]. The steady-state torque value is determined from the frictional conditions at the contact interface. Predicted Dahl torque loops obeying these observations show reasonable correlation with experimental traces (see Fig 8-3 and 8-4).

**Model Equations**

$$\frac{dT}{d\theta} = \gamma \left( T_s - T \operatorname{sgn}(\dot{\theta}) \right)^\beta \quad ; \quad \gamma = \frac{s}{T_s + |T_p|}$$

where:

s = slope at reversal

$T_s$ = maximum dahl friction torque

$T_p$ = value of torque at turnaround

**Energy Loss**
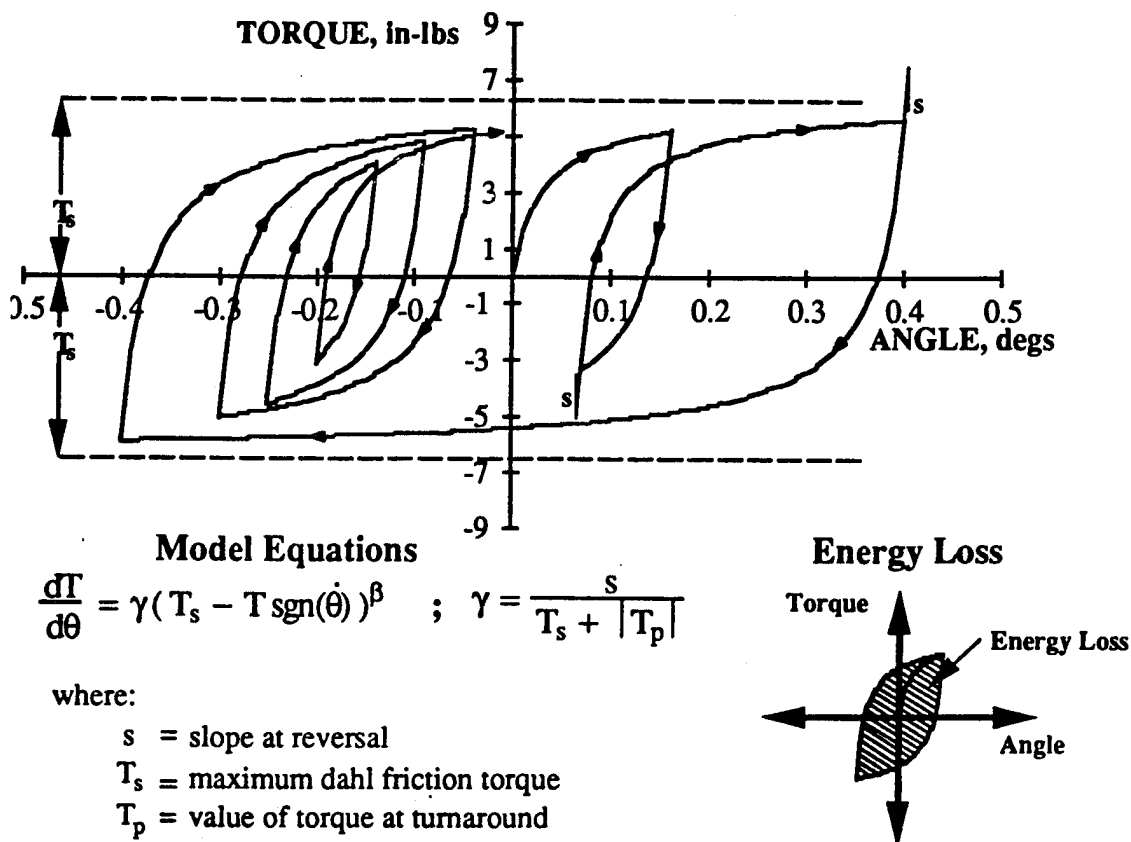
Fig. 8-3 Dahl Friction Model
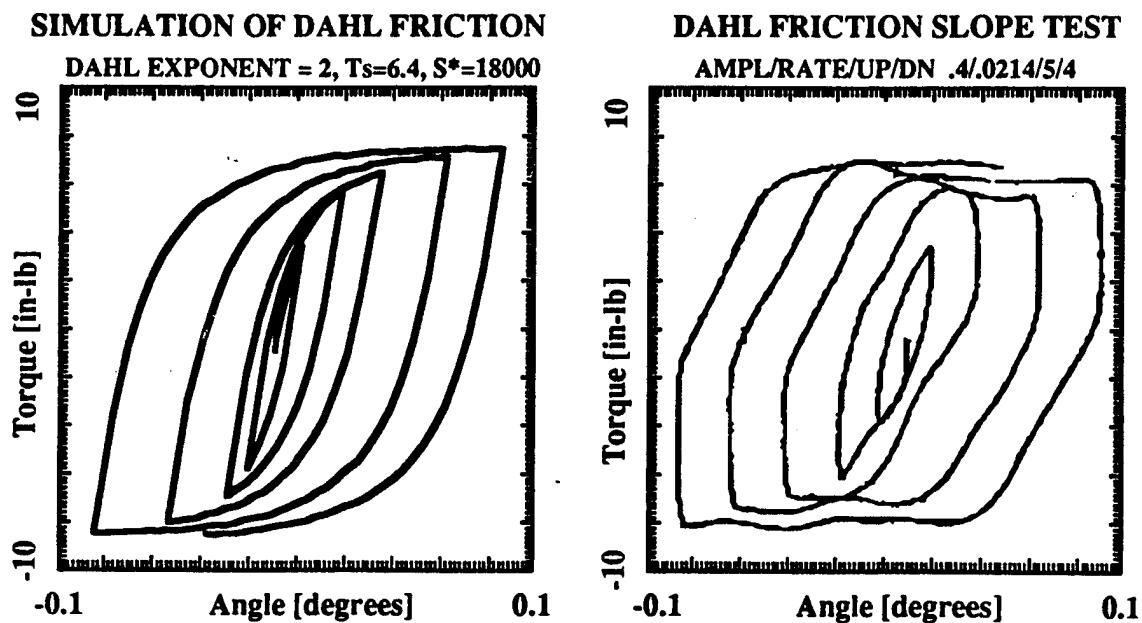


Fig. 8-4 Dahl Friction: Simulated and Experimental

- 231 -

**Torque Hash** During tracking or slewing, bearing torque variations or "hash" can cause appreciable pointing or jitter errors due to their magnitude, unpredictability, and frequency content. In particular, during a constant velocity scan, the primary bearing disturbance source is from the torque hash. For many spacecraft gimbal applications the combination of the bearing geometry and the specified gimbal slewing speed produce torque hash frequencies that are at or very close to the closed loop bandwidth of the control system and, as a result, are very difficult to attenuate.

## NCT FILM+VESPEL CAGE+MoS2 COATED BALLS
### 1/4 Hz continuous, 13k cycles
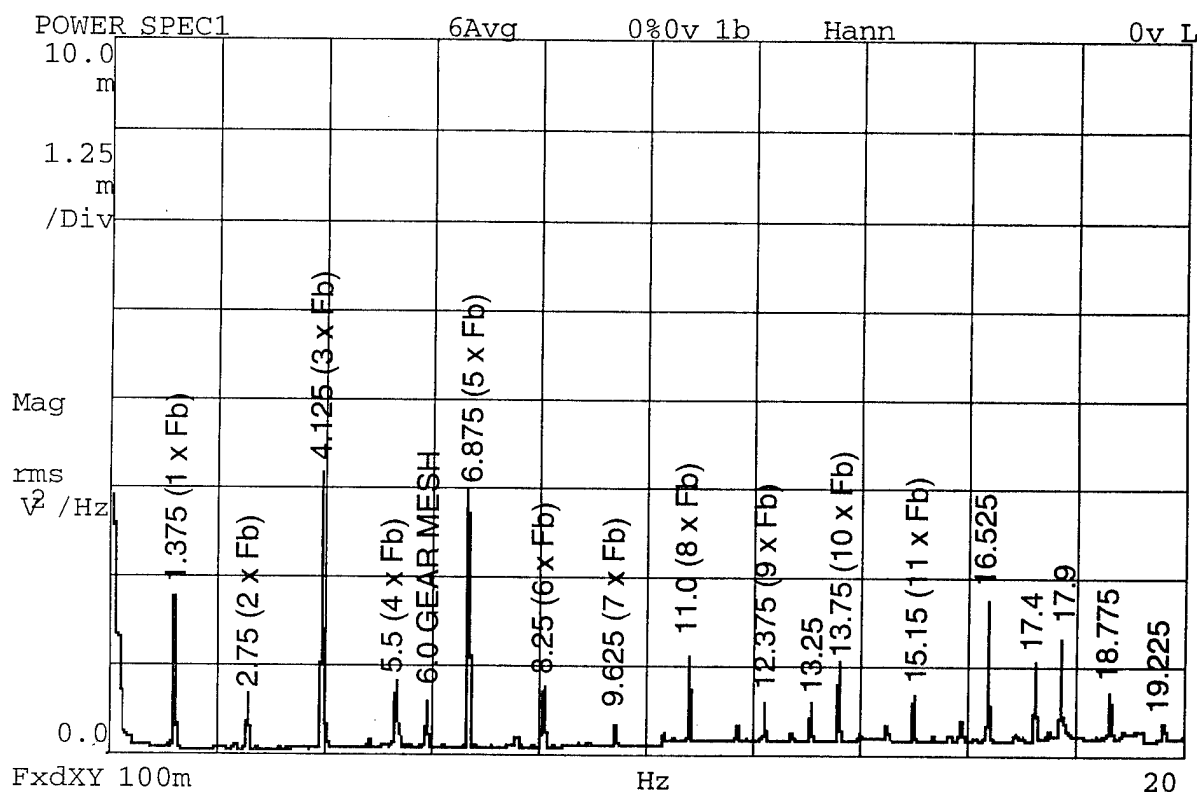


**Fig. 8-5   Bearing Critical Frequencies**

Spectral analysis of the bearing torque vs. time data reveals the frequency dependent sinusoidal nature of the bearing torque disturbance. From test data it was observed that the frequency content of the torque hash is a function of bearing geometry, loading conditions, and bearing angular velocity [8-4] (see Fig. 8-5). An LMSC code, which predicts the characteristic bearing frequencies based on information of the bearings internal geometry correlates very well with experimental data (see Fig. 8-6).

## CRITICAL BEARING DISTURBANCE FREQUENCIES [Hz]
### 1/4 Hz continuous, 13k cycles

|  | 1 Defect | 2 Defects | 3 Defects | 4 Defects | 5 Defects | 6 Defects |
|---|---|---|---|---|---|---|
| Cage Defect | 0.10 | 0.21 | 0.31 | 0.41 | 0.52 | 0.62 |
| Defect on Ball | 1.38 | 2.75 | 4.13 | 5.50 | 6.88 | 8.26 |
| Defect on Outer Race | 1.24 | 2.49 | 3.75 | 4.98 | 6.22 | 7.47 |
| Defect on Inner Race | 1.76 | 3.51 | 5.27 | 7.02 | 8.78 | 10.53 |

**Fig. 8-6  Predicted Frequencies from LMSC Code**

Test data in the form of a Torque  PSD or Power Series (PS) is back transformed into its time domain equivalent amplitude Ai  and frequency fi  components for i=1,n the number of harmonic disturbances.  The time dependent sine functions operate at a frequencies which are the ratio of the instantaneous shaft speed in the simulation to the shaft speed at which the spectral data was gathered at .

$$f_i^{simulation} = f_i^{test} \frac{\omega_{shaft}^{simulation}}{\omega_{shaft}^{test}}$$

In the simulation, the torque hash is modeled by summing a sine series where the frequencies are set equal to the scaled values calculated above.  A random phase angle in included since the spectral data in the form of a PSD or PS contains no phase information between the disturbances.

$$T_{hash}(t) = \sum_{i=1}^{n} A_i \sin(2\pi f_i t + \phi_i)$$

The magnitude of the individual terms are set according to the spectral test data obtained from flight quality bearings.  In order to simulate the ball-race slip the amplitude, frequency, and phase of each torque hash sine term is slowly modulated.

**Angular Runout**  Since the races and balls of a bearing are not perfectly round, the bearing rotation axis will move as the bearing rotates.  The movement, or runout, of the rotation axis will have a radial and angular component that are determined by the size and frequency of the out-of-roundness of the affected bearing elements.  The runout can affect gimbal pointing and tracking ability and should be considered when assessing gimbal performance.

The runout model used in the simulation is described by an angular and radial runout component.  Forces and torques are applied to the bearing races that produce static deflections and rotations equal to the radial and angular runout errors of the unloaded bearing.  The frequency and direction of the applied forces and torques are functions of the bearing angular velocity and position.

<u>Viscous Friction</u>  Friction torque from viscous drag of liquid lubricated bearings contributes significantly to bearing torque at high bearing angular velocities. The viscous torque contribution at low angular velocities or for solid lubricated bearings is generally small, but has been included within the bearing model of the simulation for completeness.

## 8.1.2  Secondary Bearing Model

<u>Structural Stiffness and Damping</u>  In most two-axis gimbal simulations, the structural stiffness and damping of the bearings are not considered. This is done to reduce the overall computational effort at the expense of also reducing simulation fidelity. A complete study of the bearings impact on gimbal performance must include the stiffness and damping of the bearings to model the dynamic coupling of the two axis gimbal. In addition, because bearing stiffness is a crucial design issue, its impact on gimbal performance must be assessed.

The stiffness and damping of the bearings are modeled as springs and dash pots in parallel. The stiffness of the bearings is a function of the bearing geometry and preload. Viscous damping internal to the bearing structural elements is assumed constant. The coupling between degrees of freedom is assumed to be negligible. As a result, the matrices that contain the stiffness and damping of the bearings have no coupling terms and, thus, are diagonal. Both the stiffness and damping matrices are defined with respect to the basis that is fixed in the outer race of each bearing. The relative inner-outer bearing race rotations are assumed to be small in the sense that higher order terms introduced from geometric or constitutive nonlinearities are insignificant in comparison to the leading order terms. This assumption is made so that the final relative inner-outer race rotation will be invariant with respect to the gimbal rotation sequence. This assumption is used only with respect to the deformation of the bearings and is not assumed in any other part of the simulation. The elements of the stiffness and damping matrices that correspond to rotation about the bearing rotation axis are set equal to zero. Any torques produced about the rotation axis are assumed to be functions of variables external to the bearings' structure and are modeled elsewhere.

<u>Cable Wrap Wind-Up</u>  The effects of cable wrap wind-up, if present, have also been included in the bearing model section of the simulation. The torque about the bearing spin axis, produced as a result of cable wind-up, can be the largest DC torque contributor within the bearing model. However, the relatively slow rotation rates of spacecraft gimbals generally cause a slow rate of change in cable wrap torque. This slow increase in torque is easily compensated for by an integral gain within the servo-control system.

Within the simulation, the cable wrap wind-up torque is described by a curve fit to experimental data [8-5]. Similar to Dahl friction, the cable wrap wind-up torque has a hysteretic component which is modeled in a similar way to Dahl friction (see Fig. 8-7).
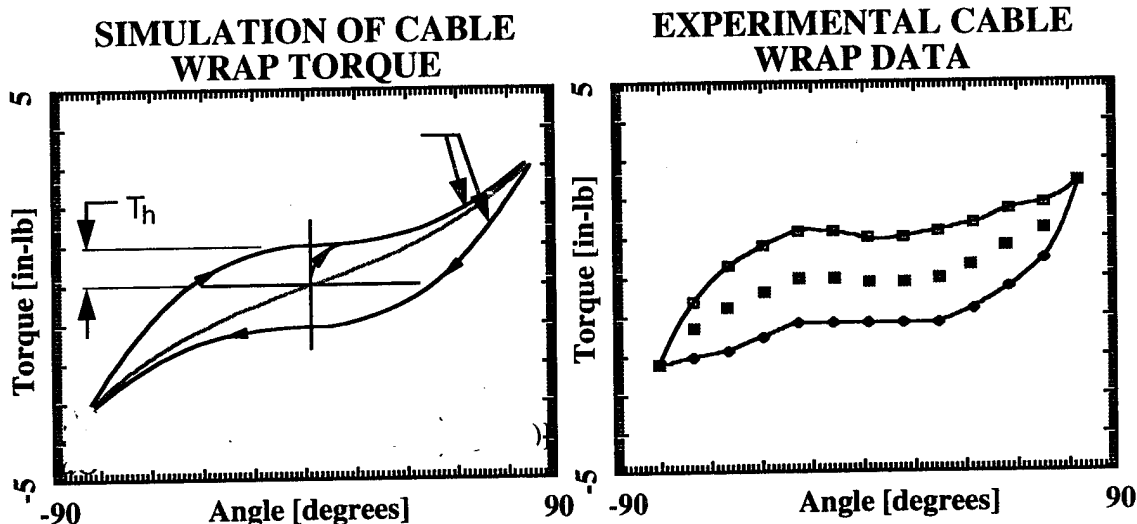
Fig. 8-7   Cable Wrap Torque Model

### 8.1.3   End-of-Life Bearing Model

Most pointing simulations consider the characteristics of undegraded components. Bearing data generated under the T/PGD program provided an opportunity to evaluate End-Of-Life pointing performance. This introduces the need for other bearing sub models to describe their anomalous behavior.

**Turnaround Torque**   Turnaround torque, sometimes called stiction, describes the apparent increase in the coulomb friction force when two adjacent surfaces exhibit a "sticking" behavior [8-6 - 8-8]. Large stiction values would not be expected for well lubricated bearings at beginning-of-life. However, after a large number of rate reversals, there is the potential for lubricant degradation which could give rise to locally higher friction and/or wear debris. In addition, unexpected torque variations such as cage friction or wear could also give rise to stiction events. Thus, stiction may correspond to end-of-life conditions and may have a significant effect on gimbal performance.

A common model of stiction assumes that adjacent surfaces will become "stuck" when the relative velocity between the sliding surfaces drops below a predetermined level [8-9]. When stiction is initiated, the frictional forces between the two sliding surfaces jumps to the static friction level which is higher than the running friction level. This commonly used model is deficient in two ways.

First , the assumption that stiction will occur when the relative sliding velocity between two surfaces in contact is low may not be correct. In situations where the sliding surfaces oscillate, such as from external vibration or intentional dithering, stiction is not initiated even though the relative sliding velocity of the two contacting surfaces passes through zero. This phenomenon suggests that the relative sliding acceleration of contacting surfaces, which, for oscillatory motion, is at a maximum when the relative sliding velocity is zero, must drop below a certain level for stiction to occur. To insure that initiation of stiction is accurately modeled, the relative acceleration of the sliding surfaces must also be considered [8-4]. The advent of stiction is, therefore, governed by two parameters that are denoted as a threshold

rate and threshold acceleration. For stiction to occur, the relative sliding velocity and acceleration must fall within an ellipse in the velocity-acceleration plane defined by the threshold rate and acceleration.

The second deficiency with the conventional theory occurs after the initiation of stiction. When stiction occurs, the stiction force is set equal to the lesser of the resultant surface shear force or the static friction force. The accelerations are set equal to zero and the relative velocity of the sliding surfaces is kept constant. As a result, the relative displacement between the sliding surfaces increases during this stiction period. This is inconsistent with the physical processes taking place. When sliding surfaces "stick" their interfaces are frozen so that the stiffness of the two sliding surfaces become coupled. This interaction is more precisely modeled by a spring with stiffness commensurate with the shear stiffness of the sliding surfaces. When the shear force between the two sliding surfaces becomes larger than the stiction breakaway torque, the spring that is used to model the stiction force is taken away so that the stiction force goes to zero (see Fig. 8-8).
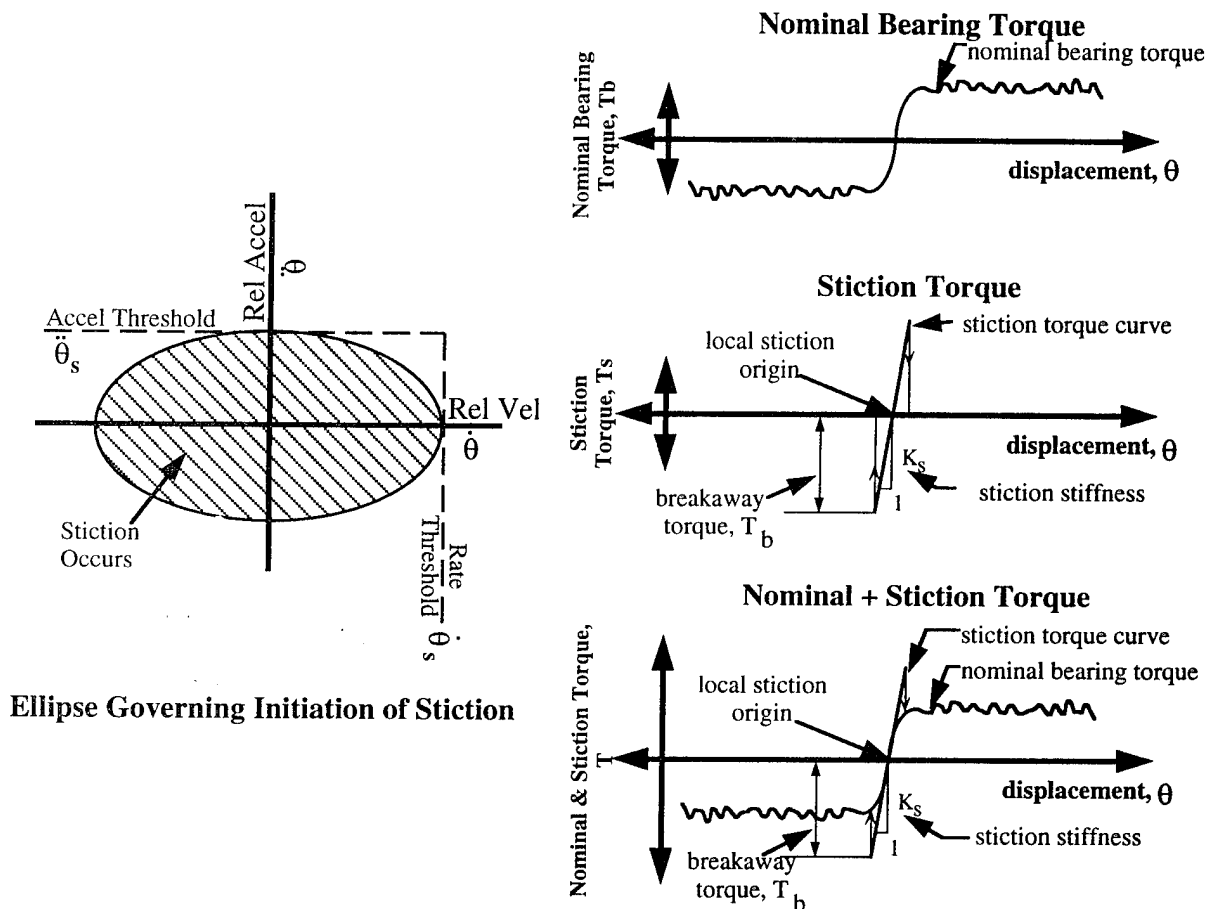


**Fig. 8-8   Turnaround (Stiction) Torque Model**

**Torque Blocking**   Torque blocking refers to the sudden increase in torque levels of a bearing that has been subjected to continual oscillatory motion. As a bearing is rotated back and forth the balls group together and can pinch the cage, causing high torque. This is a result of the unsymmetrical motion of the balls with respect to the bearing rotation. This phenomenon causes the bearing torque to rise sharply at the end of travel regions of the oscillating bearing. This behavior, if left unchecked, can seriously degrade the performance

of a precision gimbal to the point where loss of mission due to excessive bearing torque can occur. [8-10] The torque blocking model is implemented by fitting an exponential function to the bearing torque data points observed during testing (see Fig. 8-9).
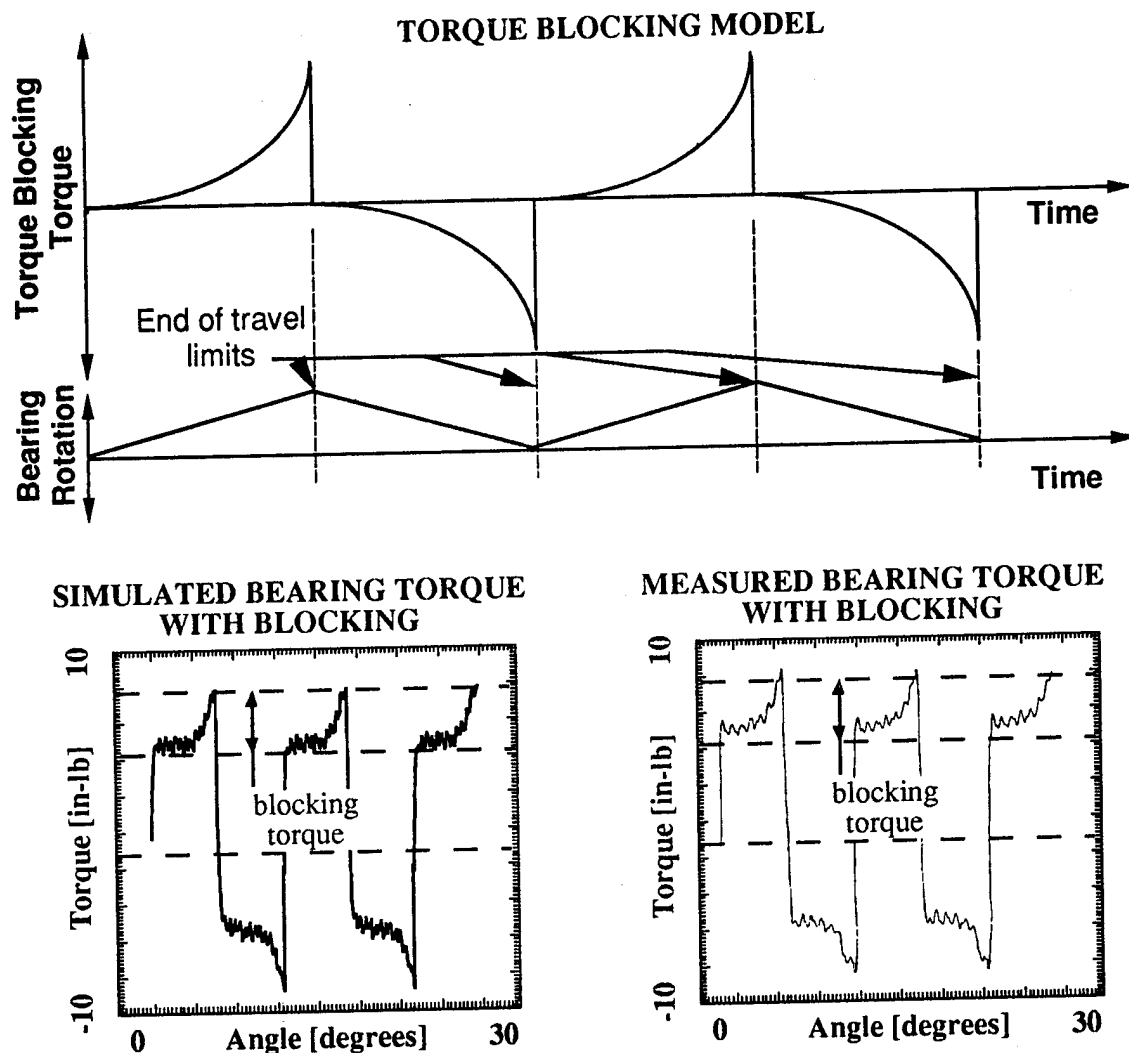


Fig. 8-9 Torque Blocking Model and Comparison with Experiment

**Torque Bump** A torque bump may occur if a bearing has undergone prolonged oscillatory motion where the amplitude of bearing motion is such that the individual ball paths have not overlapped each other. Debris and/or lubricant may build up between ball tracks during the oscillatory motion and may cause significant torque "bumps" when the bearing is slewed through a large angle over the debris. The torque bump model is implemented by inserting a skewed haversine function to model the torque profile at the bearing torque bump locations (see Fig. 8-10).

The figure shows:

$$T = A_{skew} ( -t^5 + 2t^3 -t ) \qquad A_{skew} = ( 1 - t )$$

with vertical axes labeled "Torque Bump Torque" and "Bearing Rotation", horizontal axes labeled "Time", and "Torque bump regions".

**Fig. 8-10    Torque Bump Model**

## 8.2  PRECISION BEARING TESTS

Test data from the precision bearing functional tests (Section 6.2) was used to validate the bearing disturbance model and to obtain parameter information on actual flight quality bearings. This data was used as input into the bearing simulation.

The precision test set up uses a rotary air rate table as the rotation platform for the bearing tests. The high stiffness (660,000 lb/in axial and 300,000 lb/in radial) and low runout ($\pm$ 0.00005") of the turntable provided a stable, low noise rotation platform to maximize the bearing torque signal to noise ratio. The rotation of the 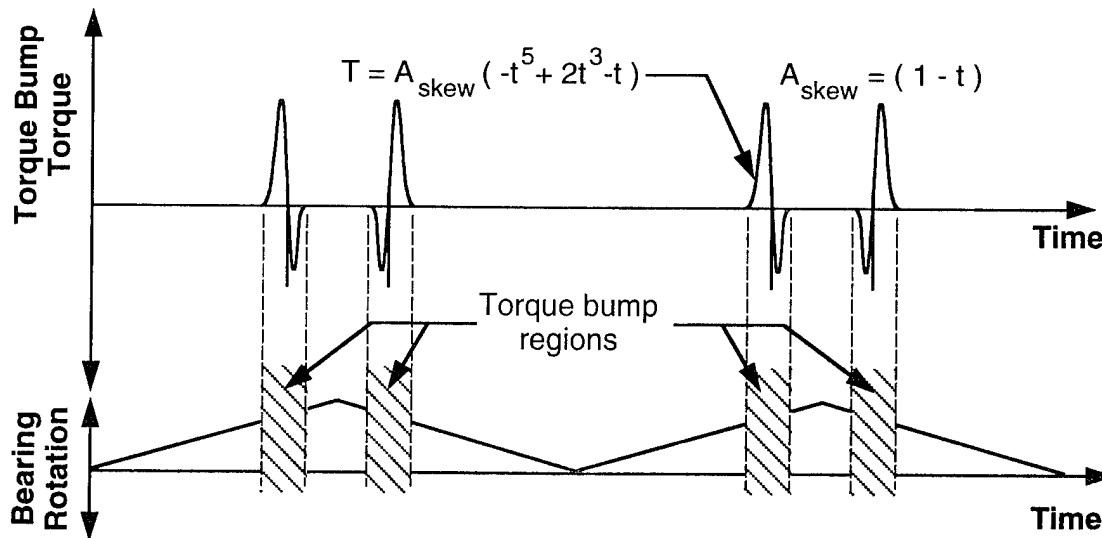turntable was controlled through an IAC-186 intelligent axis controller. The IAC-186 is a 16 bit controller provides a 0.5 millisecond servo rate for precise positioning control. An RE 36000 line encoder with tachometer feedback provided rotation information to the IAC-186 controller which relayed feedback commands to a low cogging INLAND DC servo motor. The position and velocity commands were entered through an IBM 386 PC via an RS232 port to the IAC-186 controller. The assembled test set up (see Fig. 8-11) provided precise rotation control and resolution (< 2 arc seconds) for bearing torque and position measurements.

Bearing angular runout measurements were obtained with an autocollimator mounted above the rotating bearing (Fig. 8-12). The autocollimator signal, processed by the X-Y indicator provided runout measurements with an accuracy of 0.2 arc-seconds and maximum frequency range in excess of 1.6 KHz.

Bearing torque ripple measurements were obtained with the precision bearing test set up in combination with a sub miniature load cell and amplifier (Fig. 8-12). The linearity of the load cell is greater than 0.5% and the output analog signal has infinite DC resolution which will result in very high accuracy bearing torque measurements. Torque ripple data was processed through an HP spectrum analyzer to obtain a frequency breakdown of the torque ripple data. .

**Fig. 8-11 Precision Bearing Test Set-Up**



Angular Runout Test  Torque Ripple Test  Dahl Friction Slope Test

**Fig. 8-12 Precision Bearing Test Configurations**

Bearing Dahl friction slope measurements were obtained with the load cell, a proximity probe, and a precision linear actuator and controller. The proximity probe has a resolution of 60 μ inch and the linear actuator and controller are capable of 0.001 inch accuracy and controllability. The linear actuator and controller was used for precise small angle excursions by coupling the bearing rotation to the linear actuator through a rigid moment arm. This arrangement will provide precise controlled rotation with 20 arc second accuracy.

The construction of the precision bearing test set up is motivated by the need to validate the bearing disturbance simulation and to obtain actual bearing parameter information as input to the bearing simulation. Once the bearing simulation has been validated, it can be used to extrapolate the performance and effect of other bearings by simply knowing the particular parameters associated with a given bearing. In addition, the data obtained for the bearings tested can be used as exact input data for other simulations.

## 8.3 GIMBAL SYSTEM SIMULATION

LMSC's in-house gimbal simulation represents the dynamics of the gimbal system including the structure, controller, actuators, and sensors as well as input disturbances from spacecraft mechanisms such as CMG bearings, and solar array drive motors. The gimbal simulation incorporates the bearing sub model described above To understand the true effects of bearing disturbances on gimbal pointing performance, one must study the effects of all error sources in addition to bearing disturbance torques.



**Fig. 8-13 Gimbal System Simulation**

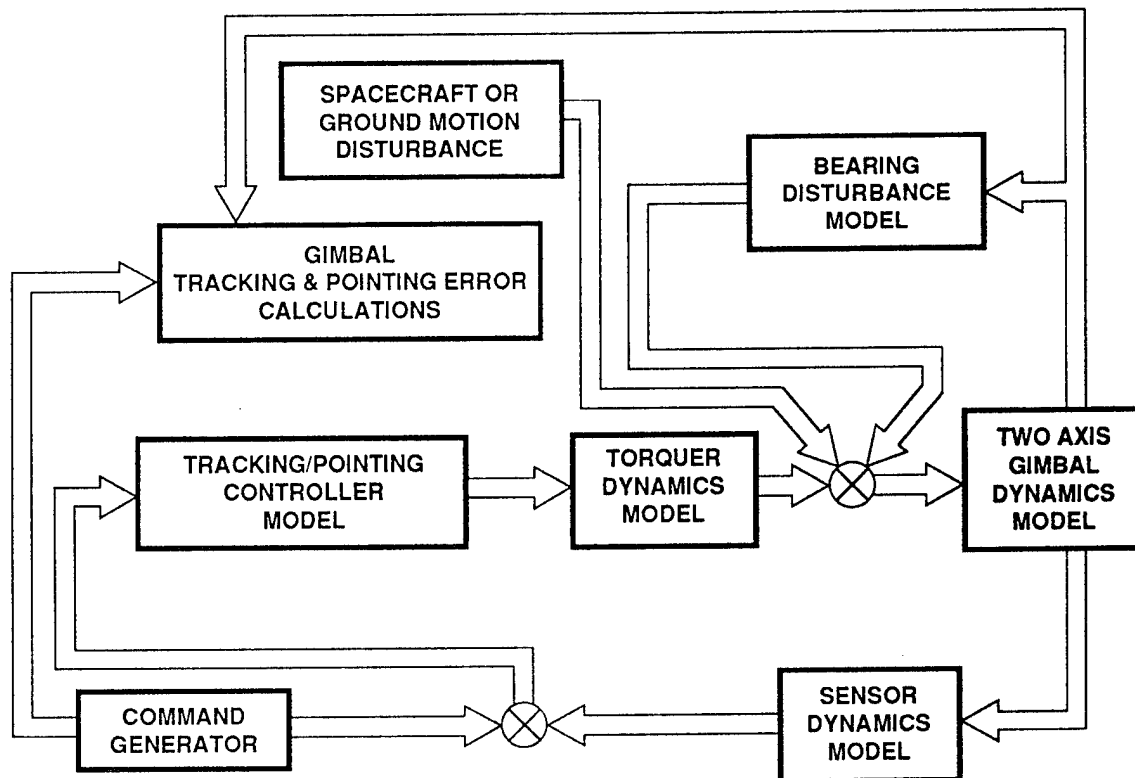### 8.3.1 Gimbal System Model
The gimbal system simulation attempts to model all of the important dynamics of a two axis space qualified gimbal. An overview of the simulation is given in Fig. 8-13. In addition to the two axis gimbal mechanical dynamics model the simulation includes: a simulation model of the sensor dynamics, including nonlinear effects such as encoder quantization, signal

delay and signal noise; a simulation model of the torquer dynamics, including back EMF, amplifier saturation, and mechanical and electrical time constant effects; a simulation model of the digital control system, including the effects of sampling rate, computational delay, and signal quantization and discretization; a simulation model of spacecraft disturbance sources such as CMG or cryo-cooler pump vibration: and, finally, the simulation model of bearing disturbance torques which is described above.

## 8.3.2 Command Generator

Simulations to date have focused on a particular scanning-pointing maneuver that was specific to the Brilliant Eyes two axis gimbal. The maneuver consisted of a reversing sweep azimuth axis motion (constant velocity with haversine reversal) coordinated with a step-stare elevation axis motion. The type of sensor and subsequently the type of raster scan that the gimbal employed is common among many spacecraft gimbals. For example, the pan/tilt scan mirrors on the NASA GOES-I and Air Force DMSP weather satellites use a two axis raster scan. The pan/tilt mirror on the SDIO proposed Brilliant Pebbles satellite used a similar profile.
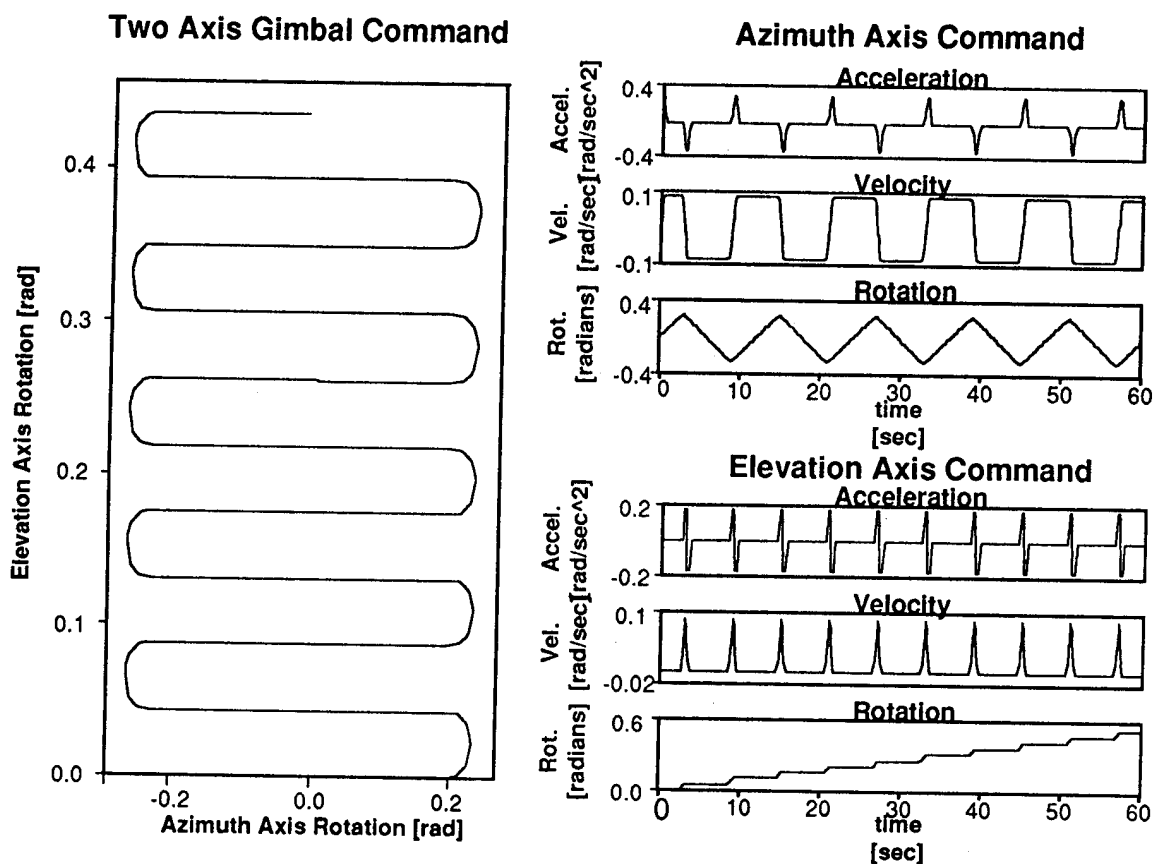
**Fig. 8-14    Gimbal Scan Maneuver**

Specifically, the commanded maneuver used in the two axis gimbal simulation for the azimuth axis consisted of a ±10° scan with constant velocity over a 5 second period with a haversine velocity profile used during reversal. The elevation axis maneuver consisted of a step of 3° which occurs simultaneously with the azimuth axis haversine reversal command. The step command is achieved through a square wave acceleration command. During the

azimuth axis constant velocity scan the elevation axis holds position in a stare mode. The scan profiles are shown in Figure 8-14.

### 8.3.3 Jitter: Pointing Error Calculation

The most frequently used figure of merit for gimbal pointing performance is jitter which is directly related to the sharpness of the sensor image. Jitter can be thought of as a measure of the high frequency component of the gimbal pointing error. More precisely, jitter is defined as the difference between the maximum and minimum peak to peak pointing error excursion during a defined scanning window. The scanning (or jitter) window can be defined over a time interval or over a scanning distance. The latter is the definition used for this study (see Fig. 8-15). Two axis jitter is calculated from the vector sum of the azimuth and elevation axis pointing errors. Jitter is one of the most important quantities in describing the performance of a gimbal system because it directly measures the errors that are the most difficult to compensate.
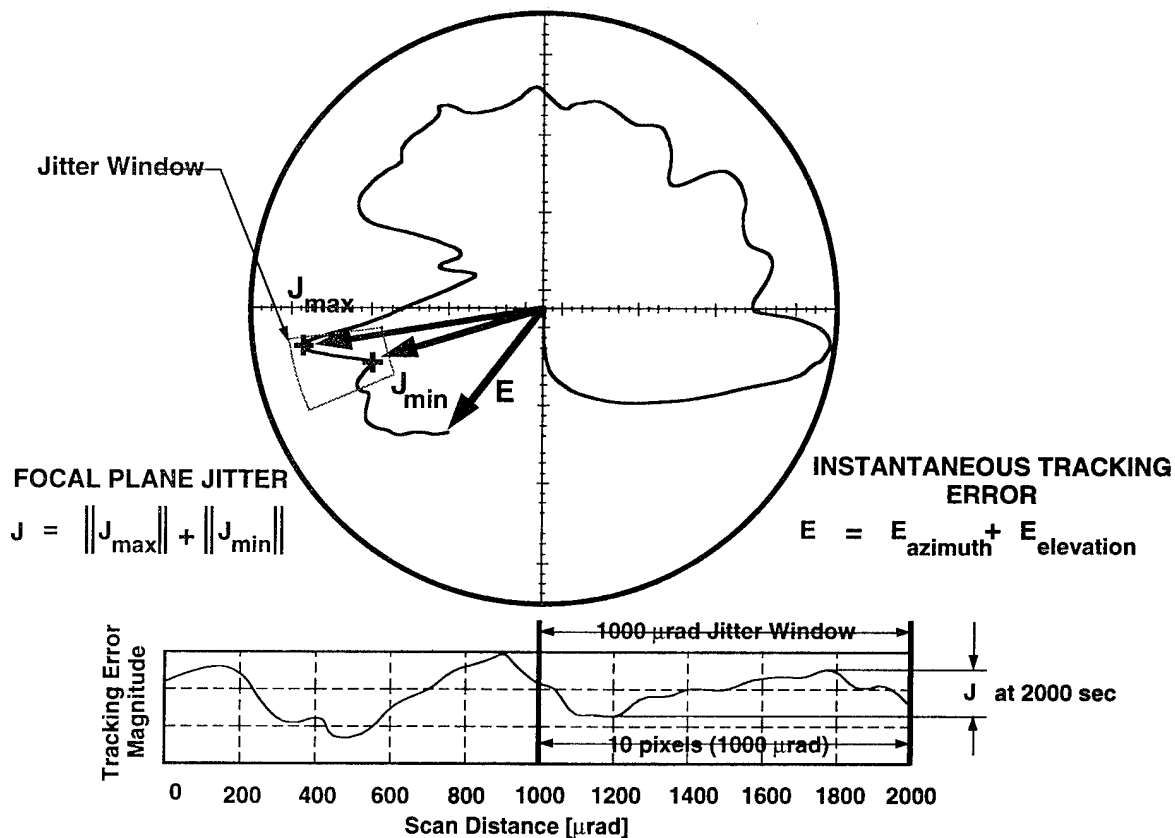


**Fig. 8-15 Two Axis Gimbal Jitter**

### 8.3.4 Effects of Bearing Failure on Gimbal Performance

Actual accelerated life test data from flight precision bearings was used as input to the bearing disturbance model to gage the effects of bearing disturbance torque on gimbal pointing performance. The bearing disturbance model's torque parameters were scaled according to a least squares approximation. The scaled bearing disturbance model was used within the

gimbal simulation to simulate the progression of gimbal performance as a flight bearing goes from beginning-of-life to end-of-life conditions. A number of different nominal gimbal configurations were simulated. The type and size of different gimbal components were varied, such as motor size, gimbal size, encoder accuracy, etc. For every case considered, the gimbal jitter increased proportionally with an increase in bearing torque. An example of the effect of bearing life cycle torque on gimbal performance is shown in Fig 8-16. Fig. 8-16 indicates that as a bearing approaches end-of-life that the increase in gimbal jitter (or decrease in gimbal performance) corresponds with the bearing torque level at a 1 to 1 ratio.
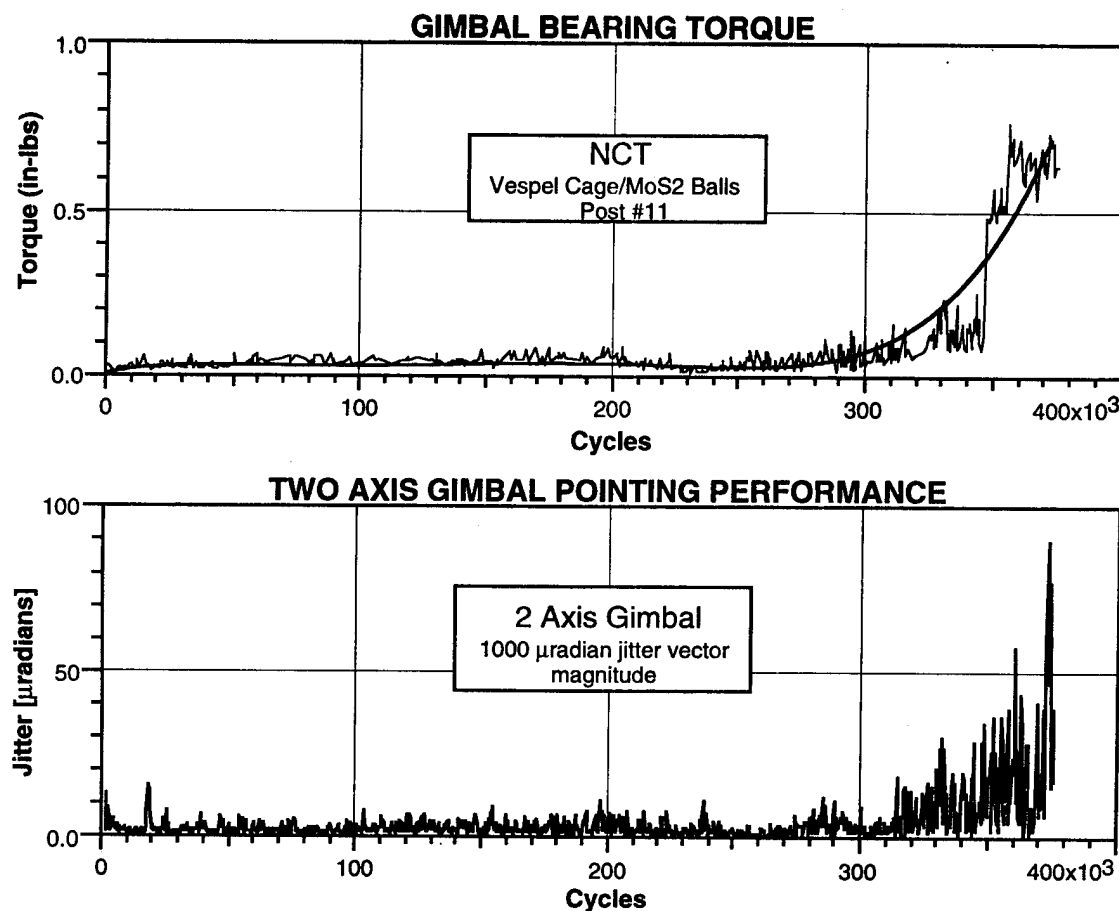


**Fig. 8-16    Loss of Sensor Function Due To Bearing Failure**

## 8.3.5    Effects of Bearing Failure on 2 Axis Gimbal Performance

The 2 axis gimbal model described in the proceeding section was used to quantify the effect of BOL versus EOL bearings on the systems jitter pointing performance. The size and mass properties the 2 axis gimbal model were chosen to be consistent with an early Brilliant Eyes Payload Gimbal concept. The azimuth axis contains a pair of 3"x5" (B117BX) angular contact bearings spread 8 inches apart. The elevation housing supports a pair of 4.75"x5.5" angular contact bearings.

Each gimbal axis is subjected to the bearing torque associated with the primary bearing disturbance model. The model consists of 7 bearing torque sub models: 1) Dahl friction; 2)

viscous friction; 3) torque hash; 4) bearing runout; 5) torque blocking; 6) torque bump; 7) and the stiction torque.

To account for the BOL and EOL bearing effects the BOL and EOL Bearing Torque PSD's presented in figure 5-34 (NCT $MoS_2$ + Vespel Cage + $MoS_2$ coated balls rotating at 1/4 Hz) were used to develop two distinctly different torque hash models. As mentioned above, the Torque PSD was back-transformed into its equivalent time domain counterpart. The amplitude and frequency of each disturbance was scaled to take into account the size difference between the 105 size bearings and the B117BX bearings.

The BOL Torque PSD and its equivalent time history is presented in Fig. 8-17. These disturbances are due mainly to the ball imperfections which occur at the harmonics associated with the ball defects frequency of 1.38 Hz.
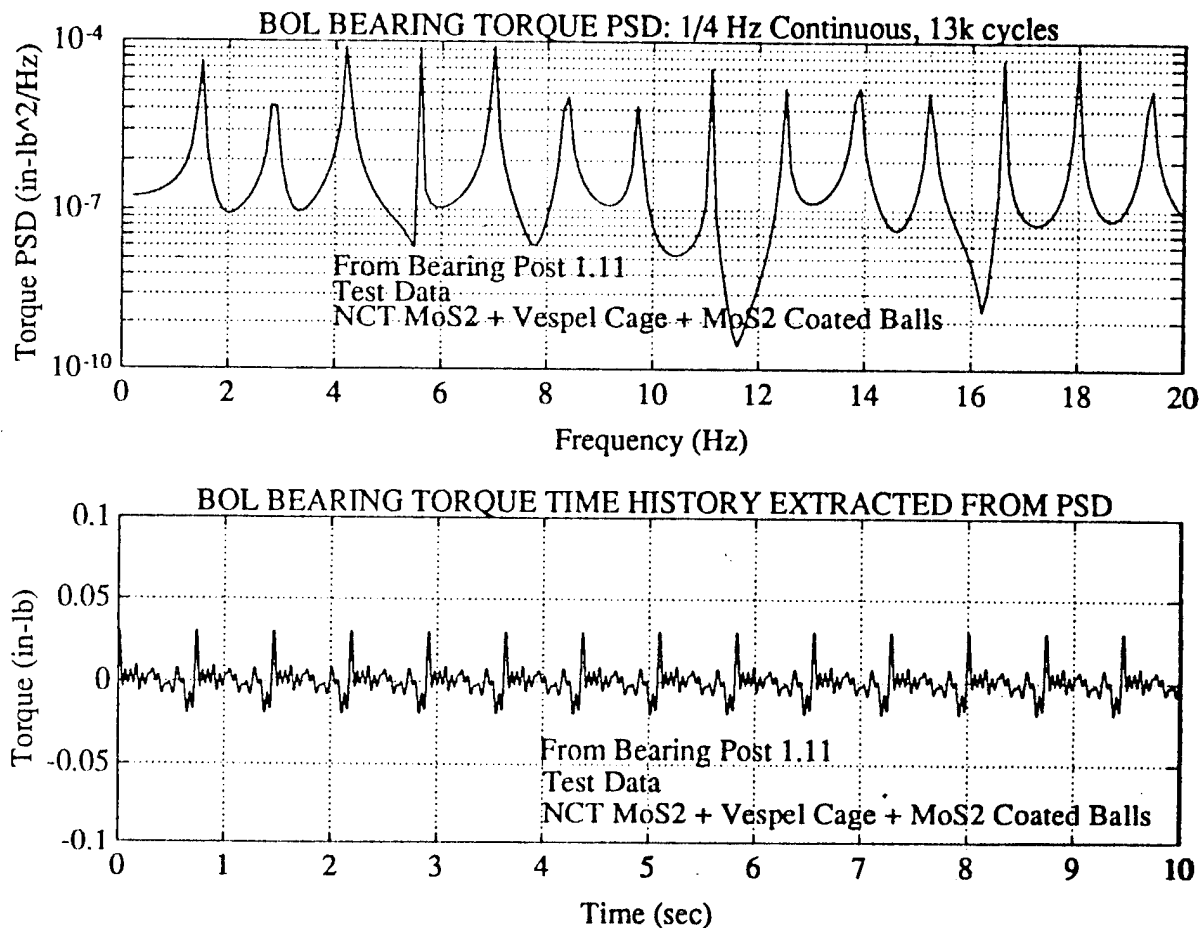


Fig. 8-17  Beginning of Life torque test data

The EOL Torque PSD and its equivalent time history are presented in Fig. 8-18. The EOL PSD is made up of the harmonics associated with the ball defects at 1.38 Hz, the inner race defects at 1.75 Hz, and the outer race defects at 1.25 Hz. As expected, the overall PSD levels as well as the spectral density of the of the EOL bearing is higher than that of the BOL bearing.
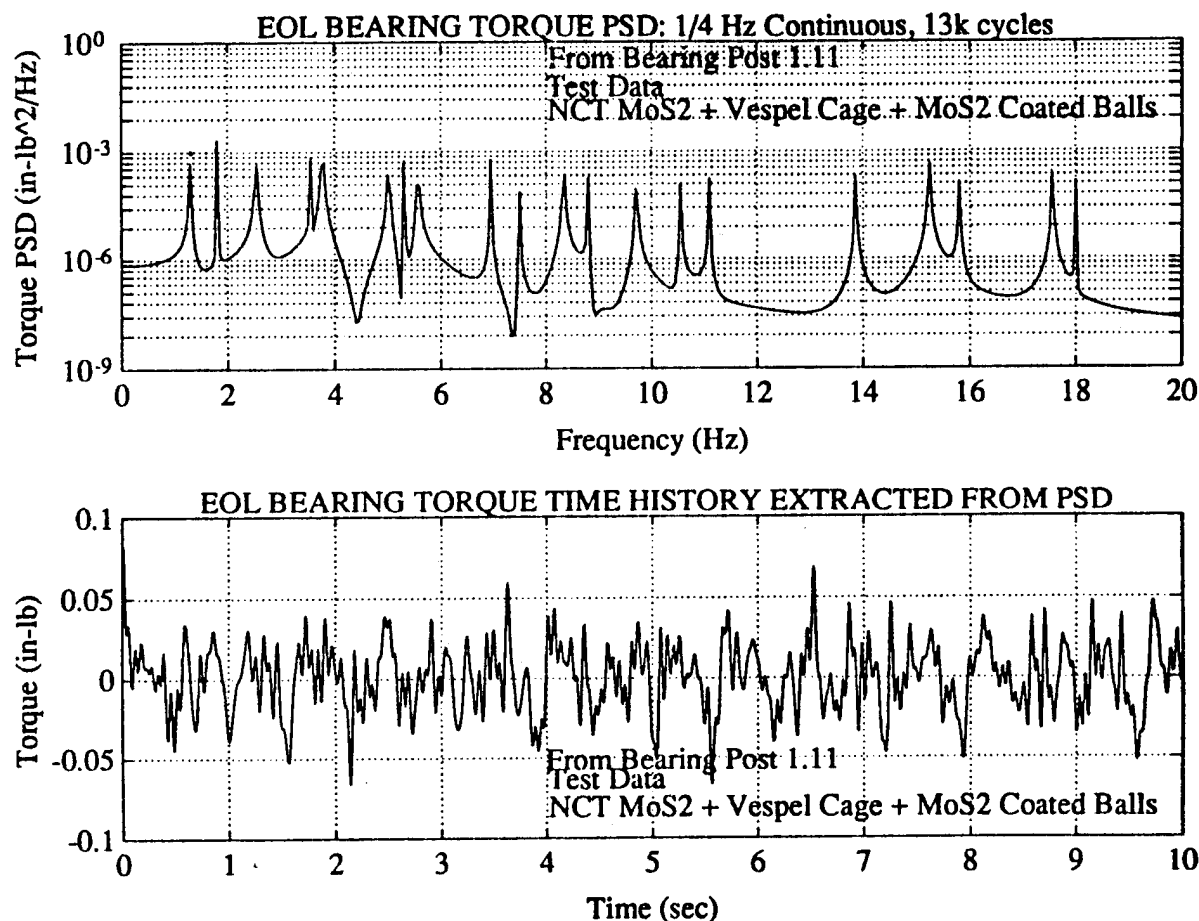


**Fig. 8-18    End of Life torque test data**

The scanning maneuver presented in Figure 8-14 was used to investigate the effect of the BOL vs. EOL bearing on sensor performance consists of the synchronized constant velocity slew about the azimuth axis (from +/- 22.5°) and the 3.0° step-stare maneuver about the elevation axis . Both of which are described in section 8.3.2.   The Jitter vs. Time plot of the BOL Bearings show a steady state jitter level of 1 μ-radians.  The larger jitter levels seen at scan reversal times are of no consequence since the sensor is inactive during scan reversal.

**Fig. 8-19   Jitter vs. Time of a BOL Bearing, Az & El Scanning**



**Fig. 8-20   Jitter vs Time of a EOL Bearing,   Az & El Scanning**

The Jitter vs. Time plot of the EOL Bearings (Fig. 8-20) also yield steady state jitter levels of 6 to 10 μ rads. Thus, the EOL bearings produce jitter which is one order of magnitude higher than its BOL counterpart. Again, the larger jitter levels seen at scan reversal times are of no consequence since the sensor is inactive during scan reversal.
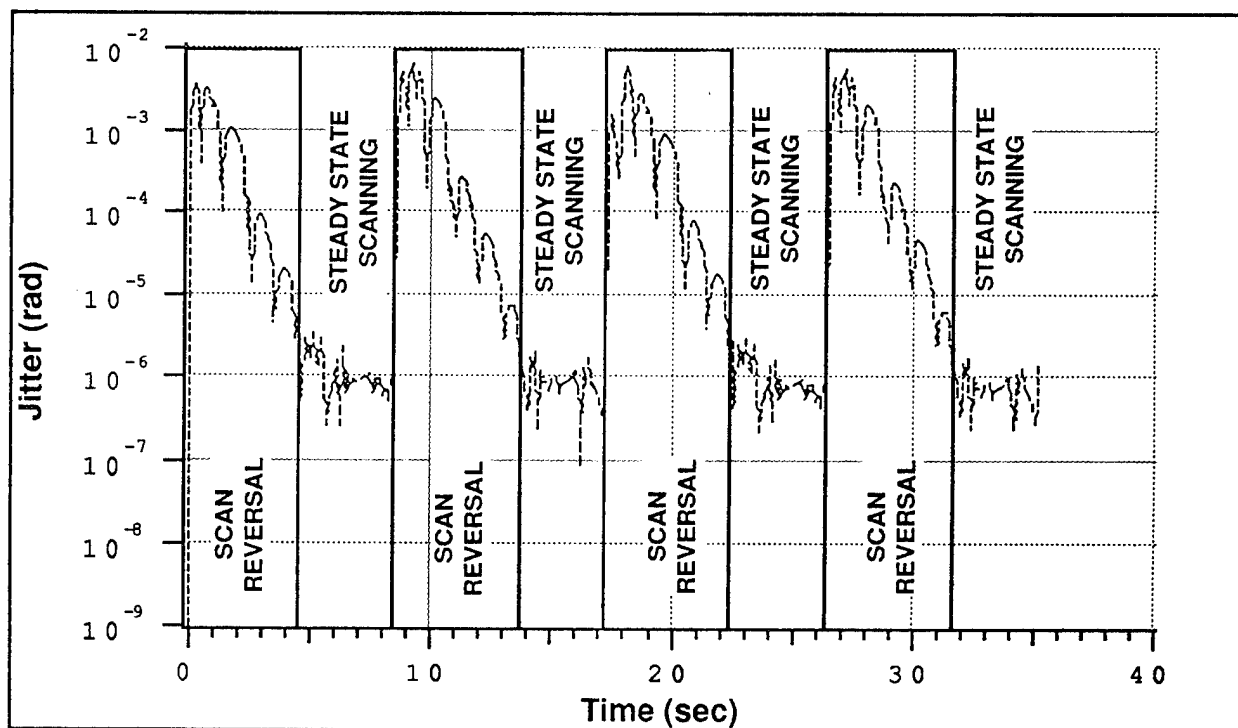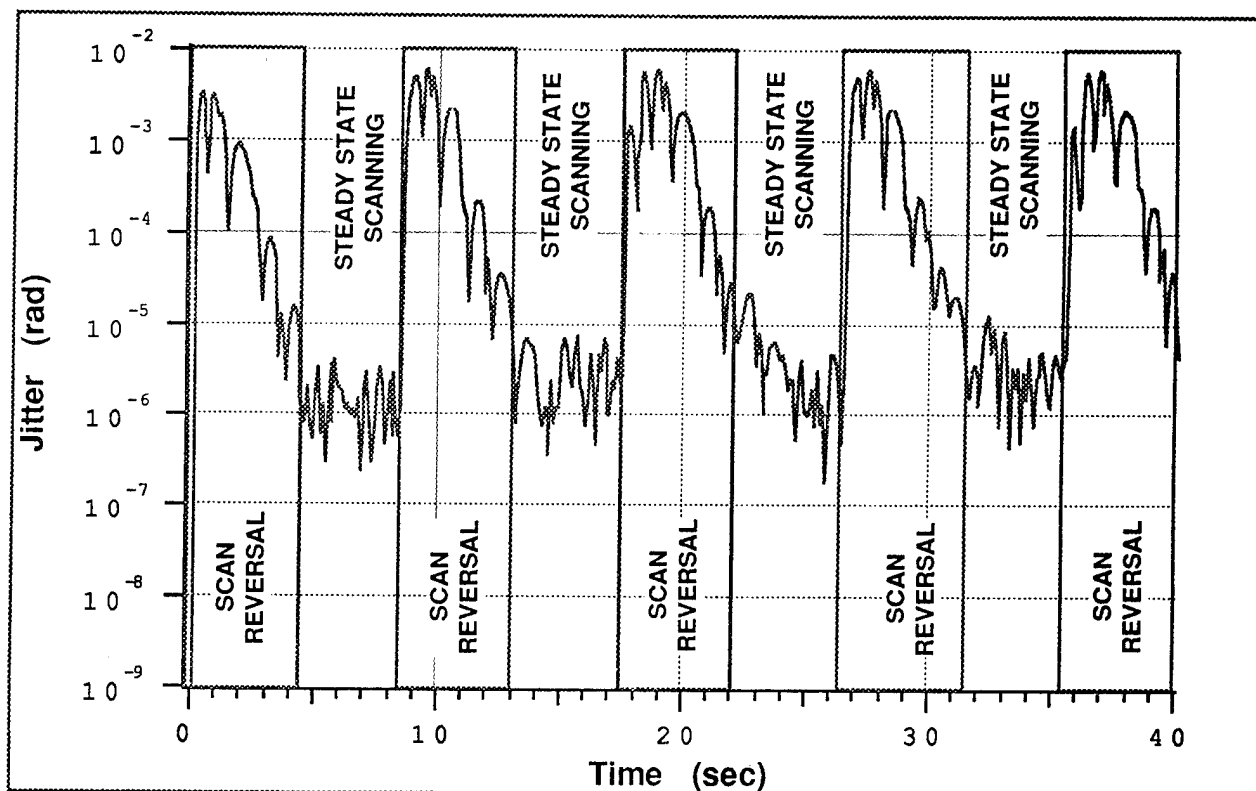
### 8.3.6 Breakdown of Gimbal Jitter Sources

A typical spacecraft gimbal has a number of different jitter (or error) sources that can degrade its performance like motor cogging, power transfer device torque such as cable wind-up, as well as spacecraft born disturbances such as CMG vibrations. Preliminary studies of the effects of various disturbance sources on the overall gimbal performance have been undertaken. Using a nominal case that closely matches the conditions of the two axis gimbal, a comparison of the contributions of bearing disturbance torque, motor cogging torque, and cable wrap wind-up was made. Initial results (see Fig. 8-21) show that the bearing is the major contributor to gimbal jitter and, therefore, a reduction in bearing disturbance torque levels could significantly improve the performance of a gimbal system. The jitter shown in Fig. 8-21 was calculated from a simulation of a constant velocity slew maneuver when the bearing torque vary the least. It should be noted that in some instances, such as when the motor cogging frequencies are very close to the control system bandwidth, the gimbal jitter contribution of the bearings may not be as high as shown in Fig. 8-21.

## JITTER SOURCE COMPARISON
### Constant Velocity Slew Mode



| DISTURBANCE SOURCE | % JITTER REDUCTION |
|---|---|
| No Bearing Torques | 71% |
| No Cable Wrap Torques | 13% |
| No Motor Cogging Torques | 10% |

10% Reduction in Bearing Torque = ~7% Jitter Reduction

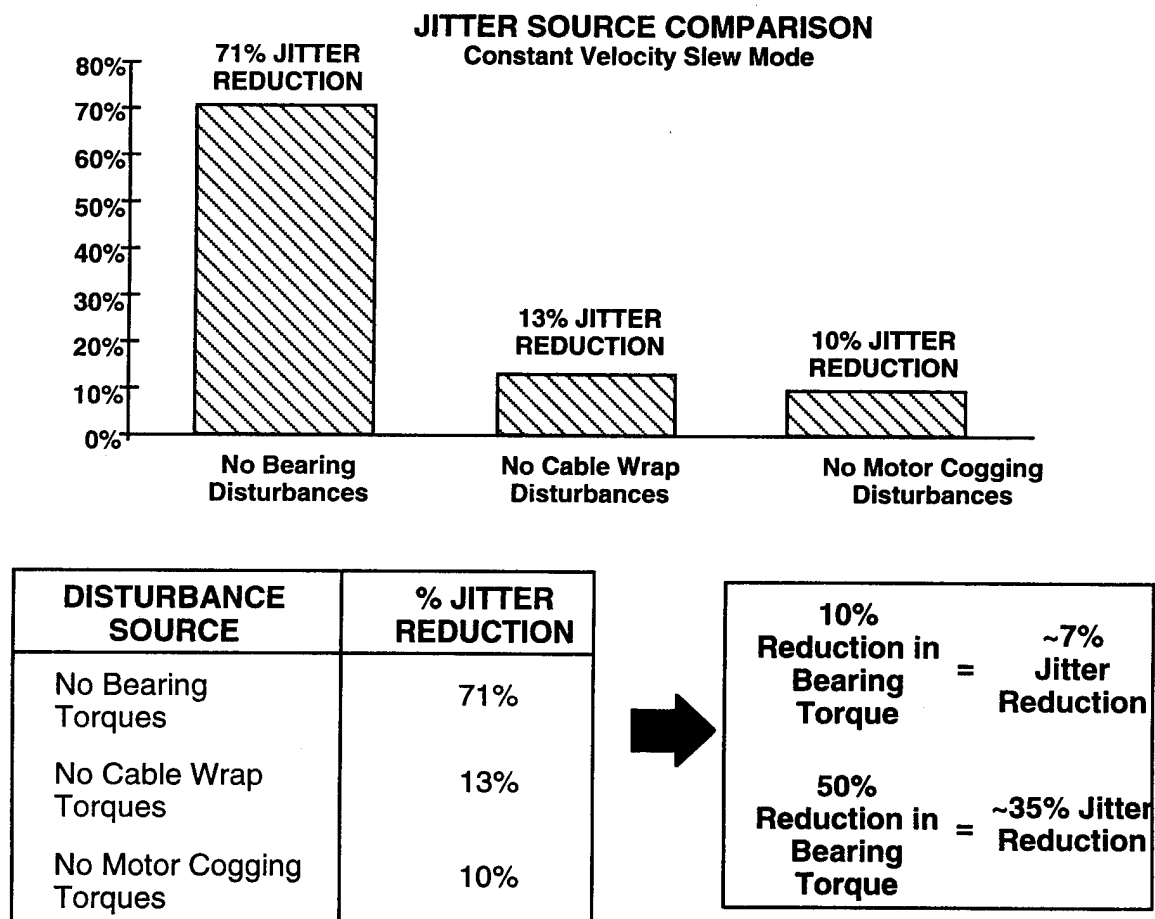50% Reduction in Bearing Torque = ~35% Jitter Reduction

**Fig. 8-21 Jitter Source Breakdown**

### 8.3.7 Gimbal Flexible Body Effects

The Tribo program was asked to help identify candidates for the bearings to be used in the two Lockheed Brilliant Eyes (BE) gimbals. Selection of bearing sizes are dependent on the required gimbal structural stiffness. This stiffness is set so sufficient separation exist between structural and servo system frequencies. The following sections describe the two payload gimbal designs that were presented to the BE Program Office. The designs were created with BE Program funds in support of their design studies.

**Gimbal Modeling** The proposed spacecraft contained two payloads each supported by a 2 axis precision gimbal. The control system bandwidth of each gimbal was on the order of 10 to 20 Hz, resulting in a gimbal design which requires that the structure modes be placed in the neighborhood of 70 to 100 Hz to avoid any coupling between the control system and structure. As with most other systems, a light weight system is desirable from the structural frequency, launch weight, and power consumption standpoints. The gimbal which supports Payload 1 is roughly 1 feet wide by 3 feet tall by 1 foot deep. The gimbal, constructed of beryllium, supports a 92 lbm payload. The payload 2 gimbal is roughly 12 inches wide, 5 inches deep, and 12 inches tall. The gimbal, constructed of aluminum, supports a 28 lbm payload.

Finite element models of two early gimbal concepts of the BE spacecraft were constructed. The stiffness of the candidate bearings were included in the form of the appropriate radial and axial stiffness terms for the elevation and azimuth axis bearings.

**Modal Analysis Results** The modal analyses of the two gimbals were performed with fixed based boundary conditions. This was accomplished by restraining the azimuth axis spacecraft interface locations. The results of the modal analysis of the payload 1 gimbal are presented in Table 8-1. The results show that the current design meets the desired structure frequency requirement of 75 to 100 Hz.

### Table 8-1. Preliminary Frequencies for the LMSC BE Payload 1 Gimbal

| Mode | Frequency | Description |
|------|-----------|-------------|
| 1 | 0.0 | Elevation axis rigid body mode |
| 2 | 0.0 | Azimuth axis rigid body mode |
| 3 | 82.9 | 1st cantilever mode YZ plane |
| 4 | 89.9 | 1st cantilever mode XZ plane |

A diagram of the 1st structural mode is presented in Fig. 8-23. The diagram contains the strain energy density distribution superimposed on the mode shape. The strain energy density distribution is typically used to identify the cause of a particular mode and also serves as a guide as to where extra material should be added to increase the structural frequency and where material may be removed from the structure without adversely affecting the stiffness of the structure.
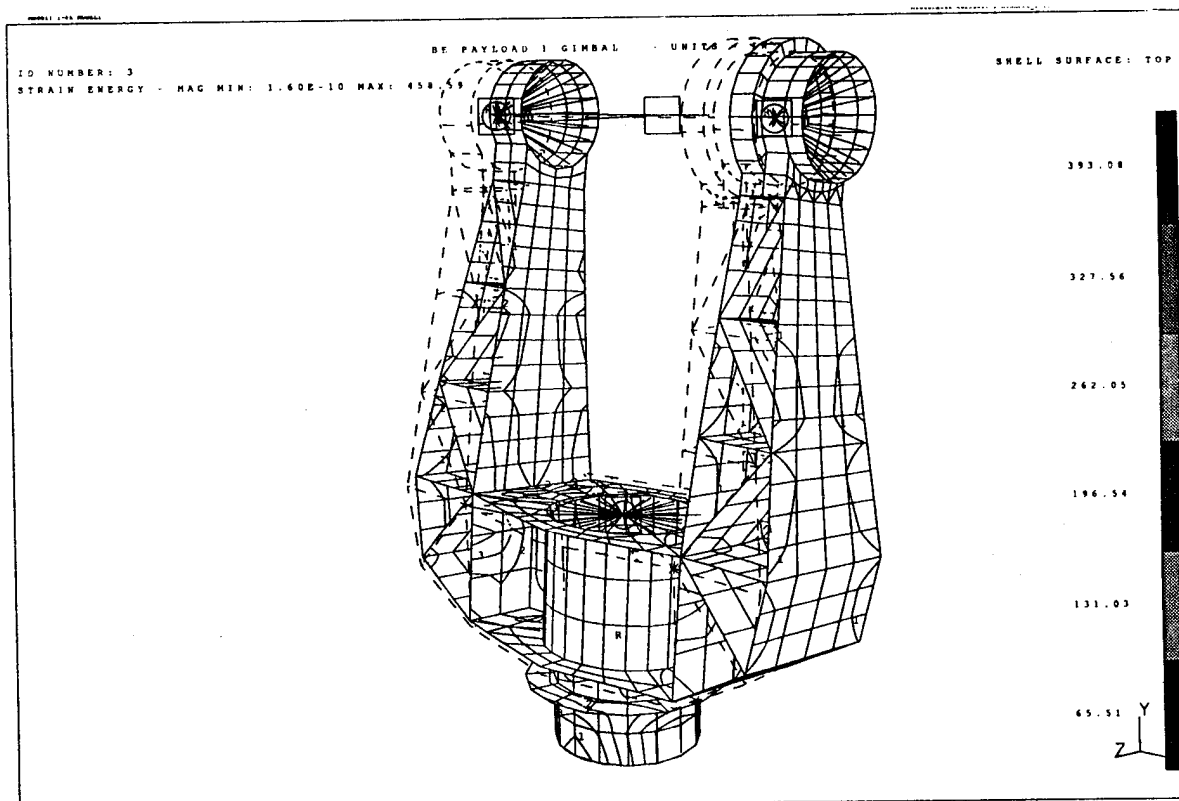


**Fig. 8-22   BE Payload 1, 1st Structural Mode 82.9 Hz**

The results of the modal analysis of the payload 2 gimbal are presented below in Table 8-2. The results show that the current design meets the desired structure frequency requirement of 100 Hz. A diagram of the 1st structural mode is presented in Fig. 8-23. Again, the diagram contains the strain energy density distribution superimposed on the mode shape.

**Table 8-2.   Preliminary Frequencies for the   LMSC BE Payload 2 Gimbal**

| Mode | Frequency | Description |
|------|-----------|-------------|
| 1 | 0.0 | Elevation axis rigid body mode |
| 2 | 0.0 | Azimuth axis rigid body mode |
| 3 | 100.6 | 1st cantilever mode YZ plane |
| 4 | 114.23 | 1st cantilever mode XZ plane |

- 249 -

The work done on the BE gimbals provided realistic structure models which can be included in future bearing simulations. Up until now the structure models used for the simulation work have been crude in comparison. The inclusion of the structure data from these model should give us a more realistic idea of the effect of the torque ripple and a high frequency structure on the gimbal pointing performance.
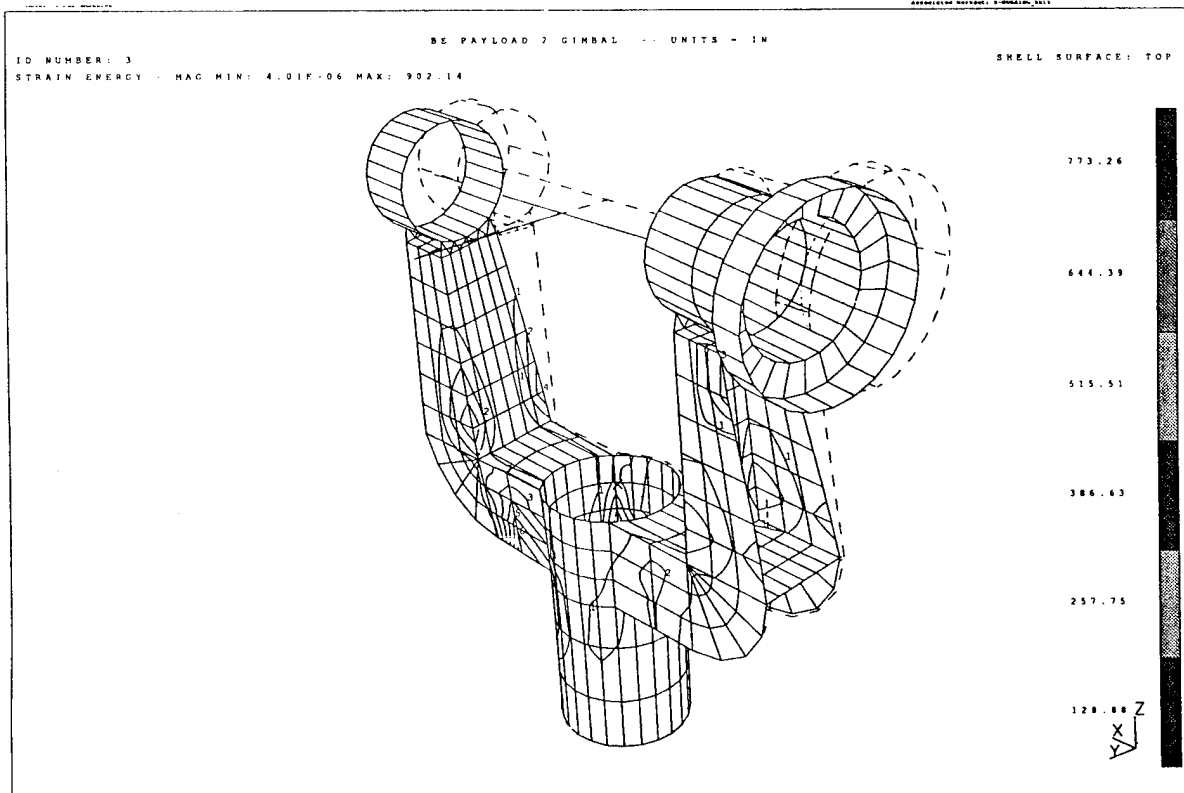


**Fig. 8-23   BE Payload 2, 1st Structural Mode 100.6 Hz**

## 8.4 LMSC HYBRID FLEXURE BEARING

The unique configuration of ball bearing and rotary flexure enables LMSC Hybrid Flexure (HF) bearing to provide low friction small angle pointing as well as large angle slew capability. The HF bearing was evaluated as an effective low friction, disturbance isolation bearing assembly for spacecraft gimbal applications.

The Hybrid Flexure bearing can be utilized in an active and passive mode. In the active mode, the rotation of the flexure cylinder is controlled through a high bandwidth servo system that attempts to zero out the relative displacement between the flexure cylinder and the gimbaled payload. In this manner, bearing disturbance torque, as well other parasitic torque such as cable wrap wind-up, are canceled or isolated from the gimbaled payload. Simulation studies have shown that the active HF bearing can attenuate spacecraft born disturbances up to 60 times greater than a standard bearing configuration (see Fig. 8-24). In particular, gimbal systems that must acquire data during maneuvers that involve velocity reversals or start-stop situations would benefit the greatest from the active HF bearing [8-4]. The large bearing torque gradients that occur during a velocity reversal or stop-start situation are canceled by the active servo system of the HF bearing. The gimbaled payload and its drive system are isolated from these large bearing torque disturbances.

The Passive Hybrid Flexure (PHF) bearing is a low cost and smaller size alternative that does not require the expensive electronics that are associated with an active servo system. Because the active cancellation of bearing disturbance torques does not occur in the passive version, there are restrictions on the type of gimbal maneuver that can be performed with the PHF bearing. During large angle slew maneuvers the PHF bearing exhibits a stick-slip phenomenon that can cause large gimbal scanning errors. As the stiffness of the flexures is increased, a threshold is crossed where the stick-slip phenomenon disappears. The value of the flexure stiffness, where the stick-slip phenomenon threshold occurs, is affected by the gimbal scan profile, the gimbal and flexure inertias, and the bearing disturbance torque parameters. For a particular gimbal, the flexure stiffness can be optimized for different gimbal scanning or pointing scenarios. For inertial pointing applications the flexure stiffness would be designed as low as possible in order to effectively isolate the payload from external spacecraft disturbances. For scanning applications, the flexure stiffness would be designed high enough to avoid the stick-slip phenomenon while still retaining some
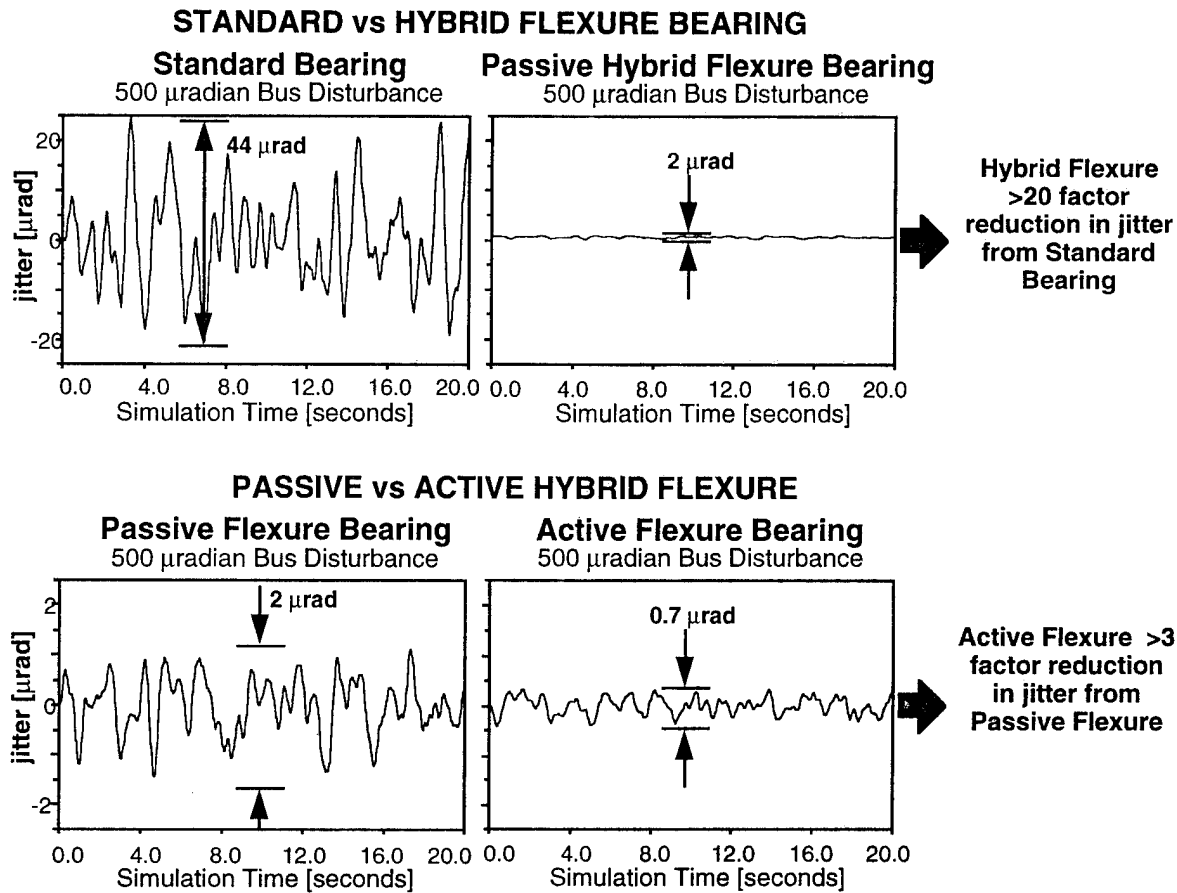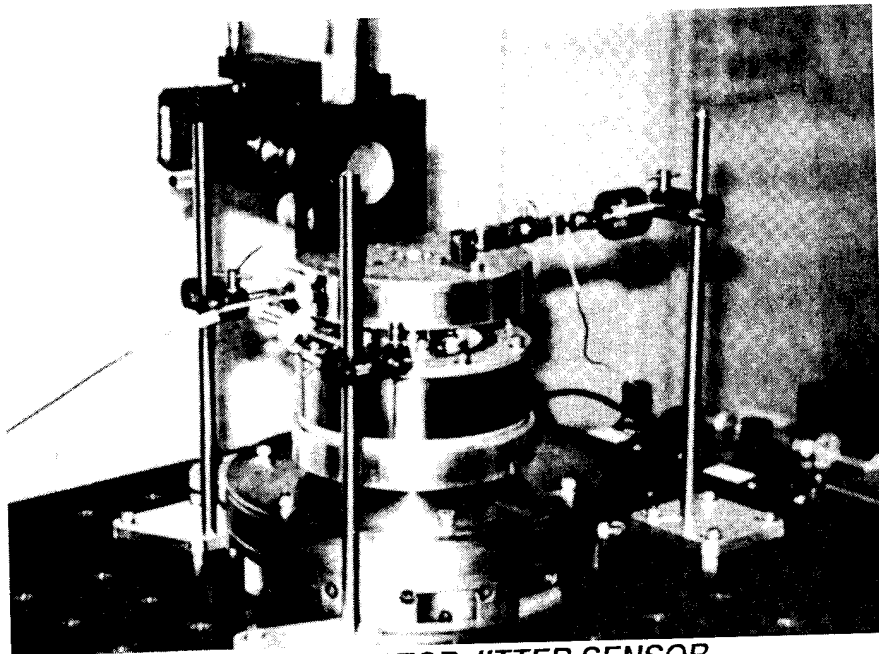
# STANDARD vs HYBRID FLEXURE BEARING

## Standard Bearing
### 500 μradian Bus Disturbance

## Passive Hybrid Flexure Bearing
### 500 μradian Bus Disturbance

**Hybrid Flexure >20 factor reduction in jitter from Standard Bearing**

## PASSIVE vs ACTIVE HYBRID FLEXURE

## Passive Flexure Bearing
### 500 μradian Bus Disturbance

## Active Flexure Bearing
### 500 μradian Bus Disturbance

**Active Flexure >3 factor reduction in jitter from Passive Flexure**

**Fig. 8-24   Hybrid Flexure Bearing Comparison**

passive isolation characteristics. In some instances, the elimination of the stick-slip phenomenon may require a very high flexure stiffness, which would eliminate the passive isolation benefits of the flexure bearing. As a result, some situations where data must be collected while the gimbal is scanning may not be appropriate applications for the passive Hybrid Flexure Bearing. However, applications such as inertial pointing are well suited for the passive Hybrid Flexure Bearing. The small gimbal rotations that are needed to compensate for spacecraft attitude adjustments or disturbances occur in the passive Hybrid Flexure Bearing's flexure range because the bearings do not rotate until the flexure torque exceeds the bearing torque. The passive Hybrid Flexure Bearing acts as a passive isolation system from the gimbaled payload to the spacecraft bus. In an inertial pointing mode, the passive Hybrid Flexure Bearing attenuates spacecraft born disturbances 20 times greater than a standard bearing (see Fig. 8-24).

In summary, the active Hybrid Flexure Bearing shows promise for all types of gimbal maneuvers while the low cost passive Hybrid Flexure Bearing shows promise for applications that involve inertial pointing.

### 8.4.1 Passive Hybrid Flexure Testbed

A optical bench testbed was constructed to evaluate the jitter reduction performance potential of the passive Hybrid Flexure Bearing. The setup used the rate table described earlier together with the autocolliminator. (Fig. 8-25). A mirror mounted on an optical bench is supported by a flexure pivot which is attached to the 5 inch test bearing. The mirror, which functionally represents the sensor on a gimbaled payload, faces an autocollimator. The autocollimator directly measures the disturbance motion (jitter) from irregular bearing torque. A reaction load cell prevents the optical bench from rotating and records bearing disturbance torque imposed on the optical bench as the bearing outer race is turned by the rotary air turntable.



NOTE: AUTO COLLIMATOR JITTER SENSOR
& OPTICAL BENCH RESTRAINED BY LOAD CELL

**Fig. 8-25.     Hybrid Flexure Bearing Test Setup Showing Optical Bench**

### 8.4.2 Test Results

The effect of varying flexure stiffness on bearing system reaction torque is shown in Fig. 8-26. Here the turntable is gimbaled back and forth through ± 5 deg., representing a possible gimbal target tracking mode. Note the considerable improvement in both torque level and disturbance torque noise acting on the optical bench as flexure pivot torsional stiffness is decreased. The performance with the "stiff" flexure approximates that of a bearing with out the passive Hybrid Flexure. In the case of the soft flexure, the full ± 5 deg. travel can be accommodated by flexure and bearing windup (Dahl friction slope region) without the balls in the bearing breaking away. Torque and torque jitter level are at least 3X smaller than for the non-passive HF bearing. For the medium and stiff flexures, ± 5 deg motion is too large and optical bench disturbance torque from the balls rotating become significant. While the soft flexure may be too radially compliant because gimbal

- 253 -

servo bandwidth considerations, a compromise between flexure stiffness and gimbal inertial pointing angle can be made. Slew speeds from 0.25 to 10 deg/sec seem to have little effect on this phenomena.
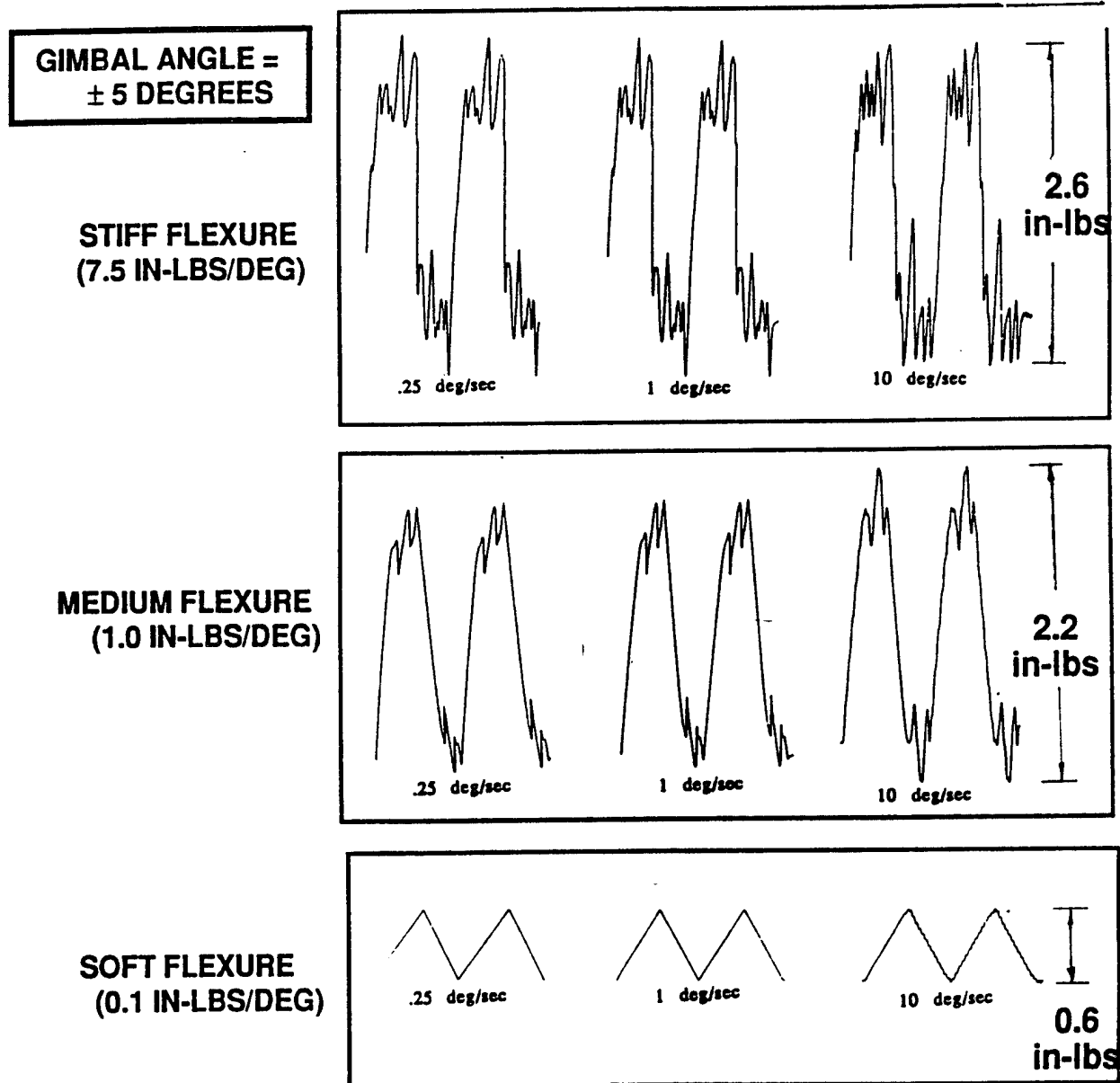
GIMBAL ANGLE =
± 5 DEGREES

STIFF FLEXURE
(7.5 IN-LBS/DEG)

2.6 in-lbs

.25 deg/sec        1 deg/sec        10 deg/sec

MEDIUM FLEXURE
(1.0 IN-LBS/DEG)

2.2 in-lbs

.25 deg/sec        1 deg/sec        10 deg/sec

SOFT FLEXURE
(0.1 IN-LBS/DEG)

.25 deg/sec        1 deg/sec        10 deg/sec

0.6 in-lbs

**Fig. 8-26.    Effect of Flexure Stiffness of Torque Jitter Performance**

In the case of large transverse slewing maneuvers, the bearing jitter levels are actually higher (not shown) with the soft flexure than with the stiff flexure. This is because the soft spring amplifies motion due to bearing torque disturbances as correctly predicted by the earlier simulations discussed above. Thus, the passive HF bearing is only recommended for staring applications such as the elevation axis

HF bearing is only recommended for staring applications such as the elevation axis hold of the BE payload having an inner nulling servo-loop. On the other hand, an active Hybrid Flexure bearing will provide significant jitter reductions in all modes of operation.

## 8.4.3 Turntable Simulation.

**Model Description** The PHF model consists of three rigid bodies which interact with each other. Body 1 consists of the rotating portion of the air bearing turntable and the bearing outer race. Body 2 consists of the bearing inner race and the inner race/flexure adapter. Body 3 consists of the optical bench platform. The mirror in conjunction with an autocollimator provide a means to evaluate optical jitter with and without the PHF in the system. The interaction torques are described below.

The primary bearing disturbance torque model is used to simulate the torque between bodies 1 and 2. The bearing model includes: 1) Dahl friction; 2) torque hash for BOL or EOL bearings; 3) angular runout; and 4) viscous friction. Specifics associated with each bearing sub-model were discussed in Section 8.1.

**Hybrid Flexure** Three different Lucas AS Flexure Pivots were used to evaluate the flexures' disturbance rejection characteristics. Flexure pivots with differing torsional stiffness were chosen for preliminary evaluation in test bed. A linear torsional stiffness model is used to simulate the flexure torque produced between bodies 2 and 3. The Lucas part numbers and stiffnesses are presented in Table 8-3.

**Table 8-3. Flexure Stiffness between The Optical Bench and the Inner Race Adapter**

| Catalog Number | Rotation Stiffness (in-lb/rad) |
|---|---|
| 5032-400 | 431 |
| 5032-600 | 53.8 |
| 5032-800 | 6.7 |

**Load Cell/Bellows** The reaction load cell is attached to flexible bellows. The two are modeled as springs in series. One end of the load cell/bellows is attached to the Optical bench while the other is rigidly restrained through its attachment to the granite block. The load-cell/bellows acts as a flexible restraint to the optical bench. It provides a mechanism for the control of the optical bench rotation when acted upon by various flexure/bearing combinations.

**Turntable Motor Cogging** Since the precision turntable is mounted on air bearings, the only major disturbance torque from the turntable itself is due to the drive motor. The brushless DC drive motor was selected to provide minimum friction drag and cogging. Preliminary estimates of the turntable motor cogging torque show that the cogging disturbance should have a frequency of 120 cycles per shaft revolution and an amplitude of 0.66 in-lbs. A properly tuned hybrid flexure should significantly reduce the jitter due to cogging.

**Test vs. Predictions** A comparison between test results (Fig. 8-27) and the predictions (Fig. 8-28) shows very good agreement. The trends observed during the test were clearly exhibited in the simulation. The model matched torque predictions in each of the flexure stiffness vs. scan rate scenarios. Scan rates of 0.25°/s, 1.0 °/s, and 10.0 °/s were used to evaluate the flexure. The simulation was able to predict both the low frequency and high frequency torque levels.
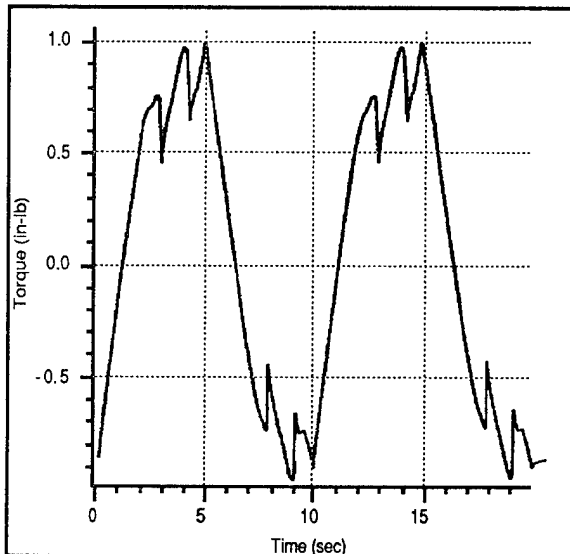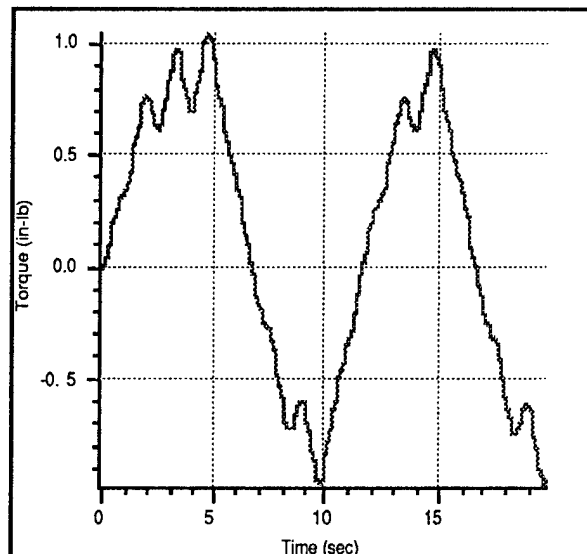


**Fig. 8-27. Test Flexure Torque**



**Fig. 8-28. Simulated Flexure Torque**

The simulations showed the same trends that were exhibited in the test data. That is, 1) the scan rate has little effect on the Flexure Torque time history; 2) the stiffer the flexure the greater the amount of bearing torque noise transmitted and the higher the torque levels; 3) the softer flexure provided enough compliance to fail break out of the bearing Dahl friction wind-up zone (this is partially due to the small scanning angle).

**Conclusions** The results show that a PHF is well suited for inertial pointing but is not recommended for high agility slewing maneuvers. For high agility slew maneuvers an active hybrid flexure design is required to attenuate jitter levels attributed to the bearing. The test results gathered also show good agreement between predicted and test flexure torque.

## 8.5 SUMMARY & CONCLUSIONS

The major accomplishments and conclusions that have come from the gimbal/bearing simulation work to date are:

- **Gimbal/Bearing Simulation**

A detailed bearing disturbance model was used to evaluate the effect of bearing torque disturbances on gimbal pointing performance. The bearing model included torque signature, Dahl friction, torque hash, runout, viscous friction, as well as end-of-life behavior such as torque blocking, torque bump, and turnaround (stiction) torque. Actual beginning and end of life test bearing data, such as runout, torque ripple, and Dahl friction, were used as input to the model.

- **Bearing End-of-Life Effects**

Predictions show that gimbal pointing performance is directly related to bearing torque disturbance levels. In simulation runs, using a number of different nominal gimbal configurations, the bearing disturbance torque level was varied based on actual torque data obtained from bearing life tests. In each instance the gimbal jitter level increased at a ratio of approximately one to one with the bearing torque level. In summary, the gimbal performance is directly linked to the bearing performance and, as a result, as the bearing reaches end of life condition, the function of the gimbal is lost.

- **Gimbal Jitter Breakdown**

Simulation results have shown that the contribution of the bearing disturbance torque to gimbal jitter can be in excess of 70% during constant velocity scans. Other disturbance sources, such as cable wrap and motor cogging, contribute less than 15%. As a result, a reduction of bearing torque levels by 50% could reduce the overall gimbal jitter by ~35%. In summary, the bearing disturbance torque is a major, if not the largest, contributor to gimbal jitter and, subsequently, improved bearing tribomaterials could significantly improve the performance of a precision gimbal system.

- **Gimbal Jitter Reduction From Hybrid Flexure Bearing**

Simulation results have shown that LMSC Hybrid Flexure Bearing concept can significantly reduce the jitter levels of gimbaled sensors. The Active Hybrid Flexure Bearing was shown to reduce gimbal jitter levels by a factor of 60 under all types of gimbal maneuvers. The low cost, Passive Hybrid Flexure Bearing was shown to reduce gimbal jitter levels of 3 to 10 times for inertial pointing applications only. Test results confirm that a soft flexure provides the greatest jitter reductions for pointing but causes degraded performance for large angle tracking.

# References for Section 8

[8-1]   Dahl, P.R., "A Solid Friction Model," AFO 4695-67-C-D158, Aerospace Corp., May 1968

[8-2]   Todd, M.J., and Johnson, K.L., "A Model For Coulomb Torque Hysteresis in Ball Bearings," Int. J. Mech. Sci. Vol. 29, No. 5, pp 339-354, 1987

[8-3]   Bearing Friction Slope Results, EM No. SL-043, Lockheed Missiles and Space Company, July 1989

[8-4]   SDIO Tribomaterials Precision Gimbal Program, Phase I Final Report, SDIO Contract Number SDIO84-89-C-0028, October 1989

[8-5]   ISF Solar Array Twistflex Torque Measurement Tests, EM No. ISF2A08, Lockheed Missiles and Space Company, December 1987

[8-6]   Rabinowicz, E., "A Study of the Stick-Slip Process," Proc. Symp. Friction and Wear, Detroit 1957

[8-7]   Singh, B.R., "Study of Critical Velocity of Stick-Slip Sliding," J. Engng. Industr., Trans. Am. Soc. Mech. Engrs., 82, 1960 Series B, 393

[8-8]   Brockley, C.A., Cameron, R. and Potter, A.F., "Friction-Induced Vibration," J. Lubric. Technol., Trans. Am. Soc. Mech. Engrs., 90, 1968 Series F, 35

[8-9]   Hughes et al., Space Station Freedom Payload Pointing System, Disturbance Environment and Pointing Performance Study, PIR 1K10-SS-251, General Electric, Astro-Space Division, May 1989

[8-10]  Loewenthal, S.H., Two Gimbal Bearing Case Studies:  Some Lessons Learned, Proc. 22nd Aerospace Mechanisms Symp. 1988. p253

## Section 9

# CONCLUSIONS

The efforts under the Tribomaterial/Precision Gimbal Program have advanced the application of ion-sputtered MoS2 films for space bearing applications. Under this effort, a considerable test data base was generated using realistic flight-like bearings, loads and operating conditions. A total of 270,000 cumulative life test hours were obtained on precision angular contact ball bearings lubricated with 33 different tribomaterial combinations (lubricant, bearing cage material, ball material or coating). Three different ion-sputtered MoS2 processes were evaluated. The information generated supports a decision when to insert these advanced tribomaterials into precision gimbal bearing assemblies.

### Accomplishments included:

- life tests to 48 million cycles conducted on a total of 55 pairs of bearings comprised of three sizes that envelope those proposed for SDIO gimbal systems.

- direct performance comparisons with test bearings lubricated with several traditional and advanced space gimbal greases.

- detailed characterization of film morphology, failure mechanisms and important film properties.

- development of two U.S. commercial sources for ion-sputtering bearings with MoS2.

- identification of producibility issues and quality control needs.

- development / evaluation of improved Hohman-antimony films with variable current deposition and more fracture resistant Ovonics films having interlayers with high gold content.

- assessment of the potential benefits of low torque bearings to gimbal pointing performance.

- generation of an extensive torque, runout, Dahl friction data base for both MoS2 and liquid lubricated bearings at both beginning and end of life.

- development of detailed bearing disturbance model for gimbal pointing simulations.

- demonstration of the torque ripple reduction benefits of the Lockheed Hybrid Flexure Bearing concept along with its associated limitations.

### Key findings include:

- MoS2 coated bearings show excellent torque performance until film failure, primarily through delamination, or until there is excessive retainer transfer film deposits.
  - failed MoS2 film can still provide long life operation as a burnished film.
  - occasional torque excursions can occur, particularly between gimbaling modes.

- Long lived bearings require replenishment from self-lubricating retainers, such as those comprised of PTFE.

- In the tests conducted here, the use of ceramic balls and those coated with MoS2 resulted in short bearing life.

- Primary torque failure mode is debris-related preload increase.
  - large diameter, hard-preloaded, thin-sectioned bearings are particularly debris-torque sensitive. Spring preloaded bearing assemblies are more tolerant.
- Over-transfer of retainer film leads to increase torque and under-transfer leads to bearing race wear.
  - a proper match between the retainer material with the $MoS_2$ film and bearing operating condition is critical for good torque performance.

## *Additional improvements to film performance and application include:*

- Development of "tougher" $MoS_2$ films that are more fracture resistant, with higher adherence and more tolerant of Hertzian stress and surface roughness.

- Better characterization of retainer transfer film lubrication, including the effects of material composition, retainer geometry-ball interaction and the effects of bearing load, speed, temperature, and gimbaling motion.

- Development of an industry standardized $MoS_2$ process specification with well defined quality control evaluation procedure.
  - tests that measure mechanical properties such as fracture toughness, hardness, and rolling contact resistance appear to be more important in process control than chemistry, texture or morphology.

- 260 -